Genome-Wide Identification and Characterization of Stimulus-Responsive Enhancers in the Nervous System

Genome-wide identification and characterization of stimulus-responsive enhancers in the nervous system

A dissertation presented

by

Athar Naveed Malik

to

The Division of Medical Sciences

in partial fulfillment of the requirements

for the degree of

Doctor of Philosophy

in the subject of

Neurobiology

Harvard University
Cambridge, Massachusetts

May 2013

Dissertation Advisor: Professor Michael Greenberg Athar Naveed Malik

Genome-wide identification and characterization

of stimulus-responsive enhancers in the nervous system

Abstract

During development, intrinsic genetic programs give rise to distinct cellular lineages through the establishment of cell type specific chromatin states. These distinct chromatin states instruct gene expression primarily through the genome-wide demarcation of enhancers. In addition to maintaining cellular identity, the chromatin state of a cell provides a platform for transcriptional responses to environmental signals. However, relatively little is known about the influence of extracellular stimuli on chromatin state at enhancers, and it is not clear which enhancers among the tens of thousands that have been recently identified function to drive stimulus-responsive transcription.

In the nervous system, the chromatin state of terminally differentiated neurons not only maintains neuronal identity but also provides a platform for sensory experience-dependent gene expression, which plays a critical role in the development and refinement of neural circuits and in long-lasting changes in neuronal function that

underlie learning, memory, and behavior. Using chromatin-immunoprecipitation followed by high through put sequencing (ChIP-Seq), we determined the effects of neuronal stimuli on the active chromatin landscape of mouse cortical neurons. We discover that stimulation with neuronal activity and brain derived neurotrophic factor (BDNF) cause rapid, widespread, and distinct changes in the acetylation of histone H3 lysine 27 (H3K27Ac) at thousands of enhancers throughout the neuronal genome. We find that functional stimulus-responsive enhancers can be identified by stimulus-inducible H3K27Ac, and we use this dynamic chromatin signature to discover neuronal enhancers that respond to neuronal activity, BDNF, or both stimuli. Finally, we investigate the transcriptional mechanisms underlying the function of stimulus responsive enhancers. We show that a subset of stimulus-responsive enhancers in the nervous system require the coordinated action of the stimulus-general transcription factor activator protein 1 (AP1) with additional stimulus-specific factors.

Our studies reveal the genome-wide basis for transcriptional specificity in response to distinct neuronal stimuli. Furthermore, the comprehensive identification of neuronal activity and BDNF-dependent enhancers in cortical neurons provides a critical resource for elucidating the role of stimulus-responsive transcription in synaptic plasticity, learning and memory, behavior, and disease. Finally, the epigenetic signature of stimulus-inducible H3K27Ac may aid in the identification and study of stimulus-regulated enhancers in other tissues.

TABLE OF CONTENTS

LIST OF FIGURES

LIST OF TABLES

DEDICATION

In the name of Allah, the Gracious, the Merciful.

The Holy Quran [1:1]

In the creation of the heavens and the earth and in the alternation of the night and the day there are indeed Signs for men of understanding; Those who remember Allah while standing, sitting, and lying on their sides, and ponder over the creation of the heavens and the earth; and say: "Our Lord, Thou hast not created this in vain; nay, Holy art Thou."

The Holy Quran [3:191-192]

Blessed is He ... Who has created seven heavens in harmony. No incongruity canst thou see in the creation of the Gracious God. Then look again. Seest thou any flaw? Aye, look again, and yet again, thy sight will only return unto thee confused and fatigued, having seen no incongruity.

The Holy Quran [67:2-5]

Say, 'My Prayer and my sacrifice and my life and my death are all for Allah, the Lord of the worlds.'

The Holy Quran [6:163]

I dedicate this thesis, everything that has led to it, and any good that may come from it, to Allah, the Lord of the worlds.

ACKNOWLEDGEMENTS

Over the course of my doctoral training, I have had the opportunity to work with and learn from many extraordinary scientists. Foremost among these individuals is my advisor Michael Greenberg. Mike accepted me into his laboratory at a time when I had little experience in molecular biology, biochemistry, genomics, or neuroscience, fields that my work in his laboratory would eventually require. Mike jokes that when I first joined the laboratory, I barely knew how to pipette. While I wouldn't go that far, I certainly realize that I had a lot to learn. Due to the opportunity that Mike gave me to train in his laboratory, I am know not only a pipetting expert, but I have also learned a great many of the diverse techniques and experimental methods used in his laboratory. But all this is technical. What I am most indebted to Mike for is shaping me as a scientist. Mike is not only a scientist of the highest caliber, he is also an extraordinary scientific mentor. One of the things that I noticed early on about Mike was that he has a clear vision of what it takes to be a successful scientist and how to train someone to get there. Mike has developed within me the intellectual qualities of independent judgment, scientific rigor, depth of thought, concentration, and hard work. Furthermore, Mike has provided me with all of the resources I could imagine to pursue my research. I always felt that if an experiment were scientifically justified, I would have the opportunity to perform it in Mike's lab. This support enabled me to pursue scientific questions in a manner limited only by my creativity and the hours of the day. This has been a great joy and privilege, and I thank Mike for providing me the opportunity to experience scientific research in such a pure form.

One of Mike's great skills as a scientist and as a mentor is to assemble individuals from diverse backgrounds into his laboratory to work together to answer scientific problems. I have had the good fortune of working with and learning a great many extraordinary people in Mike's laboratory. I will start at the beginning of my tenure in the lab, when I had the opportunity to rotate with Yingxi Lin, then a postdoctoral fellow in the lab. Yingxi taught me to be persistent and optimistic, even in the face of failed experiments. She also helped me perform my first ChIP experiments during my rotation. Little did I know that that would serve as a foundation for my later work in the lab! For all this, I thank her. When I first joined the lab, I had the opportunity to work with Steven Flavell, a senior graduate student in the lab. Steve taught me the importance of cultivating good scientific habits, reading scientific literature, and thinking creatively about scientific problems, and I thank him for these important lessons.

After working with Steve, I worked largely independently for a time but then had the opportunity to work with a research assistant, Alex Rubin. Alex has been a pleasure to work with and has been a model research assistant. Alex learns quickly and can function independently. Because of his tremendous efficacy within the lab, I have often gotten overenthusiastic about the experiments that Alex and I might be able to do within a short period of time. Alex has somehow been able to keep up with most of my experimental enthusiasm, but has also kept me grounded in what we might be able to realistically accomplish. For all this, I thank Alex.

One of the challenges in the generation of genomic data is its analysis. As I have generated a substantial amount of genomic data during my doctoral research, analyzing

it has been a considerable challenge. I am indebted to Martin Hemberg, a postdoctoral fellow who has been a longstanding bioinformatics collaborator throughout my doctoral research. Martin has been a great help in performing analyses of genomic data and has taught me a great deal in this regard. I thank Martin for his past and continuing support. In addition to Martin, I would like to thank research scientist David Harmin and postdoctoral fellow Kai-How Farh for their help with various genomic analyses and for helpful discussions. I am also indebted to the course instructors for "Integrated Statistical Analysis of Genome Scale Data," a course I took at Cold Spring Harbor Laboratory in the summer of 2011. They provided me with a foundation upon which I build the skills necessary to analyze genomic data.

I have recently had the opportunity to begin working closely with Thomas Vierbuchen, a talented new postdoctoral fellow in the lab. Tommy has helped with various experiments and plans to continue some of the research that I have been working on in the laboratory after I leave. It has been a pleasure to work with Tommy and I thank him for his help, his advice, and for always being willing to share his perspective on science.

Through collaborations, I had the opportunity to work with Bulent Ataman, Michael Soskis, Vijay Ganesh, and Milena Andzelm. I have learned from all of these excellent scientists and have greatly valued the chance to share in the excitement of their scientific projects. I thank them for giving me these opportunities. Milena has also been my bay-mate for many years and I thank her for her scientific input as well as her helpful discussions on science, careers, and life.

During an earlier part of my doctoral research, I embarked upon studying the role of AP1 transcription factors in synapse development. This led me to eventually perform physiological recordings of miniature inhibitory post-synaptic currents from CA1 pyramidal cells in hippocampal organotypic slice cultures that had been biolistically transfected with shRNA constructs targeting AP1 transcription factors. I thank Brenda Bloodgood, a former postdoctoral fellow, for teaching me to do these technically challenging experiments, and to analyze the resulting data.

While I did not have the opportunity to formally work with them, several other members of the Greenberg laboratory have supported me and have contributed to my development as a scientist. Seth Margolis was a great support to me. He was always willing to listen, to discuss ideas for experiments, and to provide encouragement along the way, and for these things I thank him. Nikhil Sharma has not only provided me critical feedback about my research but has also shaped me as a scientist by emphasizing to me the necessity of focusing on the science above all else, and thinking deeply about scientific questions. I thank him for these lessons and for his inspirational example. Henry Ho has been longstanding colleague in the lab. He has always been willing to answer my questions and taught me through his example about the true meaning of dedication to science. Jesse Gray has provided me with excellent feedback at various stages during my doctoral research and has taught me to intelligently adapt new technologies to answer scientific questions, and for these things I thank him. Harrison Gabel has provided me with important scientific input at various stages of my doctoral research, has taught me to weigh the potential benefits of an experiment by the time and effort it will take to get an answer, and has provided me with company during

our summer at the CSHL course and at triathlons around Massachusetts. For all these things, I thank him. John Salogiannis has been my classmate and friend from the beginning of graduate school. I thank him for his support and his advice. Mike Soskis and Alan Mardinly, the two graduate students in Mike's lab who most recently defended their PhD's, have provided me with advice and support as I have assembled my thesis and for this I sincerely thank them.

I must also thank all other Greenberg lab members, past and present, for making the lab such a great place to train as a scientist. These include former fellow graduate students Paul Greer, Betty Hong, Jay Bikoff, Sonia Cohen, and Ray Shao; current graduate students Emi Ling, Caleigh-Mandel Brehm, Mike Susman, Benyam Kinde, and Shela Durresi; former postdoctoral fellows Tae-Kyung Kim, Yong-Chao Ma, Joe Zhou, Zak Wills, and Sarah Ross; current postdoctoral fellows Dan Ebert, Rock Liao, Ivo Spiegel, Xu Tao, Tim Cherry, and Gabriella Boulting; our lab administrators Shannon Robichaud, Valorie Kopp-Aharonov, and Janine Zieg; our grants specialist Eric Griffith; our mouse specialist Pingping Zhang; our antibody specialist Linda Hu; and our mouse neuron dissection specialist Sara Vasquez.

I would like to thank all the faculty and programs that have advised me during my PhD, including the Harvard Medical School Neurobiology Ph.D. Program including Richard Born, Rachel Wilson, and Karen Harmin; my Dissertation Advisory Committee members David Clapham, Azad Bonni, and Joshua Kaplan; the Harvard Medical School M.D./Ph.D. program including Christopher A. Walsh, Steven Blacklow, Thomas Michel, David Frank, Marcia Goldberg, Robin Lichtenstein, and Linda Burnley; the Harvard Medical School HST M.D. Program including David Cohen, Richard Mitchell, Joseph

Bonventre, and Patty Cunningham; and my Dissertation Defense Committee members David Clapham, Christopher A. Walsh, Richard Young, and Bradley Bernstein.

I would like to also thank influential mentors and teachers from my past who developed within me an excitement for scientific research, including my undergraduate research advisor Jennifer Elisseeff, my high school physics teacher Mr. Martell, and my high school introduction to physical science teacher Mr. Coleman.

Finally, I would like to thank my family who has supported me unconditionally during my training, with encouragement, belief in me, and prayers. My father Nasir and my mother Nuzhat were my first and most important teachers, mentors, and supporters. I am indebted to them for instilling within me the desire and the ambition to pursue knowledge for the benefit of mankind. My older brother Ahmad and my younger sisters Lubna and Atiya, have all supported me throughout my training. I am extremely thankful to them and grateful to have them in my life. I also thank my larger family within my religious community, the Ahmadiyya Muslim Community, for their constant support and prayers. And, in the end, I must thank God for his grace and mercy and for everything He has provided for me to be writing this thesis.

ATTRIBUTIONS

All work in this thesis was initiated by Athar Malik. Athar Malik conceived and designed all experiments, performed all ChIP-Seq and RNA-Seq experiments, performed the majority of the bioinformatic analyses of ChIP-Seq and RNA-Seq data, assisted with luciferase reporter assays and analysis of luciferase reporter data, and wrote the thesis. Alex Rubin performed the majority of luciferase reporter assays and analysis of luciferase reporter data. Thomas Vierbuchen cloned the AP1 dominant negative *A-Fos* and assisted with luciferase reporter assays. Martin Hemberg and David Harmin assisted with bioinformatics analyses. Michael Greenberg supervised all research.

1 GENERAL INTRODUCTION

The nervous system enables higher organisms to not only sense and respond to the environment, but also to learn from and remember past experiences. Importantly, these fundamental functions of the nervous system are emergent properties that derive from the ability of individual neurons to sense, respond, and adapt to sensory stimuli. A characteristic component of the neuronal response and adaptation to extracellular stimuli is new gene transcription. This phenomenon, first discovered over 25 years ago, is now know to play a critical role in the development and function of the nervous system, and perturbations in this program of gene expression are thought to contribute to neurological disease. Despite great progress over the past decades in understanding the mechanisms underlying stimulus-dependent programs of gene expression, major question remain. How is neuronal chromatin affected by extracellular stimuli? What are the enhancers in the genome that drive stimulus-dependent transcription? What is the regulatory logic of these elements? How are specific transcriptional responses generated for different stimuli? What transcription factors play a role in generating these responses? How do multiple transcription factors work together to achieve this purpose? What are the effector molecules regulated by stimulus-responsive transcription factors that mediate adaptive cellular responses to neuronal activity? These are some of the questions that have motivated my thesis work.

1.1 DISCOVERY OF STIMULUS-RESPONSIVE TRANSCRIPTION IN THE NERVOUS SYSTEM

Stimulus-responsive transcription in the nervous system was discovered nearly 30 years ago with the discovery of neuronal activity-dependent transcription of the *c-Fos* gene. Stimulation of neuronal cells with either the cholinergic agonist nicotine or membrane depolarization with elevated extracellular concentrations of potassium chloride (KCl) was shown induce transcription of *c-Fos* (Greenberg et al., 1986). In addition to discovering this phenomenon, this first study also showed several key characteristics of neuronal activity-dependent transcription. Activity-dependent transcription was shown to be rapid, occurring with 5 minutes of stimulation. Furthermore, activity-dependent transcription was shown to be transient, lasting approximately 30 minutes after stimulus onset. Finally, activity-dependent transcription was shown to be dependent on extracellular calcium, being abolished when cells were cultured in the presence of the calcium chelator ethylene glycol tetraacetic acid (EGTA). It is interesting to note that this influential study that set the ground for many subsequent discoveries in the nervous system was done in neuronally differentiated PC12 cells. PC12 cells are a cell line derived from a rat pheochromocytoma, which is a neuroendocrine tumor of the medulla of the adrenal gland. Previous work had shown that these cells differentiate into neuronal cells when exposed to nerve growth factor, establishing PC12 cells as a useful culture system to study neuronal cells (Greene and Tischler, 1976). While the initial discovery of neuronal activity-dependent transcription was made in this somewhat artificial cell culture system, neuronal activity-dependent transcription was subsequently observed in many

additional contexts, demonstrating the power of simplified model systems to observe and study biological phenomena.

Soon after the initial discovery of activity-dependent induction of *c-Fos* in PC12 cells *in vitro*, several groups observed *c-Fos* induction in response to activity in cultured primary neurons *in vitro* (Hunt et al., 1987; Szekely et al., 1987) and in response to diverse stimuli in the nervous system *in vivo* (Morgan and Curran, 1991). Many of the stimuli that have been shown to induce *c-Fos* in the nervous system in-vivo are stimuli that increase neuronal activity or activate particular neural circuits. Such stimuli include the convulsant pentylenetetrazol (Morgan et al., 1987; Saffen et al., 1988; Sonnenberg et al., 1989a; Sonnenberg et al., 1989b; Sonnenberg et al., 1989c), the stimulant kainic acid (Le Gal La Salle, 1988; Popovici et al., 1990; Sonnenberg et al., 1989b), electrical stimulation (Daval et al., 1989; Douglas et al., 1988; Dragunow and Robertson, 1987; Hunt et al., 1987; Sagar et al., 1988; Sharp et al., 1989b; Shin et al., 1990; Sonnenberg et al., 1989b; White and Gall, 1987; Winston et al., 1990; Wisden et al., 1990), the glutamate neurotransmitter receptor agonist N-methyl-D-aspartic acid (NMDA) (Cole et al., 1989; Kaczmarek et al., 1988; Sonnenberg et al., 1989b), the γ-aminobutyric acid receptor (GABAR) antagonist picrotoxin (Sonnenberg et al., 1989b), D1-dopamine receptor agonists (Robertson et al., 1989a; Robertson et al., 1989b), β-adrenergic receptor agonists (Gubits et al., 1989), the opiate analgesic morphine (Chang et al., 1988), opiate withdrawal (Hayward et al., 1990), nociceptive and peripheral stimulation (Bullitt, 1989; Draisci and Iadarola, 1989; Menetrey et al., 1989; Presley et al., 1990; Wisden et al., 1990), and light stimulation (Aronin et al., 1990; Rea, 1989; Rusak et al., 1990; Sagar et al., 1988). In addition to the above stimuli that increase

neuronal activity and activate neural circuits, additional stimuli not directly related to neuronal activity have also been shown to induce *c-Fos* in the nervous system *in vivo*, including surgical lesions and nerve transections (Dragunow and Robertson, 1988; Sharp et al., 1989a; Sharp et al., 1989c), cerebral ischemia (Jorgensen et al., 1989; Onodera et al., 1989), heat stress (Dragunow et al., 1989), adrenalectomy (Jacobson et al., 1990), intracortical NGF injections (Sharp et al., 1989a), and even intracortical saline injections (Kaczmarek et al., 1988). These data suggest that new gene transcription is a general hallmark of a stimulated neuron. The nature of the stimulus does not appear to matter. Whether a neuron is stimulated with a physiological stimulus, a pathological stimulus, a stimulus related to neuronal activity, or a stimulus unrelated to neuronal activity, genes such as *c-Fos* are induced.

It is important to note that *c-Fos* is not unique in its transcriptional induction by neuronal activity. Soon after the discovery of the activity-dependent transcription of *c-Fos*, other genes were also shown to be induced in response to neuronal activity, including *c-Jun*, *JunB*, and *Egr1* (Saffen et al., 1988; Sukhatme et al., 1988). More recently, investigators have systematically characterized hundred of genes that are induced in neurons in response to neuronal activity (Altar et al., 2004; Hong et al., 2004; Li et al., 2004; Nedivi et al., 1993; Park et al., 2006). Genes induced in the nervous system in response to stimuli can be divided into two waves of induced genes. The first wave of genes, termed immediate early genes, consists of genes like *c-Fos* that are expressed rapidly (within minutes) and transiently in response to stimuli. The second wave of genes, termed late response genes, consists of genes like brain-derived neurotrophic factor (BDNF) that are expressed more slowly (over hours) in response to

stimuli. In general, the transcription of immediate early genes does not require new protein synthesis while the transcription of late response genes does require new protein synthesis. Many immediate early genes encode transcription factors that have been proposed to regulate the transcription of late response genes. Late response genes, in turn, are generally thought to encode molecules that effect longer lasting changes within the cell (Sheng and Greenberg, 1990).

Importantly, the stimulus-dependent induction of *c-Fos* and other genes is not limited to the nervous system. Even before *c-Fos* was shown to be induced by neuronal activity in neuronal cells, it was shown to be induced by serum and growth factors in fibroblasts (Greenberg and Ziff, 1984; Muller et al., 1984). *c-Fos* has also been shown to be induced in numerous other diverse circumstances, including cellular differentiation (Mitchell et al., 1985; Muller et al., 1985), wounding of a fibroblast monolayer (Verrier et al., 1986), thyroid hormone stimulation of thyroid cells (Colletta et al., 1986), IL-1 stimulation of lymphocytes (Kovacs et al., 1986), IGF-1 stimulation of skeletal muscle (Ong et al., 1987), growth hormone releasing hormone stimulation of pituitary cells (Billestrup et al., 1987), heat shock stimulation of HeLa cells (Andrews et al., 1987), follicle stimulating hormone stimulation of Sertoli cells (Hall et al., 1988), interferon stimulation of various cells (Wan et al., 1988), and steroid and growth factor stimulation of breast cancer cells (Wilding et al., 1988). The diverse circumstances in which *c-Fos* is induced suggests that C-FOS may play a critical role in the cellular response to many extracellular signals in many cell types, and that C-FOS may be performing a stimulus-general function that is required for the cellular response to stimulation.

1.2 FUNCTION OF STIMULUS-RESPONSIVE TRANSCRIPTION IN THE NERVOUS SYSTEM

As soon as *c-Fos* and other genes were shown to be induced in response to neuronal activity, there was great interest in understanding the function of stimulus-responsive transcription in the nervous system. Neurons were known to exhibit rapid responses to synaptic stimulation that could be explained by the opening of ligand gated ion channels or second-messenger mediated intracellular signaling. However, neurons were also known to exhibit slower, long-term responses to synaptic stimulation that could not be explained by the same mechanisms. At an organismal level, one of the most interesting long-term responses of the nervous system is memory. An appealing hypothesis was that stimulus-responsive genes might underlie memory by facilitating adaptive changes in nervous system structures such as synapses (Morgan and Curran, 1989, 1991; Sheng and Greenberg, 1990). A large body of work has supported roles for stimulus-responsive transcription in memory and synapse development and function (Flavell and Greenberg, 2008; Greer and Greenberg, 2008).

1.2.1 Role in long-term memory

Interestingly, even before the discovery of stimulus-responsive transcription in the nervous system and the speculation that this program of gene expression might contribute to memory, experiments suggested that new protein synthesis was critical for long-term memory. In a classic paper published over twenty years before the discovery

of activity-dependent transcription of *c-Fos* in the nervous system, investigators demonstrated that intracortical injections of the protein synthesis inhibitor puromycin in mice caused a loss of memory in a behavioral task (Flexner et al., 1963). This suggested that new protein synthesis was an important component of the mechanisms giving rise to memory. Subsequently, a large number of studies provided evidence that extensive inhibition of protein synthesis in the brain through injection of various protein synthesis causes loss of long-term memory, without causing changes in short-term memory or gross changes in behavior (Davis and Squire, 1984).

Further evidence for the role of new gene transcription in memory came from work done in the sea snail *Aplysia californica*, reviewed in (Kandel, 2001). When the siphon of the snail is touched, the snail exhibits a protective reflex that leads to withdrawal of the gills, similar to how someone might withdraw one's hand after touching a hot object. The length of time the gills remain retracted serves as an indication of learning by the snail. Normally, the withdrawal reflex leads to retraction of the gills for approximately 10 seconds. However, if the tail of the snail is shocked (indicating to the snail a dangerous environment), the subsequent withdrawal reflex leads to retraction of the gill and siphon for a longer period of time, in a process called sensitization. Furthermore, the animal remembers the shock and exhibits sensitization to subsequent stimuli. One shock will create a short-term memory that will lead to sensitization for a few minutes. Multiple shocks can create a long-term memory that can lead to sensitization for several days. The discovery of the neural circuitry underlying this reflex behavior (Byrne et al., 1978; Hawkins et al., 1981; Kupfermann et al., 1974) enabled the discovery that short-term and long-term sensitization lead to the

strengthening of synaptic connections between sensory and motor neurons, termed heterosynaptic facilitation (Abrams et al., 1984; Brunelli et al., 1976; Castellucci et al., 1970; Frost et al., 1985; Hawkins et al., 1981; Pinsker et al., 1973). These discoveries led to the hypothesis that heterosynaptic facilitation at the cellular level may underlie sensitization seen at the behavioral level. By studying the neural circuit underlying the gill withdrawal reflex, investigators showed that short-term heterosynaptic facilitation does not require new protein synthesis whereas long-term heterosynaptic facilitation does require new protein synthesis (Montarolo et al., 1986). These results paralleled the results seen in mice with intracortical injections of protein synthesis inhibitors and supported a role for new protein synthesis in a cellular correlate of memory. These findings suggested that proteins synthesized during and soon after learning were critical for the establishment of long-term memory. Given that stimulation of neuronal circuits during memory formation gives rise to activity-dependent gene expression, it was hypothesized that this program of gene expression played a role in memory. It wasn't until later, however, that this hypothesis could be formally tested with studies of the activity-dependent transcription factor CREB (cyclic AMP response element binding protein) in this process.

As investigators began to appreciate the role of new protein synthesis in long-term memory, details began to emerge regarding the underlying molecular mechanisms. Studies of the neural circuit underlying the gill withdrawal reflex showed that the neurotransmitter serotonin mediates long-term heterosynaptic facilitation in Aplysia (Montarolo et al., 1986) and that a second messenger downstream of serotonin, cyclic AMP, was itself capable of producing long-term heterosynaptic facilitation (Schacher et

al., 1988; Scholz and Byrne, 1988). These data suggested that the gene-products important for long-term heterosynaptic facilitation might be inducible by cAMP. It turned out that at this time, separate studies had identified the transcription factor CREB, or the cyclic AMP response element binding protein, as an important activator gene transcription in response to cAMP signaling (Montminy et al., 1986). These discoveries provided investigators with a potential molecular handle to study the role of stimulus-responsive transcription in memory. The first evidence that CREB plays a role in learning and memory came from a study in which investigators showed that Aplysia neurons contained CREB-like proteins and that injection of oligonucleotides of the cyclic AMP response element to which these proteins bind into the nucleus of Aplysia sensory neurons blocked long-term heterosynaptic facilitation without affecting short-term heterosynaptic facilitation (Dash et al., 1990). Separate studies had shown that CREB was also as an important activator of *c-Fos* transcription in mammalian cells in response to extracellular stimuli (Sheng et al., 1988) (see section 1.3.1 Initial insights from the *c-Fos* promoter). Hence, the CREB protein appeared to be an important regulator of long-term adaptations in Aplysia as well activity-dependent transcription in the mammalian nervous system. Experiments done in genetically modified mice have supported a role for CREB in mammalian long-term plasticity and memory. Mutation of *Creb* in mice resulted in defective long-term memory and long lasting long-term potentiation (L-LTP), a cellular correlate of long-term memory, with no affect on short-term memory or short term synaptic plasticity (Bourtchuladze et al., 1994). Furthermore, transgenic mice overexpressing a constitutively active form of CREB exhibit L-LTP in response to weak stimuli that would not normally elicit L-LTP (Barco et al., 2002). These data suggest that CREB plays an important role in long-term

cellular adaptations to stimuli and long-term memory. Since these processes require new protein synthesis and since CREB is a transcription factor regulated by extracellular stimuli, these results also implicate stimulus-responsive transcription in long-term cellular adaptations to stimuli and long-term memory.

1.2.2 Role in dendritic and synaptic development

In addition to playing a role in long-term cellular adaptations to stimuli and long-term memory, stimulus-responsive transcription also has been shown to play important roles in development of dendrites and synapses that underlie these long-term phenomena. The most convincing evidence supporting a role of stimulus-responsive transcription in dendritic and synaptic development has come from detailed studies of these processes in the context of genetic alterations to stimulus-responsive genes. For example the activity-dependent transcription factors CREB, CREST, and NEUROD have all been shown to play important roles in dendritic development (Aizawa et al., 2004; Gaudilliere et al., 2004; Redmond et al., 2002; Wayman et al., 2006). Furthermore, genes whose transcription is regulated by neuronal activity, such as the microRNA miRNA132 and candidate plasticity gene 15 (*Cpg15*), have also been shown to regulate dendritic remodeling (Cantallops et al., 2000; Nedivi et al., 1998; Vo et al., 2005; Wayman et al., 2008). Similarly, neuronal activity-dependent genes have also been shown to play important roles in synapse development. The neuronal activity-dependent transcription factor MEF2 has been shown to negatively regulate excitatory synapse number (Barbosa et al., 2008; Flavell et al., 2006). Furthermore, the protein

products of the activity-regulated genes *Arc*, *Homer1a*, *Npas4*, and *Plk2* have all been shown to regulate various aspects of synapse development (Chowdhury et al., 2006; Lin et al., 2008; Pak and Sheng, 2003; Rial Verde et al., 2006; Sala et al., 2003). These studies have demonstrated that neuronal stimulus-responsive transcription plays critical roles in the development of both dendrites and synapses in the nervous system.

1.3 REGULATION OF STIMULUS-RESPONSIVE TRANSCRIPTION IN THE NERVOUS SYSTEM

Because neuronal stimulus-responsive transcription plays important roles in the development and function of the nervous system, there has been great interest in understanding the molecular mechanisms underlying this program of gene expression. Early work focused on studying the promoters of stimulus-responsive genes. This yielded important insights into the proximal cis-acting elements and proximally bound trans-acting factors that regulate stimulus-responsive transcription. With the development of chromatin and transcription factor signatures that identify enhancers, and sequencing technologies that enable their unbiased genome-wide identification, recent studies have begun to identify distal enhancer elements that may also regulate stimulus-responsive transcription. Since enhancers are though to be the main drivers of specificity in gene expression, their identification and study is an important step in understanding the regulation of stimulus-responsive transcription in the nervous system.

1.3.1 Initial insights from the *c-Fos* promoter

Soon after the discovery of the stimulus-dependent transcription of the *c-Fos* gene, investigators sought to understand the mechanisms by which *c-Fos* was inducibly transcribed in response to stimuli. Initial studies demonstrated that plasmids containing several hundred base pairs of sequence upstream of the *c-Fos* transcriptional

start site were sufficient to generate stimulus-responsive transcription similar to that exhibited by *c-Fos in vivo* (Deschamps et al., 1985; Treisman, 1985). Deletion analysis of the *c-Fos* promoter revealed cis-acting regulatory elements that were critical for stimulus-dependent transcription of *c-Fos*. Promoter deletion analyses demonstrated that *c-Fos* induction from serum stimulation in fibroblasts required an element termed the serum response element (SRE) (Greenberg et al., 1987; Treisman, 1985). Subsequent experiments employing DNA affinity chromatography discovered the trans-acting transcription factor that bound to the SRE, the serum response factor (SRF) (Treisman, 1987). The SRE was subsequently shown to be required for calcium-dependent transcription of *c-Fos* (Misra et al., 1994) and SRF was subsequently shown to be required for activity-dependent induction of *c-Fos* in the nervous system (Ramanan et al., 2005). These experiments provided evidence that SRF plays an important role in regulating transcriptional responses to neuronal activity by binding to SRE sites near the promoters of target genes, such as *c-Fos*.

Separate deletion analyses of the *c-Fos* promoter revealed an additional cis-acting element required for calcium-dependent induction of the *c-Fos* gene. Deletion experiments demonstrated that *c-Fos* induction in response to depolarization in PC12 cells required an element termed the calcium response element (CaRE) (Sheng et al., 1988), which bound to the transcription factor CREB (Sheng et al., 1990). Previous experiments had established a role for cAMP responsive transcriptional activation by CREB at the cyclic AMP response element (CRE) (Montminy and Bilezikjian, 1987; Montminy et al., 1986). Together, these experiments demonstrated a role for CREB in transcriptional activation in response to elevations in both cAMP and calcium, and

provided evidence that CREB plays a role in regulating transcriptional responses to neuronal activity by binding to CaRE/CRE sites near the promoters of target genes, such as *c-Fos*.

Careful analyses of the sequences within the *c-Fos* promoter provided important insights into the cis-regulatory elements and trans-acting factors that drive *c-Fos* expression in response to extracellular stimuli. Importantly, the discovery of SRF and CREB proved to not only be important in understanding the stimulus-responsive transcription of *c-Fos*, but also of other stimulus-responsive genes. For example, the SRF knockout animal exhibited no induction of not only *c-Fos* but also the immediate early genes *FosB*, *Egr1*, *Egr2*, *c-Jun*, *JunB*, *Arc*, *ActB*, and *Actg1* in response to electroconvulsive shock (Ramanan et al., 2005). This suggested that SRF is a broadly important regulator of activity-dependent transcription in the nervous system. Genome-wide analysis of CREB target genes has demonstrated hundreds of genes that require CREB for transcription in response to the cAMP agonist forskolin (Zhang et al., 2005). While these studies suggest that SRF and CREB are both broadly important in generating stimulus-responsive transcriptional programs, the genome-wide sets of transcriptional target genes for these factors in the nervous system have not been defined.

1.3.2 Discovery of enhancer elements

As initial understanding of the regulation of stimulus-responsive transcription from the promoter regions of c-fos and other genes was developing, the contribution of

enhancers to transcriptional regulation was just beginning to be appreciated. Enhancers were first discovered through studies of β-globin gene regulation (Banerji et al., 1981). Investigators studying the expression of the β-globin gene from plasmids containing a 4.7 kb long segment of chromosomal DNA encompassing the β-globin gene found that expression of β-globin was increased a remarkable 200 fold when the plasmid also contained a 72 bp sequence of DNA derived from Simian virus 40 (SV40). Because of its remarkable ability to enhance β-globin gene transcription, this element was referred to as an enhancer. The investigators also showed that the SV40 enhancer functioned to increase β-globin gene transcription independent of its distance from the promoter and in either sequence orientation relative to the promoter (Banerji et al., 1981). These are now known to be important and defining properties of enhancers.

After the discovery of viral enhancers (Banerji et al., 1981; Moreau et al., 1981), metazoan enhancers were discovered (Banerji et al., 1983; Gillies et al., 1983) thus generalizing the relevance of enhancers to transcriptional regulation. Subsequently, several additional endogenous enhancers have been studied in detail, including the β-globin locus control region (Bender et al., 2000; Grosveld et al., 1987; Hardison et al., 1997; Moon and Ley, 1990), a limb bud enhancer for the *Sonic hedgehog* (*Shh*) gene (Lettice et al., 2003; Sagai et al., 2005), the interferon-β enhancer (Munshi et al., 1999; Panne, 2008), and the sparkling eye enhancer of the Drosophila *dPax2* gene (Evans et al., 2012). These studies have established the importance of enhancers to gene regulation and have begun to elucidate the principles underlying enhancer function. However, a major hurdle in understanding the function of enhancers and the contribution of enhancers to specific programs of gene expression, such as neuronal

stimulus regulated transcription, has been the identification of enhancer elements within the genome. Enhancers are short DNA sequences, approximately several hundred base pairs in length, that are embedded within the genome. Because enhancers lack defining characteristics, they cannot be identified within the genome on the basis of their sequence alone. Recently, however, great advances have been made in the identification of enhancers within the genome (Buecker and Wysocka, 2012). These advances, described in the introduction to the next chapter of my thesis, have facilitated my work on the identification and characterization of functional stimulus-responsive enhancers in the nervous system.

2 GENOME-WIDE IDENTIFICATION OF STIMULUS-RESPONSIVE ENHANCERS IN THE NERVOUS SYSTEM

2.1 SUMMARY

Normal brain development and function require stimulus-responsive programs of gene expression, but the impact of neuronal stimuli on chromatin, and the specific enhancers that regulate stimulus-responsive programs of gene expression are poorly understood. Here, we discover that stimulation with neuronal activity and brain derived neurotrophic factor (BDNF) cause rapid, widespread, and distinct changes in the acetylation of histone H3 lysine 27 (H3K27Ac) at thousands of promoters and enhancers throughout the neuronal genome. We find that functional stimulus-responsive enhancers can be specifically identified by stimulus-inducible H3K27Ac, and we use this dynamic chromatin signature to discover enhancers that respond to activity, BDNF, or both. This discovery of these enhancers reveals the genome-wide basis for transcriptional specificity in response to distinct stimuli. Furthermore, this work provides a critical resource to begin understanding the cis-regulatory elements that transform sensory experience into specific transcriptional programs that facilitate long-lasting changes in neuronal function. Finally, stimulus-inducible H3K27Ac may aid in the identification and study of stimulus-regulated enhancers in other tissues.

2.2 INTRODUCTION

During development, transcriptional programs give rise to distinct cellular lineages through the establishment of cell type specific chromatin states (Davidson, 2010; Ho and Crabtree, 2010; Kouzarides, 2007; Lee and Young, 2013). These distinct chromatin signatures instruct gene expression primarily through the genome-wide demarcation of enhancers, cis regulatory-elements that act at a distance to regulate gene transcription (Buecker and Wysocka, 2012; Bulger and Groudine, 2011; Levine, 2010; Ong and Corces, 2011; Spitz and Furlong, 2012; Visel et al., 2009b). Recent efforts to identify enhancers using genome-wide sequencing techniques have led to the discovery of hundreds of thousands of cis-regulatory elements (Consortium et al., 2012; Heintzman et al., 2007; Shen et al., 2012). Despite this progress, relatively little is known about the influence of extracellular stimuli on chromatin state at enhancers, and it is not clear which enhancers among the hundreds of thousands that have been identified function to promote stimulus-dependent transcription.

In the nervous system, the chromatin state of terminally differentiated neurons must not only maintain neuronal identity but also allow for sensory-experience-dependent transcription (Borrelli et al., 2008; Day and Sweatt, 2011; Dulac, 2010; Graff and Tsai, 2013; Kandel, 2001). In response to sensory experience, strong bursts of synaptic activity induce a program of gene expression in excitatory neurons that is required for proper development and refinement of neural circuits and for long-lasting changes in neuronal function that underlie learning, memory, and behavior (Greer and Greenberg, 2008; Leslie and Nedivi, 2011). Studies of this neuronal activity-dependent

gene program have primarily focused on signaling to promoter bound transcription factors (Alberini, 2009; Lyons and West, 2011). The release of the neurotransmitter glutamate at synapses leads to membrane depolarization of the post-synaptic neuron, triggering calcium influx through L-type voltage gated calcium channels. The influx of calcium then leads to activation of a complex signaling network that induces the post-translational modification of promoter bound transcription factors that initiate multiple waves of gene expression

In addition to these critical signaling events at the promoters of activity-regulated genes, signaling to enhancers contributes to activity-dependent gene expression, although there has been little progress towards characterizing the function of activity-regulated enhancers because it has been difficult to identify these elements within the genome. However, recent genome-wide studies in a variety of cell types have characterized chromatin and transcription factor signatures that now allow for the comprehensive identification of enhancers. For example, enhancers have been identified on the basis of their hypersensitivity to DNAseI digestion, enrichment of monomethylation of lysine 4 on histone H3 (H3K4Me1), enrichment of acetylation of lysine 27 on histone H3, and their ability to bind the transcriptional coactivators CBP/P300 (Consortium et al., 2012; Creyghton et al., 2010; Heintzman et al., 2009; Rada-Iglesias et al., 2011; Visel et al., 2009a). However, all enhancers are not functionally equivalent. The cellular repertoire of enhancers consists of both enhancers that are thought to be poised for future activation, and enhancers that are currently active (Rada-Iglesias et al., 2011). Poised enhancers are typically identified by their enrichment for H3K4me1, whereas active enhancers exhibit additional features (i.e.

CBP/P300 binding, eRNA transcription, H3K27Ac). H3K27Ac has been shown to be present specifically at active enhancers and not poised enhancers, and thus has been used in several studies of developmentally regulated enhancers to identify active enhancers genome-wide (Creyghton et al., 2010; Mikkelsen et al., 2010; Rada-Iglesias et al., 2012; Rada-Iglesias et al., 2011).

Several studies have recently identified enhancers within the nervous system (Kim et al., 2010; Shen et al., 2012; Visel et al., 2013). While most of these studies have not attempted to understand the enhancers within the genome that contribute to stimulus-dependent transcription in the nervous system, one recent study used H3K4Me1 enrichment and inducible CBP binding to identify nearly 12,000 putative neuronal activity-dependent enhancers (Kim et al., 2010). However, this number far exceeds the number of activity-regulated genes in excitatory neurons, suggesting that many of these enhancers may not directly contribute to activity-dependent transcription. Thus, it remains unclear whether all or a subset of these enhancers actually function to drive neuronal activity-dependent gene expression. The activity-regulated regulated enhancers identified in excitatory neurons thus far appear to be heterogeneous in terms of the transcription factors they bind and their ability to recruit RNA polymerase and drive transcription of enhancer associated RNAs (eRNAs). This suggests that these CBP-bound enhancers may not all function in the same manner. While some of these enhancers might mediate activity-dependent gene transcription, others could respond to distinct stimuli such as neurotrophic factors. It is also possible that some of the CBP-bound enhancers do not directly regulate stimulus-dependent gene transcription and instead might be constitutively active or inactive under the conditions studied.

Consistent with these possibilities, studies of developmentally regulated enhancers have shown that not all CBP/P300 bound enhancers are active (Rada-Iglesias et al., 2011; Visel et al., 2009a). It is not clear if these observations apply to stimulus-responsive enhancers in terminally differentiated cell types since to date no chromatin or transcription factor signatures have been defined that identify which of the tens of thousands of enhancers within a cell function to drive stimulus-responsive gene transcription.

In this study we determined the effects of neuronal activity on the active chromatin landscape of mouse cortical neurons. We find that neuronal activity can induce rapid changes in H3K27Ac at thousands of neuronal enhancers throughout the genome. Notably, increases in H3K27Ac occur specifically at enhancers that function to promote activity-dependent gene transcription. We observed overlapping but distinct changes in H3K27Ac at enhancers in response to stimulation with brain derived neurotrophic factor (BDNF), revealing the genome-wide basis for transcriptional specificity in response to distinct stimuli. Our studies reveal a previously underappreciated heterogeneity among active enhancers in terms of their responsiveness to stimuli. Furthermore, the comprehensive identification of neuronal activity and BDNF-dependent enhancers in cortical neurons provides a critical resource for elucidating the role of stimulus-responsive transcription in synaptic plasticity, behavior and disease. Finally, the epigenetic signature of acutely inducible H3K27Ac may aid in the identification and study of stimulus-regulated enhancers in other tissues.

2.3 RESULTS

2.3.1 H3K27Ac changes rapidly in response to neuronal activity

Despite progress in identifying enhancers in the nervous system, no study has systematically determined which of the tens of thousands of enhancers that have been identified function to drive stimulus-responsive transcription. We hypothesized that characterizing the active enhancer landscape before and after neuronal activity might enable us to identify the set of enhancers that respond to activity. To test this hypothesis, we used ChIP-Seq to measure the genomic distribution of the active chromatin associated chromatin mark H3K27Ac in mouse cortical neurons before and after two hours of membrane depolarization with elevated extracellular potassium chloride (KCl). Exposure of neuronal cultures to KCl is a well-established in vitro experimental paradigm that mimics neuronal activity *in vivo* by inducing membrane depolarization, calcium influx through L-type voltage-sensitive calcium channels, and calcium-dependent changes in gene transcription. We performed two independent bioreplicates of ChIP-Seq before and after membrane depolarization with KCl, and found that the signal for H3K27Ac was highly correlated in separate bioreplicates in each condition (Figure 2.1, Spearman's rho ρ=0.83 between –KCl experiments, ρ=0.86 between +KCl experiments). This suggested that H3K27Ac signal in our experiments was replicable across experiments. As a result, we pooled both bioreplicates for subsequent analyses.

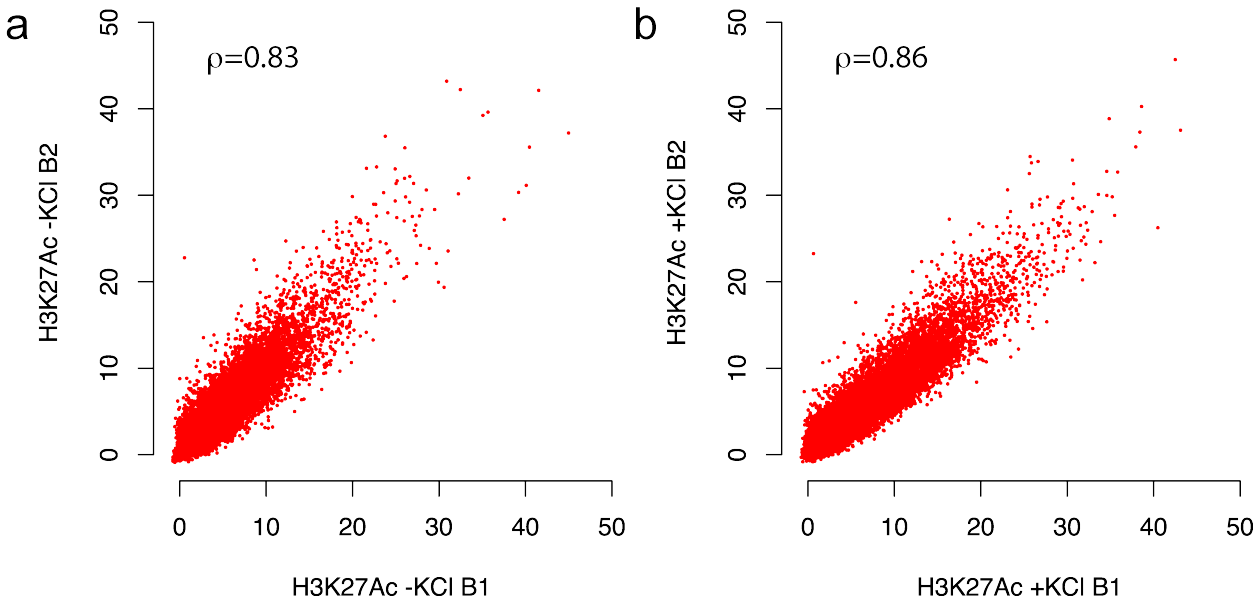

Figure 2.1: Comparison of H3K27Ac signal in two independent experiments before and after membrane depolarization with KCl

(a) H3K27Ac ChIP-Seq signal in mouse cortical neurons before membrane depolarization (-KCl) in two independent experiments (bioreplicate 1, B1; bioreplicate 2, B2), quantified at all H3K27Ac peaks in the genome. H3K27Ac signal was highly correlated between experiments, Spearman's rho ρ=0.83. (b) H3K27Ac ChIP-Seq signal in mouse cortical neurons after 2 hours of membrane depolarization (+KCl) in two independent experiments (bioreplicate 1, B1; bioreplicate 2, B2), quantified at all H3K27Ac peaks in the genome. H3K27Ac signal was highly correlated between experiments, Spearman's rho ρ=0.86. In both plots, each point represents the H3K27Ac signal quantified within a 2kb window surrounding an enhancer center.

After pooling both H3K27Ac bioreplicates (B1 and B2) in each condition (-KCl and +KCl), we identified regions of significant H3K27Ac enrichment in each condition (-KCl and +KCl) by calling H3K27Ac peaks using MACS with a significance threshold of p=1e-5. We then asked how the genomic distribution of H3K27Ac peaks compared before and after membrane depolarization with KCl. To investigate this, we classified all H3K27Ac peaks in each condition based on their location relative to genes in the NCBI Reference Sequence Database (RefSeq). H3K27Ac peaks were classified as being proximal if they were within 1kb of an annotated transcriptional start site (TSS). H3K27Ac peaks were classified as being distal if they were greater than 1kb from an annotated transcriptional start site (TSS). Distal H3K27Ac peaks were further classified as intragenic if they occurred within a RefSeq gene, or as extragenic if they did not occurred within a RefSeq gene. We found that both before and after membrane depolarization, the majority of H3K27Ac peaks occurred distal to RefSeq TSSs (Figure 2.2, 65% distal peaks –KCl, 63% distal peaks +KCl). Furthermore, the genomic distribution of H3K27Ac peaks was similar before and after depolarization. Before depolarization (-KCl), 35% of H3K27Ac peaks were proximal, 32% of H3K27Ac peaks were distal intragenic, and 33% of peaks were distal extragenic. After depolarization (+KCl), 37% of H3K27Ac peaks were proximal, 33% of H3K27Ac peaks were distal intragenic, and 30% of peaks were distal extragenic. This suggested that the overall distribution of H3K27Ac peaks within the genome did not change with neuronal activity.

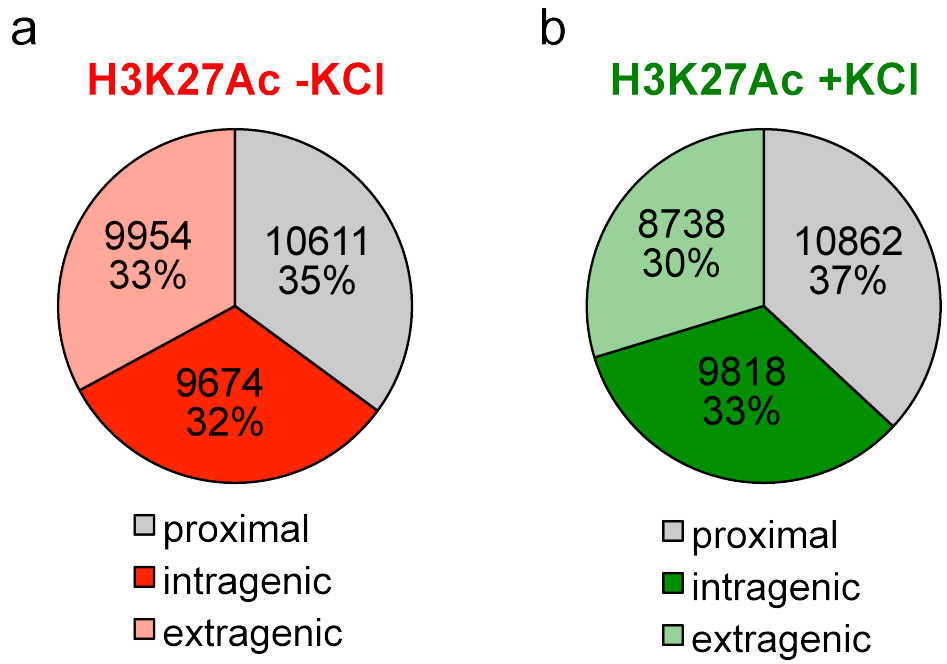

Figure 2.2: Genomic distribution of H3K27Ac peaks before and after membrane depolarization with KCl

(a) Genomic distribution of H3K27Ac peaks before membrane depolarization with KCl (-KCl). The majority of peaks occur distal to RefSeq TSSs, with 32% of distal peaks occurring within genes (intragenic) and 33% of distal peaks occurring outside of genes (extragenic). (b) Genomic distribution of H3K27Ac peaks after membrane depolarization with KCl (+KCl). The majority of peaks occur distal to RefSeq TSSs, with 33% of distal peaks occurring within genes (intragenic) and 30% of distal peaks occurring outside of genes (extragenic).

While the overall genomic distribution of H3K27Ac peaks did not change with neuronal activity, we asked whether the levels of H3K27Ac changed in response to neuronal activity at individual enhancer elements. This raises the question of how individual enhancer elements should be identified. H3K27Ac enrichment distal to promoter regions has been used to identify enhancers, but H3K27Ac enrichment often occurs over broad regions of the genome and can encompass multiple regulatory elements. Furthermore, the accurate localization of individual enhancers within regions of H3K27Ac enrichment can prove difficult. Distal regions of open chromatin identified by DNaseI hypersensitivity (DHS) have also been used to identify enhancers. Compared to H3K27Ac, DHS provides the benefit of narrow peaks that allow for accurate localization of regulatory elements. However, distal DNaseI hypersensitivity is not specific to enhancers and can indicate the presence of various distal cis-regulatory elements, such as silencers and insulators (Gross and Garrard, 1988). We found that 98.6% of all H3K27Ac peaks within our system overlapped with previously generated DHS data from brain tissues by the ENCODE consortium (Consortium, 2011), and reasoned that enhancers within our system could be comprehensively, specifically, and accurately identified by integrating our H3K27Ac data with this brain DHS data.

To identify individual enhancer elements within our system, we isolated the set of distal (>1kb from a RefSeq TSS) DHS sites that overlapped with our H3K27Ac peaks. To determine the effect of neuronal activity on H3K27Ac at individual enhancers, we quantified the levels of H3K27Ac at individual enhancer elements throughout the genome. While the enhancer-associated chromatin mark H3K4Me1 was largely similar at neuronal enhancers before and after neuronal activity (Figure 2.3a, Spearman's rank

correlation coefficient ρ= 0.96, 0.97 in two independent experiments), we found that H3K27Ac levels at neuronal enhancers exhibited substantially more variability before and after neuronal activity (Figure 2.3b, ρ=0.53, 0.58 in two independent experiments). H3K27Ac levels at neuronal enhancers also exhibited substantial variability before and after neuronal activity in the merged dataset of both H3K27Ac bioreplicates (Figure 2.3c, ρ=0.53). H3K27Ac appeared to increase and decrease at thousands of neuronal enhancers and activity-dependent increases in H3K27Ac seemed to occur both at active enhancers that displayed H3K27Ac prior to stimulation and at poised enhancers that did not display H3K27Ac prior to stimulation (Figure 2.3c). Inspection of individual loci revealed strikingly different H3K27Ac behaviors at neuronal enhancers that appeared similar based on other chromatin modifications, transcription factor binding events, and DNaseI hypersensitivity (Figure 2.4). Neuronal enhancers that appeared otherwise similar exhibited increasing H3K27Ac, high unchanging H3K27Ac, decreasing H3K27Ac, or no H3K27Ac in response to neuronal activity (Figure 2.4). Hence, H3K27Ac levels changed rapidly and dramatically at thousands of neuronal enhancers in response to activity, while H3K4Me1 levels were largely constant. Furthermore, neuronal enhancers exhibit significant heterogeneity in both the levels of H3K27Ac and also the dynamics of H3K27Ac in response to neuronal activity. This suggested that neuronal enhancers might be heterogeneous in their function and in their responsiveness to neuronal activity.

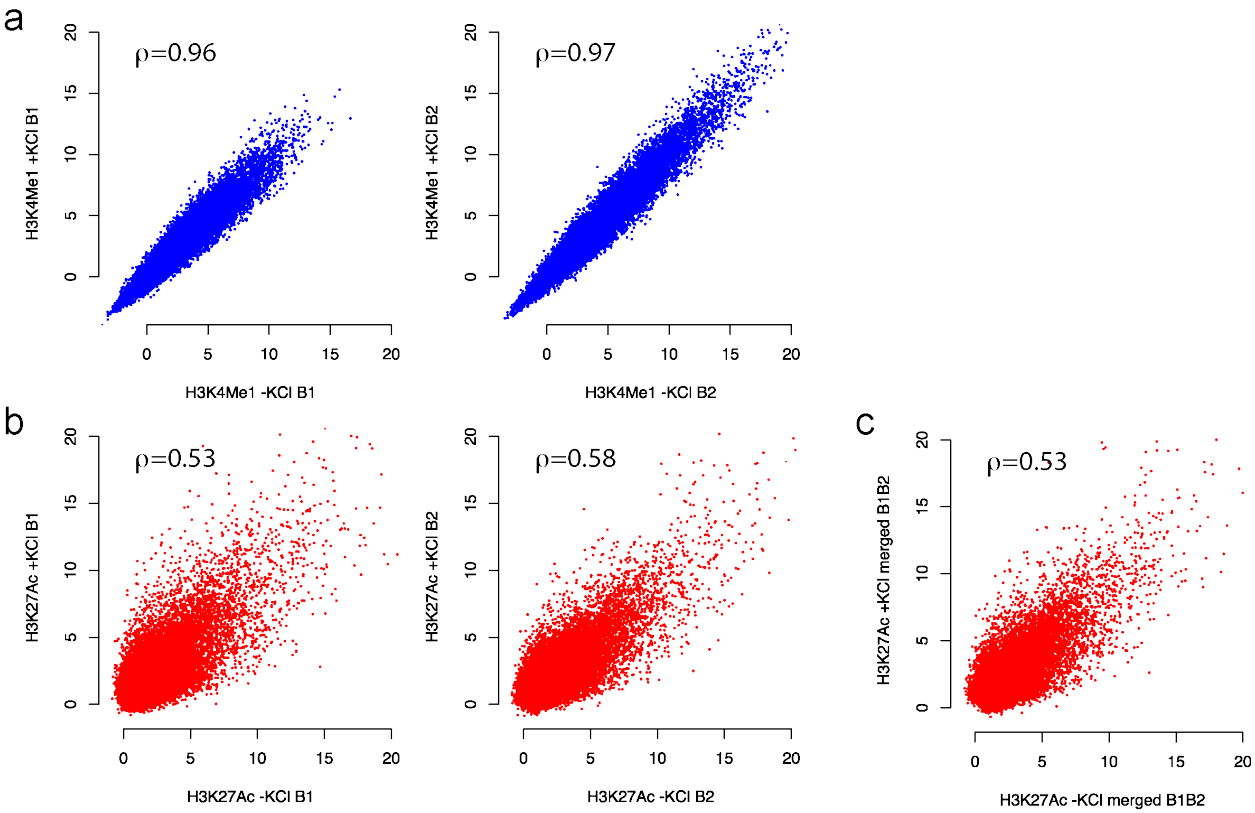

Figure 2.3: Chromatin modifications at neuronal enhancers before and after membrane depolarization

Levels and correlation of histone modifications at neuronal enhancers (defined by H3K27Ac enrichment and DNaseI hypersensitivity) throughout the genome before membrane depolarization (-KCl) and after membrane depolarization (+KCl) in two independent experiments (bioreplicate 1, B1; bioreplicate 2, B2). (a) H3K24Me1 levels. (b) H3K27Ac levels. (c) Levels and correlation of H3K27Ac at neuronal enhancers (defined by H3K27Ac enrichment and DNaseI hypersensitivity) throughout the genome before membrane depolarization (-KCl) and after membrane depolarization (+KCl) in the pooled datasets (merged B1B2).

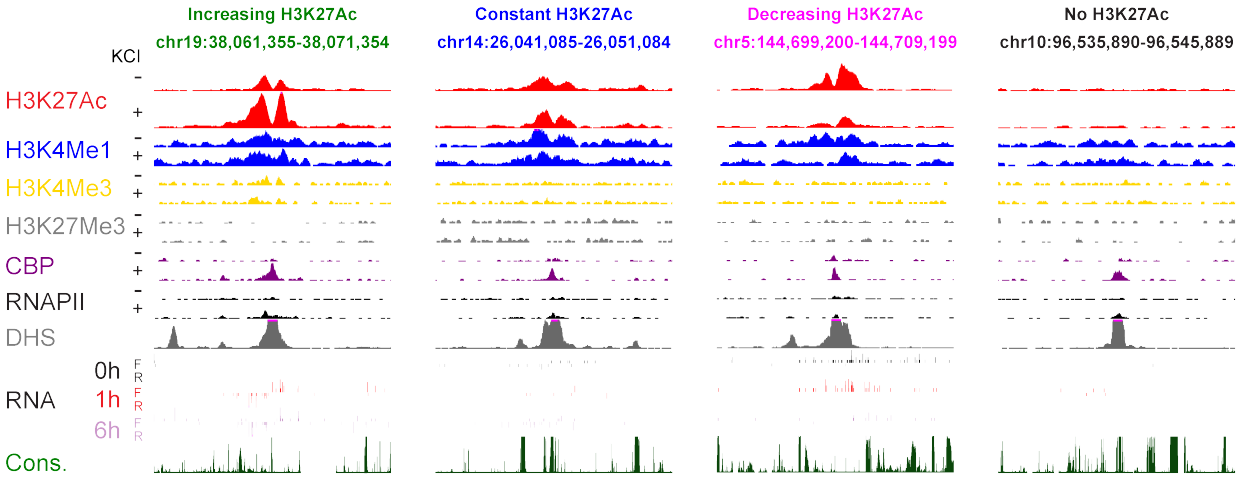

Figure 2.4: Individual enhancers exhibit different H3K27Ac behaviors in response to membrane depolarization

Genome browser views of ChIP-Seq and RNA-Seq tracks at examples of individual neuronal enhancers exhibiting increasing H3K27Ac, constant high H3K27Ac, decreasing H3K27Ac, or no H3K27Ac in response to membrane depolarization with KCl. Other chromatin marks displayed include the enhancer associated H3K4Me1, the promoter associated H3K4Me3, and the repressive chromatin associated H3K27Me3. Transcription factor binding events displayed include the transcriptional coactivator CREB-binding protein (CBP), and RNA polymerase II (RNAPII). For all chromatin marks and transcription factors, ChIP-Seq tracks display input-normalized reads from neurons stimulated with 0 hours ('-') or two hours ('+') of KCl. RNA sequencing tracks display sequencing reads aligning to forward (F) and reverse strands (R) of the genome from neurons stimulated with 0, 1, or 6 hours of KCl. Also displayed are DNaseI hypersensitivity signal from adult mouse cerebrum and vertebrate conservation by PhastCons.

To gain initial insight into how neuronal activity-dependent changes in H3K27Ac at enhancers might relate to activity-dependent programs of gene expression, we inspected the locus of the canonical activity-dependent gene *c-Fos*. Previous studies in neurons have observed increases in histone acetylation in response to physiological stimuli at the promoters of stimulus-responsive genes (Guan et al., 2009; Guan et al., 2002; Levenson et al., 2004). Consistent with previous studies, we found that levels of H3K27Ac increased at the *c-Fos* promoter in response to neuronal activity. We also found that levels of H3K27Ac increased at four nearby enhancers in response to neuronal activity (Figure 2.5). This suggested that neuronal activity-dependent gene expression might correlate with increasing H3K27Ac in response to neuronal activity and that neuronal enhancers that contribute to activity-dependent gene expression may exhibit increasing H3K27Ac in response to neuronal activity.

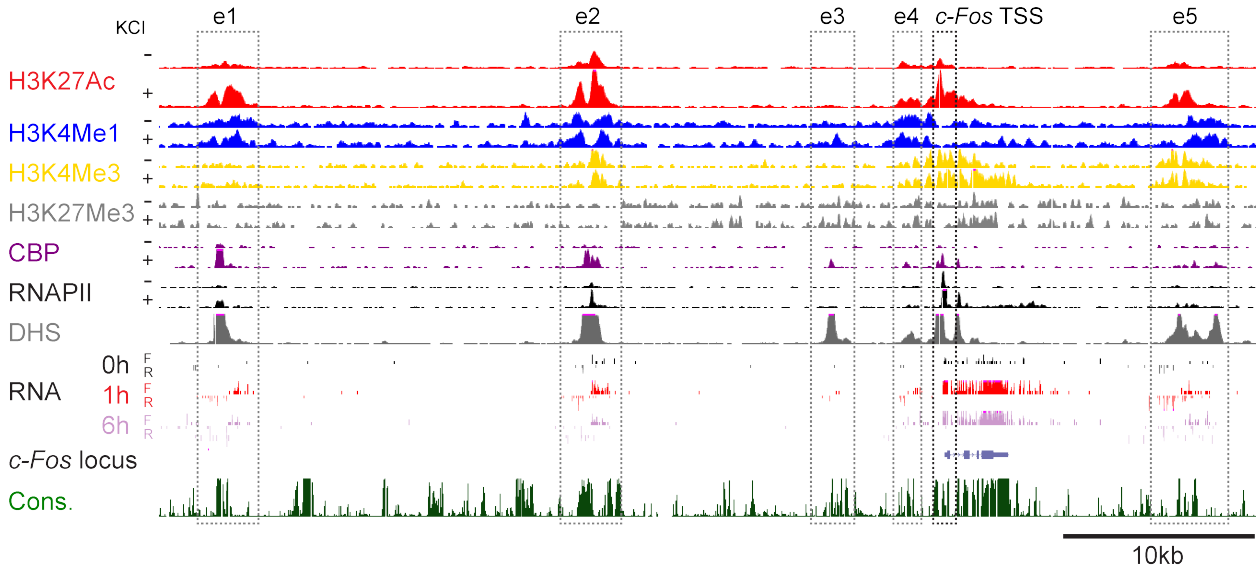

Figure 2.5: Enhancers near the *c-Fos* gene exhibit increases in H3K27Ac in response to membrane depolarization

Genome browser view of ChIP-Seq and RNA-Seq tracks at the *c-Fos* locus. Neuronal activity-dependent increases in H3K27Ac levels are seen at the *c-Fos* transcriptional start site (TSS) and at four nearby enhancers (e1,2,4,5). For all chromatin marks and transcription factors, ChIP-Seq tracks display input-normalized reads from neurons stimulated with 0 hours ('-') or two hours ('+') of KCl. RNA sequencing tracks display sequencing reads aligning to forward (F) and reverse strands (R) of the genome from neurons stimulated with 0, 1, or 6 hours of KCl.

2.3.2 Inducible H3K27Ac identifies functional neuronal activity-responsive enhancers

To determine if increases in H3K27Ac occurred at enhancers associated with activity-induced genes genome-wide, we first classified enhancers into different groups based on their differential H3K27Ac responses to neuronal activity. We selected three subsets of enhancers that exhibited the most distinct H3K27Ac dynamics in response to neuronal activity: enhancers with increasing H3K27Ac (n=2868), enhancers with decreasing H3K27Ac (n=3746), and enhancers with high constant levels of H3K27Ac before and after neuronal activity (n=1395) (Figure 2.6a; see methods). For comparison, we also included a fourth group of enhancers that had H3K4Me1, exhibited inducible binding of the transcriptional coactivator CBP in response to neuronal activity, but had no appreciable H3K27Ac before or after neuronal activity (n=3223) (Figure 2.6a). This fourth group was included because a previous report classified these elements as neuronal activity-dependent enhancers (Kim et al., 2010). Average profiles of H3K27Ac ChIP-Seq signal for each group of neuronal enhancers displayed clearly different H3K27Ac behaviors in response to neuronal activity (Figure 2.6b). This suggested that these enhancer groups could be meaningfully used to determine whether neuronal enhancers with different H3K27Ac behaviors are associated with different transcriptional functions within the nervous system.

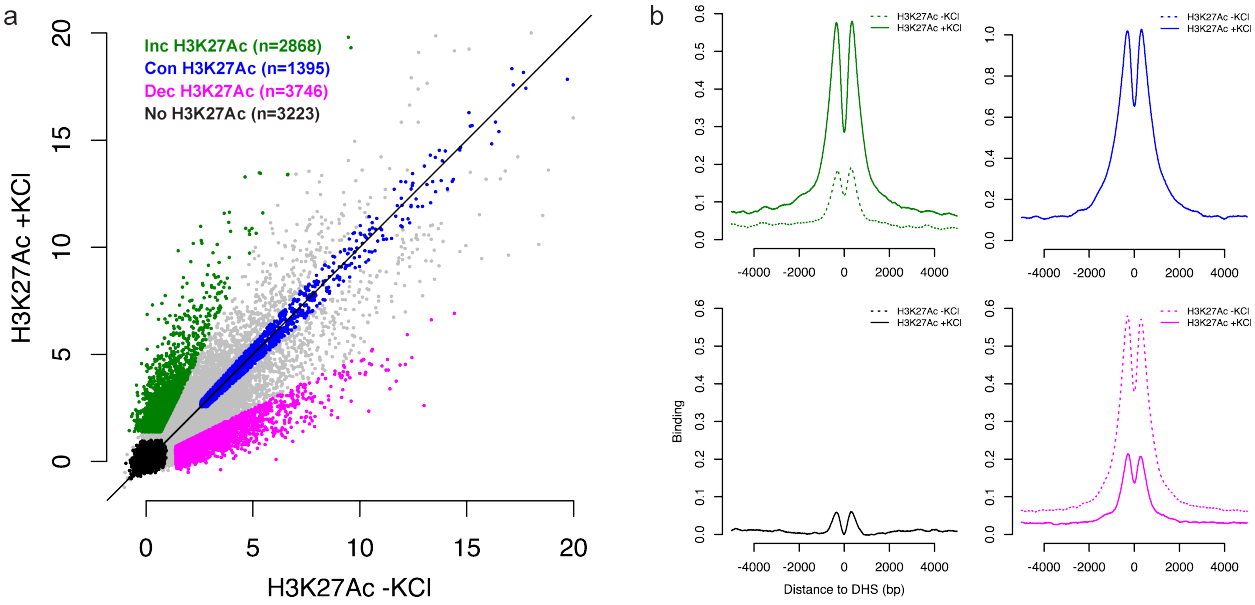

Figure 2.6: Classification of neuronal enhancers with different H3K27Ac behaviors

(a) Classification of neuronal enhancers into subgroups with distinct H3K27Ac behaviors. Enhancers with increasing H3K27Ac, high constant H3K27Ac, decreasing H3K27Ac, or no H3K27Ac in response to neuronal activity were classified into separate groups. Each point represents the input normalized H3K27Ac signal quantified within a 2kb window surrounding an enhancer center, with the x-axis value representing the signal before membrane depolarization (-KCl) and the y-axis value representing the signal after two hours of membrane depolarization with KCl (+KCl). (b) Average profiles of H3K27Ac ChIP-Seq signal at each subgroup of enhancers before membrane depolarization (dashed lines) and after membrane depolarization (solid lines). The y-axis represents the level of H3K27Ac signal, displayed as the mean number of input-normalized H3K27Ac ChIP-Seq reads for each subgroup of enhancers. H3K27Ac signal at enhancers was aligned by the centers DNaseI hypersensitive sites.

We hypothesized that different H3K27Ac behaviors were likely to reflect different transcriptional functions for these enhancers, and that only neuronal enhancers with increasing H3K27Ac in response to neuronal activity would promote gene expression in response to neuronal activity. To determine the contribution of each subset of enhancers to neuronal gene expression, we performed transcriptome sequencing (RNA-Seq) in untreated or KCl-depolarized cortical neurons (0, 1, and 6 hours of KCl). Then, for each subset of enhancers, we assessed the expression of nearby genes and the expression of enhancer associated RNAs (eRNAs), which are thought to occur at enhancers actively engaged in transcriptional regulation (Kim et al., 2010; Wang et al., 2011). Strikingly, we found that both nearest gene expression and eRNA transcription closely paralleled the H3K27Ac behaviors observed at each subset of enhancers (Figure 2.7a,b). As expected enhancers with high unchanging H3K27Ac were near genes that exhibited significantly higher levels of expression and had higher levels of eRNA transcription than enhancers lacking H3K27Ac, consistent with their classification as active enhancers (Figure 2.7a,b). Notably, only enhancers with increasing H3K27ac in response to neuronal activity were associated with activity-dependent increases in the expression of nearby genes and eRNAs (Figure 2.7a,b), suggesting that this subset of enhancers may function specifically to promote neuronal activity dependent gene expression. Thus, while a large number of active enhancers can be identified by their enrichment for H3K27Ac, profiling H3K27Ac in response to neuronal activity revealed that these enhancers differ considerably from one another not only in their levels of H3K27Ac but also in the expression of nearby genes and in the transcription of eRNAs. By measuring H3K27Ac levels before and after a neuronal activity and classifying enhancers based on their H3K27Ac dynamics, we find that only enhancers with activity-

dependent increases in H3K27Ac appear to contribute to neuronal activity-dependent transcription. Our data further suggests that while inducible CBP binding in response to neuronal activity has previously been used to identify neuronal activity-dependent enhancers, this is clearly not a specific marker. While enhancers with inducible H3K27Ac exhibited greater CBP binding than other acetylated enhancer classes, enhancers from all four classes exhibited some level of inducible CBP binding (Figure 2.7c). Furthermore, enhancers that lacked H3K27Ac but exhibited inducible robustly CBP binding were not associated with genomic correlates of activity-dependent enhancer function (Figure 2.7c). This suggested that inducible H3K27Ac is a much more specific and predictive marker of functional neuronal activity-dependent enhancers than inducible coactivator binding.

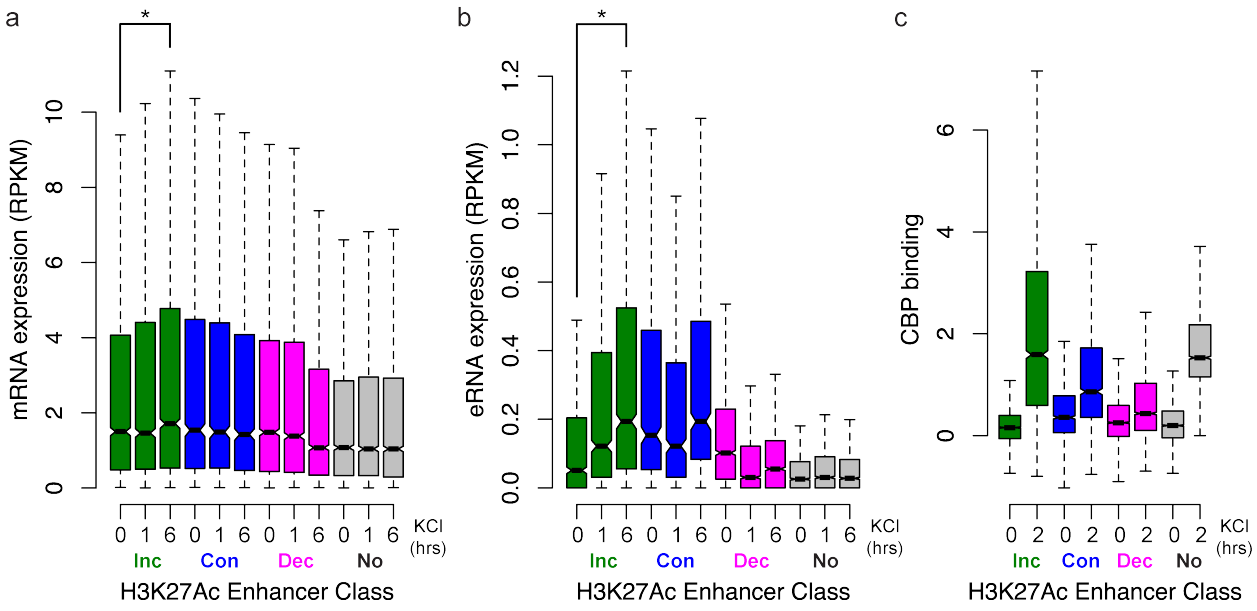

Figure 2.7: Enhancers with different H3K27Ac behaviors correlate with different patterns of transcription in the genome

(a) Boxplot of expression of nearest genes for each H3K27Ac enhancer class. mRNA expression is displayed as reads per kilobase per million mapped reads (RPKM). Nearest genes with nonzero expression by RNA-SEQ were used for this analysis. Expression of the set of genes nearest each enhancer class was assessed at 0, 1, and 6 hours after membrane depolarization with KCl. (b) Boxplot of eRNA expression for each H3K27Ac enhancer class. eRNA expression is displayed as reads per kilobase per million mapped reads (RPKM). eRNA expression for each enhancer was calculated as the number of reads within a 4kb window surrounding the enhancer center. For this analysis, only extragenic enhancers were used. Expression of eRNAs for each enhancer class was assessed at 0, 1, and 6 hours after membrane depolarization with KCl. (c) Boxplot of CBP binding for each H3K27Ac enhancer class before membrane depolarization (0hr KCl) and after membrane depolarization (2hr KCl). CBP binding at each enhancer was calculated as the number of input normalized ChIP-Seq reads within an 800bp window surrounding the enhancer center. * indicates $p < 2.2 \times 10^{-16}$ in paired Wilcoxon test.

2.3.3 Functional testing of enhancers in response to neuronal activity

While genomic correlates of enhancer activity suggested that only enhancers with neuronal activity-dependent increases in H3K27Ac function to promote activity-dependent transcription, we sought to directly test the ability of each class of enhancers to drive transcription in an activity-dependent manner. To accurately measure activity-regulated transcriptional changes, we developed a neuronal activity-regulated luciferase reporter based on the upstream regulatory region of the neuronal activity-regulated gene neuronal pentraxin-2 (*Nptx2*, Figure 2.8a). *Nptx2* encodes a secreted synaptic protein that can bind to and induce clustering of AMPA receptors to regulate homeostatic scaling of excitatory synapses within the nervous system (Chang et al., 2010). We discovered a putative enhancer ~3kb upstream of the *Nptx2* transcriptional start site (TSS). The 4.4kb sequence upstream of the *Nptx2 TSS* was able to drive activity-dependent expression of a luciferase reporter gene in a manner that depended critically upon the presence of the upstream enhancer (Figure 2.8b). We used this reporter to test the ability of enhancers from each of the four H3K27Ac enhancer classes to promote neuronal activity-regulated transcription by replacing the *Nptx2* enhancer with enhancers from each of the four H3K27Ac enhancer classes and measuring activity-dependent induction of the reporter. While our genomic analyses suggested that many enhancers inducibly bound by CBP may not contribute to neuronal activity-dependent gene expression, we sought to directly test this by selecting enhancers from each H3K27Ac enhancers class that were inducibly bound by CBP. As a result, we replaced the *Nptx2* enhancer with inducibly CBP-bound enhancers from each H3K27Ac group. We then transfected the reporter constructs into mouse cortical neuron cultures, and

then measured reporter activity induced by 6 hours of depolarization with KCl. Strikingly, all enhancers that exhibited increasing H3K27Ac signal in response to neuronal activity drove robust activity-dependent transcription of the reporter (14/14; 100% with >2 fold induction with KCl; Figure 2.8b), whereas nearly all other enhancers failed to do so, despite their recruitment of CBP (1/28; 3.6% with >2 fold induction with KCl; Figure 2.8b).

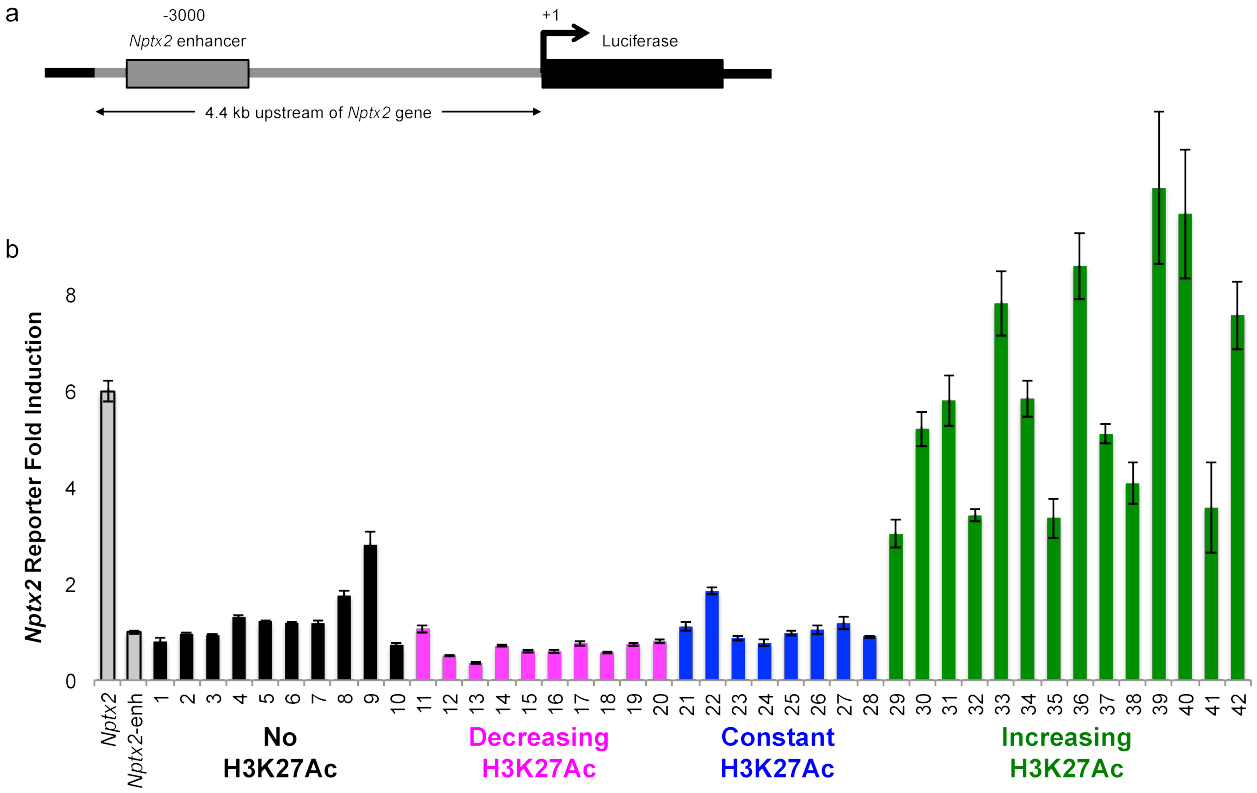

Figure 2.8: Functional testing of neuronal enhancers with different H3K27Ac behaviors

(a) Schematic of *Nptx2* reporter. The 4.4kb sequence upstream of the mouse *Nptx2* gene was cloned into a luciferase reporter construct. Approximately 3kb upstream of the *Nptx2* TSS is an enhancer element, identified by DNaseI hypersensitivity, CBP binding, and H3K27Ac. (b) Luciferase reporter data for the *Nptx2* reporter, reported as the fold induction of reporter activity in mouse cortical neurons after 6 hours of depolarization with KCl relative to 0 hours. The wild-type *Nptx2* reporter is able to induce activity-dependent reporter expression (*Nptx2*). However, if the *Nptx2* enhancer is deleted, the reporter no longer induces activity-dependent reporter expression (*Nptx2*-enh). Inducibly CBP-bound enhancers from the four H3K27Ac enhancer classes were cloned into the *Nptx2* reporter, replacing the *Nptx2* enhancer, and tested for their ability to induce activity-dependent reporter expression. Only enhancers exhibiting increasing H3K27Ac with neuronal activity consistently drove reporter expression in response to neuronal activity. $n \geq 3$ for all enhancers tested.

Across all enhancers tested, neuronal activity-dependent changes in H3K27Ac correlated much more strongly with reporter activity (Spearman's rank correlation coefficient ρ=0.88; Figure 2.9a), than did changes in CBP (ρ=0.65; Figure 2.9b), or changes in RNAPII (ρ=0.34; Figure 2.9c), which has been previously shown to inducibly bind to enhancers (Kim et al., 2010). This suggested that only enhancers that exhibit activity-dependent increases in H3K27ac function to drive activity-regulated gene transcription and further supported inducible H3K27Ac as a much more specific and predictive marker of functional neuronal activity-dependent enhancers than inducible coactivator binding or RNAPII binding. Thus, we concluded that the dynamic chromatin signature of increasing H3K27Ac is a specific and predictive marker of functional neuronal activity-dependent enhancers.

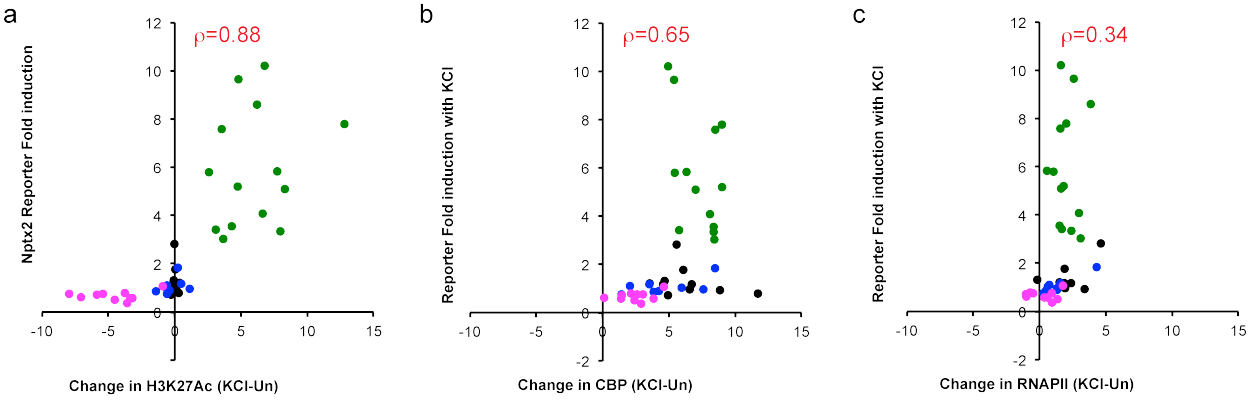

Figure 2.9: Correlation between reporter induction and genomic variables by ChIP-Seq

The *Nptx2* reporter fold induction of each enhancer displayed in Figure 2.8b was plotted against the change in H3K27Ac (a), change in CBP (b), or change in RNAPII (c) seen at that enhancer. Green, blue, magenta, and black points represent enhancers with increasing, constant, decreasing, or no H3K27Ac ChIP-Seq signal in response to neuronal activity. ρ indicates Spearman's rank correlation coefficient for the two variables plotted in each panel.

During development, enhancer elements are thought to be the principal determinants of cell-type specific gene expression. However, numerous studies of neuronal activity-regulated transcription have demonstrated that the promoters of activity-regulated genes are sufficient to drive activity-dependent expression under some conditions (Alberini, 2009; Robertson et al., 1995). This brings into question whether activity-dependent enhancers serve as determinants of stimulus-responsiveness or if they simply amplify transcription from activity-regulated promoters. To gain some insight into this question, we asked whether the ability of activity-responsive enhancers to promote neuronal activity-regulated transcription depended upon their pairing with the activity-regulated *Nptx2* promoter. We cloned four enhancers from each H3K27Ac class into two additional luciferase reporter vectors containing heterologous promoters not known to drive neuronal activity-dependent transcription: an SV40 promoter and a minimal TATA box containing promoter. We hypothesized that if activity-dependent enhancers instructed the transcriptional response to neuronal activity, they would be able to drive activity-dependent transcription from heterologous promoters. However, if activity-dependent enhancers simply amplified promoter driven transcriptional responses to neuronal activity, we hypothesized that they would not be able to drive activity-dependent transcription from heterologous promoters. We found that enhancers with increasing H3K27Ac in response to neuronal activity were able to drive robust activity-dependent reporter expression when paired with either the SV40 promoter (Figure 2.10c,d) or the minimal TATA box promoter (Figure 2.10e,f). While the minimal TATA box containing promoter was weaker than the other promoters (Figure 2.10e,f), enhancer-driven reporter expression for the *Nptx2* reporter and the SV40 were strongly correlated with one

another (ρ=0.95; Figure 2.11), suggesting that the ability to activate transcription in response to neuronal activity was intrinsic to the enhancer element itself, with minimal contribution from the promoter. These results suggest that neuronal activity-dependent enhancers play a significant role in instructing activity-dependent gene expression, rather than functioning to merely amplify transcription from activity-regulated promoters. Furthermore, since enhancers not exhibiting increasing H3K27Ac levels in response to neuronal activity did not drive activity-dependent expression of the other reporter constructs tested (Figure 2.10c-f), these results provide additional evidence from independent reporter contexts that only enhancers with increasing H3K27Ac in response to neuronal activity are able to drive activity-dependent transcription.

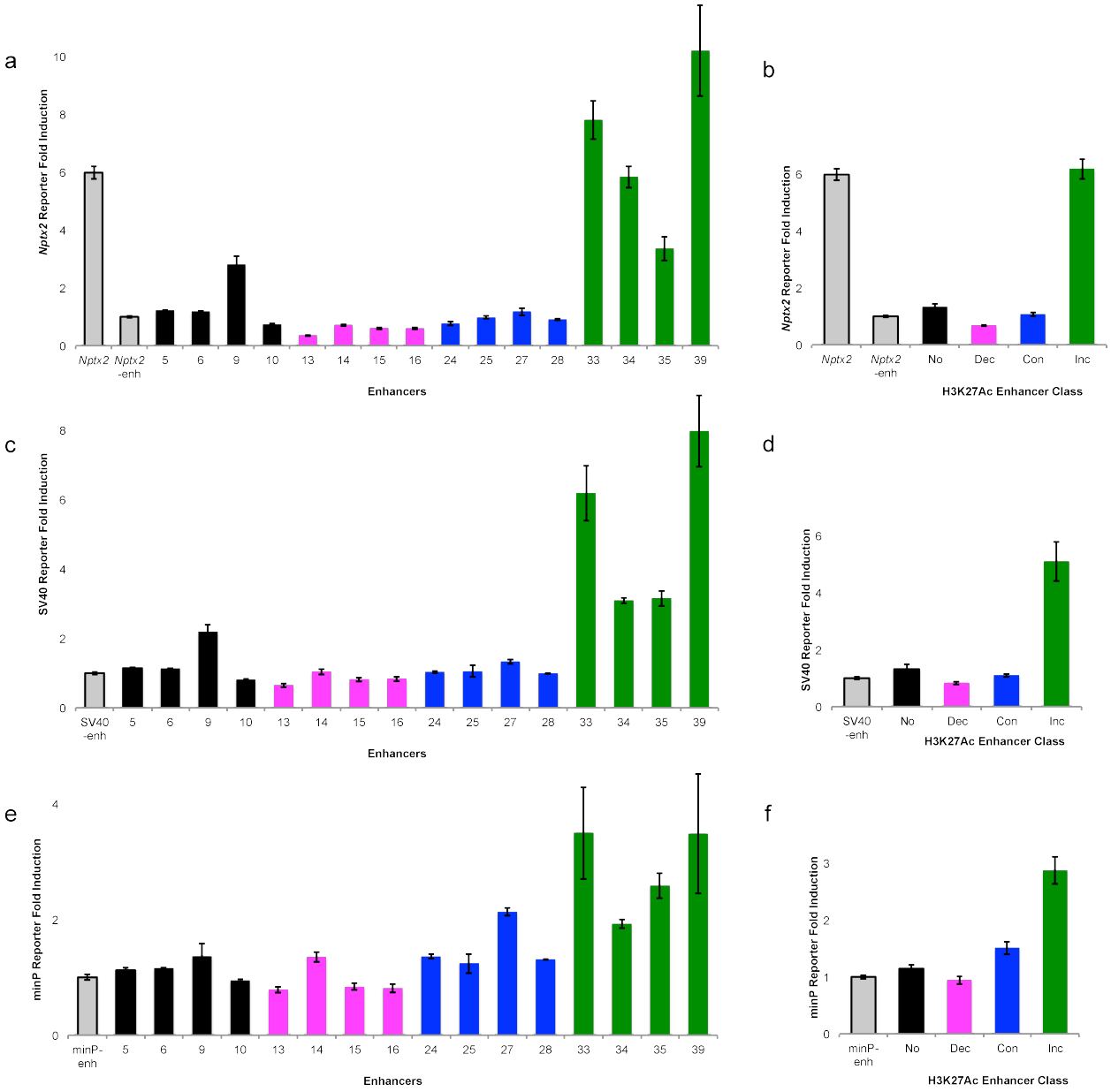

Figure 2.10: Functional testing of neuronal enhancers in different reporter constructs

Luciferase data from neuronal enhancers from each of the four H3K27Ac enhancer classes cloned into either the *Nptx2* reporter containing the *Nptx2* enhancer (a, b), an SV40 promoter reporter (c, d), or a minimal TATA box containing promoter reporter (e, f). Reporter activity is reported as the fold induction of reporter activity in mouse cortical neurons after 6 hours of depolarization with KCl relative to 0 hours of depolarization with KCl. Panels a, c, and e show data for individual enhancers. Panels b, d, and f represent average reporter induction for all enhancers in each enhancer class. $n \geq 3$ for all enhancers tested.

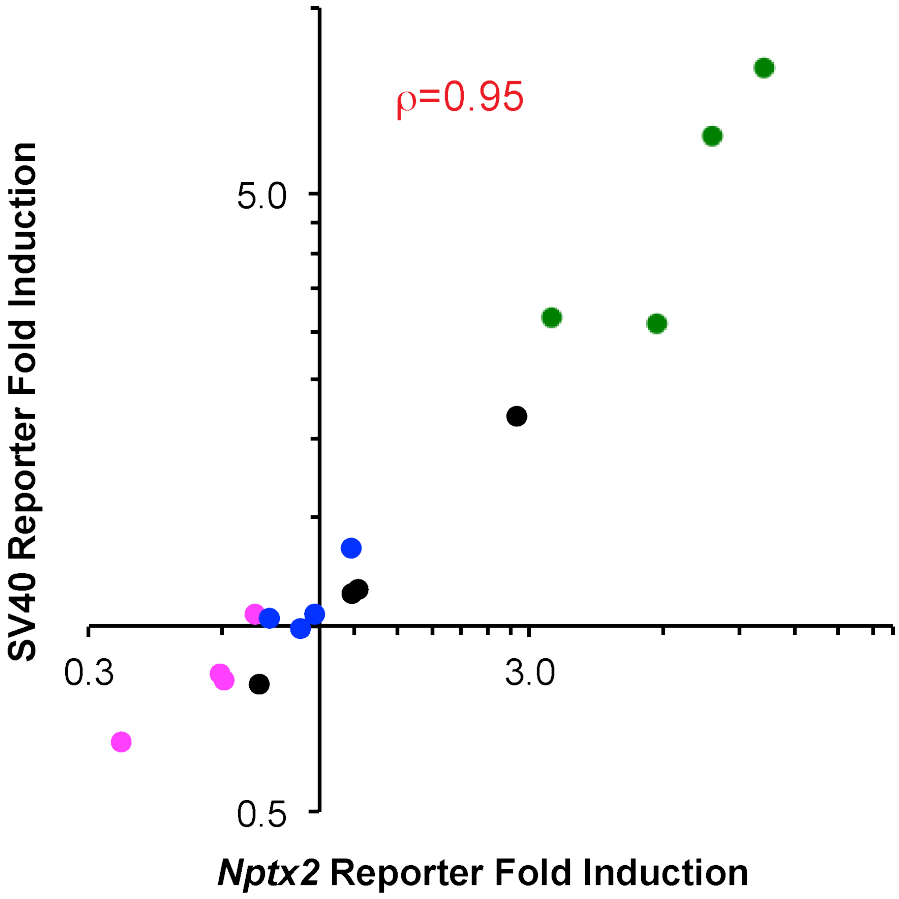

Figure 2.11: Enhancers drive very similar levels of activity-dependent reporter expression independent of the promoter

For each enhancer displayed in Figure 2.10, the fold induction of the SV40 reporter (displayed in Figure 2.10c) was plotted against the fold induction of the *Nptx2* reporter (displayed in Figure 2.10a). Green, blue, magenta, and black points represent enhancers with increasing, constant, decreasing, or no H3K27Ac ChIP-Seq signal in response to neuronal activity. For greater clarity, the data is presented on a log-log scale. ρ indicates Spearman's rank correlation coefficient between reporter inductions plotted.

2.3.4 Neuronal activity-dependent enhancers are increasingly used during brain development

While we were able to use H3K27Ac to identify neuronal activity-dependent enhancers in our *in vitro* culture system with KCl stimulation, we sought to evaluate whether these enhancers were also activity-dependent *in vivo*. To assess the *in vivo* utilization of our neuronal activity-dependent enhancers, we integrated our datasets with H3K27Ac and DNaseI hypersensitivity (DHS) datasets generated by other laboratories from mouse brain tissues at different stages in development (Consortium, 2011; Shen et al., 2012). We reasoned that since activity levels within the brain increase over development, evaluating the H3K27Ac and DNaseI hypersensitivity (DHS) signal at our enhancers at different stages in development could shed light on the utilization of these enhancers with increasing levels of activity exhibited over development *in vivo*. We found individual examples of enhancers that exhibited increasing H3K27Ac levels in response to KCl stimulation that also exhibited increasing H3K27Ac levels and DHS signal with brain development (Figure 2.12a). We quantified H3K27Ac levels and DHS signal at all activity-dependent enhancers we previously identified and found that these enhancers exhibited significantly more H3K27Ac (Figure 2.12b) and DHS (Figure 2.12c) in adult brain tissue compared to embryonic brain tissue. This suggested that, genome-wide, neuronal activity-dependent enhancers identified in our system are not only utilized in the brain *in vivo*, but are increasingly utilized as the brain becomes more active during development.

Figure 2.12: Activity-dependent enhancers are increasing utilized during brain development

(a) Genome browser views of ChIP-Seq tracks at examples of activity-dependent enhancers that exhibit increasing H3K27Ac and DNAseI hypersensitivity (DHS) with brain development. (b) Quantification of H3K27Ac signal at all activity-dependent enhancers in the genome at two stages of brain development. (c) Quantification of DHS signal at all activity-dependent enhancers in the genome at two stages of brain development. In (b) and (c), * indicates $P < 2.2x10^{-16}$ by paired Wilcoxon signed rank test.

2.3.5 Distinct yet overlapping enhancers drive activity-dependent and BDNF-dependent transcriptional programs

While the dynamic chromatin signature of stimulus-inducible H3K27Ac enabled us to identify the subset of neuronal enhancers that function to promote neuronal activity-dependent transcription, it is not clear whether this group of enhancers contains all stimulus-responsive enhancers in neurons or if different stimuli might induce distinct changes to the active enhancer landscape. Neurons must respond to a diverse array of stimuli with appropriate transcriptional changes to function properly *in vivo*. However, the mechanisms by which different extracellular stimuli instruct distinct programs of gene expression are poorly understood. Furthermore, how cis-regulatory elements at stimulus responsive genes activate transcription in response to diverse stimuli is not clear. For example, at genes that are upregulated in response to several distinct stimuli in neurons (such as *c-Fos*), it is not clear whether the response to all stimuli is driven by one multifunctional enhancer or if each stimulus activates a distinct enhancer element to drive transcription. At a mechanistic level, the cis-acting DNA sequences that determine why some enhancers respond to stimuli and others do not are poorly characterized (Evans et al., 2012). Attempts to understand these issues have been limited by challenges in the unbiased, genome-wide identification of the enhancers relevant for stimulus-responsive gene transcription. Our discovery of a dynamic chromatin signature that can accurately identify neuronal activity-regulated enhancers genome-wide provides a potential solution to this problem. Therefore, we sought to utilize this signature to identify neuronal enhancers that respond to an additional stimulus. This would enable a more detailed study of the general principles underlying

stimulus-responsive enhancer function and could help begin to decipher the specific mechanisms that drive transcriptional changes in response to neuronal activity.

Brain derived neurotrophic factor (BDNF) is a particularly important extracellular signal for nervous system development and functional plasticity (Hong et al., 2008; Park and Poo, 2013). Like neuronal activity, BDNF signaling can induce new gene transcription in neurons, although BDNF is thought to regulate a distinct program of gene expression (Gaiddon et al., 1996; Watson et al., 2001). We utilized the dynamic chromatin signature of stimulus-inducible H3K27Ac to identify the set of poised and active enhancers that respond to BDNF stimulation. We performed ChIP-Seq to measure genome-wide levels of H3K27Ac in mouse cortical neurons before and after stimulation with BDNF. In response to BDNF treatment we observed dynamic changes in H3K27Ac across the genome (Spearman rank correlation coefficient ρ=0.39; Figure 2.13a). First, we selected a subset of enhancers that exhibited inducible H3K27Ac (n=2134) using the same criteria to what was used for the set identified for neuronal activity (Figure 2.13b; see methods). The 4.4kb sequence upstream of the *Nptx2* TSS was able to drive BDNF-dependent expression of a luciferase reporter gene in a manner that depended critically upon the presence of the upstream enhancer (Figure 2.14). To test the ability of enhancers with increasing H3K27Ac with BDNF stimulation to promote neuronal BDNF-regulated transcription, we replaced the *Nptx2* enhancer with enhancers with increasing H3K27Ac and measured BDNF-dependent induction of the reporter. Similar to what was observed for neuronal activity, we found that enhancers with increasing H3K27Ac levels in response to BDNF stimulation were able to drive BDNF-dependent expression of the *Nptx2* reporter (Figure 2.14), providing direct

evidence that many of these enhancers function to promote BDNF-dependent transcription. Therefore, the dynamic chromatin signature of stimulus-inducible H3K27Ac was able to accurately identify BDNF responsive enhancers.

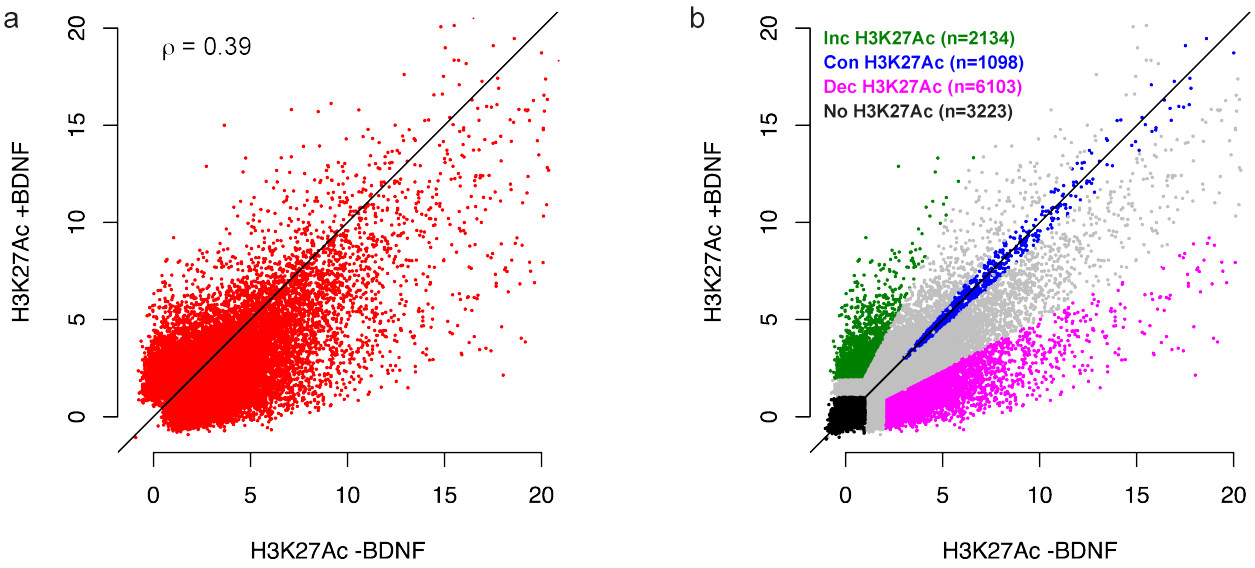

Figure 2.13: H3K27Ac at neuronal enhancers before and after BDNF stimulation

(a) Levels and correlation of H3K27Ac at neuronal enhancers (defined by H3K27Ac enrichment and DNaseI hypersensitivity) throughout the genome before BDNF stimulation (-BDNF) and after BDNF stimulation (+BDNF), Spearman's rho ρ=0.39. (b) Classification of neuronal enhancers into subgroups with distinct H3K27Ac behaviors in response to BDNF stimulation. Enhancers with increasing H3K27Ac, high constant H3K27Ac, decreasing H3K27Ac, or no H3K27Ac in response to BDNF stimulation were classified into separate groups. Each point in both panels represents the input normalized H3K27Ac signal quantified within a 2kb window surrounding an enhancer center, with the x-axis value representing the signal before BDNF stimulation (-BDNF) and the y-axis value representing the signal after two hours of BDNF stimulation (+BDNF).

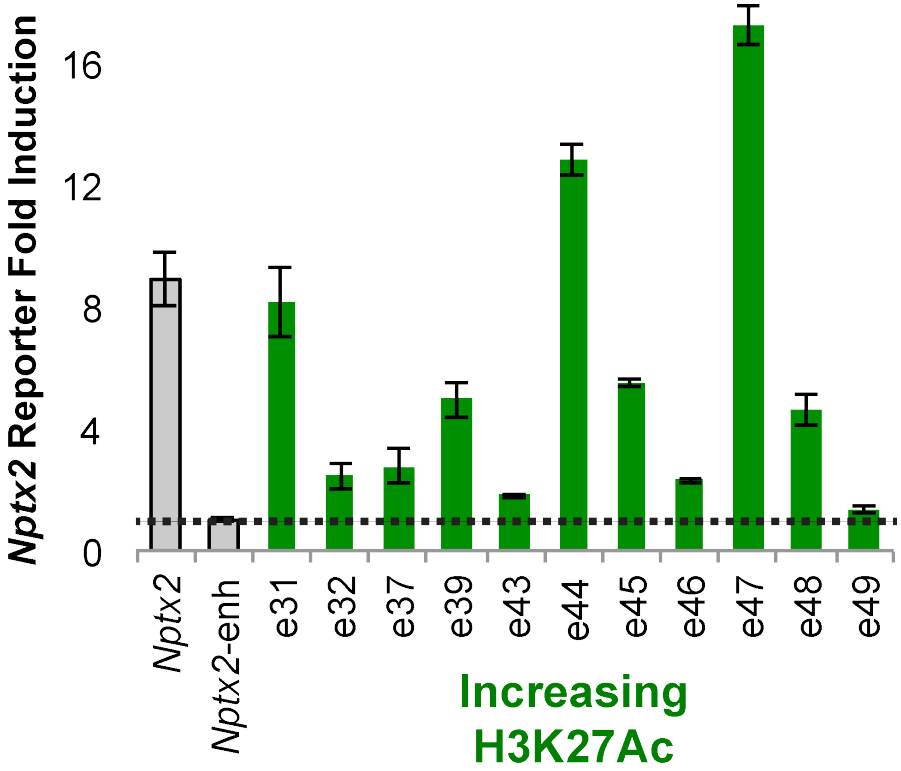

Figure 2.14: Functional testing of neuronal enhancers with increasing H3K27Ac with BDNF stimulation

Luciferase reporter data for the *Nptx2* reporter, reported as the fold induction of reporter activity in mouse cortical neurons after 6 hours of BDNF stimulation relative to 0 hours. The wild-type *Nptx2* reporter is able to induce BDNF-dependent reporter expression (*Nptx2*). However, if the *Nptx2* enhancer is deleted, the reporter no longer induces BDNF-dependent reporter expression (*Nptx2*-enh). Enhancers exhibiting increasing H3K27Ac in response to BDNF stimulation were cloned into the *Nptx2* reporter, replacing the *Nptx2* enhancer, and tested for their ability to induce BDNF-dependent reporter expression. $n \geq 3$ for all enhancers tested.

The ability to accurately identify stimulus-responsive enhancers also provides the novel opportunity to study the properties of BDNF enhancers and compare their properties with those of neuronal activity-dependent enhancers. Having identified two sets of stimulus-responsive enhancers in the nervous system, we next asked whether stimulus-responsive enhancers responded to a single stimulus or could respond to multiple stimuli. We reasoned that initial insight into the question of stimulus-responsiveness of enhancers might be obtained by examining the enhancers near genes that exhibit different stimulus-responsive patterns of expression. We investigated dynamics of H3K27Ac at enhancers near *Npas4*, a gene that is known to be preferentially induced by neuronal activity (Lin et al., 2008), *Arc*, which is preferentially induced in response to BDNF (Kawashima et al., 2009), and *c-Fos*, which is induced in response to both neuronal activity and BDNF (Bonni et al., 1995) (Figure 2.15). We discovered that the enhancers near these genes had H3K27Ac dynamics consistent with their stimulus-responsive patterns of expression. Several putative enhancers near the *Npas4* gene exhibited inducible H3K27Ac only in response to neuronal activity (Figure 2.15, left). Similarly, a well-characterized enhancer (Kawashima et al., 2009) upstream of the *Arc* gene exhibited inducible H3K27Ac only in response to BDNF (Figure 2.15, center). Interestingly, enhancers near the *c-Fos* gene exhibited distinct patterns of H3K27Ac in response to different stimuli. Two enhancers upstream of the *c-Fos* TSS exhibited inducible H3K27Ac specifically in response to neuronal activity while one enhancer downstream of the TSS exhibited inducible H3K27Ac in response to both neuronal activity and BDNF (Figure 2.15, right). These loci demonstrate that while some neuronal stimulus-responsive enhancers respond to specific stimuli, others can respond to multiple stimuli.

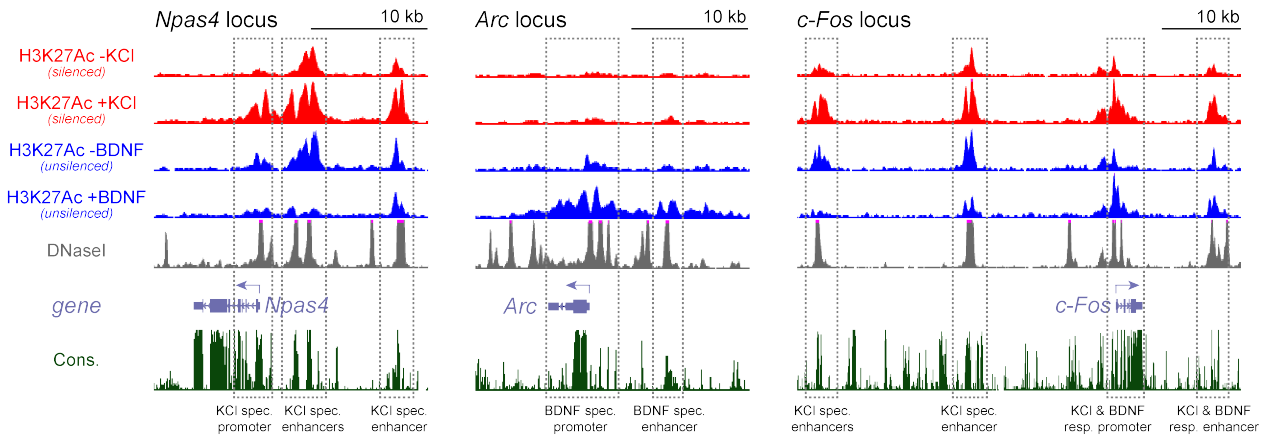

Figure 2.15: Differential changes in H3K27Ac with KCl and BDNF stimulation

Genome browser views of H3K27Ac ChIP-Seq tracks at the *Npas4* locus (left), the *Arc* locus (center), and the *c-Fos* locus (right). ChIP-Seq tracks display input-normalized H3K27Ac ChIP-Seq reads from neurons from the indicated stimulation conditions. Also displayed are DNaseI hypersensitivity signal from adult mouse cerebrum and vertebrate conservation by PhastCons. Dashed boxes identify regulatory elements with different stimulus-responsive changes in H3K27Ac.

From inspection of individual genetic loci, it was clear that while some neuronal stimulus-responsive enhancers respond to specific stimuli, others can respond to multiple stimuli. We sought to characterize neuronal enhancers throughout the genome that exhibited differential responses to neuronal activity and BDNF. At a genomic level, a distinct yet overlapping set of DNaseI hypersensitive sites exhibited increases in H3K27Ac in response to neuronal activity and BDNF. Thus, we hypothesized that by identifying all neuronal enhancers in the genome with different stimulus responsive properties, we could begin to understand the mechanisms by which enhancers respond to specific stimuli. In order to accomplish this, we first identified all neuronal activity-responsive (n=2261; Figure 2.16a), BDNF-responsive (n=1560; Figure 2.16b), or activity and BDNF responsive enhancers (n=404; Figure 2.16c) based on the inducibility of H3K27Ac at these enhancers in response to KCl, BDNF, or both. Average profiles of H3K27Ac ChIP-Seq signal for each group of neuronal enhancers displayed clearly different H3K27Ac behaviors in response to neuronal activity and BDNF (Figure 2.16).

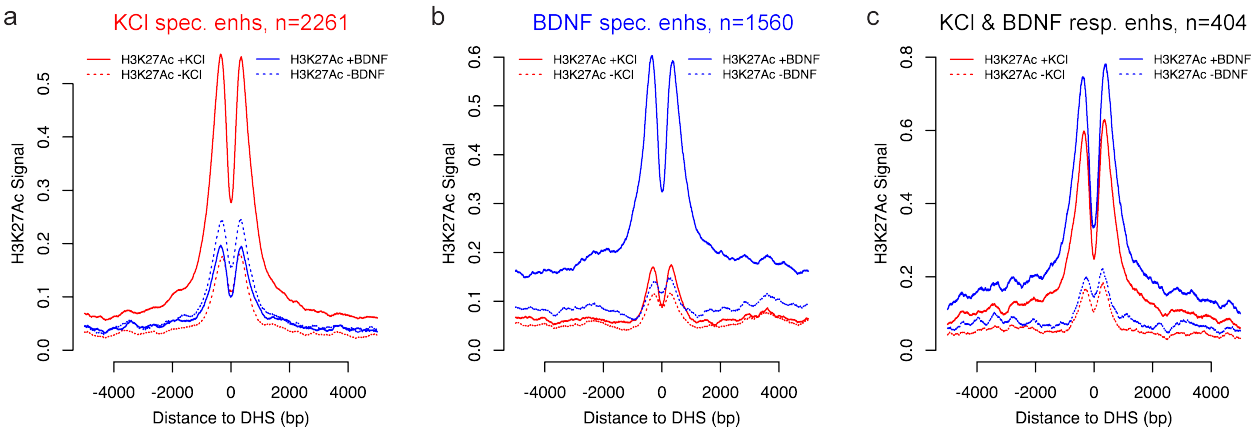

Figure 2.16: Identification of neuronal enhancers with differential responses to neuronal activity and BDNF stimulation

Average profiles of H3K27Ac ChIP-Seq signal at KCl specific enhancers (a), BDNF specific enhancers (b), or KCl and BDNF responsive enhancers (c). The y-axis represents the level of H3K27Ac signal, displayed as the mean number of input-normalized H3K27Ac ChIP-Seq reads at each subgroup of enhancers. H3K27Ac signal at enhancers was aligned by the centers DNaseI hypersensitive sites. H3K27Ac signal at enhancers is displayed before KCl depolarization (dashed red line), after KCl depolarization (solid red line), before BDNF stimulation (dashed blue line), or after BDNF stimulation (solid blue line).

For each set of enhancers, the changes in H3K27Ac in response to each stimulus predicted the stimulus-specific changes in transcription, as assessed by functional testing of these enhancers in *Nptx2* luciferase reporter assays (Figure 2.17). This suggested that dynamic stimulus-dependent changes in H3K27Ac can not only accurately identify stimulus-responsive enhancers but can also accurately identify enhancers throughout the genome that respond differentially to distinct stimuli.

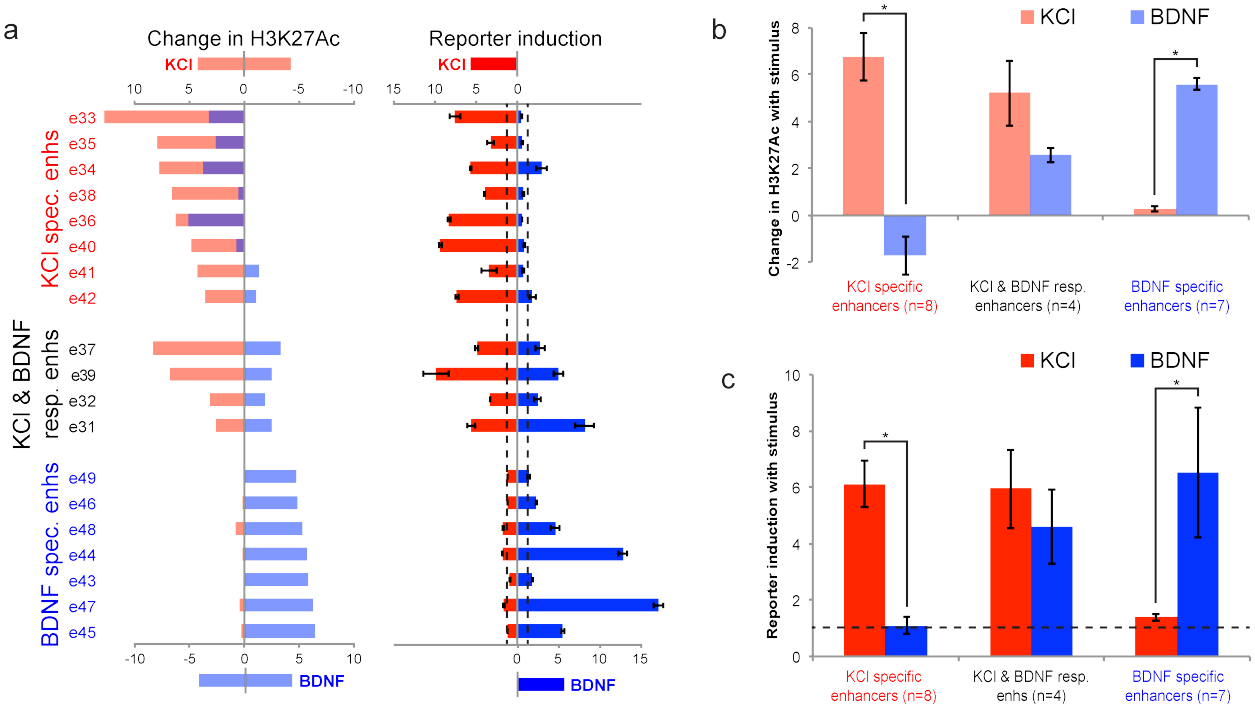

Figure 2.17: Functional testing of enhancers with differential responses to neuronal activity and BDNF stimulation

Neuronal enhancers with differential H3K27Ac behaviors in response to neuronal activity and BDNF were cloned into the *Nptx2* luciferase reporter and tested for their ability to induce reporter expression in response to KCl, BDNF, or both (a). (b) Average change in H3K27Ac for all enhancers in each stimulus-responsive enhancer class shown in (a). (c) Average reporter induction for all enhancers in each stimulus-responsive enhancer class shown in (a).

Having identified neuronal enhancers that respond to either neuronal activity or BDNF, we asked whether these different sets of enhancers contribute to stimulus-dependent transcriptional programs with different biological functions within the neuron. We did this by assessing whether activity-responsive and BDNF responsive enhancers were associated with genes of distinct functional annotations by performing ontology analysis with the Genomic Regions Enrichment of Annotations Tool (GREAT) (McLean et al., 2010). Each class of enhancers was associated with neuronal cellular components, biological processes, mouse phenotypes, and disease ontologies, consistent with specific functions of these enhancers in neurons (Table 1). However, there was little overlap in the specific categories enriched from each group (Table 1), consistent with the differences in the physiological functions of neuronal activity and BDNF. Closer analysis of the enriched terms for each class of enhancers revealed possible differences in the biological functions of stimulus-dependent transcriptional programs induced by neuronal activity and BDNF (Table 1). While activity-responsive enhancers were linked to genes that localize to dendritic compartments and play a role in behavior, BDNF-responsive enhancers were linked to genes that localize to vesicles and play a role in signaling. Enriched terms also revealed distinct mouse phenotypes and human diseases associated with each set of enhancers. While activity-responsive enhancers were linked to abnormal brain morphology and psychiatric disease, BDNF-responsive enhancers were linked to abnormal synapse function and cancer and neurodegenerative disease. These data suggest that dynamic stimulus-dependent changes in H3K27Ac can not only accurately identify enhancers throughout the genome that respond differentially to distinct stimuli, but that these different sets of enhancers may contribute to different biological functions within the neuron.

Table 1: KCl and BDNF specific enhancers are linked to genes with distinct functional annotations

KCl and BDNF specific enhancers were analyzed using the Genomic Regions Enrichment of Annotations Tool (GREAT). Both KCl specific and BDNF specific enhancers were linked to genes with nervous system-related annotations but these classes of enhancers differed in the specific annotations that were most enriched within each ontology category. Only the top three most significant terms are displayed for each ontology category.

Ontology Category	KCl-specific enhancers		BDNF-specific enhancers	
	Term	P-value	Term	P-value
GO Cellular Component	dendrite	8.7E-14	neuron projection	7.9E-18
	dendritic shaft	2.7E-10	cytoplasmic membrane-bounded vesicle	5.6E-15
	dendritic spine	4.0E-10	membrane-bounded vesicle	5.9E-15
GO Biological Process	adult behavior	5.4E-15	regulation of signaling	1.3E-39
	behavior	5.6E-14	regulation of response to stimulus	6.4E-39
	locomotory behavior	1.6E-11	regulation of signal transduction	2.0E-32
Mouse Phenotype	convulsive seizures	1.1E-13	abnormal synaptic transmission	1.9E-22
	abnormal limbic system morphology	2.2E-12	abnormal CNS synaptic transmission	4.9E-22
	abnormal hippocampus morphology	2.7E-12	abnormal long term potentiation	1.5E-17
Disease Ontology	bipolar disease	7.8E-10	astrocytoma	5.9E-09
	mood disease	1.1E-09	tauopathy	2.8E-08
	spinal cord disease	9.8E-07	substance-related disease	3.4E-07

2.4 DISCUSSION

In neurons, extracellular stimuli can induce specific and temporally regulated changes in gene expression that correlate with the formation and functional plasticity of synaptic connections in developing and adult brains (Loebrich and Nedivi, 2009). In order to identify and begin to understand the cis-regulatory elements that function to instruct the temporally and spatially circumscribed induction of activity-regulated transcription in neurons, we utilized genome-scale tools to map enhancer elements in cortical neurons. While previous studies have begun to identify neuronal enhancers, the enhancers that function to promote stimulus-responsive transcription within the nervous system have not been specifically identified. This is in part because no chromatin signature has been described for the specific identification of this subset of enhancers. We demonstrate that membrane depolarization with KCl and stimulation with BDNF can both induce rapid changes in H3K27Ac at thousands of enhancer elements within the genome. We further show that stimulus-responsive enhancers within the nervous system can be specifically identified on the basis of the dynamic chromatin signature of stimulus-inducible H3K27Ac. We utilized this dynamic chromatin signature to comprehensively identify and characterize functional KCl and BDNF responsive enhancer elements in mouse cortical neurons. These enhancers are sufficient to drive robust and stimulus-specific reporter expression in cortical neurons *in vitro*. Furthermore, these enhancers are associated with genes with distinct functional annotations, suggesting that KCl and BDNF responsive enhancers play distinct biological functions within the neuron. Finally, by integrating our data with epigenomic data from other studies, we have gained insight into the cis-regulatory logic

of activity-regulated transcriptional control and have identified thousands of previously uncharacterized neuronal enhancer elements.

2.4.1 Rapid changes in H3K27Ac at neuronal enhancers

In the nervous system, it has been proposed that long-term changes in synaptic function associated with learning and memory might arise in part from stable changes in chromatin modifications that serve as a molecular "mnemonic" devices (Day and Sweatt, 2011; Graff and Tsai, 2013). Interestingly, global levels of histone acetylation occur in brain regions that are strongly activated during specific experimental behavioral paradigms (Day and Sweatt, 2011; Graff and Tsai, 2013; Peleg et al., 2010). Furthermore, reduction or removal of histone deacetylase activity using genetic methods or treatment with HDAC inhibitors has been shown to increase memory formation and long-term potentiation (Graff and Tsai, 2013; Guan et al., 2009). It will be interesting to explore the possibility that HDAC inhibitors might influence learning and memory by acting to increase the magnitude or half-life of inducible acetylation at stimulus-responsive enhancers, which could lead to changes in the kinetics of stimulus-regulated gene transcription, decreases in the levels of stimulation required to induce stimulus-regulated gene transcription, or ectopic activation of genes that are not activity-regulated under physiological conditions.

2.4.2 Heterogeneity among active neuronal enhancers

Previous studies that have identified active enhancers within the nervous system have using distal enrichment of H3K27Ac. However, these studies have treated neuronal enhancers as a homogeneous population. We find that neuronal enhancers are quite heterogeneous, both in terms of their response to extracellular stimuli as well as their stimulus specificity. Our data suggest a previously underappreciated diversity of cis-regulatory function among enhancers defined as "active" using H3K27Ac enrichment, and suggest that by profiling enhancer activity both during differentiation and in specific stimulus paradigms it will be possible to further classify active enhancers into discrete functional classes. A recent report suggests that in macrophages, prolonged stimulation with an inflammatory stimulus induces the activation of "latent" enhancer elements, which exhibit none of the chromatin marks associated with poised enhancer elements (e.g. H3K4me1, nucleosome depletion) prior to exposure to inflammatory stimuli (Ostuni et al., 2013). These latent enhancers were suggested to function to prime specific genes for increased expression following a transient stimulus, which the authors suggest might provide a chromatin-based mechanism for storing information about prior exposure to environmental stimuli. However, when tested in luciferase reporter assays, only ~50% of these regions can drive stimulus responsive transcription, suggesting that a substantial portion of these elements are not acutely involved in stimulus-regulated transcription and are potentially more important for stimulus-induced phenotypic plasticity. In the brain, sensory experience can induce long-lasting changes in neuronal morphology, synapse number and plasticity, and survival, but the potential for this limited plasticity is balanced by the need to tightly

and stably regulate neuronal fate for the entire lifespan of the organism (Dulac, 2010). Further studies will be required to unravel the connection between synaptic activity and the active enhancer repertoire during brain development and function *in vivo* to determine whether neurons also utilize stimulus-responsive "latent" enhancers. It will be similarly interesting to investigate whether any observed differences in stimulus-responsive enhancer "latency" represents a physiologically relevant difference between the function of stimulus responsive transcription in macrophages and neurons.

2.4.3 Novel tools to study the role of activity-regulated gene transcription in nervous system development and plasticity

The induction of stimulus-regulated transcription occurs specifically in neurons that are highly active during a defined behavior (Alberini, 2009; Lyons and West, 2011). The induction of immediate early genes such as *c-Fos*, *FosB*, *JunB*, *Nur77*, *Zif268* and *Npas4 in vivo* has been used as a tool to specifically mark the neurons involved in the circuitry governing a defined behavior. The ability of enhancers to integrate various transcription factor inputs and signal responsive cues can also be repurposed to develop tools to drive reporter gene expression or Cre recombinase in specific cell populations *in vivo*, providing genetic access to specific neuronal circuits. Similarly, in order to rigorously study the function of stimulus regulated genes it will be necessary to remove the enhancer(s) that specifically control a gene's induction in order to disentangle the stimulus-dependent and stimulus-independent effects on synaptic function of these often pleiotropic factors (e.g. BDNF, see Hong et al., 2008). Historically it has been

difficult to separate the activity-regulated function of many genes from their functions in neural development, so the ability to functionally separate these features will become critical for future studies to determine the contribution of specific activity-regulated genes to learning and memory *in vivo*. Given recent efforts to establish *in vitro* stem cell models of neurological disorders that affect synaptic plasticity and function *in vivo*, activity-responsive enhancers could provide useful tools for the characterization of the *in vitro* maturation of various types of neurons derived from embryonic stem cell differentiation protocols (Dolmetsch and Geschwind, 2011; Ming et al., 2011).

2.5 Materials and Methods

2.5.1 Mouse cortical cultures

Embryonic day 16.5 (E16.5) C57BL/6 embryonic mouse cortices were dissected and then dissociated for 10 minutes in 1× Hank's Balanced Salt Solution (HBSS) containing 20 mg/mL trypsin (Worthington Biochemicals) and 0.32 mg/mL L-cysteine (Sigma). Trypsin treatment was terminated by washing dissociated cells three times for two minutes each in dissociation medium consisting of 1× HBSS containing 10 mg/mL trypsin inhibitor (Sigma). Cells were then triturated using a flame-narrowed Pasteur pipette to fully dissociate cells. After dissociation, neurons in were kept on ice in dissociation medium until plating. Cell culture plates were pre-coated overnight with a solution containing 20 ug/mL poly-D-lysine (Sigma) and 4 ug/mL mouse laminin (Invitrogen) in water. Prior to plating neurons, cell culture plates were washed three times with sterile distilled water and washed once with Neurobasal Medium (Life Technologies). Neurons were grown in neuronal medium consisting of Neurobasal Medium containing B27 supplement (2%; Invitrogen), penicillin-streptomycin (50 g/ml penicillin, 50 U/mL streptomycin, Sigma) and glutamine (1 mM, Sigma). At the time of plating, cold neuronal medium was added to neurons in dissociation medium to dilute neurons to the desired concentration. Neurons were subsequently plated and placed in a cell culture incubator that maintained a temperature of 37 degrees C and a CO2 concentration of 5%. Two hours after plating neurons, medium was completely aspirated from cells and replaced with fresh warm neuronal medium. Neurons were grown *in vitro* until the seventh day *in vitro* (DIV7).

2.5.1.1 Mouse cortical cultures for ChIP-Seq experiments

For ChIP-Seq experiments, mouse cortical neurons were plated at an approximate density of 4×10^7 on 15-cm dishes. Neurons were plated in 30mL neuronal medium. Ten mL of the medium was replaced with 12ml fresh warm medium on DIV3 and DIV6.

2.5.1.2 Mouse cortical cultures for luciferase reporter assays

For luciferase reporter assays, mouse cortical neurons were plated at an approximate density of 3×10^5 per well on 24-well plates. Neurons were plated in 500 uL neuronal medium. On the DIV3, 100 uL fresh warm medium was added to neurons. On DIV5 neurons were transfected (see section on transfection). At the completion of transfection, conditioned medium containing 15% fresh medium was returned to neurons.

2.5.2 Stimulation with potassium chloride (KCl)

Prior to KCl depolarization, neurons were quieted with 1 μM tetrodotoxin (TTX, Fisher) and 100 μM DL-2-amino-5-phosphopentanoic acid (DL-AP5, Fisher). Neurons were subsequently stimulated by adding warmed KCl depolarization buffer (170 mM KCl, 2 mM CaCl2, 1 mM MgCl2, 10 mM HEPES) directly to the neuronal culture, to final concentration of 31% in the neuronal culture medium within the culture plate or well.

2.5.2.1 KCl stimulation for ChIP-Seq experiments

For KCl depolarization of neurons for ChIP-Seq experiments, DIV 6 neurons were quieted overnight with 1 μM TTX and 100 μM DL-AP5. The next morning, neurons were left silenced (-KCl condition) or stimulated for 2 hours with KCl (+KCl condition).

2.5.2.2 KCl stimulation for luciferase reporter assays

For KCl depolarization of neurons for luciferase reporter assays, DIV 7 neurons were quieted for two hours with 1 μM TTX and 100 μM DL-AP5. Two hours later, neurons were left silenced (-KCl condition) or stimulated for 6 hours with KCl (+KCl condition).

2.5.3 Stimulation with brain derived neurotrophic factor (BDNF)

2.5.3.1 BDNF stimulation for ChIP-Seq experiments

For BDNF stimulation of neurons for ChIP-Seq experiments, the volume of conditioned medium on DIV6 neurons was reduced to 25 mL. On DIV7, neurons were left in a basal condition (-BDNF condition) or stimulated for 2 hours with 50ng/mL recombinant human BDNF (Fisher) (+BDNF condition).

2.5.3.2 BDNF stimulation for luciferase reporter assays

For BDNF stimulation of neurons for luciferase reporter assays, DIV7 neurons were left in a basal condition (-BDNF condition) or stimulated for 6 hours with 50ng/mL recombinant human BDNF (Fisher) (+BDNF condition).

2.5.4 H3K27Ac Chromatin immunoprecipitation sequencing (ChIP-Seq)

Forty million mouse cortical neurons cultured to *in vitro* day 7 were used for each ChIP-Seq library construction. Typically 20-40 million cortical neurons were used for a single ChIP experiment. To cross-link protein-DNA complexes, media was removed from neuronal cultures and crosslinking-buffer (0.1 M NaCl, 1 mM EDTA, 0.5 mM EGTA, 25 mM HEPES-KOH, pH 8.0) containing 1% formaldehyde was added for 10 minutes at room temperature. Cross-linking was quenched by adding 125 mM glycine for five minutes at RT. Cells were then rinsed three times in ice-cold PBS containing complete protease inhibitor cocktail tablets (Roche) and collected by scraping. Cells were pelleted and either stored at -80 degrees C until use or immediately processed. Cell pellets were lysed by 20 cell pellet volumes (CPVs) of buffer 1 (50 mM HEPES-KOH, pH 7.5, 140 mM NaCl, 1 mM EDTA, pH 8.0, 10 % Glycerol, 0.5 % NP-40, 0.25 % Triton X-100, complete protease inhibitor cocktail) for 10 min at 4 degrees C. Nuclei were then pelleted by centrifugation at 3000 rpm for 10 min at 4 degrees C. The isolated nuclei were rinsed with 20 CPVs of buffer 2 (200 mM NaCl, 1 mM EDTA, pH 8.0, 0.5 mM EGTA, pH 8.0, 10 mM Tris-HCl, pH 8.0, complete protease inhibitor cocktail) for 10 min at RT and re-pelleted. Next, 4 CPVs of buffer 3 (1 mM EDTA, pH 8.0, 0.5 mM

EGTA, pH 8.0, 10 mM Tris-HCl, pH 8.0, complete protease inhibitor cocktail) were added to the nuclei and sonication was carried out using a Misonix 3000 Sonicator (Misonix) set at a power setting of 7.5 (equivalent to 24 watts). 20 pulses of 15 seconds each were delivered at this setting, which resulted in genomic DNA fragments with sizes ranging from 200 bp to 2 kb. Insoluble materials were removed by centrifugation at 20,000 rpm for 10 min at 4 degrees C. The supernatant was transferred to a new tube and the final volume of the resulting nuclear lysate was adjusted to 1 mL by adding buffer 3 supplemented with 0.3 M NaCl, 1 % Triton X-100, 0.1 % Deoxycholate. The lysate was pre-cleared by adding 100 uL of pre-rinsed Protein A/G Agarose (Sigma) per 1 ml of the lysate and incubating for 1 hour at 4 degrees C. After pre-clearing, ten percent of the ChIP sample (50 uL from 500 uL lysate) was saved as input material. The remaining lysate was incubated with 0.5 ug H3K27Ac antibody ab4729 (Abcam) for immunoprecipitation. The antibody incubation was carried out overnight at 4 degrees C. The next day, 30 uL of pre-rinsed Protein A/G PLUS Agarose beads (Santa Cruz Biotechnology) was added to each ChIP reaction and further incubated for 1 hour at 4 degrees C. The beads bound by immune-complexes were pelleted and washed twice with each of the following buffers: low salt buffer (0.1% SDS, 1% Triton X-100, 2mM EDTA, 20mM Tris-HCl, pH 8.1, 150mM NaCl), high salt buffer (0.1% SDS, 1% Triton X-100, 2mM EDTA, 20mM Tris-HCl, pH 8.1, 500mM NaCl) and LiCl buffer (0.25M LiCl, 1% IGEPAL CA630, 1% deoxycholic acid (sodium salt), 1mM EDTA, 10mM Tris, pH 8.1). In each wash, the beads were incubated with wash buffer for 10 min at 4 degrees C while nutating. The washed beads were then rinsed once with 1x TE buffer (10 mM Tris-HCl, pH 8.0, 1 mM EDTA). The immunoprecipitated material was eluted from the beads twice by adding 100 uL of elution buffer (10 mM Tris-HCl, pH 8.0, 1 mM EDTA, pH 8.0,

1 % SDS) to each ChIP reaction and incubating the sample at 65 degree C for 30 min with brief vortexing every 2 min. 150 uL of elution buffer was also added to the saved input material (50 uL) and this sample was processed together with the ChIP samples. The eluates were combined and crosslinking was reversed by incubation at 65 degrees C overnight. The next day, 7 ug RNase A (affinity purified, 1mg/mL; Invitrogen) was added to each sample and samples were incubated for 37 degrees C for one hour. Then, 7 uL Proteinase K (RNA grade, 20mg/mL; Invitrogen) was added to each sample and samples were incubated at 55 degrees C for two hours. The immunoprecipitated genomic DNA fragments were then extracted once with Phenol:Chloroform:Isoamyl Alcohol (25:24:1, pH 7.9; Life Technologies) and then back extracted with water. The resulting genomic DNA fragments were then purified using the QIAquick PCR purification kit (Qiagen) and DNA fragments were eluted in 100 ul of Buffer EB (elution buffer consisting of 10 mM Tris-HCl, pH 8.5, Qiagen). Samples were assessed for enrichment by quantitative PCR using primers to different genomic regions. Samples with significant enrichment over negative regions were submitted to the Beijing Genomic Institute (BGI) for 50 base pair single end sequencing on the Illumina Hiseq 2000 platform. For each sample, over 20 million clean reads were obtained.

2.5.5 ChIP-Seq analysis

2.5.5.1 Initial processing

Sequencing data was obtained from BGI in gzipped fastq file format. Files were transferred and unzipped. Then, sequencing reads were aligned to the July 2007

assembly of the mouse genome (NCBI 37, mm9) using the Burrows-Wheeler Aligner (BWA) (Li and Durbin, 2009) with default settings. The resulting bwa files were then converted to sam files and uniquely mapped reads were extracted from the sam files. Sam files of the uniquely mapped reads were then converted to bam files. Bam files were then used for peak calling using Model-based Analysis of ChIP-Seq (MACS) (Zhang et al., 2008) with the following parameters: -f BAM -g mm --nomodel --shiftsize=150.

2.5.5.2 Visualizing ChIP-Seq data on the UCSC genome browser

ChIP-Seq bam files were converted to bigwig track format to display the number of input normalized ChIP-Seq reads, normalized to 20 million total reads.

2.5.5.3 Identifying enhancers by integrating DNaseI hypersensitivity data with H3K27Ac ChIP-Seq data

DNaseI hypersensitivity (DHS) identified by using ENCODE consortium DHS peaks data from embryonic day 14.5 whole brain, embryonic day 18.5 whole brain, and adult 8 week cerebrum was assessed for overlap with H3K27Ac peaks. First, the genomic ranges of DHS peaks from adult 8week cerebrum in all three bioreplicates were concatenated and merged. Then, merged ranges that overlapped with peaks in three out of three DHS bioreplicates were computed (8wk_merged_overlappingwithB1B2B3). Similarly, merged ranges that overlapped with two out of two bioreplicates from embryonic day 18.5 (e18.5_merged_overlappingwithB1B2) and merged ranges that overlapped with two out of two bioreplicates from embryonic day 14.5 (e14.5_merged_overlappingwithB1B2) were obtained. Then DHS peaks overlapping

with H3K27Ac were obtained through iterations of assessing overlap between the datasets. First, the DHS peaks in 8wk_merged_overlappingwithB1B2B3 that overlapped with H3K27Ac peaks (in the –KCl, +KCl, -BDNF, or +BDNF conditions) were isolated. Then, the DHS peaks in e18.5_merged_overlappingwithB1B2 that overlapped with the remaining H3K27Ac peaks were isolated. Then, the DHS peaks in e14.5_merged_overlappingwithB1B2 that overlapped with the remaining H3K27Ac peaks were isolated. Then, the DHS peaks in the first bioreplicate from 8-week cerebrum that overlapped with the remaining H3K27Ac peaks were isolated. Then, the DHS peaks in the second bioreplicate from 8-week cerebrum that overlapped with the remaining H3K27Ac peaks were isolated. Then, the DHS peaks in the third bioreplicate from 8-week cerebrum that overlapped with the remaining H3K27Ac peaks were isolated. Then, the DHS peaks in the first bioreplicate from e18.5 whole brain that overlapped with the remaining H3K27Ac peaks were isolated. Then, the DHS peaks in the second bioreplicate from e18.5 whole brain that overlapped with the remaining H3K27Ac peaks were isolated. Then, the DHS peaks in the first bioreplicate from e14.5 whole brain that overlapped with the remaining H3K27Ac peaks were isolated. Then, the DHS peaks in the second bioreplicate from e14.5 whole brain that overlapped with the remaining H3K27Ac peaks were isolated. Then, CBP peaks previously identified in our system (Kim et al., 2010) that overlapped with the remaining H3K27Ac peaks were isolated. This iterative procedure was used rather than simply assessing overlap between H3K27Ac signal and either the union or intersection of all DHS data to increase accuracy of calling overlaps and to reduce the multiplicity of DHS peaks associated with H3K27Ac peaks. In the end, 98.6% of H3K27Ac peaks were found to overlap with DHS peaks, with an average of 1.39 DHS peaks per H3K27Ac peak. Each DHS peak that

overlapped with H3K27Ac and existed greater than 1kb from an annotated RefSeq TSS was taken to be an enhancer for subsequent analyses.

2.5.5.4 Characterization of genomic distribution of enhancers

H3K27Ac peaks were classified based on their location relative to genes in the NCBI Reference Sequence Database (RefSeq). H3K27Ac peaks were classified as being proximal if they were within 1kb of an annotated transcriptional start site (TSS). H3K27Ac peaks were classified as being distal if they were greater than 1kb from an annotated transcriptional start site (TSS). Distal H3K27Ac peaks were further classified as intragenic if they occurred within a RefSeq gene, or as extragenic if they did not occurred within a RefSeq gene.

2.5.5.5 Quantification of ChIP-Seq signal at enhancers

For chromatin modifications (H3K4Me1, H3K27Ac), the number of input-normalized ChIP-Seq reads within a two kb window centered on each enhancer was taken to be the ChIP-Seq signal at the enhancer. For transcription factors (CBP), the number of input-normalized ChIP-Seq reads within an 800 bp window centered on each enhancer was taken to be the ChIP-Seq signal at the enhancer.

2.5.5.6 Classification of enhancers with distinct H3K27Ac behaviors

Enhancers were classified into different categories based on the behavior of the quantified H3K27Ac signal at each enhancer. Enhancers were classified as having increasing H3K27Ac if they exhibited a two fold or greater increase in H3K27Ac signal

with stimulation and if the stimulated signal for H3K27Ac was not within the bottom quartile of H3K27Ac signal at all enhancers identified in the stimulated condition. Enhancers were classified as having decreasing H3K27Ac if they exhibited a two fold or greater decrease in H3K27Ac signal with stimulation and if the unstimulated signal for H3K27Ac was not within the bottom quartile of H3K27Ac signal at all enhancers identified in the unstimulated condition. Enhancers were classified as having constant H3K27Ac if they exhibited H3K27Ac signal in the top quartile of all enhancers identified in both the unstimulated and stimulated conditions and if the H3K27Ac signal changed by 10% or less with stimulation. Enhancers were classified as having no H3K27Ac if they were identified previously on the basis of inducible CBP binding and enrichment for H3K4Me1 (Kim et al., 2010) but did not overlap with H3K27Ac peaks within the H3K27Ac datasets generated in this study.

2.5.6 RNA-Seq analysis

RNA-Seq data from a previous study (Kim et al., 2010) was analyzed and integrated into this study. For nearest gene analyses, the nearest gene (with nonzero expression) to an enhancer was linked to that enhancer and the expression of the genes nearest to each class of enhancers was characterized. For eRNA analysis, the number of RNA-Seq reads within a four kb window centered on each extragenic enhancer was taken to be the eRNA signal at the enhancer.

2.5.7 Luciferase reporter assays

2.5.7.1 Nptx2 reporter plasmid design

All luciferase reporter plasmids used were newly developed for this study. Most luciferase reporter plasmids used were based on the *Nptx2* gene, and hence this reporter was termed the *Nptx2* reporter. To develop the *Nptx2* reporter, we cloned the 4355 bp region upstream of the *Nptx2* coding sequence from C57BL/6 purified mouse genomic DNA between the NheI and EcoRV restriction sites within the multiple cloning site of the promoterless pGL4.11 reporter plasmid (Promega) using the primers shown in Table 2, with 5' clamp shown in red, NheI and EcoRV sites shown in green.

Table 2: Primers used to clone the *Nptx2* upstream regulatory region into pGL4.11

Primer	Sequence (5' → 3')
Forward primer	5' GCGCGCTAGCTTCCTGGCTTGTAGTGACCT 3'
Reverse primer	5' GCGCGATATCCTCGCTGACCTGTGTGCTCACTTCA 3'

pGL4.11 was chosen as the host plasmid since it contained the luc2P reporter gene, which contains an hPEST protein destabilization sequence. We found that the luc2P reporter responded more quickly and with greater magnitude to stimuli than luc2 reporters. Using PCR driven overlap extension (Heckman and Pease, 2007), the *Nptx2* reporter was then modified so that the 1216 bp *Nptx2* upstream enhancer (located -3607 to -2391 relative to the start of the *Nptx2* coding sequence) was replaced with a multiple cloning site containing SbfI, PacI, PmeI, and AscI restrictions sites. In order to do this, the primers shown in Table 3 were used (A, B, C, D nomenclature same as described in

(Heckman and Pease, 2007)), with 5' clamp shown in red; NheI and EcoRV sites shown in green; SbfI, PacI, PmeI, and AscI sites shown in blue; and spacers shown in orange.

Table 3: Primers used to replace the *Nptx2* upstream enhancer with a multiple cloning site

Primer	Sequence (5' → 3')
A	5' GCGCGCTAGCTTCCTGGCTTGTAGTGACCT 3'
B	5' GGCGCGCCACACGTTTAAACGCGCTTAATTAAGTGTCCTGCAGGTTGTGTGAGACACTGTTTCCA 3'
C	5' CCTGCAGGACACTTAATTAAGCGCGTTTAAACGTGTGGCGCGCCAGCTAGTAACAGTTGGCATT 3'
D	5' GCGCGATATCCTCGCTGACCTGTGTGCTCACTTCA 3'

The multiple cloning site was inserted into the *Nptx2* upstream regulatory region to create a modified *Nptx2* reporter so that various enhancers could be easily cloned into this multiple cloning site. We verified that the modified *Nptx2* reporter in which the Nptx2 enhancer had been cloned into the multiple cloning site had the same inducibility as the wild-type *Nptx2* reporter (data not shown). This suggested that the multiple cloning site did not affect the function of the reporter and that other enhancers could be similarly cloned into this multiple cloning site without adverse affects on enhancer function.

2.5.7.2 Alternate reporter plasmid design

We generated 2 additional reporter constructs by modifying pGL4.24 (Promega), a luciferase reporter containing a minimal TATA box containing promoter but not containing any enhancer elements. To facilitate cloning of enhancers from the Nptx2 reporter plasmid into this plasmid, we first modified this plasmid by adding a multiple

cloning site containing SbfI, PacI, PmeI, and AscI sites between BamHI and SalI sites downstream of the firefly luciferase gene (pGL4.24_minP_MCS). This multiple cloning site was added by annealing together two oligonucleotides containing the multiple cloning site as well as overhanging BamHI and SalI restriction sites, and then ligating this annealed product into pGL4.24 backbone that had been cut with BamHI and SalI. The sequences of the oligonucleotides are shown in Table 4, with BamHI and SalI sites shown in green and SbfI, PacI, PmeI, and AscI sites shown in blue.

Table 4: Primers used to introduce a multiple cloning site into pGL4.24

Primer	Sequence (5' → 3')
F	5' GATCCGACACCTGCAGGACACTTAATTAAGCGCGTTTAAACGTGTGGCGCGCCATCGG 3'
R	5' TCGACCGATGGCGCGCCACACGTTTAAACGCGCTTAATTAAGTGTCCTGCAGGTGTCG 3'

We then further modified pGL4.24_minP_MCS by removing the minimal TATA box containing promoter from this plasmid and replacing this promoter with an SV40 promoter from another Promega luciferase reporter, the pGL3-Promoter Vector. This cloning was achieved by using BglII and NcoI restriction sites flanking both promoter regions. This resulted in the generation of a separate reporter construct, pGL4.24_SV40_MCS, with which enhancer activity could be assessed.

2.5.7.3 Enhancer sequences

Enhancer with different H3K27Ac behaviors were cloned between the SbfI and AscI sites within the multiple cloning site of the modified *Nptx2* reporter. Cloned enhancer regions varied in size but were approximately 1kb in length. The following enhancers were cloned in this way using the primers listed in Table 5, with 5' clamp shown in red and SbfI and AscI sites shown in blue.

Table 5: Primers to clone neuronal enhancers with different H3K27Ac behaviors

Note that enhancers e31, e32, e37, e39, all cloned initially because they displayed increasing H3K27Ac in response to KCl, also displayed increasing H3K27Ac in response to BDNF. As a result, these enhancers were subsequently used in BDNF experiments in Figure 2.14 and Figure 2.17.

Enhancer category	Name	Forward primer (5' → 3')	Reverse primer (5' → 3')
No H3K27Ac (with KCl stimulation)	e1	GCGTCCTGCAGGTAAACAGTTCTAGTTCTGGG	GTATGGCGCGCCAATGAGCTTCTGTGAAGGAA
	e2	GCGCCCTGCAGGTGTTATTGTCCAATGCGTAG	GTATGGCGCGCCCATGGTGCCCACACTCATGT
	e3	GCGTCCTGCAGGCTGCTCAGTAAGAGATATCA	GTATGGCGCGCCTAGATCCCAGGTAGATACTCA
	e4	GCGTCCTGCAGGCAGAATGGAGCAAACTGGGT	GTATGGCGCGCCGACTTGGTGAAGATGAGGGT
	e5	GCGTCCTGCAGGGTGTGAGTAAGTGTGAGTGC	GTATGGCGCGCCGACCTGGAGTGCTTAATCTG
	e6	GCGTCCTGCAGGAGCAGCCAGTAGAAGACTCT	GTATGGCGCGCCCCTAGTCTTGAAGAGGGTCA
	e7	GCGTCCTGCAGGAGATACTAGGAACAGGGAGG	GTATGGCGCGCCAGTCTCTACTGGCTGTGTCT
	e8	GCGTCCTGCAGGGAGCTTGGAGGGTAGATACA	GTATGGCGCGCCGGTGGTGGTACCACAAATAG
	e9	GCGTCCTGCAGGTCCTATGGCAAGTGCCTAGA	GCATGGCGCGCCCCAGTCATTGAACATTCTCC
	e10	GCGTCCTGCAGGTGATTTGGTTCCTAGAGCCC	GTATGGCGCGCCTTACTGCAGAGCTCAGATGC
Constant H3K27Ac (with KCl stimulation)	e11	GCGTCCTGCAGGCATATGTGTGCACGCACATG	GTATGGCGCGCCCCAAACTTTTCTGCTTTCAC
	e12	GCGTCCTGCAGGAGGCGACAGAACGATATTAA	GTATGGCGCGCCTTATCCTTCAAGCAAGTCTG
	e13	GCGTCCTGCAGGGAGTGGCTTCCATCCCATTT	GCATGGCGCGCCGGGATGATCCTGTTAGATAG
	e14	GCGTCCTGCAGGAAGTCAGGCACCAAGTTCTG	GTATGGCGCGCCCAGTGACCGTTAGCAGCTAA
	e15	GCGTCCTGCAGGTCAGTGAAAGGTGCTAGCTG	GTATGGCGCGCCCACTGAGTAAGACAGAGGTG
	e16	GCGTCCTGCAGGGTGACTATAGAGAGTTGCCC	GTATGGCGCGCCTTAGCTTCGTGACACTGCCA
	e17	GCGTCCTGCAGGAGCTTGGAGGAATGTCAGCT	GTATGGCGCGCCGAAGGAGTGGCTTAGACACT
	e18	GCGTCCTGCAGGTGGTTAGCCTCAGCGACATA	GTATGGCGCGCCCCATCTGCTAGGAAGTCTCA
Decreasing H3K27Ac (with KCl stimulation)	e19	GCGTCCTGCAGGTAGTGAGCCTGTAGCTGAAA	GTATGGCGCGCCAGAGCAAAGGCATGTTTACT
	e20	GCGTCCTGCAGGGACTGTAGGGAAGGAATTGC	GTATGGCGCGCCGCAATTGTGCCGAATACCTG
	e21	GCGTCCTGCAGGTTACGCAACCCATCCGTCAA	GTATGGCGCGCCCATTAGGAGCTAGAGACAGC
	e22	GCGTCCTGCAGGTCCTAGCCAACCACTCTCAA	GTATGGCGCGCCTTGACATCCAGACTGACCTG
	e23	GCGTCCTGCAGGCATACGATTAATGCTCTCCAG	GTATGGCGCGCCCCAGCTTTGCAAAGAGTTGC
	e24	GCGTCCTGCAGGGACGTTTGGATAGCATGCCA	GTATGGCGCGCCCCATTTCACAGATCCTCACC
	e25	GCGTCCTGCAGGCTCAATGCAAAGGGCAGTGT	GTATGGCGCGCCTGGCACTGGGTAATGAACCA
	e26	GCGTCCTGCAGGGCCACTGAAATAACACAGCC	GTATGGCGCGCCATCATGGGAACAGCAACCAG
	e27	GCGTCCTGCAGGCAAATACACGGCATGCTCCA	GTATGGCGCGCCGCGTGTGTGTAATGAGAGAG
	e28	GCGTCCTGCAGGGACTCAACATACAGCCAAAGC	GTATGGCGCGCCGTCTCAGGACAACCTGATTG
Increasing H3K27Ac (with KCl stimulation)	e29	GCGTCCTGCAGGAACTTTGATTTCGGAACCCT	GTATGGCGCGCCCACCGAATTCTTTCCTTCTT
	e30	GCGTCCTGCAGGAATTCAGGCCCTAAGTCACC	GTATGGCGCGCCTAAAGTAAGAGCTAGGGAGA
	e31	GCGTCCTGCAGGCATCTGTCATCTCTTGAAAG	GTATGGCGCGCCAATGTGCCATTGTGGTACTT
	e32	GCGACCTGCAGGATCTTCTGATCATTGGCCTT	GTATGGCGCGCCTTGGAGCCAATTAGGAAGAA
	e33	GCGTCCTGCAGGAATAGCAGTTAGGTGCCCAA	GTATGGCGCGCCCTCCTGAGATACATCTGCCA
	e34	GCGTCCTGCAGGTCACAGGCAGTAGACAAGGG	GTATGGCGCGCCCCTCCATCTGAAGAGGTTCC
	e35	GCGTCCTGCAGGGAAAGCTGAGCACTTTGGCA	GTATGGCGCGCCCCATATGTCAGATTGCTGCC
	e36	GCGTCCTGCAGGCCATCCTCATTTCTCTCTCC	GTATGGCGCGCCATTCCCAGCAATGTGAGGGA
	e37	GCGTCCTGCAGGTTGTTCTGTGTGACAACGGG	GTATGGCGCGCCTGGCACCAGATCTGCACTAA
	e38	GCGTCCTGCAGGAAAGGCATAATAGGGGTGGG	GTATGGCGCGCCGGTCCTGTAAGGAACCTTGT
	e39	GCGTCCTGCAGGAGCAAGTAGAGACGGGAAAG	GTATGGCGCGCCCCTGACTTGTGGTTGTTACC
	e40	GCGTCCTGCAGGCATGCATGTGGGAAGACTTG	GTATGGCGCGCCGATGACATTCAAGTCCGTGG
	e41	GCGTCCTGCAGGTTCTGAAGTTTGCTGCCACC	GTATGGCGCGCCCTACCTCATCATCCTCTCAG
	e42	GCGTCCTGCAGGTTGGTAGACCAGGGACTTCT	GCATGGCGCGCCGTAACTAGGGAAAGTGCTTC
Increasing H3K27Ac (with BDNF stimulation)	e43	GCGTCCTGCAGGACATACAGAAGCCAGGAGAG	GTATGGCGCGCCAGCAGGTCAAGGCCTTGTGT
	e44	GCGTCCTGCAGGGCAGAGTTACGAACCAGGAA	GTATGGCGCGCCAACCAGAGCTCTAGGGTACA
	e45	GCGTCCTGCAGGTGACATCAGAGCTGATGTGG	GTATGGCGCGCCCTGACTTGGGTAGGCATGTT
	e46	GCGTCCTGCAGGGACCAAGCCTCATGAACTCA	GTATGGCGCGCCTCTAGTCTCCTCATCACTGG
	e47	GCGTCCTGCAGGCAGTTACCAACTTGATGGGG	GTATGGCGCGCCTTGTCCAAAGCAGGATGAGC
	e48	GCGTCCTGCAGGTTACAGCCAGGAGTCTCCAA	GTATGGCGCGCCTAAAAGGAGAGGGATGGCTG
	e49	GCGTCCTGCAGGGCACAGCAGGTAGACTCATA	GTATGGCGCGCCCAAGGCTCTGCCCTAAAGAA

2.5.7.4 Transfection

Mouse cortical neurons plated on 24 well plates at a density of approximately $3x10^5$ neurons per well were transfected for luciferase reporter assays using Lipofectamine 2000 Reagent (Invitrogen), generally according to the manufacter's protocol. Briefly, DNA mixes were made immediately preceding the transfection consisting of 1ug total plasmid DNA/well diluted in Neurobasal medium (Life Technologies). DNA typically consisted of 450ng firefly luciferase reporter DNA, 50ng pGL4.74 renilla luciferase reporter DNA (Promega), and 500ng empty pCS2 plasmid (Rupp et al., 1994; Turner and Weintraub, 1994) as filler DNA. Lipofectamine was used at 2uL/well and was diluted in Neurobasal medium just before the transfection. Within each experiment, all conditions were transfected in two to three independent wells, for technical duplicates or triplicates. Thirty minutes prior to the addition of Lipofectamine to neurons, the culture medium was removed and replaced with warmed Neurobasal medium. At this time, neurons were returned to the incubator and DNA mixes were added to diluted Lipofectamine in a drop-wise manner. After thirty minutes of incubation, DNA-Lipofectamine mixes were added to neurons, again in a drop-wise manner. The cells were left to incubate with the DNA-Lipofectamine mix for two hours, after which the transfection medium was replaced with supplemented conditioned neuronal medium.

2.5.7.5 Sample collection and luciferase assay

After stimulation, neurons were lysed using Passive Lysis Buffer (Dual-Luciferase Reporter Assay System, Promega). Lysates were then collected in microcentrifuge tubes

and frozen at -20 degrees C. At the time of performing the luciferase assay, neuronal lysates were thawed, briefly vortexed, briefly spun down, and then 20uL of each sample was added to one well of Costar White Polystyrene 96-well Assay Plates (Corning). The reagents to run the luciferase assay, Luciferase Assay Reagent II (LARII) and Stop & Glo Reagent (Dual-Luciferase Reporter Assay System, Promega), were aliquoted and thawed according to the manufacturer's protocol. The luciferase assay was performed using the Synergy 4 Hybrid Microplate Reader (BioTek), with 100uL of LARII and Stop & Glo Reagent injected per well. Data was subsequently downloaded and analyzed using Microsoft Excel.

2.5.7.6 Statistical Analyses of Luciferase Assay Data

Using the Dual-Luciferase Reporter Assay System, we recorded *Firefly (FF)* and *Renilla (Ren)* luminescence from each well. To correct for variations in transfection efficiency and cell lysate generation, the *Firefly* values were normalized to *Renilla* luminescence within each well, generating a ratio of *FF/Ren*. The stimulus-dependent fold induction of each reporter plasmid was obtained by dividing the (+ stimulus) *FF/Ren* value by the (- stimulus) value. To isolate the induction due to the enhancer, the fold induction of an enhancer reporter was divided by the fold induction of the appropriate backbone into which the enhancer was cloned, giving fold induction relative to backbone. Fold induction relative to backbone is the value shown in all figures containing luciferase reporter data. All error bars shown are standard error of biological replicates.

2.5.8 GREAT analysis

Functional annotations of genes linked to stimulus-responsive enhancers was investigated with the Genomic Regions Enrichment of Annotations Tool (GREAT) (McLean et al., 2010). For the analysis, the following settings were used: species assembly: Mouse: NCBI build 37 (UCSC mm9, Jul/2007); test regions: BED file containing genomic locations of stimulus inducible enhancers; background regions: whole genome; association rule setting: basal plus extension including 20 kb upstream, 20 kb downstream, plus distal up to 250 kb, and including curated regulatory domains. Ontology categories investigated include cellular components, biological processes, mouse phenotypes, and disease ontologies.

3 TRANSCRIPTIONAL MECHANISMS UNDERLYING STIMULUS-RESPONSIVE ENHANCERS IN THE NERVOUS SYSTEM

3.1 SUMMARY

Normal brain development and function require stimulus-responsive programs of gene expression, but how neuronal stimuli interface with stimulus-responsive enhancers to regulate gene expression is poorly understood. We have recently shown that functional stimulus-responsive enhancers can be identified by stimulus-inducible H3K27Ac, and we used this dynamic chromatin signature to discover enhancers that respond to activity, BDNF, or both. Here, we investigate the transcriptional mechanisms that underlie stimulus-responsive enhancer function in the nervous system. We show that stimulus-responsive enhancers require the coordinated action of the stimulus-general transcription factor activator protein 1 (AP1) with additional stimulus-specific factors. This work provides important insights into the cis-acting elements at stimulus-responsive enhancers that together with the trans-acting factors that bind to these elements transform sensory experience into specific transcriptional programs that facilitate long-lasting changes in neuronal function.

3.2 INTRODUCTION

Enhancers consist of binding sites for multiple families of transcription factors, the binding of which function synergistically to promote transcription at promoters of target genes (Spitz and Furlong, 2012). The exact complement of transcription factors recruited to enhancers determines when and where an enhancer is active. Much of what we know about the transcriptional mechanisms comes from studies of a few enhancers in detail. Recently, genome-wide methods have been developed to comprehensively identify the enhancer elements within the genome. These methods have been used to catalog enhancer elements in various cells and tissues in different organisms. Furthermore, genomic characterization has led to new understanding of how enhancer elements function and contribute to the establishment and maintenance of cellular identity. However, enhancers also play an important role in transcriptional responses to extracellular stimuli. Only recently have studies attempted to identify and characterize enhancers that contribute to stimulus-responsive programs of gene expression.

Stimulus responsive enhancers play an important role in the nervous system. In response to sensory experience, strong bursts of synaptic activity induce a program of gene expression in excitatory neurons that is required for proper development and refinement of neural circuits and for long-lasting changes in neuronal function that underlie learning, memory, and behavior. Studies of this neuronal activity-dependent gene program have primarily focused on signaling to promoter bound transcription factors. The release of the neurotransmitter glutamate at synapses leads to membrane depolarization of the post-synaptic neuron, triggering calcium influx through L-type

voltage gated calcium channels. The influx of calcium then leads to activation of a complex signaling network that induces the post-translational modification of promoter bound transcription factors that initiate multiple waves of gene expression. In addition to these critical signaling events at the promoters of activity-regulated genes, signaling to enhancers contributes to activity-dependent gene expression, although there has been little progress towards characterizing the function of activity-regulated enhancers because it has been difficult to identify these elements within the genome.

Recently, we have discovered that the dynamic chromatin signature of stimulus-inducible H3K27Ac specifically identifies functional stimulus-responsive enhancers. We employed this dynamic chromatin signature to identify neuronal enhancers that respond to neuronal activity, BDNF stimulation, or both. Here, we characterize the transcriptional mechanism underlying these stimulus-responsive enhancers within the nervous system. We identify the transcription factor motifs enriched at neuronal stimulus-responsive enhancers. We further study the binding of activity-dependent transcription factors predicted to bind to stimulus-responsive enhancers. The motif for the stimulus-responsive transcription factor activator protein 1 (AP1) is enriched at neuronal enhancers that respond to activity and those that respond to BDNF stimulation. AP1 transcription factors within the Fos family of transcription factors bind to stimulus responsive enhancers in response to neuronal activity and BDNF stimulation. We show that AP1 is necessary but not sufficient at a subset of enhancers for their response to both neuronal activity and BDNF stimulation. These data demonstrate that AP1 functions as a stimulus-general transcription factor that coordinates stimulus-responsive transcription at enhancers with other stimulus-specific

factors. These findings begin to elucidate the transcriptional mechanisms underlying stimulus responsive enhancers within the nervous system. These mechanisms will be important to not only understand how these elements function, but also to begin to understand how sequence variation at stimulus-responsive enhancers affects their function and may contribute to human variation and disease.

3.3 RESULTS

3.3.1 Sequence determinants of stimulus-responsive enhancers

To begin to understand the sequence determinants and transcription factors that regulate the function of stimulus-responsive enhancers, we performed *de novo* motif analysis on enhancers with different stimulus-responsive properties. Given that we had previously shown that reporter activity driven by enhancer elements appeared to be intrinsic to the sequence of these elements rather than genomic context or chromatin structure, we reasoned that de novo motif discovery might enable us to find important sequence determinants that drive distinct patterns of enhancer activity. De-novo motif analysis was performed using Multiple Em for Motif Elicitation (MEME) (Bailey and Elkan, 1994), beginning with neuronal enhancers that respond to membrane depolarization with elevated extracellular potassium chloride (KCl). Enhancers with increasing H3K27Ac in response to neuronal depolarization showed enrichment for motifs for the neuronal-activity regulated transcription factors AP-1, MEF2, and CREB (Figure 3.1a), suggesting that these transcription factors may drive neuronal activity-regulated transcriptional programs via enhancer mediated mechanisms. The AP1 transcription factor complex generally consists of dimers of FOS and JUN family transcription factors, many of which are canonical immediate early genes that are rapidly expressed in a protein synthesis-independent manner in response to extracellular stimuli in diverse cell types (Eferl and Wagner, 2003; Greenberg and Ziff, 1984; Sheng and Greenberg, 1990). MEF2 family transcription factors (MEF2A-D) are known to be activated via dephosphorylation in response to neuronal activity and to

play an important role in activity-dependent transcription in the nervous system (Barbosa et al., 2008; Flavell et al., 2006; Potthoff and Olson, 2007). The transcription factor CREB is known to be activated by phosphorylation in response to neuronal activity and to play an important role in activity-dependent transcription in the nervous system (Gonzalez and Montminy, 1989; Sheng et al., 1991). Notably, none of these activity-dependent transcription factor motifs were significantly enriched among enhancers with constant or decreasing levels of H3K27Ac, suggesting that the transcription factors that bind these motifs may function specifically at activity-responsive enhancers within the genome.

In addition to these activity-dependent transcription factor motifs, we also noted enrichment at activity-responsive enhancers for additional motifs for developmental transcription factors (Figure 3.1b). For example, we found that the X-box motif and the E-box motif were both significantly enriched among stimulus-responsive enhancers. These motifs are known to be bound by RFX and proneural bHLH transcription factors, respectively, both of which have been implicated in neuronal differentiation and development. RFX1 binding (as well as the X-box motif) has been shown to be enriched at active enhancers in cultured neural progenitor cells (Creyghton et al., 2010). Numerous bHLH transcription factors have also been shown to be expressed in neural progenitor cells (e.g. ASCL1, NGN1, NGN2) and differentiated neurons (e.g. NGN2, NEUROD, NHLH) and in many cases have been shown to play critical roles during nervous system development (Bertrand et al., 2002). Thus, neuronal stimulus-responsive enhancers may achieve tissue specificity through the action of RFX1 and proneural bHLH transcription factors at these enhancers, although further studies will

be required to understand how these and other transcription factors establish the active enhancer landscape in neurons.

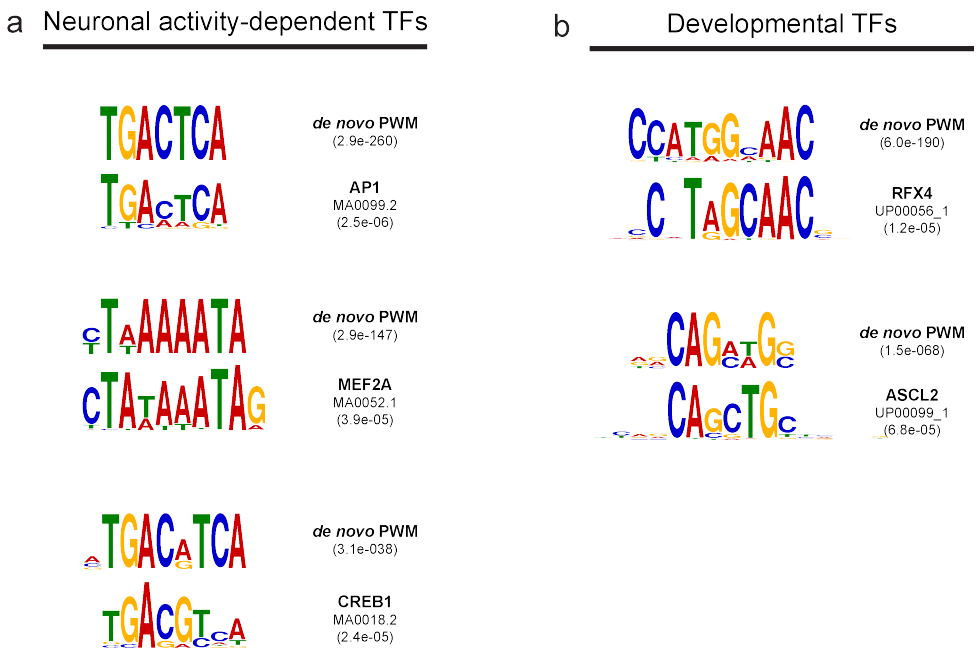

Figure 3.1: Motifs enriched among neuronal activity-responsive enhancers

To understand the sequence determinants that contribute to the function of neuronal activity-responsive enhancers, we performed de novo motif analysis of the DNA sequences from all neuronal enhancers exhibiting increasing H3K27Ac levels in response to neuronal activity. De-novo motif analysis was performed using Multiple Em for Motif Elicitation (MEME) (Bailey and Elkan, 1994). The position weight matrices (PWM) for top neuronal activity-dependent transcription factor motifs (a) and the top developmental transcription factor motifs (b) identified by MEME are displayed, along with the E value reported by MEME for each de novo PWM. In addition, for each de novo PWM, the most similar PWM in the JASPAR or UniPROBE transcription factor motif databases, identified using TOMTOM (Gupta et al., 2007), is displayed.

Having characterized the transcription factor motifs and binding events enriched at neuronal activity-responsive enhancers, we next investigated the transcription factor motifs present at neuronal BDNF-responsive enhancers by performing de novo motif analysis on this set of enhancers. Surprisingly, the most enriched motif at BDNF-responsive enhancers was the same motif that was enriched at neuronal activity-responsive enhancers, the AP-1 motif (Figure 3.2b, top). Furthermore, the AP1 motif was also the most significantly enriched motif at neuronal enhancers exhibiting increasing H3K27Ac in response to neuronal activity but not BDNF (activity-specific enhancers; Figure 3.2a, bottom), increasing H3K27Ac in response to BDNF but not neuronal activity (BDNF-specific enhancers; Figure 3.2b, bottom), and increasing H3K27Ac in response to neuronal activity and BDNF (KCl and BDNF inducible enhancers; Figure 3.2c). This suggested that AP1 transcription factors may play a critical role in mediating transcriptional responses at enhancers to multiple stimuli.

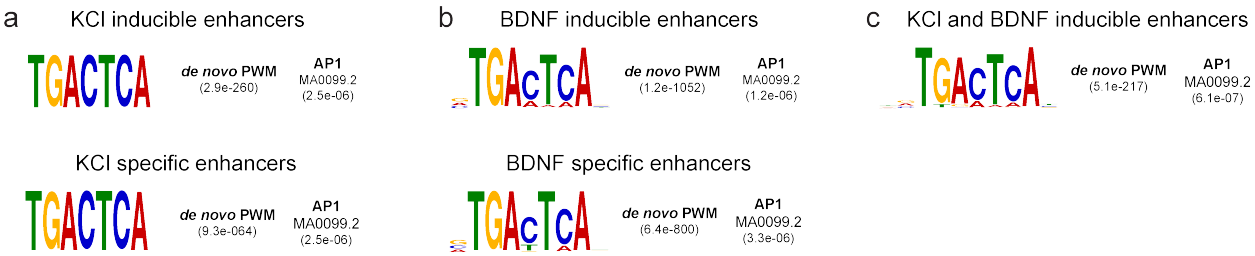

Figure 3.2: AP1 is the most significantly enriched motif at all classes of neuronal stimulus-responsive enhancers

De novo motif analysis of the DNA sequences from neuronal enhancers exhibiting increasing H3K27Ac levels in response to neuronal activity (a), BDNF (b), or both (c). De-novo motif analysis was performed using Multiple Em for Motif Elicitation (MEME) (Bailey and Elkan, 1994). The position weight matrices (PWM) for top neuronal transcription factor motifs are displayed, along with the E value reported by MEME for each de novo PWM. In addition, for each de novo PWM, the most similar PWM in the JASPAR or UniPROBE transcription factor motif databases, identified using TOMTOM (Gupta et al., 2007), is displayed.

3.3.2 Transcription factor binding to activity-responsive enhancers

Given the enrichment of activity-regulated transcription factor motifs at enhancers with increasing H3K27Ac in response to activity, we asked whether the transcription factors corresponding to these motifs would show greater binding at these enhancers. First, we performed ChIP-Seq for MEF2A and MEF2D before and after neuronal depolarization and found that these activity-dependent transcription factors were enriched at enhancers with increasing H3K27Ac in response to neuronal depolarization (Figure 3.3). We further integrated our H3K27Ac data with previously generated ChIP-Seq data for CREB, NPAS4, CBP, and RNAPII (Kim, 2010) in order to more thoroughly investigate the contribution of activity-regulated transcription factor binding to inducible H3K27ac at enhancers. Interestingly, all of these transcription factors also showed significantly more binding to enhancers with increasing H3K27Ac compared to other enhancers (Figure 3.3). Binding of the stimulus regulated transcription factor SRF was not enriched at enhancers with increasing H3K27ac, in line with the SRF motif not being significantly enriched these enhancers. Hence, many but not all activity-dependent transcription factors in the nervous system show not only enrichment of their motifs but also increased binding to activity-dependent enhancers in the genome. This suggests that several activity-dependent transcription factors collaborate at enhancers to regulate neuronal activity-dependent transcription, and that many such transcription factors may drive activity-dependent transcription via enhancer-mediated mechanisms.

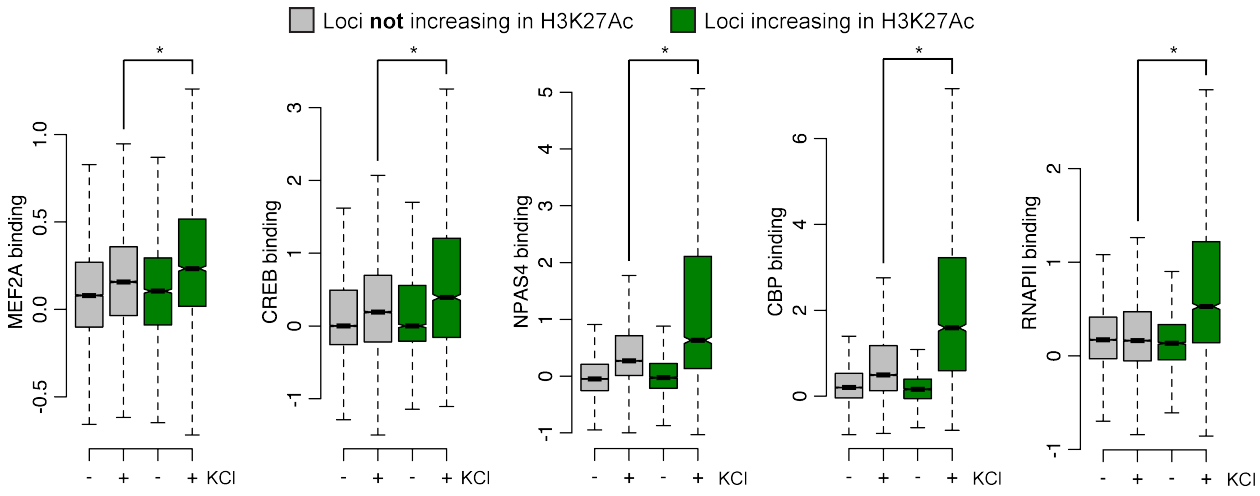

Figure 3.3: Neuronal activity-responsive enhancers are enriched for binding by neuronal activity-dependent transcription factors

ChIP-Seq was performed (MEF2A) or analyzed (CREB, NPAS4, CBP, RNAPII) for the displayed transcription factors. Input normalized ChIP-Seq reads within an 800bp window surrounding each enhancer center were quantified at enhancers with increasing H3K27Ac or other enhancers, before and after membrane depolarization with KCl. Data is displayed in boxplots and * indicates $p < 2.2 \times 10^{-16}$ in paired Wilcoxon test.

Given that our genomic analyses suggested that neuronal activity-responsive enhancers are enriched for binding by neuronal activity-dependent transcription factors, we asked whether this enrichment could be seen at any individual loci of neuronal activity regulated genes. Two intragenic enhancers within the genomic locus for the activity-regulated neuronal gene *Prkg2* reflect the preferential and activity-dependent binding of several activity-dependent transcription factors at enhancers with increasing but not constant H3K27Ac in response to membrane depolarization (Figure 3.4).

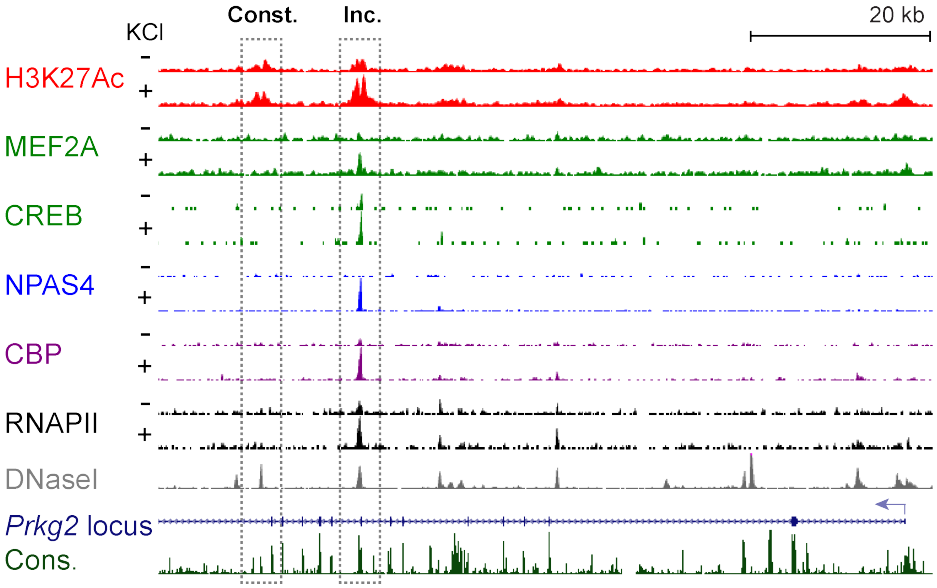

Figure 3.4: Activity-dependent transcription factor binding at the *Prkg2* locus

Genome browser view of ChIP-Seq tracks for the indicated factors at the activity-regulated *Prkg2* locus. ChIP-Seq tracks display input-normalized H3K27Ac ChIP-Seq reads from neurons before membrane depolarization (-KCl) or after membrane depolarization (+KCl). Also displayed are DNaseI hypersensitivity signal from adult mouse cerebrum and vertebrate conservation by PhastCons. Dashed boxes identify regulatory elements with different stimulus-responsive changes in H3K27Ac. Activity-dependent transcription factors (MEF2A, CREB, Cs, NPAS4) and general transcription factors (CBP, RNAPII) exhibit activity-dependent binding at the enhancer with increasing H3K27Ac in response to neuronal activity ('Inc.') but not at the enhancer with constant H3K27Ac in response to neuronal activity ('Con.').

3.3.3 AP1 is required for both neuronal activity-dependent and BDNF-dependent enhancer function

Given the enrichment of the AP1 motif at enhancers that respond to neuronal activity or BDNF and the lack of enrichment for the AP1 motif in active enhancers at which H3K27Ac did not change in response to either stimuli, we reasoned that the AP1 transcription factor complex may be critical for stimulus-responsive enhancers to promote transcription in response to extracellular stimuli. This would represent a novel mechanism for AP1 transcription factors in the nervous system, as AP1 has long been assumed to function at the promoters of neuronal activity-regulated genes to regulate transcription. First, we sought to characterize AP1 transcription factor binding to stimulus-responsive enhancers. Since FOS transcription factors have been shown to be an important component of the AP1 complex with important roles in the nervous system (Brown et al., 1996; Fleischmann et al., 2003; Jin et al., 2002; Zhang et al., 2002), we focused on members of this family of transcription factors. We first asked which *Fos* genes exhibited significant inducibility in response to extracellular stimuli, reasoning that inducible FOS transcription factors are likely to contribute to stimulus-dependent transcriptional control mediated by the AP-1 complex. Using RNA-Seq data we generated from mouse cortical neurons after 0, 1, or 6 hours of stimulation with KCl or BDNF, we characterized the expression of the genes of the four FOS family transcription factors: *c-Fos*, *FosB*, *Fosl1*, and *Fosl2*. We found that *c-Fos* and *FosB* were the most robustly induced *Fos* family members in response to stimuli, being similarly induced by KCl and BDNF (Figure 3.5). As a result, we chose to focus on these transcription factors.

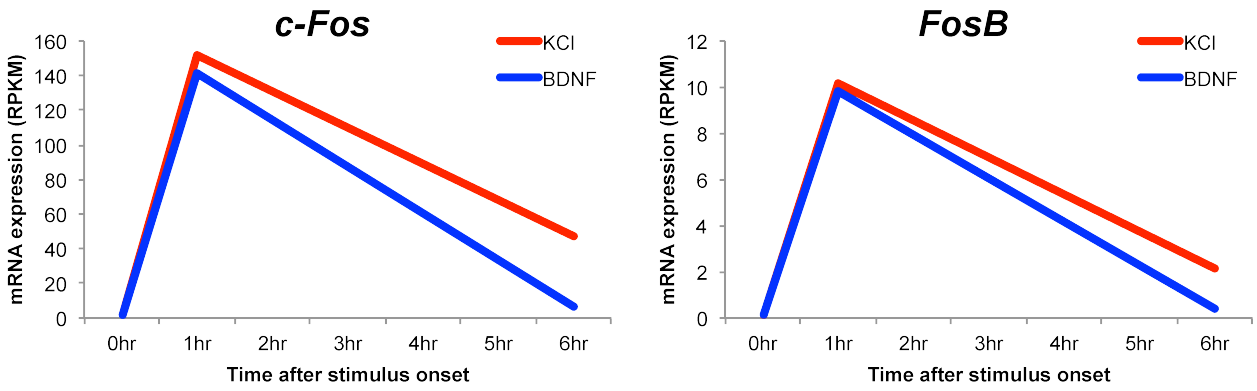

Figure 3.5: *c-Fos* and *FosB* are induced in response to both KCl and BDNF stimulation

RNA-Seq data from mouse cortical neurons stimulated with 0, 1, 6 hours KCl or 0, 1, 6 hours BDNF was analyzed to assess the levels of expression of genes in the *Fos* family of transcription factors. *c-Fos* and *FosB* (displayed) were the most inducible transcription factors and were found to be similarly induced in response to both KCl and BDNF. mRNA is expressed as reads per kilobase per million mapped reads (RPKM).

Since *c-Fos* and *FosB* were the most inducible AP1 transcription factors within the *Fos* family of transcription factors (by both KCl and BDNF stimulation), we next sought to characterize the binding of these transcription factors by ChIP-Seq in response to both KCl and BDNF stimulation. We first characterized binding in response to KCl. Using two independent C-FOS antibodies, we identified only 654 C-FOS peaks prior to KCl stimulation but identified 16,131 C-FOS peaks after KCl stimulation, consistent with the low baseline levels of C-FOS expression and the strong inducibility of C-FOS in response to neuronal activity. Furthermore, levels of C-FOS binding at C-FOS peaks exhibited strong inducibility with KCl stimulation (Figure 3.6a). In order to further confirm the specificity of these peaks, we performed an additional ChIP-Seq experiment for C-FOS and found that the majority of these peaks replicated in an independent experiment (79%). We also performed ChIP-Seq for C-FOS from neuronal

cultures expressing a lentiviral shRNA knockdown construct targeting *c-Fos*. C-FOS ChIP-Seq signal was substantially reduced by *c-Fos* RNAi throughout the genome (Figure 3.6b) and the majority of C-FOS peaks identified exhibited significantly reduced C-FOS signal after *c-Fos* knockdown (71%). Finally, we performed *de* novo motif analysis on the set of 16,131 peaks and found that the AP1 motif was the most strongly enriched motif within this set of loci. These data suggest that we were able to identify a high confidence set of C-FOS binding sites within the genome that were reproducible and specific.

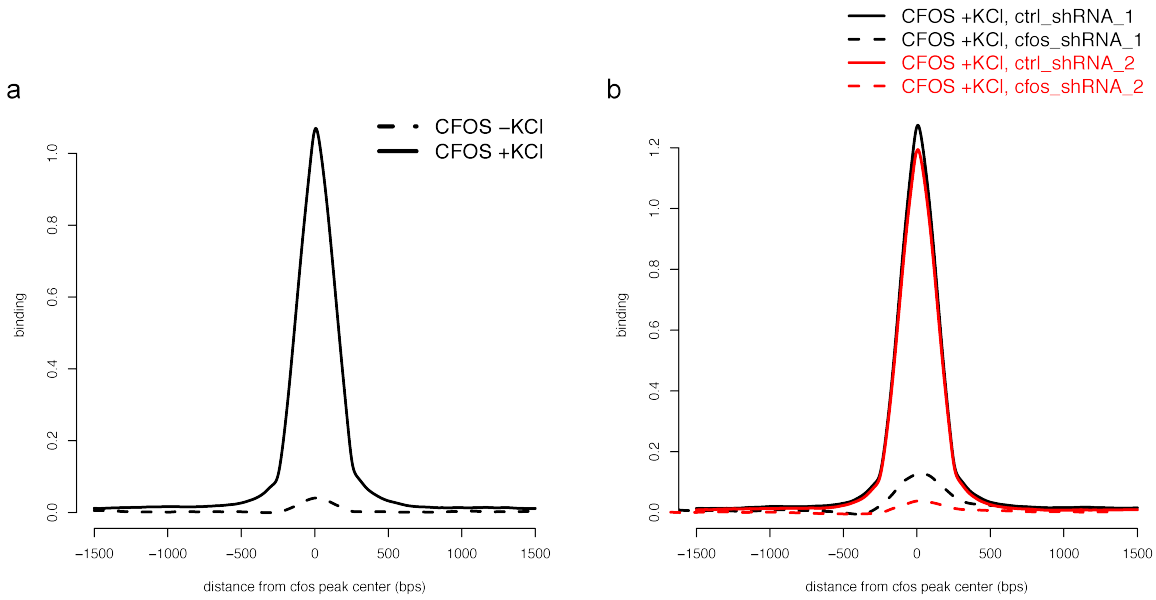

Figure 3.6: ChIP-Seq signal for C-FOS is inducible and specific in response to KCl stimulation

(a) C-FOS ChIP-Seq was performed in mouse cortical neurons before membrane depolarization with KCl (-KCl) and after membrane depolarization with KCl (+KCl). Average profiles of input-normalized C-FOS ChIP-Seq signal before membrane depolarization (dashed lines) and after membrane depolarization (solid lines) are shown. (b) C-FOS ChIP-Seq was also performed after membrane depolarization with KCl in mouse cortical neurons that had been infected with lentivirus expressing either a control shRNA or an shRNA targeting *c-Fos*, in two independent experiments. Average profiles of C-FOS ChIP-Seq signal from control RNAi lentivirus infected neurons (dashed lines) and C-FOS RNAi lentivirus infected neurons (solid lines) are shown.

Having identified a high confidence set of C-FOS binding sites, we asked where C-FOS binding occurred within the genome. While we found the AP1 motif to be enriched at enhancers, AP1 factors have been long thought to act at promoters of target genes. An analysis of the genomic location of our rigorously defined set of C-FOS binding sites indicated that C-FOS binding was observed predominantly at gene distal sites across the genome, with the vast majority of peaks occurring greater than 1kb from an annotated TSS (82% of all replicating peaks, 94% of replicated peaks reduced by RNAi; Figure 3.7a). Analysis of a similarly verified set of high confidence FOSB peaks (n=8687; see methods) indicated that FOSB binding also occurred almost exclusively at sites greater than 1kb from an annotated TSS (96% of replicating peaks; Figure 3.7b). This strongly suggested that in our system, the AP1 transcription factors C-FOS and FOSB generally do not bind to promoters but rather bind to regions of the genome distant to promoters.

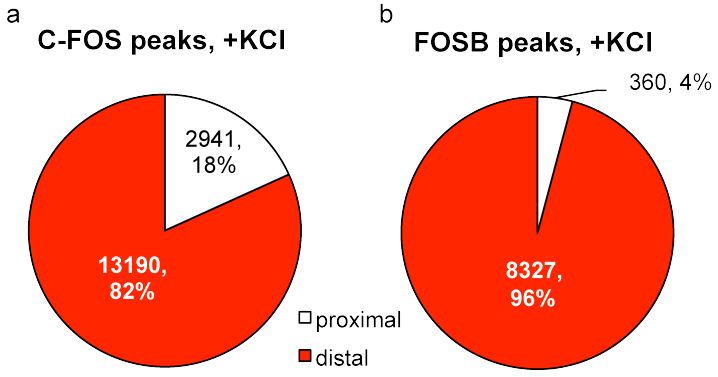

Figure 3.7: Genomic distribution of C-FOS and FOSB peaks after stimulation with KCl

ChIP-Seq for C-FOS and FOSB were performed before and after stimulation with KCl and peaks were called with MACS (Zhang et al., 2008). Peaks called after stimulation with KCl were then classified as proximal if they occurred within 1kb of an annotated RefSeq TSS, and as distal if they occurred outside of this window. The majority of C-FOS (a) and FOSB (b) peaks occur distal to TSSs.

Since the AP1 motif was enriched at stimulus-responsive enhancers, we hypothesized that C-FOS and FOSB binding to gene distal regions may be occurring at enhancers. Characterization of the chromatin modifications and transcription factor binding at distal C-FOS peaks demonstrated enrichment for enhancer associated H3K4Me1 (Figure 3.8a), H3K27Ac (Figure 3.8b), and CBP (Figure 3.8c), suggesting that C-FOS and binds to enhancers. Thus, in our system, FOS transcription factors appear to bind to enhancers rather than promoters in response to neuronal activity.

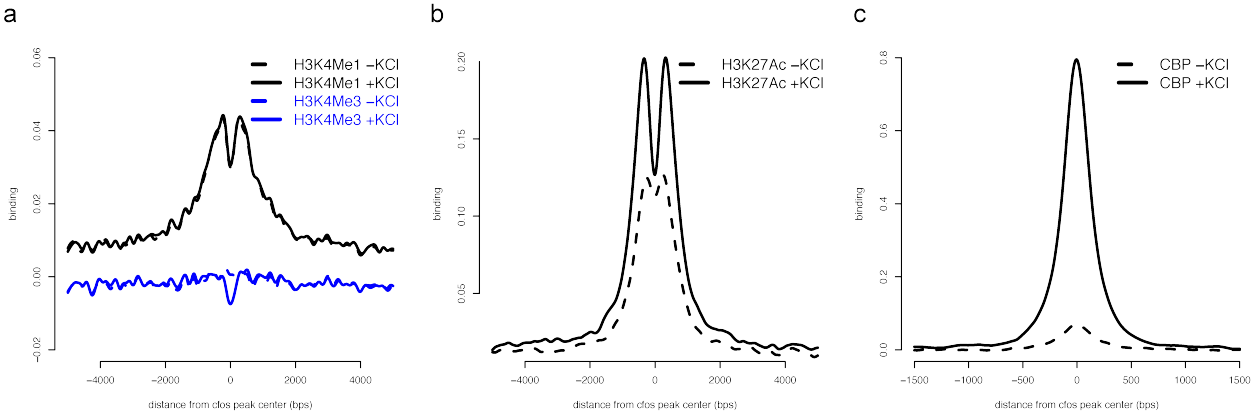

Figure 3.8: Distal C-FOS peaks induced by KCl exhibit features of enhancers

Chromatin modifications and transcription factor binding was assessed at distal C-FOS peaks within the genome before membrane depolarization (-KCl, dashed lines) and after membrane depolarization (+KCl, solid lines). (a) C-FOS peaks exhibit enrichment for the enhancer associated chromatin mark H3K4Me1 but not the promoter associated chromatin mark H3K4Me3. (b) C-FOS peaks exhibit enrichment for the active enhancer associated chromatin mark H3K27Ac, and H3K27Ac increases at C-FOS peaks with KCl stimulation. (c) C-FOS peaks exhibit enrichment for the transcriptional coactivator CBP with KCl stimulation. The y-axis for all plots represents the level of ChIP-Seq signal for the indicated factor, displayed as the mean number of input-normalized H3K27Ac ChIP-Seq reads at C-FOS peaks within the genome.

Given the enrichment of the AP1 motif among not only activity-responsive enhancers but also BDNF-responsive enhancers, and given our ability to detect bona fide C-FOS and FOSB binding by ChIP-Seq, we sought to characterize the binding of each of these factors in response to BDNF. We hypothesized that C-FOS and FOSB binding in response to BDNF would also occur at enhancers within the neuronal genome. We performed ChIP-Seq for each factor in response to BDNF. In BDNF stimulated neurons, we identified 15057 C-FOS peaks (93% gene distal; Figure 3.9a) and 13362 FOSB peaks (96% gene distal; Figure 3.9b), indicating that FOS transcription factors function primarily at gene distal regulatory elements in response to both neuronal activity and BDNF. These data strongly suggest that the current model of FOS function through promoters needs to be revisited.

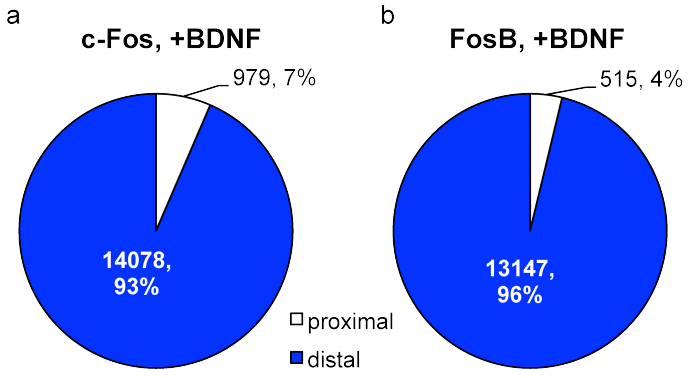

Figure 3.9: Genomic distribution of C-FOS and FOSB peaks after stimulation with BDNF

ChIP-Seq for C-FOS and FOSB were performed before and after stimulation with BDNF and peaks were called with MACS (Zhang et al., 2008). Peaks called after stimulation with BDNF were then classified as proximal if they occurred within 1kb of an annotated RefSeq TSS, and as distal if they occurred outside of this window. The majority of C-FOS (a) and FOSB (b) peaks occur distal to TSSs.

Having shown that FOS transcription factors bind predominantly to gene distal regions within the genome likely to be enhancers, we next determined the extent to which FOS transcription factors bound to neuronal stimulus-responsive enhancers. We assessed C-FOS binding at neuronal stimulus-responsive enhancers. We found significant enrichment for C-FOS binding at KCl and BDNF responsive enhancers (Figure 3.10). Furthermore, we found that a significant percentage of stimulus-responsive enhancers overlapped with C-FOS or FOSB peaks (39% of activity-responsive enhancers, 61% of BDNF-responsive enhancers). These large percentages further suggest that FOS transcription factors likely contribute significantly to the function of both activity-responsive and BDNF-responsive enhancers.

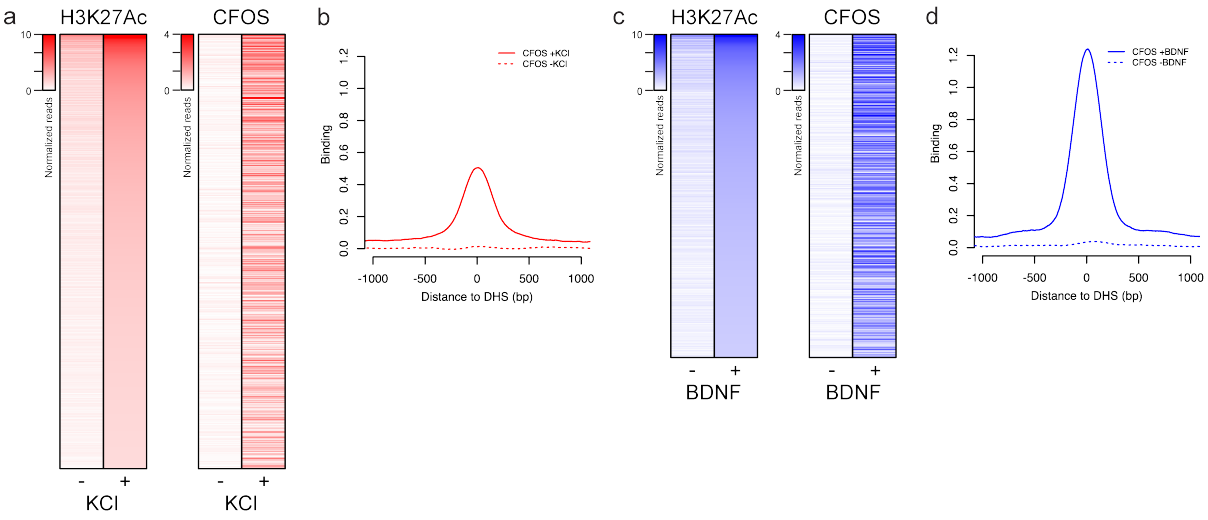

Figure 3.10: C-FOS binding at stimulus-responsive enhancers

(a) Heatmap of H3K27Ac and C-FOS binding before and after KCl stimulation at KCl responsive enhancers, sorted by magnitude of H3K27Ac after KCl stimulation. (b) Average profile of input-normalized C-FOS ChIP-Seq signal before membrane depolarization (dashed lines) and after membrane depolarization (solid lines). (c) Heatmap of H3K27Ac and C-FOS binding before and after BDNF stimulation at BDNF responsive enhancers, sorted by magnitude of H3K27Ac after BDNF stimulation. (d) Average profile of input-normalized C-FOS ChIP-Seq signal before BDNF stimulation (dashed lines) and after BDNF stimulation (solid lines).

Importantly, a large percentage of stimulus-responsive enhancers were not bound by FOS transcription actors, suggesting that FOS-independent mechanisms may exist to activate enhancers in response to stimuli. This is to be expected since enhancers that are needed to express *Fos* transcription factors in response to stimuli are unlikely to require FOS for this response. There are likely distinct enhancers that function to activate the distinct waves of transcription that have been shown to occur in response to extracellular stimulation.

Interestingly, we found that a significant percentage of C-FOS and FOSB peaks in the genome did not occur at stimulus-responsive enhancers or at regions with any appreciable H3K27Ac. We asked whether these FOS binding sites functioned to regulate stimulus responsive transcription. We cloned several such loci into reporter constructs and found that none of these loci were able to drive transcription in an activity-dependent manner. This suggested that only a subset of all C-FOS and FOSB binding sites within the genome might contribute to stimulus-responsive transcription.

Since the AP1 transcription factors C-FOS and FOSB bind to stimulus-responsive enhancers within the genome, we hypothesized that AP1 may play a critical role in the function of these enhancers. To directly assess whether AP1 contributes to neuronal stimulus-inducible enhancer activity, we asked whether binding of the AP1 complex is necessary for the function of these enhancers. To accomplish this, we tested the function of *Nptx2* reporter plasmids containing eight separate stimulus-inducible enhancers with canonical AP1 motifs that also exhibited high levels of binding by AP1 components (measured by ChIP-Seq). We disrupted the function of AP1 at these functional enhancers by either subtly mutating the AP1 motifs to block AP-1 binding or

by co-transfecting the dominant negative AP1 protein A-FOS (Ahn et al., 1998; Olive et al., 1997) with the *Nptx2* reporter. We found that both manipulations significantly reduced activity-dependent and BDNF-dependent expression of each reporter tested, often down to levels exhibited by the reporter in the absence of any enhancer, suggesting that in some cases the AP1 motif is strictly required to achieve any enhancer activity.

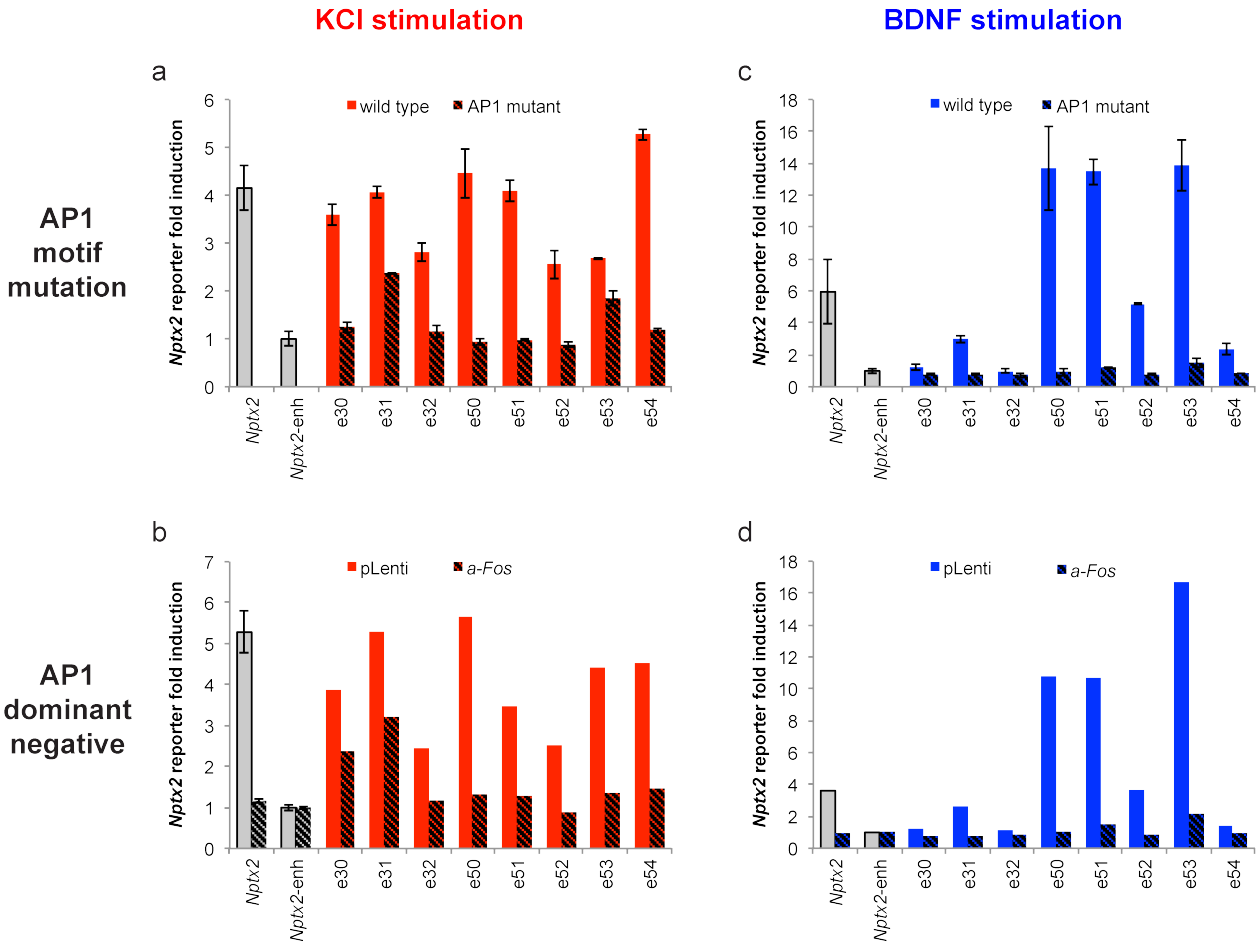

Figure 3.11: AP1 is critical for the function of KCl and BDNF responsive enhancers

The impact of AP1 motif mutations (a, c) and expression of the AP1 dominant negative *A-Fos* (b, d) on the function of eight enhancers containing AP1 sites and exhibiting binding by FOS transcription factors were assessed. Luciferase reporter data of each enhancer within the *Nptx2* reporter is shown, reported as the fold induction of reporter activity in mouse cortical neurons after 6 hours of stimulation with KCl (a, b) or BDNF (c, d) relative to 0 hours. n=3 in panels a and c. n=1 in panels b and d.

Importantly, not all enhancers exhibiting inducible H3K27Ac in response to extracellular stimuli were sensitive to AP1 manipulations. Several enhancers with increasing H3K27Ac and robust reporter expression in response to neuronal activity were not affected by the AP1 dominant negative *A-Fos* in reporter assays (Figure 3.12). This not only provided evidence of the specificity of the function of the A-FOS dominant negative protein, but also suggested that AP1 independent mechanisms likely exist to enable enhancers to respond to neuronal activity. This is consistent with our earlier observations that not all enhancers with increasing H3K27Ac were bound by FOS transcription factors.

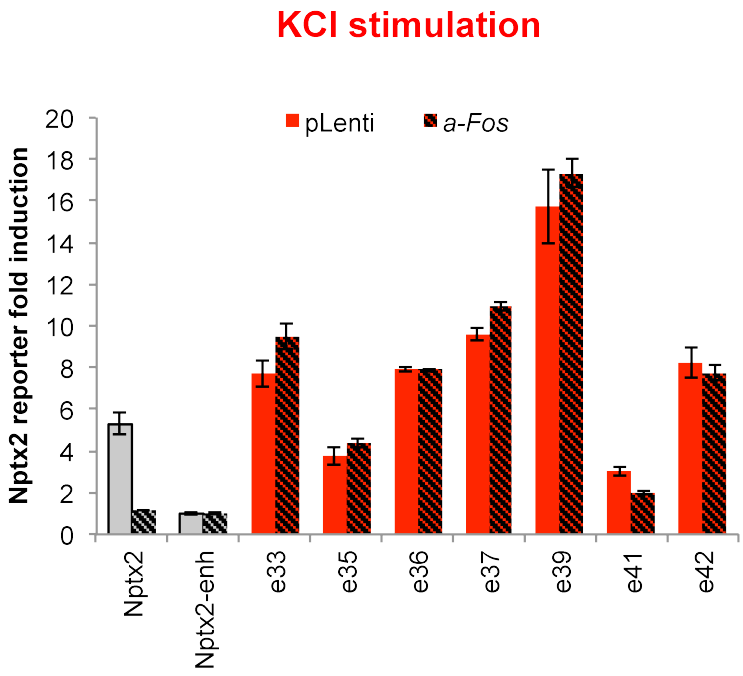

Figure 3.12: AP1 is not required at all KCl responsive enhancers

The expression of the AP1 dominant negative *A-Fos* has no impact on the function of seven enhancers that exhibit increasing H3K27Ac in response to neuronal activity and display responsiveness to KCl when cloned into the *Nptx2* luciferase reporter. Luciferase reporter data of each enhancer within the *Nptx2* reporter is shown, reported as the fold induction of reporter activity in mouse cortical neurons after 6 hours of stimulation with KCl relative to 0 hours. n=3 for all plasmids tested.

These data reveal a critical requirement for AP1 transcription factors at a subset of stimulus-responsive enhancers. Furthermore, these data suggest that AP1 plays a critical role in the function of enhancers with diverse stimulus-responsive properties, such as responsiveness to activity or BDNF. Given that AP1 transcription factors are expressed in a wide variety of cells in response to numerous extracellular stimuli, AP1 may play a critical role in the acquisition of stimulus-responsiveness of enhancers in multiple cellular contexts.

3.3.4 C-FOS regulates stimulus-responsive gene expression in the nervous system

C-FOS and other activity-regulated components of the AP1 complex bind to neuronal activity-dependent enhancers and abrogation of the binding of these components to enhancers through AP1 motif mutations leads to significant reductions in activity-dependent reporter induction. These data suggest that C-FOS may be important for neuronal activity-dependent enhancers. Since neuronal activity-dependent enhancers are associated with neuronal activity-dependent gene expression (Figure 2.7), we hypothesized that C-FOS may play a critical role in driving neuronal activity-dependent gene expression. To test this hypothesis directly, we performed genome-wide microarray analysis on neuronal RNA obtained from mouse cortical neurons that had been stimulated with 0, 1, 3, or 6 hours of KCl and infected with lentivirus expressing either a control RNAi or c-Fos RNAi. Western blot analysis of protein lysates obtained from simultaneously infected and stimulated cortical neurons

demonstrated that c-Fos RNAi was effective and specific. At each stimulus timepoint tested, c-Fos RNAi significantly reduced levels of C-FOS protein without affecting levels of the related FOSB protein, levels of activity-dependent posttranslational modifications, or cell viability as assessed by levels of β-actin (Figure 3.13).

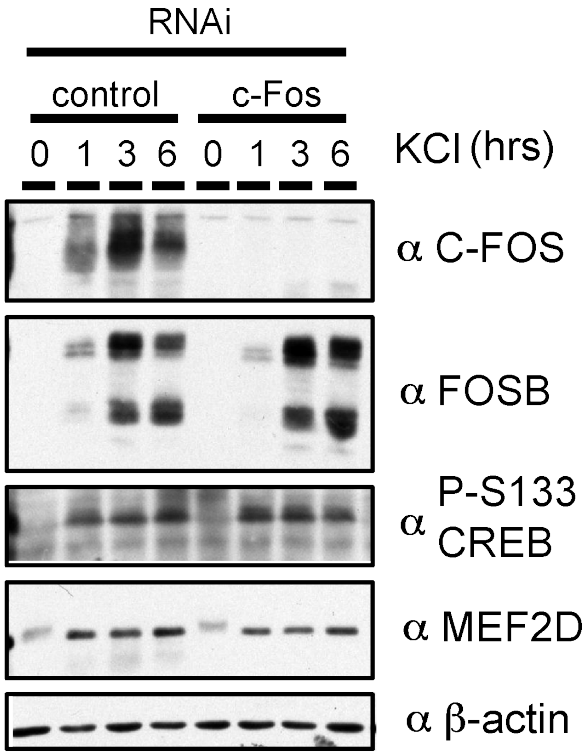

Figure 3.13: c-Fos RNAi effectively and specifically reduces levels of C-FOS protein

Western blot analysis of protein lysates obtained from mouse cortical neurons that had been stimulated with 0, 1, 3, or 6 hours of KCl and infected with lentivirus expressing either a control RNAi or c-Fos RNAi. At each stimulus timepoint tested, c-Fos RNAi significantly reduced levels of C-FOS protein without affecting levels of the related FOSB protein, levels of activity-dependent posttranslational modifications, or cell viability as assessed by levels of β-actin.

Since C-FOS protein levels appear greatest after 3 hours of stimulation among the timepoints tested in this experiment (Figure 3.13), we hypothesized that the greatest effects on activity-dependent gene expression would be seen after 3 or 6 hours of KCl stimulation. Analysis of the 1, 3, and 6 hour fold inductions of all expressed genes revealed, with the greatest misregulation seen after 6 hours of KCl stimulation (Figure 6B, an increasing number of genes that were less inducible with c-Fos RNAi compared to control RNAi red).

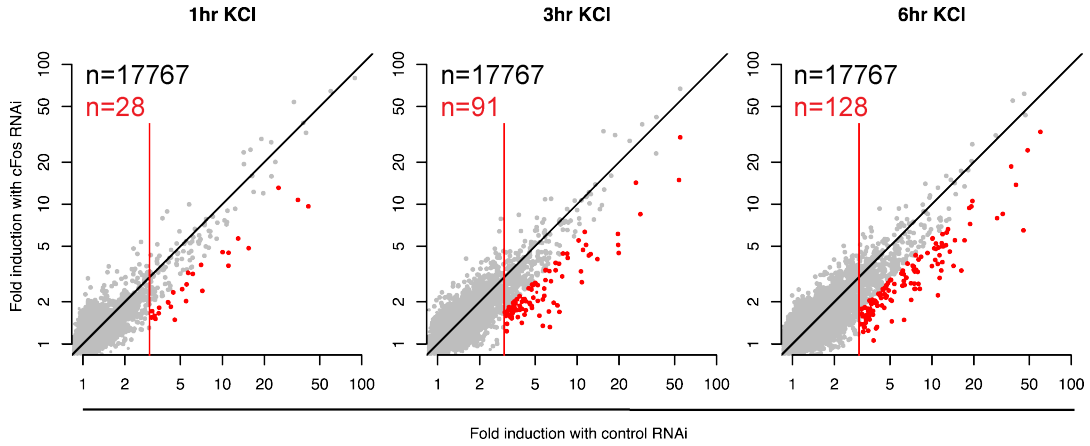

Figure 3.14: Genome-wide microarray analysis with c-Fos RNAi

Genome-wide microarray analysis was performed on neuronal RNA obtained from mouse cortical neurons that had been stimulated with 0, 1, 3, or 6 hours of KCl and infected with lentivirus expressing either a control RNAi or c-Fos RNAi. Scatterplots show fold induction of gene expression at 1, 3, or 6 hrs after KCl stimulation relative to 0 hrs (unstimulated neurons) for all expressed genes (n=17767). In order to be considered expressed, a gene must have been detected by a probe in both microarray bioreplicates at at least one of the timepoints assessed and must have achieved a minimal expression value of 250. The x-axis displays the fold induction exhibited in neurons infected with control RNAi. The y-axis displays the fold induction exhibited in neurons infected with c-Fos RNAi. The diagonal black line represents unity (y=x). The vertical red line represents a three-fold cutoff for fold induction with control RNAi. Red points represent genes induced at least three fold with control RNAi and exhibited a reduced fold induction by at least 1.75 fold with c-Fos RNAi. An increasing number of genes were less inducible with c-Fos RNAi compared to control RNAi with increasing time after KCl stimulation (red numbers).

Investigation of genes misregulated with c-Fos RNAi revealed several genes with known functions in the nervous system including the postsynaptic scaffolding protein *Grasp* that has been shown to regulate metabotropic glutamate receptors (Kitano et al., 2002), the secreted protein *Nptx2* that has been shown to regulate AMPA receptor clustering (O'Brien et al., 2002; O'Brien et al., 1999) and homeostatic scaling (Chang et al., 2010), the hormone *Igf1* that has been shown to be important for brain development (Beck et al., 1995; Fernandez and Torres-Aleman, 2012), and the chromatin regulator *Hdac9* that has been shown to be highly expressed within the nervous system (Zhou et al., 2001) and regulate dendrite development (Sugo et al., 2010) (Figure 3.15a). While these and other important neuronal genes were misregulated with c-Fos RNAi, we sought to determine which genes may be direct targets of C-FOS within neurons. We hypothesized that direct targets may be identifiable not only on the basis of misexpression with c-Fos RNAi but also on the basis of a nearby activity-dependent enhancer bound by C-FOS. To investigate this possibility, we integrated our microarray data with our ChIP-Seq data and assessed the genomic regions surrounding these putative C-FOS target genes. We found that each of these genes was near an activity-regulated enhancer bound by C-FOS and other activity-dependent AP1 transcription factors (Figure 3.15b). This suggested that these genes may indeed be direct transcriptional targets of C-FOS. The identification of high confidence C-FOS target genes using integrated analysis of gene expression and ChIP-Seq data enables us to begin to understand the effector genes regulated by immediate early genes in the nervous system and how immediate early genes may mediate adaptive changes in the nervous system in response to neuronal activity.

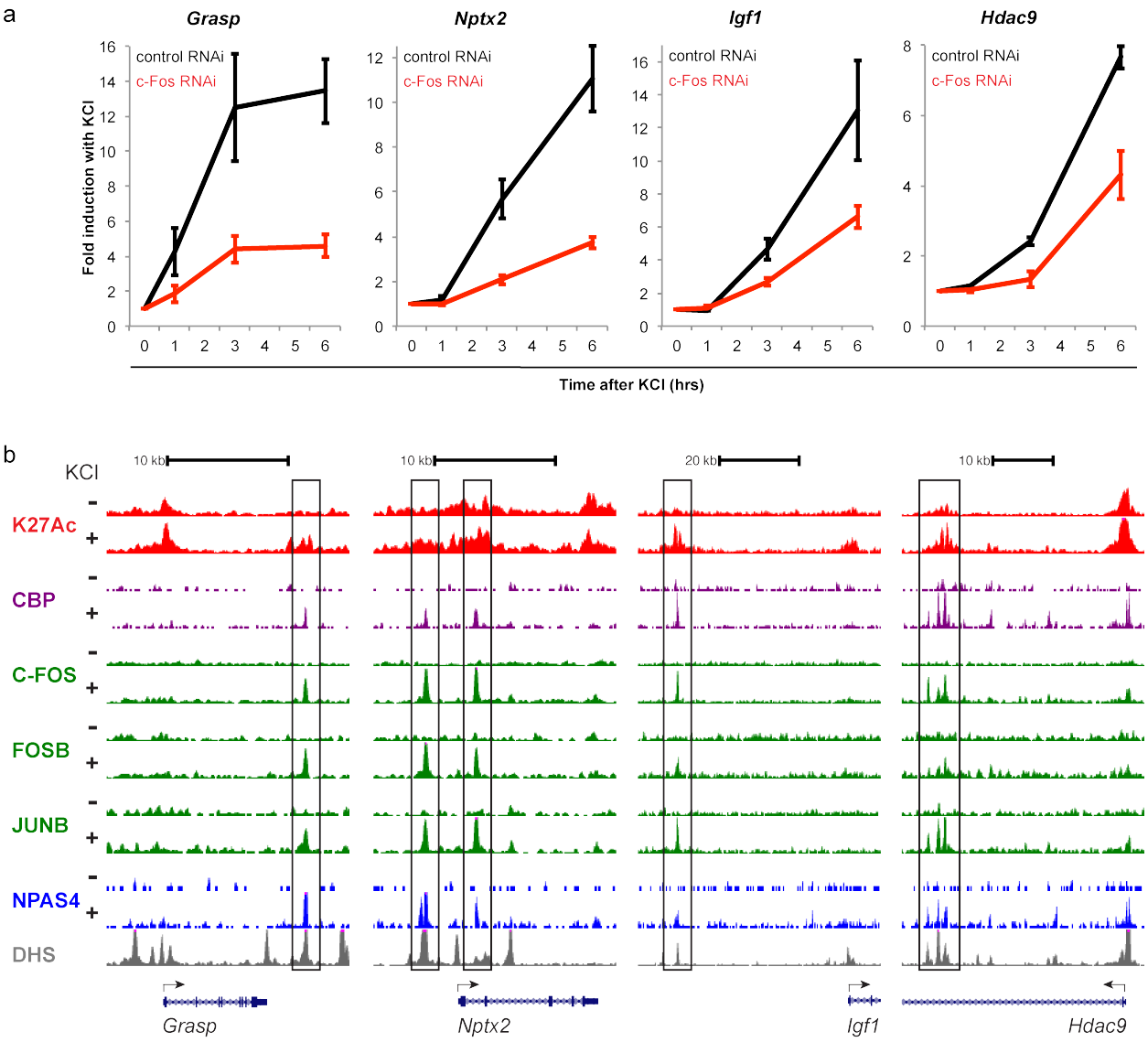

Figure 3.15: High confidence C-FOS target genes with important functions in the nervous system

(a) Lineplots of fold induction of *Grasp*, *Nptx2*, *Igf1*, and *Hdac9* after 1, 3, or 6 hours of KCl stimulation (relative to 0 hrs) in neurons that had been infected with lentivirus expressing control RNAi (black line) or c-Fos RNAi (red line). Data is plotted as the average of two microarray bioreplicates +/- SEM. (b) Genome browser views of ChIP-Seq data at *Grasp*, *Nptx2*, *Igf1*, and *Hdac9* loci. All four of these genes are near enhancers that display increasing H3K27Ac in response to KCl stimulation and are bound by C-FOS and other inducible AP1 transcription factors. For all chromatin marks and transcription factors, ChIP-Seq tracks display input-normalized reads from neuronas stimulated with 0 hours ('-') or two hours ('+') of KCl.

3.3.5 Functional dissection of stimulus responses of the *Nptx2* enhancer

While our data reveal that AP1 is required for enhancer responses to neuronal activity and BDNF, it is not clear if AP1 is sufficient to generate these responses or if other transcription factors are also required. We sought to understand this issue by dissecting the function of a neuronal stimulus-responsive enhancer. We hypothesized that an enhancer that responded to both neuronal activity and BDNF might require AP1 to respond to each stimulus and might require additional stimulus-specific transcription factors to induce H3K27Ac at enhancers that respond to only one stimulus. We further hypothesized that mechanisms that enable an enhancer to respond to neuronal activity might be distinct from the mechanisms that enable an enhancer to respond to BDNF. To test these hypotheses, we chose to study the *Nptx2* enhancer, which served as the basis for our luciferase reporter construct. The *Nptx2* gene is robustly expressed in cortical neurons in response to both neuronal activity and BDNF, with highest expression at 6hrs, and greater expression in response to BDNF stimulation than KCl stimulation (Figure 3.16a). The enhancer ~3kb upstream of the *Nptx2* gene exhibits inducible H3K27Ac in response to neuronal activity and BDNF (Figure 3.16b) and is required for the response of the *Nptx2* reporter to both stimuli in a reporter assay (Figure 3.11a,c). The *Nptx2* enhancer also exhibits robust binding of the AP1 transcription factors C-FOS and FOSB in response to each stimulus (Figure 3.16b and data not shown). All of these data suggest that the *Nptx2* enhancer may be useful for determining how neuronal stimulus-responsive enhancers function to contribute to stimulus-responsive transcription in the nervous system.

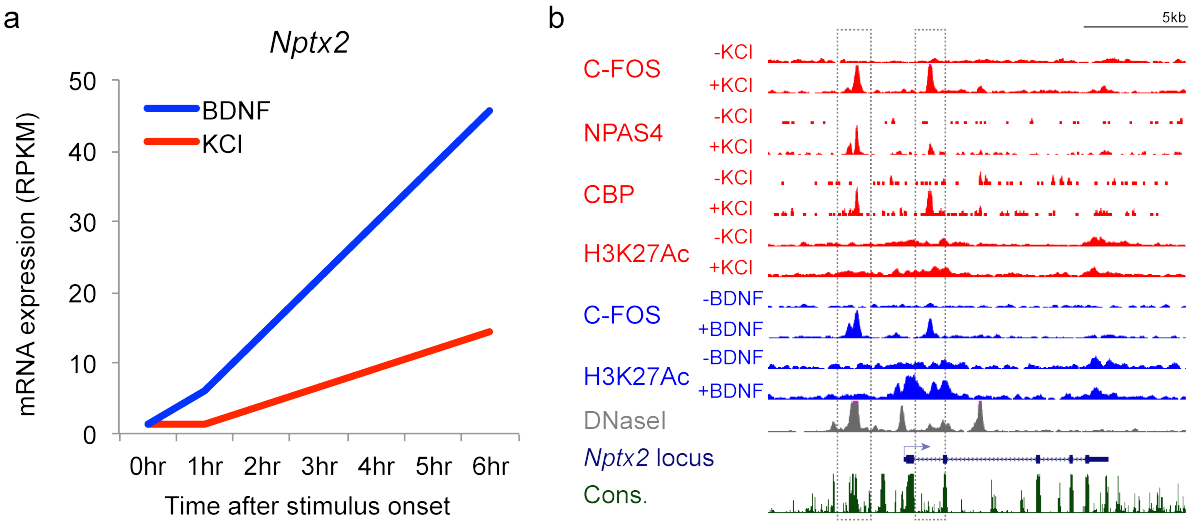

Figure 3.16: Characterization of *Nptx2* expression and *Nptx2* locus

(a) RNA-Seq data from mouse cortical neurons stimulated with 0, 1, 6 hours KCl or 0, 1, 6 hours BDNF was analyzed to assess the levels of expression of *Nptx2*. *Nptx2* is induced in response to both KCl and BDNF stimulation but is more induced in response to BDNF. mRNA is expressed as reads per kilobase per million mapped reads (RPKM). (b) Genome browser view of ChIP-Seq tracks for the indicated factors at the stimulus-regulated *Nptx2* locus. ChIP-Seq tracks display input-normalized ChIP-Seq reads from neurons before membrane depolarization (-KCl), after two hours of membrane depolarization (+KCl), before BDNF stimulation (-BDNF), or after two hours of BDNF stimulation (+BDNF). Also displayed are DNaseI hypersensitivity signal from adult mouse cerebrum and vertebrate conservation by PhastCons. Dashed boxes identify nearby enhancer elements.

We utilized the *Nptx2* reporter to dissect the function of the *Nptx2* enhancer. We first sought to identify the core element within the enhancer that was sufficient to generate transcriptional responses to neuronal activity and BDNF. To do this, we first generated truncation mutants of the *Nptx2* enhancer and measured the ability of each mutant to respond to neuronal activity and BDNF in reporter assays. We found that a core 180bp region retained the full activity of the full-length enhancer, suggesting that the sequence determinants that give rise to neuronal activity-dependent and BDNF-dependent responses from this enhancer reside within this region of the enhancer (Figure 3.17).

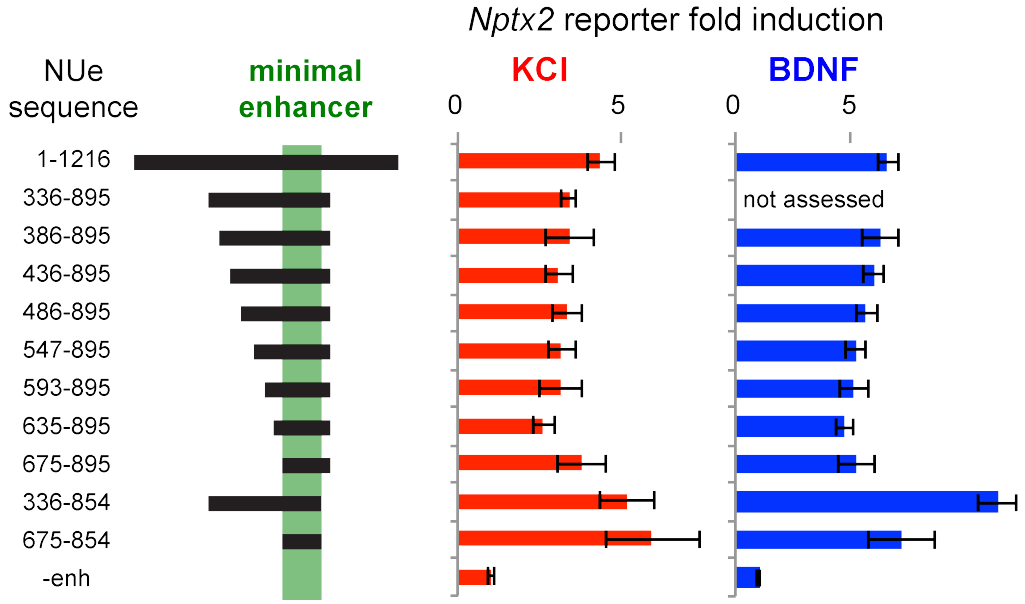

Figure 3.17: Identification of the minimal sequence within the *Nptx2* upstream enhancer that drives responses to both KCl and BDNF

Luciferase reporter data for truncation mutants of the *Nptx2* upstream enhancer (NUe) cloned into the *Nptx2* reporter, reported as the fold induction of reporter activity in mouse cortical neurons after 6 hours of KCl or BDNF stimulation relative to 0 hours. Error bars represent standard error of the mean (S.E.M.). n ≥ 3 for all enhancers tested.

To discover motifs in an unbiased fashion that contribute to the function of the Nptx2 enhancer, we comprehensively scrambled the sequence of a minimized version of the enhancer and measured the ability of mutant enhancer sequences to respond to neuronal activity and BDNF in reporter assays. We scrambled approximately 7-10 base pairs at a time by converting all adenine nucleotides to cytosine nucleotides (A→C), all cytosine nucleotides to adenine nucleotides (C→A), all thymine nucleotides to guanine nucleotides (T→G), and all guanine nucleotides to thymine nucleotides (G→T). We found several regions within the enhancer whose mutation reduced reporter expression by more than 50% compared to the wild type sequence (Figure 3.18). Some stretches of sequence appeared to be important for the response of the *Nptx2* enhancer to both KCl and BDNF, while other sequences appeared to be important for the response to either KCl or BDNF. Closer inspection of the critical sequences revealed three AP1 motifs within the enhancer that appeared to be critical for the responses to both KCl and BDNF (Figure 3.18). This suggested that AP1 might be important for generating responses to both KCl and BDNF at the *Nptx2* enhancer, consistent with our earlier findings about AP1.

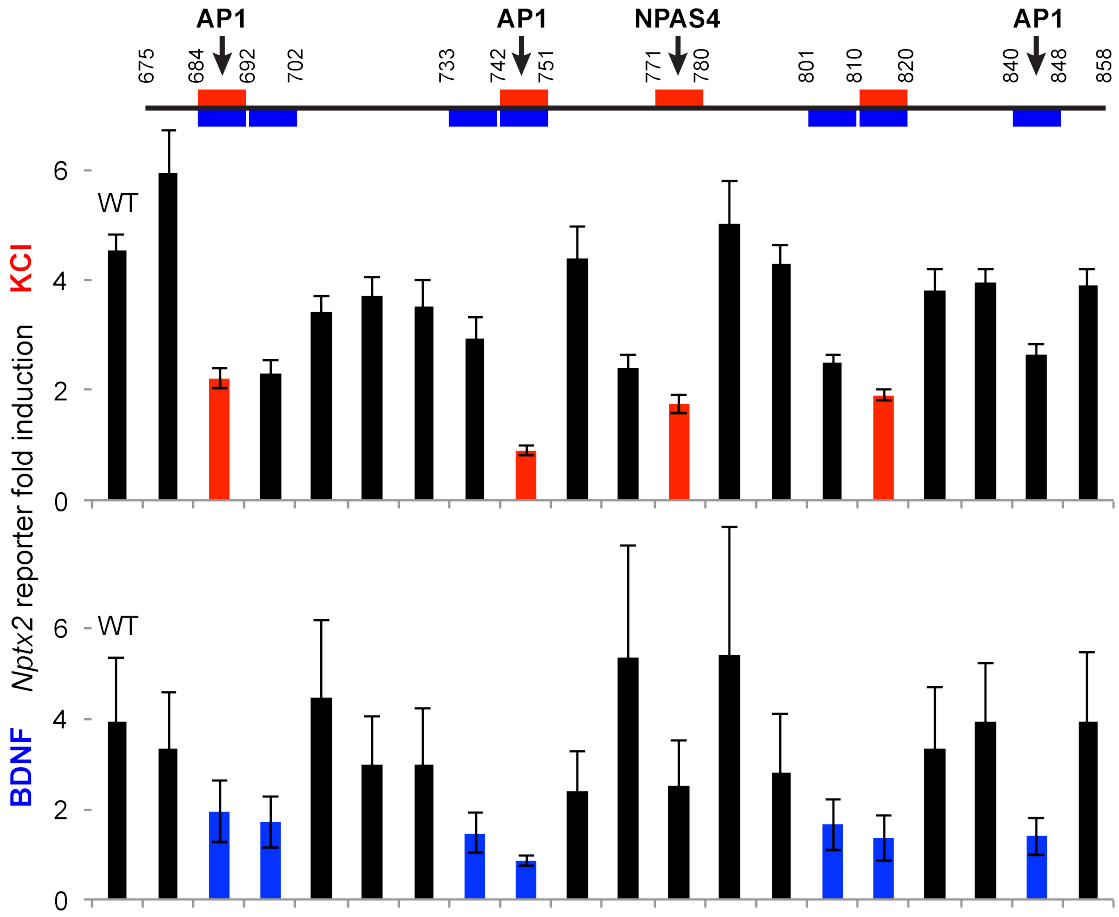

Figure 3.18: Comprehensive scrambling of the *Nptx2* enhancer reveals sequences important for responsiveness to KCl and BDNF

A minimized version of the *Nptx2* enhancer (schematic, top) was scrambled 7-10 base pairs at a time and the ability of each mutant to drive luciferase reporter expression in response to KCl (top bar graph) and BDNF (bottom bar graph) was assessed. Sequences whose mutation reduced reporter expression by more than 50% are highlighted in red for KCl and blue for BDNF. Luciferase activity is reported as the fold induction of reporter activity in mouse cortical neurons after 6 hours of KCl or BDNF stimulation relative to 0 hours. Error bars represent standard error of the mean (S.E.M.). n ≥ 3 for all enhancers tested with KCl, n ≥ 3 for all enhancers tested with BDNF.

To determine the functional contribution of each AP1 site while minimally impacting the sequence of the *Nptx2* enhancer, we subtly mutated each AP1 motif within the full length *Nptx2* enhancer, which included four AP1 motifs in total. A single base pair mutation of the second nucleotide of the AP1 motif from G to A has previously been shown to abrogate AP1 activity, and we independently confirmed that this subtle manipulation of AP1 sites phenocopied the effect of deletion of the entire AP1 site. Using AP1 single base pair point mutations, we found that both AP1 motifs that appeared to be critical for generating responses of the *Nptx2* enhancer to KCl and BDNF in our scrambling experiments were critical to generate responses to neuronal activity and BDNF (AP1 #2,3; Figure 3.19a, b). The AP1 site not contained within the minimal enhancer region (AP1 #1) and the AP1 site that appeared to impact BDNF but not KCl responsiveness of the *Nptx2* enhancer in our scrambling experiments (AP1 #4) did not appear to contribute significantly to the responsiveness of the *Nptx2* enhancer to either KCl or BDNF. Mutation of individual AP1 motifs reduced reporter expression to different extents, and mutation of all four AP1 motifs within the *Nptx2* enhancer eliminated nearly all reporter expression induced by both activity and BDNF. These data indicate that AP1 is required for responses of the *Nptx2* enhancer to both neuronal activity and BDNF. Interestingly, while the AP1 motifs within the *Nptx2* enhancer appear to contribute variably to the magnitude of the stimulus response, they do not appear to be used differentially in the context of different stimuli. This suggests that AP1 may function similarly in the context of different stimuli, and that other factors may collaborate with AP1 to generate responses to specific stimuli.

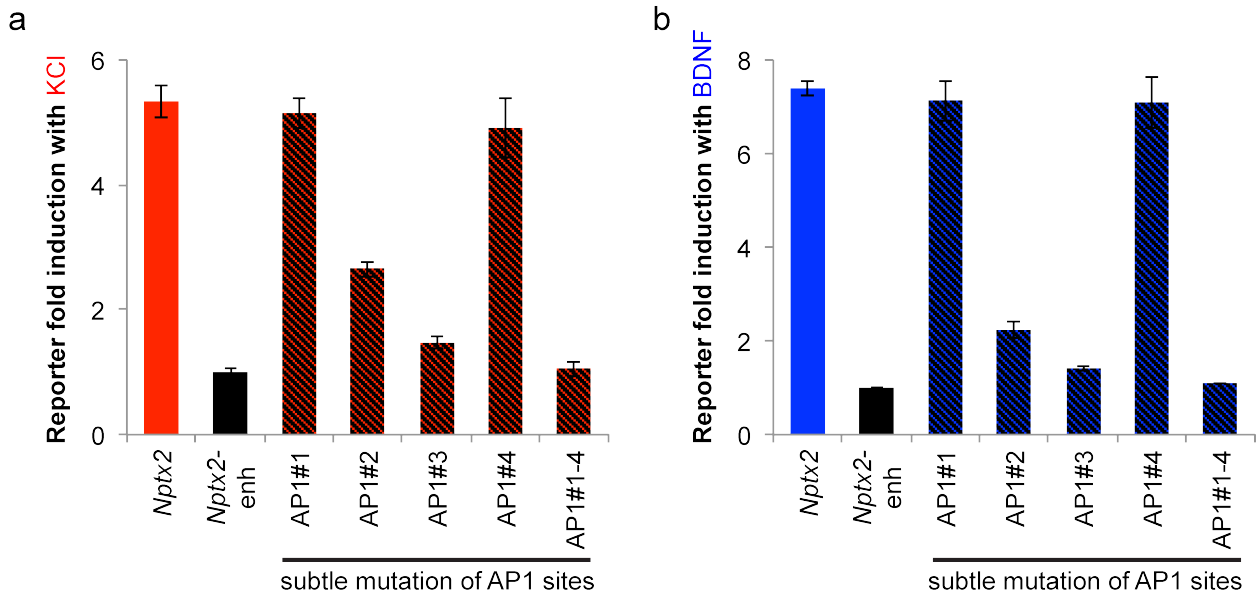

Figure 3.19: Functional contribution of individual AP1 sites to the responsiveness of the *Nptx2* enhancer to KCl and BDNF

AP1 sites within the *Nptx2* enhancer were subtly mutated (T**G**AGTCA→T**A**AGTCA) individually (AP#1, AP1#2, AP1#3, AP1#4) or all together (AP1#1-4) and the ability of each mutant to drive luciferase reporter expression in response to KCl (a) and BDNF (b) was assessed. Luciferase activity is reported as the fold induction of reporter activity in mouse cortical neurons after 6 hours of KCl or BDNF stimulation relative to 0 hours. Error bars represent standard error of the mean (S.E.M.). $n \geq 3$ for all enhancers tested.

Having demonstrated that AP1 plays a critical role in the responsiveness of the *Nptx2* enhancer to both activity and BDNF, we asked whether AP1 was sufficient to drive responses to these stimuli. To test this possibility, we mutated the entire sequence of a minimized version of the *Nptx2* enhancer outside of the critical AP1 sites and tested whether the AP1 sites (retained with their native spacing and GC content) were sufficient to retain responsiveness to neuronal activity or BDNF. We found that scrambling the non-AP1 sequence of the enhancer eliminated responses to both activity and BDNF, suggesting that AP1 motifs are not sufficient to drive stimulus-responses of this enhancer and that additional sequences within the enhancer are required to generate stimulus responses.

To discover additional motifs that may contribute to the stimulus-responsive function of this enhancer, we searched the sequences identified in our scrambling experiment (Figure 3.18) for known transcription factor motifs other than AP1. Interestingly, we found that a sequence within the *Nptx2* enhancer that appeared to be important for responses of this enhancer to KCl but not BDNF contained a "TCGTG" motif that has been shown to be the preferred motif for NPAS4 (Ooe et al, 2004 PMID: 14701734). ChIP-Seq data also revealed that the *Nptx2* enhancer is bound by NPAS4 in response to neuronal activity (Figure 3.16b). NPAS4 is a basic helix loop helix PAS domain containing (bHLH-PAS) transcription factor that is expressed specifically in the nervous system in response to neuronal activity (Lin et al., 2008). Thus, we hypothesized that NPAS4 might also contribute to the ability of stimulus-responsive enhancers to respond to neuronal activity. To test this hypothesis, we abrogated the

function of NPAS4 at the *Nptx2* enhancer by mutating the NPAS4 motif from the enhancer and by depleting NPAS4 levels by RNAi (Figure 3.20).

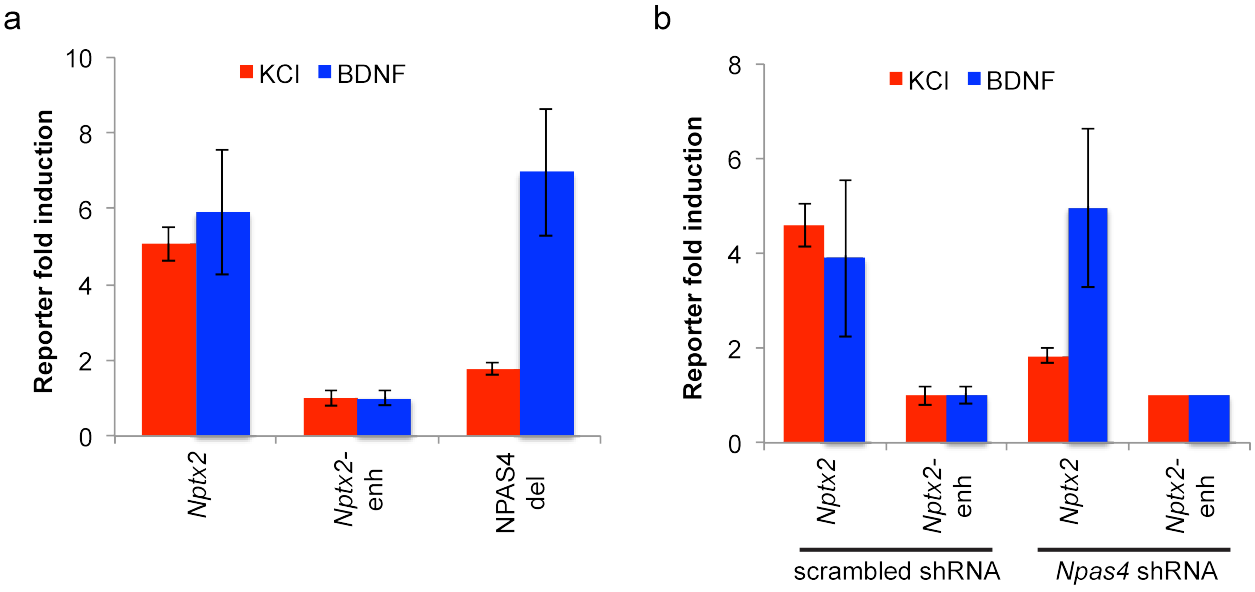

Figure 3.20: NPAS4 contributes to the KCl but not BDNF responsiveness of the *Nptx2* enhancer

(a) The putative NPAS4 motif within the *Nptx2* enhancer was deleted (NPAS4 del) and the ability of this mutant to drive luciferase reporter expression in response to KCl and BDNF was assessed. (b) The activity of the Nptx2 reporter in response to KCl and BDNF was assessed in neurons that had been transfected with scrambled shRNA or *Npas4* shRNA. Luciferase activity is reported as the fold induction of reporter activity in mouse cortical neurons after 6 hours of KCl or BDNF stimulation relative to 0 hours. Error bars represent standard error of the mean (S.E.M.). $n \geq 3$ for all enhancers tested.

We found that both manipulations significantly reduced the activity-dependent expression of the reporter, but neither manipulation significantly reduced the BDNF-dependent expression of the reporter. This suggested that the *Nptx2* enhancer requires NPAS4 to respond to neuronal activity but not to respond to BDNF. Consistent with this possibility, data from a previous study shows that *Nptx2* is less induced by neuronal activity after *Npas4* RNAi (Lin et al., 2008). On the genome scale, analysis of the NPAS4 ChIP-Seq data indicated that Npas4 was bound preferentially to neuronal activity-dependent enhancers compared to other neuronal enhancers, providing further evidence that NPAS4 may be important for neuronal activity-dependent enhancer function.

These data together reveal that AP1 family transcription factors and NPAS4 collaborate to promote stimulus responsive transcription through enhancers. AP1 is required for both activity-dependent and BDNF dependent responses while NPAS4 is required for only the activity-dependent response. These experiments begin to elucidate how stimulus-dependent and stimulus specific transcriptional responses are generated within the nervous system. Further experiments will be required to reveal the additional determinants of stimulus-responsiveness of neuronal enhancers.

3.3.6 NPAS4 and CBP collaborate with C-FOS to drive activity-dependent enhancers

Our data from the functional dissection of the *Nptx2* enhancer revealed a critical role for NPAS4 is driving enhancer responses to neuronal activity. To evaluate whether

NPAS4 and other factors collaborated with C-FOS to drive neuronal activity-dependent enhancers throughout the genome, we assessed the binding of NPAS4 and other transcription factors to C-FOS bound loci throughout the genome, reasoning that significant binding of transcription factors with C-FOS may indicate a function with C-FOS. Using previously generated data from our system (Kim et al., 2010), we found significant binding for both NPAS4 and CBP at C-FOS peaks within the genome. This suggested that NPAS4 and CBP may collaborate with C-FOS to drive neuronal activity-dependent enhancers.

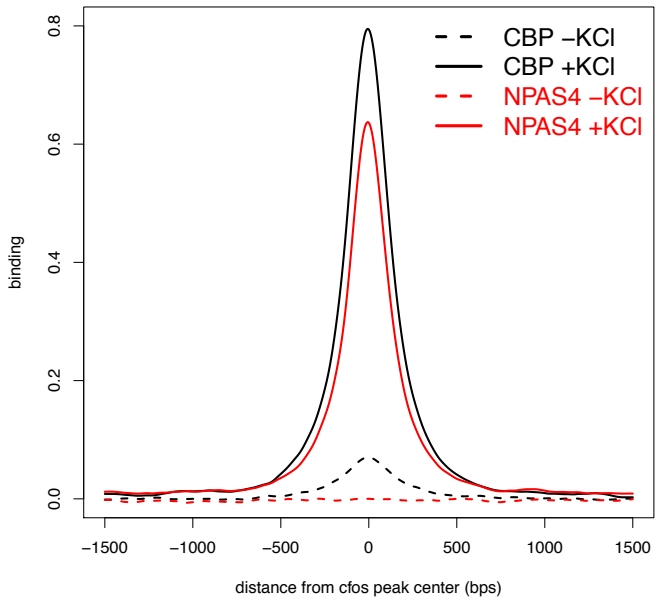

Figure 3.21: ChIP-Seq signal for NPAS4 and CBP and C-FOS peaks

Previously generated ChIP-Seq data for CBP and NPAS4 (Kim et al., 2010) was analyzed to evaluate the binding of these factors at sites of C-FOS binding throughout the genome. Average profiles of input-normalized CBP (black) and NPAS4 (red) ChIP-Seq signal before KCl stimulation (dashed lines) and after KCl stimulation (solid lines) are shown. Here, sites of C-FOS binding are defined as regions of the genome that exhibited a called C-FOS peak in three or more out of four separate C-FOS ChIP-Seq bioreplicates that were reduced by 50% or more in two out of two c-Fos RNAi ChIP-Seq bioreplicates.

We hypothesized that if CBP and NPAS4 collaborated with C-FOS to drive neuronal activity-dependent enhancers, we may expect a higher percentage of loci bound by C-FOS/NPAS4/CBP to exhibit increasing H3K27Ac in response to neuronal activity than loci bound by C-FOS but not NPAS4 or CBP. To investigate this possibility, we evaluated the H3K27Ac behaviors of C-FOS peaks that were bound without NPAS4 and CBP or were bound with NPAS4 and CBP. We found that while only 5% of C-FOS peaks that were not bound by NPAS4 and CBP exhibited increasing H3K27Ac in response to neuronal activity, a striking 47% of C-FOS peaks that were bound by NPAS4 and CBP exhibited increasing H3K27Ac in response to neuronal activity. This suggested that sites within the genome that are bound by C-FOS/NPAS4/CBP are nearly 10 times more likely to function as neuronal activity-dependent enhancers than sites within the genome bound by C-FOS but not NPAS4 or CBP. This suggested that NPAS4 and CBP may collaborate with C-FOS to drive neuronal activity-dependent enhancers throughout the genome. Additional experiments will have to be done to understand the specific function of each of these factors in neuronal activity-dependent enhancer function.

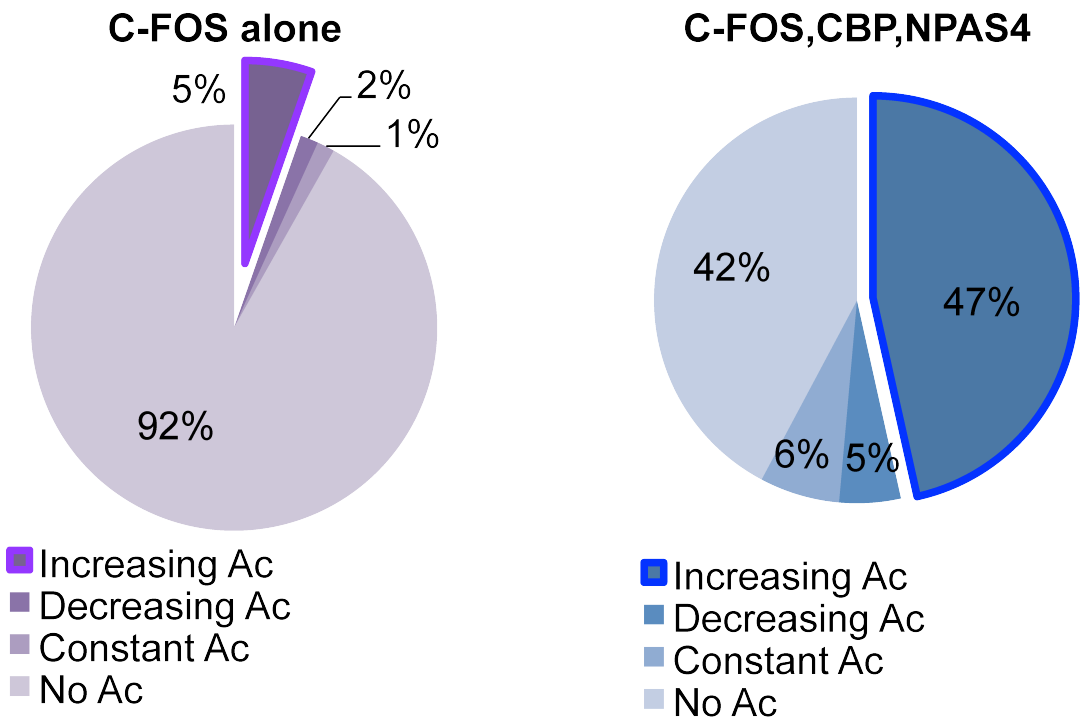

Figure 3.22: H3K27Ac behaviors at loci bound by different complements of transcription factors

The H3K27Ac behaviors of C-FOS peaks that were bound without NPAS4 and CBP (left panel) or were bound with NPAS4 and CBP (right panel) were investigated. While only 5% of C-FOS peaks that were not bound by NPAS4 and CBP exhibited increasing H3K27Ac in response to neuronal activity, a striking 47% of C-FOS peaks that were bound by NPAS4 and CBP exhibited increasing H3K27Ac in response to neuronal activity

3.4 DISCUSSION

We have recently discovered that stimulus-responsive enhancers can be identified on the basis of rapidly increasing H3K27Ac levels in response to stimulation. We employed this dynamic chromatin signature to identify stimulus-responsive enhancers within the nervous system that respond to neuronal activity and BDNF stimulation. Here, we characterized the transcriptional mechanisms underlying activity-responsive and BDNF-responsive neuronal enhancers. We find that the AP1 transcription factor complex plays an important role at neuronal enhancers that respond to neuronal activity, BDNF, or both. We show that the AP1 motif is the most significantly enriched motif at all subsets of neuronal stimulus-responsive enhancers, that the AP1 transcription factors C-FOS and FOSB bind to stimulus-responsive enhancers, and that AP1 is required for responses to both neuronal activity and BDNF stimulation at a subset of neuronal enhancers. By dissecting the function of the activity and BDNF responsive *Nptx2* enhancer, we confirm the necessity of the AP1 transcription factor in coordinating responses to activity and BDNF and also show that AP1 is not sufficient to generate responses to these stimuli. AP1 must coordinate with other stimulus-specific transcription factors to generate stimulus-responses at enhancers. In the case of the *Nptx2* enhancer, AP1 coordinates with the activity-specific transcription factor NPAS4 to generate responses to neuronal activity. These results begin to elucidate the transcriptional mechanisms underlying stimulus-responsive enhancers within the nervous system.

3.4.1 Multiple transcriptional mechanisms underlying stimulus responsive enhancers

While AP1 transcription factors play a critical role at a subset of neuronal enhancers, transcriptional mechanisms independent of AP1 also exist to drive stimulus responses at enhancers. We show that not all stimulus responsive enhancers are bound by FOS transcription factors and not all stimulus responsive enhancers are affected by the expression of a potent AP1 dominant negative transcription factor. Hence, other mechanism likely exists at these enhancers. This is consistent with the observation that multiple waves of transcription occur in response to extracellular stimuli. Extracellular stimuli rapidly activate pre-existing transcription factors (such as CREB, MEF2, and SRF) within the cell that drive a first wave of transcription. Many genes expressed in this first wave of transcription encode transcription factors (such as FOS, JUN, and NPAS4) that, once expressed, activate a second wave of transcription in response to extracellular stimuli. It is possible that the assessment of H3K27Ac 2 hours after stimulation with KCl or BDNF best reveals active enhancers mediating the second wave of transcription. This may be why AP1 appears to play a dominant role within the enhancers characterized in this study. Assessment of inducible H3K27Ac at earlier time points after stimulation may better enable the understanding of AP1-independent mechanisms at stimulus-responsive enhancers.

3.4.2 Role of AP1 at neuronal stimulus-responsive enhancers

While we find AP1 to play a critical role at neuronal stimulus-responsive enhancers, this is in stark contrast to historical studies of AP1. Since enhancers have been difficult to identify until recently, historically much of the work on AP1 has focused on promoter elements that contain AP1 motifs. The presence of AP1 motifs within promoter regions, the importance of these motifs in reporter assays, and the ability of AP1 transcription factors to bind these motifs in gel-shift assays was all taken as evidence that AP1 functioned predominantly at promoters of target genes to regulate transcription. However, the studies that proposed this mechanism of function, being done long ago, were not able to demonstrate binding of AP1 transcription factors to promoters in neurons *in vivo*. Here, we present for the first time ChIP-Seq data from mouse cortical neurons that clearly demonstrates that the vast majority of C-FOS and FOSB binding does not occur at promoter regions. Furthermore, we find no evidence of C-FOS or FOSB binding at the promoters of reported FOS target genes in the nervous system. For example, the first reported target gene for FOS in the nervous system was proenkephalin (Sonnenberg et al., 1989c). The study that reported this target gene suggested that FOS bound to AP1 motifs near the promoter to regulate expression of this gene. However, we find no evidence of C-FOS or FOSB binding at the promoter of this gene in any of our ChIP-Seq bioreplicates in response to neuronal activity or BDNF. While proenkephalin or other proposed target genes may be regulated by FOS transcription factors, our data suggests that the mechanisms of such regulation do not occur at promoters but likely occur at enhancers.

3.4.3 Genetic control of activity-regulated enhancers and human disease

We have found that the human versions of many of our identified mouse activity-regulated enhancers can drive reporter expression in response to depolarization when introduced into cultured mouse neurons (data not shown), which suggests that many of these regions might be functionally conserved between mouse and human. Thus, the ability to identify a refined set of functional stimulus responsive enhancers should permit an accurate identification of activity-regulated enhancers in human neurons. Instances in which function is not conserved could provide insights into how the transcriptional responses of human neurons to synaptic activity have evolved. Changes in the activity-regulated gene program during human evolution might allow for adaptations in synaptic plasticity and function that are thought to be critical for human specific cognitive abilities (Dolmetsch and Geschwind, 2011; Konopka and Geschwind, 2010). We have begun to elucidate how these elements are regulated by activity-dependent transcription factors in mouse and how various transcription factor motifs correlate with inducible acetylation. These data could be potentially utilized to better interpret the potential functional consequences of human single nucleotide polymorphisms (SNPs) in these regulatory regions (Maurano et al., 2012). Indeed, the majority of variants within the genome appear to be in noncoding regions. As a result, human variation at enhancer elements may contribute to different traits, common diseases, and rare diseases. Exome sequencing studies of autistic individuals and their unaffected relatives have largely failed to identify recurrent de novo coding mutations that can explain the disease burden, indicating that non-coding variation could potentially play an important role in the genetics of autism (Buxbaum et al., 2012).

Given the proposed importance of synaptic signaling in autism spectrum disorders (Ebert and Greenberg, 2013), the identification of the cis-regulatory control of human activity-regulated transcription could provide a critical resource for the further elucidation of the genetics of these disorders.

3.5 Materials and Methods

3.5.1 Mouse cortical cultures

Embryonic day 16.5 (E16.5) C57BL/6 embryonic mouse cortices were dissected and then dissociated for 10 minutes in 1× Hank's Balanced Salt Solution (HBSS) containing 20 mg/mL trypsin (Worthington Biochemicals) and 0.32 mg/mL L-cysteine (Sigma). Trypsin treatment was terminated by washing dissociated cells three times for two minutes each in dissociation medium consisting of 1× HBSS containing 10 mg/mL trypsin inhibitor (Sigma). Cells were then triturated using a flame-narrowed Pasteur pipette to fully dissociate cells. After dissociation, neurons in were kept on ice in dissociation medium until plating. Cell culture plates were pre-coated overnight with a solution containing 20 ug/mL poly-D-lysine (Sigma) and 4 ug/mL mouse laminin (Invitrogen) in water. Prior to plating neurons, cell culture plates were washed three times with sterile distilled water and washed once with Neurobasal Medium (Life Technologies). Neurons were grown in neuronal medium consisting of Neurobasal Medium containing B27 supplement (2%; Invitrogen), penicillin-streptomycin (50 g/ml penicillin, 50 U/mL streptomycin, Sigma) and glutamine (1 mM, Sigma). At the time of plating, cold neuronal medium was added to neurons in dissociation medium to dilute neurons to the desired concentration. Neurons were subsequently plated and placed in a cell culture incubator that maintained a temperature of 37 degrees C and a CO2 concentration of 5%. Two hours after plating neurons, medium was completely aspirated from cells and replaced with fresh warm neuronal medium. Neurons were grown *in vitro* until the seventh day *in vitro* (DIV7).

3.5.1.1 Mouse cortical cultures for ChIP-Seq experiments

For ChIP-Seq experiments, mouse cortical neurons were plated at an approximate density of 4×10^7 on 15-cm dishes. Neurons were plated in 30mL neuronal medium. Ten mL of the medium was replaced with 12ml fresh warm neuronal medium on DIV3 and DIV6.

3.5.1.2 Mouse cortical cultures for luciferase reporter assays

For luciferase reporter assays, mouse cortical neurons were plated at an approximate density of 3×10^5 per well on 24-well plates. Neurons were plated in 500 ul neuronal medium. On the DIV3, 100 uL fresh warm medium was added to neurons. On DIV5 neurons were transfected (see section on transfection). At the completion of transfection, conditioned medium containing 15% fresh neuronal medium was returned to neurons.

3.5.1.3 Mouse cortical cultures for microarray experiments

For microarray experiments, mouse cortical neurons were plated at an approximate density of 3×10^5 per well on 24-well plates. Neurons were plated in 500 ul neuronal medium. On the DIV5, neurons were infected for 6 hours with viral supernatant containing lentivirus expressing either a control RNAi or c-Fos RNAi. At the completion of infection, wells were washed three times with warmed neuronal medium, and then conditioned medium containing 15% fresh medium was returned to neurons. Four wells were used for each condition: one well was used to obtain protein lysates for western blot, three wells were used to obtain RNA for microarrays.

3.5.2 Stimulation with potassium chloride (KCl)

Prior to KCl depolarization, neurons were quieted with 1 μM tetrodotoxin (TTX, Fisher) and 100 μM DL-2-amino-5-phosphopentanoic acid (DL-AP5, Fisher). Neurons were subsequently stimulated by adding warmed KCl depolarization buffer (170 mM KCl, 2 mM CaCl2, 1 mM MgCl2, 10 mM HEPES) directly to the neuronal culture, to final concentration of 31% in the neuronal culture medium within the culture plate or well.

3.5.2.1 KCl stimulation for ChIP-Seq experiments

For KCl depolarization of neurons for ChIP-Seq experiments, DIV 6 neurons were quieted overnight with 1 μM TTX and 100 μM DL-AP5. The next morning, neurons were left silenced (-KCl condition) or stimulated for 2 hours with KCl (+KCl condition).

3.5.2.2 KCl stimulation for luciferase reporter assays

For KCl depolarization of neurons for luciferase reporter assays, DIV 7 neurons were quieted for two hours with 1 μM TTX and 100 μM DL-AP5. Two hours later, neurons were left silenced (-KCl condition) or stimulated for 6 hours with KCl (+KCl condition).

3.5.2.3 KCl stimulation for microarray experiments

For KCl depolarization of neurons for microarray experiments, DIV 7 neurons were quieted for two hours with 1 μM TTX and 100 μM DL-AP5. Two hours later, neurons were left silenced (0 hour condition) or stimulated for 1, 3, or 6 hours with KCl.

3.5.3 Stimulation with brain derived neurotrophic factor (BDNF)

3.5.3.1 BDNF stimulation for ChIP-Seq experiments

For BDNF stimulation of neurons for ChIP-Seq experiments, the volume of conditioned medium on DIV6 neurons was reduced to 25 mL. On DIV7, neurons were left in a basal condition (-BDNF condition) or stimulated for 2 hours with 50ng/mL recombinant human BDNF (Fisher) (+BDNF condition).

3.5.3.2 BDNF stimulation for luciferase reporter assays

For BDNF stimulation of neurons for luciferase reporter assays, DIV7 neurons were left in a basal condition (-BDNF condition) or stimulated for 6 hours with 50ng/mL recombinant human BDNF (Fisher) (+BDNF condition).

3.5.4 Lentivirus infection

The pLLx3.7 backbone was used for generation of lentivirus as previously described (Lois et al., 2002; Rubinson et al., 2003).

3.5.5 H3K27Ac Chromatin immunoprecipitation sequencing (ChIP-Seq)

Forty million mouse cortical neurons cultured to *in vitro* day 7 were used for each ChIP-Seq library construction. Typically 20-40 million cortical neurons were used for a single ChIP experiment. To cross-link protein-DNA complexes, media was removed

from neuronal cultures and crosslinking-buffer (0.1 M NaCl, 1 mM EDTA, 0.5 mM EGTA, 25 mM HEPES-KOH, pH 8.0) containing 1% formaldehyde was added for 10 minutes at room temperature. Cross-linking was quenched by adding 125 mM glycine for five minutes at RT. Cells were then rinsed three times in ice-cold PBS containing complete protease inhibitor cocktail tablets (Roche) and collected by scraping. Cells were pelleted and either stored at -80 degrees C until use or immediately processed. Cell pellets were lysed by 20 cell pellet volumes (CPVs) of buffer 1 (50 mM HEPES-KOH, pH 7.5, 140 mM NaCl, 1 mM EDTA, pH 8.0, 10 % Glycerol, 0.5 % NP-40, 0.25 % Triton X-100, complete protease inhibitor cocktail) for 10 min at 4 degrees C. Nuclei were then pelleted by centrifugation at 3000 rpm for 10 min at 4 degrees C. The isolated nuclei were rinsed with 20 CPVs of buffer 2 (200 mM NaCl, 1 mM EDTA, pH 8.0, 0.5 mM EGTA, pH 8.0, 10 mM Tris-HCl, pH 8.0, complete protease inhibitor cocktail) for 10 min at RT and re-pelleted. Next, 4 CPVs of buffer 3 (1 mM EDTA, pH 8.0, 0.5 mM EGTA, pH 8.0, 10 mM Tris-HCl, pH 8.0, complete protease inhibitor cocktail) were added to the nuclei and sonication was carried out using a Misonix 3000 Sonicator (Misonix) set at a power setting of 7.5 (equivalent to 24 watts). 20 pulses of 15 seconds each were delivered at this setting, which resulted in genomic DNA fragments with sizes ranging from 200 bp to 2 kb. Insoluble materials were removed by centrifugation at 20,000 rpm for 10 min at 4 degrees C. The supernatant was transferred to a new tube and the final volume of the resulting nuclear lysate was adjusted to 1 mL by adding buffer 3 supplemented with 0.3 M NaCl, 1 % Triton X-100, 0.1 % Deoxycholate. The lysate was pre-cleared by adding 100 ul of pre-rinsed Protein A/G Agarose (Sigma) per 1 ml of the lysate and incubating for 1 hour at 4 degrees C. After pre-clearing, ten percent of the ChIP sample (50 ul from 500 ul lysate) was saved as input material. The

remaining lysate was incubated with 4 ug antibodies for immunoprecipitation. The antibodies used in this study are shown in Table 6:

Table 6: Antibodies used for ChIP-Seq experiments

Transcription factor	Antibody or antibodies used
MEF2A	Custom
MEF2D	Custom
C-FOS	sc52, sc7202 (Santa Cruz)
FOSB	sc7203 (Santa Cruz)

The antibody incubation was carried out overnight at 4 degrees C. The next day, 30 ul of pre-rinsed Protein A/G PLUS Agarose beads (Santa Cruz Biotechnology) was added to each ChIP reaction and further incubated for 1 hour at 4 degrees C. The beads bound by immune-complexes were pelleted and washed twice with each of the following buffers: low salt buffer (0.1% SDS, 1% Triton X-100, 2mM EDTA, 20mM Tris-HCl, pH 8.1, 150mM NaCl), high salt buffer (0.1% SDS, 1% Triton X-100, 2mM EDTA, 20mM Tris-HCl, pH 8.1, 500mM NaCl) and LiCl buffer (0.25M LiCl, 1% IGEPAL CA630, 1% deoxycholic acid (sodium salt), 1mM EDTA, 10mM Tris, pH 8.1). In each wash, the beads were incubated with wash buffer for 10 min at 4 degrees C while nutating. The washed beads were then rinsed once with 1x TE buffer (10 mM Tris-HCl, pH 8.0, 1 mM EDTA). The immunoprecipitated material was eluted from the beads twice by adding 100 ul of elution buffer (10 mM Tris-HCl, pH 8.0, 1 mM EDTA, pH 8.0, 1 % SDS) to each ChIP reaction and incubating the sample at 65 degree C for 30 min with brief vortexing every 2 min. 150 ul of elution buffer was also added to the saved input material (50 ul) and this sample was processed together with the ChIP samples. The eluates were combined and crosslinking was reversed by incubation at 65 degrees C overnight. The next day, 7 ug RNase A (affinity purified, 1mg/mL; Invitrogen) was added to each

sample and samples were incubated for 37 degrees C for one hour. Then, 7 uL Proteinase K (RNA grade, 20mg/mL; Invitrogen) was added to each sample and samples were incubated at 55 degrees C for two hours. The immunoprecipitated genomic DNA fragments were then extracted once with Phenol:Chloroform:Isoamyl Alcohol (25:24:1, pH 7.9; Life Technologies) and then back extracted with water. The resulting genomic DNA fragments were then purified using the QIAquick PCR purification kit (Qiagen) and DNA fragments were eluted in 100 ul of Buffer EB (elution buffer consisting of 10 mM Tris-HCl, pH 8.5, Qiagen). Samples were assessed for enrichment by quantitative PCR using primers to different genomic regions. Samples with significant enrichment over negative regions were submitted to the Beijing Genomic Institute (BGI) for 50 base pair single end sequencing on the Illumina Hiseq 2000 platform. For each sample, over 20 million clean reads were obtained.

3.5.6 ChIP-Seq analysis

3.5.6.1 Initial processing

Sequencing data was obtained from BGI in gzipped fastq file format. Files were transferred and unzipped. Then, sequencing reads were aligned to the July 2007 assembly of the mouse genome (NCBI 37, mm9) using the Burrows-Wheeler Aligner (BWA) (Li and Durbin, 2009) with default settings. The resulting bwa files were then converted to sam files and uniquely mapped reads were extracted from the sam files. Sam files of the uniquely mapped reads were then converted to bam files. Bam files

were then used for peak calling using Model-based Analysis of ChIP-Seq (MACS) (Zhang et al., 2008) with the following parameters: -f BAM -g mm.

3.5.6.2 Visualizing ChIP-Seq data on the UCSC genome browser

ChIP-Seq bam files were converted to bigwig track format to display the number of input normalized ChIP-Seq reads, normalized to 20 million total reads.

3.5.6.3 Characterization of genomic distribution of FOS binding sites

C-FOS and FOSB peaks were classified based on their location relative to genes in the NCBI Reference Sequence Database (RefSeq). Peaks were classified as being proximal if they were within 1kb of an annotated transcriptional start site (TSS). H3K27Ac peaks were classified as being distal if they were greater than 1kb from an annotated transcriptional start site (TSS).

3.5.6.4 Quantification of ChIP-Seq signal at enhancers

For transcription factors (MEF2A, MEF2D, C-FOS, FOSB), the number of input-normalized ChIP-Seq reads within an 800 bp window centered on each enhancer was taken to be the ChIP-Seq signal at the enhancer.

3.5.7 Luciferase reporter assays

3.5.7.1 Nptx2 reporter plasmid design

All luciferase reporter plasmids used were newly developed for this study. Most luciferase reporter plasmids used were based on the *Nptx2* gene, and hence this reporter was termed the *Nptx2* reporter. To develop the *Nptx2* reporter, we cloned the 4355 bp region upstream of the *Nptx2* coding sequence from C57BL/6 purified mouse genomic DNA between the NheI and EcoRV restriction sites within the multiple cloning site of the promoterless pGL4.11 reporter plasmid (Promega) using the primers shown in Table 7, with 5' clamp shown in red, NheI and EcoRV sites shown in green:

Table 7: Primers used to clone the *Nptx2* upstream regulatory region into pGL4.11

Primer	Sequence (5' → 3')
Forward primer	5' GCGCGCTAGCTTCCTGGCTTGTAGTGACCT 3'
Reverse primer	5' GCGCGATATCCTCGCTGACCTGTGTGCTCACTTCA 3'

pGL4.11 was chosen as the host plasmid since it contained the luc2P reporter gene, which contains an hPEST protein destabilization sequence. We found that the luc2P reporter responded more quickly and with greater magnitude to stimuli than luc2 reporters. Using PCR driven overlap extension (Heckman and Pease, 2007), the *Nptx2* reporter was then modified so that the 1216 bp *Nptx2* upstream enhancer (located -3607 to -2391 relative to the start of the *Nptx2* coding sequence) was replaced with a multiple cloning site containing SbfI, PacI, PmeI, and AscI restrictions sites. In order to do this, the primers shown in Table 8 were used (A, B, C, D nomenclature same as described in (Heckman and Pease, 2007)), with 5' clamp shown in red; NheI and EcoRV sites shown in green; SbfI, PacI, PmeI, and AscI sites shown in blue; and spacers shown in orange.

Table 8: Primers used to replace the *Nptx2* upstream enhancer with a multiple cloning site

Primer	Sequence (5' → 3')
A	5' GCGCGCTAGCTTCCTGGCTTGTAGTGACCT 3'
B	5' GGCGCGCCACACGTTTAAACGCGCTTAATTAAGTGTCCTGCAGGTTGTGTGAGACACTGTTTCCA 3'
C	5' CCTGCAGGACACTTAATTAAGCGCGTTTAAACGTGTGGCGCGCCAGCTAGTAACAGTTGGCATT 3'
D	5' GCGCGATATCCTCGCTGACCTGTGTGCTCACTTCA 3'

The multiple cloning site was inserted into the *Nptx2* upstream regulatory region to create a modified *Nptx2* reporter so that various enhancers could be easily cloned into this multiple cloning site. We verified that the modified *Nptx2* reporter in which the Nptx2 enhancer had been cloned into the multiple cloning site had the same inducibility as the wild-type *Nptx2* reporter (data not shown). This suggested that the multiple cloning site did not affect the function of the reporter and that other enhancers could be similarly cloned into this multiple cloning site without adverse affects on enhancer function.

3.5.7.2 Enhancer sequences for wild-type of mutated C-FOS bound enhancers

Activity-dependent enhancers containing AP1 sites, exhibiting reproducible and specific binding by the AP1 transcription factor C-FOS, were cloned between the SbfI and AscI sites within the multiple cloning site of the modified *Nptx2* reporter. For most enhancers, we observed that the trough between H3K27Ac peak shoulders as well as DNAseI hypersensitivity typically could be localized to a region less than 500bp. As a result, we synthesized approximately 500 bp genomic blocks for each enhancer of interest using gBlocks Gene Fragments (IDT). For each enhancer, we designed a wild-type version and a version of the enhancer in which the AP1 sites were mutated by one

base pair (T**G**AGTCA→T**A**AGTCA), which has been shown previously to abrogate AP1 binding (Risse et al., 1989). These gBlocks are shown in Table 9, with the clamp shown in bold, the SbfI site in green, and the AscI site in red.. In the case where no gBlock is shown, the sequence was obtained via PCR.

Table 9: gBlocks designed to create wild-type and AP1 mutant versions of 8 neuronal enhancers

Enh	500bp gBlock	AP1 mutant gBlock
e4	**GCGTCCTGCAGG**cagagagctgcctatgcgtctatttatgtctcactggccaaaacttactcac atgtctacccctcaaagaaagtaagaatgtcttctattatttgggtgactcatctagccaATGAGCAG GAAGAGAGTGAAATGTGGGGTGCGCCAGACTCTCCCAGCCATAGAGC ATCACGCCAAAATGTGGAAACAGCAAAGCAAACCCCTGGGAAGCCAGC CGCCCAGCCTGTGTGAGTCACACAACTCGGTGACTCACTCCCGCCCCC AGAGCTTGTCAGTGCAGCTGAGTTTCTCAGCATCGTGAAACTTAAGAG ATTGCTAAAATAGTCACCGCTCTGGATGGTGTGCTCCTGGATGCAAAG CATCTACTTAGCATTTAGCATGTTTCCTAAGTGTCCAAATTACATGTTT CACACAAAAATTACCGTCTCTGTCAAGCACTAAAGGTAAATGCTCTTTA ACATCAACAGTTACTTCAG**GGCGCGCC**ATAC	**GCGTCCTGCAGG**cagagagctgcctatgcgtctatttatgtctcactggccaaaactaactcacatg tctacccctcaaagaaagtaagaatgtcttctattatttgggtaactcatctagccaATGAGCAGGAAG AGAGTGAAATGTGGGGTGCGCCAGACTCTCCCAGCCATAGAGCATCACGC CAAAATGTGGAAACAGCAAAGCAAACCCCTGGGAAGCCAGCCGCCCAGCC TGTGTaAGTCACACAACTCGGTaACTCACTCCCGCCCCCAGAGCTTGTCAG TGCAGCTGAGTTTCTCAGCATCGTGAAACTTAAGAGATTGCTAAAATAGTC ACCGCTCTGGATGGTGTGCTCCTGGATGCAAAGCATCTACTTAGCATTTA GCATGTTTCCTAAGTGTCCAAATTACATGTTTCACACAAAAATTACCGTCT CTGTCAAGCACTAAAGGTAAATGCTCTTTAACATCAACAGTTACTTCAG**G GCGCGCC**ATAC
e16	No wild-type gBlock ordered; wild-type sequence was obtained by PCR	**GCGTCCTGCAGG**TTAGATGTGCCCAGAGAACGCTTGTTTGCTTTCAGTG CCCCTAAATTACAATTCTTTGTGCACTTCCTGTTTCACAGTTAATGGCTGA GATCTGTGACTCTAGCAACACTGTTGTTTTTCACTCCAGTCCGTTTCTGCT AGAAACTACGCAGCCTGTGTACTGTCTGGAACATGTTGCACGCATGTGCT TTGAGAAGAACAGCATGCATAGCTaACTAATTTCAAAAACAGCCTATTTAT AGTCCTTCAGAGTAATTGTCAGACACTTGGTCTGTGCGCTTTTGCTCACGT CATGTGGATCAACATGGCTTTTTAAATGGAGATAAATTGTTTTTTATGTGT GGGTaATTCATTTGATACTTCTCTATAAATTCATACCCCAACTGTGTCTCTG AAGTaTGTCACTGCAGTAATAGCCCAGGGAGGAGTTTTCAACAATTAGCAT TGGATTCAATATGAGATGGTGCTTTAGAGAA**GGCGCGCC**ATAC
e17	**GCGTCCTGCAGG**CATAATCATTTTGGAAAATTCAGTTTCAGCACAGA GATTTACAAAAGCCCAGCGGATCCTTTTGTCATCCAGCCTAAGTATTTA CCGGGTGCCCTTAGGGTGCCTAATACTGGATGAGACTGCTTTTGTGAG CAAGCCAGCGGGTCCTCAGCCATGAAAATAGAAATTTAATCACTTGCT CATCCAAGCATTTCCCTTCTGCTTCTGCAATATGCTTTTTTTGTGTGTG TGAATGACTAACCAAACGCTACAAAGAGCTTTCAGGTCCGGGCTGAAG ATGCGGGGAGGAGAGATGACTCATCCCTCTGACGTCAGAGCCTCCTTC CTTTCAGAGGCGGAGGAAGAGAGTGGCAAAGGCCTGACAGAAAGGAG AATGACCCAAATGCCCTCCTGAGAACTGTGTGGGTCAGAACTGCTTCC TCCTCCCCCGCCAGGCAAAGATGATTATCACTCAAAGTTTAAACTGTG AAATTTCG**GGCGCGCC**ATAC	**GCGTCCTGCAGG**CATAATCATTTTGGAAAATTCAGTTTCAGCACAGAGA TTTACAAAAGCCCAGCGGATCCTTTTGTCATCCAGCCTAAGTATTTACCGG GTGCCCTTAGGGTGCCTAATACTGGATGAGACTGCTTTTGTGAGCAAGCC AGCGGGTCCTCAGCCATGAAAATAGAAATTTAATCACTTGCTCATCCAAGC ATTTCCCTTCTGCTTCTGCAATATGCTTTTTTTGTGTGTGTaAATaACTAAC CAAACGCTACAAAGAGCTTTCAGGTCCGGGCTGAAGATGCGGGGAGGAG AGATaACTCATCCCTCTGACGTCAGAGCCTCCTTCCTTTCAGAGGCGGAGG AAGAGAGTGGCAAAGGCCTGACAGAAAGGAGAATGACCCAAATGCCCTCC TGAGAACTGTGTGGGTCAGAACTGCTTCCTCCTCCCCCGCCAGGCAAAGA TGATTATaACTCAAAGTTTAAACTGTGAAATTTCG**GGCGCGCCATAC**
e18	**GCGTCCTGCAGG**CTTTATTTGGAATATTTCCGTTTCTTCTGACATTTA GTGAGCCGCTAGAGAAAGCTGATGCGCGTAGCCTGCTGTCTTTTACAT CAGTTATTTAGTGAGTCGAGCAAGAATACATTAGGCCTATTTTTAGCA TGTTCTTTCTTATAAGCGCATCATGAACGTCAGAGAGTCTTAgcagcctcac taatgtgggaagtgaacttgtcagatatcagttcctctgcagggtcaggcttaattgaaacgccgagatg gagataggaaccacactaaagaaaactccaagtgattcaaggagtggtatttataaacctgagtcagc agtgaatcagctctcaagtgggggctcaggggacTGCTTGGTTAAAGCGACAACAAAG CCAAATTGAAGCTGAGCCCGCCCGCCTGGGCTTCTTGTTCGATATCCT GGGTTTTCTCTGGAATTACTGCTGTACCTCTGCAGAAGTCTGAGGAG**G GCGCGCC**ATAC	**GCGTCCTGCAGG**CTTTATTTGGAATATTTCCGTTTCTTCTGACATTTAGT GAGCCGCTAGAGAAAGCTGATGCGCGTAGCCTGCTGTCTTTTACATCAGT TATTTAGTaAGTCGAGCAAGAATACATTAGGCCTATTTTTAGCATGTTCTT TCTTATAAGCGCATCATGAACGTCAGAGAGTCTTAgcagcctcactaatgtgggaagt gaacttgtcagatatcagttcctctgcagggtcaggcttaattgaaacgccgagatggagatagggaaccaca ctaaagaaaactccaagtaattcaaggagtggtatttataaacctaagtcagcagtaaatcagctctcaagtg ggggctcaggggacTGCTTGGTTAAAGCGACAACAAAGCCAAATTGAAGCTGAG CCCGCCCGCCTGGGCTTCTTGTTCGATATCCTGGGTTTTCTCTGGAATTAC TGCTGTACCTCTGCAGAAGTCTGAGGAG**GGCGCGCCATAC**
e28		
e29	**GCGTCCTGCAGG**CAGTGCTAAAAAGCTTACAGAGATTGTCTGGCAA GCACTGAAATATAAAAATTTACTGAAAGCTGAAGACTAATTTAGAAGT GTGTTTTAAAAAGAACTCGTTGCCTAGGCTTTTTGGTGCTACCCATTAA ACAAACAAATGTTGCTAATGTTAAAATGTGATTAGACCTAGTCAAATA GACAAACATCTCTAATGTAACGCATAAGCATTACAGCAAGCACGATGA CACAGAAAGTGAGTCATCTGTGTCTGAGAGATGCCTGGAATTCTGTGA CTCAATGCTCACAATACTATGAAGCTATTTTATGACTCATACAAACATA GCATTCTTCTATGCAAATCAAAATAAAAGGGAATTAATTAATAATGAA AGAAAAAATACAGATCTTATTTCACTCTACTAGAGTTCAACACTGAAAA TTAGGCATTAAAATAGCTAAAAGTCCCTTTAGTAAAATATGGCTTTAAA ACTTAT**GGCGCGCC**ATAC	**GCGTCCTGCAGG**CAGTGCTAAAAAGCTTACAGAGATTGTCTGGCAAGCA CTGAAATATAAAAATTTACTGAAAGCTGAAGACTAATTTAGAAGTGTGTTT TAAAAAGAACTCGTTGCCTAGGCTTTTTGGTGCTACCCATTAAACAAACAA ATGTTGCTAATGTTAAAATGTGATTAGACCTAGTCAAATAGACAAACATCT CTAATGTAACGCATAAGCATTACAGCAAGCACGATaACACAGAAAGTaAGT CATCTGTGTCTGAGAGATGCCTGGAATTCTGTaACTCAATGCTCACAATAC TATGAAGCTATTTTATaACTCATACAAACATAGCATTCTTCTATGCAAATCA AAATAAAAGGGAATTAATTAATAATGAAAGAAAAAATACAGATCTTATTTC ACTCTACTAGAGTTCAACACTGAAAATTAGGCATTAAAATAGCTAAAAGTC CCTTTAGTAAAATATGGCTTTAAAACTTAT**GGCGCGCC**ATAC
e30	**GCGTCCTGCAGG**GCATTGCTACTAGGTGATATAAATGAAATGTCATT TCACTTCACAGAAGGAGCTGCCAGTTATTTTGCATAACAGACCAAGAA TGAAAAGGATCATTTTGTACTGTTAAAGCCTTTGAGAGGAAGTGATCT ATAACATGGAACTGAACAGGAAACTTCTTAAAGCAAGCCTGAGTCACT GCAAGCActcagaaagacagctgtgactcatcacaggtcacccagaggctggggctagagctgga aatagaacacagacctcggcctttttctccccacctacttcctctgACGACTTACATCGATCTG TTGAGTCATGAGACCATAACGTAGTGCAGCTGTTTCCTGAACAGCTTT TCATTAAGGATTTTTGGCTTGTTCTAGTTTACTCAGCAGAAGCAGTACT TACTAAAGAGGCATTGAATTTTTATGCAGTGAACAAAGAAGCTAAGAA ATGCAACAACAGAATTTGCTTACA**GGCGCGCC**ATAC	**GCGTCCTGCAGG**GCATTGCTACTAGGTGATATAAATGAAATGTCATTTC ACTTCACAGAAGGAGCTGCCAGTTATTTTGCATAACAGACCAAGAATGAA AAGGATCATTTTGTACTGTTAAAGCCTTTGAGAGGAAGTGATCTATAACAT GGAACTGAACAGGAAACTTCTTAAAGCAAGCCTaAGTCACTGCAAGCActca gaaagacagctgtaactcatcacaggtcacccagaggctggggctagagctggaaatagaacacagacctc ggccttttctccccacctacttcctctgACGACTTACATCGATCTGTTaAGTCATGAGACC ATAACGTAGTGCAGCTGTTTCCTGAACAGCTTTTCATTAAGGATTTTTGGC TTGTTCTAGTTaACTCAGCAGAAGCAGTACTTACTAAAGAGGCATTGAATT TTTATGCAGTGAACAAAGAAGCTAAGAAATGCAACAACAGAATTTGCTTA CA**GGCGCGCC**ATAC
e31	**GCGTCCTGCAGG**aaaccctgaGACAGCAAGGATTACAAAAATGTCTAAA ATTTTTGGGATCTAGTATTATGATTTTCATCATTCTATAATGTGAACAT ATGTTAAAGTGCTACACTGGACCCATAATTTTAGTAATTACAGCAATAC TTTCTAATTTTAAGTTCAACACATTTTATTTGAATCATCAGAGACTTGT GCCAGAAAGCAAACATCTTAGTTCTTAAATGTGTTCTATCTTTAAAATG TCTTTGCTAATTTAAATAGGAAAAATGTTTAGTTGATTCAATGATTCAG TCGGTGGTAATGATGTAATTCAGTGAATCATAGCTCTCCCTTCTTTCTT CTCACAGTAACTCTAGATTTGATAGTGTTTGAAAATCTTTTGGTTATTT TAAAAAACTCTGAATGAGACATAGAGTTCTGAATTCTAAGGAAAGTAC ACAGCAAGGCGGCACCAAAGGTCTATTCTTCTGTTAAGTAGTAGCAAG **GGCGCGCC**ATAC	**GCGTCCTGCAGG**aaaccctgaGACAGCAAGGATTACAAAAATGTCTAAAAT TTTTGGGATCTAGTATTATGATTTTCATCATTCTATAATGTGAACATATGT TAAAGTGCTACACTGGACCCATAATTTTAGTAATTACAGCAATACTTTCTA ATTTTAAGTTCAACACATTTTATTTaAATCATCAGAGACTTGTGCCAGAAA GCAAACATCTTAGTTCTTAAATGTGTTCTATCTTTAAAATGTCTTTGCTAAT TTAAATAGGAAAAATGTTTAGTTaATTCAATaATTCAGTCGGTGGTAATGA TGTAATTCAGTaAATCATAGCTCTCCCTTCTTTCTTCTCACAGTAACTCTAG ATTTGATAGTGTTTGAAAATCTTTTGGTTATTTTAAAAAACTCTGAATGAG ACATAGAGTTCTGAATTCTAAGGAAAGTACACAGCAAGGCGGCACCAAAG GTCTATTCTTCTGTTAAGTAGTAGCAAG**GGCGCGCC**ATAC

Due to a low quantity of gBlock DNA provided, we also designed primers to PCR amplify the desired sequence from gBlock fragments. These primers are shown in Table 10, with the clamp shown in red, and the SbfI and AscI sites shown in blue.

Table 10: PCR primers to amplify gBlock fragments

Enh	Forward primer (5' → 3')	Reverse primer (5' → 3')
e4	GCGTCCTGCAGGCAGAGAGCTGCCTATGCGTC	GTATGGCGCGCCCTGAAGTAACTGTTGATGTT
e16	GCGTCCTGCAGGTTAGATGTGCCCAGAGAACG	GTATGGCGCGCCTTCTCTAAAGCACCATCTCA
e17	GCGTCCTGCAGGCATAATCATTTTGGAAAATT	GTATGGCGCGCCCGAAATTTCACAGTTTAAAC
e18	GCGTCCTGCAGGCTTTATTTGGAATATTTCCG	GTATGGCGCGCCCTCCTCAGACTTCTGCAGAG
e28	GCGTCCTGCAGGCCATTTCTCTTTCCTCCCCA	GTATGGCGCGCCGGACCCCTACCTCTCACTTT
e29	GCGTCCTGCAGGCAGTGCTAAAAAGCTTACAG	GTATGGCGCGCCATAAGTTTTAAAGCCATATT
e30	GCGTCCTGCAGGGCATTGCTACTAGGTGATAT	GTATGGCGCGCCTGTAAGCAAATTCTGTTGTT
e31	GCGTCCTGCAGGAAACCCTGAGACAGCAAGGA	GTATGGCGCGCCCTTGCTACTACTTAACAGAA

3.5.7.3 Generation and use of the AP1 dominant negative A-Fos

A plasmid containing N-terminal Flag-tagged *A-Fos* (Ahn et al., 1998; Olive et al., 1997) was obtained from Addgene (Plasmid #33353, Addgene). The *A-Fos* gene was PCR amplified and cloned into a custom designed pLenti-GB-hUb-IRES-EGFP lentiviral vector between the human Ubiquitin C promoter and the IRES sequence using AscI and EcoR1 sites. For use in a luciferase assay, the 500ng filler pCS2 DNA was replaced 250ng pCS2, 125 ng empty pLenti-GB-hUb-IRES-EGFP vector, and 125ng *A-Fos*. This was compared to a condition transfected with 250ng pCS2, 250 ng empty pLenti-GB-hUb-IRES-EGFP vector.

3.5.7.4 Nptx2 upstream enhancer truncations

To identify the minimal enhancer element within the Nptx2 upstream enhancer capable of driving stimulus-responsive transcription, we first minimized the Nptx2 reporter to 560bp, removing the regions further outside the H3K27Ac trough and DNAseI hypersensitive site. In an attempt to truncate the *Nptx2* enhancer further, we

sequentially removed about 50bp at a time. We designed eight constructs to clone from the *Nptx2* reporter, the primers for which are listed in Table 11.

Table 11: Primers to truncate the *Nptx2* enhancer to identify the minimal sequence capable of driving stimulus-responsive transcription

	Forward primer (5' -> 3')	Reverse primer (5' -> 3')
NUe560bp	**GCGT**CCTGCAGGTGAAATTCAGCACCGAGGAT	**GTAT**GGCGCGCCTTCTTCCTCACAGCACAGAA
mNUedel1	**gcatgt**CCTGCAGGCCTTGAATTCCGTGCTATTGAGCAC	**gcatgt**GGCGCGCCTTCTTCCTCACAGCACAGAAACCGTCC
mNUedel2	**gcatgt**CCTGCAGGTGGCTAAGAGGGGAGGAAATGC	**gcatgt**GGCGCGCCTTCTTCCTCACAGCACAGAAACCGTCC
mNUedel3	**gcatgt**CCTGCAGGGATAGGTTCTTCTGACATCGTGGTGG	**gcatgt**GGCGCGCCTTCTTCCTCACAGCACAGAAACCGTCC
mNUedel4	**gcatgt**CCTGCAGGTGCATGTGAGAAAGAACCAGGGAGCC	**gcatgt**GGCGCGCCTTCTTCCTCACAGCACAGAAACCGTCC
mNUedel5	**gcatgt**CCTGCAGGTGGAGGTAGAACAGCTCATTAGG	**gcatgt**GGCGCGCCTTCTTCCTCACAGCACAGAAACCGTCC
mNUedel6	**gcatgt**CCTGCAGGGGTTAAGTCTGTACCCGGCTCT	**gcatgt**GGCGCGCCTTCTTCCTCACAGCACAGAAACCGTCC
mNUedel7	**gcatgt**CCTGCAGGGCCGACATAGTGAATGAGTGGG	**gcatgt**GGCGCGCCTTCTTCCTCACAGCACAGAAACCGTCC
mNUedel8	**gcatgt**CCTGCAGGTGAAATTCAGCACCGAGGATAGTTCC	**gcatgt**GGCGCGCCGCGTGCATGACTCACCCTACCCA
NUe180bp	**gcatgt**CCTGCAGGGCCGACATAGTGAATGAGTGGG	**gcatgt**GGCGCGCCGCGTGCATGACTCACCCTACCCA

3.5.7.5 Nptx2 reporter scrambling

To identify the crucial sequences within the minimized *Nptx2* enhancer that contributed to the responsiveness of this enhancer to KCl and BDNF stimulation, we sequentially scrambled ~7-10 bases at a time from an already minimized reporter. As before, we designed genomic blocks (gBlocks Gene Fragments, IDT) containing the scrambled mutations that we used as PCR templates. gBlocks were PCR amplified using a common forward primer (5' ttcctggcttgtagtgacct 3') and a common reverse primer (5' agcaagccttgttgtttctg 3'). The gBlocks are shown in Table 12.

Table 12: gBlock sequences synthesized to comprehensively scramble the minimal *Nptx2* enhancer

Name	primer/gBlock
5_mNUeSCRATtoCG-9--1	ttcctggcttgtagtgacctGCGTCCTGCAGGTAATCACGCGTGAATGAGTGGGTGGTTACTATGCTGTTGCACCGGTTACACTAAGAGATTAGGTGGCAGTG ATTCACTGCTGCAGATCTGCACGACTTTCTCAAGTAGCAGAAAAATCTGTGGGCCCTGGGCTCTGTCACTCGCACAGCCCTTCTCATGGGTAGGGT GAGTCATGCACGCAGGATCTTTCAGGTGGACGGTTTCTGTGCTGTGAGGAAGAAGGCGCGCCATACcagaaacaacaaggcttgct
6_mNUeSCRATtoCG1-9	ttcctggcttgtagtgacctGCGTCCTGCAGGGCCGACATATGTCCGTCTTGGGTGGTTACTATGCTGTTGCACCGGTTACACTAAGAGATTAGGTGGCAGTG ATTCACTGCTGCAGATCTGCACGACTTTCTCAAGTAGCAGAAAAATCTGTGGGCCCTGGGCTCTGTCACTCGCACAGCCCTTCTCATGGGTAGGGT GAGTCATGCACGCAGGATCTTTCAGGTGGACGGTTTCTGTGCTGTGAGGAAGAAGGCGCGCCATACcagaaacaacaaggcttgct
7_mNUeSCRATtoCG10-19	ttcctggcttgtagtgacctGCGTCCTGCAGGGCCGACATAGTGAATGAGGTTTGTTGGCCTATGCTGTTGCACCGGTTACACTAAGAGATTAGGTGGCAGTG ATTCACTGCTGCAGATCTGCACGACTTTCTCAAGTAGCAGAAAAATCTGTGGGCCCTGGGCTCTGTCACTCGCACAGCCCTTCTCATGGGTAGGGT GAGTCATGCACGCAGGATCTTTCAGGTGGACGGTTTCTGTGCTGTGAGGAAGAAGGCGCGCCATACcagaaacaacaaggcttgct
8_mNUeSCRATtoCG20-29	ttcctggcttgtagtgacctGCGTCCTGCAGGGCCGACATAGTGAATGAGTGGGTGGTTAAGCGTAGTGGGCACCGGTTACACTAAGAGATTAGGTGGCAGT GATTCACTGCTGCAGATCTGCACGACTTTCTCAAGTAGCAGAAAAATCTGTGGGCCCTGGGCTCTGTCACTCGCACAGCCCTTCTCATGGGTAGG GTGAGTCATGCACGCAGGATCTTTCAGGTGGACGGTTTCTGTGCTGTGAGGAAGAAGGCGCGCCATACcagaaacaacaaggcttgct
9_mNUeSCRATtoCG30-39	ttcctggcttgtagtgacctGCGTCCTGCAGGGCCGACATAGTGAATGAGTGGGTGGTTACTATGCTGTTTACAATTGGCCACTAAGAGATTAGGTGGCAGTG ATTCACTGCTGCAGATCTGCACGACTTTCTCAAGTAGCAGAAAAATCTGTGGGCCCTGGGCTCTGTCACTCGCACAGCCCTTCTCATGGGTAGGGT GAGTCATGCACGCAGGATCTTTCAGGTGGACGGTTTCTGTGCTGTGAGGAAGAAGGCGCGCCATACcagaaacaacaaggcttgct
10_mNUeSCRATtoCG40-49	ttcctggcttgtagtgacctGCGTCCTGCAGGGCCGACATAGTGAATGAGTGGGTGGTTACTATGCTGTTGCACCGGTTAACAGCCTCTCTTAGGTGGCAGTG ATTCACTGCTGCAGATCTGCACGACTTTCTCAAGTAGCAGAAAAATCTGTGGGCCCTGGGCTCTGTCACTCGCACAGCCCTTCTCATGGGTAGGGT GAGTCATGCACGCAGGATCTTTCAGGTGGACGGTTTCTGTGCTGTGAGGAAGAAGGCGCGCCATACcagaaacaacaaggcttgct
11_mNUeSCRATtoCG50-59	ttcctggcttgtagtgacctGCGTCCTGCAGGGCCGACATAGTGAATGAGTGGGTGGTTACTATGCTGTTGCACCGGTTACACTAAGAGAGGCTTGTTACGTG ATTCACTGCTGCAGATCTGCACGACTTTCTCAAGTAGCAGAAAAATCTGTGGGCCCTGGGCTCTGTCACTCGCACAGCCCTTCTCATGGGTAGGGT GAGTCATGCACGCAGGATCTTTCAGGTGGACGGTTTCTGTGCTGTGAGGAAGAAGGCGCGCCATACcagaaacaacaaggcttgct
12_mNUeSCRATtoCG60-68	ttcctggcttgtagtgacctGCGTCCTGCAGGGCCGACATAGTGAATGAGTGGGTGGTTACTATGCTGTTGCACCGGTTACACTAAGAGATTAGGTGGCATGT CGGACATGCTGCAGATCTGCACGACTTTCTCAAGTAGCAGAAAAATCTGTGGGCCCTGGGCTCTGTCACTCGCACAGCCCTTCTCATGGGTAGGG TGAGTCATGCACGCAGGATCTTTCAGGTGGACGGTTTCTGTGCTGTGAGGAAGAAGGCGCGCCATACcagaaacaacaaggcttgct
13_mNUeSCRATtoCG69-80	ttcctggcttgtagtgacctGCGTCCTGCAGGGCCGACATAGTGAATGAGTGGGTGGTTACTATGCTGTTGCACCGGTTACACTAAGAGATTAGGTGGCAGTG ATTCACGTAGTACTCGAGGCACGACTTTCTCAAGTAGCAGAAAAATCTGTGGGCCCTGGGCTCTGTCACTCGCACAGCCCTTCTCATGGGTAGGG TGAGTCATGCACGCAGGATCTTTCAGGTGGACGGTTTCTGTGCTGTGAGGAAGAAGGCGCGCCATACcagaaacaacaaggcttgct
14_mNUeSCRATtoCG81-87	ttcctggcttgtagtgacctGCGTCCTGCAGGGCCGACATAGTGAATGAGTGGGTGGTTACTATGCTGTTGCACCGGTTACACTAAGAGATTAGGTGGCAGTG ATTCACTGCTGCAGATCTTACATCATTTCTCAAGTAGCAGAAAAATCTGTGGGCCCTGGGCTCTGTCACTCGCACAGCCCTTCTCATGGGTAGGGT GAGTCATGCACGCAGGATCTTTCAGGTGGACGGTTTCTGTGCTGTGAGGAAGAAGGCGCGCCATACcagaaacaacaaggcttgct
15_mNUeSCRATtoCG88-97	ttcctggcttgtagtgacctGCGTCCTGCAGGGCCGACATAGTGAATGAGTGGGTGGTTACTATGCTGTTGCACCGGTTACACTAAGAGATTAGGTGGCAGTG ATTCACTGCTGCAGATCTGCACGACGGGAGACCTGAGCAGAAAAATCTGTGGGCCCTGGGCTCTGTCACTCGCACAGCCCTTCTCATGGGTAGGG TGAGTCATGCACGCAGGATCTTTCAGGTGGACGGTTTCTGTGCTGTGAGGAAGAAGGCGCGCCATACcagaaacaacaaggcttgct
16_mNUeSCRATtoCG98-107	ttcctggcttgtagtgacctGCGTCCTGCAGGGCCGACATAGTGAATGAGTGGGTGGTTACTATGCTGTTGCACCGGTTACACTAAGAGATTAGGTGGCAGTG ATTCACTGCTGCAGATCTGCACGACTTTCTCAAGTCTACTCCCCCTCTGTGGGCCCTGGGCTCTGTCACTCGCACAGCCCTTCTCATGGGTAGGGT GAGTCATGCACGCAGGATCTTTCAGGTGGACGGTTTCTGTGCTGTGAGGAAGAAGGCGCGCCATACcagaaacaacaaggcttgct
17_mNUeSCRATtoCG108-117	ttcctggcttgtagtgacctGCGTCCTGCAGGGCCGACATAGTGAATGAGTGGGTGGTTACTATGCTGTTGCACCGGTTACACTAAGAGATTAGGTGGCAGTG ATTCACTGCTGCAGATCTGCACGACTTTCTCAAGTAGCAGAAAAAGAGTGTTTAACTGGGCTCTGTCACTCGCACAGCCCTTCTCATGGGTAGGG TGAGTCATGCACGCAGGATCTTTCAGGTGGACGGTTTCTGTGCTGTGAGGAAGAAGGCGCGCCATACcagaaacaacaaggcttgct
18_mNUeSCRATtoCG118-127	ttcctggcttgtagtgacctGCGTCCTGCAGGGCCGACATAGTGAATGAGTGGGTGGTTACTATGCTGTTGCACCGGTTACACTAAGAGATTAGGTGGCAGTG ATTCACTGCTGCAGATCTGCACGACTTTCTCAAGTAGCAGAAAAATCTGTGGGCCAGTTTAGAGTTCACTCGCACAGCCCTTCTCATGGGTAGGG TGAGTCATGCACGCAGGATCTTTCAGGTGGACGGTTTCTGTGCTGTGAGGAAGAAGGCGCGCCATACcagaaacaacaaggcttgct
19_mNUeSCRATtoCG128-137	ttcctggcttgtagtgacctGCGTCCTGCAGGGCCGACATAGTGAATGAGTGGGTGGTTACTATGCTGTTGCACCGGTTACACTAAGAGATTAGGTGGCAGTG ATTCACTGCTGCAGATCTGCACGACTTTCTCAAGTAGCAGAAAAATCTGTGGGCCCTGGGCTCTGGACAGATACAAGCCCTTCTCATGGGTAGGG TGAGTCATGCACGCAGGATCTTTCAGGTGGACGGTTTCTGTGCTGTGAGGAAGAAGGCGCGCCATACcagaaacaacaaggcttgct
20_mNUeSCRATtoCG138-147	ttcctggcttgtagtgacctGCGTCCTGCAGGGCCGACATAGTGAATGAGTGGGTGGTTACTATGCTGTTGCACCGGTTACACTAAGAGATTAGGTGGCAGTG ATTCACTGCTGCAGATCTGCACGACTTTCTCAAGTAGCAGAAAAATCTGTGGGCCCTGGGCTCTGTCACTCGCACCTAAAGGAGAATGGGTAGGG TGAGTCATGCACGCAGGATCTTTCAGGTGGACGGTTTCTGTGCTGTGAGGAAGAAGGCGCGCCATACcagaaacaacaaggcttgct
21_mNUeSCRATtoCG148-156	ttcctggcttgtagtgacctGCGTCCTGCAGGGCCGACATAGTGAATGAGTGGGTGGTTACTATGCTGTTGCACCGGTTACACTAAGAGATTAGGTGGCAGTG ATTCACTGCTGCAGATCTGCACGACTTTCTCAAGTAGCAGAAAAATCTGTGGGCCCTGGGCTCTGTCACTCGCACAGCCCTTCTCCGTTTGCTTGT GAGTCATGCACGCAGGATCTTTCAGGTGGACGGTTTCTGTGCTGTGAGGAAGAAGGCGCGCCATACcagaaacaacaaggcttgct
22_mNUeSCRATtoCG157-165	ttcctggcttgtagtgacctGCGTCCTGCAGGGCCGACATAGTGAATGAGTGGGTGGTTACTATGCTGTTGCACCGGTTACACTAAGAGATTAGGTGGCAGTG ATTCACTGCTGCAGATCTGCACGACTTTCTCAAGTAGCAGAAAAATCTGTGGGCCCTGGGCTCTGTCACTCGCACAGCCCTTCTCATGGGTAGGTG TCTGACGGCACGCAGGATCTTTCAGGTGGACGGTTTCTGTGCTGTGAGGAAGAAGGCGCGCCATACcagaaacaacaaggcttgct
23_mNUeSCRATtoCG166-175	ttcctggcttgtagtgacctGCGTCCTGCAGGGCCGACATAGTGAATGAGTGGGTGGTTACTATGCTGTTGCACCGGTTACACTAAGAGATTAGGTGGCAGTG ATTCACTGCTGCAGATCTGCACGACTTTCTCAAGTAGCAGAAAAATCTGTGGGCCCTGGGCTCTGTCACTCGCACAGCCCTTCTCATGGGTAGGGT GAGTCATTACATACTTCTCTTTCAGGTGGACGGTTTCTGTGCTGTGAGGAAGAAGGCGCGCCATACcagaaacaacaaggcttgct
24_mNUeSCRATtoCG176-185	ttcctggcttgtagtgacctGCGTCCTGCAGGGCCGACATAGTGAATGAGTGGGTGGTTACTATGCTGTTGCACCGGTTACACTAAGAGATTAGGTGGCAGTG ATTCACTGCTGCAGATCTGCACGACTTTCTCAAGTAGCAGAAAAATCTGTGGGCCCTGGGCTCTGTCACTCGCACAGCCCTTCTCATGGGTAGGGT GAGTCATGCACGCAGGAGAGGGACTTGGGACGGTTTCTGTGCTGTGAGGAAGAAGGCGCGCCATACcagaaacaacaaggcttgct
25_mNUeSCRATtoCG186-195	ttcctggcttgtagtgacctGCGTCCTGCAGGGCCGACATAGTGAATGAGTGGGTGGTTACTATGCTGTTGCACCGGTTACACTAAGAGATTAGGTGGCAGTG ATTCACTGCTGCAGATCTGCACGACTTTCTCAAGTAGCAGAAAAATCTGTGGGCCCTGGGCTCTGTCACTCGCACAGCCCTTCTCATGGGTAGGGT GAGTCATGCACGCAGGATCTTTCAGGTTTCATTGGGATGTGCTGTGAGGAAGAAGGCGCGCCATACcagaaacaacaaggcttgct
26_mNUeSCRATtoCG196-212	ttcctggcttgtagtgacctGCGTCCTGCAGGGCCGACATAGTGAATGAGTGGGTGGTTACTATGCTGTTGCACCGGTTACACTAAGAGATTAGGTGGCAGTG ATTCACTGCTGCAGATCTGCACGACTTTCTCAAGTAGCAGAAAAATCTGTGGGCCCTGGGCTCTGTCACTCGCACAGCCCTTCTCATGGGTAGGGT GAGTCATGCACGCAGGATCTTTCAGGTGGACGGTTTCGTGTAGTGTCTTCCTCCGGCGCGCCATACcagaaacaacaaggcttgct

3.5.7.6 Mutating AP1 motifs within the Nptx2 enhancer

We observed four AP1 motifs within the full-length 1216bp *Nptx2* enhancer. Using PCR driven overlap extension (Heckman and Pease, 2007), we sequentially mutated the second base pair of each AP1 motif with a mutation (TGAGTCA→TAAGTCA) that has been previously shown to abrogate the binding of AP1 (Risse et al., 1989). In order to do this, the primers shown in Table 13 were used (A, B, C, D nomenclature same as described in (Heckman and Pease, 2007)), with 5' clamp shown in red.

Table 13: Primers to subtly mutate each AP1 motif present within the sequence of the *Nptx2* enhancer

Primer	Sequence (5' → 3')
A	5' GCGTCCTGCAGGCAGAAACAACAAGGCTTGCT 3'
D	5' GTATGGCGCGCCTACTAGCTAAGTGGTTTGGG 3'
AP1 #1 B	CTTCCTGCAAACA**TGACTTA**GGAACTATCCTCGGTGCTGA
AP1 #1 C	CGAGGATAGTTCC**TAAGTCA**TGTTTGCAGGAAGCTGTCCT
AP1 #2 B	GATCCTGCGTGCA**TGACTTA**CCCTACCCATGAGAAGGGCT
AP1 #2 C	CTCATGGGTAGGG**TAAGTCA**TGCACGCAGGATCTTTCAGG
AP1 #3 B	AGATCTGCAGCAG**TGAATTA**CTGCCACCTAATCTCTTAGT
AP1 #3 C	GATTAGGTGGCAG**TAATTCA**CTGCTGCAGATCTGCACGAC
AP1 #4 B	CCAGCCGACATAG**TAAATGA**GTGGGTGGTTACTATGCTGT
AP1 #4 C	AGTAACCACCCAC**TCATTTA**CTATGTCGGCTGGTCCCGGG

3.5.7.7 Mutating the NPAS4 motif within the Nptx2 reporter

Using PCR driven overlap extension (Heckman and Pease, 2007), we deleted a putative NPAS4 binding site located directly under the ChIP-Seq peak. In order to do this, the primers shown in Table 14 were used (A, B, C, D nomenclature same as described in (Heckman and Pease, 2007)), with 5' clamp shown in red.

Table 14: Primers used to delete NPAS4 motif from *Nptx2* enhancer

Primer	Sequence (5' → 3')
A	5' GCGTCCTGCAGGCAGAAACAACAAGGCTTGCT 3'
B	5' TTTTCTGCTACTTGAGAAAGCAGATCTGCAGCAGTGAATC 3'
C	5' GATTCACTGCTGCAGATCTGCTTTCTCAAGTAGCAGAAAA 3'
D	5' GTATGGCGCGCCTACTAGCTAAGTGGTTTGGG 3'

3.5.7.8 Transfection

Mouse cortical neurons plated on 24 well plates at a density of approximately $3x10^5$ neurons per well were transfected for luciferase reporter assays using Lipofectamine 2000 Reagent (Invitrogen), generally according to the manufacter's protocol. Briefly, DNA mixes were made immediately preceding the transfection consisting of 1ug total plasmid DNA/well diluted in Neurobasal medium (Life Technologies). DNA typically consisted of 450ng firefly luciferase reporter DNA, 50ng pGL4.74 renilla luciferase reporter DNA (Promega), and 500ng empty pCS2 plasmid (Rupp et al., 1994; Turner and Weintraub, 1994) as filler DNA. Lipofectamine was used at 2uL/well and was diluted in Neurobasal medium just before the transfection. Within each experiment, all conditions were transfected in two to three independent wells, for technical duplicates or triplicates. Thirty minutes prior to the addition of Lipofectamine to neurons, the culture medium was removed and replaced with warmed Neurobasal medium. At this time, neurons were returned to the incubator and DNA mixes were added to diluted Lipofectamine in a drop-wise manner. After thirty minutes of incubation, DNA-Lipofectamine mixes were added to neurons, again in a drop-wise manner. The cells were left to incubate with the DNA-Lipofectamine mix for two hours, after which the transfection medium was replaced with supplemented conditioned neuronal medium.

3.5.7.9 Sample collection and luciferase assay

After stimulation, neurons were lysed using Passive Lysis Buffer (Dual-Luciferase Reporter Assay System, Promega). Lysates were then collected in microcentrifuge tubes and frozen at -20 degrees C. At the time of performing the luciferase assay, neuronal lysates were thawed, briefly vortexed, briefly spun down, and then 20uL of each sample was added to one well of Costar White Polystyrene 96-well Assay Plates (Corning). The reagents to run the luciferase assay, Luciferase Assay Reagent II (LARII) and Stop & Glo Reagent (Dual-Luciferase Reporter Assay System, Promega), were aliquoted and thawed according to the manufacturer's protocol. The luciferase assay was performed using the Synergy 4 Hybrid Microplate Reader (BioTek), with 100uL of LARII and Stop & Glo Reagent injected per well. Data was subsequently downloaded and analyzed using Microsoft Excel.

3.5.7.10 Statistical Analyses of Luciferase Assay Data

Using the Dual-Luciferase Reporter Assay System, we recorded *Firefly (FF)* and *Renilla (Ren)* luminescence from each well. To correct for variations in transfection efficiency and cell lysate generation, the *Firefly* values were normalized to *Renilla* luminescence within each well, generating a ratio of *FF/Ren*. The stimulus-dependent fold induction of each reporter plasmid was obtained by dividing the (+ stimulus) *FF/Ren* value by the (- stimulus) value. To isolate the induction due to the enhancer, the fold induction of an enhancer reporter was divided by the fold induction of the appropriate backbone into which the enhancer was cloned, giving fold induction relative to backbone. Fold induction relative to backbone is the value shown in all figures

containing luciferase reporter data. All error bars shown are standard error of biological replicates.

3.5.8 DNA Microarrays and data analysis

For all microarray experiments, total RNA was purified using RNeasy mini kits (Qiagen). Ten micrograms of RNA was hybridized to Affymetrix Mouse Genome 430 2.0 Array with Affymetrix processing. To identify activity-regulated genes regulated by C-FOS, mouse cortical neurons were cultured for 5 days, infected with lentivirus expressing control or c-Fos RNAi, and then depolarized with mM KCl for 0, 1, 3, or 6 hours. Two microarray bioreplicates were performed for all conditions. The DNA-Chip (dChip) software package (Li and Wong, 2001) was used to analyze the microarray data. Genes were considered C-FOS targets if they met the following criteria: (1) the gene was present and expressed at a level of at least 250 at at least one of the timepoints in both bioreplicates of the experiment, (2) there was at least a 3-fold induction of the gene relative to the 0 hour timepoint, (3) there was at least a 1.75 fold reduction in the induction of the gene with c-Fos RNAi compared to control RNAi.

3.5.9 *de novo* motif analysis

For de novo motif analysis, MEME (Bailey and Elkan, 1994) was used to analyze the 200 bps surrounding enhancer centers. The following parameters were used: -dna -mod anr -nmotifs 15 -minw 5 -maxw 10 -revcomp.

4 GENERAL DISCUSSION

The work presented in this thesis advances our understanding of stimulus responsive enhancers in the nervous system. By discovering that H3K27Ac changes rapidly at neuronal enhancers, and that stimulus-dependent increases in H3K27Ac at neuronal enhancers can be used to identify enhancers that function to promoter stimulus-responsive transcription, we now have a much more accurate picture of the enhancers that respond to stimuli. We used the dynamic chromatin signature of stimulus-inducible H3K27Ac to identify and characterize neuronal enhancers that respond to neuronal activity (modeled *in vitro* by the application of KCl) as well as neuronal enhancers that respond to BDNF. We now know that neuronal enhancers can respond to specific stimuli or to multiple stimuli and that activity and BDNF responsive enhancers are linked to genes with distinct functions. We also know that the function of neuronal stimulus responsive enhancers appears to be intrinsic to the DNA sequence of these enhancers. Because of this, understanding the sequences that give rise to stimulus responsiveness of enhancers should be computationally and experimentally tractable. We have begun to understand the sequence determinants of stimulus responsive enhancers by performing *de novo* motif finding and studying the function of neuronal stimulus responsive enhancers in luciferase reporter assays *in vitro*, a system in which stimulus-responsive enhancer function can be effectively recapitulated. These approaches have shown that AP1 transcription factors play a critical role in the function of a subset of stimulus-responsive enhancers. One enhancer context in which AP1 is required is the enhancer upstream of the neuronal stimulus-regulated gene *Nptx2*. We

have begun to understand the sequence determinants underlying the *Nptx2* enhancer. This work has revealed the critical importance of AP1 for the KCl and BDNF-dependent responses of this enhancer, but has also revealed that AP1 is insufficient to drive the responses of this enhancer to either KCl or BDNF. At the *Nptx2* enhancer, both AP1 and NPAS4 are required for responses to neuronal activity, but these two factors are still insufficient to drive activity-dependent responses from the *Nptx2* enhancer. Further work will be required to understand the additional factors that collaborate with AP1 and NPAS4 to drive responses to activity, and the factors that collaborate with AP1 to drive responses to BDNF. These advances in our understanding of stimulus-responsive enhancers in the nervous system were possible because of the approaches that we employed to study this biology. However, there are limitations to the experiments we have performed and conclusions we are able to draw from these experiments. We would like to discuss some of the advantages and limitations of the methods we have used to study stimulus-responsive transcription in the nervous system.

4.1 ADVANTAGES AND LIMITATIONS OF THE EXPERIMENTS PERFORMED IN THIS THESIS

4.1.1 *In vitro* studies

4.1.1.1 Advantages of in vitro studies

While all of the work described in this thesis has been performed in primary mouse cortical neurons, all experiments have been done using these neurons *in vitro*. Studying neuronal stimulus-responsive transcriptional regulation *in vitro* has several advantages. First, neurons from a single source can be plated onto multiple cell culture dishes that can be treated differently and then compared with one another. In studying stimulus-responsive transcription, this is of critical importance. All stimulus-responsive phenomena require the comparison of a stimulated state with an unstimulated state. To isolate the effects of the stimulus, stimulated and unstimulated cells need to be as similar to one another as possible. In practice, the only way for this to be achieved is through *in vitro* experiments. In experiments that I did not describe in this thesis, I have characterized stimulus-responsive transcription *in vivo* using kainic acid-induced seizures in mice. All experiments were performed on mice from a pure C57BL/6 genetic background that were litter-mates born and raised to the time of the experiment in the same cage. Despite their identical genetic background and identical environment from birth, these mice exhibited significant variability in the levels of immediate-early gene protein products (such as CFOS, FOSB, JUNB, and NPAS4) induced in response to seizure, assessed by western blot. This could be due to differences between the mice,

such as differences is nourishment and development. It is often observed that some mice within a litter are larger and better nourished than others. Alternatively, differences in the inducibility of immediate early genes could be due to differences in the stimulation of different mice. This brings me to the second major advantage of studying neuronal stimulus-responsive transcription *in vitro*: the ability to uniformly and reproducibly stimulate cells.

Stimulating neurons *in vitro* by adding the stimulus directly to the neuronal cell culture medium allows for uniform and reproducible stimulation. In contrast, stimulating mice to study neuronal stimulus-responsive transcription *in vivo* is extremely challenging. To study robust transcriptional responses, we and others have employed kainic acid induced seizures in juvenile or adult mice. However, the delivery of kainate by subcutaneous injections, is inherently variable. The site of injection, the depth of injection, the volume of injected liquid that remains within the animal, can all vary considerably and lead to significant differences in the level of seizure induced in the animal. After subcutaneous kainate injections, some mice begin to visibly seize after 10 minutes, other mice begin to seize after 30 minutes, and some mice never display visible seizure-related behaviors. This variability contributes to variability in seizure induced transcriptional programs activated in the nervous system, thus making it extremely difficult to achieve reproducible results. This challenge in achieving reproducible stimulation brings me to the third major advantage of studying neuronal stimulus-responsive transcription *in vitro*: the ability to perform and compare experimental manipulations with one another.

In vitro neuronal cultures can be easily experimentally manipulated to study mechanisms underlying stimulus-responsive transcription. By employing lentivirus containing shRNA to knockdown particular protein products, or cDNAs to overexpress particular protein products, the role of candidate proteins in stimulus-responsive transcription can be studied. In this thesis, we have begun using these tools to understand the role of AP1 transcription factors in neuronal stimulus-responsive transcription. While methods exist to study gene function *in vivo* (such as the generation of transgenic mouse lines, in utero electroporation of knockdown or overexpressing plasmids, or stereotactic viral injections), these methods are more challenging and time consuming than *in vitro* approaches. Furthermore, the inability to consistently and reproducibly stimulate animals *in vivo* becomes a major issue. For example, if a gene is knocked down via virally delivered shRNA in one animal *in vivo*, the relevant control is another animal that has been infected with a control shRNA. However, if these two animals cannot be similarly stimulated *in vivo*, the control animal differs from the experimental animal, and the effects of the knockdown cannot be rigorously assessed.

4.1.1.2 Limitations of in vitro studies

While there are many advantages of employing an *in vitro* approach to study stimulus responsive transcription within the nervous system, as detailed above, there are also important limitations to this approach. While *in vitro* neuronal cultures recapitulate many aspects of neuronal biology, including stimulus-responsive transcription, this is clearly an artificial system. Normally neurons form and maintain precise synaptic contacts with other neurons, and precise cellular contacts with glial

cells, through a carefully orchestrated process of development within the three dimensional environment of a brain that is nourished by blood and cerebrospinal fluid. In contrast, when neurons are cultured in vitro, they are stripped of their synaptic and cellular contacts through harsh trituration, plated on a two dimensional plastic surface, and grown in culture medium in an incubator. This artificiality *in vitro* will cause differences in neuronal function compared to *in vivo*. As a result, any phenomenon observed *in vitro* should be demonstrated *in vivo* in to ensure that it is not a artifact of the *in vitro* system.

Another disadvantage of *in vitro* studies of stimulus responsive transcription is that there is no way to physiologically stimulate cells *in vitro*. Normally, the brain is activated by sensory experience which in turn activates specific neural circuits within the brain. When studying cortical neurons *in vitro*, not only are there no sensory inputs to speak of, neural circuits and synaptic connectivity are completely disorganized. As a result, any stimulation of neurons in vitro is artificial. We have utilized the extracellular potassium chloride (KCl) to depolarize neurons and mimic neuronal activity. While KCl does depolarize neurons, it does so by depolarizing the neuronal membrane as a whole rather than by activating neurotransmitter gated ion channels at synapses as occurs in vivo. Hence, KCl is an artificial stimulus of neurons grown in an artificial system. Nonetheless, KCl has proved to be a useful discovery tool for many activity-dependent phenomena that have been recapitulated *in vivo* with physiological stimuli.

4.1.2 Chromatin immunoprecipitation (ChIP)

4.1.2.1 Advantages of ChIP

ChIP has emerged as one of the most powerful tools available to survey transcription factor binding and chromatin modifications in the genome. ChIP enables transcription factor binding and chromatin modifications to be assessed in vivo. When combined with high throughput sequencing, ChIP enables genome-wide assessments of transcription factor binding events and chromatin modifications. Furthermore, ChIP is a relatively simple assay that can be easily scaled to investigate multiple proteins of histone modifications simultaneously.

4.1.2.2 Limitations of ChIP

While ChIP has significant advantages, it also has limitations that need to be kept in mind. First of all, ChIP is normally performed under crosslinking conditions to maintain protein-DNA interactions through the experiment. Crosslinking can introduce artifacts causing a locus within the genome to appear artificially enriched for certain transcription factor binding events or chromatin modifications, when it is only in proximity to a locus truly exhibiting these features. ChIP also relies on antibodies that recognize the desired epitope within the cell. All antibodies bind nonspecifically to proteins within the cell, as any silver stain of an immunoprecipitation will demonstrate. Hence, it is not always clear if a signal in a ChIP experiment is due to the immunoprecipitation of the desired epitope or of another protein. For these reasons, it is preferable to utilize multiple pieces of evidence to confirm a result by ChIP. In the

case of ChIP for transcription factors, it can be useful to assess whether known motifs for the transcription factor are enriched underneath ChIP signal and if the signal is specific to the protein of interest by performing ChIP using the same antibody in cells in which that protein has been knocked down or knocked out. We have utilized both motif enrichment and ChIP from shRNA infected cells to increase our confidence in our ChIP results for C-FOS and FOSB in this work.

Another limitation of ChIP is the fact that it is a biochemical assay that provides the average signal over millions of cells (ChIP experiments done for the work described in this thesis were done with 20 million neurons). As a result ChIP does not provide information about the variability that may exist between cells processed together or at the two alleles of each locus within a cell. If the two alleles of a locus vary in sequence, allele specificity can be studied using high throughput sequencing.

Finally, ChIP, in particular ChIP-SEQ, is a variable assay. It is essential that bioreplicates be performed to ensure that a given peak or region of enrichment is reproducible. We have performed multiple bioreplicates of our H3K27Ac and transcription factor ChIP experiments in this work.

4.1.3 Luciferase reporter assays

4.1.3.1 Advantages of luciferase reporter assays

Luciferase reporter assays provide several advantages for studying gene expression and the function of DNA sequences. Luciferase reporter assays provide high sensitivity, a wide dynamic range, and easy methodology. Furthermore, luciferase

reporter assays enable direct investigations into the function of sequences of regulatory DNA, unlike studies of endogenous gene expression. Finally, since luciferase reporter plasmids can be delivered to cells via transfection or infection, luciferase reporter assays enable signaling to DNA sequences to be studied in the context of the cell and its environment. In comparison, studies of transcription using reconstituted systems in vitro do not enable one to study transcriptional regulation in the context of normal cellular signaling.

4.1.3.2 Limitations of luciferase reporter assays

While luciferase reporter assays offer several advantages, these assays are artificial. DNA cloned into a plasmid is very different than DNA that exists within the cell as part of chromatin. In the cell, modifications of chromatin during development instruct programs of gene expression. Luciferase plasmids lack the normal chromatin structure of cellular DNA and as a result lack this important regulatory component. As a result, DNA sequences that are normally not available for transcription actor binding can be exposed in luciferase reporters causing ectopic activity to be observed from a DNA sequence. As a result, luciferase data alone should not be taken to indicate activity in the context of the cell. In the case of our work, we couple luciferase reporter assays with ChIP-Seq data obtained *in vivo* to increase our confidence in our findings. It is only because the stimulus-responsive enhancers we have identified exhibit both increasing H3K27Ac within the neuron as well as the ability to drive stimulus responsive reporter expression within a plasmid that we take these enhancers to promote stimulus-responsive gene expression with the neuron. Still, luciferase reporter assays do not inform us of endogenous gene expression directly. For example, while many of the

enhancers cloned in this work are active in luciferase reporter assays, we still do not know which genes within the cell these enhancers may regulate. Further studies will be required to understand the specific contributions of the stimulus responsive enhancers we have identified to stimulus-responsive transcription within the neuron.

4.2 FUTURE DIRECTIONS

The work I have performed for my thesis has advanced our understanding of stimulus-responsive enhancers in the nervous system. It is bittersweet that my work has opened more questions than it has answered. It is sweet because I take this as an indication that these findings will have importance for developing further understanding of this biology. However, it is also bitter because I will not be able to myself continue performing these experiments to find out the answers. Hopefully others will be motivated to do so! Here, I outline the most interesting future directions that I see from this point that I would pursue if I could have more time in the laboratory.

4.2.1 Demonstrating stimulus-inducible H3K27Ac in the nervous system *in vivo*

As mentioned above, there are limitations to the findings we have obtained from our experiments *in vitro*. It will be important to determine whether we detect changes in H3K27Ac in the nervous system in vivo. This can be done using strong, artificial stimuli such as kainic acid induced seizures, or using more physiological stimuli, such as enriched environment or light exposure after dark rearing. Investigating stimulus-inducible H3K27Ac in vivo also opens the door to the exciting possibility of identifying and studying enhancers that are activated *in vivo* in response to specific stimuli or within particular brain regions.

4.2.2 Performing H3K27Ac at different time points after stimulation

As mentioned earlier in the thesis, multiple waves of transcription occur in response to extracellular stimulation. A first wave of transcription mediated by pre-existing transcription factors within the cell (such as CREB, MEF2, and SRF) occurs rapidly. Among the genes expressed in this first wave of transcription are transcription factors (such as C-FOS, FOSB, JUNB, and NPAS4) that activate a subsequent wave of transcription. In this work, we have only investigated H3K27Ac at 0 hours or 2 hours after sustained stimulation. It could be interesting to perform H3K27Ac ChIP-Seq at several additional time points after sustained stimulation or a brief pulse of stimulation. Such experiments may demonstrate that some enhancers exhibit inducible H3K27Ac early after a stimulus, while other enhancers may exhibit inducible H3K27Ac later after a stimulus. Such a finding may enable us to distinguish the enhancers that function to promote the first wave of transcription from those that promote the second wave of transcription, and study these two classes of enhancers separately. We have observed that only a subset of neuronal stimulus-responsive enhancers are bound by AP1 transcription factors and appear sensitive to the AP1 dominant negative *A-Fos*. It is possible that enhancers mediating the first wave of transcription do not require AP1 while enhancers mediating the second wave of transcription do require AP1. These interesting possibilities can only be explored if better temporal resolution of changes in H3K27Ac after stimulation is achieved. It may be the case that stimulus-responsive enhancers exhibit even greater diversity of responses than just early and late inducibility. Some enhancers may be activated transiently while others may exhibit longer lasting activity after a stimulus. Performing H3K27Ac ChIP-Seq at additional time points will

not only reveal if this is the case but will also enable us to begin understanding the sequences and transcription factors that give rise to diverse temporal responses from enhancers.

4.2.3 Better understanding the mechanisms underlying stimulus-responsive enhancers

While we have shown that AP1 plays critical roles at a subset of activity and BDNF responsive neuronal enhancers, the exact contribution of AP1 to enhancer function is not clear. Whether AP1 binding is necessary for recruitment of other transcription factors, recruitment of CBP/P300, activation of CBP/P300, deposition of H3K27Ac, or looping to target promoters is not clear. Insight into these questions can be achieved by delivering the AP1 dominant negative A-Fos to neurons via lentiviral infection, thereby disrupting the activity of AP1, and assessing any number of variables from transcription factor binding, to looping interactions, to gene expression. Furthermore, more work will be needed to understand the additional transcription factors that drive stimulus-responsive enhancers, and the contribution of each of these factors to enhancer function. Additional factors could be identified computationally based on presence of motifs, biochemically based on mass spectrometry of factors bound to AP1 factors or to stimulus responsive enhancers, or based on a candidate approach. Hopefully, detailed investigations at individual enhancers, such as the *Nptx2* enhancer, will shed light onto not only the additional transcription factors that drive stimulus-responsive enhancers, but also the cis regulatory logic of enhancer function and stimulus-specific transcriptional responses.

4.2.4 Performing H3K27Ac ChIP-Seq in response to stimuli in human neurons

Recently, it has become feasible to obtain and culture human neurons in vitro. This provides the exciting possibility of performing H3K27Ac ChIP-Seq in human neurons in response to stimuli. This would not only enable the identification of stimulus-responsive enhancers in human neurons, it would also enable comparisons to be made between mouse and human. Such comparisons would not only be interesting from an evolutionary standpoint, they could also shed light onto the cis-regulatory logic of stimulus-responsive enhancers. Any variations in the H3K27Ac behaviors at orthologous enhancers in human and mouse could then be attempted to be understood on the basis of the variation in the underlying orthologous sequences. Similarly, if H3K27Ac ChIP-Seq is done from human neurons obtained from different individuals for whom whole genome sequencing is also obtained, the contribution of human variation to enhancer function can be studied using H3K27Ac as a readout. This need not be limited to stimulus responsive enhancers, and could be done for constitutively active enhancers as well. Studies performed in human neurons may enable us to begin to understand the functional contribution of sequence variation to gene regulation and human cognition.

5 REFERENCES

Abrams, T.W., Castellucci, V.F., Camardo, J.S., Kandel, E.R., and Lloyd, P.E. (1984). Two endogenous neuropeptides modulate the gill and siphon withdrawal reflex in Aplysia by presynaptic facilitation involving cAMP-dependent closure of a serotonin-sensitive potassium channel. Proceedings of the National Academy of Sciences of the United States of America *81*, 7956-7960.

Ahn, S., Olive, M., Aggarwal, S., Krylov, D., Ginty, D.D., and Vinson, C. (1998). A dominant-negative inhibitor of CREB reveals that it is a general mediator of stimulus-dependent transcription of c-fos. Molecular and cellular biology *18*, 967-977.

Aizawa, H., Hu, S.C., Bobb, K., Balakrishnan, K., Ince, G., Gurevich, I., Cowan, M., and Ghosh, A. (2004). Dendrite development regulated by CREST, a calcium-regulated transcriptional activator. Science *303*, 197-202.

Alberini, C.M. (2009). Transcription factors in long-term memory and synaptic plasticity. Physiological reviews *89*, 121-145.

Altar, C.A., Laeng, P., Jurata, L.W., Brockman, J.A., Lemire, A., Bullard, J., Bukhman, Y.V., Young, T.A., Charles, V., and Palfreyman, M.G. (2004). Electroconvulsive seizures regulate gene expression of distinct neurotrophic signaling pathways. The Journal of neuroscience : the official journal of the Society for Neuroscience *24*, 2667-2677.

Andrews, G.K., Harding, M.A., Calvet, J.P., and Adamson, E.D. (1987). The heat shock response in HeLa cells is accompanied by elevated expression of the c-fos proto-oncogene. Molecular and cellular biology *7*, 3452-3458.

Aronin, N., Sagar, S.M., Sharp, F.R., and Schwartz, W.J. (1990). Light regulates expression of a Fos-related protein in rat suprachiasmatic nuclei. Proceedings of the National Academy of Sciences of the United States of America *87*, 5959-5962.

Bailey, T.L., and Elkan, C. (1994). Fitting a mixture model by expectation maximization to discover motifs in biopolymers. Proceedings / International Conference on Intelligent Systems for Molecular Biology ; ISMB International Conference on Intelligent Systems for Molecular Biology *2*, 28-36.

Banerji, J., Olson, L., and Schaffner, W. (1983). A lymphocyte-specific cellular enhancer is located downstream of the joining region in immunoglobulin heavy chain genes. Cell *33*, 729-740.

Banerji, J., Rusconi, S., and Schaffner, W. (1981). Expression of a beta-globin gene is enhanced by remote SV40 DNA sequences. Cell *27*, 299-308.

Barbosa, A.C., Kim, M.S., Ertunc, M., Adachi, M., Nelson, E.D., McAnally, J., Richardson, J.A., Kavalali, E.T., Monteggia, L.M., Bassel-Duby, R., *et al.* (2008). MEF2C, a transcription factor that facilitates learning and memory by negative regulation of synapse numbers and function. Proceedings of the National Academy of Sciences of the United States of America *105*, 9391-9396.

Barco, A., Alarcon, J.M., and Kandel, E.R. (2002). Expression of constitutively active CREB protein facilitates the late phase of long-term potentiation by enhancing synaptic capture. Cell *108*, 689-703.

Beck, K.D., Powell-Braxton, L., Widmer, H.R., Valverde, J., and Hefti, F. (1995). Igf1 gene disruption results in reduced brain size, CNS hypomyelination, and loss of hippocampal granule and striatal parvalbumin-containing neurons. Neuron *14*, 717-730.

Bender, M.A., Bulger, M., Close, J., and Groudine, M. (2000). Beta-globin gene switching and DNase I sensitivity of the endogenous beta-globin locus in mice do not require the locus control region. Molecular cell *5*, 387-393.

Bertrand, N., Castro, D.S., and Guillemot, F. (2002). Proneural genes and the specification of neural cell types. Nature reviews Neuroscience *3*, 517-530.

Billestrup, N., Mitchell, R.L., Vale, W., and Verma, I.M. (1987). Growth hormone-releasing factor induces c-fos expression in cultured primary pituitary cells. Molecular endocrinology *1*, 300-305.

Bonni, A., Ginty, D.D., Dudek, H., and Greenberg, M.E. (1995). Serine 133-phosphorylated CREB induces transcription via a cooperative mechanism that may confer specificity to neurotrophin signals. Molecular and cellular neurosciences *6*, 168-183.

Borrelli, E., Nestler, E.J., Allis, C.D., and Sassone-Corsi, P. (2008). Decoding the epigenetic language of neuronal plasticity. Neuron *60*, 961-974.

Bourtchuladze, R., Frenguelli, B., Blendy, J., Cioffi, D., Schutz, G., and Silva, A.J. (1994). Deficient long-term memory in mice with a targeted mutation of the cAMP-responsive element-binding protein. Cell *79*, 59-68.

Brown, J.R., Ye, H., Bronson, R.T., Dikkes, P., and Greenberg, M.E. (1996). A defect in nurturing in mice lacking the immediate early gene fosB. Cell *86*, 297-309.

Brunelli, M., Castellucci, V., and Kandel, E.R. (1976). Synaptic facilitation and behavioral sensitization in Aplysia: possible role of serotonin and cyclic AMP. Science *194*, 1178-1181.

Buecker, C., and Wysocka, J. (2012). Enhancers as information integration hubs in development: lessons from genomics. Trends in genetics : TIG *28*, 276-284.

Bulger, M., and Groudine, M. (2011). Functional and mechanistic diversity of distal transcription enhancers. Cell *144*, 327-339.

Bullitt, E. (1989). Induction of c-fos-like protein within the lumbar spinal cord and thalamus of the rat following peripheral stimulation. Brain research *493*, 391-397.

Buxbaum, J.D., Daly, M.J., Devlin, B., Lehner, T., Roeder, K., State, M.W., and Autism Sequencing, C. (2012). The autism sequencing consortium: large-scale, high-throughput sequencing in autism spectrum disorders. Neuron *76*, 1052-1056.

Byrne, J.H., Castellucci, V.F., and Kandel, E.R. (1978). Contribution of individual mechanoreceptor sensory neurons to defensive gill-withdrawal reflex in Aplysia. Journal of neurophysiology *41*, 418-431.

Cantallops, I., Haas, K., and Cline, H.T. (2000). Postsynaptic CPG15 promotes synaptic maturation and presynaptic axon arbor elaboration in vivo. Nature neuroscience *3*, 1004-1011.

Castellucci, V., Pinsker, H., Kupfermann, I., and Kandel, E.R. (1970). Neuronal mechanisms of habituation and dishabituation of the gill-withdrawal reflex in Aplysia. Science *167*, 1745-1748.

Chang, M.C., Park, J.M., Pelkey, K.A., Grabenstatter, H.L., Xu, D., Linden, D.J., Sutula, T.P., McBain, C.J., and Worley, P.F. (2010). Narp regulates homeostatic scaling of

excitatory synapses on parvalbumin-expressing interneurons. Nature neuroscience *13*, 1090-1097.

Chang, S.L., Squinto, S.P., and Harlan, R.E. (1988). Morphine activation of c-fos expression in rat brain. Biochemical and biophysical research communications *157*, 698-704.

Chowdhury, S., Shepherd, J.D., Okuno, H., Lyford, G., Petralia, R.S., Plath, N., Kuhl, D., Huganir, R.L., and Worley, P.F. (2006). Arc/Arg3.1 interacts with the endocytic machinery to regulate AMPA receptor trafficking. Neuron *52*, 445-459.

Cole, A.J., Saffen, D.W., Baraban, J.M., and Worley, P.F. (1989). Rapid increase of an immediate early gene messenger RNA in hippocampal neurons by synaptic NMDA receptor activation. Nature *340*, 474-476.

Colletta, G., Cirafici, A.M., and Vecchio, G. (1986). Induction of the c-fos oncogene by thyrotropic hormone in rat thyroid cells in culture. Science *233*, 458-460.

Consortium, E.P. (2011). A user's guide to the encyclopedia of DNA elements (ENCODE). PLoS biology *9*, e1001046.

Consortium, E.P., Dunham, I., Kundaje, A., Aldred, S.F., Collins, P.J., Davis, C.A., Doyle, F., Epstein, C.B., Frietze, S., Harrow, J.*, et al.* (2012). An integrated encyclopedia of DNA elements in the human genome. Nature *489*, 57-74.

Creyghton, M.P., Cheng, A.W., Welstead, G.G., Kooistra, T., Carey, B.W., Steine, E.J., Hanna, J., Lodato, M.A., Frampton, G.M., Sharp, P.A.*, et al.* (2010). Histone H3K27ac separates active from poised enhancers and predicts developmental state. Proceedings of the National Academy of Sciences of the United States of America *107*, 21931-21936.

Dash, P.K., Hochner, B., and Kandel, E.R. (1990). Injection of the cAMP-responsive element into the nucleus of Aplysia sensory neurons blocks long-term facilitation. Nature *345*, 718-721.

Daval, J.L., Nakajima, T., Gleiter, C.H., Post, R.M., and Marangos, P.J. (1989). Mouse brain c-fos mRNA distribution following a single electroconvulsive shock. Journal of neurochemistry *52*, 1954-1957.

Davidson, E.H. (2010). Emerging properties of animal gene regulatory networks. Nature *468*, 911-920.

Davis, H.P., and Squire, L.R. (1984). Protein synthesis and memory: a review. Psychological bulletin *96*, 518-559.

Day, J.J., and Sweatt, J.D. (2011). Epigenetic mechanisms in cognition. Neuron *70*, 813-829.

Deschamps, J., Meijlink, F., and Verma, I.M. (1985). Identification of a transcriptional enhancer element upstream from the proto-oncogene fos. Science *230*, 1174-1177.

Dolmetsch, R., and Geschwind, D.H. (2011). The human brain in a dish: the promise of iPSC-derived neurons. Cell *145*, 831-834.

Douglas, R.M., Dragunow, M., and Robertson, H.A. (1988). High-frequency discharge of dentate granule cells, but not long-term potentiation, induces c-fos protein. Brain research *464*, 259-262.

Dragunow, M., Currie, R.W., Robertson, H.A., and Faull, R.L. (1989). Heat shock induces c-fos protein-like immunoreactivity in glial cells in adult rat brain. Experimental neurology *106*, 105-109.

Dragunow, M., and Robertson, H.A. (1987). Kindling stimulation induces c-fos protein(s) in granule cells of the rat dentate gyrus. Nature *329*, 441-442.

Dragunow, M., and Robertson, H.A. (1988). Brain injury induces c-fos protein(s) in nerve and glial-like cells in adult mammalian brain. Brain research *455*, 295-299.

Draisci, G., and Iadarola, M.J. (1989). Temporal analysis of increases in c-fos, preprodynorphin and preproenkephalin mRNAs in rat spinal cord. Brain research Molecular brain research *6*, 31-37.

Dulac, C. (2010). Brain function and chromatin plasticity. Nature *465*, 728-735.

Ebert, D.H., and Greenberg, M.E. (2013). Activity-dependent neuronal signalling and autism spectrum disorder. Nature *493*, 327-337.

Eferl, R., and Wagner, E.F. (2003). AP-1: a double-edged sword in tumorigenesis. Nature reviews Cancer *3*, 859-868.

Evans, N.C., Swanson, C.I., and Barolo, S. (2012). Sparkling insights into enhancer structure, function, and evolution. Current topics in developmental biology *98*, 97-120.

Fernandez, A.M., and Torres-Aleman, I. (2012). The many faces of insulin-like peptide signalling in the brain. Nature reviews Neuroscience *13*, 225-239.

Flavell, S.W., Cowan, C.W., Kim, T.K., Greer, P.L., Lin, Y., Paradis, S., Griffith, E.C., Hu, L.S., Chen, C., and Greenberg, M.E. (2006). Activity-dependent regulation of MEF2 transcription factors suppresses excitatory synapse number. Science *311*, 1008-1012.

Flavell, S.W., and Greenberg, M.E. (2008). Signaling mechanisms linking neuronal activity to gene expression and plasticity of the nervous system. Annual review of neuroscience *31*, 563-590.

Fleischmann, A., Hvalby, O., Jensen, V., Strekalova, T., Zacher, C., Layer, L.E., Kvello, A., Reschke, M., Spanagel, R., Sprengel, R.*, et al.* (2003). Impaired long-term memory and NR2A-type NMDA receptor-dependent synaptic plasticity in mice lacking c-Fos in the CNS. The Journal of neuroscience : the official journal of the Society for Neuroscience *23*, 9116-9122.

Flexner, J.B., Flexner, L.B., and Stellar, E. (1963). Memory in mice as affected by intracerebral puromycin. Science *141*, 57-59.

Frost, W.N., Castellucci, V.F., Hawkins, R.D., and Kandel, E.R. (1985). Monosynaptic connections made by the sensory neurons of the gill- and siphon-withdrawal reflex in Aplysia participate in the storage of long-term memory for sensitization. Proceedings of the National Academy of Sciences of the United States of America *82*, 8266-8269.

Gaiddon, C., Loeffler, J.P., and Larmet, Y. (1996). Brain-derived neurotrophic factor stimulates AP-1 and cyclic AMP-responsive element dependent transcriptional activity in central nervous system neurons. Journal of neurochemistry *66*, 2279-2286.

Gaudilliere, B., Konishi, Y., de la Iglesia, N., Yao, G., and Bonni, A. (2004). A CaMKII-NeuroD signaling pathway specifies dendritic morphogenesis. Neuron *41*, 229-241.

Gillies, S.D., Morrison, S.L., Oi, V.T., and Tonegawa, S. (1983). A tissue-specific transcription enhancer element is located in the major intron of a rearranged immunoglobulin heavy chain gene. Cell *33*, 717-728.

Gonzalez, G.A., and Montminy, M.R. (1989). Cyclic AMP stimulates somatostatin gene transcription by phosphorylation of CREB at serine 133. Cell *59*, 675-680.

Graff, J., and Tsai, L.H. (2013). Histone acetylation: molecular mnemonics on the chromatin. Nature reviews Neuroscience *14*, 97-111.

Greenberg, M.E., Siegfried, Z., and Ziff, E.B. (1987). Mutation of the c-fos gene dyad symmetry element inhibits serum inducibility of transcription in vivo and the nuclear regulatory factor binding in vitro. Molecular and cellular biology *7*, 1217-1225.

Greenberg, M.E., and Ziff, E.B. (1984). Stimulation of 3T3 cells induces transcription of the c-fos proto-oncogene. Nature *311*, 433-438.

Greenberg, M.E., Ziff, E.B., and Greene, L.A. (1986). Stimulation of neuronal acetylcholine receptors induces rapid gene transcription. Science *234*, 80-83.

Greene, L.A., and Tischler, A.S. (1976). Establishment of a noradrenergic clonal line of rat adrenal pheochromocytoma cells which respond to nerve growth factor. Proceedings of the National Academy of Sciences of the United States of America *73*, 2424-2428.

Greer, P.L., and Greenberg, M.E. (2008). From synapse to nucleus: calcium-dependent gene transcription in the control of synapse development and function. Neuron *59*, 846-860.

Gross, D.S., and Garrard, W.T. (1988). Nuclease hypersensitive sites in chromatin. Annual review of biochemistry *57*, 159-197.

Grosveld, F., van Assendelft, G.B., Greaves, D.R., and Kollias, G. (1987). Position-independent, high-level expression of the human beta-globin gene in transgenic mice. Cell *51*, 975-985.

Guan, J.S., Haggarty, S.J., Giacometti, E., Dannenberg, J.H., Joseph, N., Gao, J., Nieland, T.J., Zhou, Y., Wang, X., Mazitschek, R., *et al.* (2009). HDAC2 negatively regulates memory formation and synaptic plasticity. Nature *459*, 55-60.

Guan, Z., Giustetto, M., Lomvardas, S., Kim, J.H., Miniaci, M.C., Schwartz, J.H., Thanos, D., and Kandel, E.R. (2002). Integration of long-term-memory-related synaptic plasticity involves bidirectional regulation of gene expression and chromatin structure. Cell *111*, 483-493.

Gubits, R.M., Smith, T.M., Fairhurst, J.L., and Yu, H. (1989). Adrenergic receptors mediate changes in c-fos mRNA levels in brain. Brain research Molecular brain research *6*, 39-45.

Gupta, S., Stamatoyannopoulos, J.A., Bailey, T.L., and Noble, W.S. (2007). Quantifying similarity between motifs. Genome biology *8*, R24.

Hall, S.H., Joseph, D.R., French, F.S., and Conti, M. (1988). Follicle-stimulating hormone induces transient expression of the protooncogene c-fos in primary Sertoli cell cultures. Molecular endocrinology *2*, 55-61.

Hardison, R., Slightom, J.L., Gumucio, D.L., Goodman, M., Stojanovic, N., and Miller, W. (1997). Locus control regions of mammalian beta-globin gene clusters: combining phylogenetic analyses and experimental results to gain functional insights. Gene *205*, 73-94.

Hawkins, R.D., Castellucci, V.F., and Kandel, E.R. (1981). Interneurons involved in mediation and modulation of gill-withdrawal reflex in Aplysia. I. Identification and characterization. Journal of neurophysiology *45*, 304-314.

Hayward, M.D., Duman, R.S., and Nestler, E.J. (1990). Induction of the c-fos proto-oncogene during opiate withdrawal in the locus coeruleus and other regions of rat brain. Brain research *525*, 256-266.

Heckman, K.L., and Pease, L.R. (2007). Gene splicing and mutagenesis by PCR-driven overlap extension. Nature protocols *2*, 924-932.

Heintzman, N.D., Hon, G.C., Hawkins, R.D., Kheradpour, P., Stark, A., Harp, L.F., Ye, Z., Lee, L.K., Stuart, R.K., Ching, C.W.*, et al.* (2009). Histone modifications at human enhancers reflect global cell-type-specific gene expression. Nature *459*, 108-112.

Heintzman, N.D., Stuart, R.K., Hon, G., Fu, Y., Ching, C.W., Hawkins, R.D., Barrera, L.O., Van Calcar, S., Qu, C., Ching, K.A.*, et al.* (2007). Distinct and predictive chromatin signatures of transcriptional promoters and enhancers in the human genome. Nature genetics *39*, 311-318.

Ho, L., and Crabtree, G.R. (2010). Chromatin remodelling during development. Nature *463*, 474-484.

Hong, E.J., McCord, A.E., and Greenberg, M.E. (2008). A biological function for the neuronal activity-dependent component of Bdnf transcription in the development of cortical inhibition. Neuron *60*, 610-624.

Hong, S.J., Li, H., Becker, K.G., Dawson, V.L., and Dawson, T.M. (2004). Identification and analysis of plasticity-induced late-response genes. Proceedings of the National Academy of Sciences of the United States of America *101*, 2145-2150.

Hunt, S.P., Pini, A., and Evan, G. (1987). Induction of c-fos-like protein in spinal cord neurons following sensory stimulation. Nature *328*, 632-634.

Jacobson, L., Sharp, F.R., and Dallman, M.F. (1990). Induction of fos-like immunoreactivity in hypothalamic corticotropin-releasing factor neurons after adrenalectomy in the rat. Endocrinology *126*, 1709-1719.

Jin, W., Zhang, J., Lou, D., Chavkin, C., and Xu, M. (2002). C-fos-deficient mouse hippocampal CA3 pyramidal neurons exhibit both enhanced basal and kainic acid-induced excitability. Neuroscience letters *331*, 151-154.

Jorgensen, M.B., Deckert, J., Wright, D.C., and Gehlert, D.R. (1989). Delayed c-fos proto-oncogene expression in the rat hippocampus induced by transient global cerebral ischemia: an in situ hybridization study. Brain research *484*, 393-398.

Kaczmarek, L., Siedlecki, J.A., and Danysz, W. (1988). Proto-oncogene c-fos induction in rat hippocampus. Brain research *427*, 183-186.

Kandel, E.R. (2001). The molecular biology of memory storage: a dialogue between genes and synapses. Science *294*, 1030-1038.

Kawashima, T., Okuno, H., Nonaka, M., Adachi-Morishima, A., Kyo, N., Okamura, M., Takemoto-Kimura, S., Worley, P.F., and Bito, H. (2009). Synaptic activity-responsive element in the Arc/Arg3.1 promoter essential for synapse-to-nucleus signaling in activated neurons. Proceedings of the National Academy of Sciences of the United States of America *106*, 316-321.

Kim, T.K., Hemberg, M., Gray, J.M., Costa, A.M., Bear, D.M., Wu, J., Harmin, D.A., Laptewicz, M., Barbara-Haley, K., Kuersten, S., *et al.* (2010). Widespread transcription at neuronal activity-regulated enhancers. Nature *465*, 182-187.

Kitano, J., Kimura, K., Yamazaki, Y., Soda, T., Shigemoto, R., Nakajima, Y., and Nakanishi, S. (2002). Tamalin, a PDZ domain-containing protein, links a protein complex formation of group 1 metabotropic glutamate receptors and the guanine nucleotide exchange factor cytohesins. The Journal of neuroscience : the official journal of the Society for Neuroscience *22*, 1280-1289.

Konopka, G., and Geschwind, D.H. (2010). Human brain evolution: harnessing the genomics (r)evolution to link genes, cognition, and behavior. Neuron *68*, 231-244.

Kouzarides, T. (2007). Chromatin modifications and their function. Cell *128*, 693-705.

Kovacs, E.J., Oppenheim, J.J., and Young, H.A. (1986). Induction of c-fos and c-myc expression in T lymphocytes after treatment with recombinant interleukin 1-alpha. Journal of immunology *137*, 3649-3651.

Kupfermann, I., Carew, T.J., and Kandel, E.R. (1974). Local, reflex, and central commands controlling gill and siphon movements in Aplysia. Journal of neurophysiology *37*, 996-1019.

Le Gal La Salle, G. (1988). Long-lasting and sequential increase of c-fos oncoprotein expression in kainic acid-induced status epilepticus. Neuroscience letters *88*, 127-130.

Lee, T.I., and Young, R.A. (2013). Transcriptional regulation and its misregulation in disease. Cell *152*, 1237-1251.

Leslie, J.H., and Nedivi, E. (2011). Activity-regulated genes as mediators of neural circuit plasticity. Progress in neurobiology *94*, 223-237.

Lettice, L.A., Heaney, S.J., Purdie, L.A., Li, L., de Beer, P., Oostra, B.A., Goode, D., Elgar, G., Hill, R.E., and de Graaff, E. (2003). A long-range Shh enhancer regulates expression in the developing limb and fin and is associated with preaxial polydactyly. Human molecular genetics *12*, 1725-1735.

Levenson, J.M., O'Riordan, K.J., Brown, K.D., Trinh, M.A., Molfese, D.L., and Sweatt, J.D. (2004). Regulation of histone acetylation during memory formation in the hippocampus. The Journal of biological chemistry *279*, 40545-40559.

Levine, M. (2010). Transcriptional enhancers in animal development and evolution. Current biology : CB *20*, R754-763.

Li, C., and Wong, W.H. (2001). Model-based analysis of oligonucleotide arrays: expression index computation and outlier detection. Proceedings of the National Academy of Sciences of the United States of America *98*, 31-36.

Li, H., and Durbin, R. (2009). Fast and accurate short read alignment with Burrows-Wheeler transform. Bioinformatics *25*, 1754-1760.

Li, H., Gu, X., Dawson, V.L., and Dawson, T.M. (2004). Identification of calcium- and nitric oxide-regulated genes by differential analysis of library expression (DAzLE). Proceedings of the National Academy of Sciences of the United States of America *101*, 647-652.

Lin, Y., Bloodgood, B.L., Hauser, J.L., Lapan, A.D., Koon, A.C., Kim, T.K., Hu, L.S., Malik, A.N., and Greenberg, M.E. (2008). Activity-dependent regulation of inhibitory synapse development by Npas4. Nature *455*, 1198-1204.

Loebrich, S., and Nedivi, E. (2009). The function of activity-regulated genes in the nervous system. Physiological reviews *89*, 1079-1103.

Lois, C., Hong, E.J., Pease, S., Brown, E.J., and Baltimore, D. (2002). Germline transmission and tissue-specific expression of transgenes delivered by lentiviral vectors. Science *295*, 868-872.

Lyons, M.R., and West, A.E. (2011). Mechanisms of specificity in neuronal activity-regulated gene transcription. Progress in neurobiology *94*, 259-295.

Maurano, M.T., Humbert, R., Rynes, E., Thurman, R.E., Haugen, E., Wang, H., Reynolds, A.P., Sandstrom, R., Qu, H., Brody, J., *et al.* (2012). Systematic localization of common disease-associated variation in regulatory DNA. Science *337*, 1190-1195.

McLean, C.Y., Bristor, D., Hiller, M., Clarke, S.L., Schaar, B.T., Lowe, C.B., Wenger, A.M., and Bejerano, G. (2010). GREAT improves functional interpretation of cis-regulatory regions. Nature biotechnology *28*, 495-501.

Menetrey, D., Gannon, A., Levine, J.D., and Basbaum, A.I. (1989). Expression of c-fos protein in interneurons and projection neurons of the rat spinal cord in response to noxious somatic, articular, and visceral stimulation. The Journal of comparative neurology *285*, 177-195.

Mikkelsen, T.S., Xu, Z., Zhang, X., Wang, L., Gimble, J.M., Lander, E.S., and Rosen, E.D. (2010). Comparative epigenomic analysis of murine and human adipogenesis. Cell *143*, 156-169.

Ming, G.L., Brustle, O., Muotri, A., Studer, L., Wernig, M., and Christian, K.M. (2011). Cellular reprogramming: recent advances in modeling neurological diseases. The Journal of neuroscience : the official journal of the Society for Neuroscience *31*, 16070-16075.

Misra, R.P., Bonni, A., Miranti, C.K., Rivera, V.M., Sheng, M., and Greenberg, M.E. (1994). L-type voltage-sensitive calcium channel activation stimulates gene expression by a serum response factor-dependent pathway. The Journal of biological chemistry *269*, 25483-25493.

Mitchell, R.L., Zokas, L., Schreiber, R.D., and Verma, I.M. (1985). Rapid induction of the expression of proto-oncogene fos during human monocytic differentiation. Cell *40*, 209-217.

Montarolo, P.G., Goelet, P., Castellucci, V.F., Morgan, J., Kandel, E.R., and Schacher, S. (1986). A critical period for macromolecular synthesis in long-term heterosynaptic facilitation in Aplysia. Science *234*, 1249-1254.

Montminy, M.R., and Bilezikjian, L.M. (1987). Binding of a nuclear protein to the cyclic-AMP response element of the somatostatin gene. Nature *328*, 175-178.

Montminy, M.R., Sevarino, K.A., Wagner, J.A., Mandel, G., and Goodman, R.H. (1986). Identification of a cyclic-AMP-responsive element within the rat somatostatin gene. Proceedings of the National Academy of Sciences of the United States of America *83*, 6682-6686.

Moon, A.M., and Ley, T.J. (1990). Conservation of the primary structure, organization, and function of the human and mouse beta-globin locus-activating regions. Proceedings of the National Academy of Sciences of the United States of America *87*, 7693-7697.

Moreau, P., Hen, R., Wasylyk, B., Everett, R., Gaub, M.P., and Chambon, P. (1981). The SV40 72 base repair repeat has a striking effect on gene expression both in SV40 and other chimeric recombinants. Nucleic acids research *9*, 6047-6068.

Morgan, J.I., Cohen, D.R., Hempstead, J.L., and Curran, T. (1987). Mapping patterns of c-fos expression in the central nervous system after seizure. Science *237*, 192-197.

Morgan, J.I., and Curran, T. (1989). Stimulus-transcription coupling in neurons: role of cellular immediate-early genes. Trends in neurosciences *12*, 459-462.

Morgan, J.I., and Curran, T. (1991). Stimulus-transcription coupling in the nervous system: involvement of the inducible proto-oncogenes fos and jun. Annual review of neuroscience *14*, 421-451.

Muller, R., Bravo, R., Burckhardt, J., and Curran, T. (1984). Induction of c-fos gene and protein by growth factors precedes activation of c-myc. Nature *312*, 716-720.

Muller, R., Curran, T., Muller, D., and Guilbert, L. (1985). Induction of c-fos during myelomonocytic differentiation and macrophage proliferation. Nature *314*, 546-548.

Munshi, N., Yie, Y., Merika, M., Senger, K., Lomvardas, S., Agalioti, T., and Thanos, D. (1999). The IFN-beta enhancer: a paradigm for understanding activation and repression of inducible gene expression. Cold Spring Harbor symposia on quantitative biology *64*, 149-159.

Nedivi, E., Hevroni, D., Naot, D., Israeli, D., and Citri, Y. (1993). Numerous candidate plasticity-related genes revealed by differential cDNA cloning. Nature *363*, 718-722.

Nedivi, E., Wu, G.Y., and Cline, H.T. (1998). Promotion of dendritic growth by CPG15, an activity-induced signaling molecule. Science *281*, 1863-1866.

O'Brien, R., Xu, D., Mi, R., Tang, X., Hopf, C., and Worley, P. (2002). Synaptically targeted narp plays an essential role in the aggregation of AMPA receptors at excitatory synapses in cultured spinal neurons. The Journal of neuroscience : the official journal of the Society for Neuroscience *22*, 4487-4498.

O'Brien, R.J., Xu, D., Petralia, R.S., Steward, O., Huganir, R.L., and Worley, P. (1999). Synaptic clustering of AMPA receptors by the extracellular immediate-early gene product Narp. Neuron *23*, 309-323.

Olive, M., Krylov, D., Echlin, D.R., Gardner, K., Taparowsky, E., and Vinson, C. (1997). A dominant negative to activation protein-1 (AP1) that abolishes DNA binding and inhibits oncogenesis. The Journal of biological chemistry *272*, 18586-18594.

Ong, C.T., and Corces, V.G. (2011). Enhancer function: new insights into the regulation of tissue-specific gene expression. Nature reviews Genetics *12*, 283-293.

Ong, J., Yamashita, S., and Melmed, S. (1987). Insulin-like growth factor I induces c-fos messenger ribonucleic acid in L6 rat skeletal muscle cells. Endocrinology *120*, 353-357.

Onodera, H., Kogure, K., Ono, Y., Igarashi, K., Kiyota, Y., and Nagaoka, A. (1989). Proto-oncogene c-fos is transiently induced in the rat cerebral cortex after forebrain ischemia. Neuroscience letters *98*, 101-104.

Ostuni, R., Piccolo, V., Barozzi, I., Polletti, S., Termanini, A., Bonifacio, S., Curina, A., Prosperini, E., Ghisletti, S., and Natoli, G. (2013). Latent enhancers activated by stimulation in differentiated cells. Cell *152*, 157-171.

Pak, D.T., and Sheng, M. (2003). Targeted protein degradation and synapse remodeling by an inducible protein kinase. Science *302*, 1368-1373.

Panne, D. (2008). The enhanceosome. Current opinion in structural biology *18*, 236-242.

Park, C.S., Gong, R., Stuart, J., and Tang, S.J. (2006). Molecular network and chromosomal clustering of genes involved in synaptic plasticity in the hippocampus. The Journal of biological chemistry *281*, 30195-30211.

Park, H., and Poo, M.M. (2013). Neurotrophin regulation of neural circuit development and function. Nature reviews Neuroscience *14*, 7-23.

Peleg, S., Sananbenesi, F., Zovoilis, A., Burkhardt, S., Bahari-Javan, S., Agis-Balboa, R.C., Cota, P., Wittnam, J.L., Gogol-Doering, A., Opitz, L., *et al.* (2010). Altered histone acetylation is associated with age-dependent memory impairment in mice. Science *328*, 753-756.

Pinsker, H.M., Hening, W.A., Carew, T.J., and Kandel, E.R. (1973). Long-term sensitization of a defensive withdrawal reflex in Aplysia. Science *182*, 1039-1042.

Popovici, T., Represa, A., Crepel, V., Barbin, G., Beaudoin, M., and Ben-Ari, Y. (1990). Effects of kainic acid-induced seizures and ischemia on c-fos-like proteins in rat brain. Brain research *536*, 183-194.

Potthoff, M.J., and Olson, E.N. (2007). MEF2: a central regulator of diverse developmental programs. Development *134*, 4131-4140.

Presley, R.W., Menetrey, D., Levine, J.D., and Basbaum, A.I. (1990). Systemic morphine suppresses noxious stimulus-evoked Fos protein-like immunoreactivity in the rat spinal cord. The Journal of neuroscience : the official journal of the Society for Neuroscience *10*, 323-335.

Rada-Iglesias, A., Bajpai, R., Prescott, S., Brugmann, S.A., Swigut, T., and Wysocka, J. (2012). Epigenomic annotation of enhancers predicts transcriptional regulators of human neural crest. Cell stem cell *11*, 633-648.

Rada-Iglesias, A., Bajpai, R., Swigut, T., Brugmann, S.A., Flynn, R.A., and Wysocka, J. (2011). A unique chromatin signature uncovers early developmental enhancers in humans. Nature *470*, 279-283.

Ramanan, N., Shen, Y., Sarsfield, S., Lemberger, T., Schutz, G., Linden, D.J., and Ginty, D.D. (2005). SRF mediates activity-induced gene expression and synaptic plasticity but not neuronal viability. Nature neuroscience *8*, 759-767.

Rea, M.A. (1989). Light increases Fos-related protein immunoreactivity in the rat suprachiasmatic nuclei. Brain research bulletin *23*, 577-581.

Redmond, L., Kashani, A.H., and Ghosh, A. (2002). Calcium regulation of dendritic growth via CaM kinase IV and CREB-mediated transcription. Neuron *34*, 999-1010.

Rial Verde, E.M., Lee-Osbourne, J., Worley, P.F., Malinow, R., and Cline, H.T. (2006). Increased expression of the immediate-early gene arc/arg3.1 reduces AMPA receptor-mediated synaptic transmission. Neuron *52*, 461-474.

Risse, G., Jooss, K., Neuberg, M., Bruller, H.J., and Muller, R. (1989). Asymmetrical recognition of the palindromic AP1 binding site (TRE) by Fos protein complexes. The EMBO journal *8*, 3825-3832.

Robertson, G.S., Herrera, D.G., Dragunow, M., and Robertson, H.A. (1989a). L-dopa activates c-fos in the striatum ipsilateral to a 6-hydroxydopamine lesion of the substantia nigra. European journal of pharmacology *159*, 99-100.

Robertson, H.A., Peterson, M.R., Murphy, K., and Robertson, G.S. (1989b). D1-dopamine receptor agonists selectively activate striatal c-fos independent of rotational behaviour. Brain research *503*, 346-349.

Robertson, L.M., Kerppola, T.K., Vendrell, M., Luk, D., Smeyne, R.J., Bocchiaro, C., Morgan, J.I., and Curran, T. (1995). Regulation of c-fos expression in transgenic mice requires multiple interdependent transcription control elements. Neuron *14*, 241-252.

Rubinson, D.A., Dillon, C.P., Kwiatkowski, A.V., Sievers, C., Yang, L., Kopinja, J., Rooney, D.L., Zhang, M., Ihrig, M.M., McManus, M.T.*, et al.* (2003). A lentivirus-based system to functionally silence genes in primary mammalian cells, stem cells and transgenic mice by RNA interference. Nature genetics *33*, 401-406.

Rupp, R.A., Snider, L., and Weintraub, H. (1994). Xenopus embryos regulate the nuclear localization of XMyoD. Genes & development *8*, 1311-1323.

Rusak, B., Robertson, H.A., Wisden, W., and Hunt, S.P. (1990). Light pulses that shift rhythms induce gene expression in the suprachiasmatic nucleus. Science *248*, 1237-1240.

Saffen, D.W., Cole, A.J., Worley, P.F., Christy, B.A., Ryder, K., and Baraban, J.M. (1988). Convulsant-induced increase in transcription factor messenger RNAs in rat brain. Proceedings of the National Academy of Sciences of the United States of America *85*, 7795-7799.

Sagai, T., Hosoya, M., Mizushina, Y., Tamura, M., and Shiroishi, T. (2005). Elimination of a long-range cis-regulatory module causes complete loss of limb-specific Shh expression and truncation of the mouse limb. Development *132*, 797-803.

Sagar, S.M., Sharp, F.R., and Curran, T. (1988). Expression of c-fos protein in brain: metabolic mapping at the cellular level. Science *240*, 1328-1331.

Sala, C., Futai, K., Yamamoto, K., Worley, P.F., Hayashi, Y., and Sheng, M. (2003). Inhibition of dendritic spine morphogenesis and synaptic transmission by activity-inducible protein Homer1a. The Journal of neuroscience : the official journal of the Society for Neuroscience *23*, 6327-6337.

Schacher, S., Castellucci, V.F., and Kandel, E.R. (1988). cAMP evokes long-term facilitation in Aplysia sensory neurons that requires new protein synthesis. Science *240*, 1667-1669.

Scholz, K.P., and Byrne, J.H. (1988). Intracellular injection of cAMP induces a long-term reduction of neuronal K+ currents. Science *240*, 1664-1666.

Sharp, F.R., Gonzalez, M.F., Hisanaga, K., Mobley, W.C., and Sagar, S.M. (1989a). Induction of the c-fos gene product in rat forebrain following cortical lesions and NGF injections. Neuroscience letters *100*, 117-122.

Sharp, F.R., Gonzalez, M.F., Sharp, J.W., and Sagar, S.M. (1989b). c-fos expression and (14C) 2-deoxyglucose uptake in the caudal cerebellum of the rat during motor/sensory cortex stimulation. The Journal of comparative neurology *284*, 621-636.

Sharp, F.R., Griffith, J., Gonzalez, M.F., and Sagar, S.M. (1989c). Trigeminal nerve section induces Fos-like immunoreactivity (FLI) in brainstem and decreases FLI in sensory cortex. Brain research Molecular brain research *6*, 217-220.

Shen, Y., Yue, F., McCleary, D.F., Ye, Z., Edsall, L., Kuan, S., Wagner, U., Dixon, J., Lee, L., Lobanenkov, V.V.*, et al.* (2012). A map of the cis-regulatory sequences in the mouse genome. Nature *488*, 116-120.

Sheng, M., Dougan, S.T., McFadden, G., and Greenberg, M.E. (1988). Calcium and growth factor pathways of c-fos transcriptional activation require distinct upstream regulatory sequences. Molecular and cellular biology *8*, 2787-2796.

Sheng, M., and Greenberg, M.E. (1990). The regulation and function of c-fos and other immediate early genes in the nervous system. Neuron *4*, 477-485.

Sheng, M., McFadden, G., and Greenberg, M.E. (1990). Membrane depolarization and calcium induce c-fos transcription via phosphorylation of transcription factor CREB. Neuron *4*, 571-582.

Sheng, M., Thompson, M.A., and Greenberg, M.E. (1991). CREB: a Ca(2+)-regulated transcription factor phosphorylated by calmodulin-dependent kinases. Science *252*, 1427-1430.

Shin, C., McNamara, J.O., Morgan, J.I., Curran, T., and Cohen, D.R. (1990). Induction of c-fos mRNA expression by afterdischarge in the hippocampus of naive and kindled rats. Journal of neurochemistry *55*, 1050-1055.

Sonnenberg, J.L., Macgregor-Leon, P.F., Curran, T., and Morgan, J.I. (1989a). Dynamic alterations occur in the levels and composition of transcription factor AP-1 complexes after seizure. Neuron *3*, 359-365.

Sonnenberg, J.L., Mitchelmore, C., Macgregor-Leon, P.F., Hempstead, J., Morgan, J.I., and Curran, T. (1989b). Glutamate receptor agonists increase the expression of Fos, Fra, and AP-1 DNA binding activity in the mammalian brain. Journal of neuroscience research *24*, 72-80.

Sonnenberg, J.L., Rauscher, F.J., 3rd, Morgan, J.I., and Curran, T. (1989c). Regulation of proenkephalin by Fos and Jun. Science *246*, 1622-1625.

Spitz, F., and Furlong, E.E. (2012). Transcription factors: from enhancer binding to developmental control. Nature reviews Genetics *13*, 613-626.

Sugo, N., Oshiro, H., Takemura, M., Kobayashi, T., Kohno, Y., Uesaka, N., Song, W.J., and Yamamoto, N. (2010). Nucleocytoplasmic translocation of HDAC9 regulates gene expression and dendritic growth in developing cortical neurons. The European journal of neuroscience *31*, 1521-1532.

Sukhatme, V.P., Cao, X.M., Chang, L.C., Tsai-Morris, C.H., Stamenkovich, D., Ferreira, P.C., Cohen, D.R., Edwards, S.A., Shows, T.B., Curran, T.*, et al.* (1988). A zinc finger-encoding gene coregulated with c-fos during growth and differentiation, and after cellular depolarization. Cell *53*, 37-43.

Szekely, A.M., Barbaccia, M.L., and Costa, E. (1987). Activation of specific glutamate receptor subtypes increases C-fos proto-oncogene expression in primary cultures of neonatal rat cerebellar granule cells. Neuropharmacology *26*, 1779-1782.

Treisman, R. (1985). Transient accumulation of c-fos RNA following serum stimulation requires a conserved 5' element and c-fos 3' sequences. Cell *42*, 889-902.

Treisman, R. (1987). Identification and purification of a polypeptide that binds to the c-fos serum response element. The EMBO journal *6*, 2711-2717.

Turner, D.L., and Weintraub, H. (1994). Expression of achaete-scute homolog 3 in Xenopus embryos converts ectodermal cells to a neural fate. Genes & development *8*, 1434-1447.

Verrier, B., Muller, D., Bravo, R., and Muller, R. (1986). Wounding a fibroblast monolayer results in the rapid induction of the c-fos proto-oncogene. The EMBO journal *5*, 913-917.

Visel, A., Blow, M.J., Li, Z., Zhang, T., Akiyama, J.A., Holt, A., Plajzer-Frick, I., Shoukry, M., Wright, C., Chen, F.*, et al.* (2009a). ChIP-seq accurately predicts tissue-specific activity of enhancers. Nature *457*, 854-858.

Visel, A., Rubin, E.M., and Pennacchio, L.A. (2009b). Genomic views of distant-acting enhancers. Nature *461*, 199-205.

Visel, A., Taher, L., Girgis, H., May, D., Golonzhka, O., Hoch, R.V., McKinsey, G.L., Pattabiraman, K., Silberberg, S.N., Blow, M.J.*, et al.* (2013). A high-resolution enhancer atlas of the developing telencephalon. Cell *152*, 895-908.

Vo, N., Klein, M.E., Varlamova, O., Keller, D.M., Yamamoto, T., Goodman, R.H., and Impey, S. (2005). A cAMP-response element binding protein-induced microRNA regulates neuronal morphogenesis. Proceedings of the National Academy of Sciences of the United States of America *102*, 16426-16431.

Wan, Y.J., Levi, B.Z., and Ozato, K. (1988). Induction of c-fos gene expression by interferons. Journal of interferon research *8*, 105-112.

Wang, D., Garcia-Bassets, I., Benner, C., Li, W., Su, X., Zhou, Y., Qiu, J., Liu, W., Kaikkonen, M.U., Ohgi, K.A.*, et al.* (2011). Reprogramming transcription by distinct classes of enhancers functionally defined by eRNA. Nature *474*, 390-394.

Watson, F.L., Heerssen, H.M., Bhattacharyya, A., Klesse, L., Lin, M.Z., and Segal, R.A. (2001). Neurotrophins use the Erk5 pathway to mediate a retrograde survival response. Nature neuroscience *4*, 981-988.

Wayman, G.A., Davare, M., Ando, H., Fortin, D., Varlamova, O., Cheng, H.Y., Marks, D., Obrietan, K., Soderling, T.R., Goodman, R.H., *et al.* (2008). An activity-regulated microRNA controls dendritic plasticity by down-regulating p250GAP. Proceedings of the National Academy of Sciences of the United States of America *105*, 9093-9098.

Wayman, G.A., Impey, S., Marks, D., Saneyoshi, T., Grant, W.F., Derkach, V., and Soderling, T.R. (2006). Activity-dependent dendritic arborization mediated by CaM-kinase I activation and enhanced CREB-dependent transcription of Wnt-2. Neuron *50*, 897-909.

White, J.D., and Gall, C.M. (1987). Differential regulation of neuropeptide and proto-oncogene mRNA content in the hippocampus following recurrent seizures. Brain research *427*, 21-29.

Wilding, G., Lippman, M.E., and Gelmann, E.P. (1988). Effects of steroid hormones and peptide growth factors on protooncogene c-fos expression in human breast cancer cells. Cancer research *48*, 802-805.

Winston, S.M., Hayward, M.D., Nestler, E.J., and Duman, R.S. (1990). Chronic electroconvulsive seizures down-regulate expression of the immediate-early genes c-fos and c-jun in rat cerebral cortex. Journal of neurochemistry *54*, 1920-1925.

Wisden, W., Errington, M.L., Williams, S., Dunnett, S.B., Waters, C., Hitchcock, D., Evan, G., Bliss, T.V., and Hunt, S.P. (1990). Differential expression of immediate early genes in the hippocampus and spinal cord. Neuron *4*, 603-614.

Zhang, J., Zhang, D., McQuade, J.S., Behbehani, M., Tsien, J.Z., and Xu, M. (2002). c-fos regulates neuronal excitability and survival. Nature genetics *30*, 416-420.

Zhang, X., Odom, D.T., Koo, S.H., Conkright, M.D., Canettieri, G., Best, J., Chen, H., Jenner, R., Herbolsheimer, E., Jacobsen, E., *et al.* (2005). Genome-wide analysis of cAMP-response element binding protein occupancy, phosphorylation, and target gene activation in human tissues. Proceedings of the National Academy of Sciences of the United States of America *102*, 4459-4464.

Zhang, Y., Liu, T., Meyer, C.A., Eeckhoute, J., Johnson, D.S., Bernstein, B.E., Nusbaum, C., Myers, R.M., Brown, M., Li, W., *et al.* (2008). Model-based analysis of ChIP-Seq (MACS). Genome biology *9*, R137.

Zhou, X., Marks, P.A., Rifkind, R.A., and Richon, V.M. (2001). Cloning and characterization of a histone deacetylase, HDAC9. Proceedings of the National Academy of Sciences of the United States of America *98*, 10572-10577.

6 APPENDIX A: STIMULUS-RESPONSIVE GENES IN THE NERVOUS SYSTEM

6.1 TOP KCL RESPONSIVE GENES

Table 15: Top 25 KCl-induced early response genes

RNA-Seq was performed from mouse cortical neurons that were stimulated with 0, 1, or 6 hours (h) of KCl or BDNF. Displayed are the top 25 KCl-induced early response genes, defined as genes with greater induction at 1 h than at 6 h after KCl stimulation. Only genes expressed in the top 50th percentile of all expressed genes within at least one of the time points (0 h, 1 h, 6 h KCl) were considered for this analysis. Genes are displayed in decreasing order of fold induction at the 1 h time point after KCl stimulation relative to the 0 h time point after KCl stimulation. mRNA expression values are reported as reads per kilobase per million mapped reads (RPKM). For each gene, gene name (Gene), NCBI GeneID, chromosome number (Ch), DNA strand (St), start and stop position are also displayed.

						KCl					BDNF				
Gene	GeneID	Ch	St	Start	Stop	0h	1h	6h	1h/0h	6h/0h	0h	1h	6h	1h/0h	6h/0h
Fosb	14282	7	-	19888045	19895394	0.11	10.13	2.15	95.08	20.16	0.15	9.79	0.39	64.10	2.58
LOC668604	668604	11	+	74985977	74986583	0.56	51.45	15.71	91.34	27.88	0.97	68.17	16.34	70.12	16.81
Fos	14281	12	+	86814851	86818219	1.68	152.20	47.73	90.68	28.44	1.77	141.48	6.66	79.80	3.75
Egr4	13656	6	-	85461116	85463536	0.11	8.02	1.15	72.03	10.30	0.28	40.55	1.93	143.89	6.86
Npas4	225872	19	-	4984355	4989971	0.26	17.84	7.23	68.63	27.83	0.45	7.49	0.41	16.76	0.92
Junb	16477	8	-	87500831	87502647	3.85	215.22	29.46	55.97	7.66	4.45	261.02	13.04	58.69	2.93
Egr2	13654	10	+	67000626	67004936	0.18	8.59	0.66	46.83	3.60	0.19	61.85	8.86	318.63	45.66
Nr4a1	15370	15	+	101097293	101105223	0.17	6.32	2.09	37.04	12.27	0.18	6.45	0.28	35.08	1.54
Klf4	16600	4	-	55540137	55545338	0.15	5.35	0.88	34.59	5.71	0.17	0.70	0.28	4.25	1.72
Maff	17133	15	+	79178108	79189506	0.35	10.42	4.07	29.69	11.60	0.44	9.23	1.29	21.20	2.96
Arc	11838	15	-	74499513	74503000	0.79	16.07	2.50	20.32	3.16	0.85	169.39	44.94	198.86	52.76
Gadd45b	17873	10	+	80392836	80394949	1.08	17.83	2.27	16.54	2.11	1.02	30.26	5.60	29.53	5.46
Ier2	15936	8	-	87183450	87186747	0.86	10.59	2.77	12.28	3.21	1.09	26.97	3.35	24.64	3.06
Nr4a2	18227	2	-	56960567	56967666	0.57	6.30	4.37	10.97	7.61	0.60	2.16	0.80	3.57	1.32
Atf3	11910	1	-	192994175	193007212	0.42	4.18	2.73	9.86	6.43	0.61	17.65	1.01	28.95	1.66
Cyr61	16007	3	-	145309940	145312945	2.56	24.09	17.07	9.42	6.67	2.61	38.64	6.60	14.80	2.53
Fbxo33	70611	12	-	60301643	60306676	1.97	13.26	5.70	6.73	2.89	2.25	9.48	3.26	4.22	1.45
Sertad1	55942	7	+	28271972	28275333	0.89	5.98	4.83	6.69	5.39	0.92	20.55	9.51	22.27	10.30
Egr1	13653	18	+	35020861	35024610	0.80	5.23	0.99	6.54	1.23	0.71	15.97	3.00	22.65	4.25
Ccnu	218630	13	+	113778010	113780986	0.28	1.81	0.42	6.39	1.48	0.28	1.72	0.14	6.11	0.50
Dusp6	67603	10	+	98725865	98730118	1.89	12.04	8.76	6.38	4.64	2.74	26.66	27.98	9.72	10.20
Tiparp	99929	3	+	65332369	65359440	5.87	25.09	11.62	4.28	1.98	5.30	21.02	16.97	3.97	3.20
Btg2	12227	1	-	135971442	135975732	5.58	23.83	8.19	4.27	1.47	5.76	98.55	6.98	17.10	1.21
Spty2d1	101685	7	-	54246068	54263579	2.15	9.12	3.66	4.25	1.71	1.99	5.85	3.01	2.94	1.51
Dusp1	19252	17	-	26642536	26645406	1.04	4.40	1.79	4.23	1.72	1.09	4.36	1.01	4.01	0.93

Table 16: Top 25 KCl-induced late response genes

RNA-Seq was performed from mouse cortical neurons that were stimulated with 0, 1, or 6 hours (h) of KCl or BDNF. Displayed are the top 25 KCl-induced late response genes, defined as genes with greater induction at 6 h than at 1 h after KCl stimulation. Only genes expressed in the top 50th percentile of all expressed genes within at least one of the time points (0 h, 1 h, 6 h KCl) were considered for this analysis. Genes are displayed in decreasing order of fold induction at the 6 h time point after KCl stimulation relative to the 0 h time point after KCl stimulation. mRNA expression values are reported as reads per kilobase per million mapped reads (RPKM). For each gene, gene name (Gene), NCBI GeneID, chromosome number (Ch), DNA strand (St), start and stop position are also displayed.

						KCl					BDNF				
Gene	GeneID	Ch	St	Start	Stop	0h	1h	6h	1h/0h	6h/0h	0h	1h	6h	1h/0h	6h/0h
Pcsk1	18548	13	+	75227435	75269946	0.23	2.46	15.92	10.56	68.39	0.30	1.13	2.01	3.78	6.74
Col10a1	12813	10	+	34109641	34118110	0.06	0.63	2.95	10.78	50.18	0.11	0.15	0.17	1.41	1.58
4931440P22Rik	71004	3	-	65331405	65334255	0.15	1.22	6.49	8.22	43.65	0.15	0.24	0.20	1.68	1.40
Bdnf	12064	2	+	109514857	109567200	0.17	0.68	6.98	4.05	41.63	0.36	0.79	3.74	2.23	10.52
Cartpt	27220	13	-	100668439	100670638	0.11	0.35	4.45	3.19	40.15	0.49	0.70	0.88	1.43	1.79
Serpinb2	18788	1	+	109412050	109422175	0.06	0.05	2.14	0.79	35.10	0.04	0.11	5.16	2.71	127.33
Acan	11595	7	+	86198369	86259985	0.06	0.07	1.91	1.03	30.25	0.11	0.16	0.50	1.39	4.39
Vgf	381677	5	+	137506165	137509221	1.27	17.51	38.31	13.79	30.18	2.41	62.99	107.36	26.17	44.61
Hspb3	56534	13	-	114453104	114453867	0.14	0.12	2.45	0.81	17.12	0.17	0.28	0.16	1.64	0.95
C030019I05Rik	320116	11	+	46049059	46053373	0.40	0.88	6.63	2.21	16.61	0.51	0.79	5.53	1.54	10.84
Gpr3	14748	4	-	132765255	132768422	0.15	0.61	1.91	4.10	12.80	0.14	1.33	0.71	9.51	5.10
Nptx2	53324	5	+	145306772	145318347	1.18	1.23	14.29	1.04	12.11	1.35	6.12	45.77	4.52	33.81
Cort	12854	4	-	148499300	148500850	0.49	0.93	5.18	1.89	10.55	1.08	1.16	1.57	1.07	1.45
Crem	12916	18	-	3266354	3327517	1.15	3.17	12.01	2.75	10.40	1.19	1.74	2.09	1.46	1.76
Nr4a3	18124	4	+	48064120	48096224	0.71	4.39	7.05	6.19	9.94	0.86	3.30	0.60	3.82	0.69
Tac1	21333	6	+	7505071	7512973	0.34	0.69	3.33	2.03	9.84	0.73	0.95	3.71	1.29	5.05
Map3k5	26408	10	+	19654278	19861529	0.61	0.60	5.67	0.98	9.27	0.87	0.77	0.99	0.88	1.14
E530001K10Rik	414123	2	-	94092031	94112239	1.18	1.59	10.52	1.34	8.91	2.29	3.23	4.41	1.41	1.93
Rgs2	19735	1	-	145847127	145851279	4.66	19.97	37.02	4.29	7.94	7.38	17.90	17.46	2.42	2.36
5430433G21Rik	319909	2	+	139503914	139584317	0.24	0.27	1.84	1.13	7.71	0.24	0.23	0.90	0.94	3.70
Tnfrsf12a	27279	17	-	23812412	23814411	0.83	1.20	6.28	1.46	7.60	0.63	6.14	11.77	9.79	18.75
Fosl2	14284	5	+	32438907	32460213	2.26	9.44	15.33	4.18	6.78	2.94	9.58	3.86	3.26	1.31
4930431J08Rik	73884	1	+	63319843	63361146	1.31	3.01	8.81	2.29	6.72	1.40	2.63	2.51	1.87	1.79
Popdc3	78977	10	+	45009111	45038256	0.34	0.35	2.25	1.02	6.55	0.28	0.35	0.57	1.22	2.02
Scg2	20254	1	-	79431244	79436665	24.41	44.14	157.97	1.81	6.47	46.02	78.42	218.83	1.70	4.76

6.2 TOP BDNF RESPONSIVE GENES

Table 17: Top 25 BDNF-induced early response genes

RNA-Seq was performed from mouse cortical neurons that were stimulated with 0, 1, or 6 hours (h) of KCl or BDNF. Displayed are the top 25 BDNF-induced early response genes, defined as genes with greater induction at 1 h than at 6 h after BDNF stimulation. Only genes expressed in the top 50th percentile of all expressed genes within at least one of the time points (0 h, 1 h, 6 h BDNF) were considered for this analysis. Genes are displayed in decreasing order of fold induction at the 1 h time point after BDNF stimulation relative to the 0 h time point after BDNF stimulation. mRNA expression values are reported as reads per kilobase per million mapped reads (RPKM). For each gene, gene name (Gene), NCBI GeneID, chromosome number (Ch), DNA strand (St), start and stop position are also displayed.

						KCl					BDNF				
Gene	GeneID	Ch	St	Start	Stop	0h	1h	6h	1h/0h	6h/0h	0h	1h	6h	1h/0h	6h/0h
Egr2	13654	10	+	67000626	67004936	0.18	8.59	0.66	46.83	3.60	0.19	61.85	8.86	318.63	45.66
Arc	11838	15	-	74499513	74503000	0.79	16.07	2.50	20.32	3.16	0.85	169.39	44.94	198.86	52.76
Egr4	13656	6	-	85461116	85463536	0.11	8.02	1.15	72.03	10.30	0.28	40.55	1.93	143.89	6.86
Fos	14281	12	+	86814851	86818219	1.68	152.20	47.73	90.68	28.44	1.77	141.48	6.66	79.80	3.75
LOC668604	668604	11	+	74985977	74986583	0.56	51.45	15.71	91.34	27.88	0.97	68.17	16.34	70.12	16.81
Fosb	14282	7	-	19888045	19895394	0.11	10.13	2.15	95.08	20.16	0.15	9.79	0.39	64.10	2.58
Junb	16477	8	-	87500831	87502647	3.85	215.22	29.46	55.97	7.66	4.45	261.02	13.04	58.69	2.93
Nr4a1	15370	15	+	101097293	101105223	0.17	6.32	2.09	37.04	12.27	0.18	6.45	0.28	35.08	1.54
Rrad	56437	8	-	107151966	107155221	0.14	0.32	0.31	2.25	2.16	0.11	3.61	3.05	32.19	27.20
Gadd45b	17873	10	+	80392836	80394949	1.08	17.83	2.27	16.54	2.11	1.02	30.26	5.60	29.53	5.46
Atf3	11910	1	-	192994175	193007212	0.42	4.18	2.73	9.86	6.43	0.61	17.65	1.01	28.95	1.66
Ier2	15936	8	-	87183450	87186747	0.86	10.59	2.77	12.28	3.21	1.09	26.97	3.35	24.64	3.06
Egr1	13653	18	+	35020861	35024610	0.80	5.23	0.99	6.54	1.23	0.71	15.97	3.00	22.65	4.25
Sertad1	55942	7	+	28271972	28275333	0.89	5.98	4.83	6.69	5.39	0.92	20.55	9.51	22.27	10.30
Maff	17133	15	+	79178108	79189506	0.35	10.42	4.07	29.69	11.60	0.44	9.23	1.29	21.20	2.96
Egr3	13655	14	+	70477252	70479964	0.44	1.19	0.32	2.70	0.72	0.42	8.06	0.74	19.28	1.78
Dusp5	240672	19	+	53603599	53616909	0.23	1.32	0.92	5.82	4.05	0.21	3.92	1.93	18.51	9.11
Btg2	12227	1	-	135971442	135975732	5.58	23.83	8.19	4.27	1.47	5.76	98.55	6.98	17.10	1.21
Npas4	225872	19	-	4984355	4989971	0.26	17.84	7.23	68.63	27.83	0.45	7.49	0.41	16.76	0.92
Axud1	215418	9	-	119880284	119893776	0.26	0.92	1.23	3.48	4.67	0.18	2.79	1.74	15.34	9.60
Cyr61	16007	3	-	145309940	145312945	2.56	24.09	17.07	9.42	6.67	2.61	38.64	6.60	14.80	2.53
Arl4d	80981	11	+	101526875	101529143	2.72	5.79	2.41	2.13	0.89	3.35	28.19	7.36	8.42	2.20
LOC100038842	100038842	11	+	101527946	101529142	2.96	6.41	2.63	2.16	0.89	3.73	31.23	8.23	8.37	2.21
Trib1	211770	15	+	59480209	59488654	0.14	0.41	0.60	2.87	4.20	0.23	1.87	0.74	8.15	3.22
Klf10	21847	15	-	38224168	38230462	2.95	2.06	1.98	0.70	0.67	2.50	19.48	17.65	7.80	7.06

Table 18: Top 25 BDNF-induced late response genes

RNA-Seq was performed from mouse cortical neurons that were stimulated with 0, 1, or 6 hours (h) of KCl or BDNF. Displayed are the top 25 BDNF-induced late response genes, defined as genes with greater induction at 6 h than at 1 h after BDNF stimulation. Only genes expressed in the top 50th percentile of all expressed genes within at least one of the time points (0 h, 1 h, 6 h BDNF) were considered for this analysis. Genes are displayed in decreasing order of fold induction at the 6 h time point after BDNF stimulation relative to the 0 h time point after BDNF stimulation. mRNA expression values are reported as reads per kilobase per million mapped reads (RPKM). For each gene, gene name (Gene), NCBI GeneID, chromosome number (Ch), DNA strand (St), start and stop position are also displayed.

						KCl					BDNF				
Gene	GeneID	Ch	St	Start	Stop	0h	1h	6h	1h/0h	6h/0h	0h	1h	6h	1h/0h	6h/0h
Areg	11839	5	+	91568641	91577458	0.01	0.09	0.44	18.39	86.80	0.01	0.20	1.82	15.18	140.00
Serpinb2	18788	1	+	109412050	109422175	0.06	0.05	2.14	0.79	35.10	0.04	0.11	5.16	2.71	127.33
Galr1	14427	18	-	82561888	82576169	0.03	0.04	0.06	1.35	1.99	0.05	0.05	3.03	1.05	66.08
Vgf	381677	5	+	137506165	137509221	1.27	17.51	38.31	13.79	30.18	2.41	62.99	107.36	26.17	44.61
Nptx2	53324	5	+	145306772	145318347	1.18	1.23	14.29	1.04	12.11	1.35	6.12	45.77	4.52	33.81
Rasl11a	68895	5	+	147656647	147659302	1.32	1.27	2.08	0.96	1.58	1.09	6.51	32.72	5.96	29.96
Emp1	13730	6	+	135312949	135333191	0.41	0.29	1.07	0.72	2.64	0.30	0.36	7.46	1.22	25.11
Tnfrsf12a	27279	17	-	23812412	23814411	0.83	1.20	6.28	1.46	7.60	0.63	6.14	11.77	9.79	18.75
Ccl2	20296	11	+	81849079	81850954	0.21	0.02	0.11	0.10	0.51	0.11	0.07	2.00	0.64	18.29
Nptx1	18164	11	-	119400033	119409134	1.32	1.86	3.08	1.41	2.33	1.40	5.29	25.48	3.77	18.16
Cckbr	12426	7	+	112574334	112584852	0.10	0.12	0.44	1.22	4.45	0.15	0.22	2.44	1.47	16.01
Nrn1	68404	13	-	36817494	36826325	1.09	1.78	6.69	1.64	6.16	1.04	4.37	16.20	4.21	15.59
Sema3e	20349	5	+	14025276	14256689	0.15	0.13	0.53	0.89	3.61	0.17	0.18	2.14	1.05	12.58
LOC100043802	100043802	9	-	113407150	113420573	0.15	0.16	0.29	1.08	1.98	0.16	0.20	1.80	1.26	11.53
Cited1	12705	X	-	99442775	99447108	0.55	0.72	2.50	1.31	4.56	0.79	0.95	8.88	1.20	11.22
C030019I05Rik	320116	11	+	46049059	46053373	0.40	0.88	6.63	2.21	16.61	0.51	0.79	5.53	1.54	10.84
Bdnf	12064	2	+	109514857	109567200	0.17	0.68	6.98	4.05	41.63	0.36	0.79	3.74	2.23	10.52
Dusp6	67603	10	+	98725865	98730118	1.89	12.04	8.76	6.38	4.64	2.74	26.66	27.98	9.72	10.20
Dusp4	319520	8	+	35870664	35882948	3.10	5.59	10.28	1.80	3.32	3.63	12.69	34.72	3.50	9.56
Il33	77125	19	+	30024140	30035208	0.18	0.15	0.11	0.85	0.62	0.18	0.22	1.75	1.19	9.48
Hsd11b1	15483	1	-	195047834	195090239	0.22	0.24	0.24	1.06	1.08	0.25	0.27	2.32	1.08	9.13
Ngfb	18049	3	+	102273851	102324928	0.57	0.40	0.92	0.71	1.62	0.49	0.59	4.47	1.20	9.10
Wnt2	22413	6	-	17938940	17980356	0.16	0.17	0.23	1.05	1.44	0.23	0.24	2.10	1.04	9.09
S100a3	20197	3	+	90404137	90406624	0.35	0.18	0.27	0.52	0.76	0.23	0.25	2.01	1.06	8.60
C1ql2	226359	1	+	122237159	122239751	0.25	0.23	0.17	0.91	0.70	0.22	0.29	1.81	1.30	8.09

6.3 UCSC GENOME BROWSER VIEWS OF CHIP-SEQ AND RNA-SEQ DATA

NEAR STIMULUS RESPONSIVE GENES IN THE NERVOUS SYSTEM

All genes listed in Appendix A are displayed on the subsequent pages, in alphabetical order.
The window displayed ranges from 50kb upstream of the gene to 50kb downstream of the gene.

For each gene, the following tracks are displayed:

1) RNA-Seq after 0 hr of KCl stimulation, silenced conditions
2) RNA-Seq after 1 hr of KCl stimulation
3) RNA-Seq after 6 hr of KCl stimulation
4) RefSeq gene
5) PhastCons vertebrate conservation
6) DNaseI hypersensitivity from embryonic 14.5 whole brain*
7) DNaseI hypersensitivity from embryonic 18.5 whole brain*
8) DNaseI hypersensitivity from 8 week adult cerebrum*
9) H3K27Ac ChIP-Seq from embryonic 14.5 whole brain*
10) H3K27Ac ChIP-Seq from 8 week adult cortex*
11) H3K27Ac ChIP-Seq in silenced conditions
12) H3K27Ac ChIP-Seq after 2hrs of KCl stimulation
13) H3K4Me1 ChIP-Seq in silenced conditions**
14) H3K4Me1 ChIP-Seq after 2hrs of KCl stimulation**
15) H3K4Me3 ChIP-Seq in silenced conditions**
16) H3K4Me3 ChIP-Seq after 2hrs of KCl stimulation**
17) H3K27Me3 ChIP-Seq in silenced conditions**
18) H3K27Me3 ChIP-Seq after 2hrs of KCl stimulation**
19) CBP ChIP-Seq in silenced conditions**
20) CBP ChIP-Seq after 2hrs of KCl stimulation**
21) CBP ChIP-Seq in silenced conditions
22) CBP ChIP-Seq after 2hrs of KCl stimulation
23) P300 ChIP-Seq in silenced conditions
24) P300 ChIP-Seq after 2hrs of KCl stimulation
25) RNAPII ChIP-Seq in silenced conditions**
26) RNAPII ChIP-Seq after 2hrs of KCl stimulation**
27) C-FOS ChIP-Seq in silenced conditions
28) C-FOS ChIP-Seq after 2hrs of KCl stimulation
29) C-FOS ChIP-Seq after 2hrs of KCl stimulation from control shRNA lentivirus infected neurons
30) C-FOS ChIP-Seq after 2hrs of KCl stimulation from *c-Fos* shRNA lentivirus infected neurons
31) FOSB ChIP-Seq in silenced conditions
32) FOSB ChIP-Seq after 2hrs of KCl stimulation
33) FOSB ChIP-Seq after 2hrs of KCl stimulation from control shRNA lentivirus infected neurons
34) FOSB ChIP-Seq after 2hrs of KCl stimulation from *FosB* shRNA lentivirus infected neurons
35) NPAS4 ChIP-Seq in silenced conditions**
36) NPAS4 ChIP-Seq after 2hrs of KCl stimulation**
37) CREB ChIP-Seq in silenced conditions**
38) CREB ChIP-Seq after 2hrs of KCl stimulation**
39) SRF ChIP-Seq in silenced conditions**
40) SRF ChIP-Seq after 2hrs of KCl stimulation**
41) MEF2A ChIP-Seq in silenced conditions
42) MEF2A ChIP-Seq after 2hrs of KCl stimulation
43) SNPs
44) RepeatMasker
45) RNA-Seq after 0 hr of BDNF stimulation, basal conditions
46) RNA-Seq after 1 hr of BDNF stimulation
47) RNA-Seq after 6 hr of BDNF stimulation
48) UCSC gene
49) PhastCons mammalian conservation
50) H3K27Ac ChIP-Seq in basal conditions
51) H3K27Ac ChIP-Seq after 2hrs of BDNF stimulation
52) C-FOS ChIP-Seq in basal conditions
53) C-FOS ChIP-Seq after 2hrs of BDNF stimulation
54) FOSB ChIP-Seq in basal conditions
55) FOSB ChIP-Seq after 2hrs of BDNF stimulation

* denotes data from ENCODE, ** denotes data from Kim et al., 2010

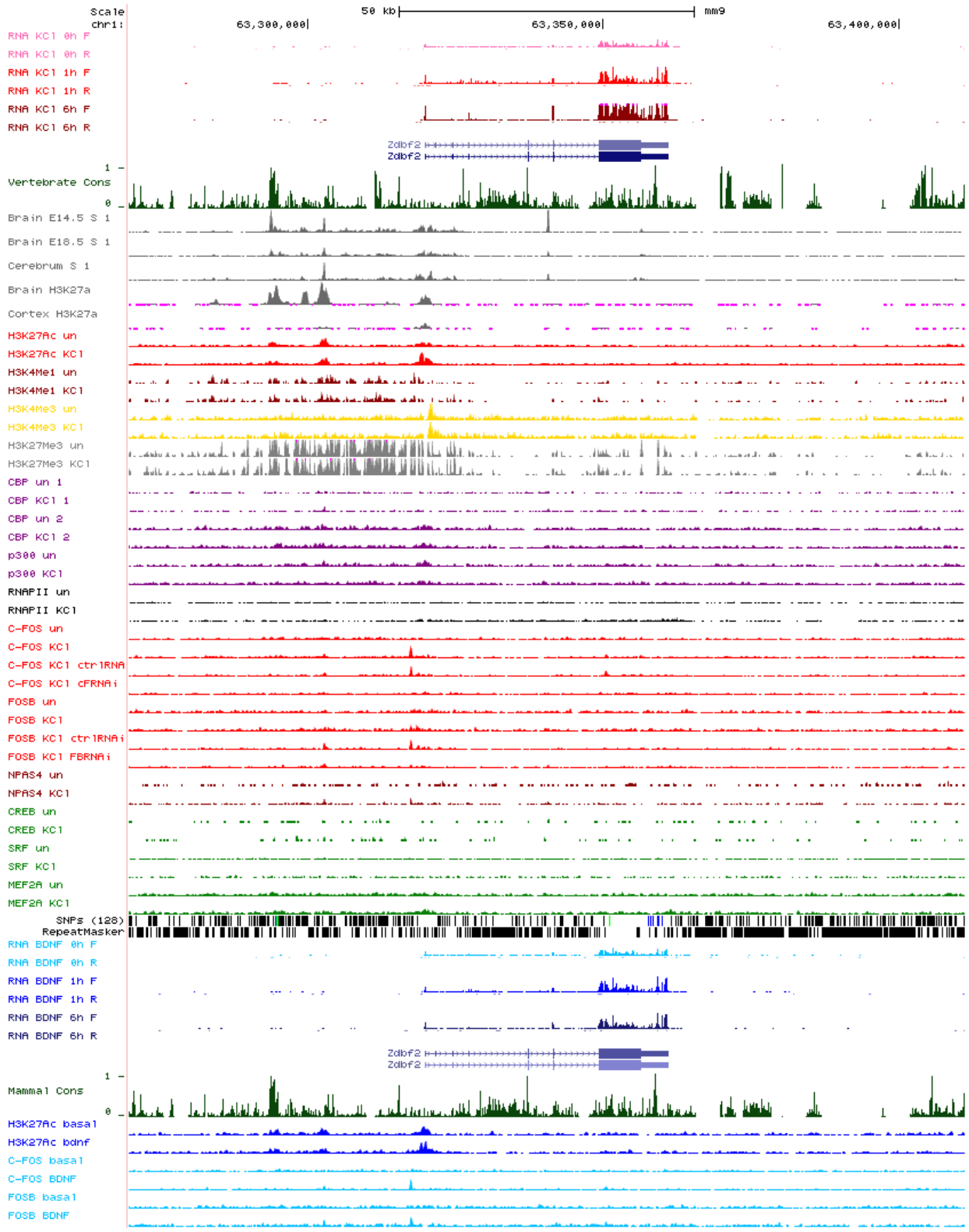

Figure 6.1: *4930431J08Rik* locus

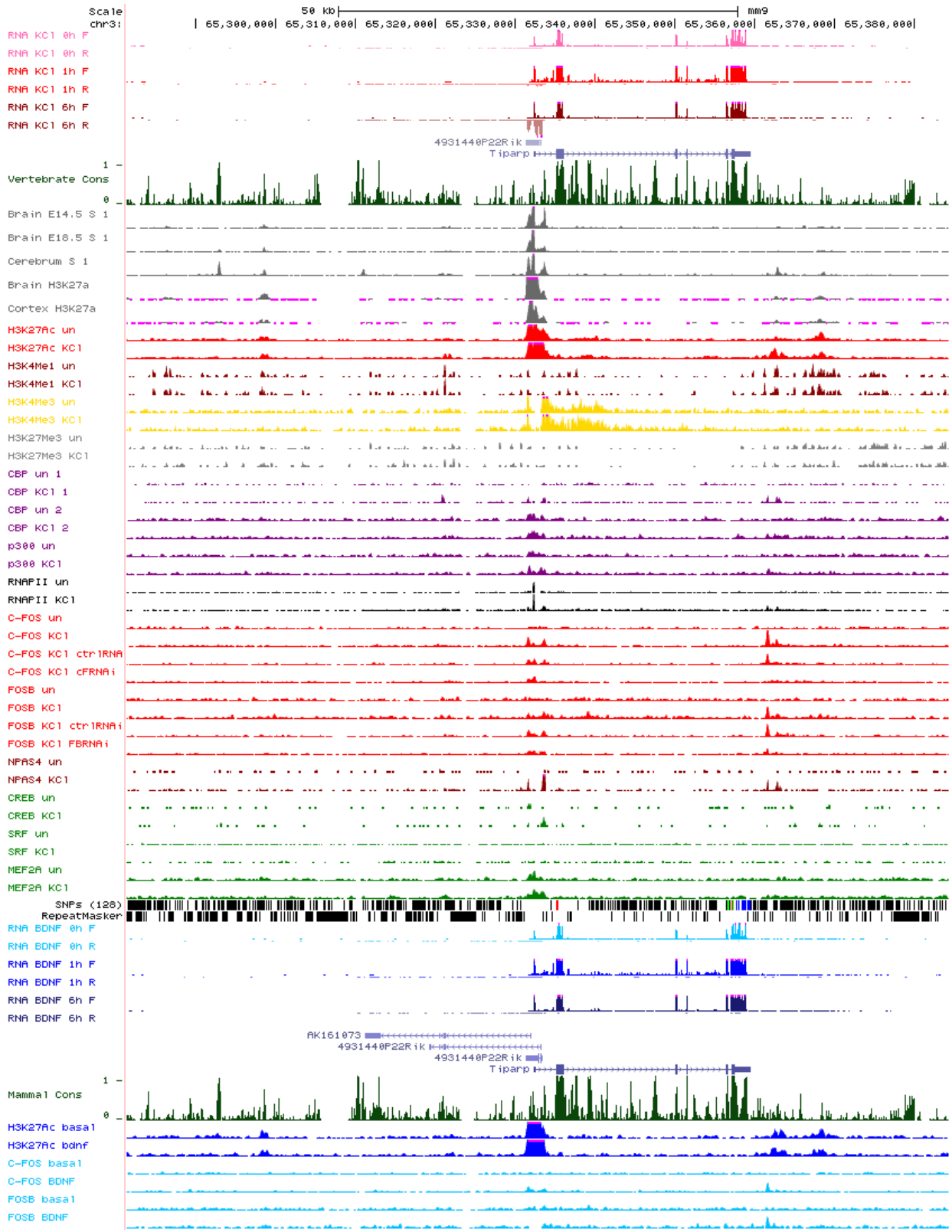

Figure 6.2: *4931440P22Rik* locus

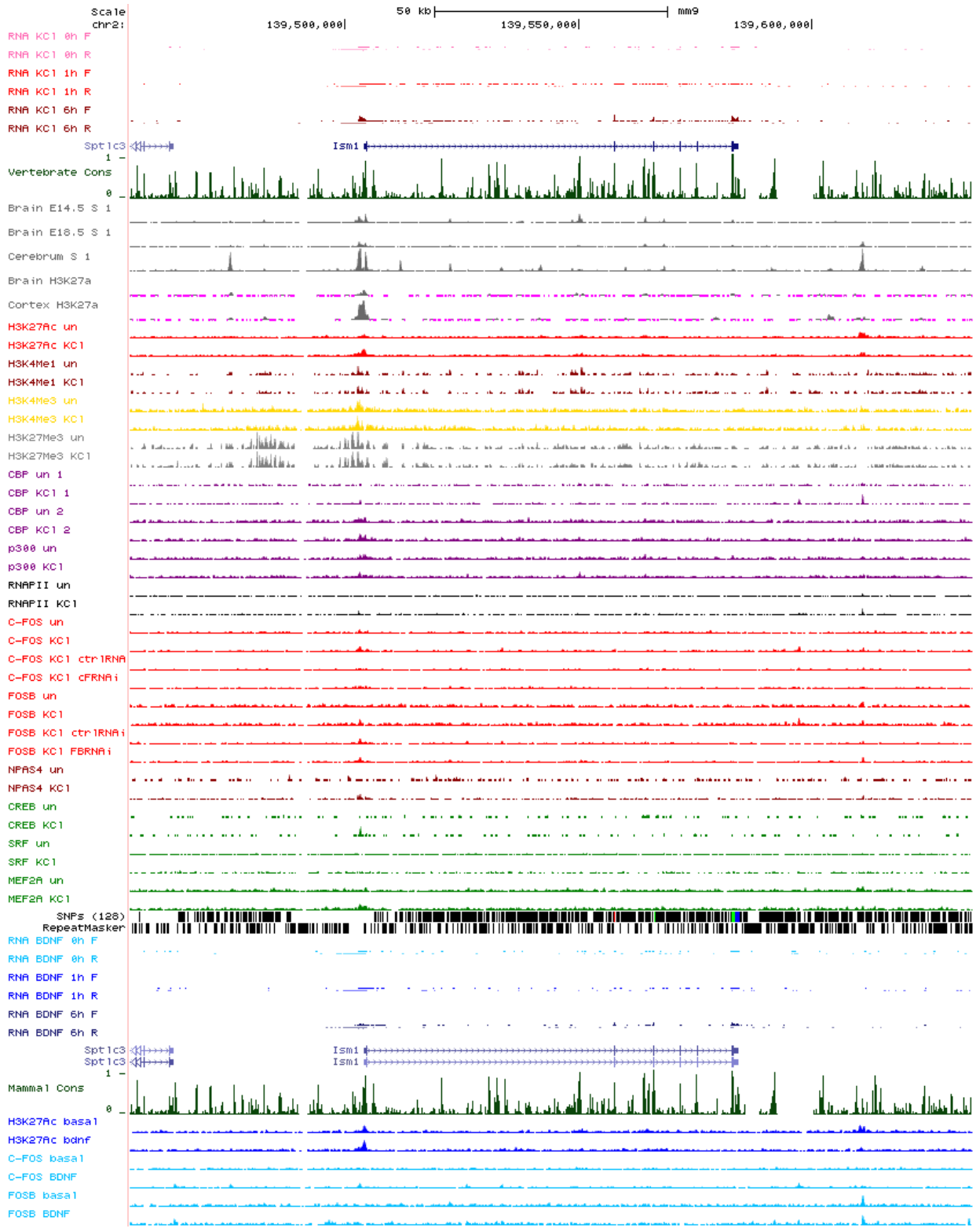

Figure 6.3: *5430433G21Rik* locus

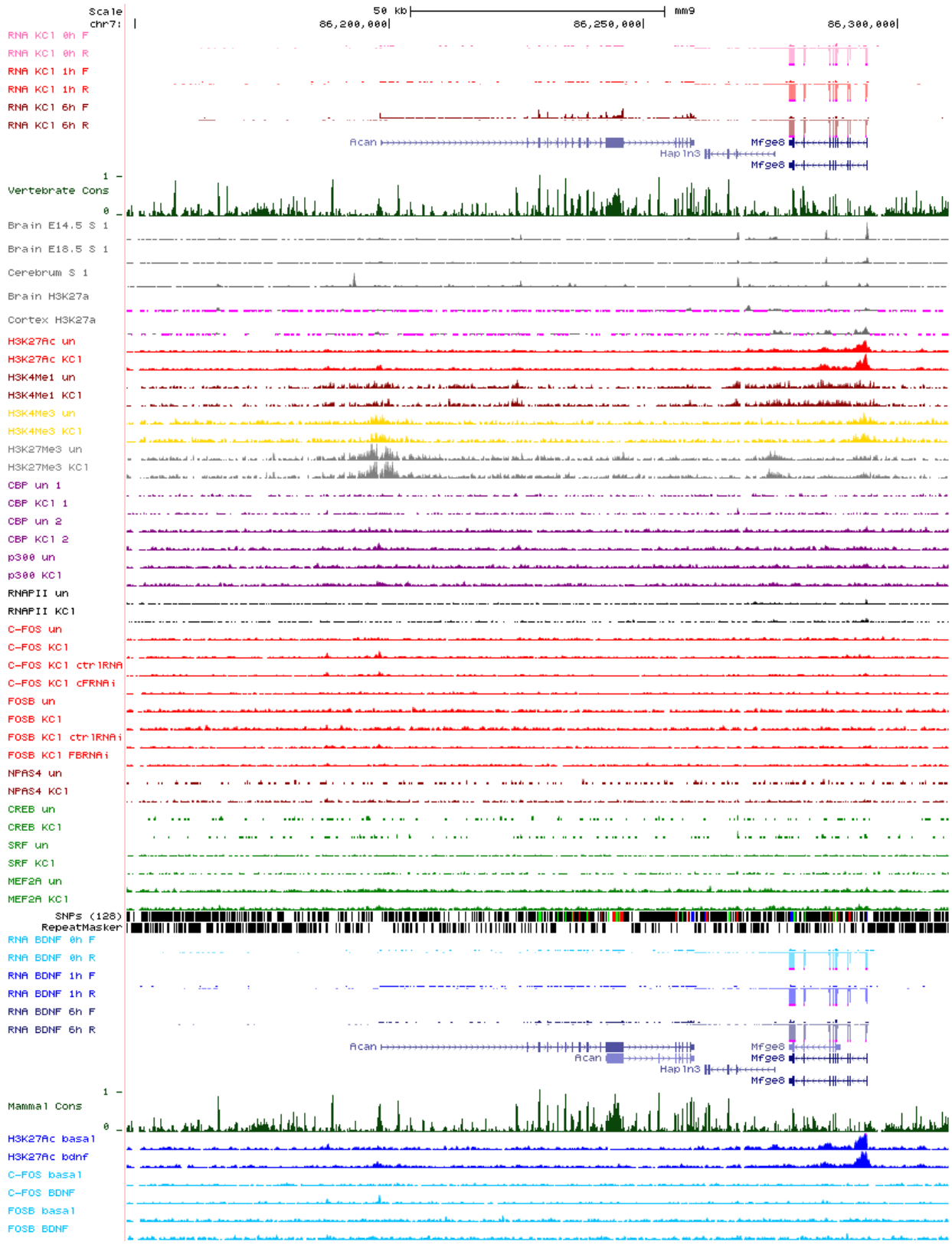

Figure 6.4: *Acan* locus

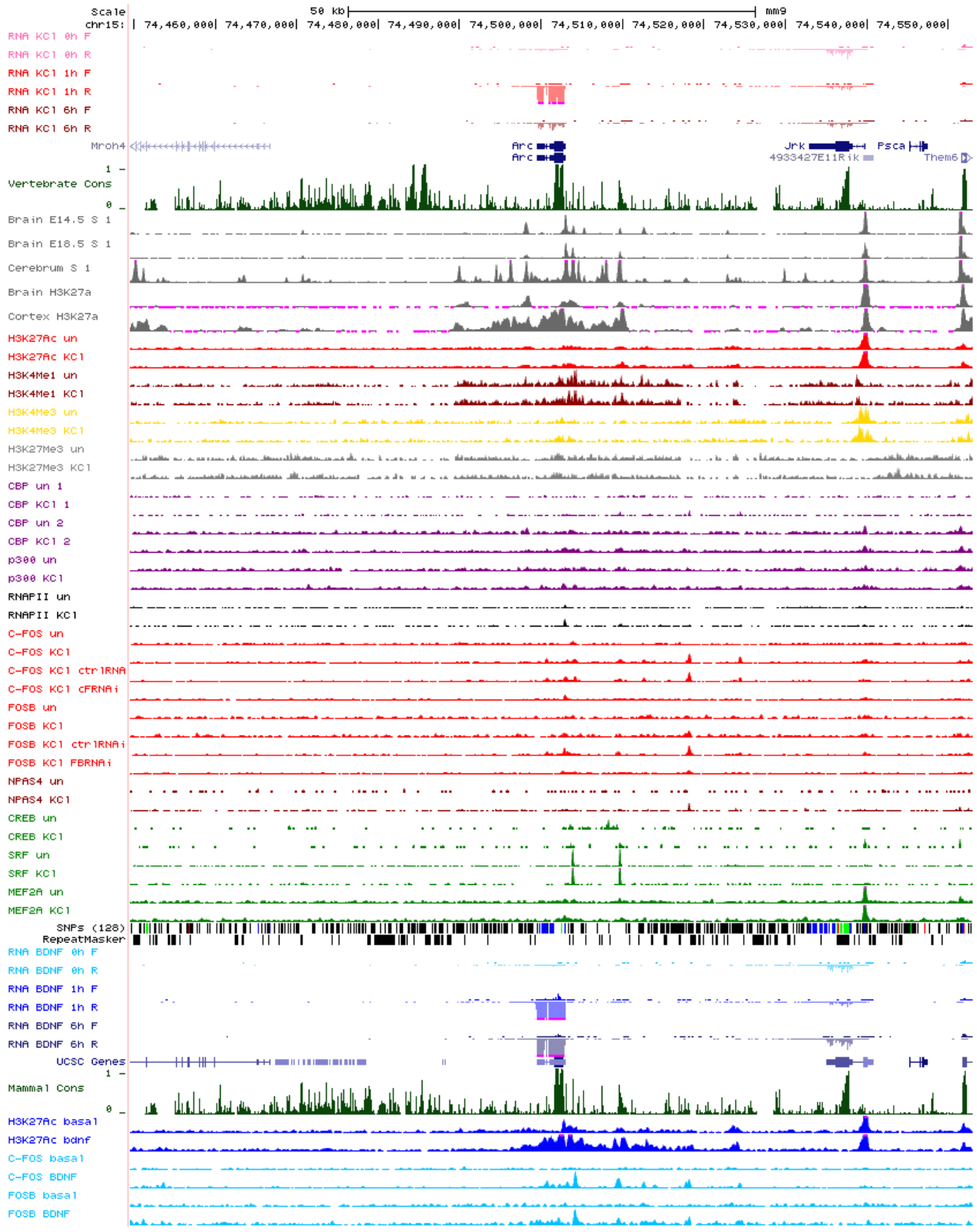

Figure 6.5: *Arc* locus

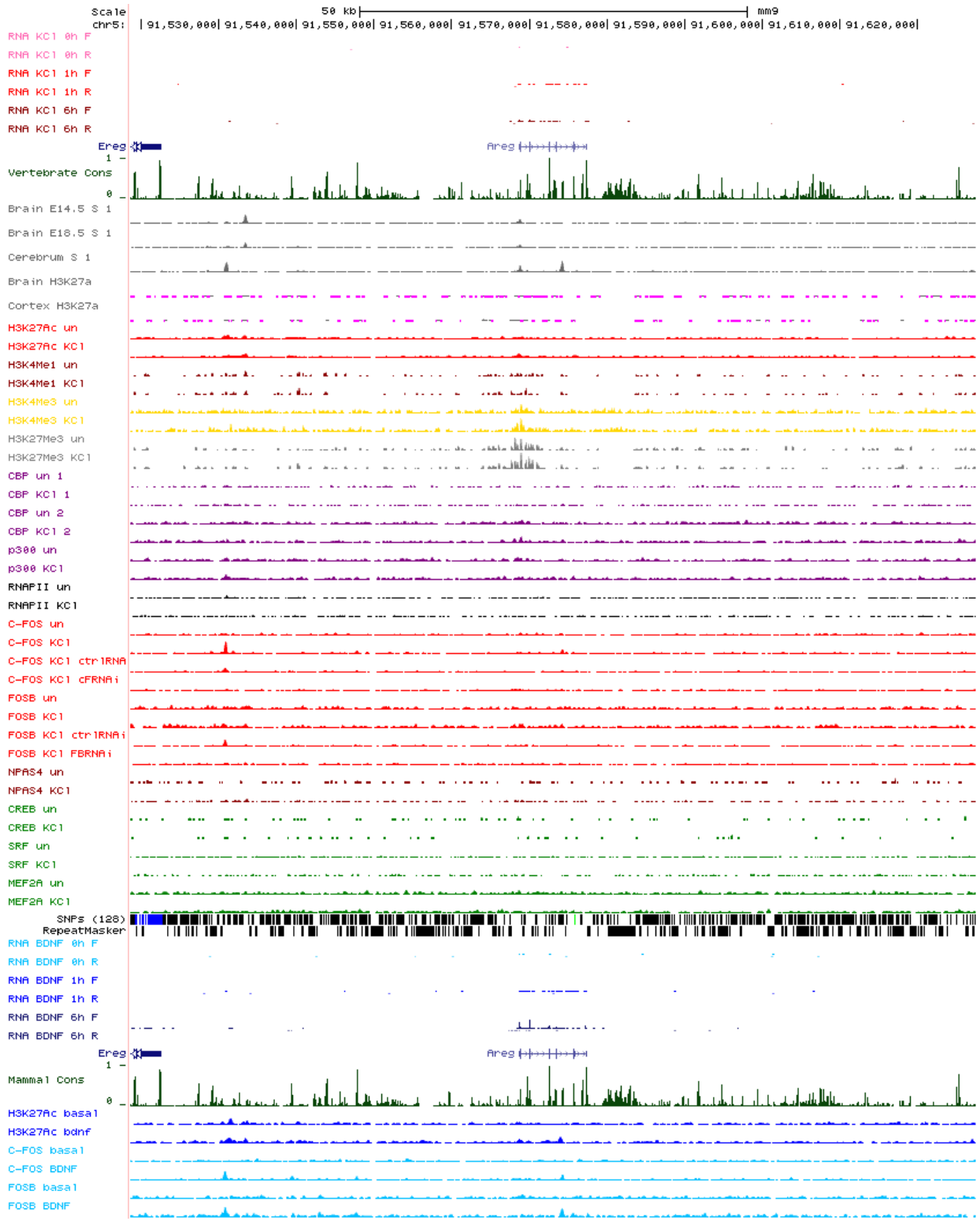

Figure 6.6: *Areg* locus

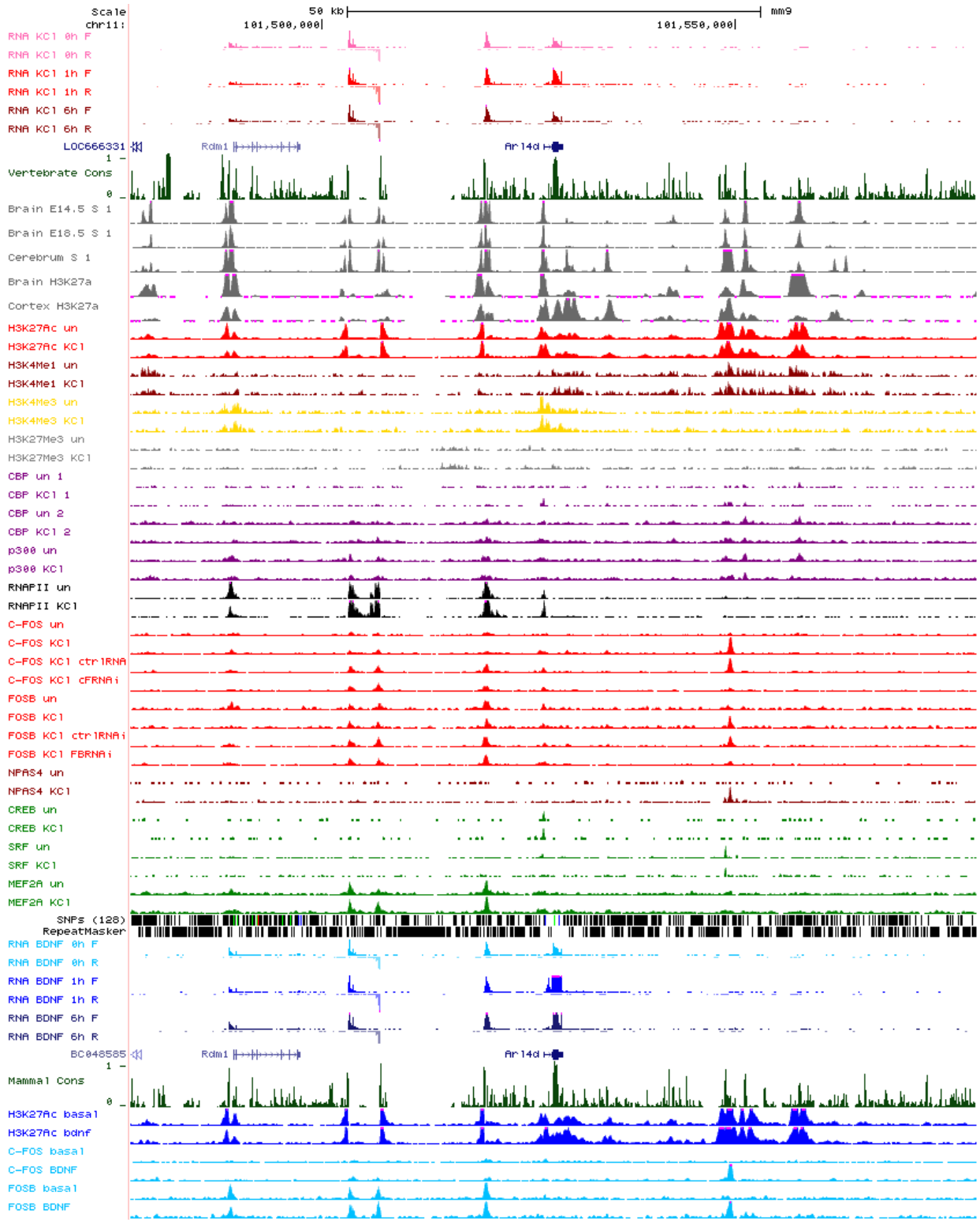

Figure 6.7: *Arl4d* locus

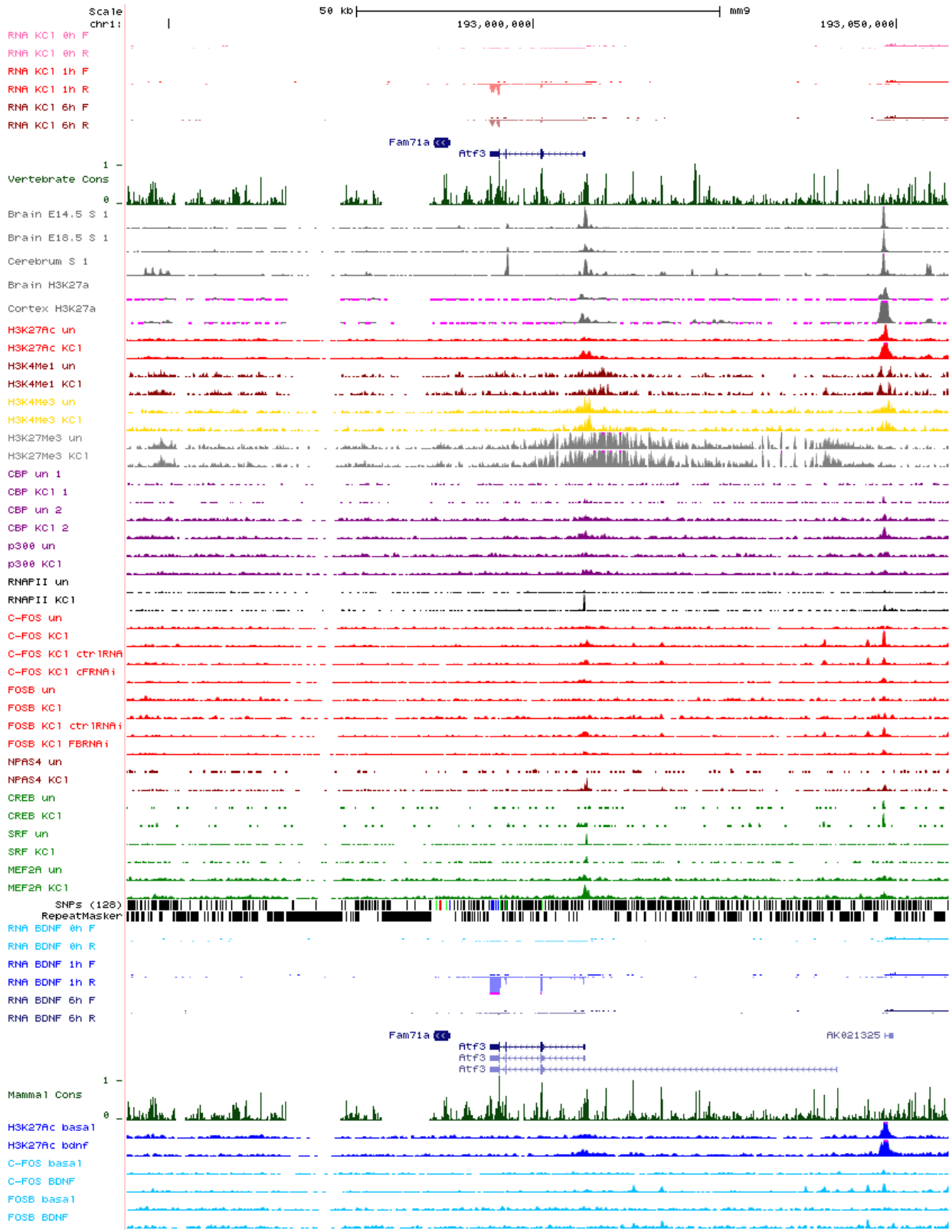

Figure 6.8: *Atf3* locus

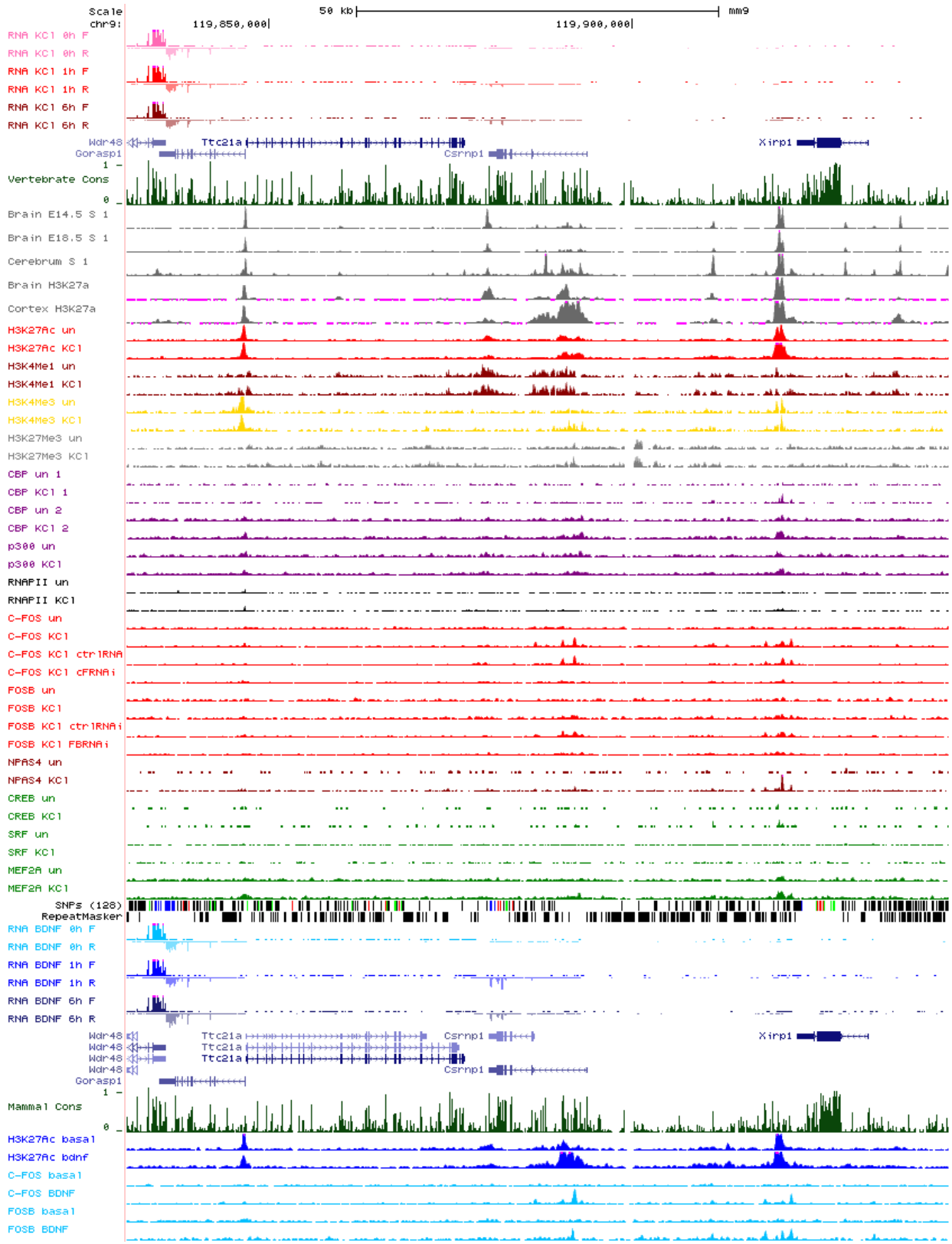

Figure 6.9: *Axud1* locus

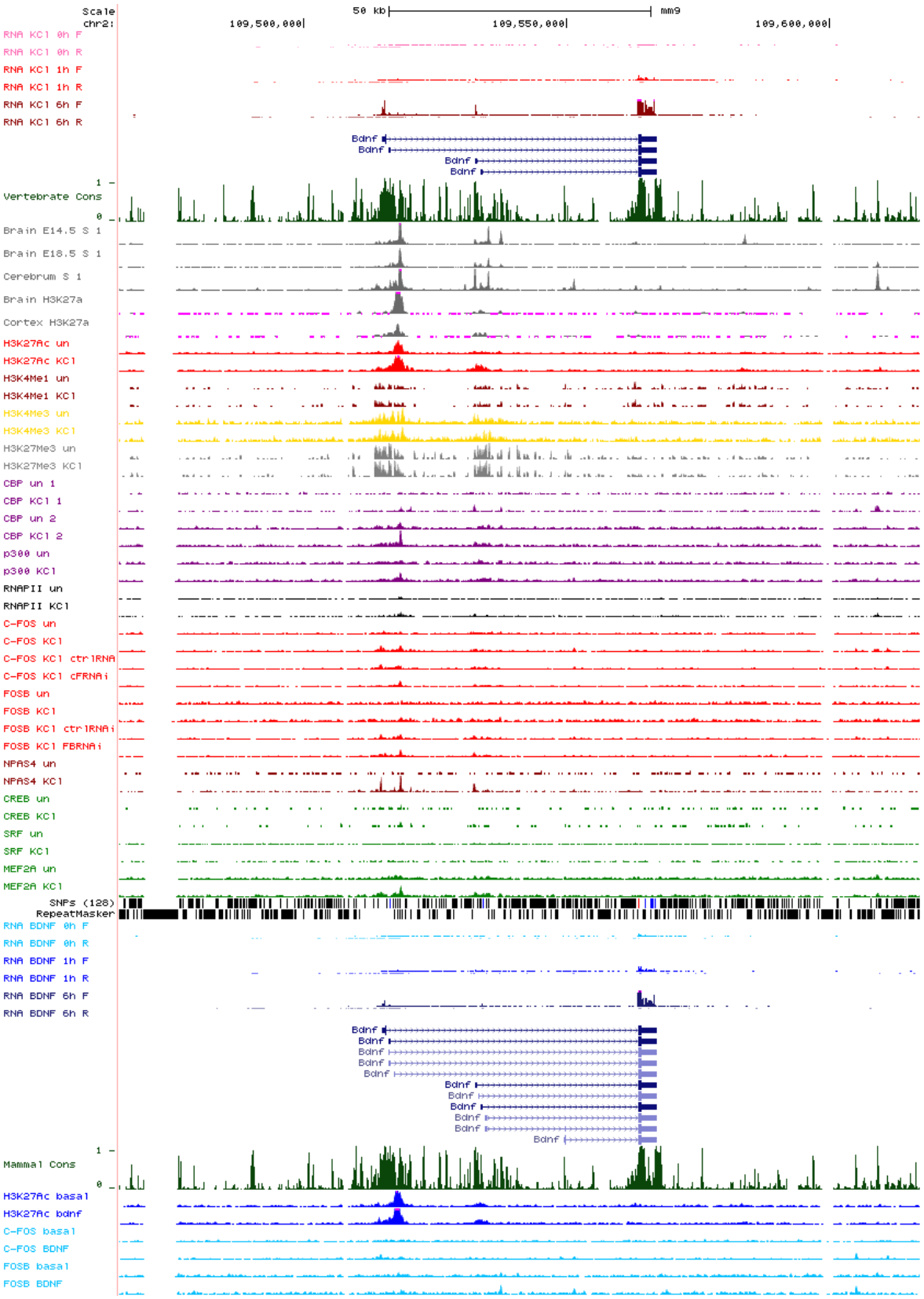

Figure 6.10: *Bdnf* locus

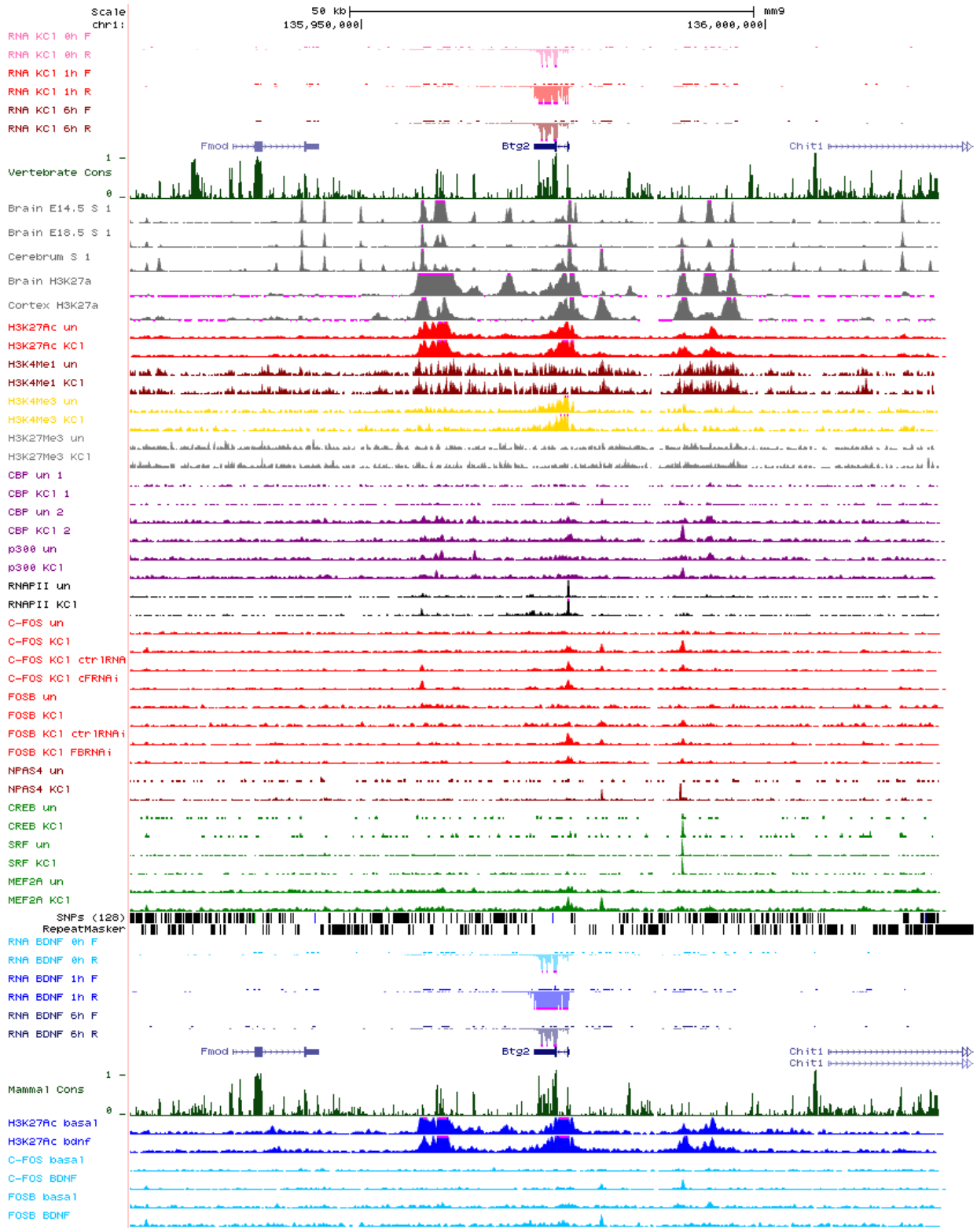

Figure 6.11: *Btg2* locus

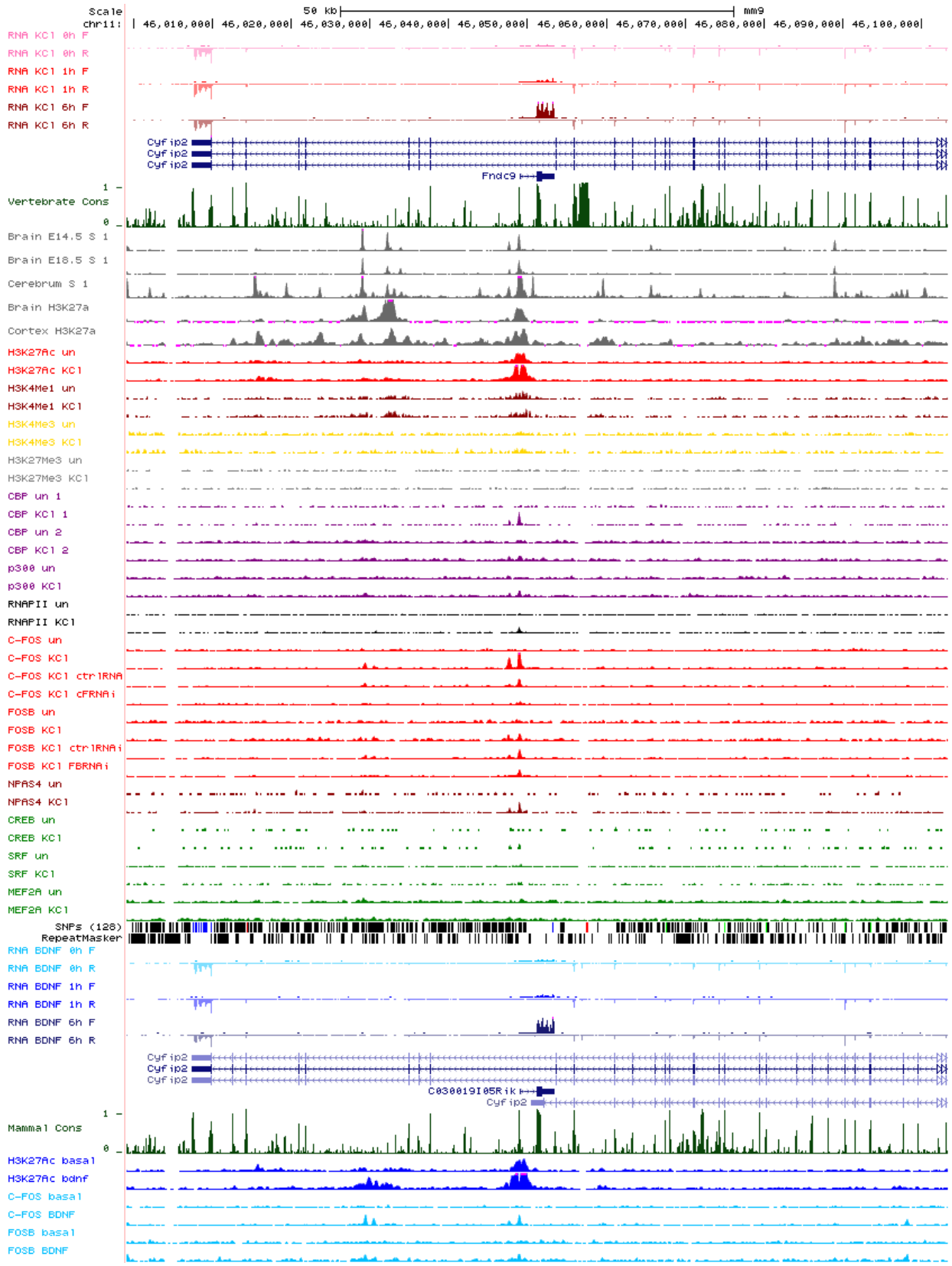

Figure 6.12: *C030019I05Rik* locus

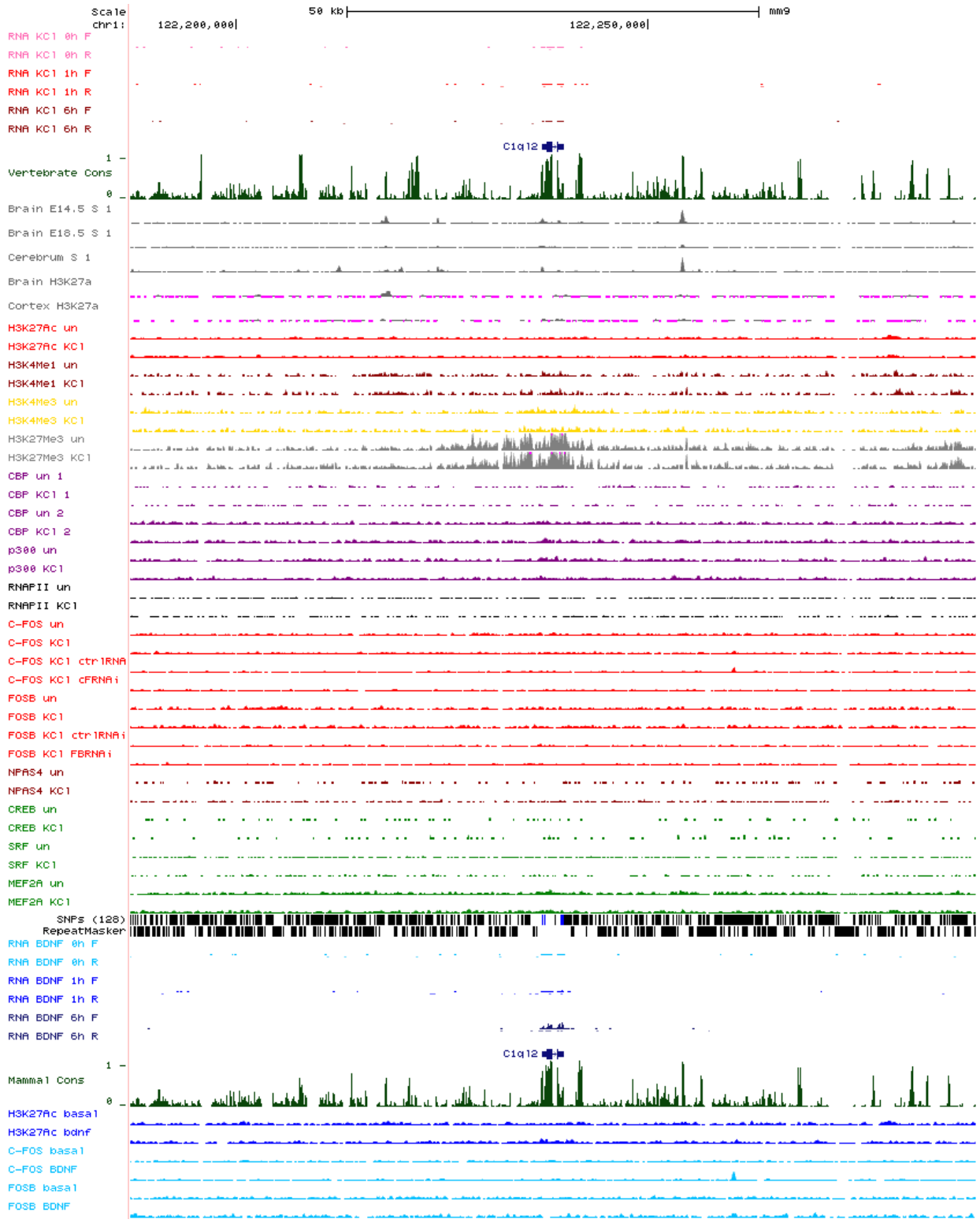

Figure 6.13: *C1ql2* locus

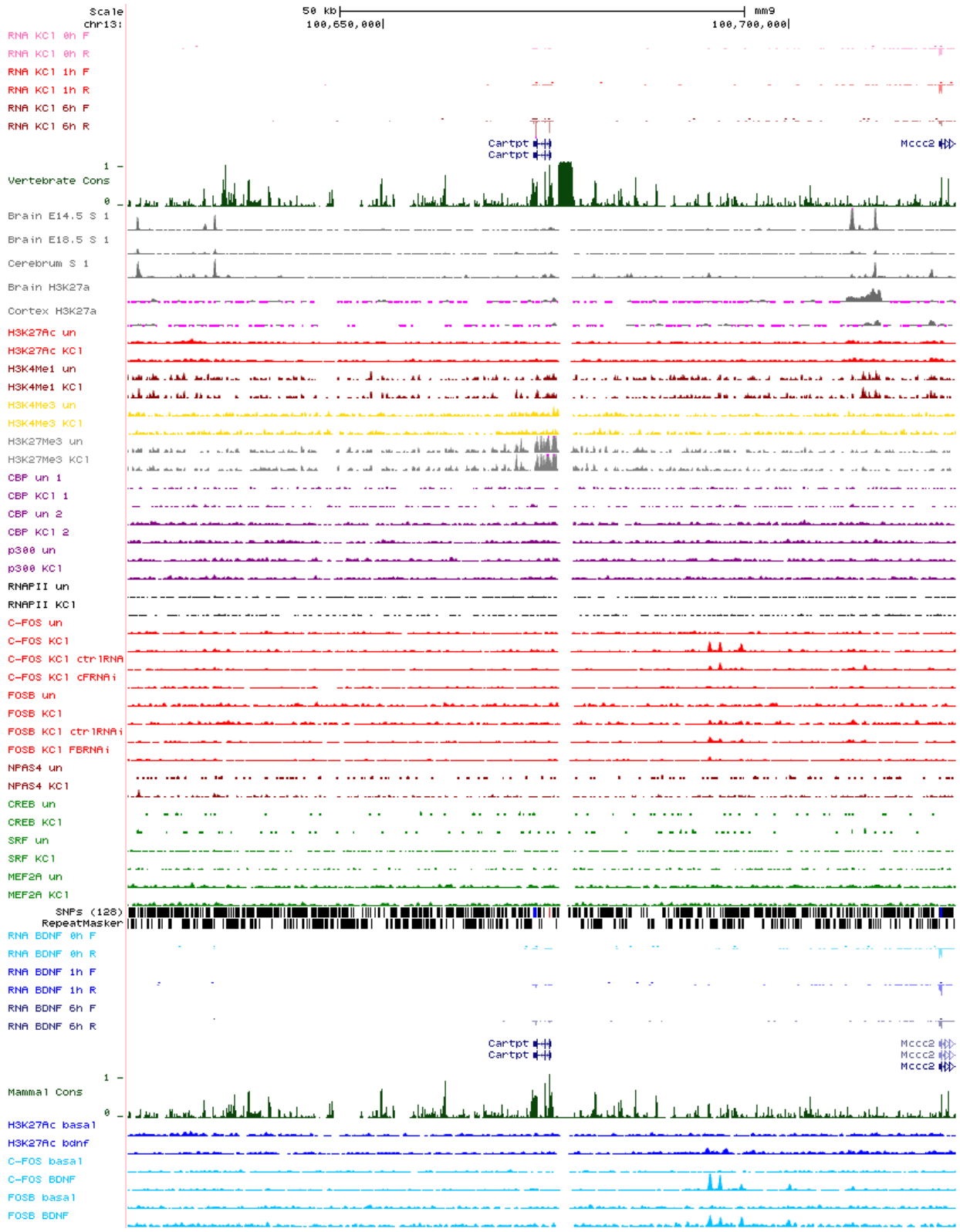

Figure 6.14: *Cartpt* locus

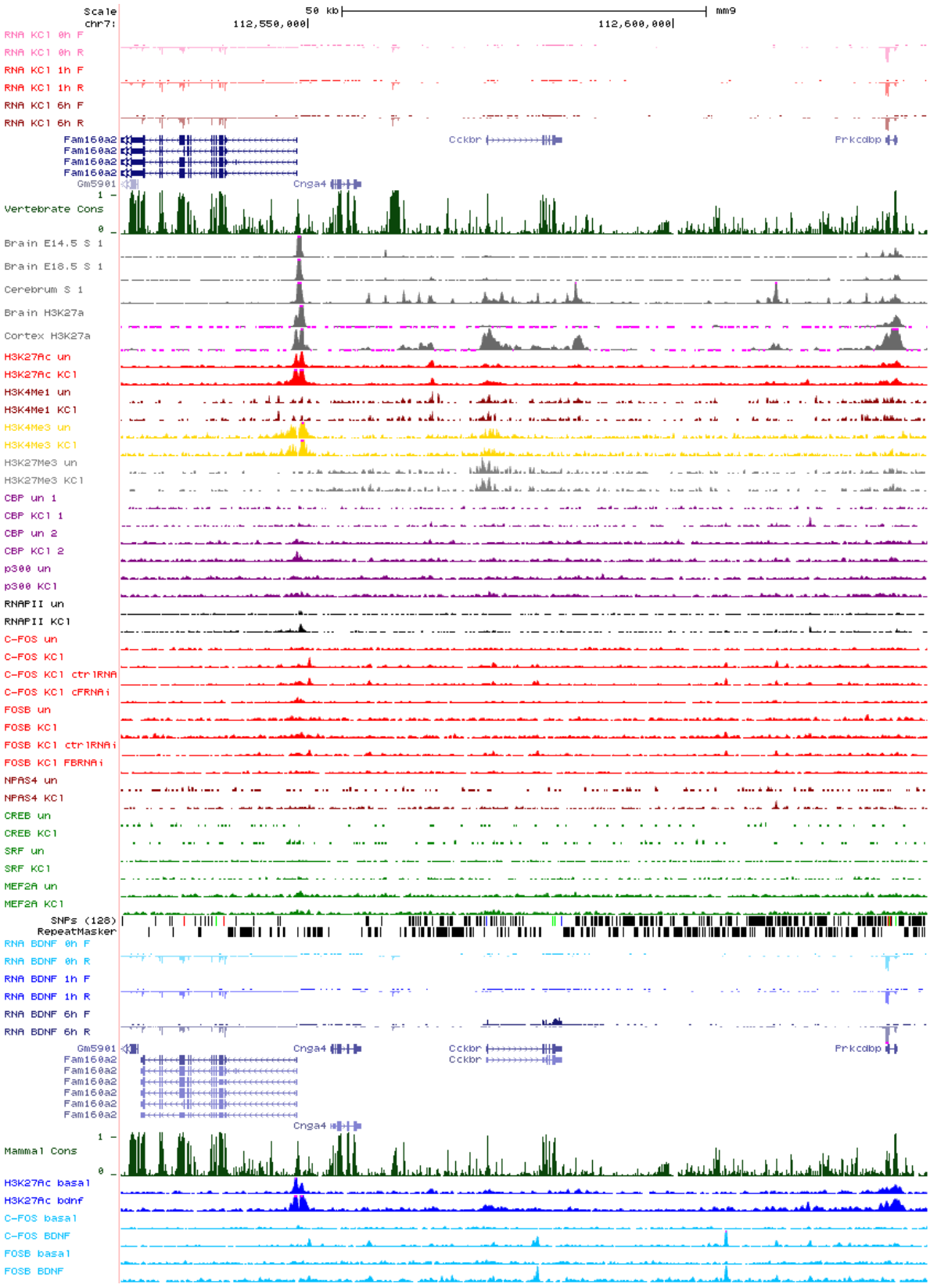

Figure 6.15: *Cckbr* locus

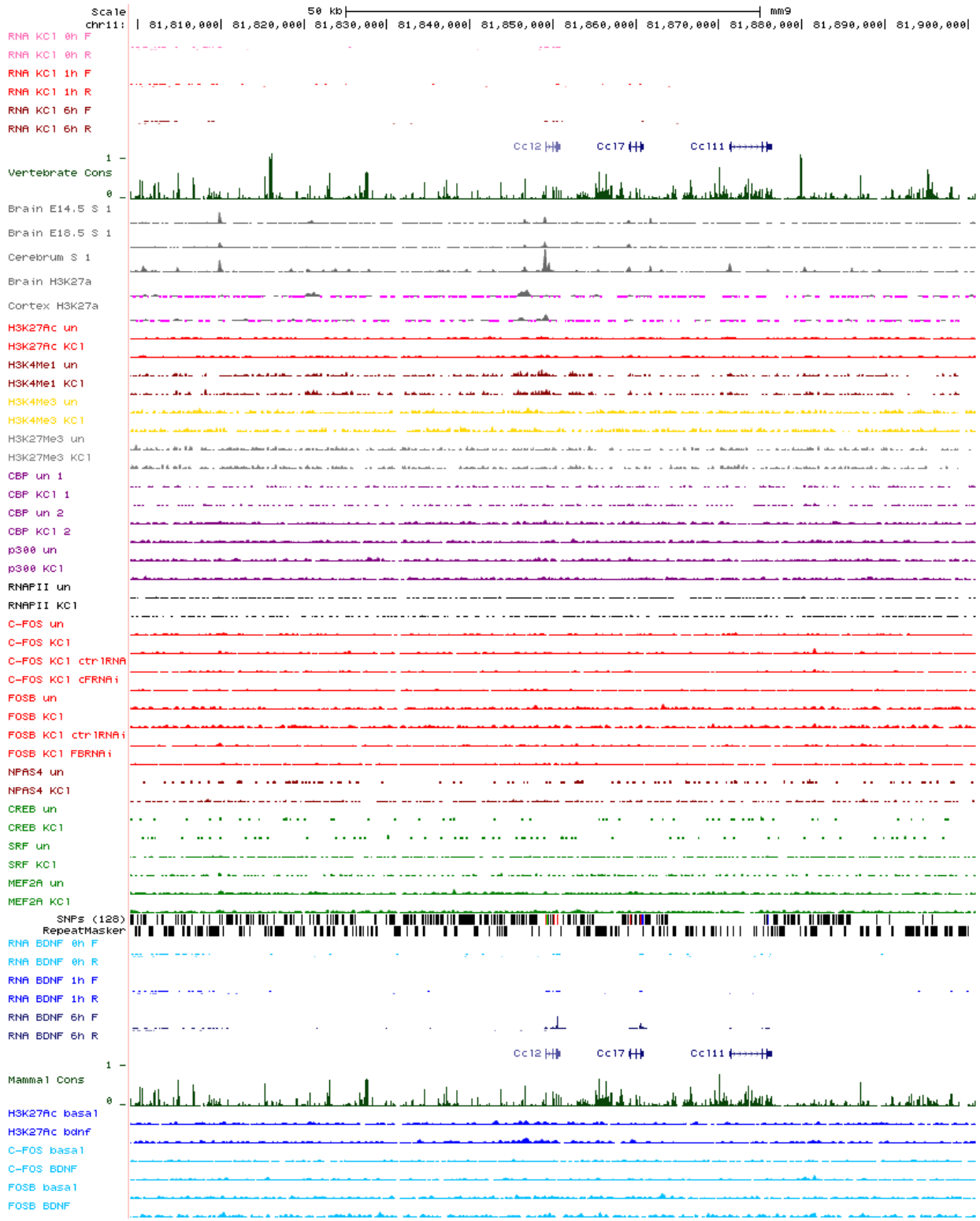

Figure 6.16: *Ccl2* locus

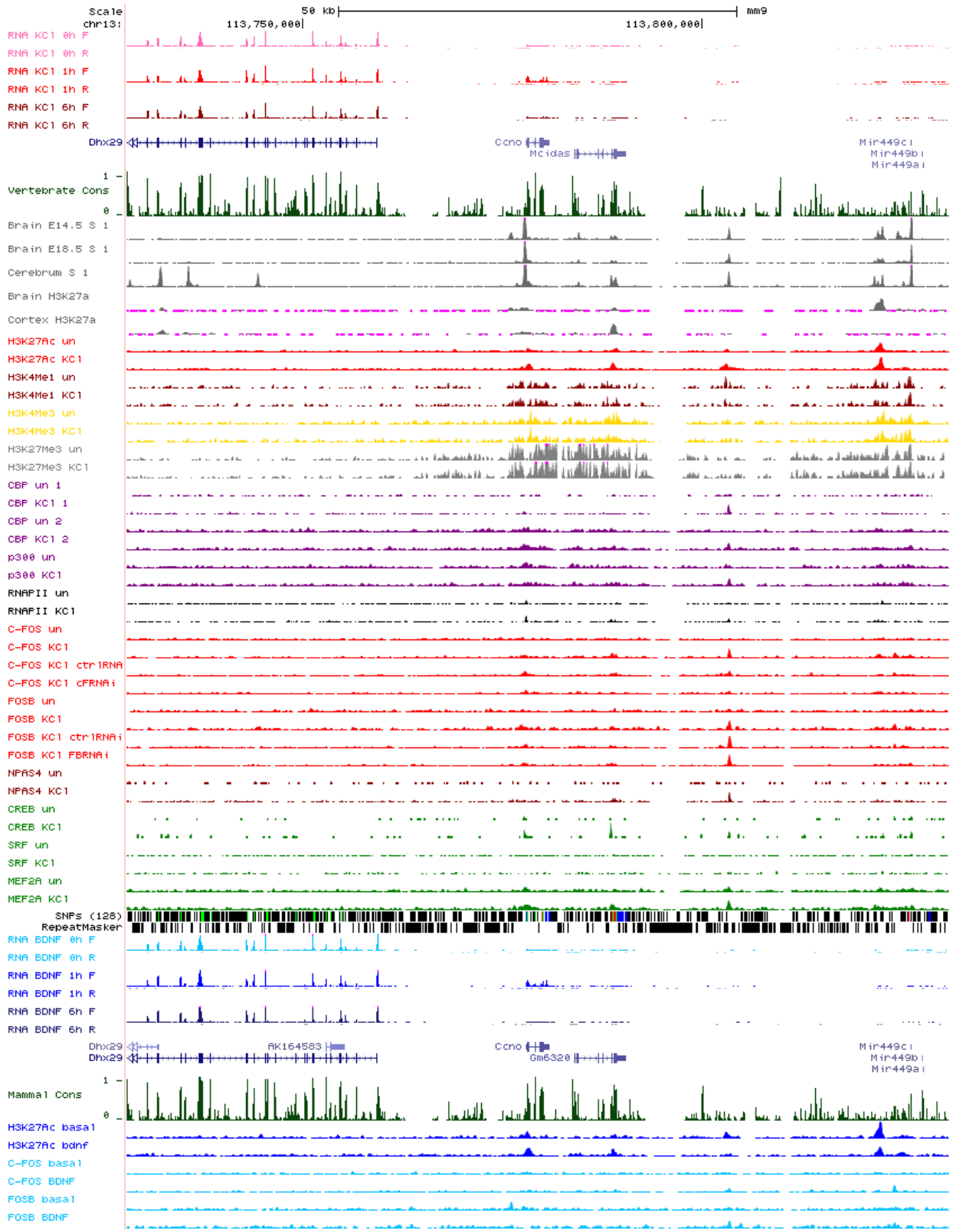

Figure 6.17: *Ccnu* locus

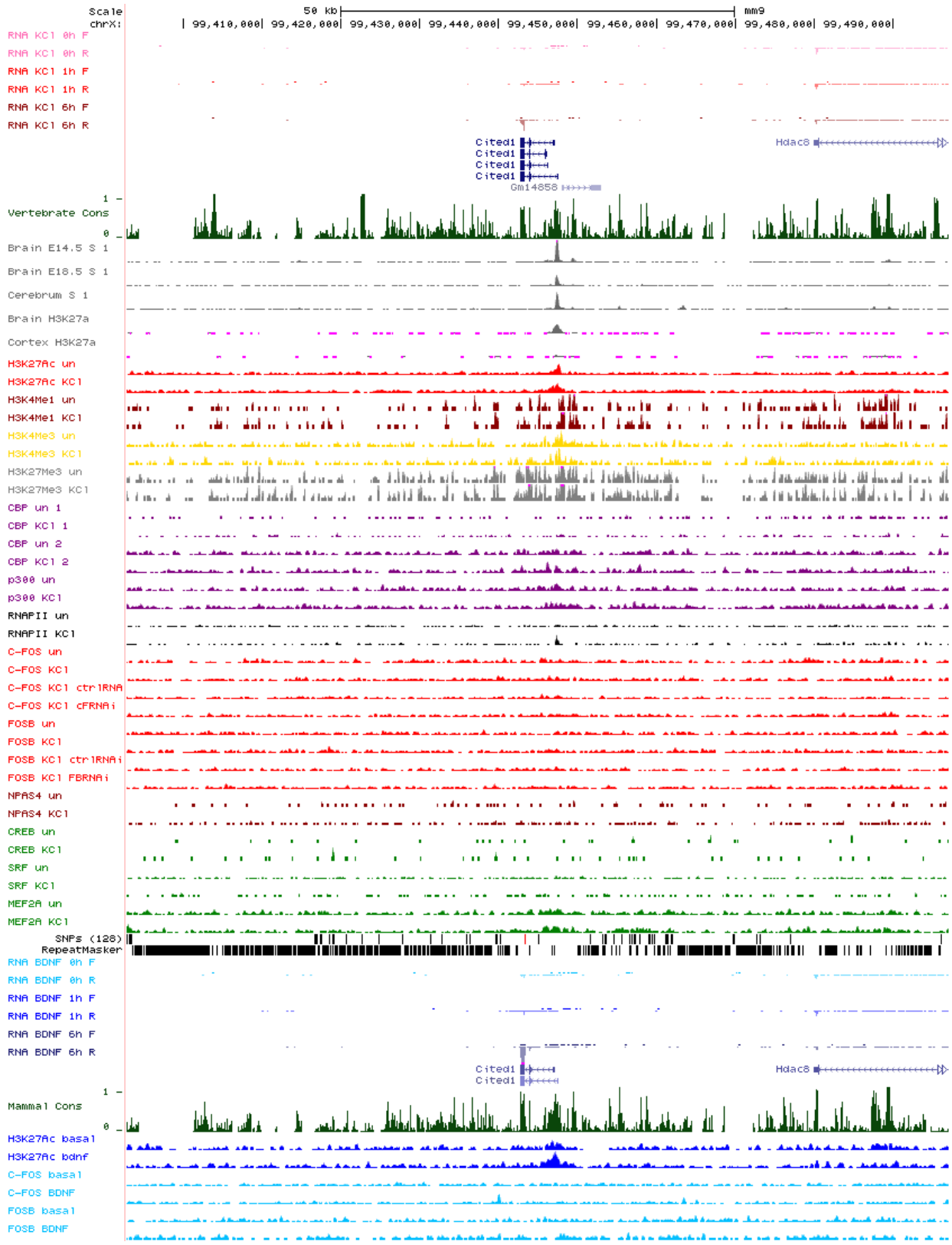

Figure 6.18: *Cited1* locus

Figure 6.19: *Col10a1* locus

Figure 6.20: *Cort* locus

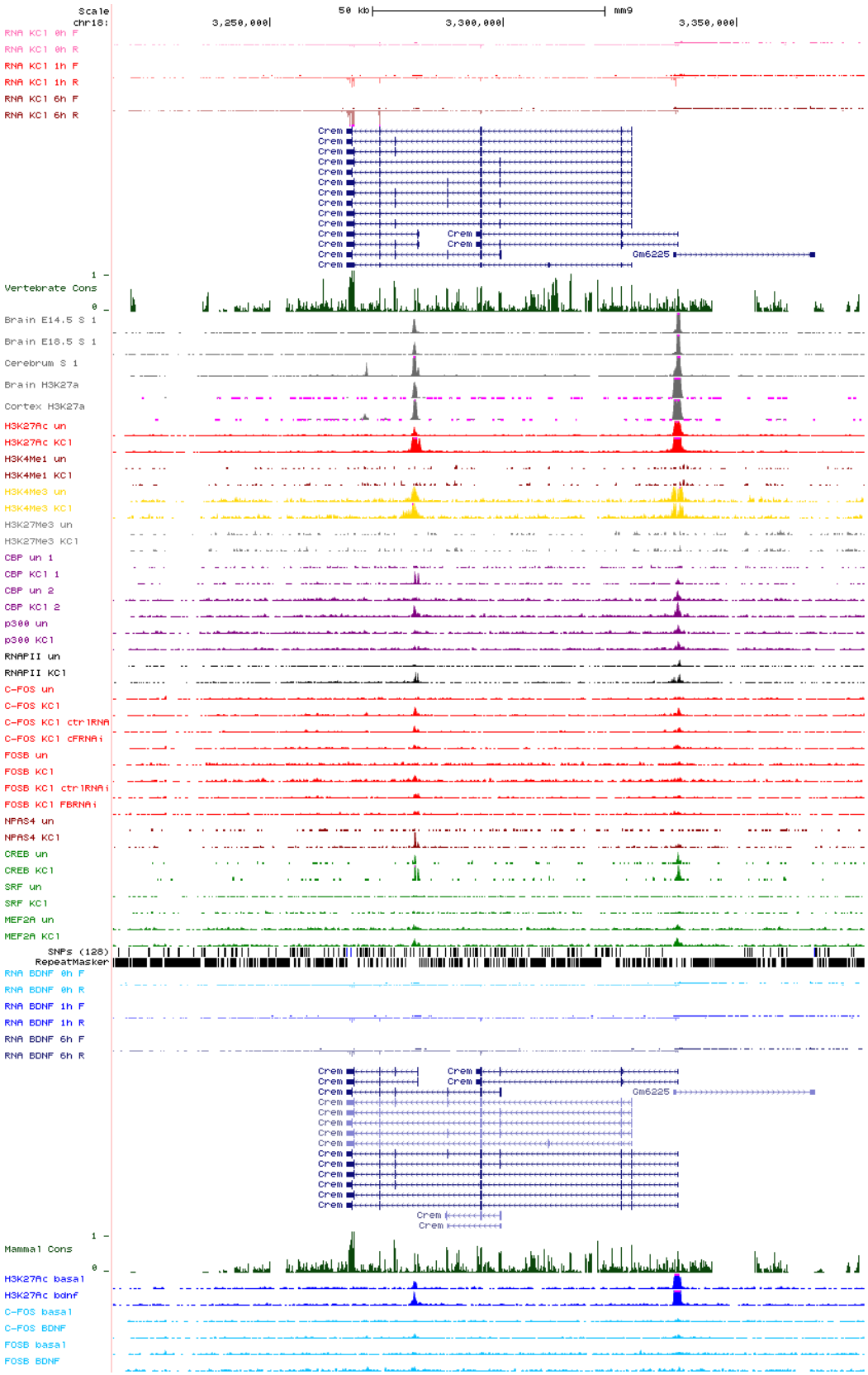

Figure 6.21: *Crem* locus

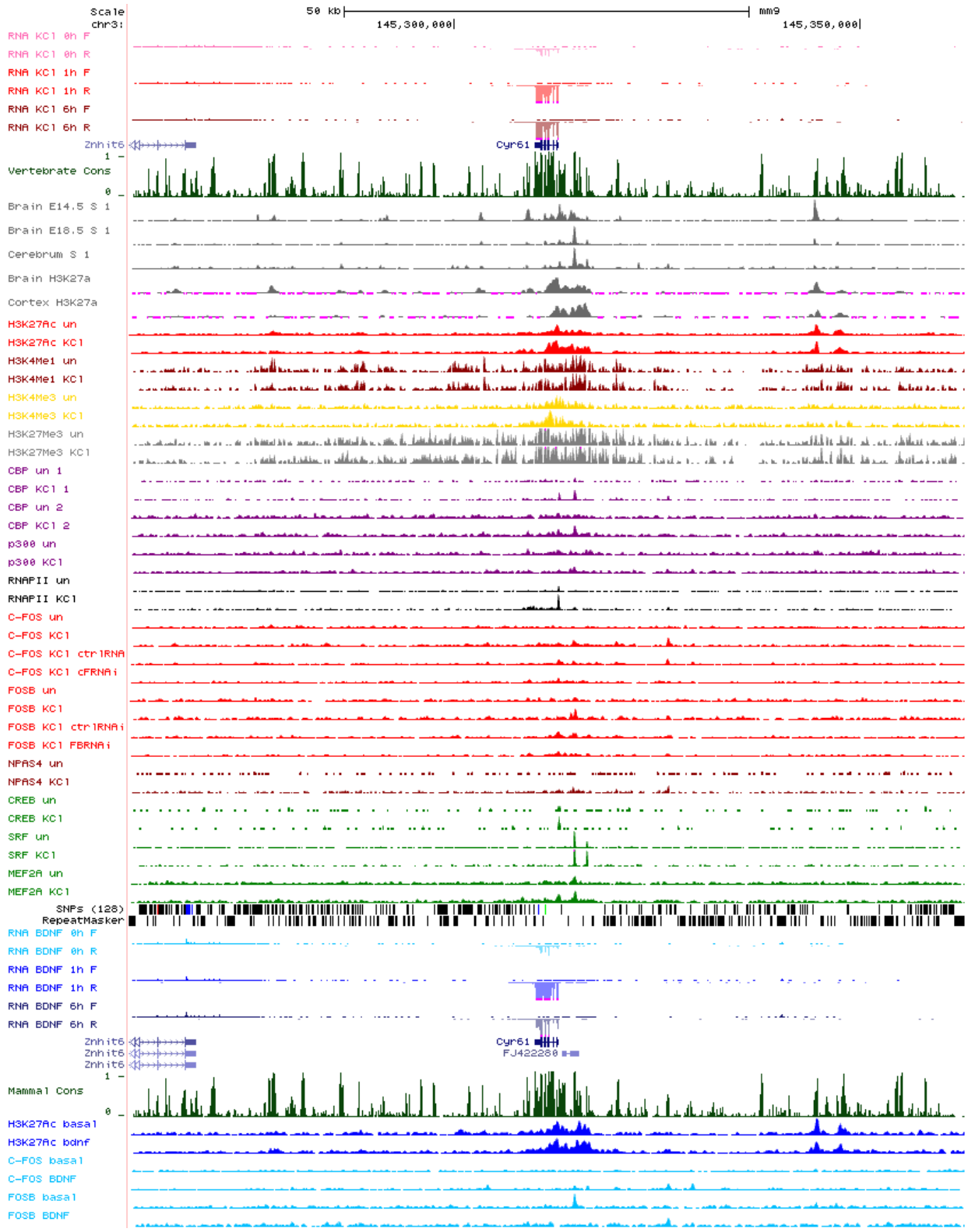

Figure 6.22: *Cyr61* locus

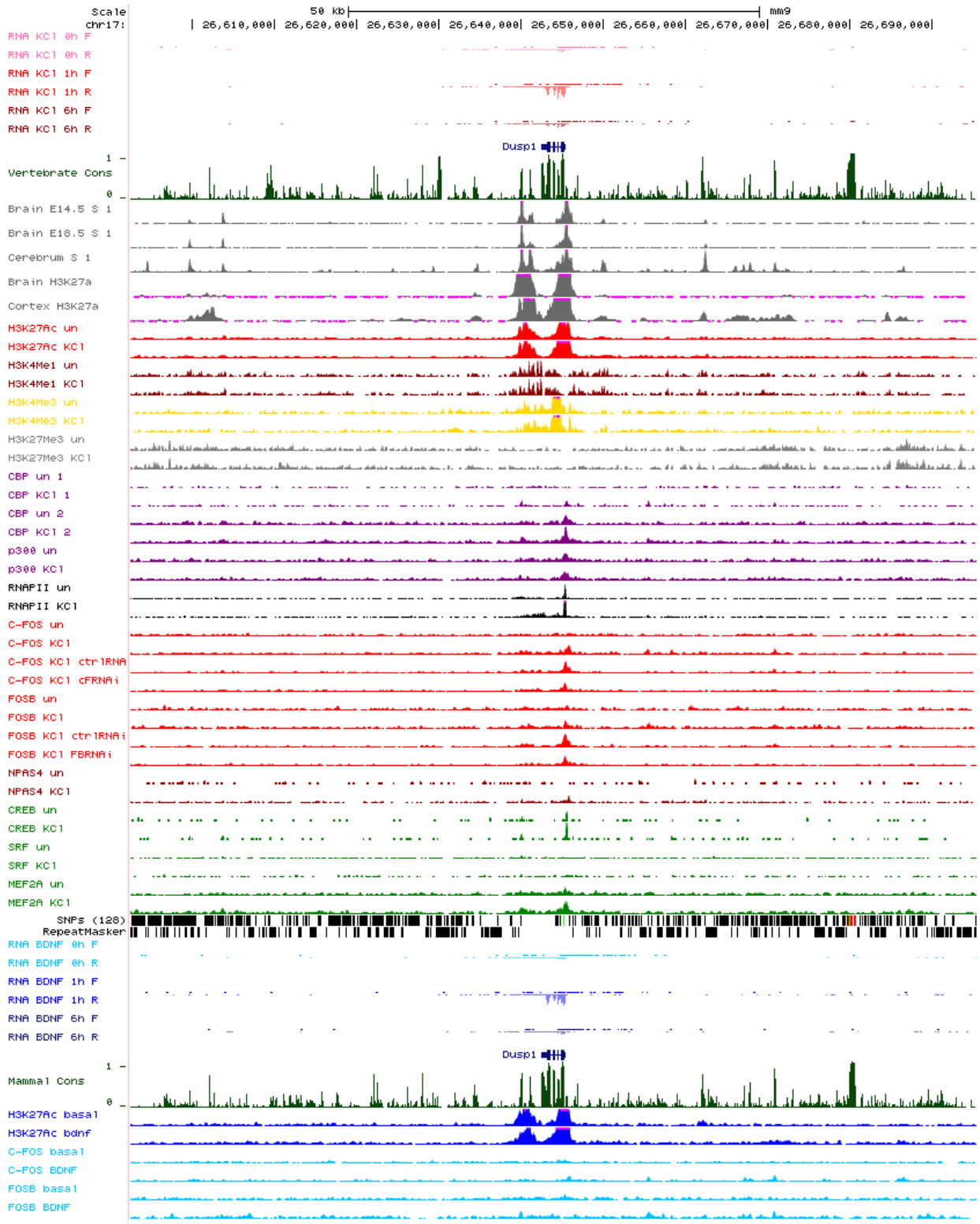

Figure 6.23: *Dusp1* locus

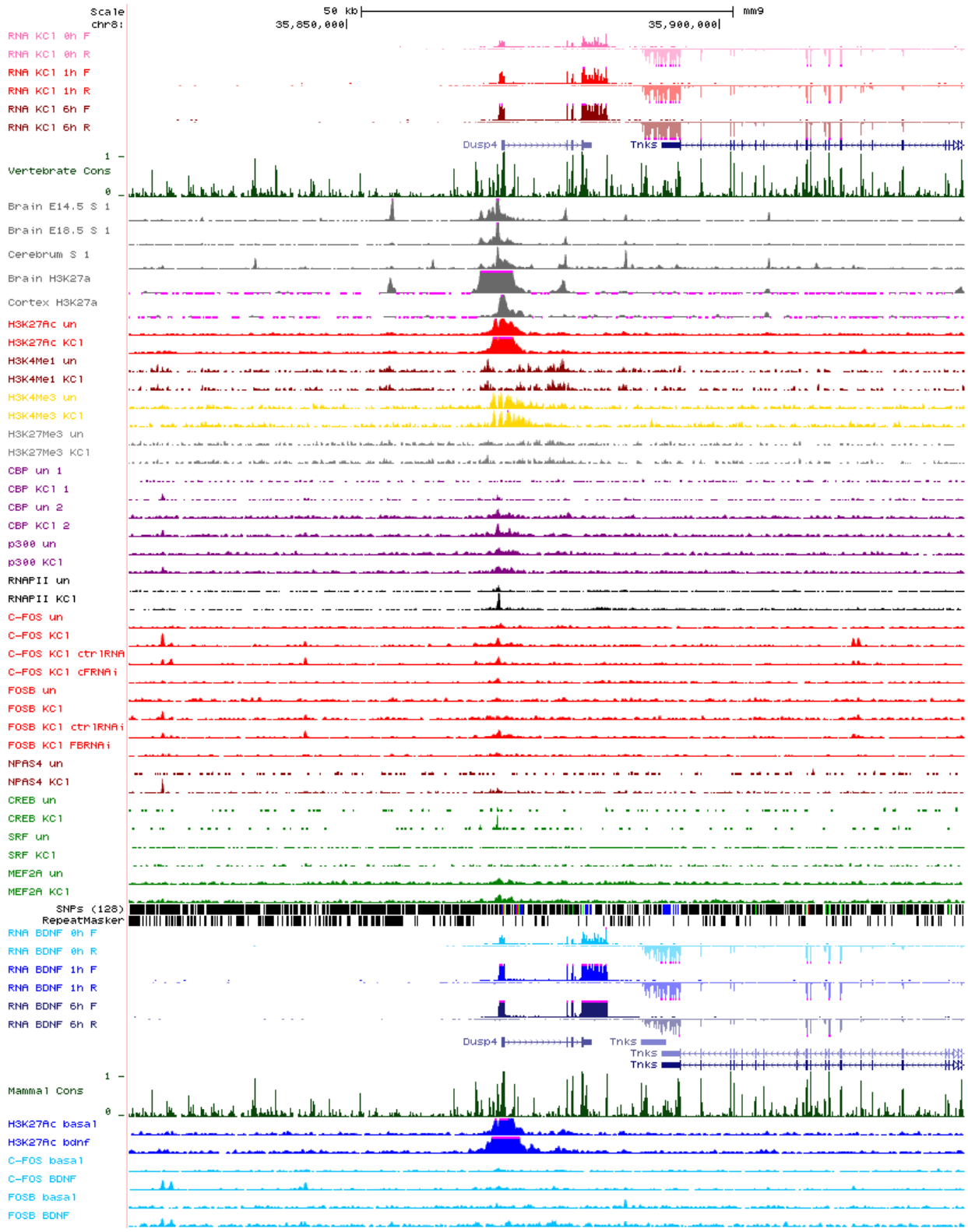

Figure 6.24: *Dusp4* locus

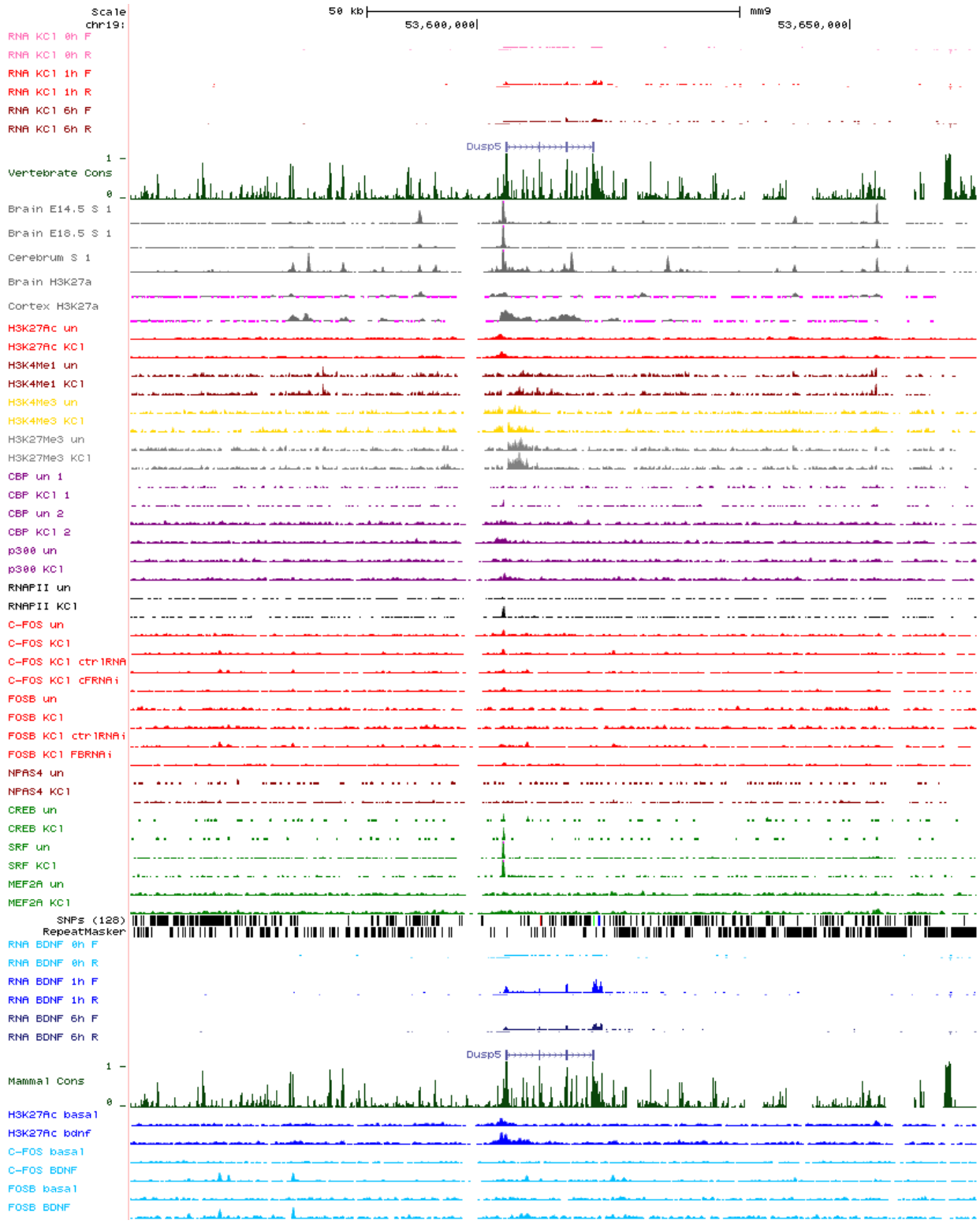

Figure 6.25: *Dusp5* locus

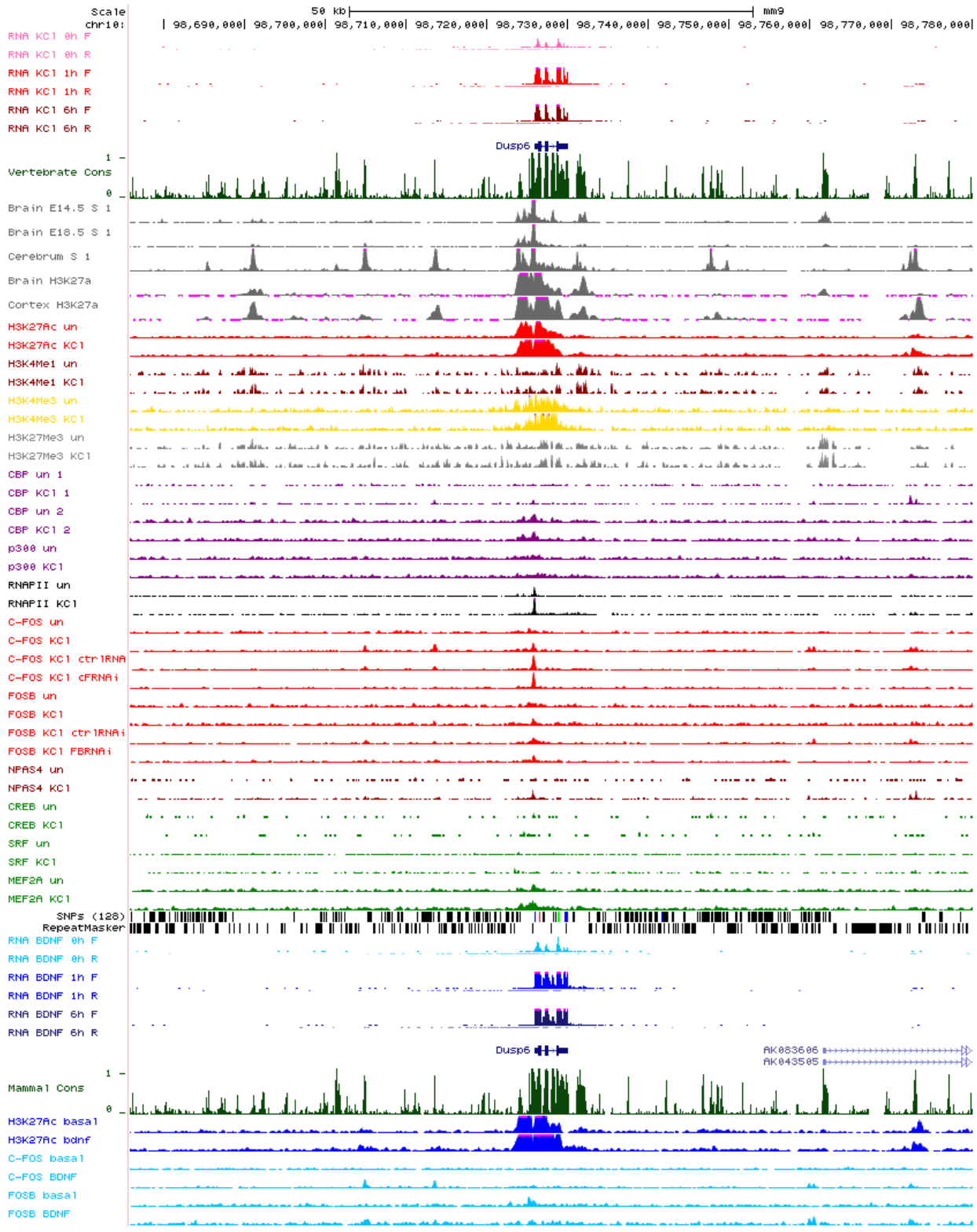

Figure 6.26: *Dusp6* locus

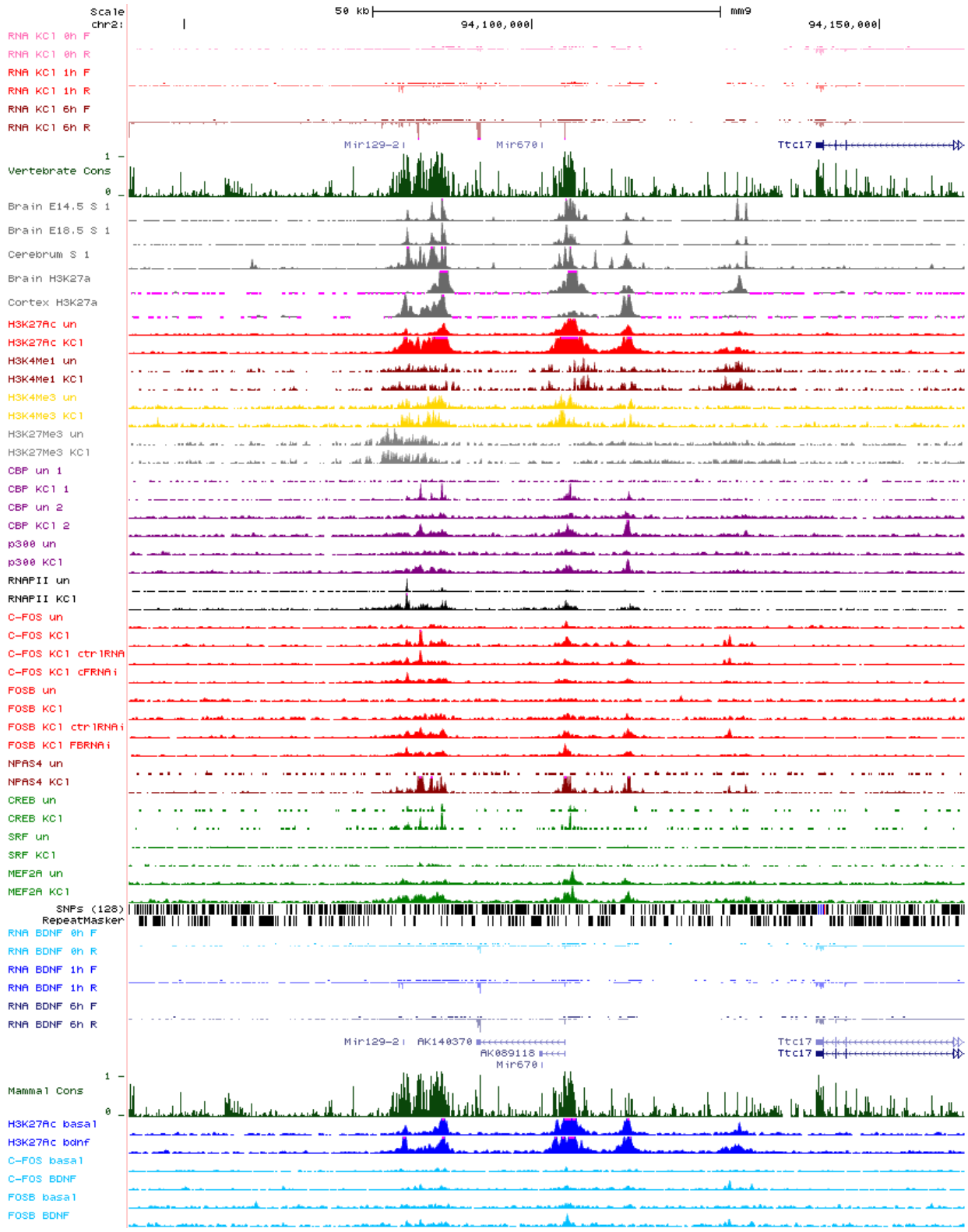

Figure 6.27: *E530001K10Rik* locus

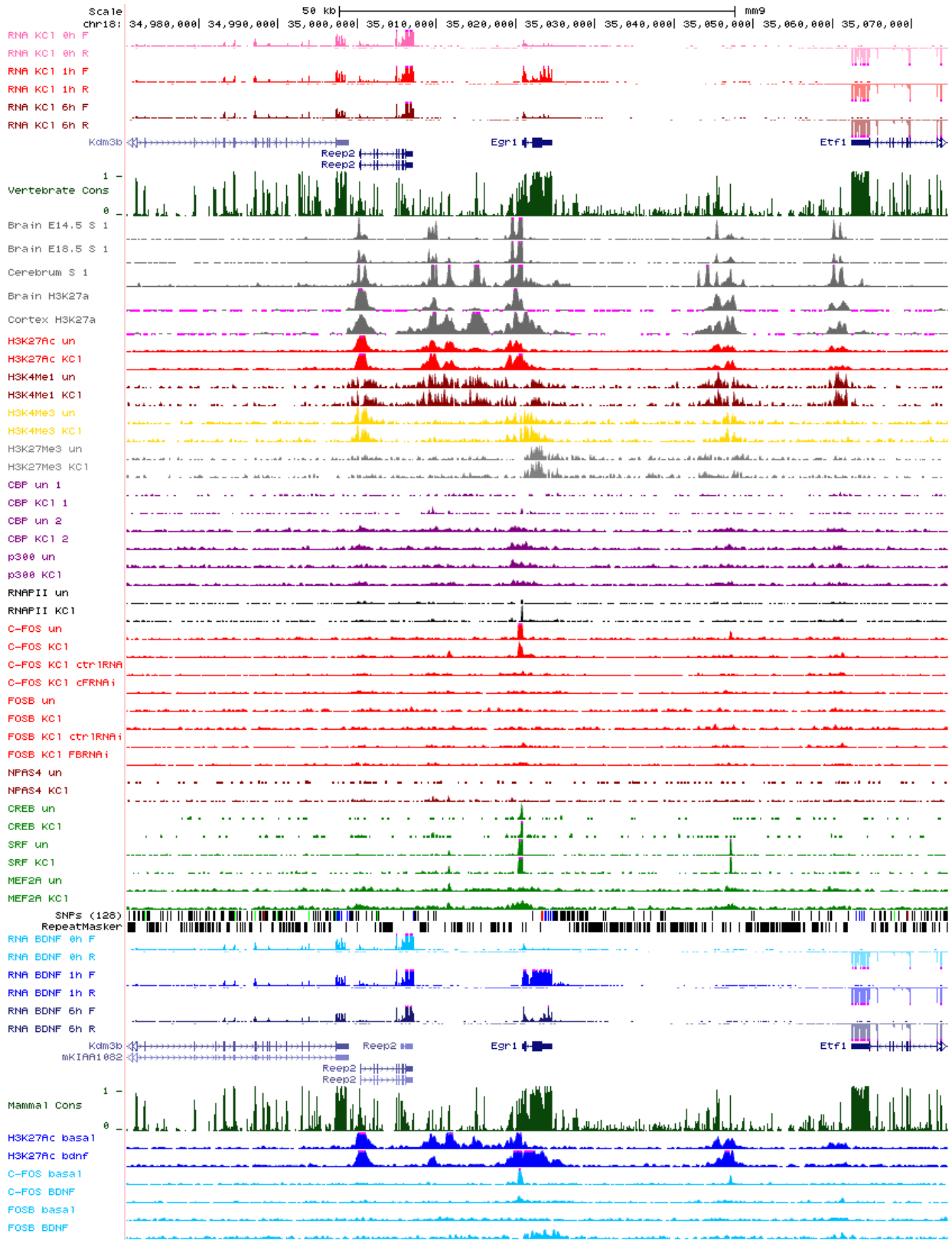

Figure 6.28: *Egr1* locus

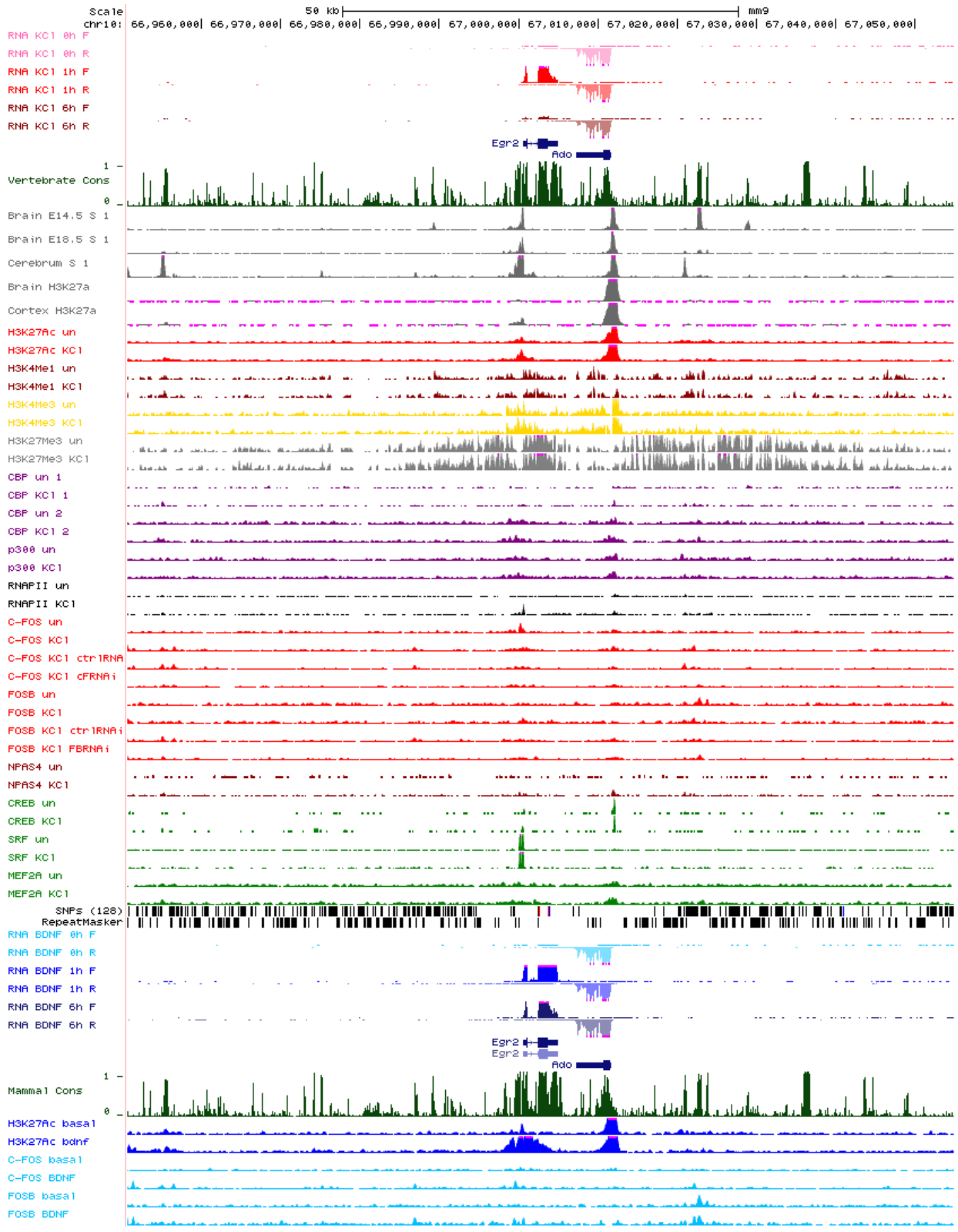

Figure 6.29: *Egr2* locus

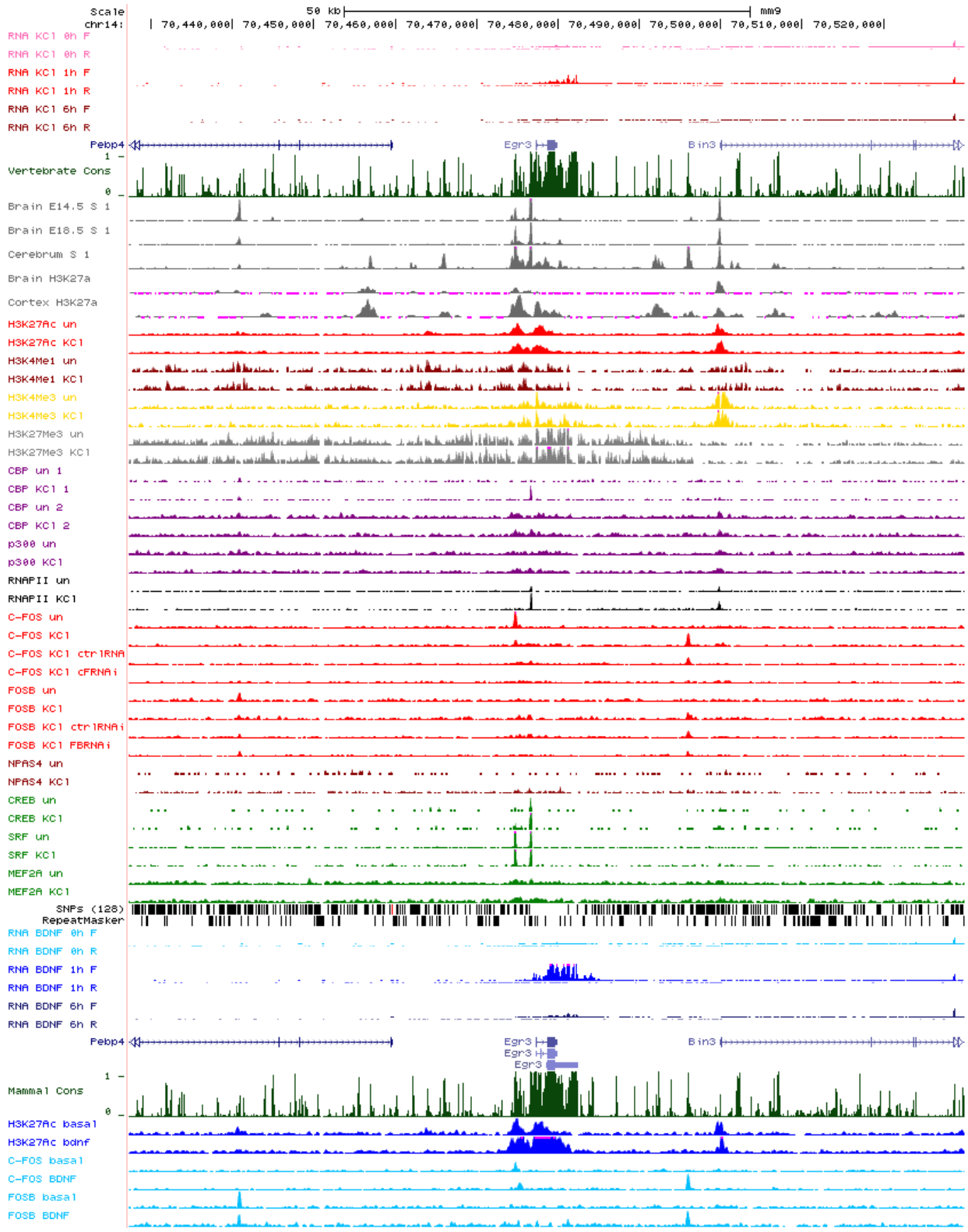

Figure 6.30: *Egr3* locus

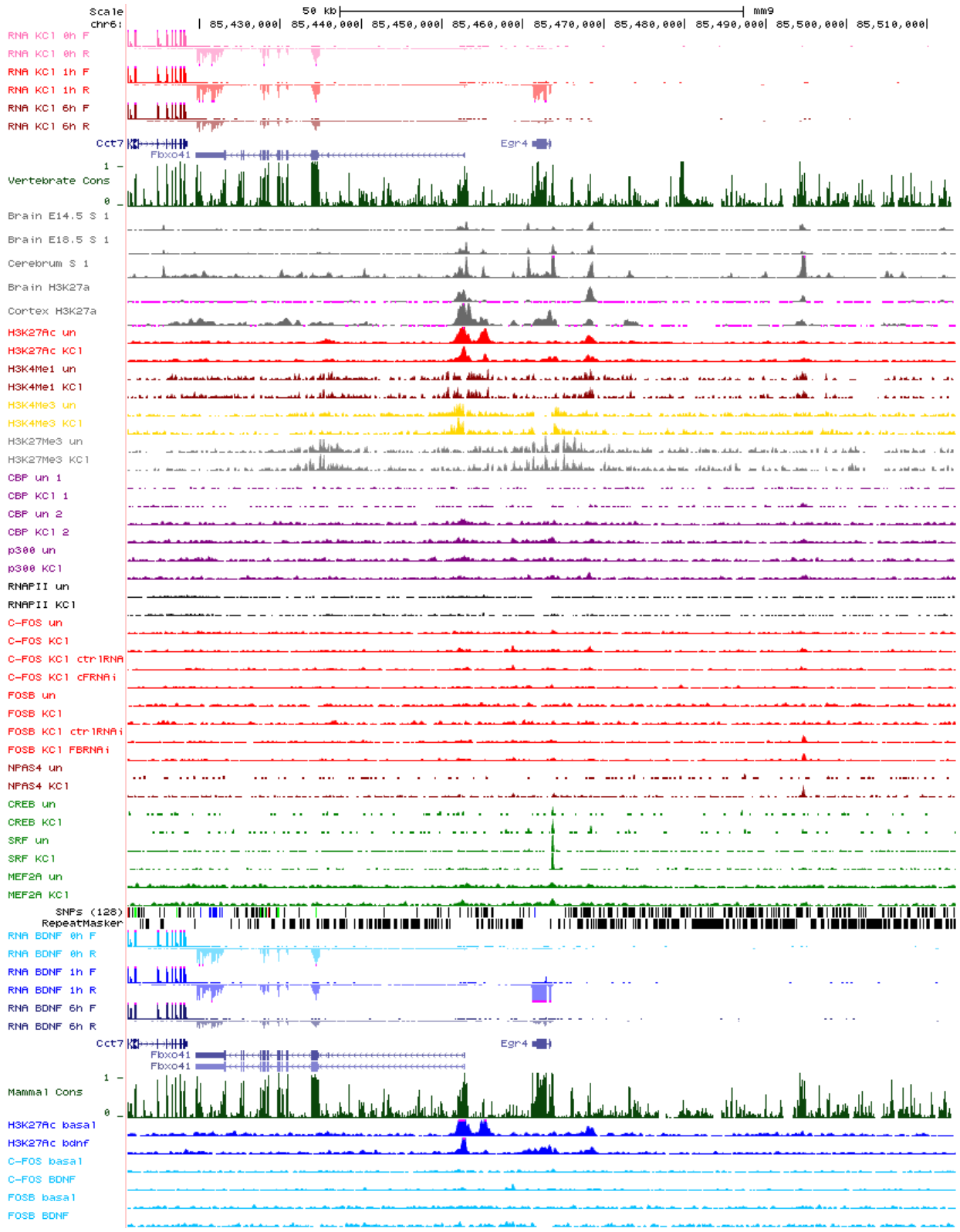

Figure 6.31: *Egr4* locus

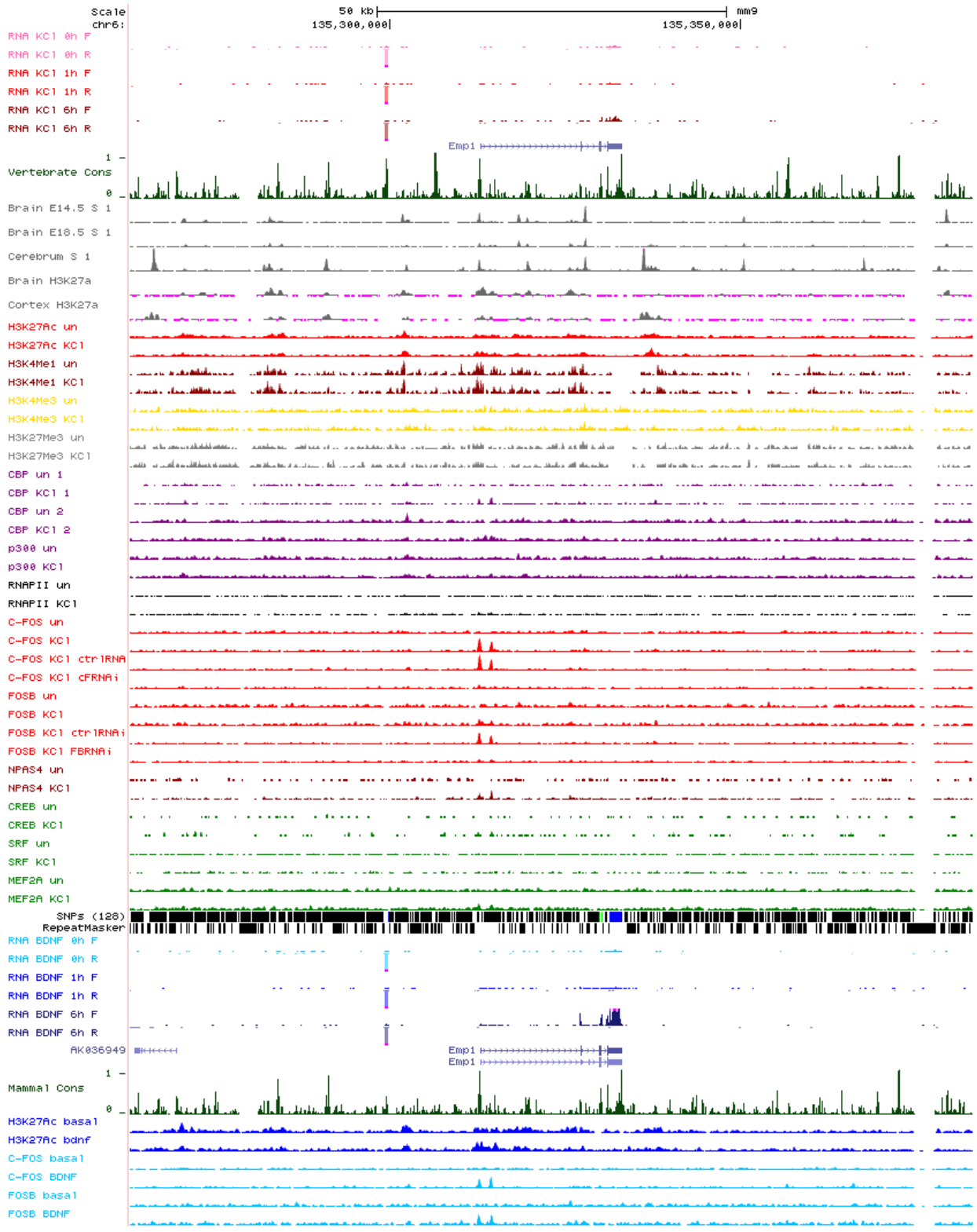

Figure 6.32: *Emp1* locus

Figure 6.33: *Fbxo33* locus

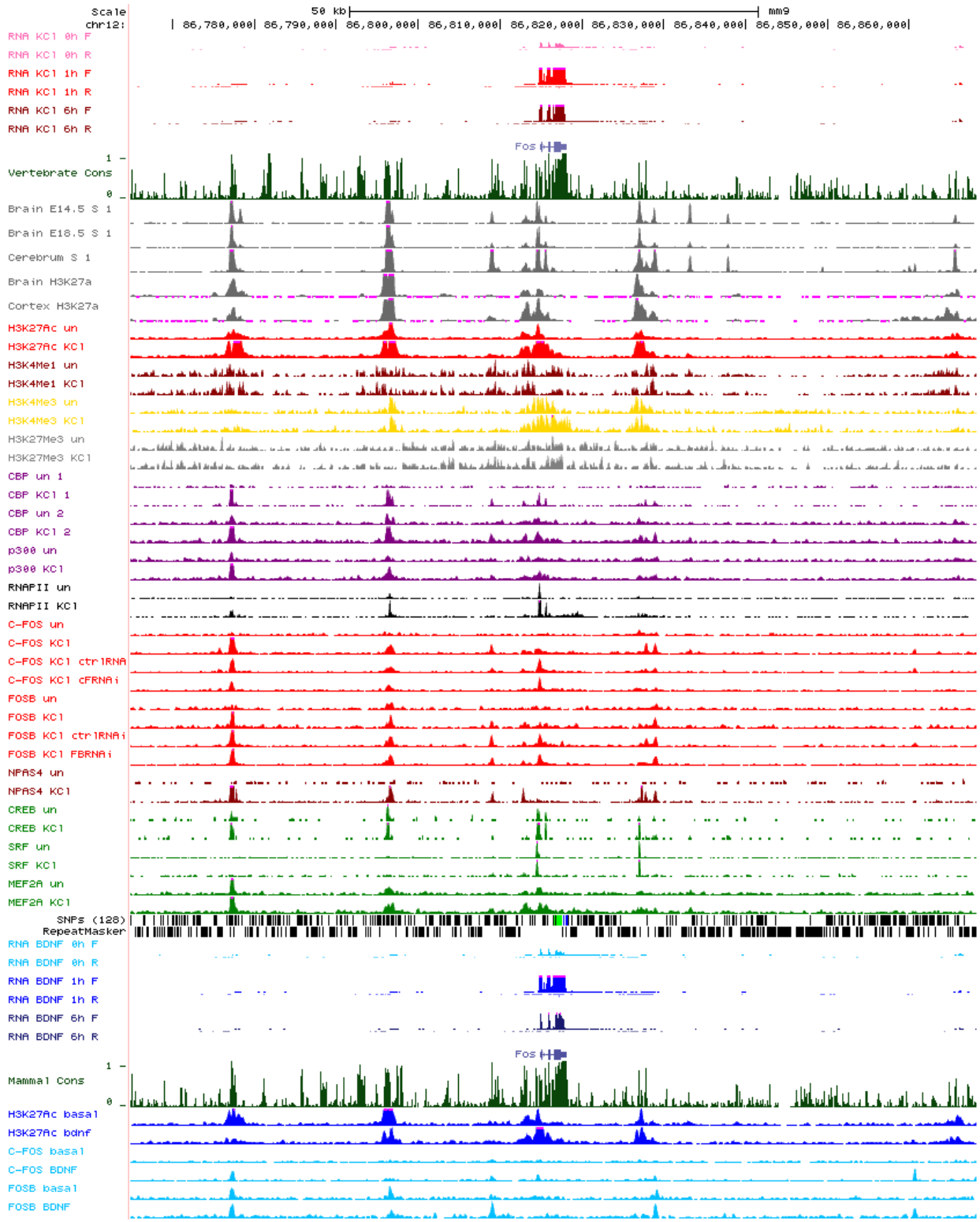

Figure 6.34: *Fos* locus

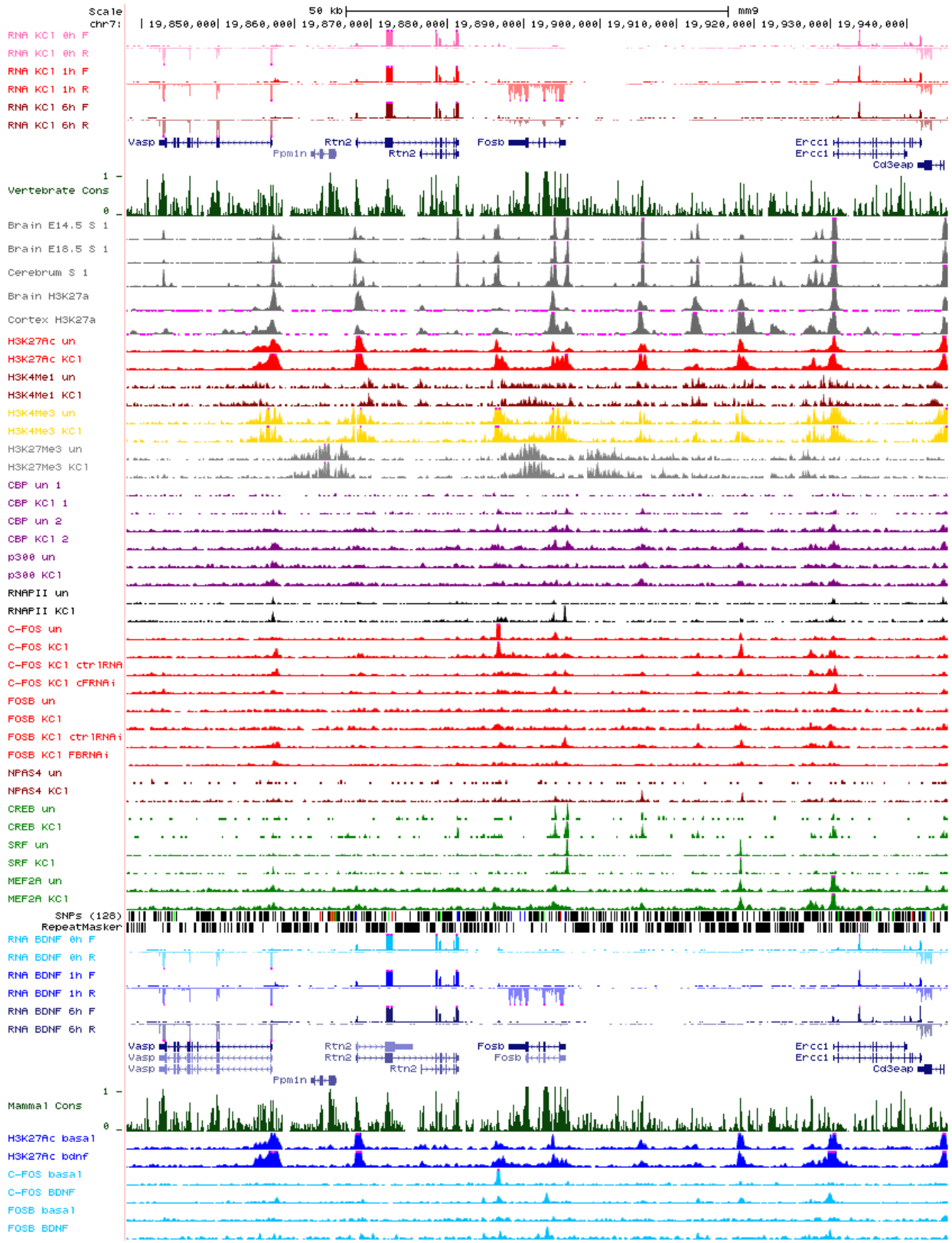

Figure 6.35: *FosB* locus

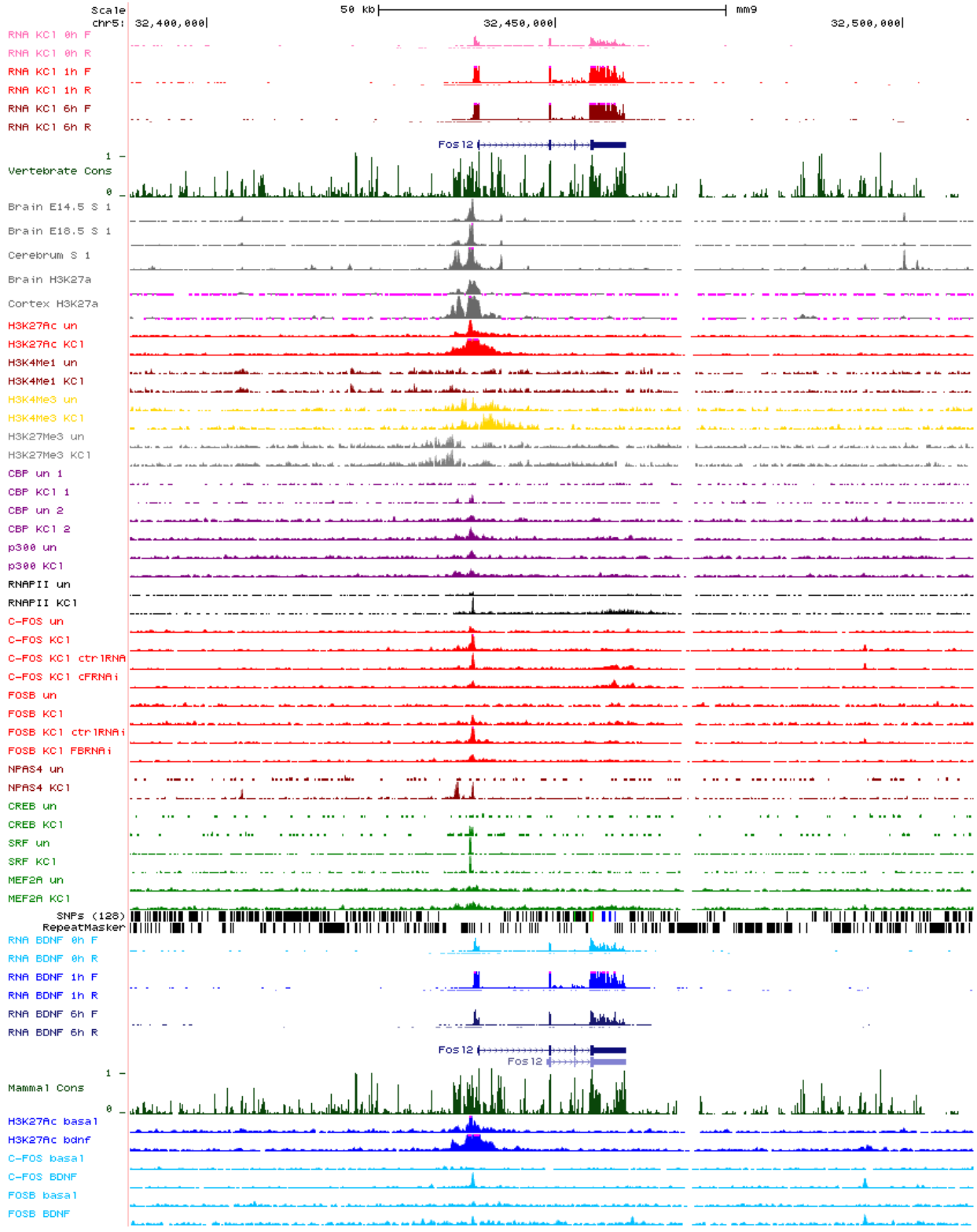

Figure 6.36: *Fosl2* locus

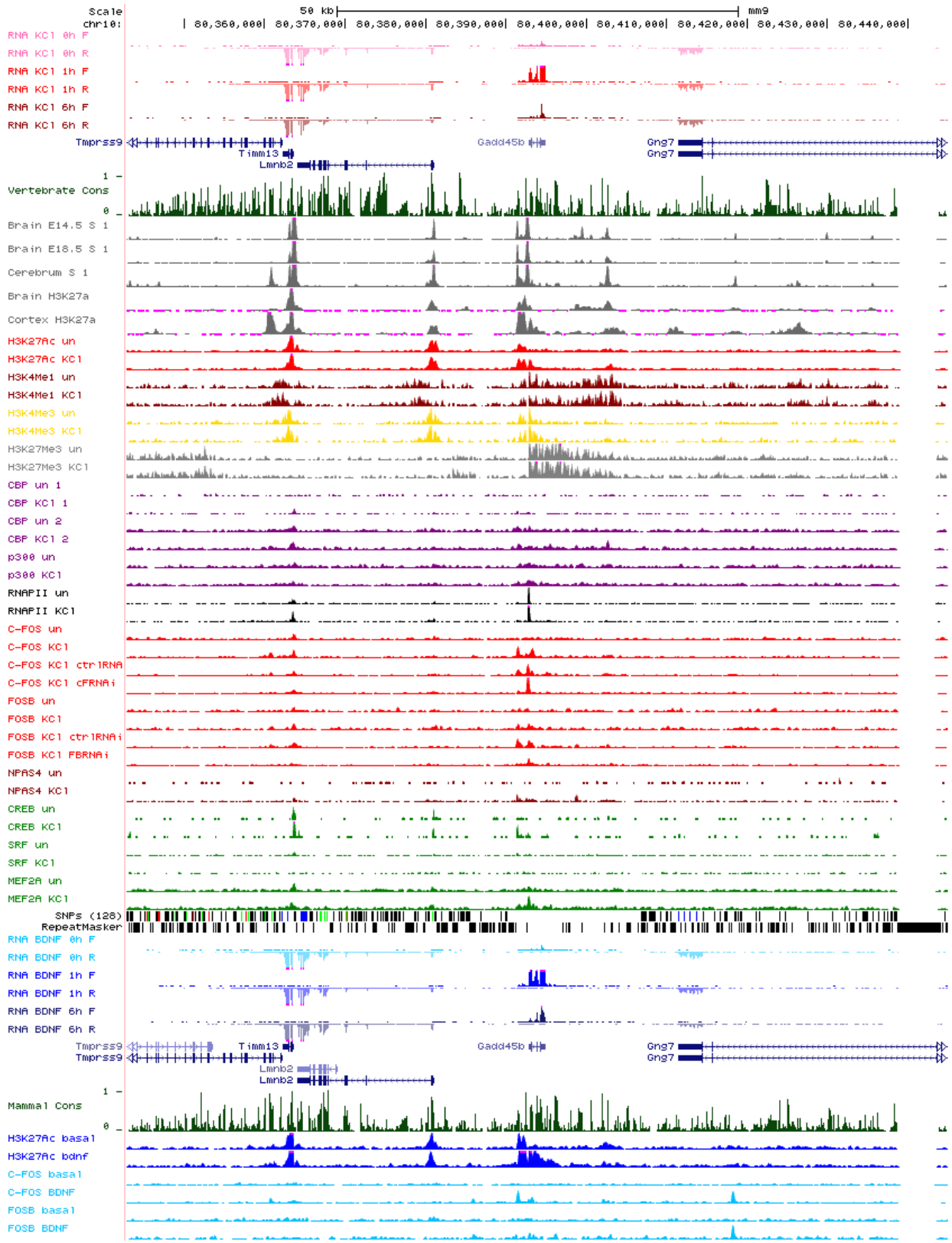

Figure 6.37: *Gadd45b* locus

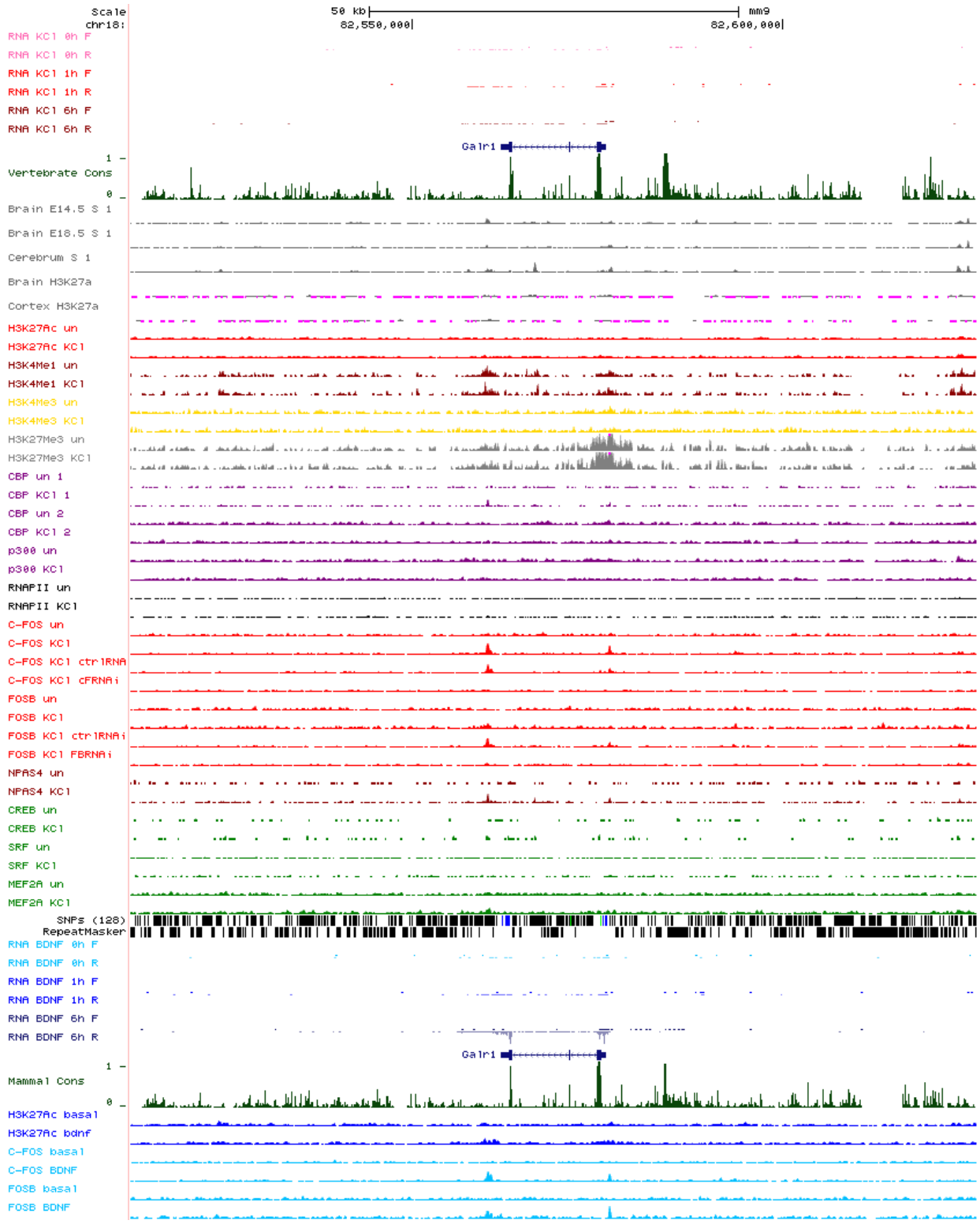

Figure 6.38: *Galr1* locus

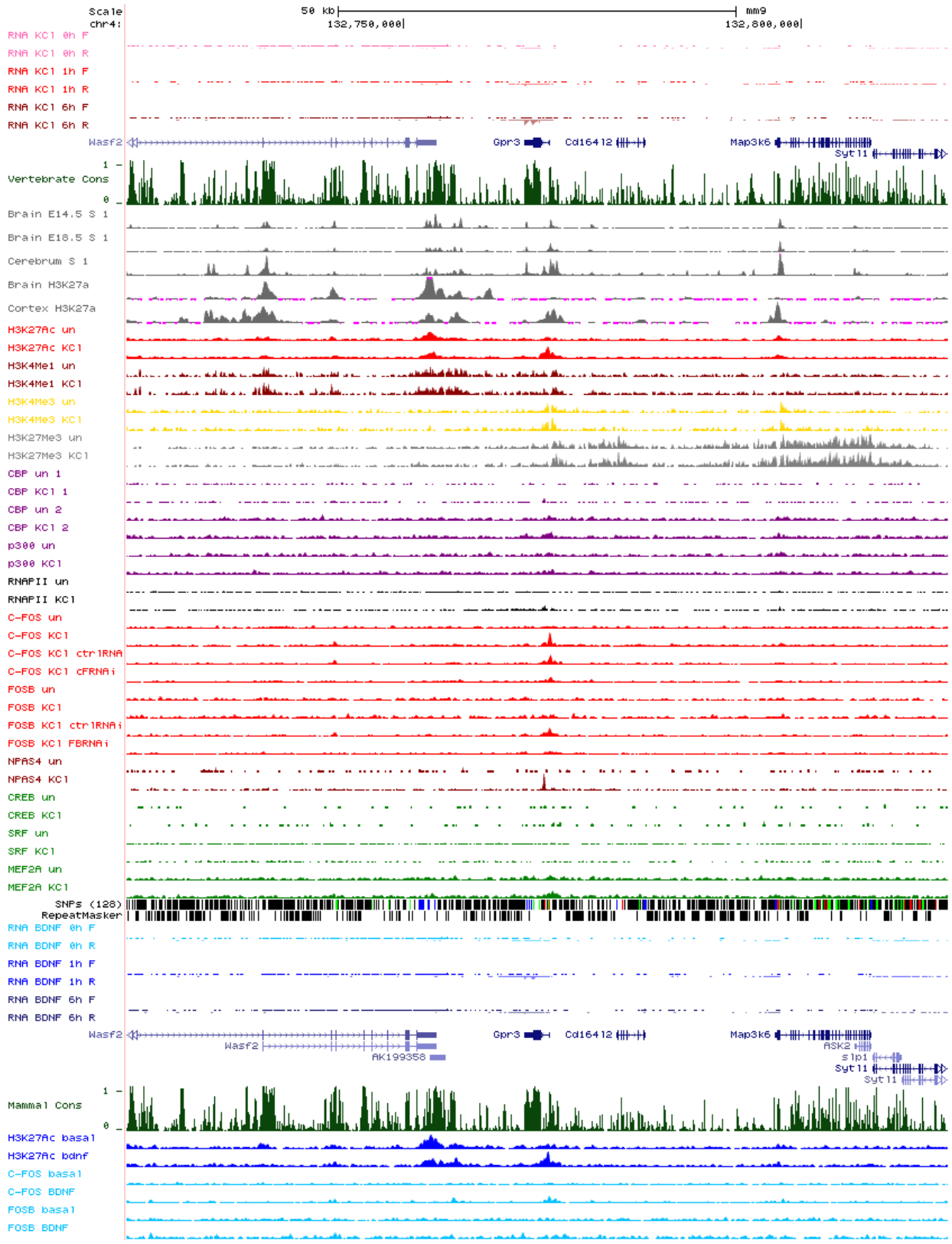

Figure 6.39: *Gpr3* locus

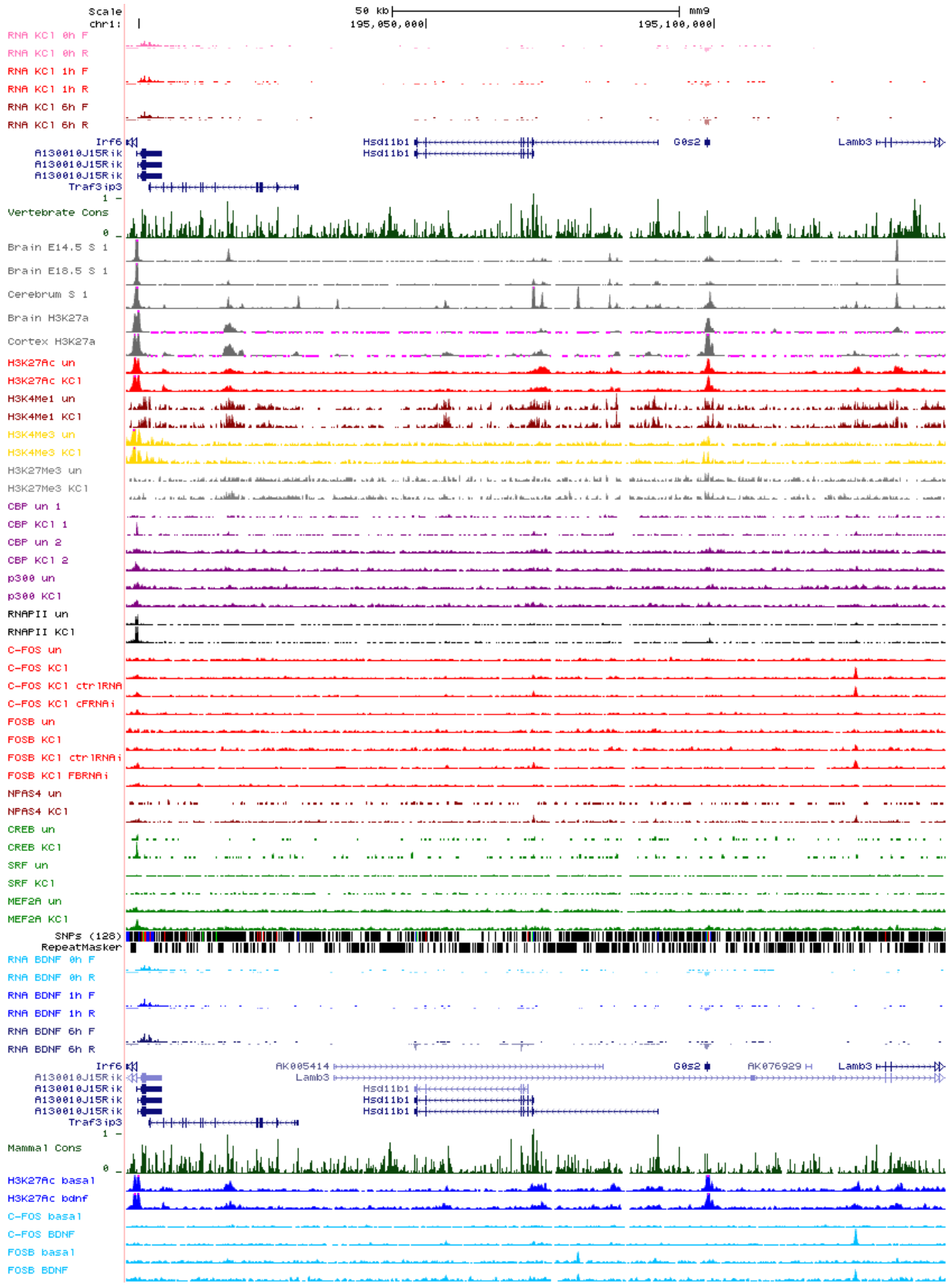

Figure 6.40: *Hsd11b1* locus

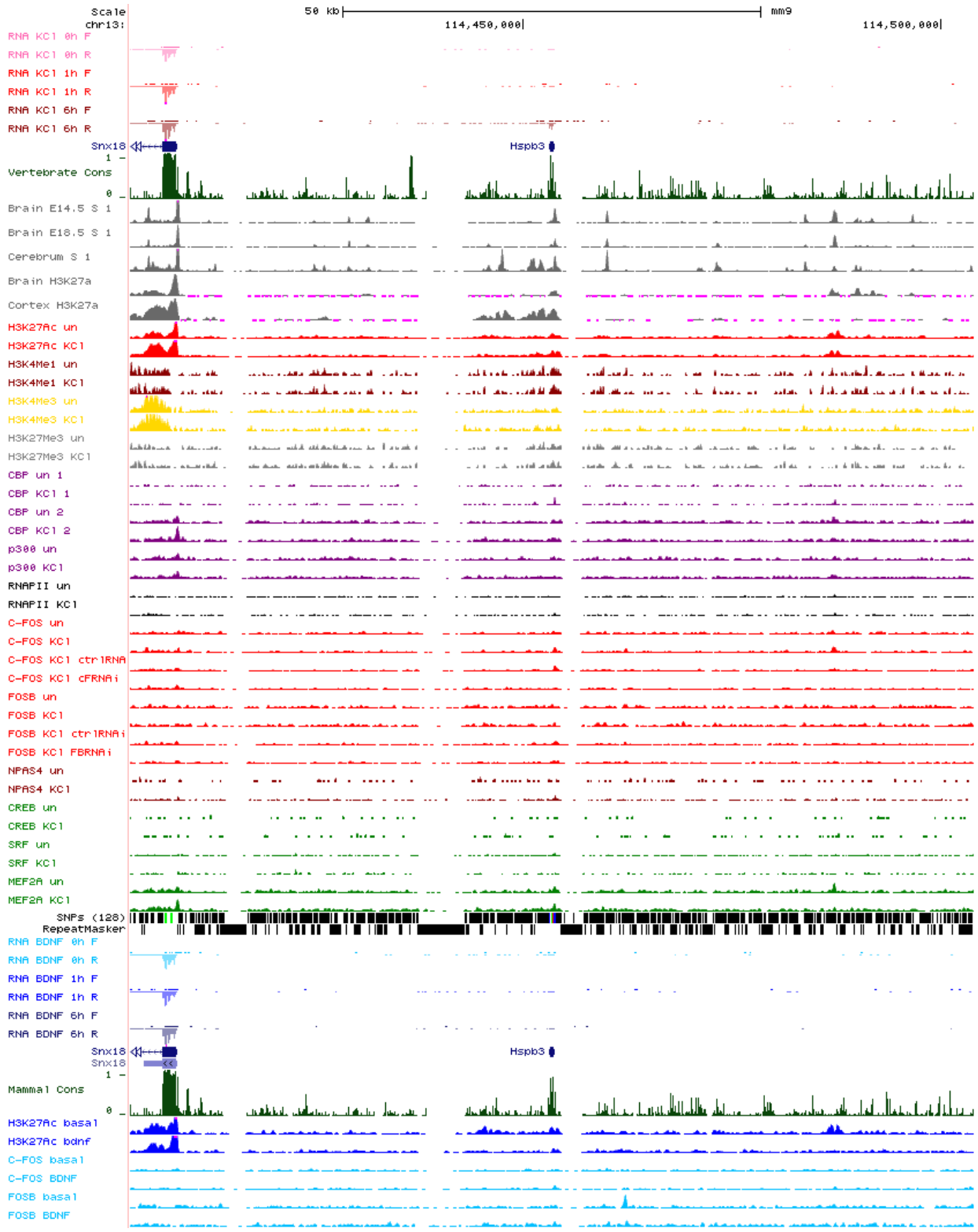

Figure 6.41: *Hspb3* locus

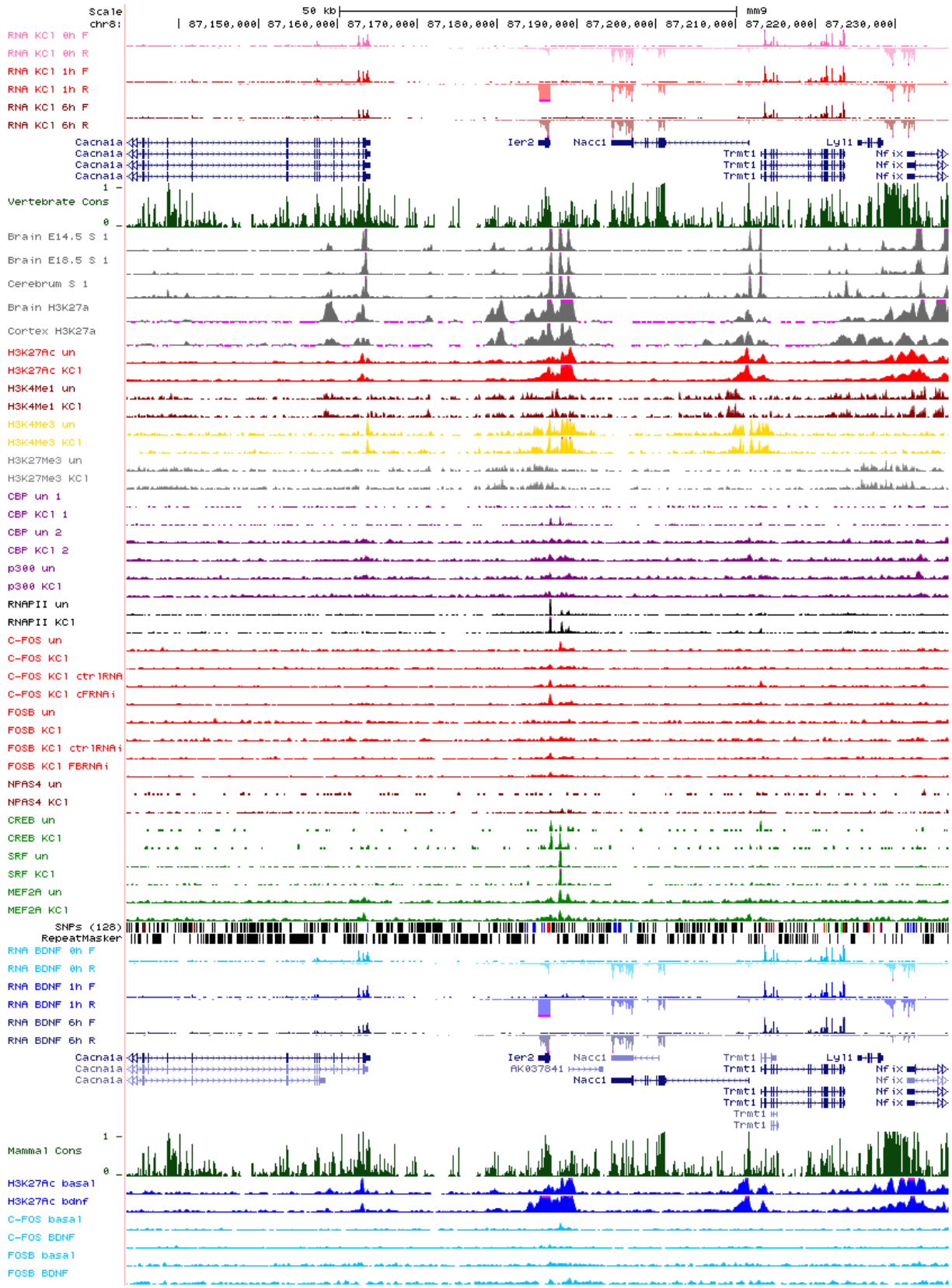

Figure 6.42: *Ier2* locus

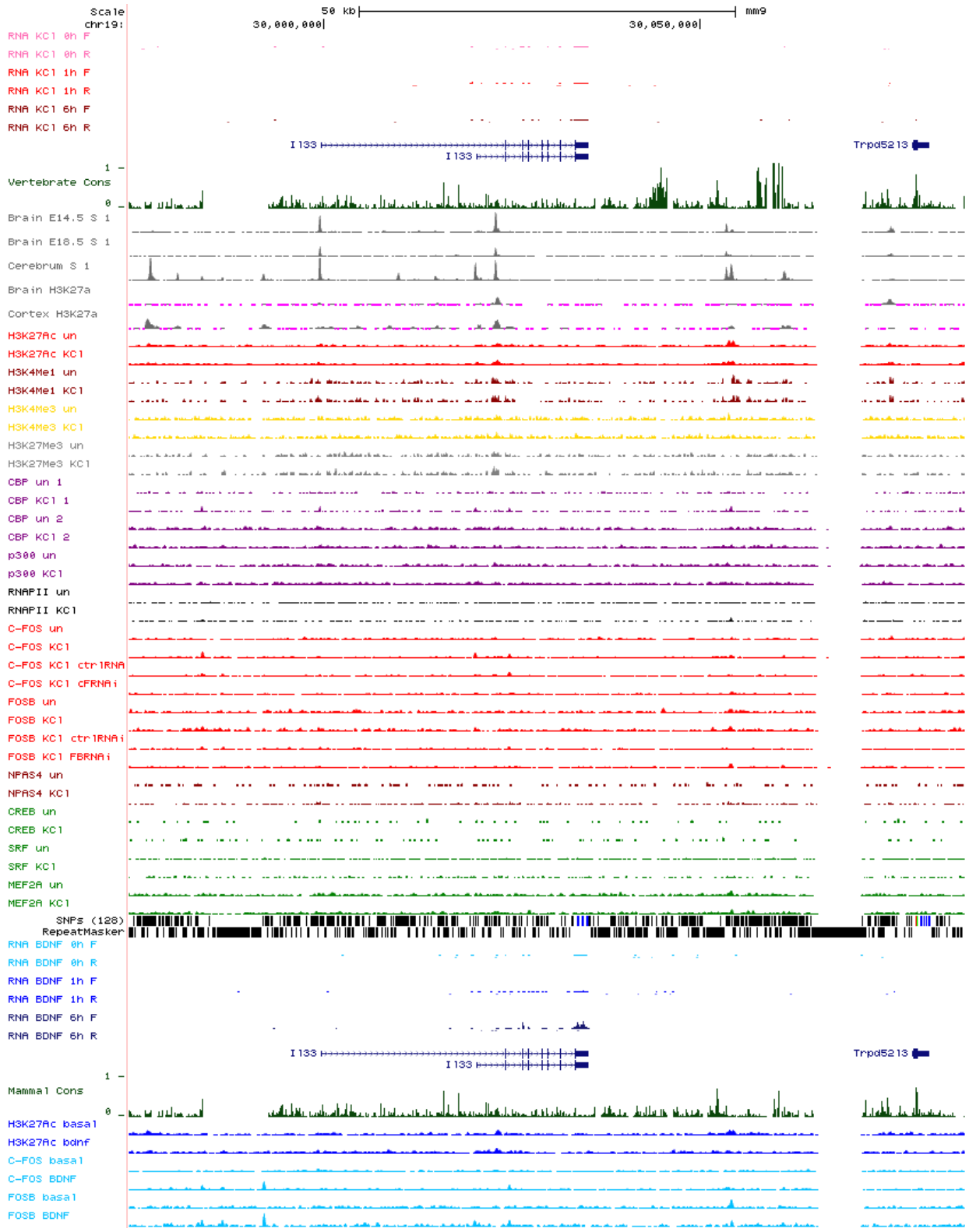

Figure 6.43: *Il33* locus

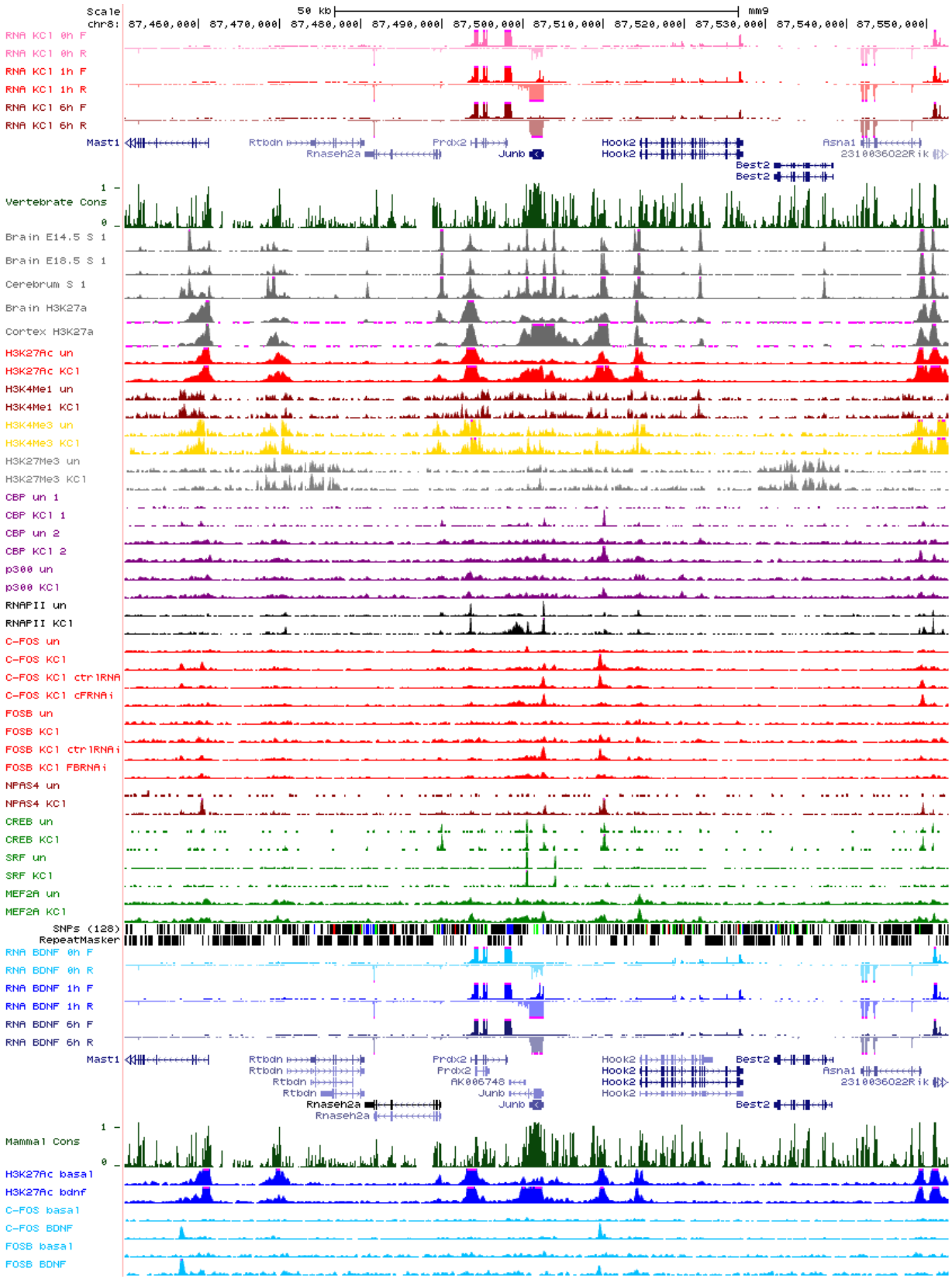

Figure 6.44: *JunB* locus

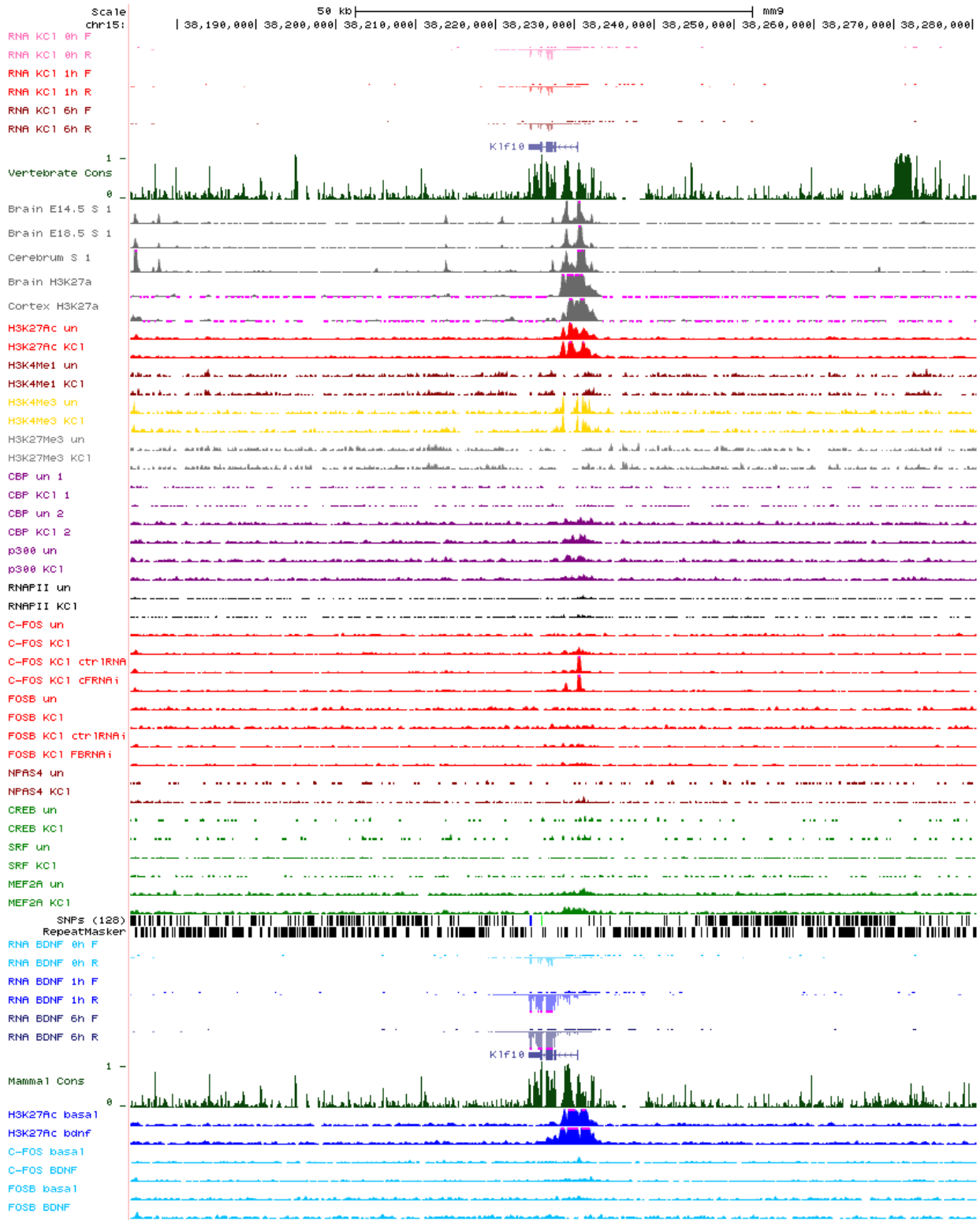

Figure 6.45: *Klf10* locus

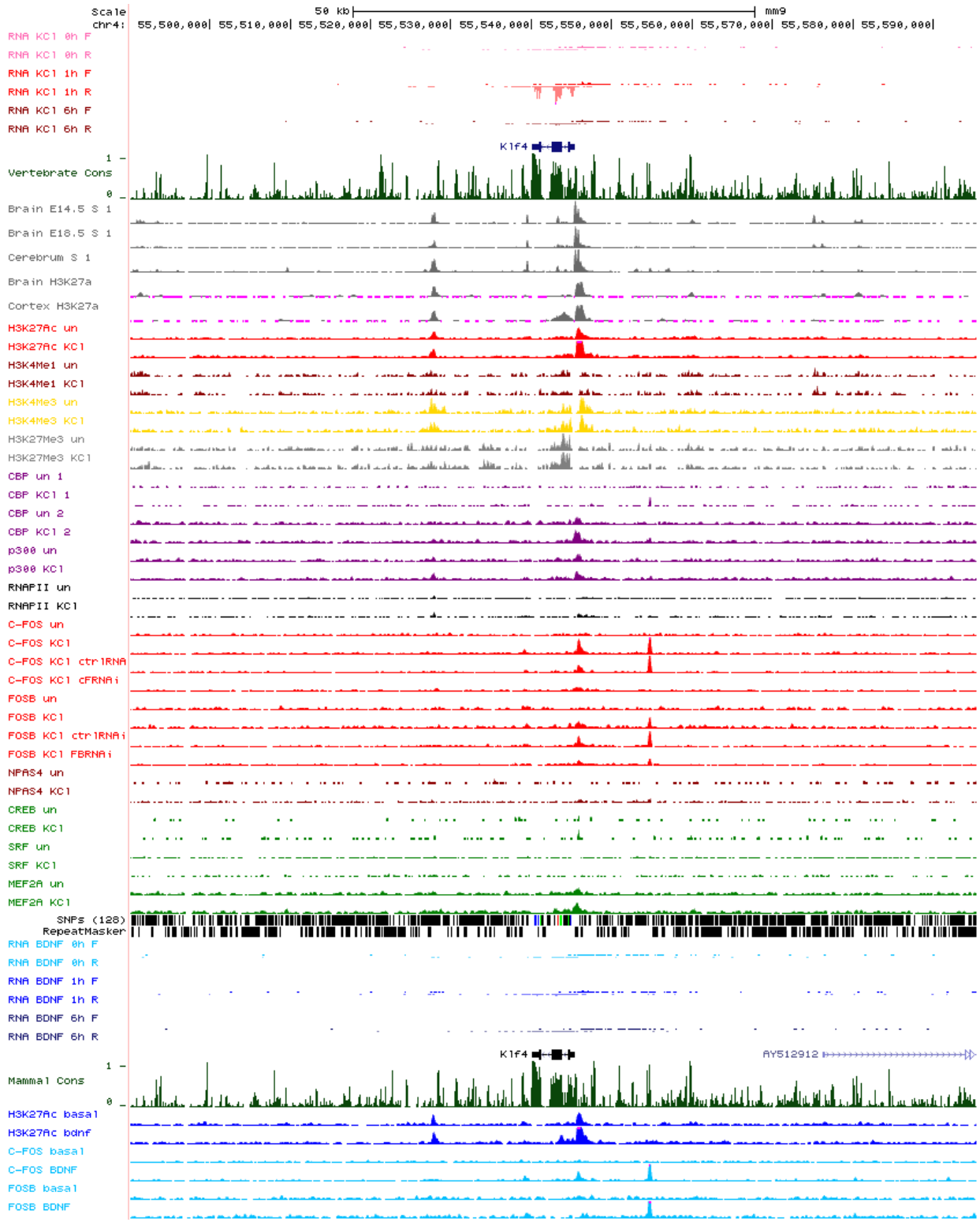

Figure 6.46: *Klf4* locus

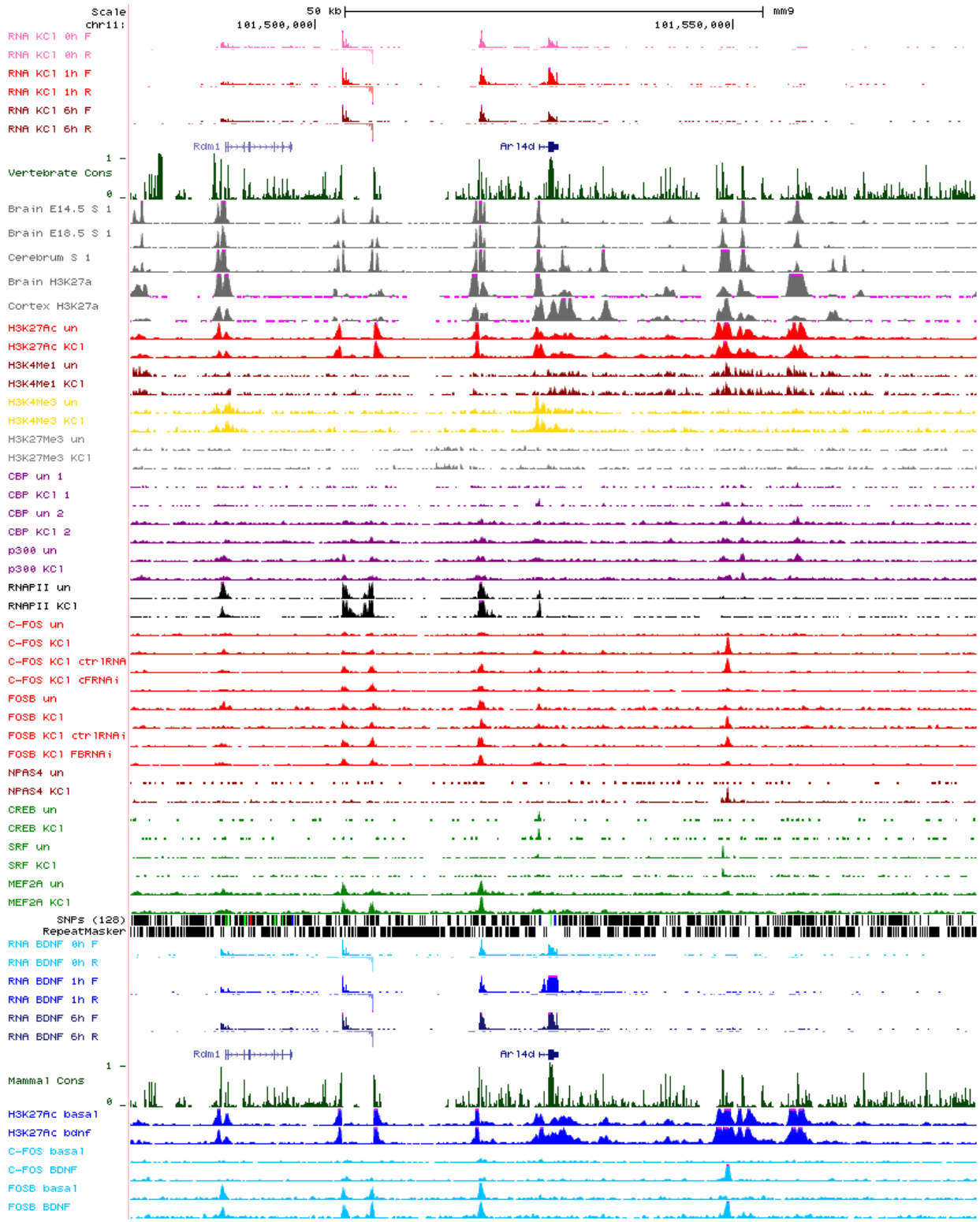

Figure 6.47: *LOC100038842* locus

Figure 6.48: *LOC100043802* locus

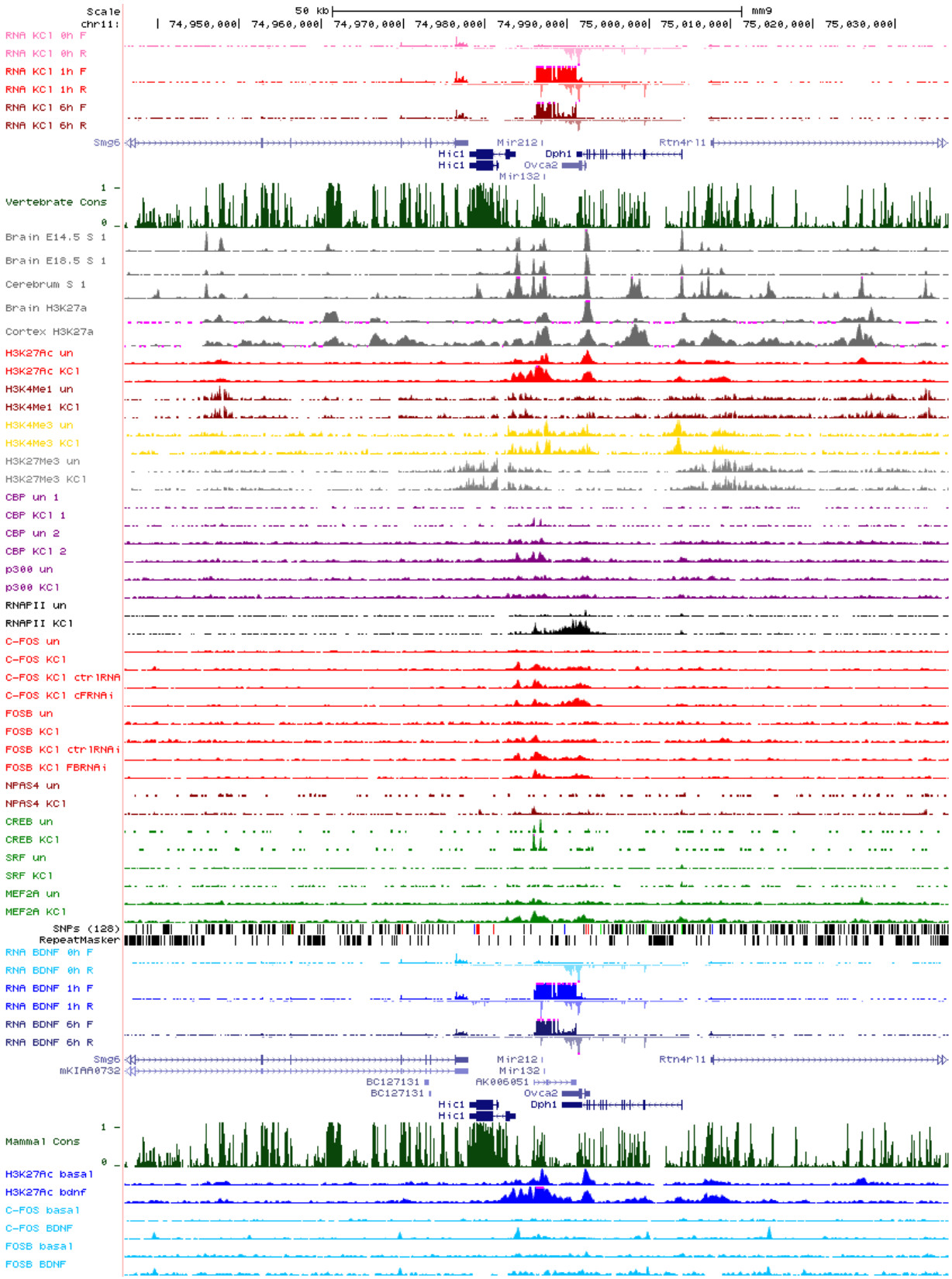

Figure 6.49: *LOC668604* locus

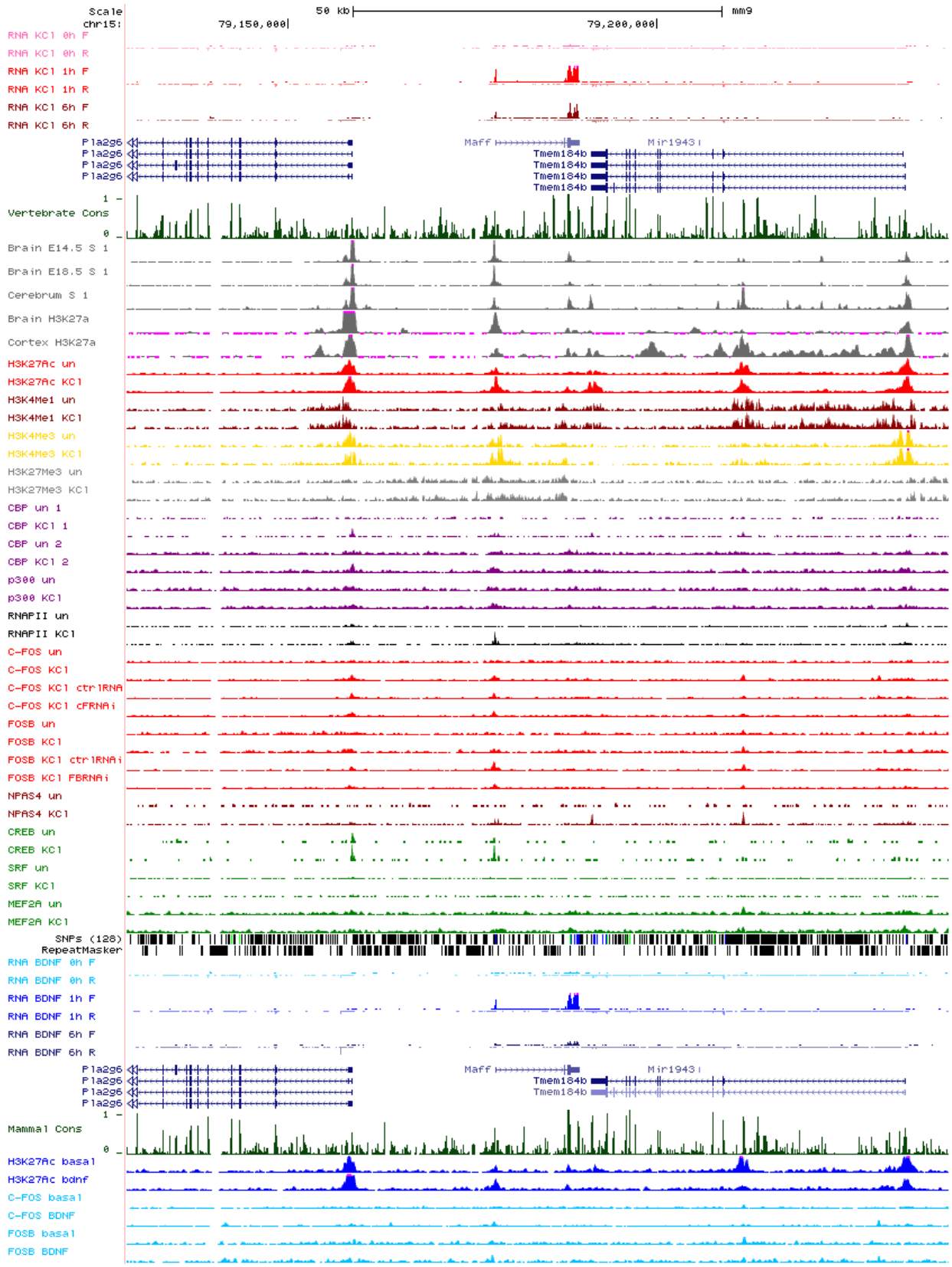

Figure 6.50: *Maff* locus

Figure 6.51: *Map3k5* locus

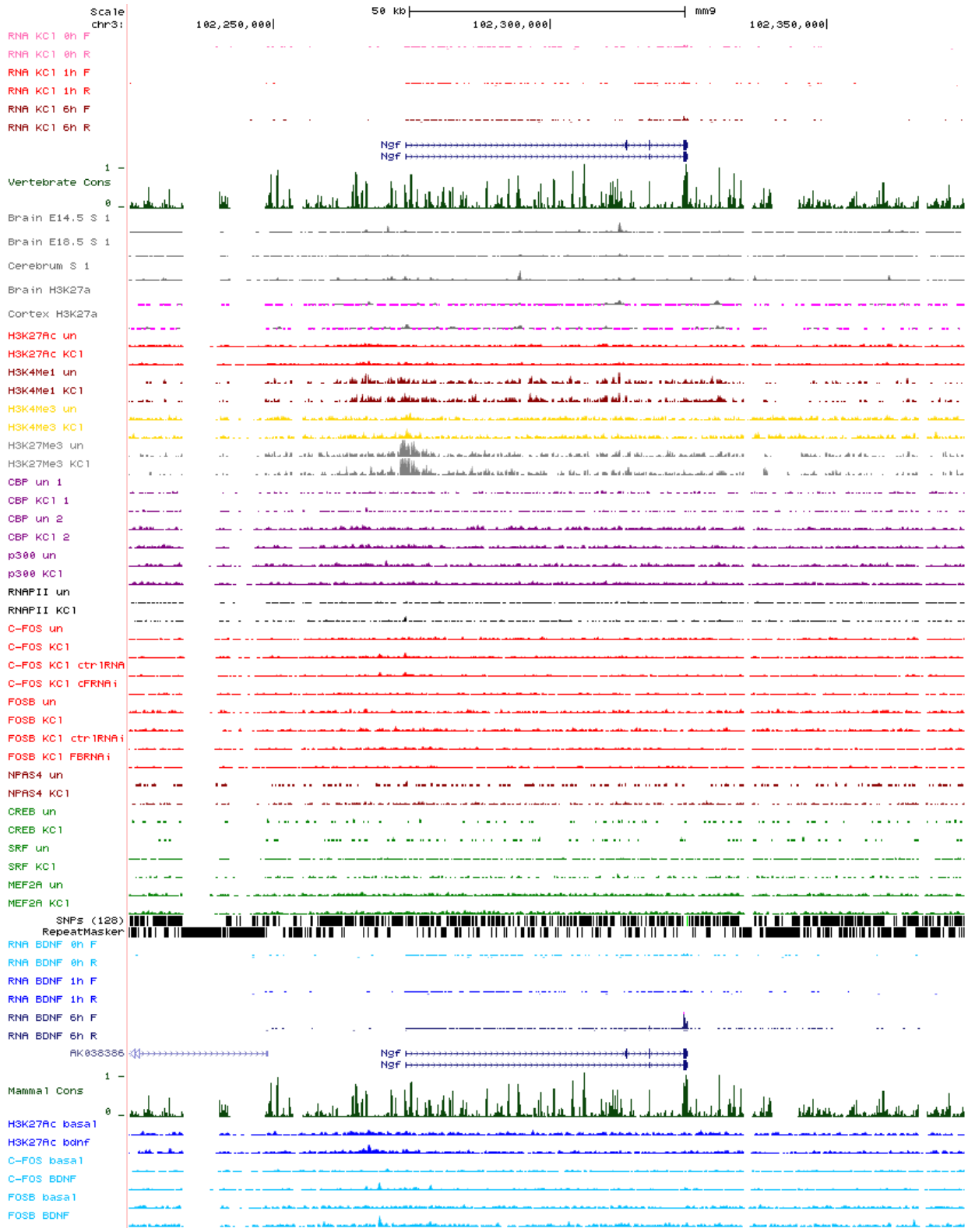

Figure 6.52: *Ngfb* locus

Figure 6.53: *Npas4* locus

Figure 6.54: *Nptx1* locus

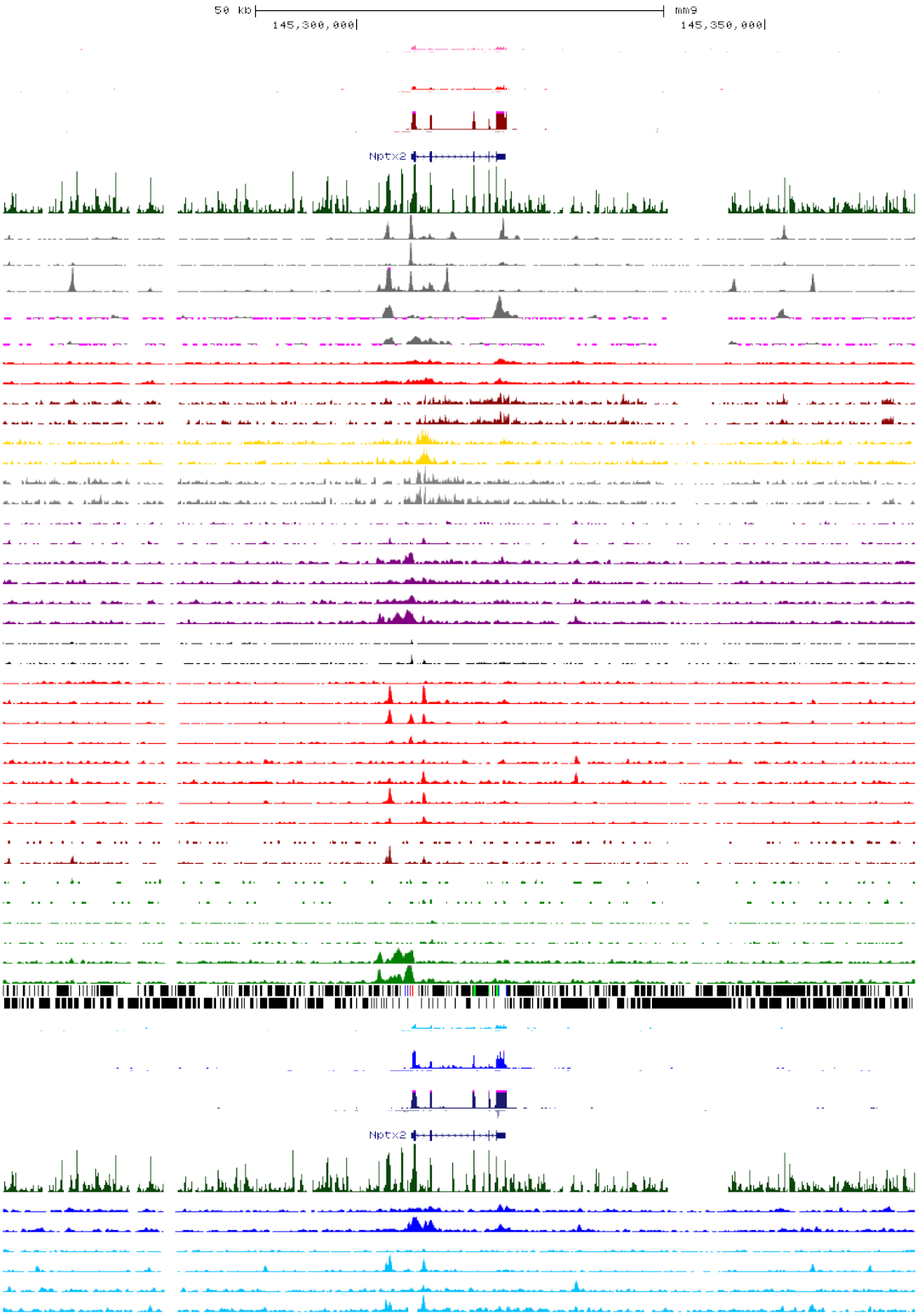

Figure 6.55: *Nptx2* locus

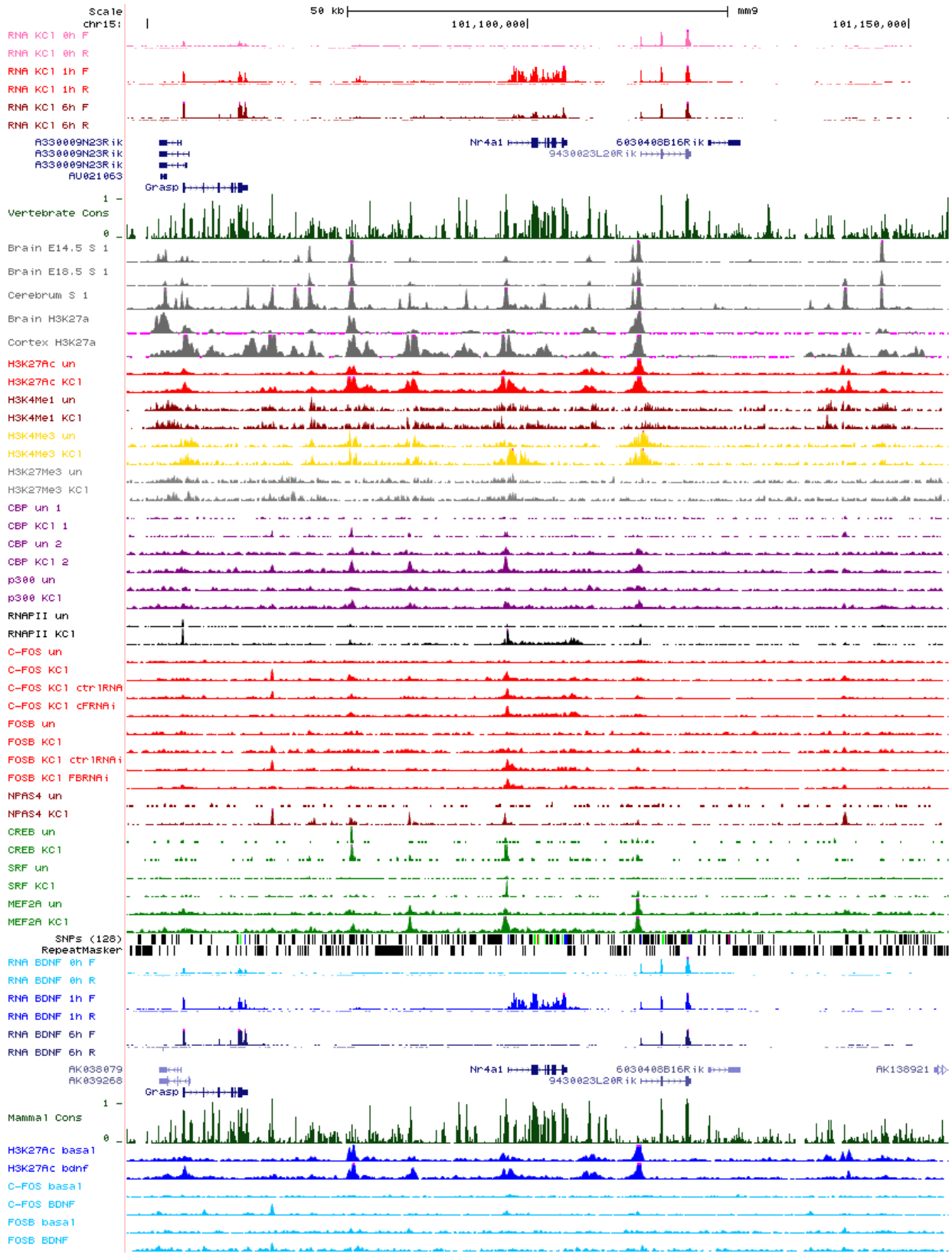

Figure 6.56: *Nr4a1* locus

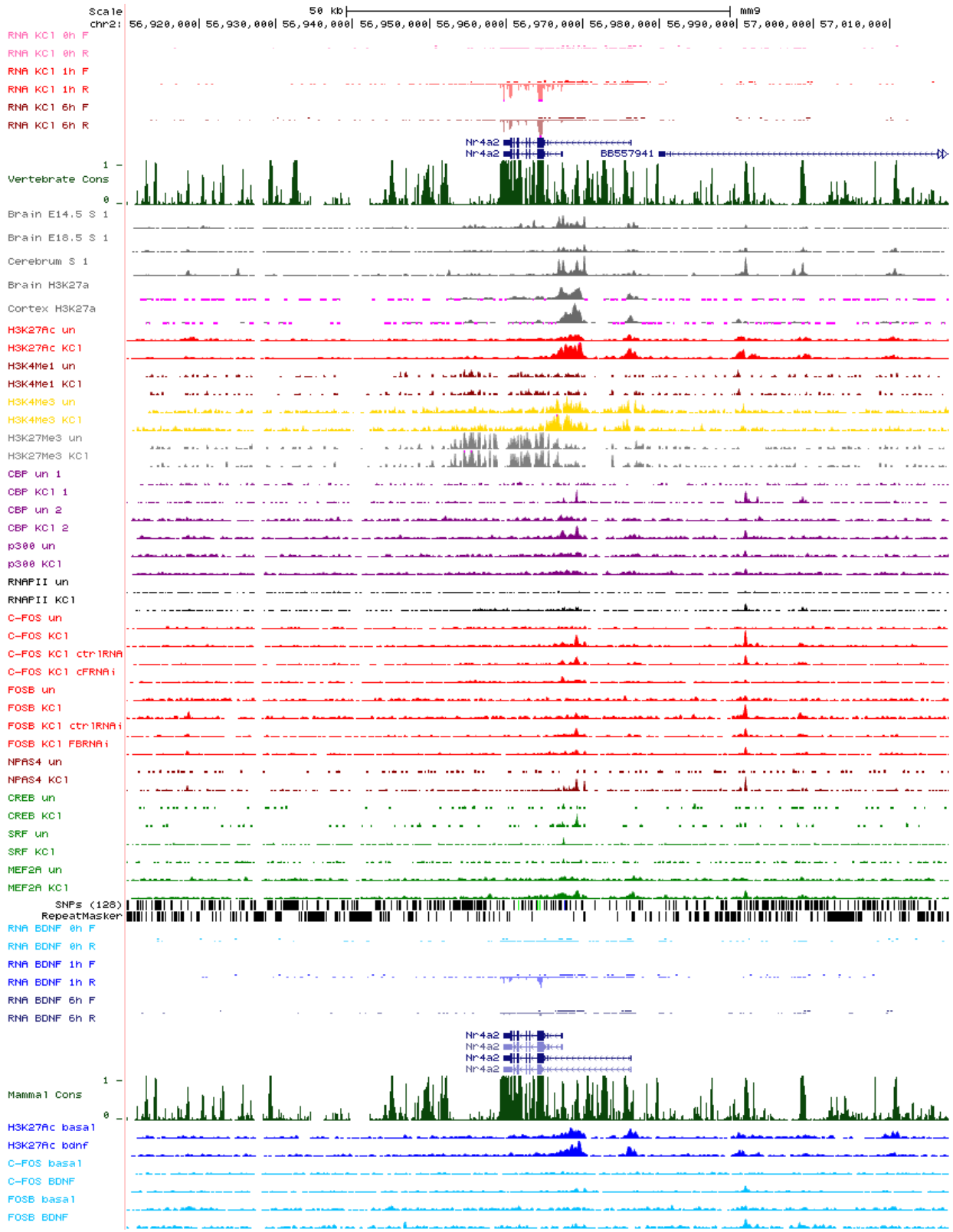

Figure 6.57: *Nr4a2* locus

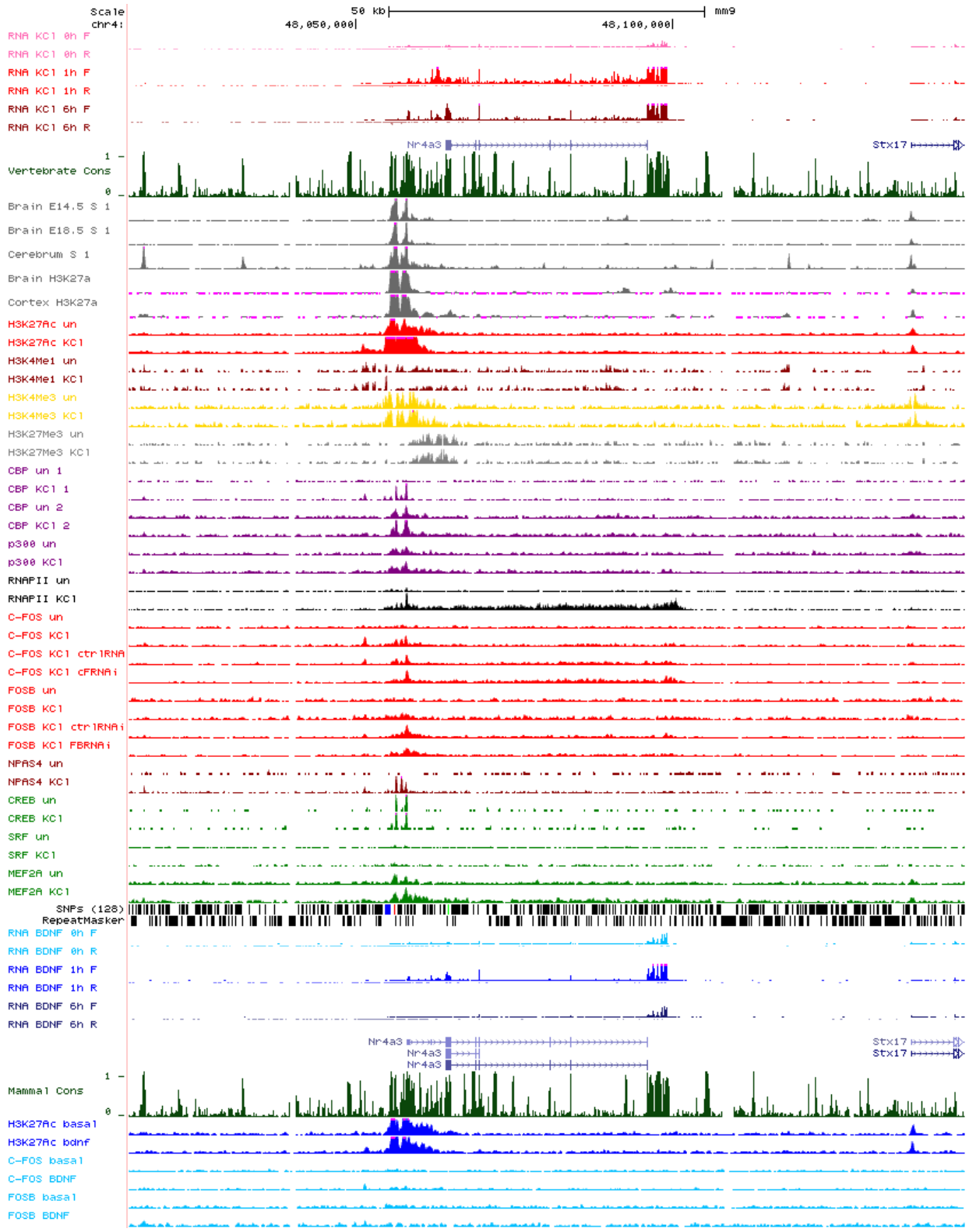

Figure 6.58: *Nr4a3* locus

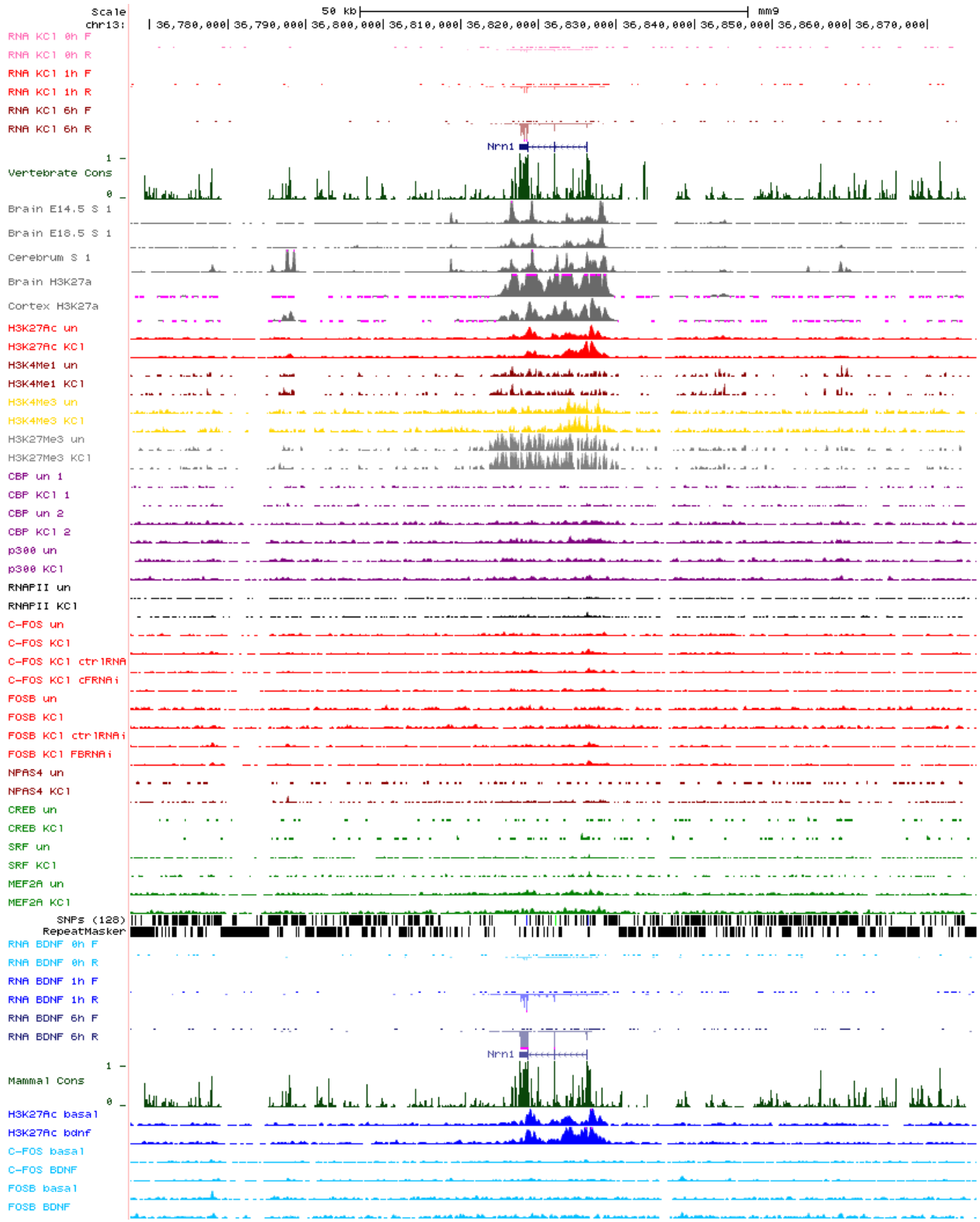

Figure 6.59: *Nrn1* locus

Figure 6.60: *Pcsk1* locus

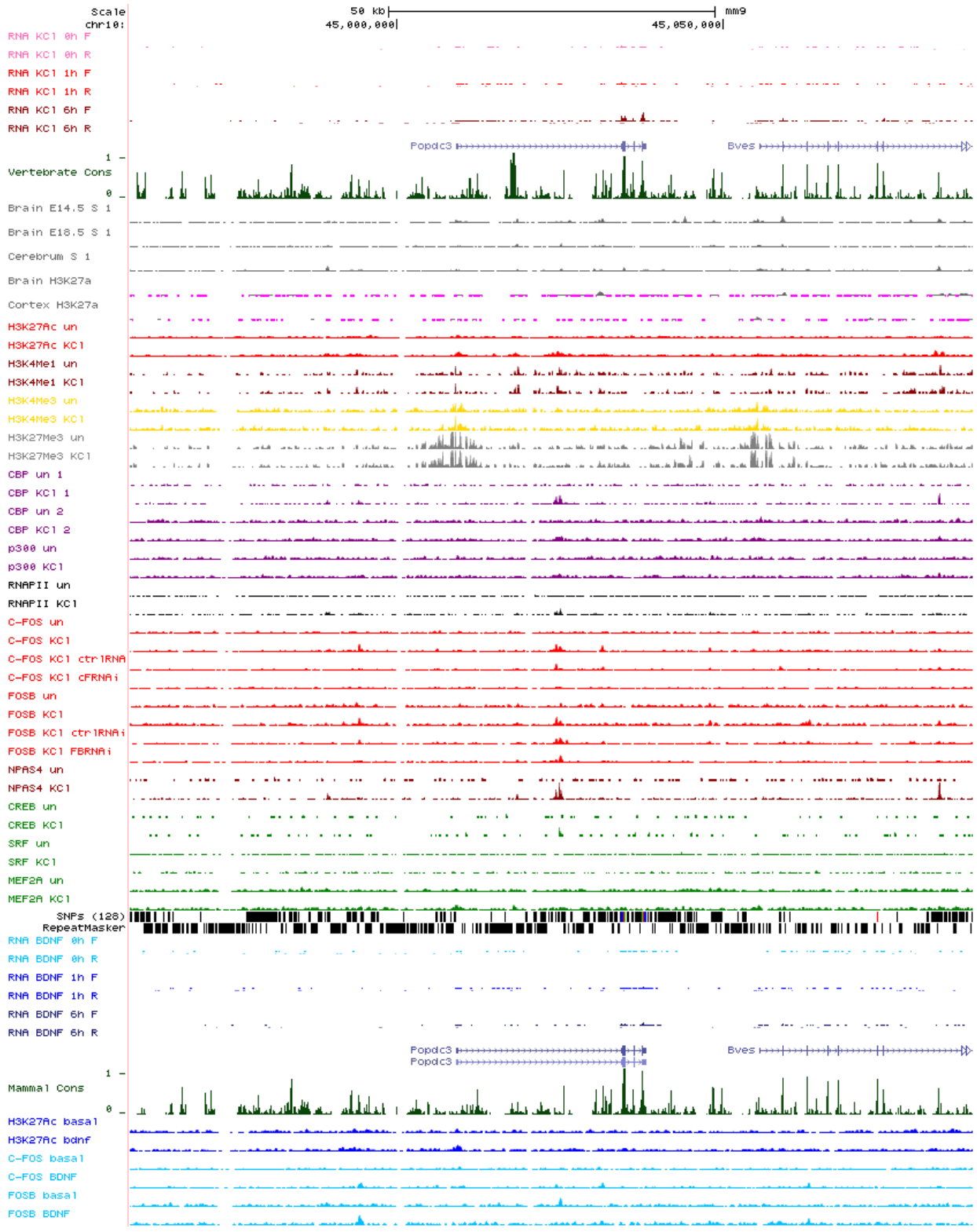

Figure 6.61: *Popdc3* locus

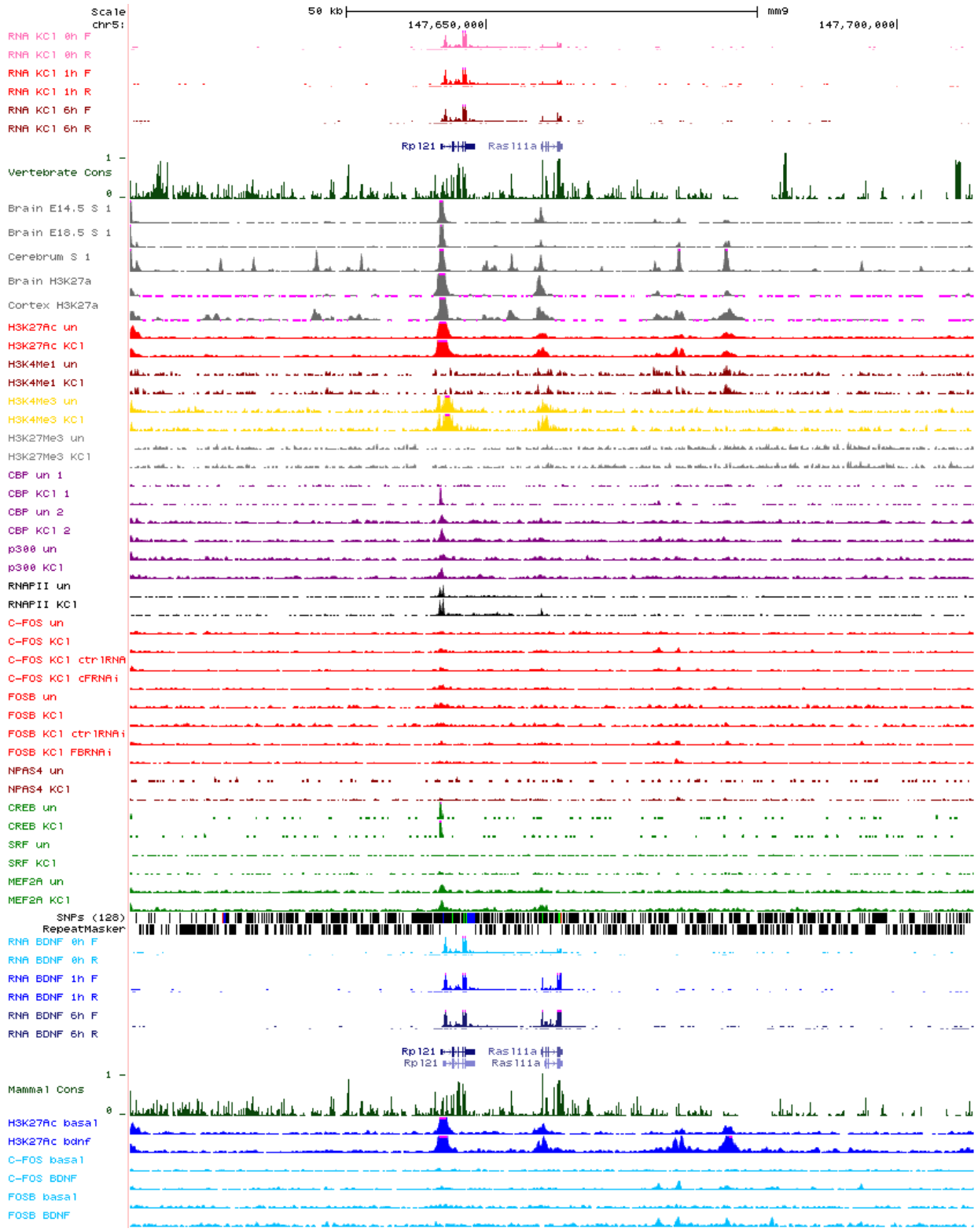

Figure 6.62: *Rasl11a* locus

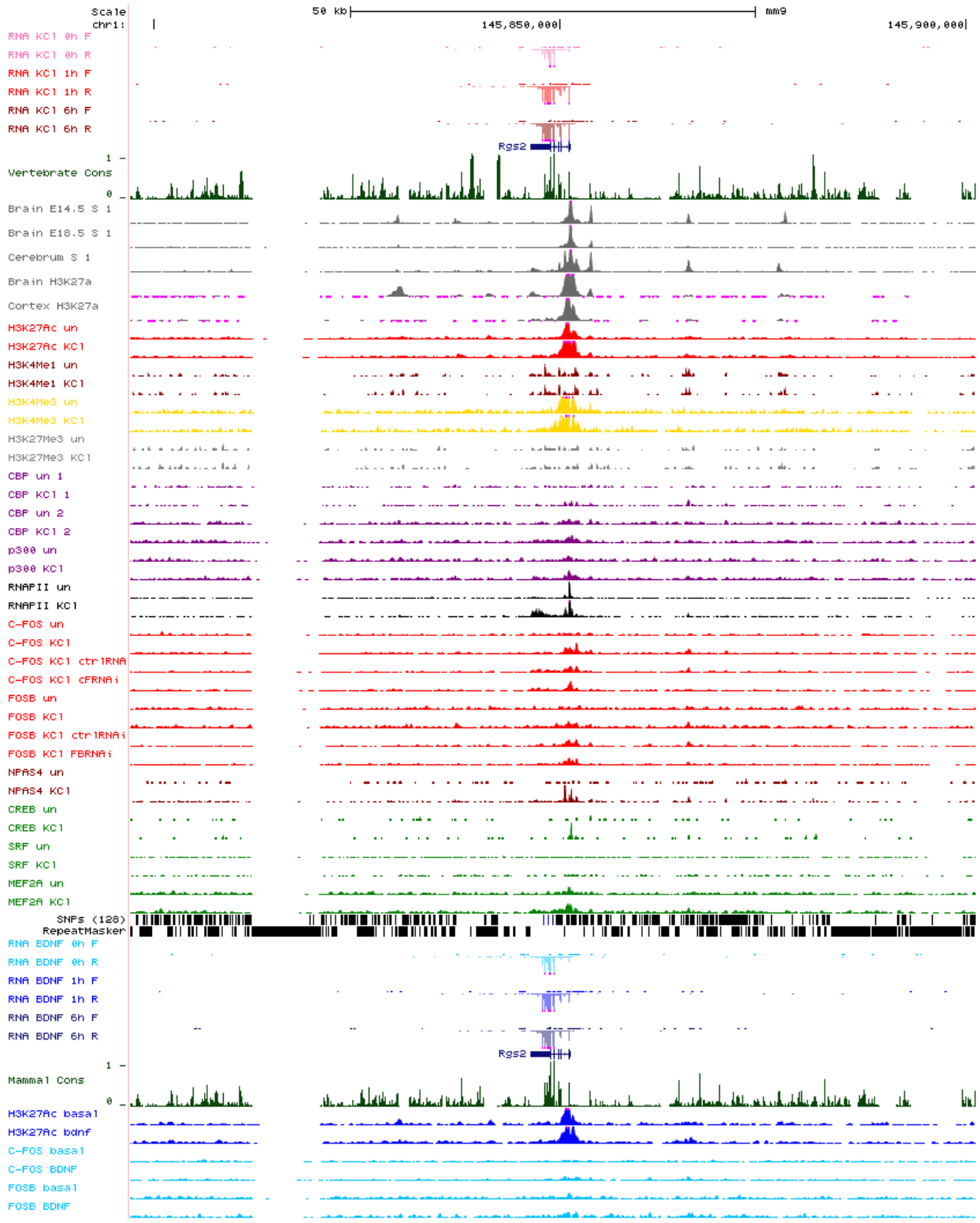

Figure 6.63: *Rgs2* locus

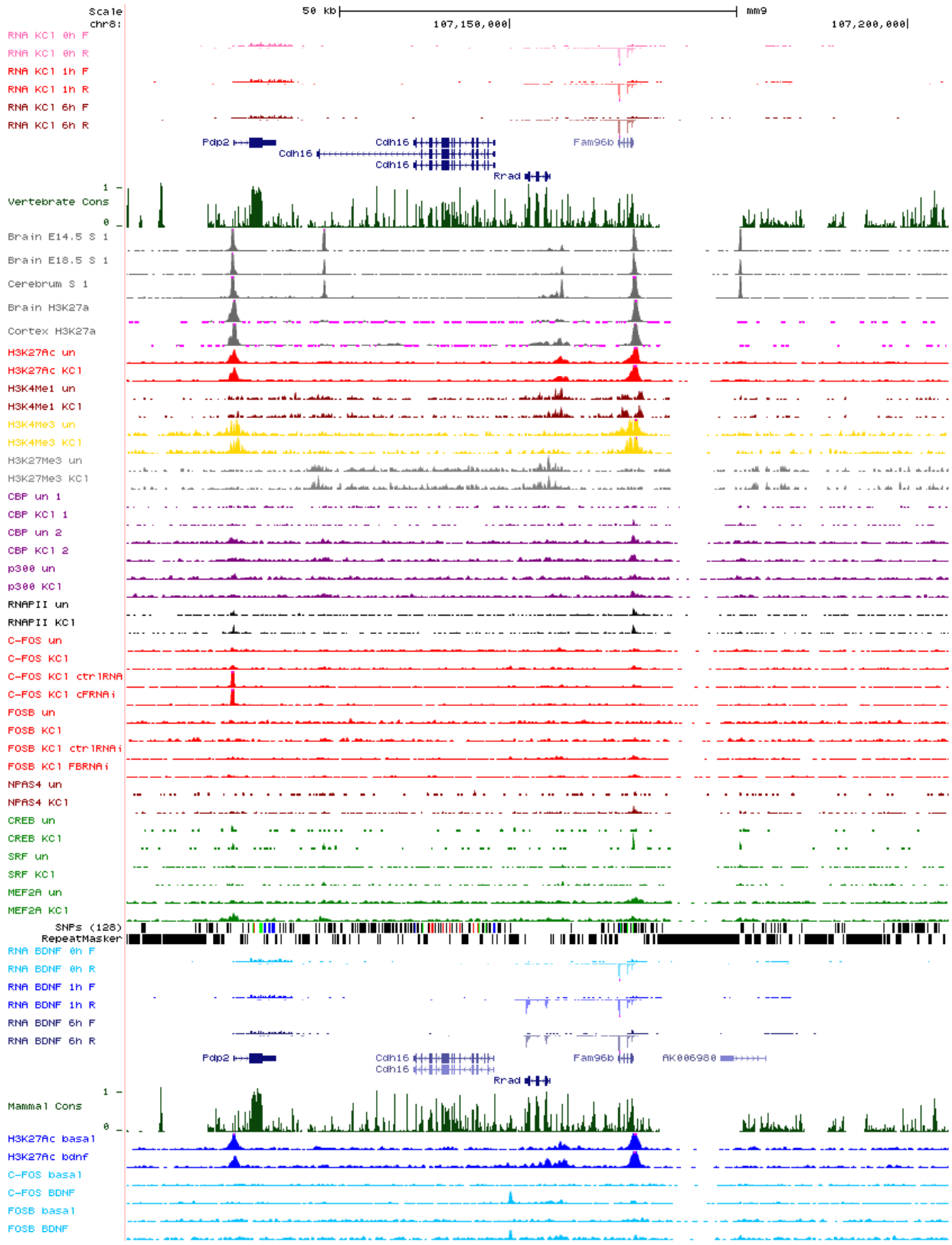

Figure 6.64: *Rrad* locus

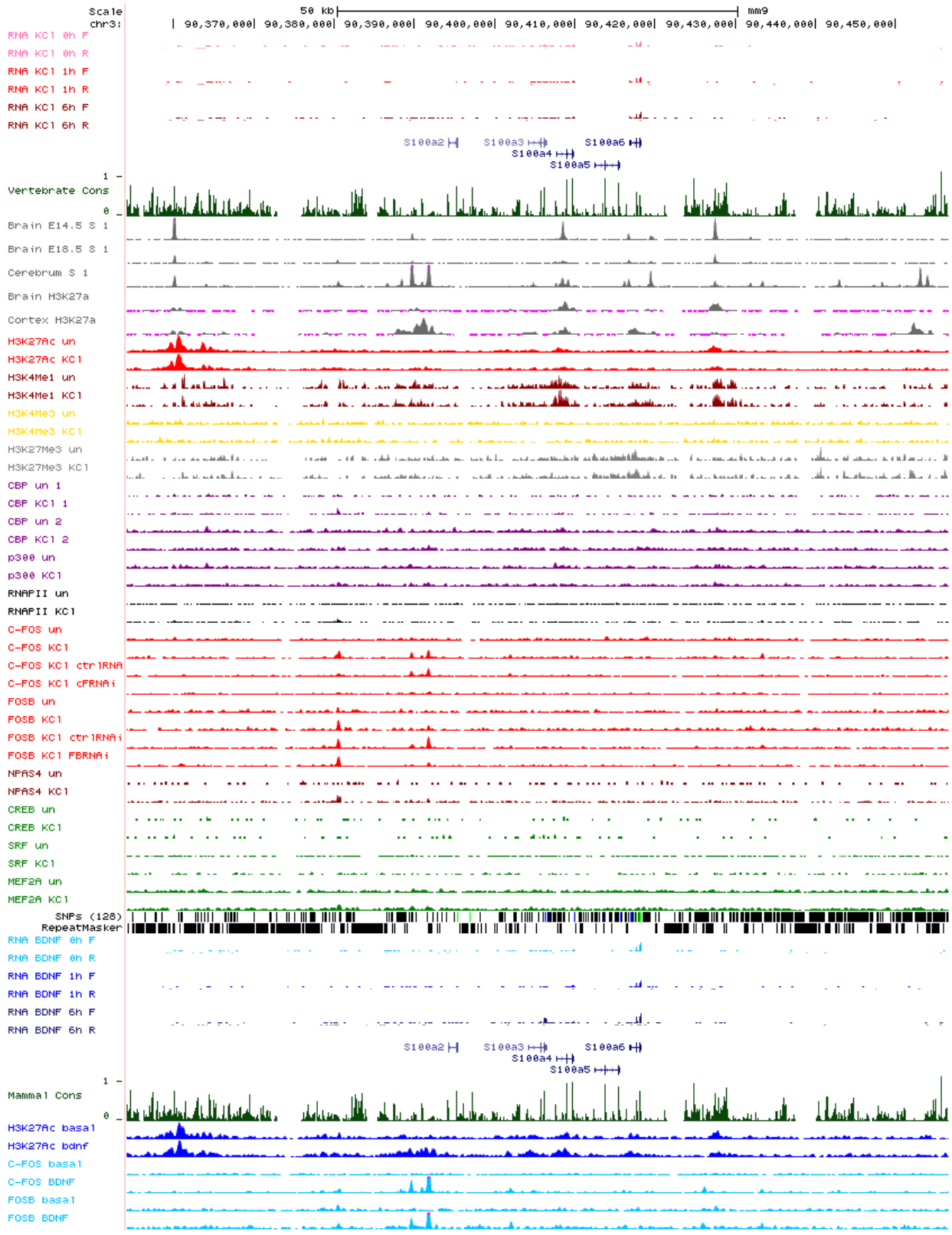

Figure 6.65: *S100a3* locus

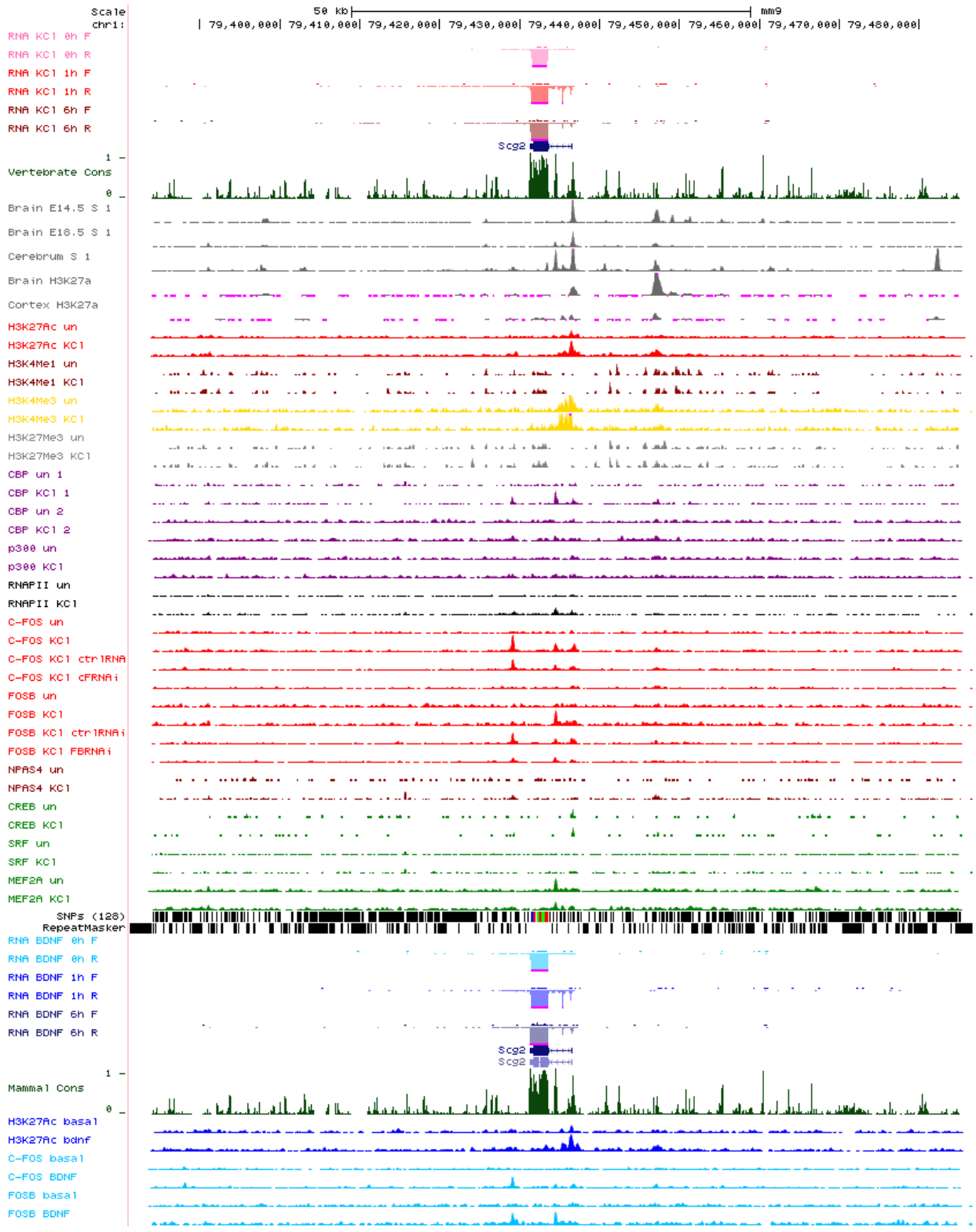

Figure 6.66: *Scg2* locus

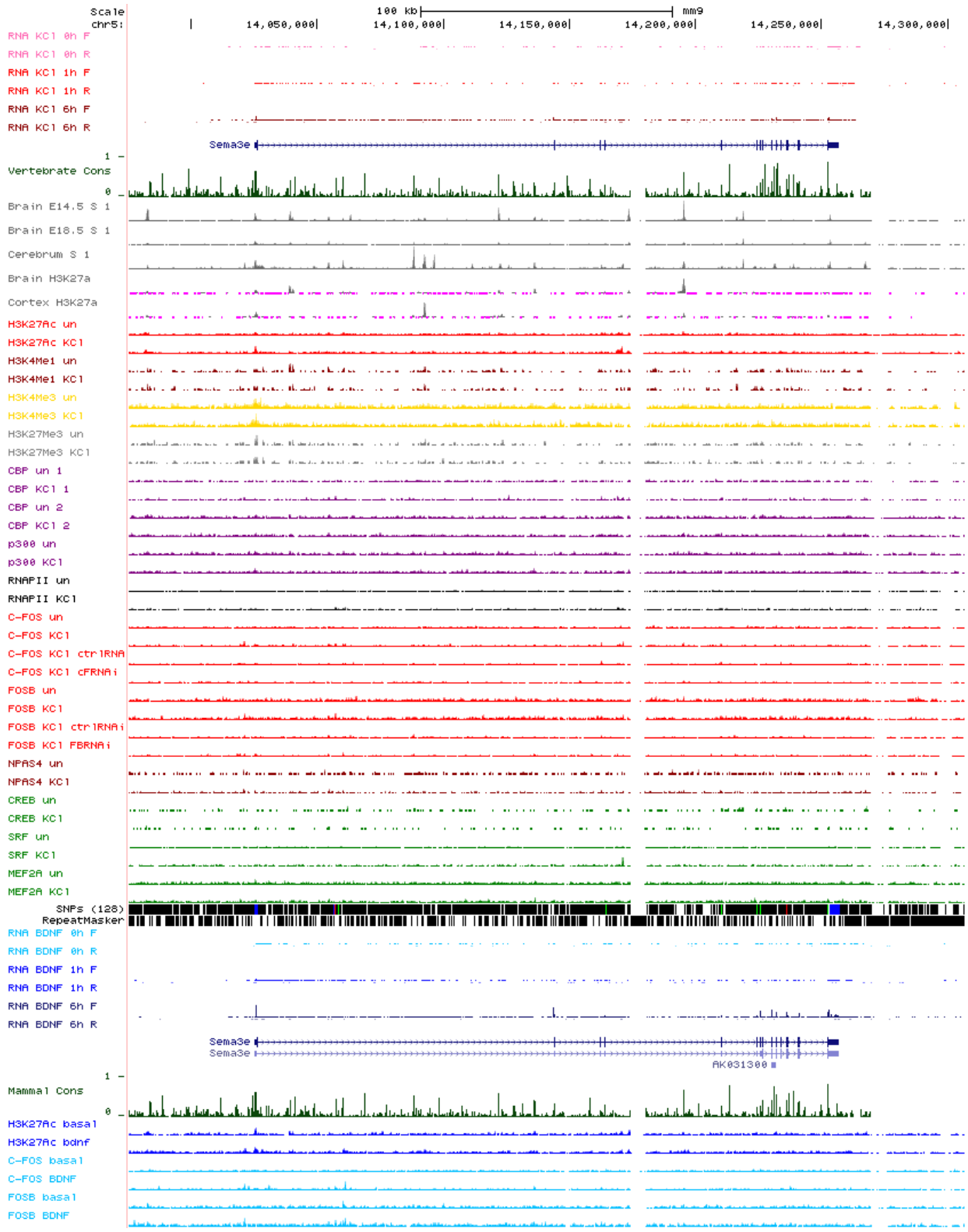

Figure 6.67: *Sema3e* locus

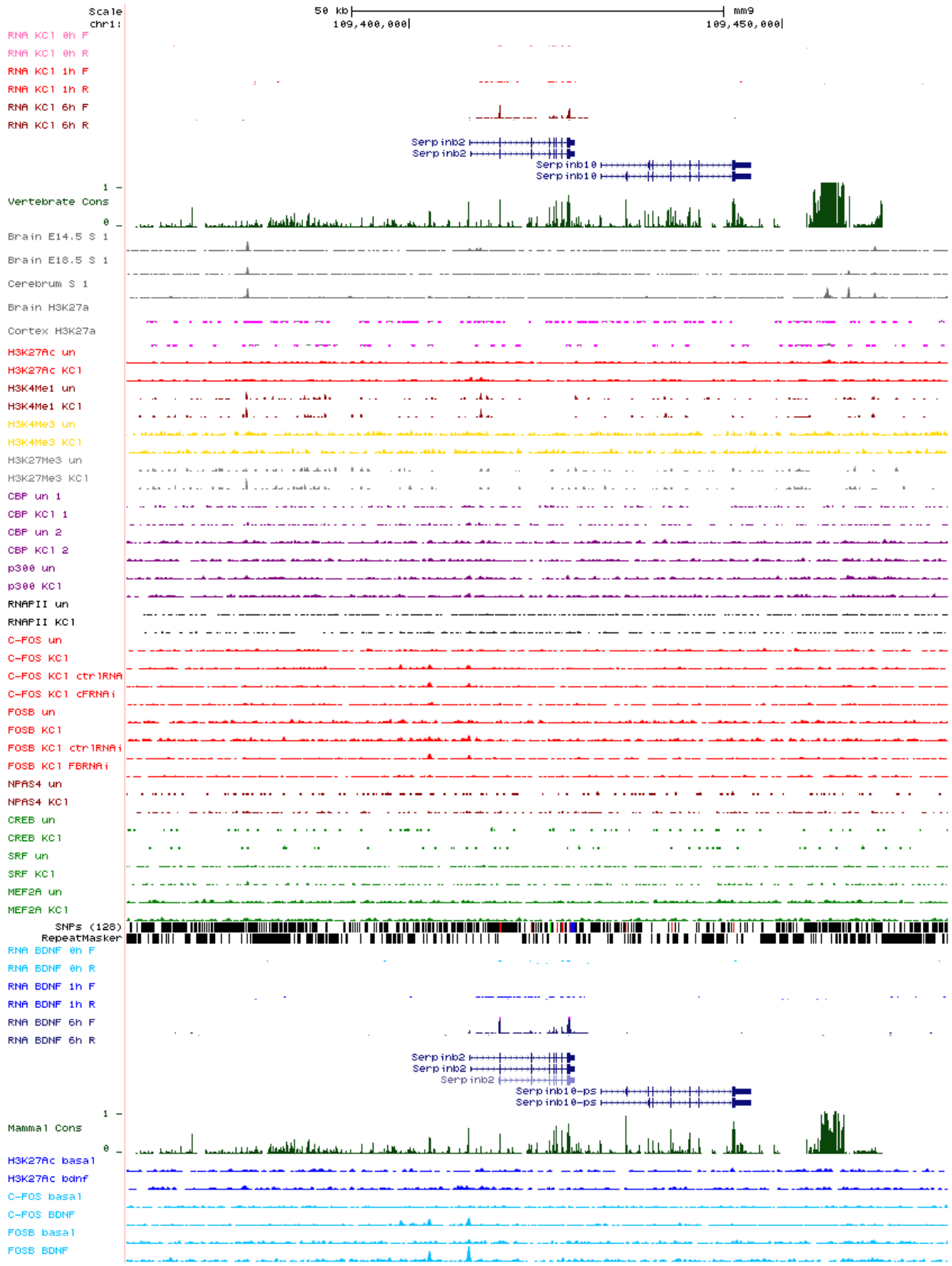

Figure 6.68: *Serpinb2* locus

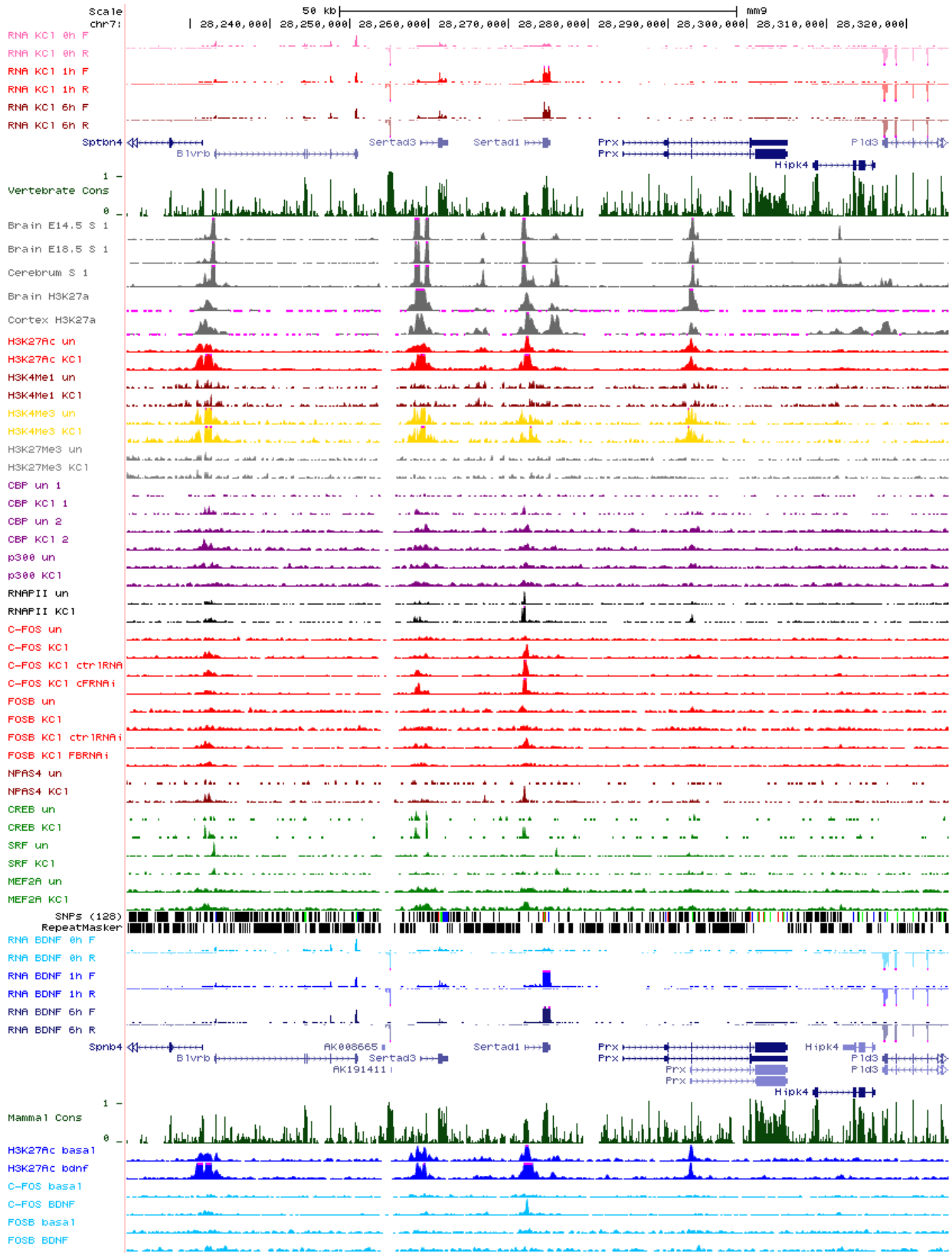

Figure 6.69: *Sertad1* locus

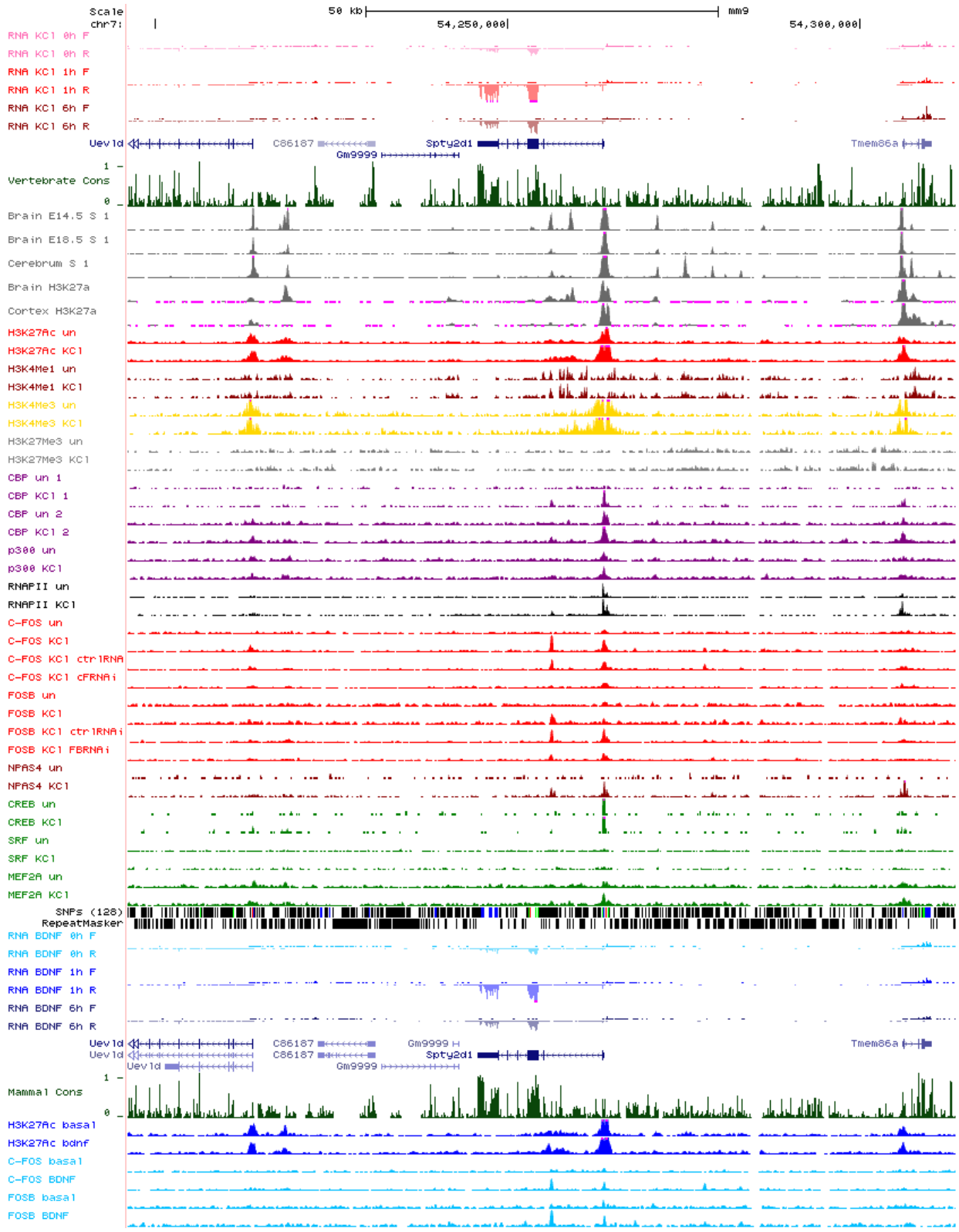

Figure 6.70: *Spty2d1* locus

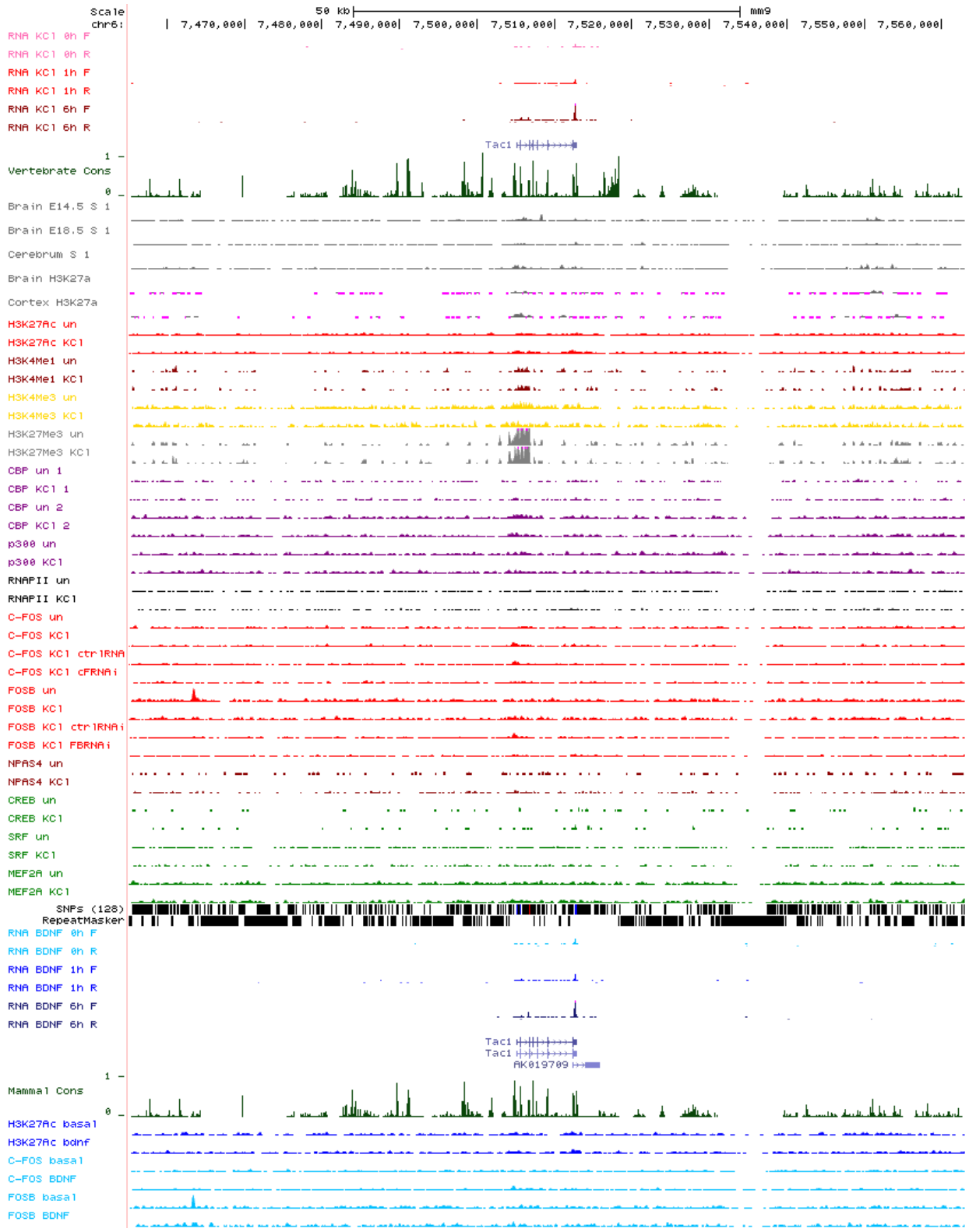

Figure 6.71: *Tac1* locus

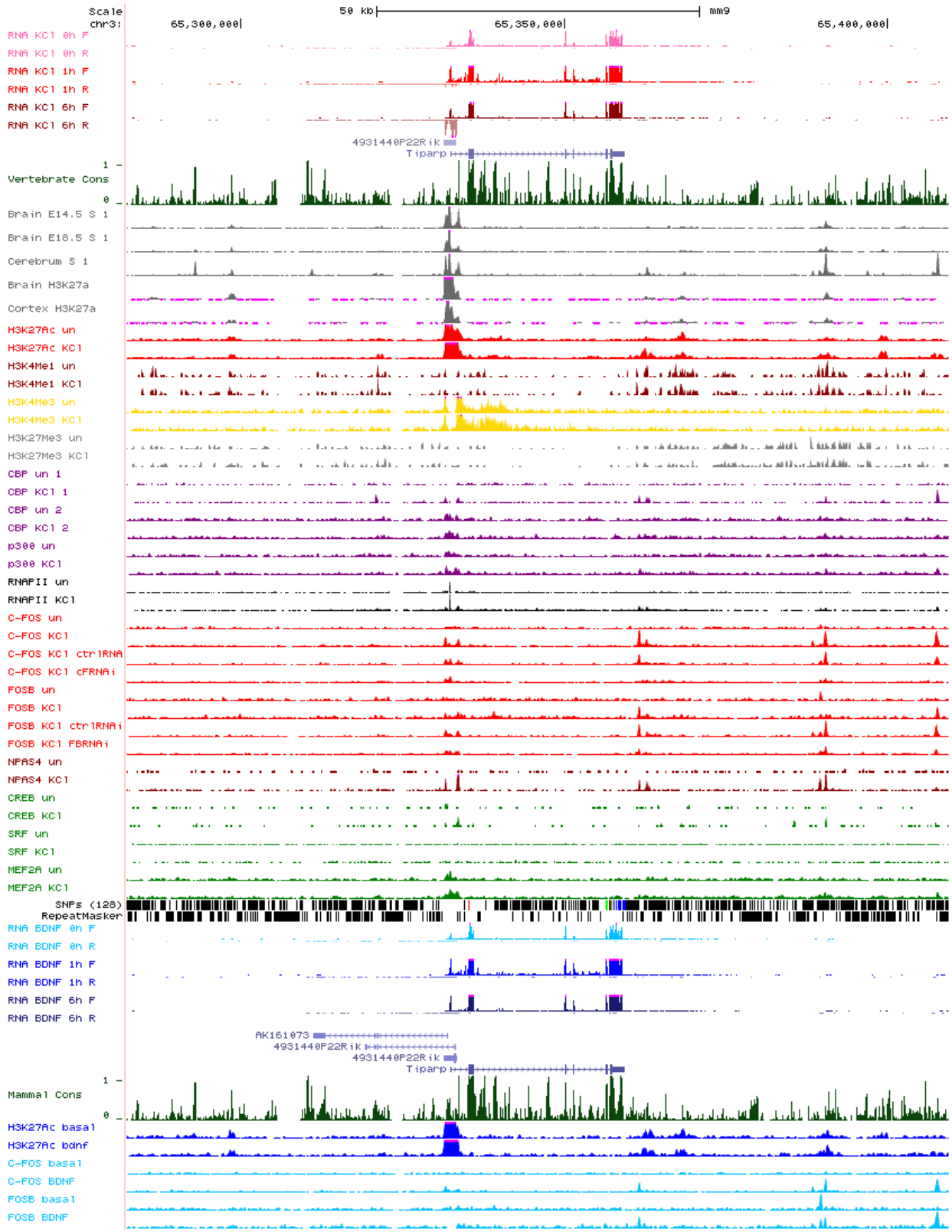

Figure 6.72: *Tiparp* locus

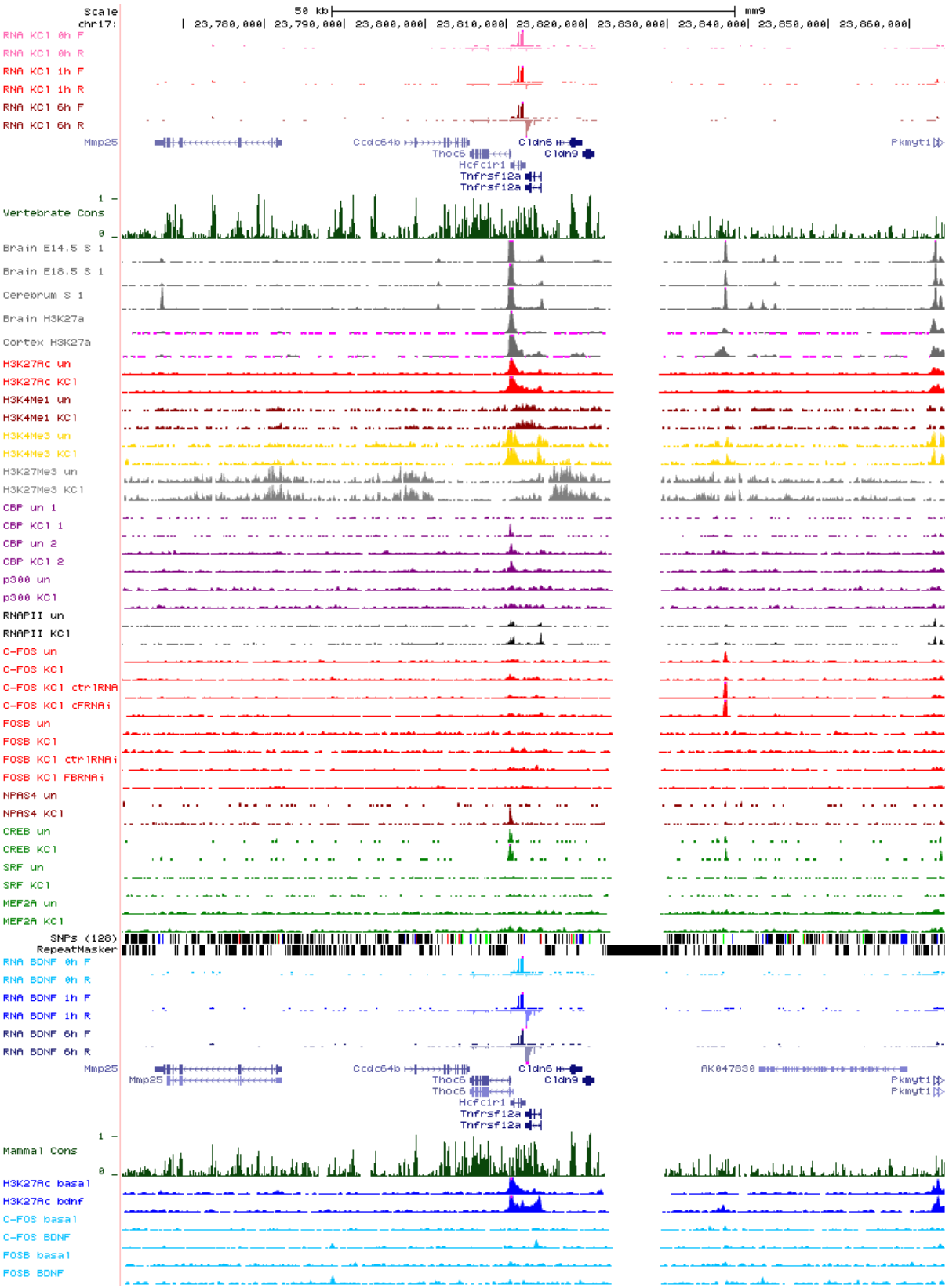

Figure 6.73: *Tnfrsf12a* locus

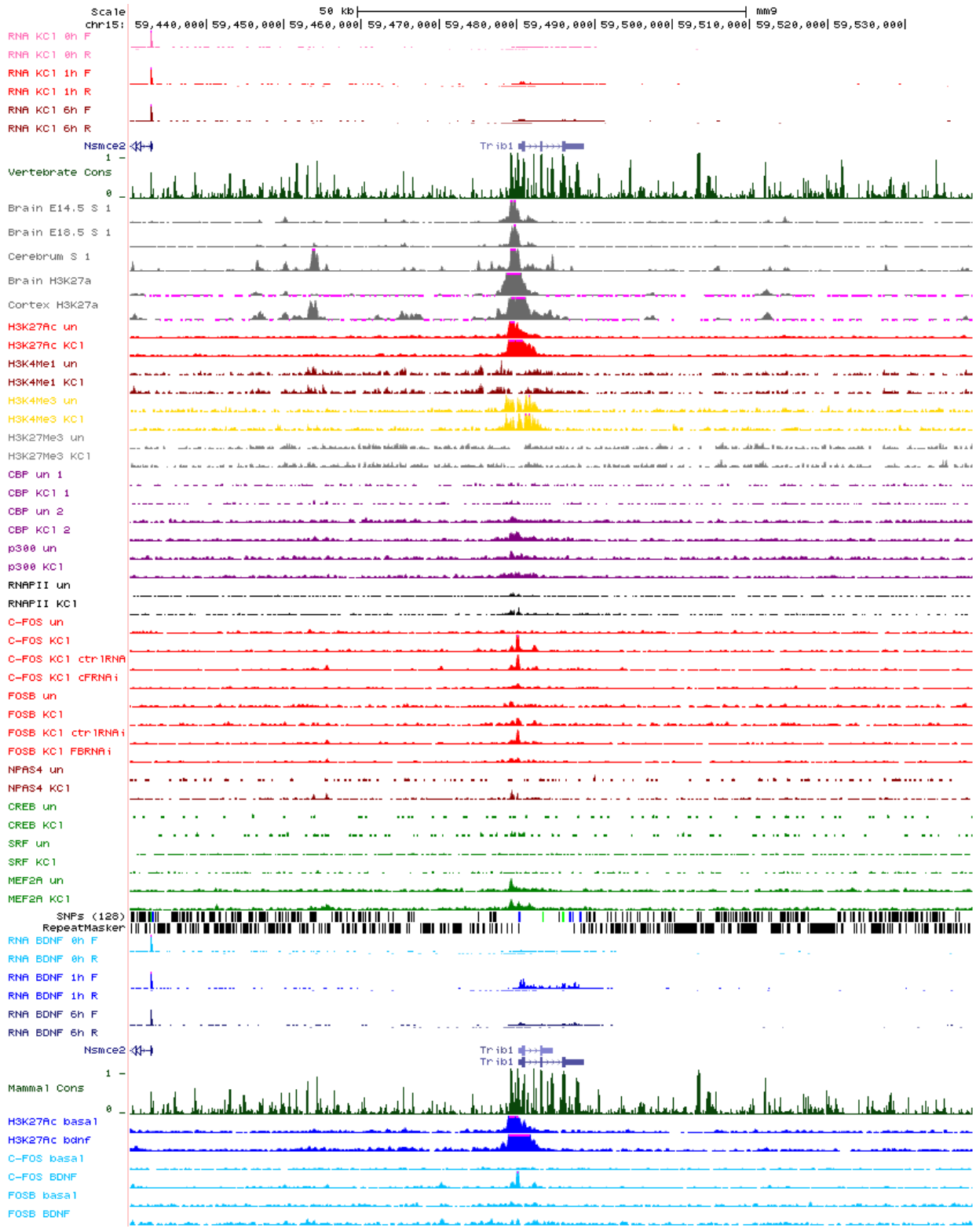

Figure 6.74: *Trib1* locus

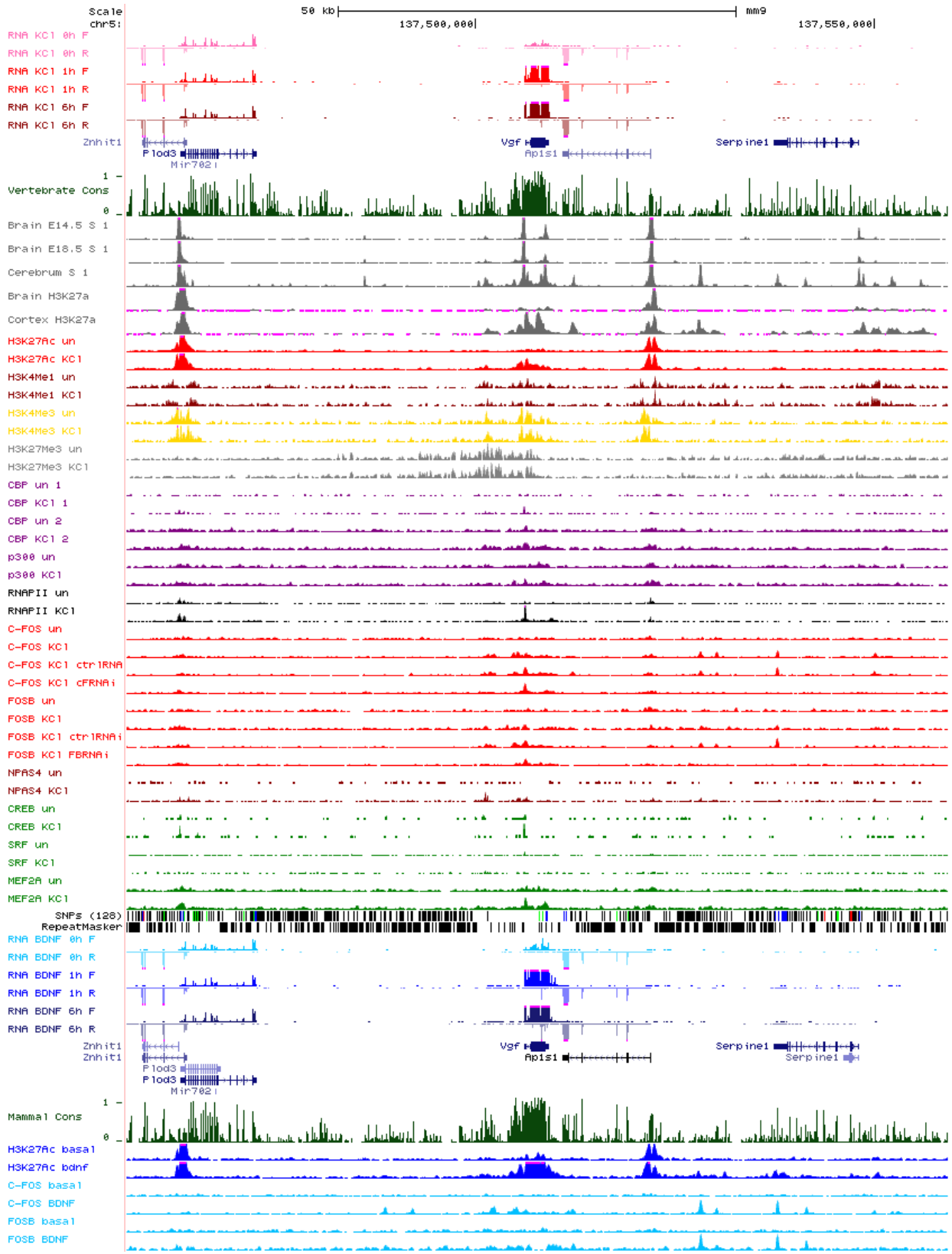

Figure 6.75: *Vgf* locus

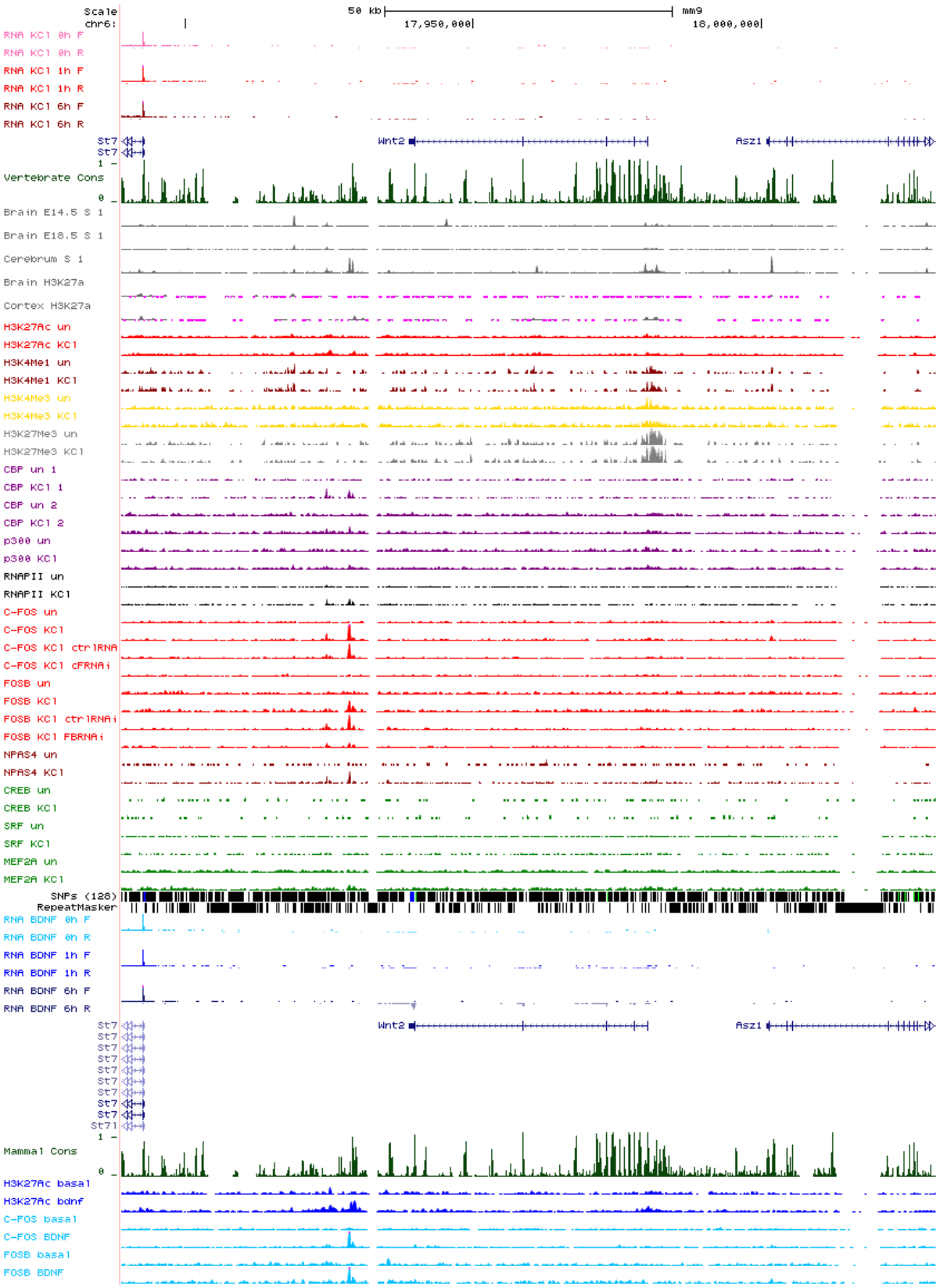

Figure 6.76: *Wnt2* locus

7 APPENDIX B: NEURONAL ENHANCERS WITH DIFFERENT H3K27AC BEHAVIORS

7.1 UCSC GENOME BROWSER VIEWS OF CHIP-SEQ AND RNA-SEQ DATA AT NEURONAL ENHANCERS WITH DIFFERENT H3K27AC BEHAVIORS

All enhancers tested in luciferase assays within this thesis are displayed on the subsequent pages, in order of enhancer number. A 20kb window surrounding each enhancer center is displayed.

For each enhancer, the following tracks are displayed:

1) RNA-Seq after 0 hr of KCl stimulation, silenced conditions
2) RNA-Seq after 1 hr of KCl stimulation
3) RNA-Seq after 6 hr of KCl stimulation
4) RefSeq gene
5) PhastCons vertebrate conservation
6) DNaseI hypersensitivity from embryonic 14.5 whole brain*
7) DNaseI hypersensitivity from embryonic 18.5 whole brain*
8) DNaseI hypersensitivity from 8 week adult cerebrum*
9) H3K27Ac ChIP-Seq from embryonic 14.5 whole brain*
10) H3K27Ac ChIP-Seq from 8 week adult cortex*
11) H3K27Ac ChIP-Seq in silenced conditions
12) H3K27Ac ChIP-Seq after 2hrs of KCl stimulation
13) H3K4Me1 ChIP-Seq in silenced conditions**
14) H3K4Me1 ChIP-Seq after 2hrs of KCl stimulation**
15) H3K4Me3 ChIP-Seq in silenced conditions**
16) H3K4Me3 ChIP-Seq after 2hrs of KCl stimulation**
17) H3K27Me3 ChIP-Seq in silenced conditions**
18) H3K27Me3 ChIP-Seq after 2hrs of KCl stimulation**
19) CBP ChIP-Seq in silenced conditions**
20) CBP ChIP-Seq after 2hrs of KCl stimulation**
21) CBP ChIP-Seq in silenced conditions
22) CBP ChIP-Seq after 2hrs of KCl stimulation
23) P300 ChIP-Seq in silenced conditions
24) P300 ChIP-Seq after 2hrs of KCl stimulation
25) RNAPII ChIP-Seq in silenced conditions**
26) RNAPII ChIP-Seq after 2hrs of KCl stimulation**
27) C-FOS ChIP-Seq in silenced conditions
28) C-FOS ChIP-Seq after 2hrs of KCl stimulation
29) C-FOS ChIP-Seq after 2hrs of KCl stimulation from control shRNA lentivirus infected neurons
30) C-FOS ChIP-Seq after 2hrs of KCl stimulation from *c-Fos* shRNA lentivirus infected neurons
31) FOSB ChIP-Seq in silenced conditions
32) FOSB ChIP-Seq after 2hrs of KCl stimulation
33) FOSB ChIP-Seq after 2hrs of KCl stimulation from control shRNA lentivirus infected neurons
34) FOSB ChIP-Seq after 2hrs of KCl stimulation from *FosB* shRNA lentivirus infected neurons
35) NPAS4 ChIP-Seq in silenced conditions**
36) NPAS4 ChIP-Seq after 2hrs of KCl stimulation**
37) CREB ChIP-Seq in silenced conditions**
38) CREB ChIP-Seq after 2hrs of KCl stimulation**
39) SRF ChIP-Seq in silenced conditions**
40) SRF ChIP-Seq after 2hrs of KCl stimulation**
41) MEF2A ChIP-Seq in silenced conditions
42) MEF2A ChIP-Seq after 2hrs of KCl stimulation
43) SNPs
44) RepeatMasker
45) RNA-Seq after 0 hr of BDNF stimulation, basal conditions
46) RNA-Seq after 1 hr of BDNF stimulation
47) RNA-Seq after 6 hr of BDNF stimulation
48) UCSC gene
49) PhastCons mammalian conservation
50) H3K27Ac ChIP-Seq in basal conditions
51) H3K27Ac ChIP-Seq after 2hrs of BDNF stimulation
52) C-FOS ChIP-Seq in basal conditions
53) C-FOS ChIP-Seq after 2hrs of BDNF stimulation
54) FOSB ChIP-Seq in basal conditions
55) FOSB ChIP-Seq after 2hrs of BDNF stimulation

* denotes data from ENCODE, ** denotes data from Kim et al., 2010

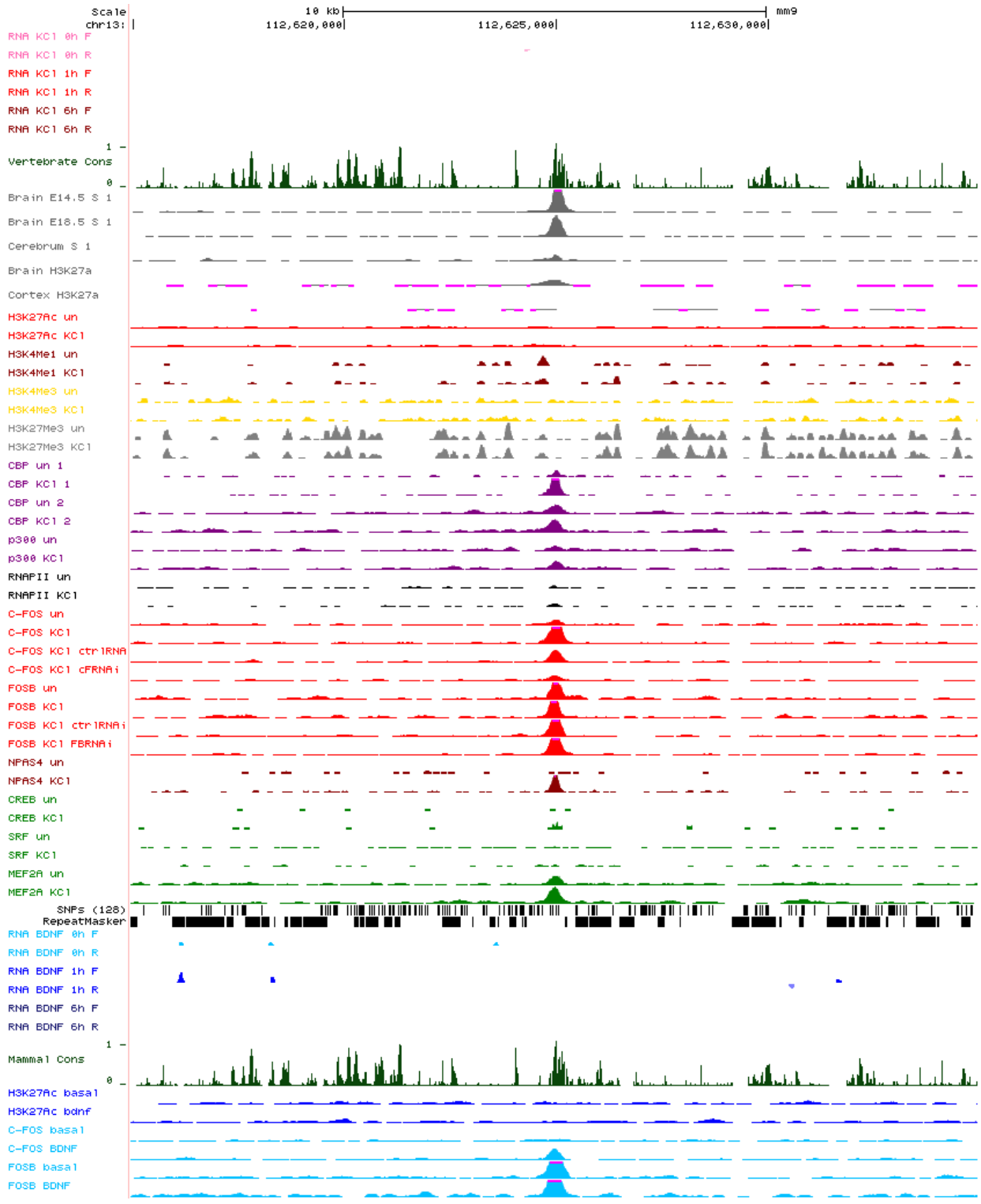

Figure 7.1: Enhancer 1 locus

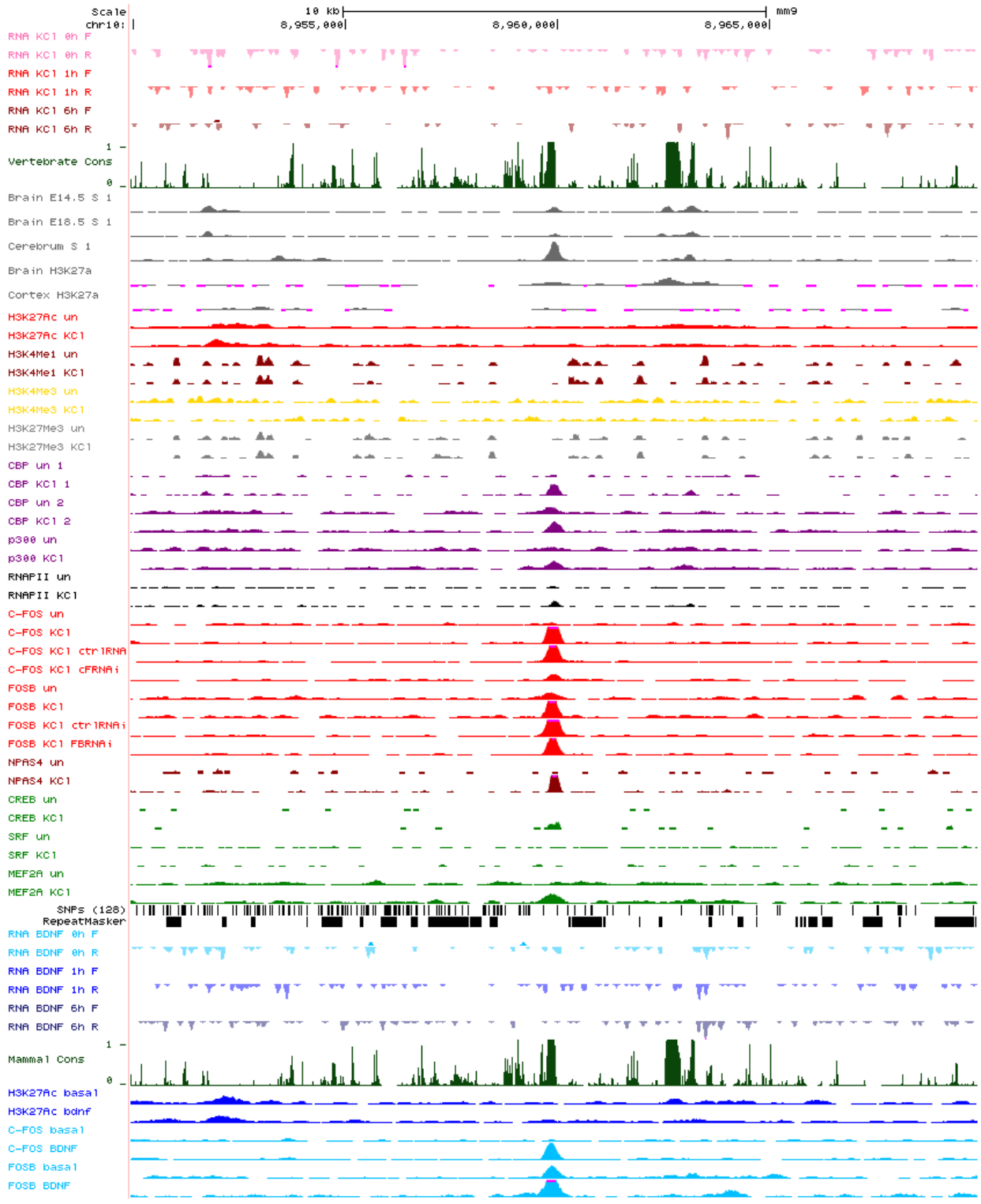

Figure 7.2: Enhancer 2 locus

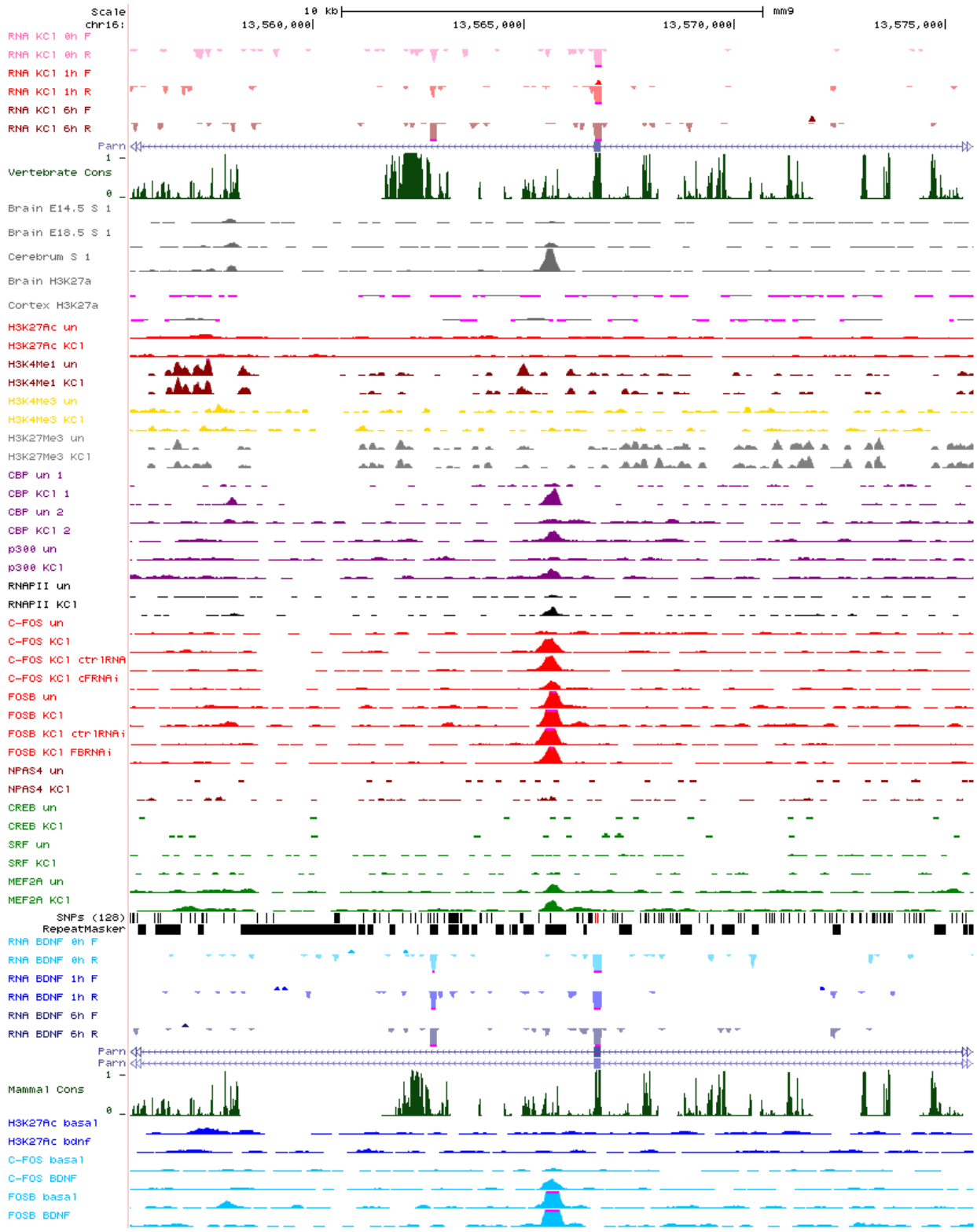

Figure 7.3: Enhancer 3 locus

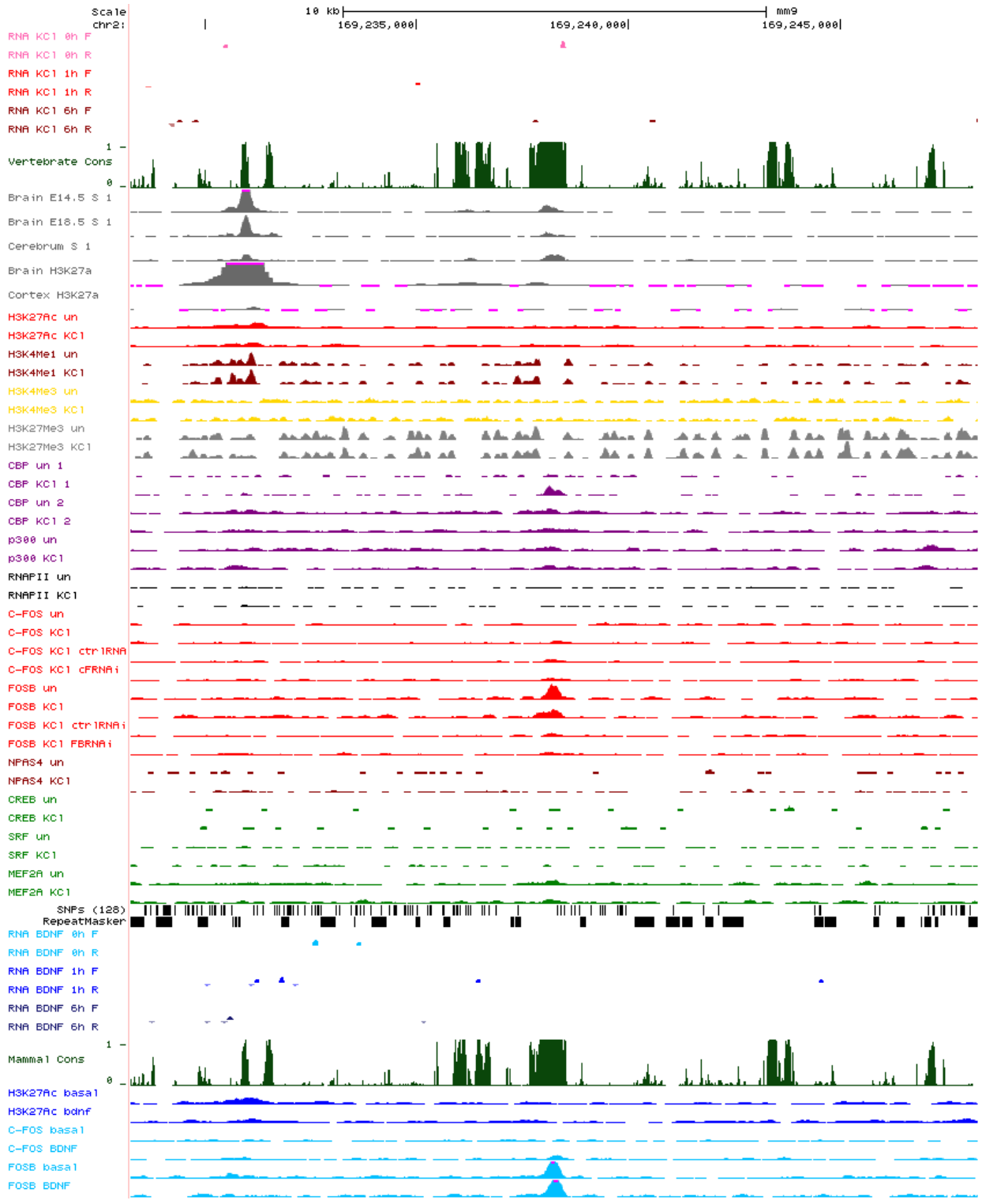

Figure 7.4: Enhancer 4 locus

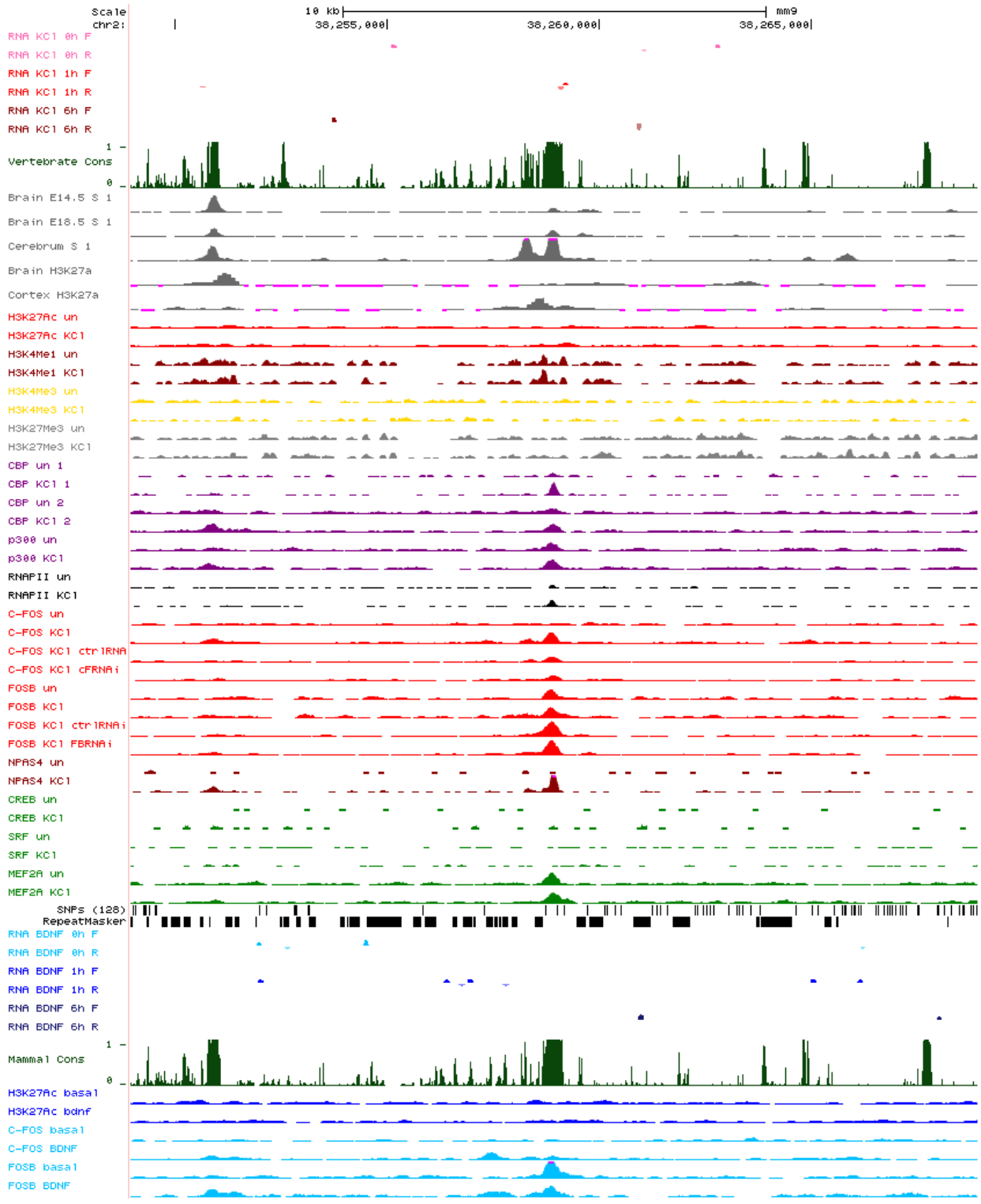

Figure 7.5: Enhancer 5 locus

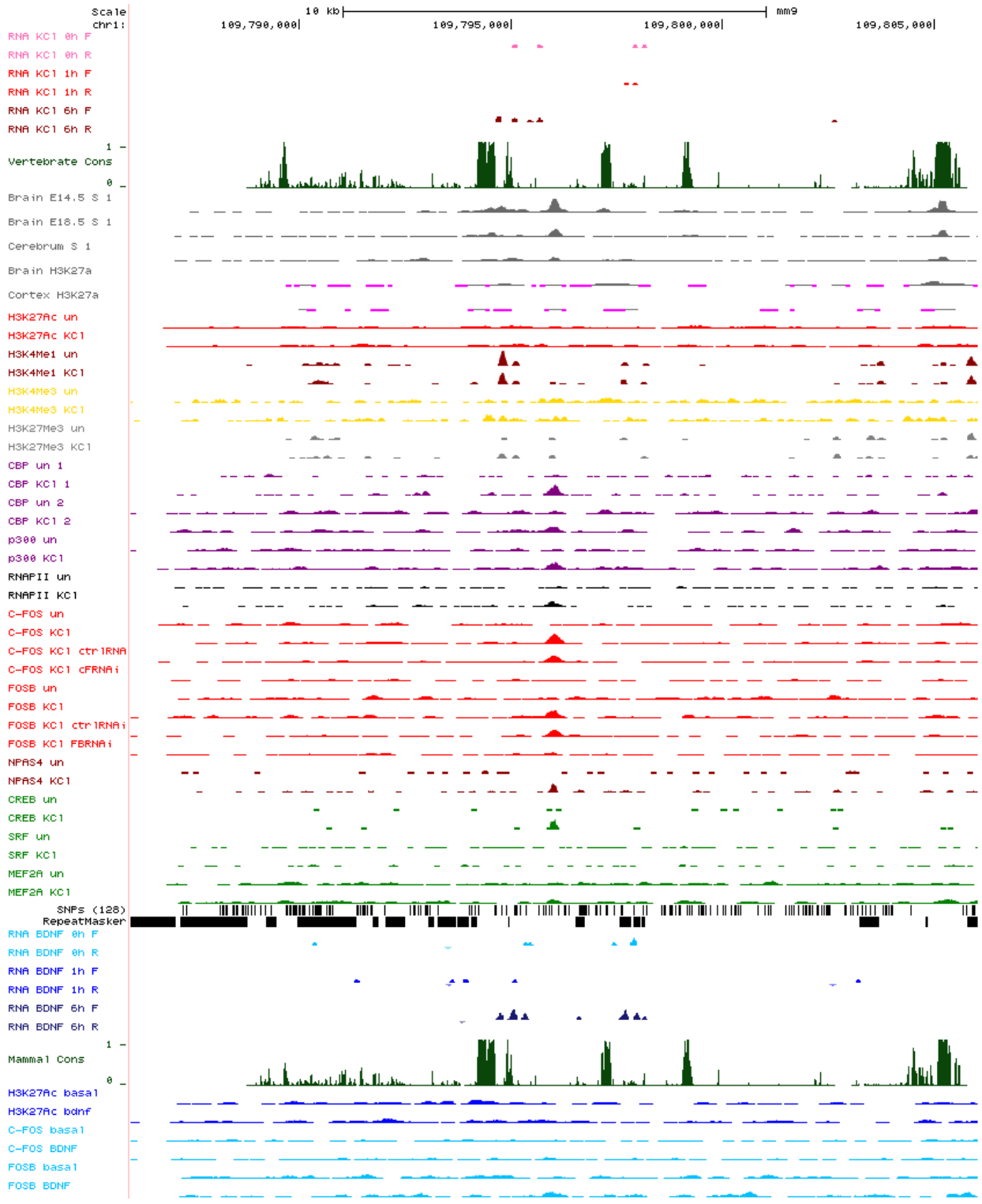

Figure 7.6: Enhancer 6 locus

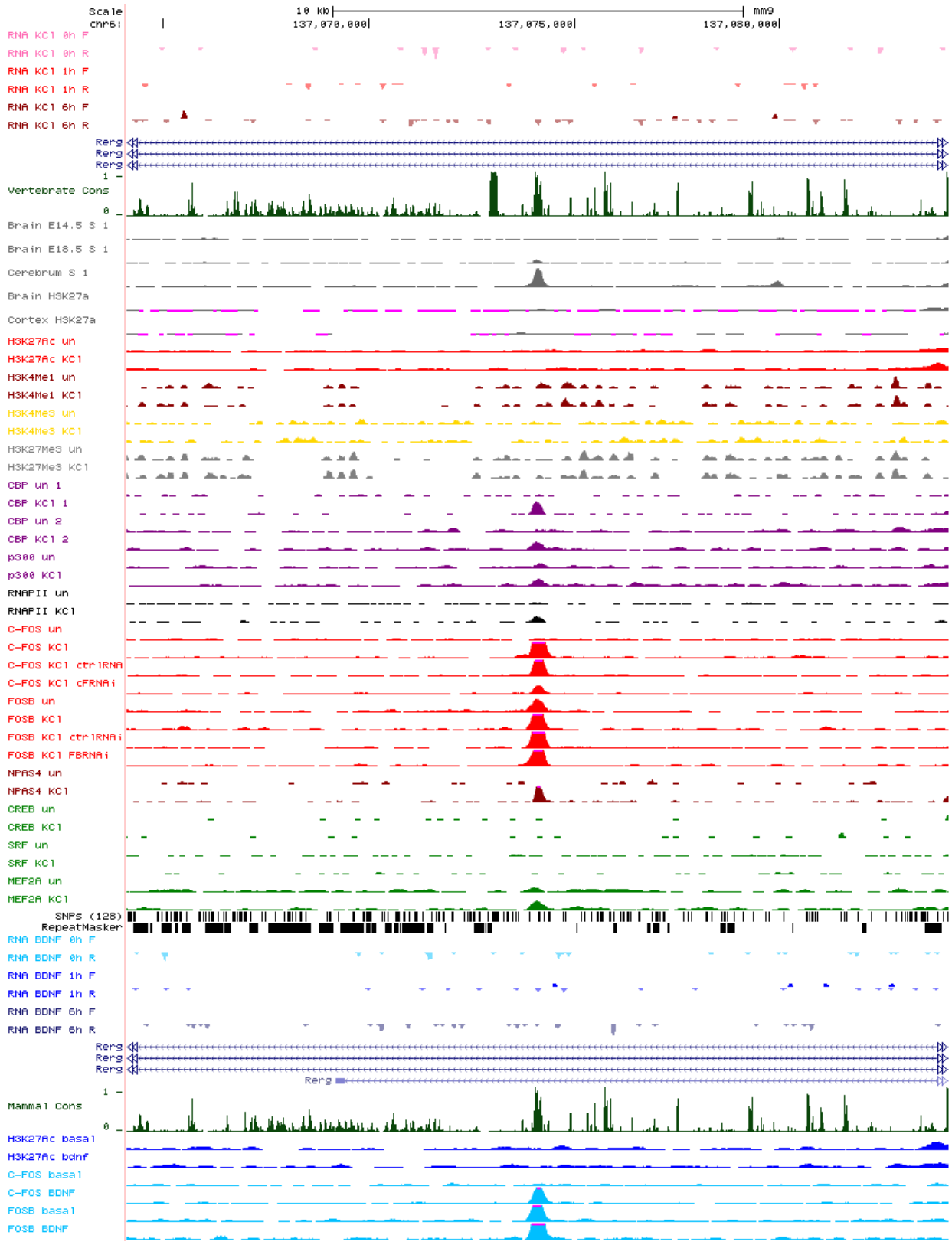

Figure 7.7: Enhancer 7 locus

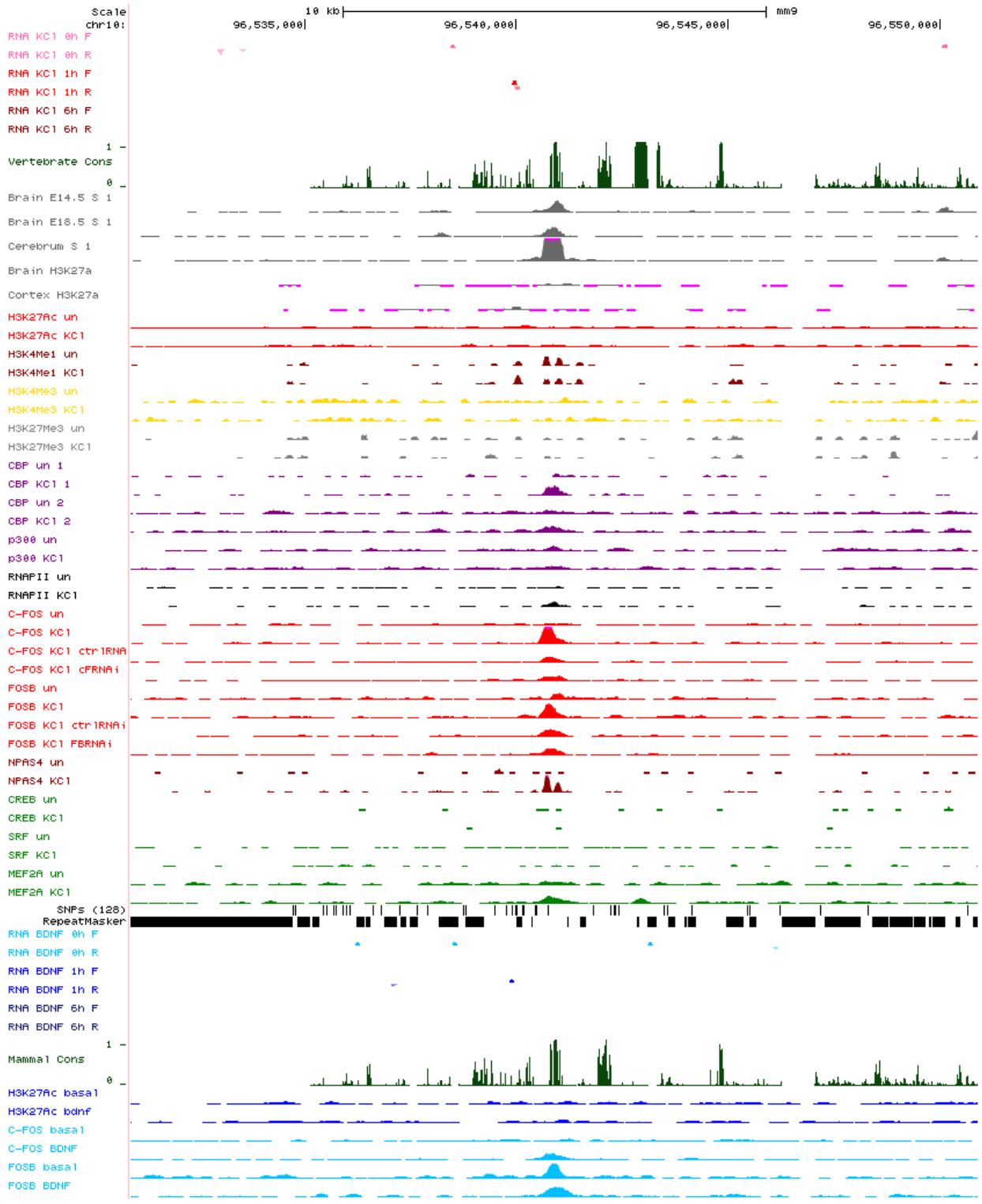

Figure 7.8: Enhancer 8 locus

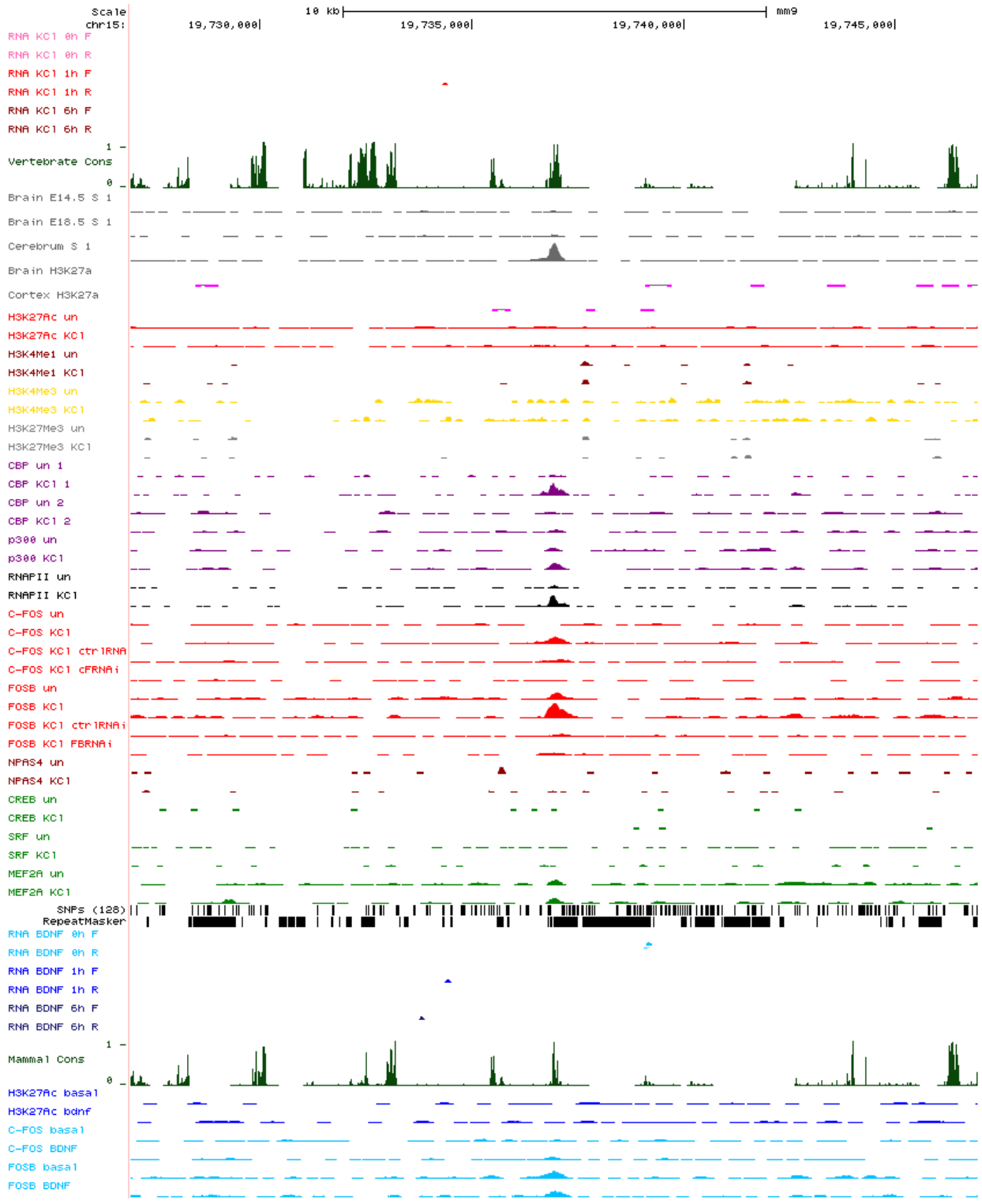

Figure 7.9: Enhancer 9 locus

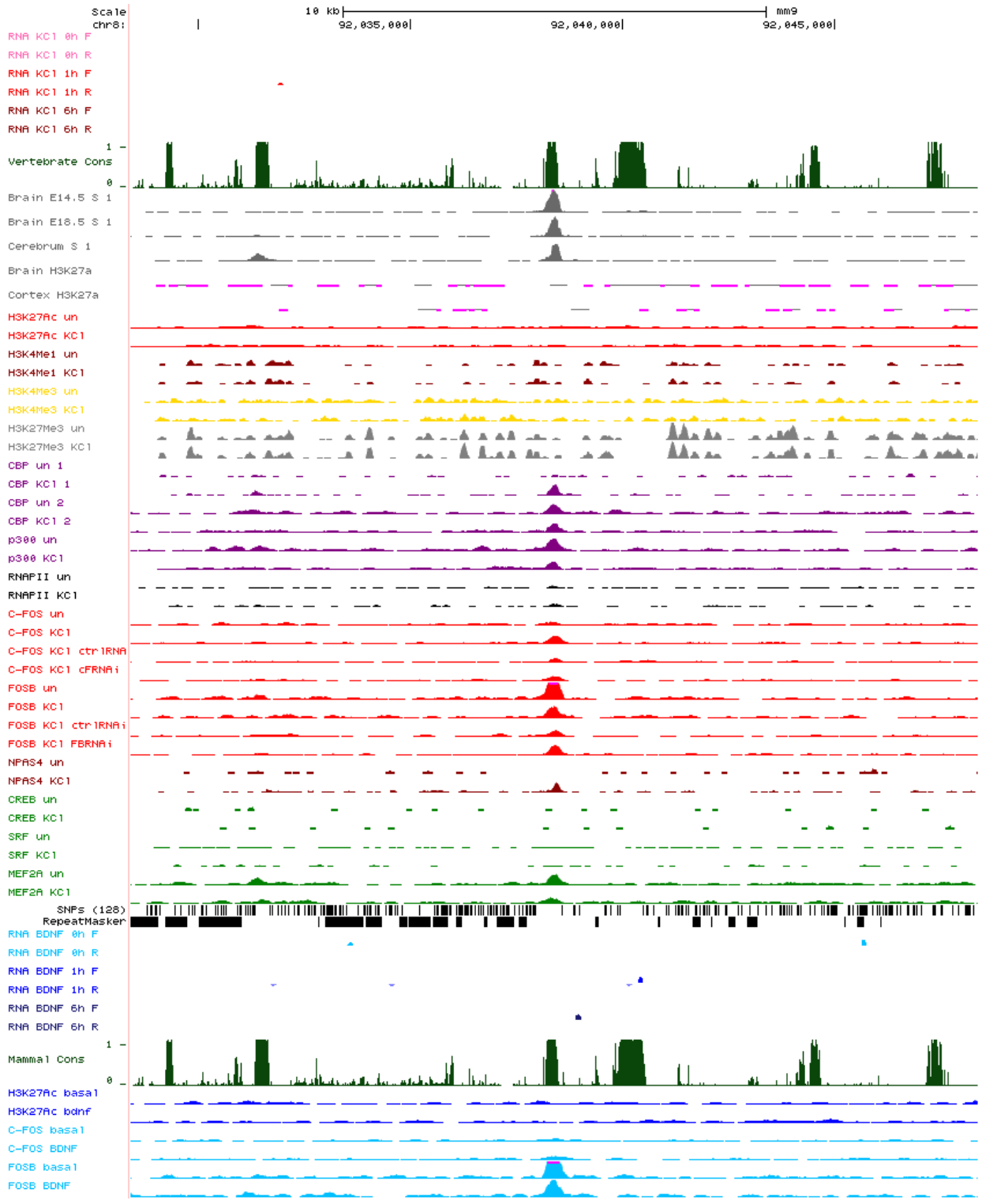

Figure 7.10: Enhancer 10 locus

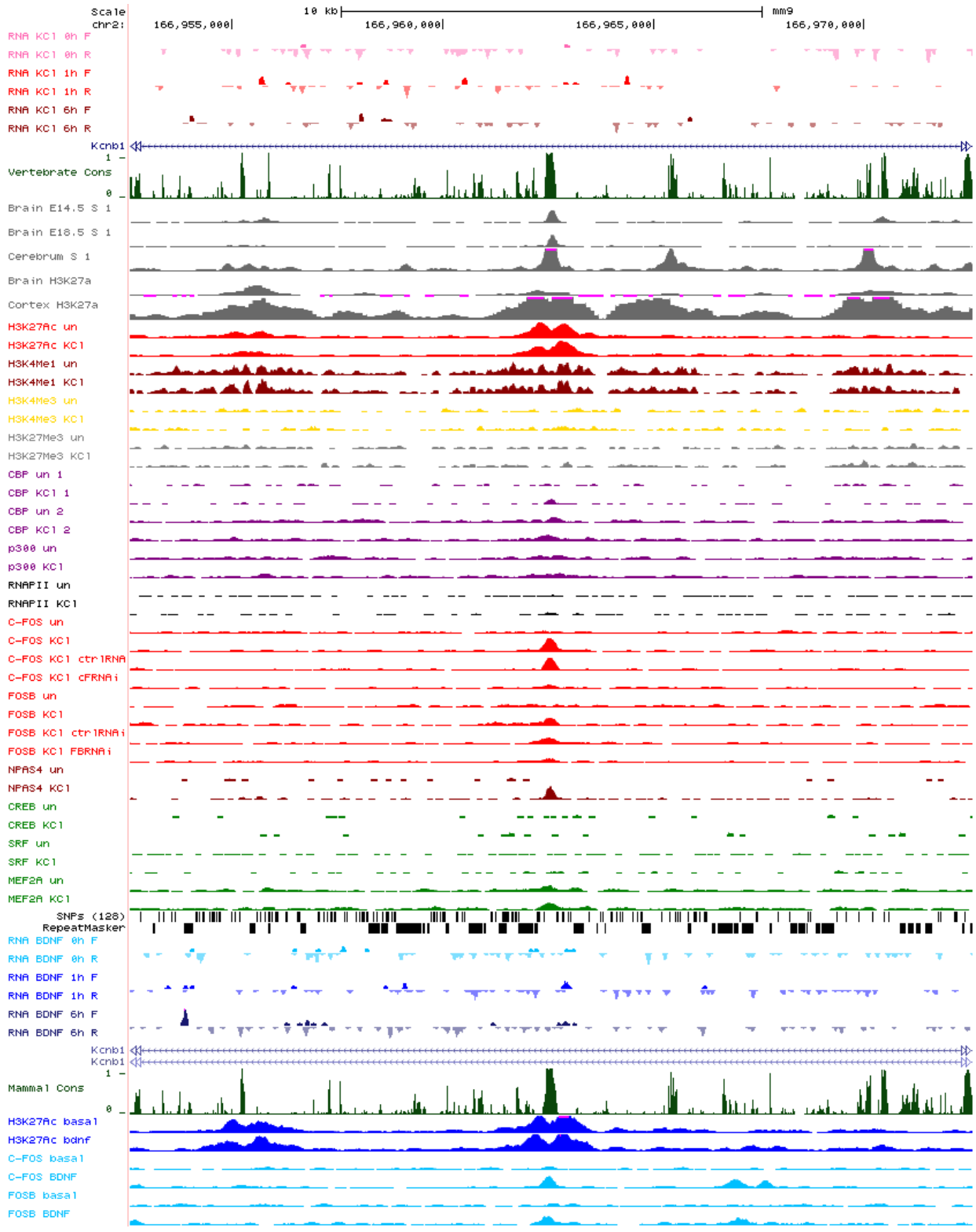

Figure 7.11: Enhancer 11 locus

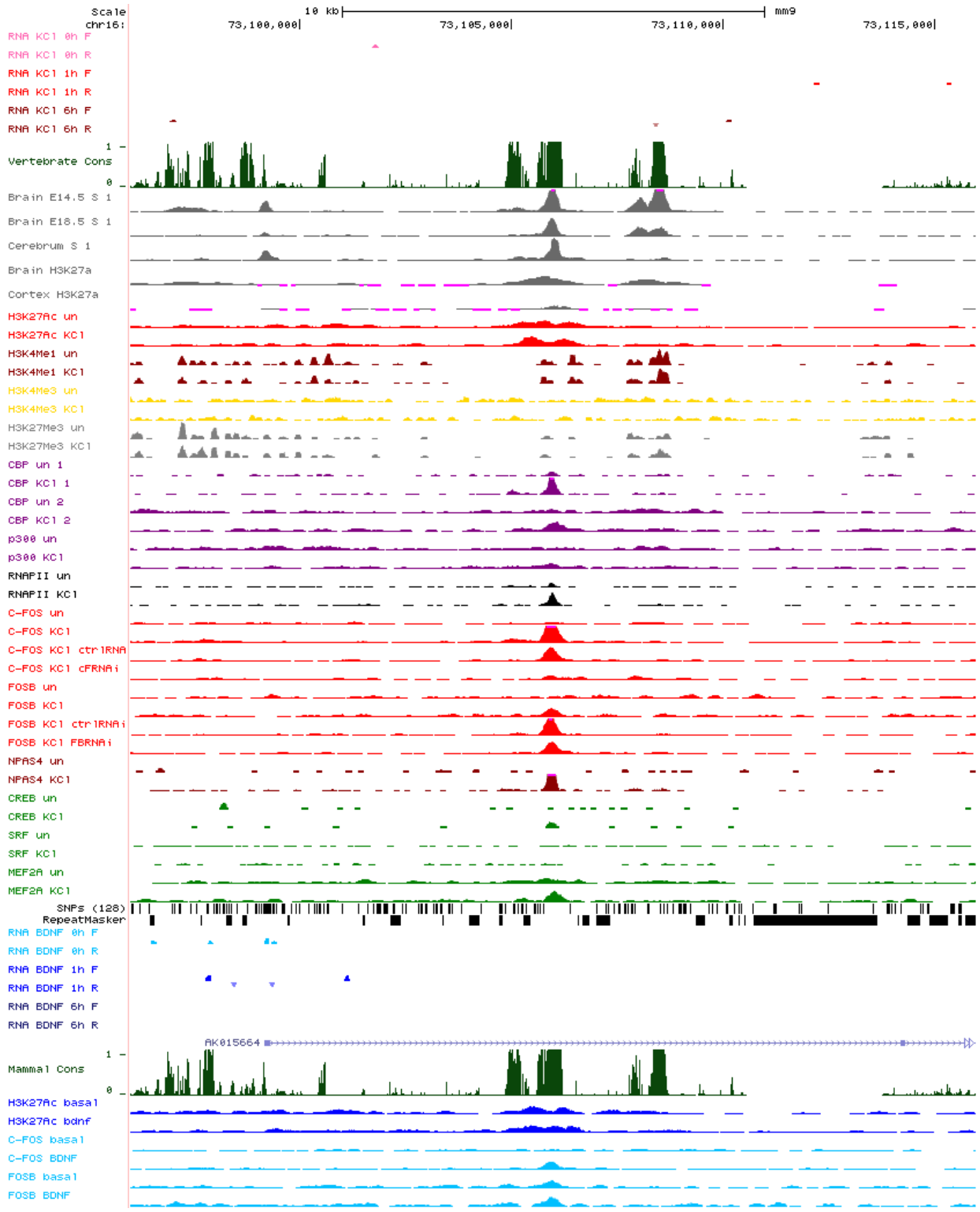

Figure 7.12: Enhancer 12 locus

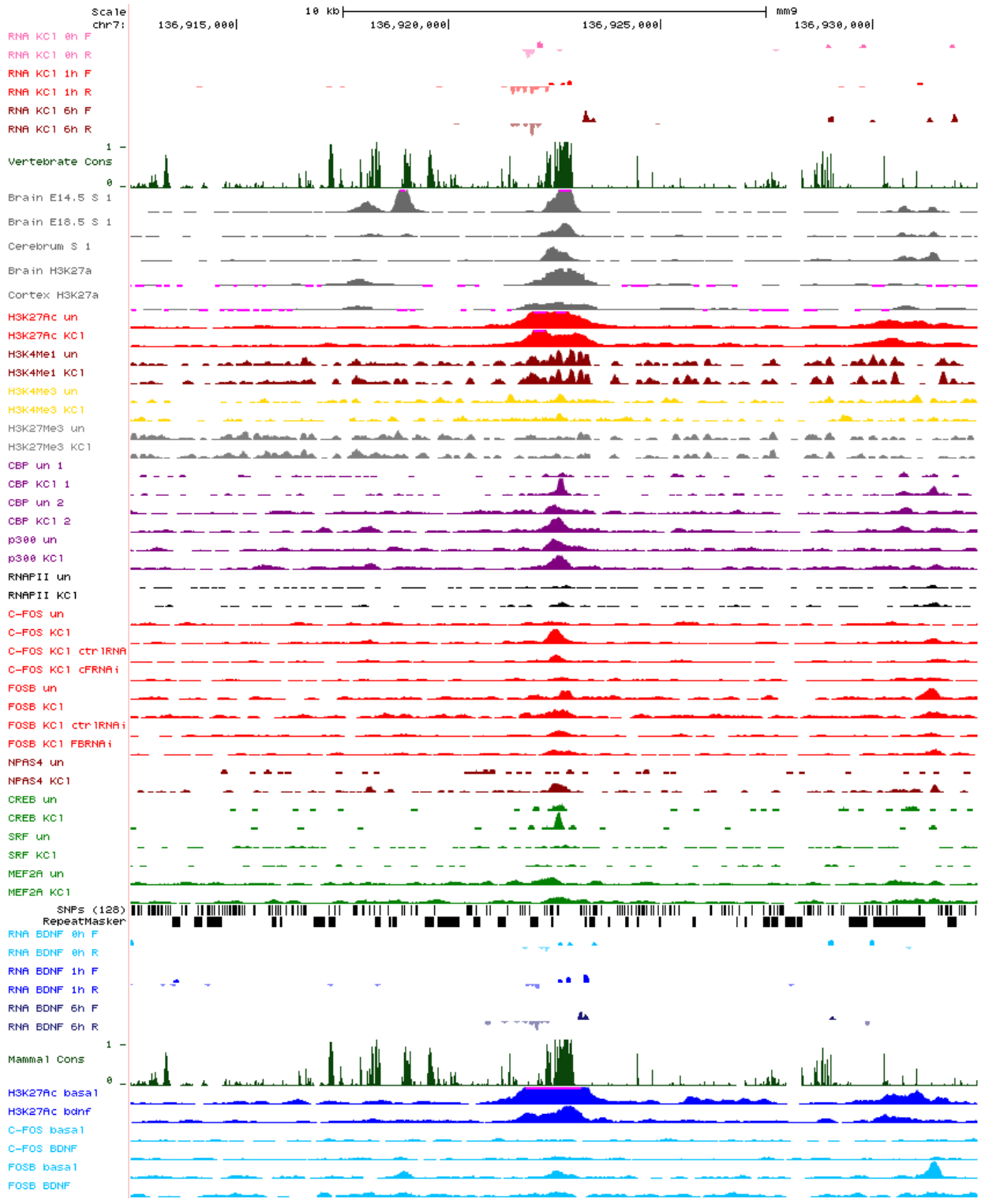

Figure 7.13: Enhancer 13 locus

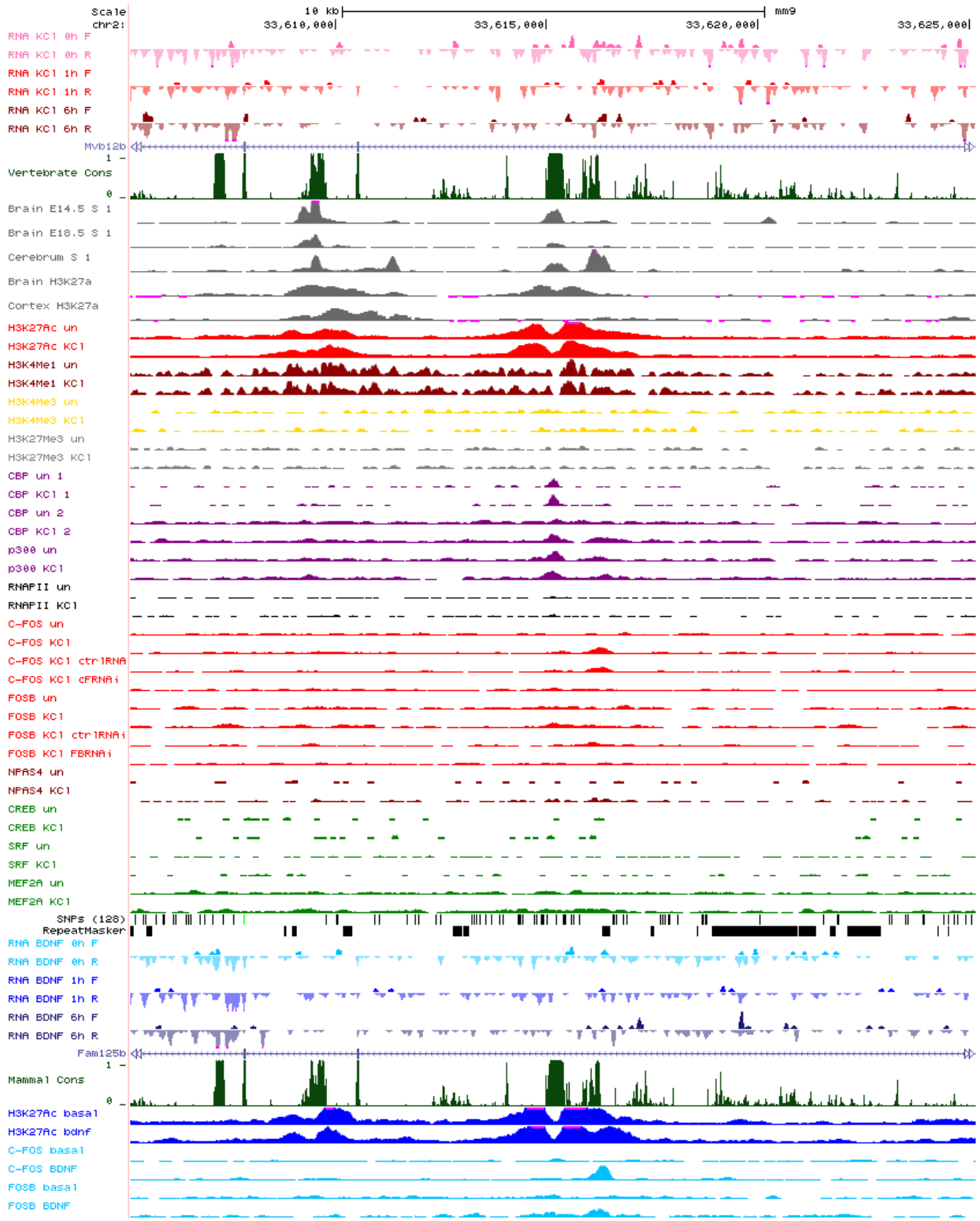

Figure 7.14: Enhancer 14 locus

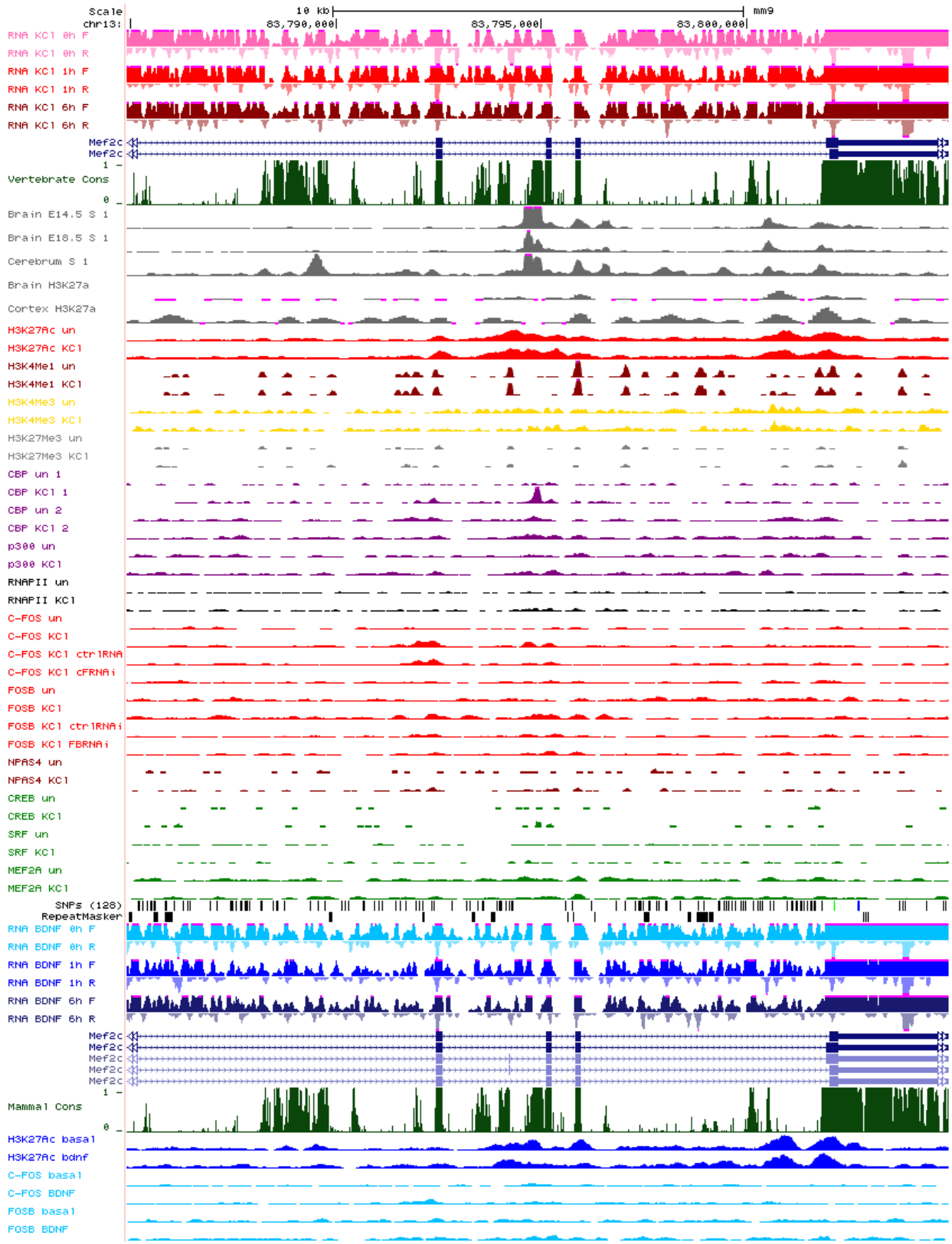

Figure 7.15: Enhancer 15 locus

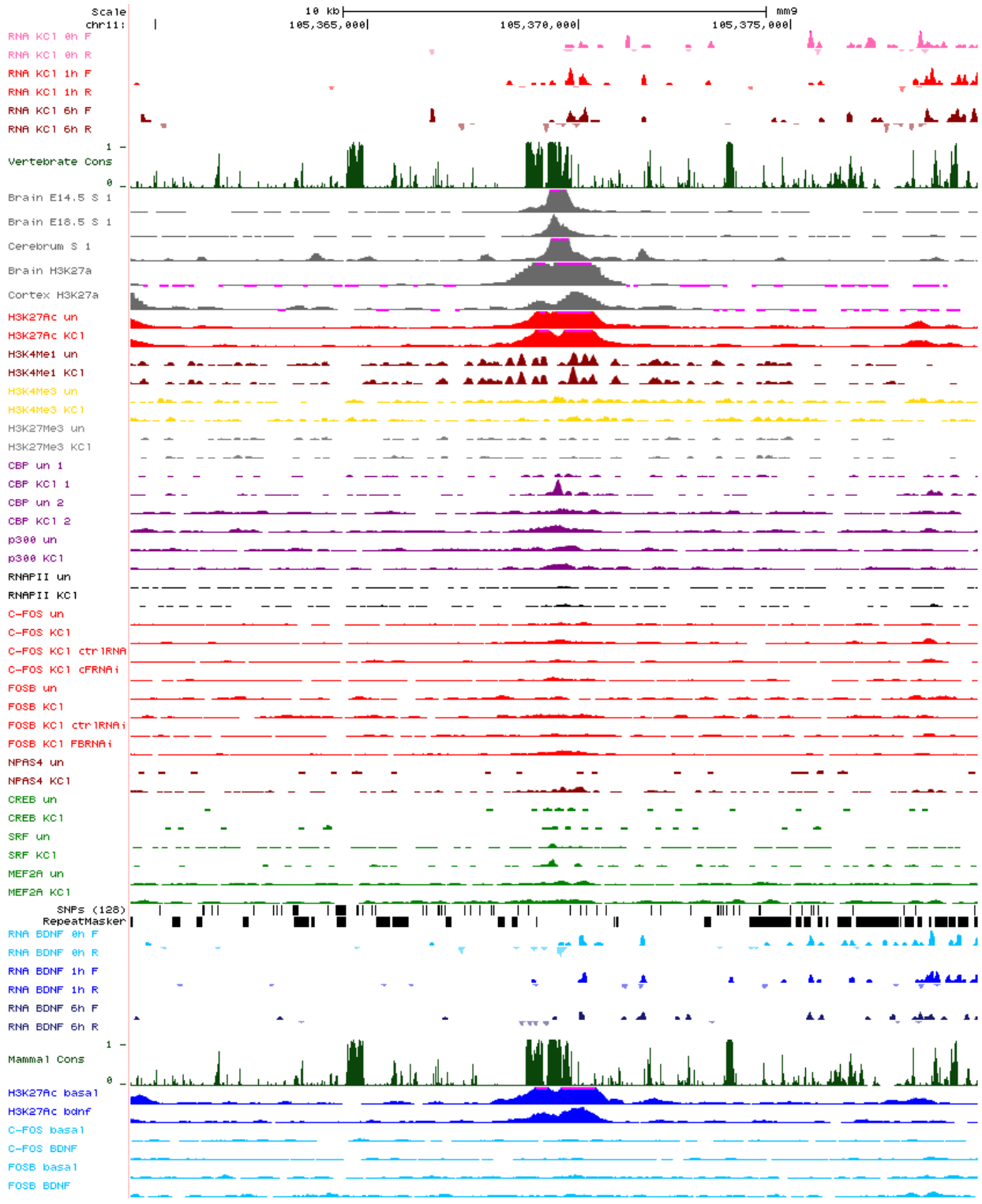

Figure 7.16: Enhancer 16 locus

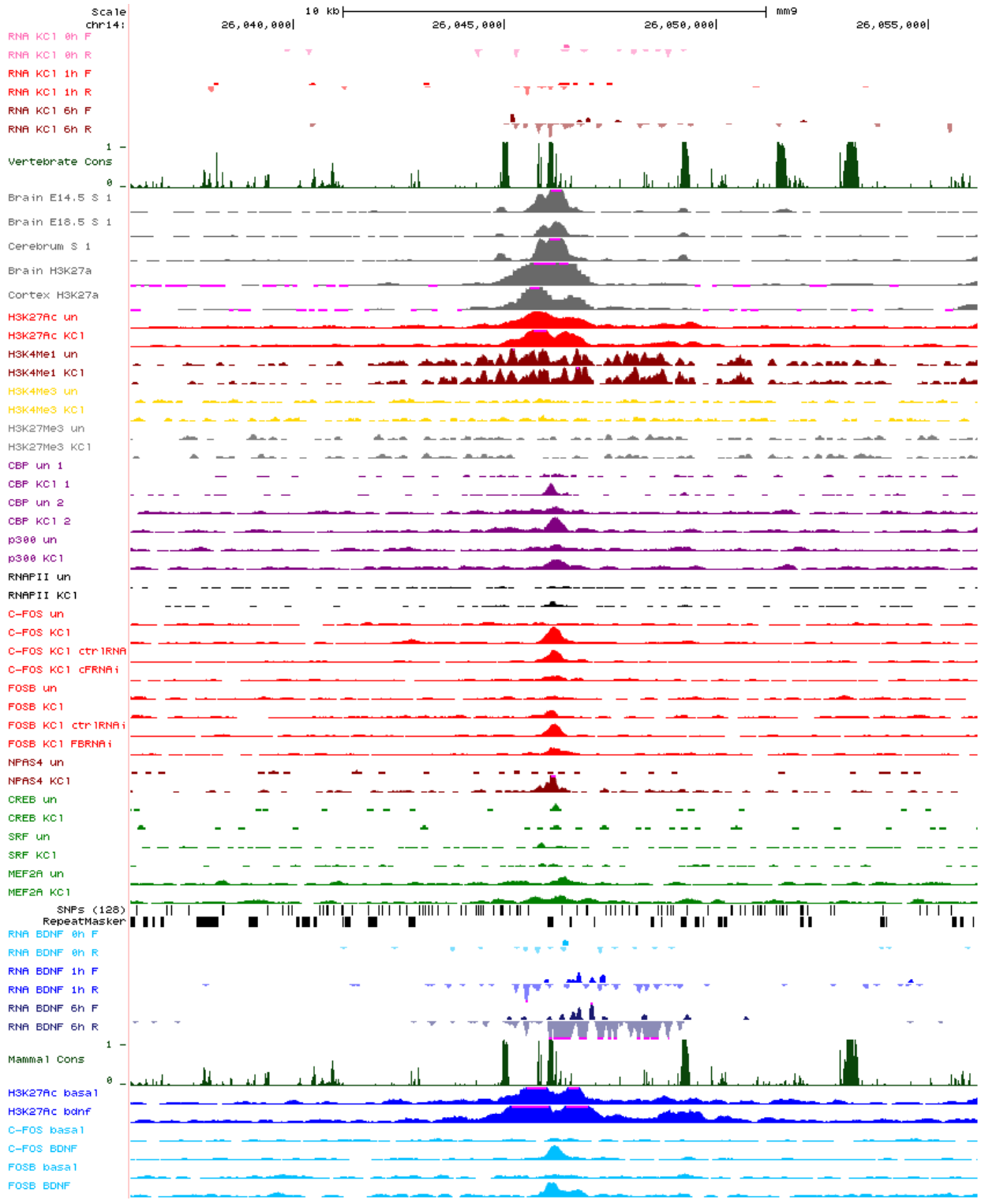

Figure 7.17: Enhancer 17 locus

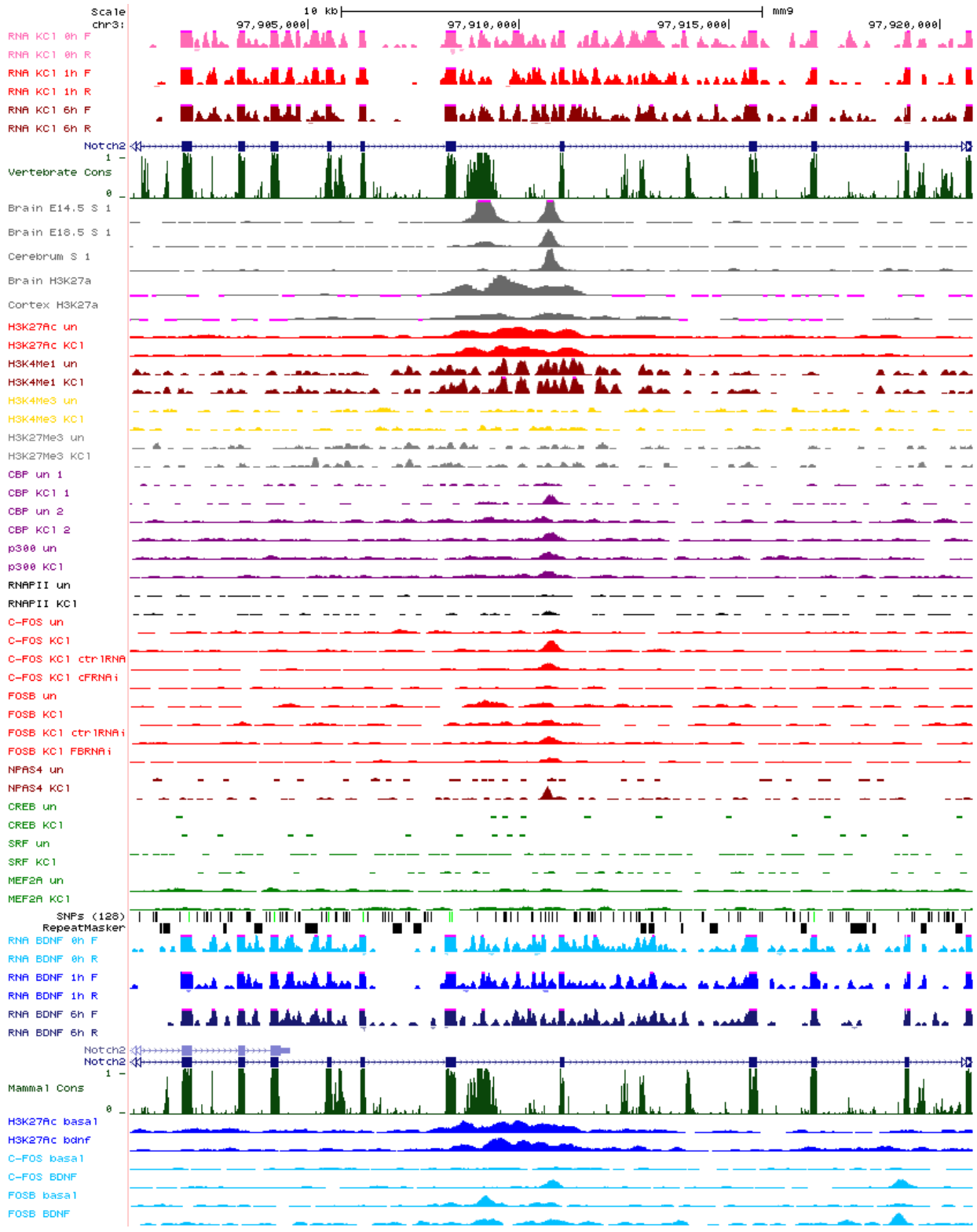

Figure 7.18: Enhancer 18 locus

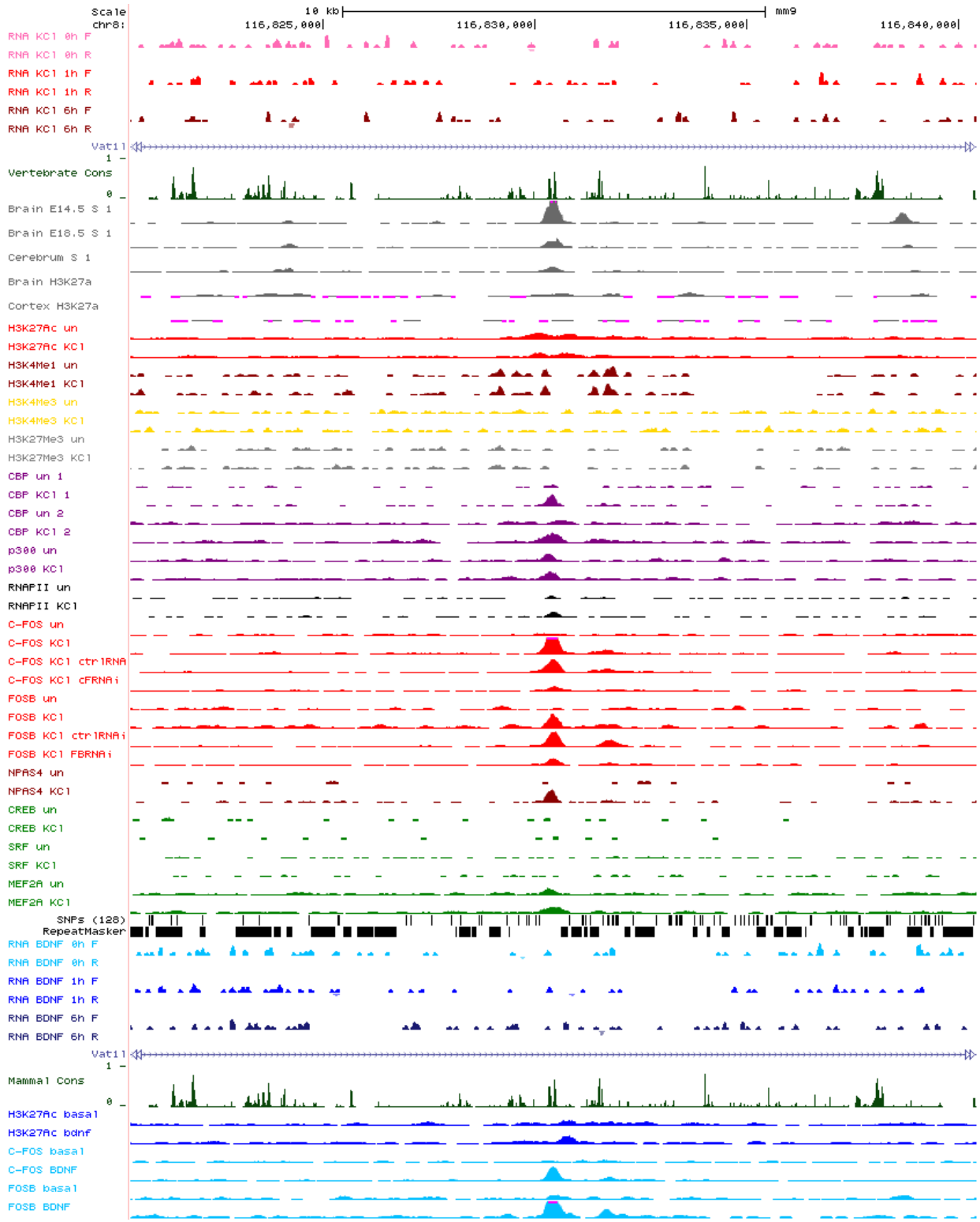

Figure 7.19: Enhancer 19 locus

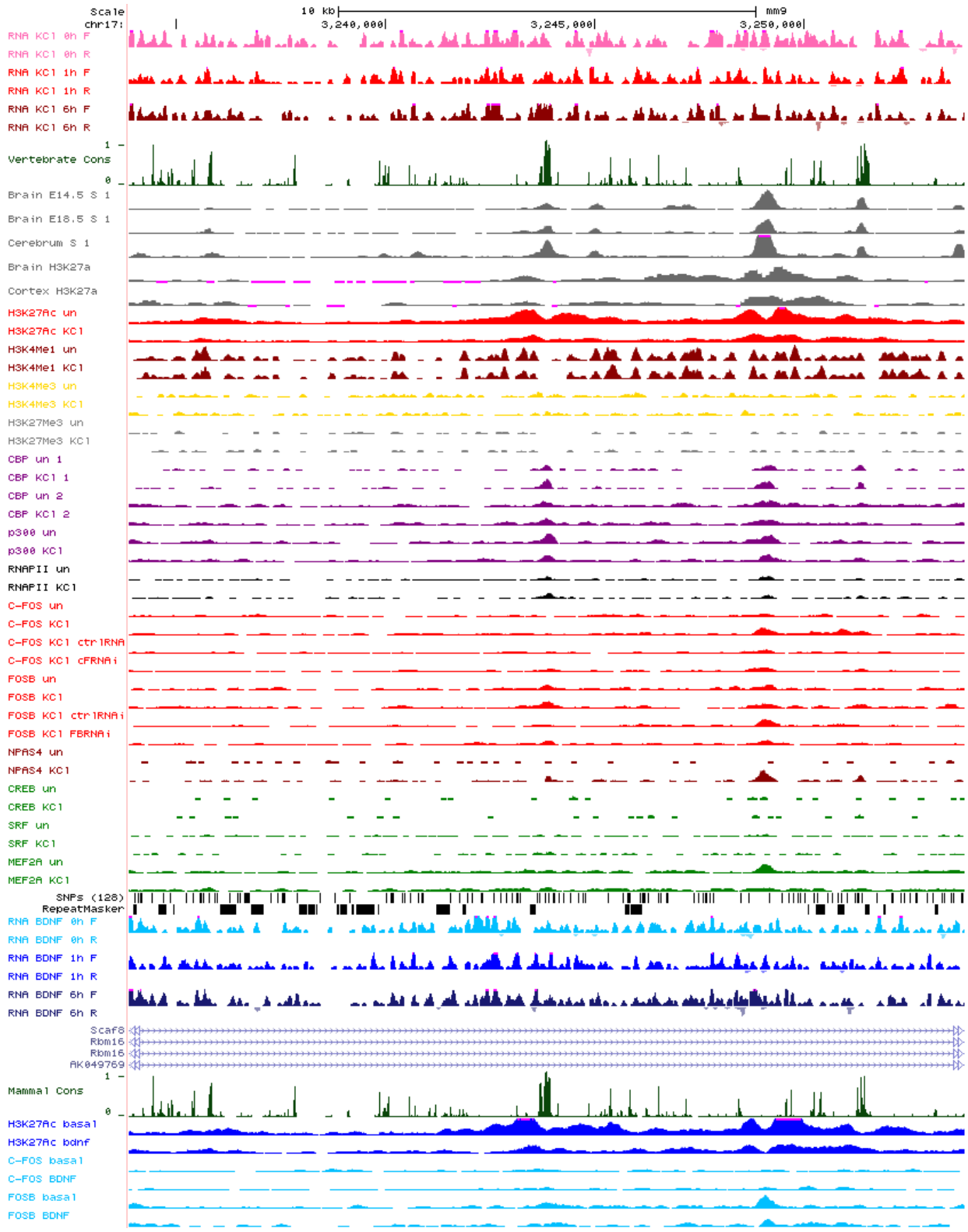

Figure 7.20: Enhancer 20 locus

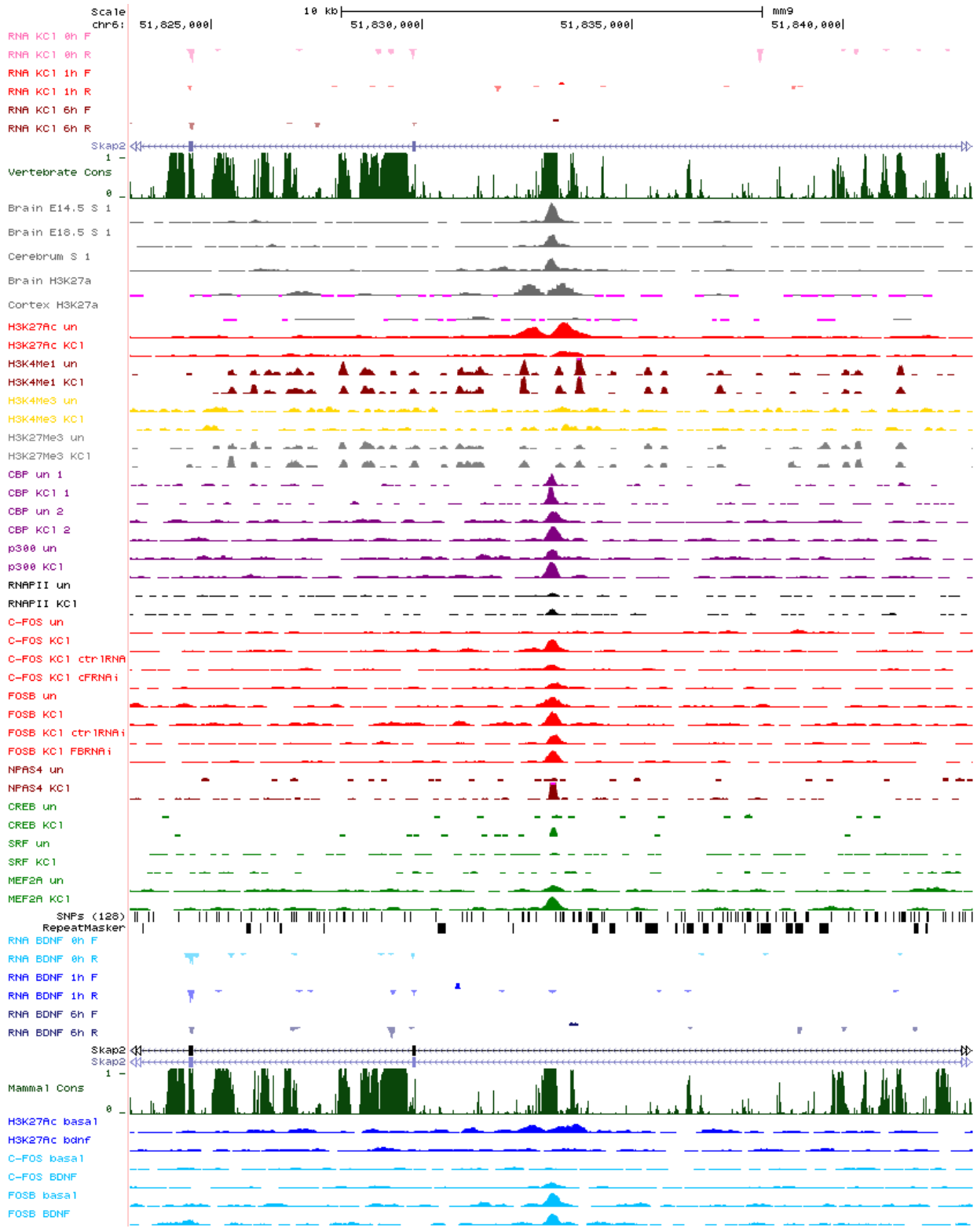

Figure 7.21: Enhancer 21 locus

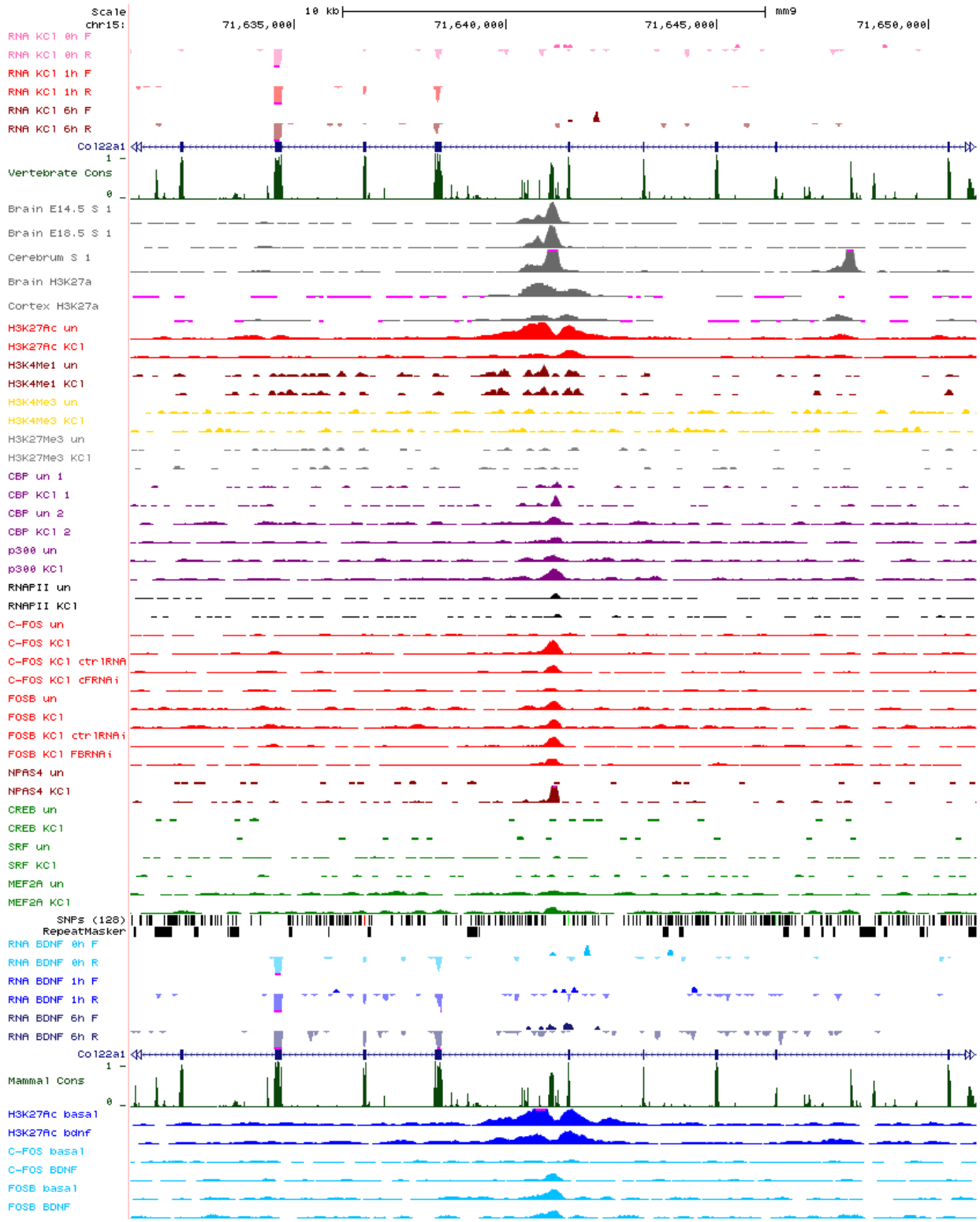

Figure 7.22: Enhancer 22 locus

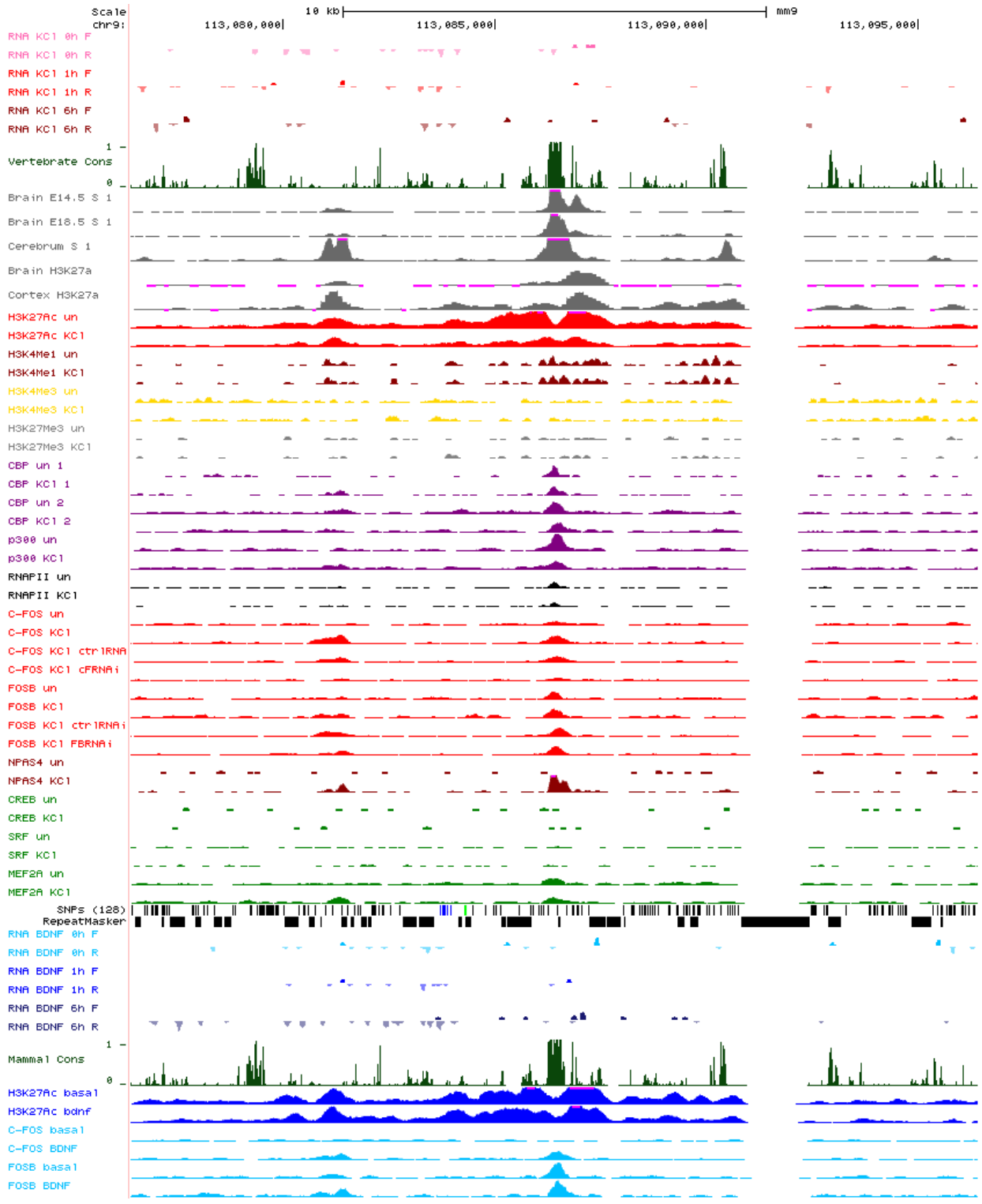

Figure 7.23: Enhancer 23 locus

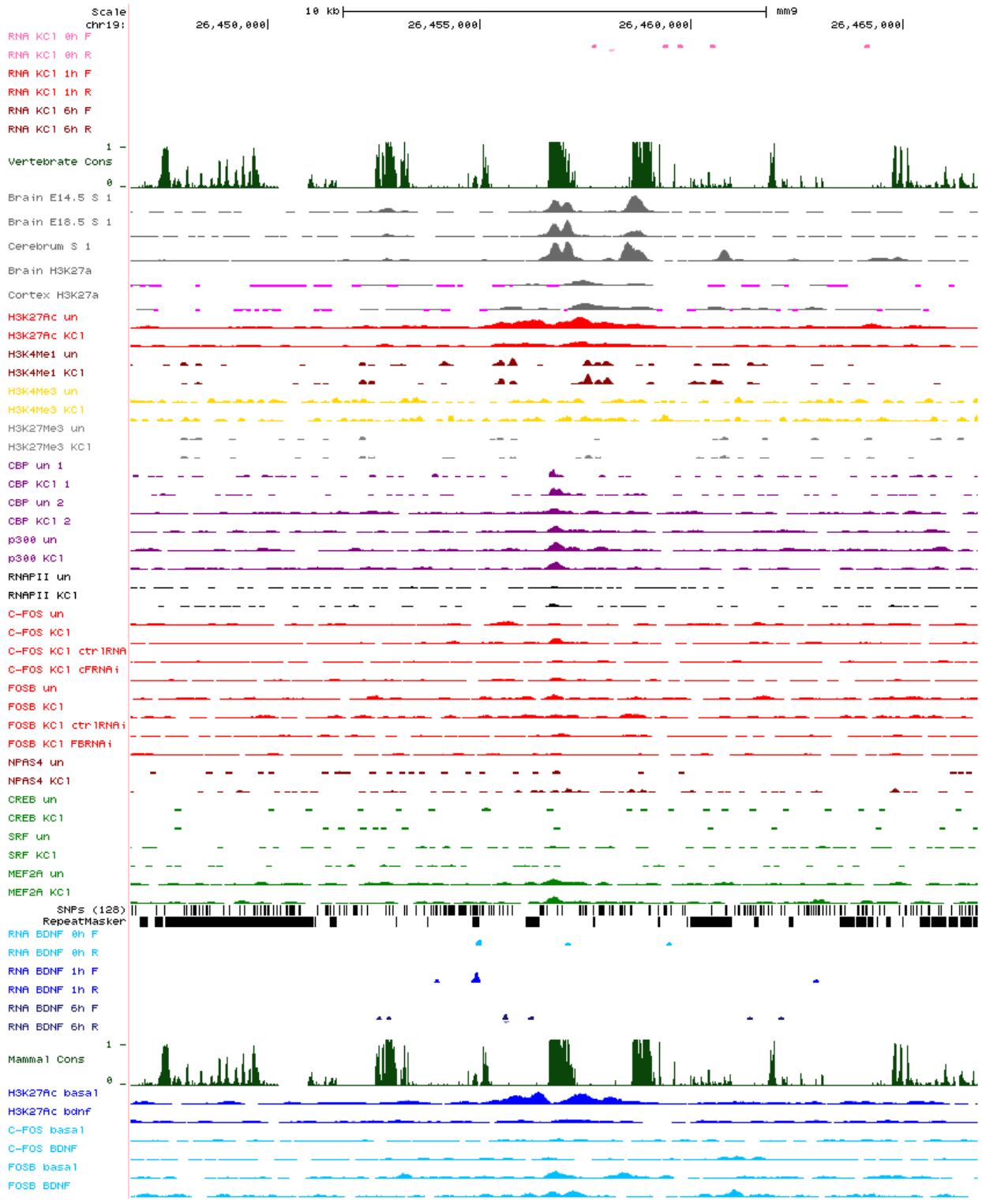

Figure 7.24: Enhancer 24 locus

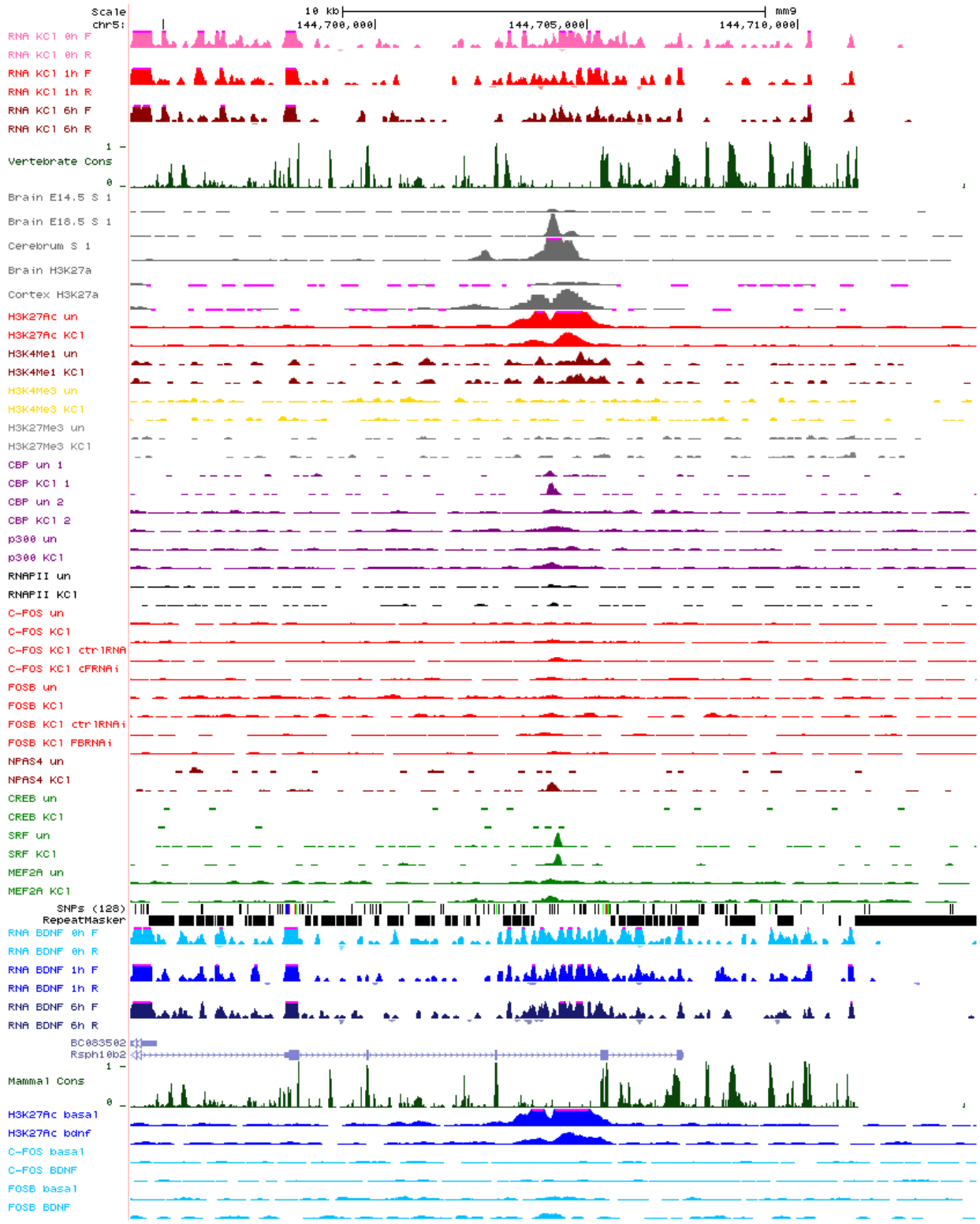

Figure 7.25: Enhancer 25 locus

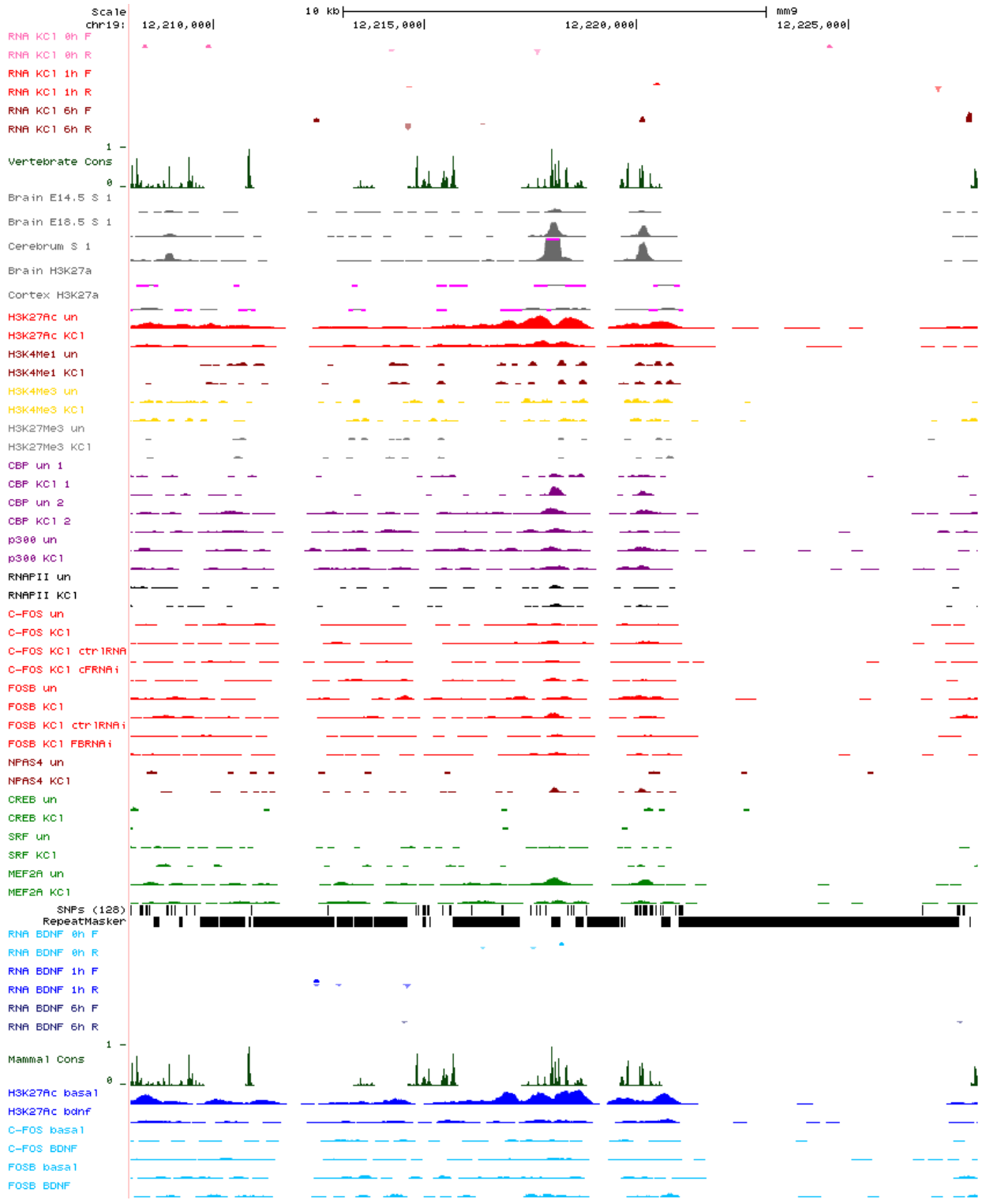

Figure 7.26: Enhancer 26 locus

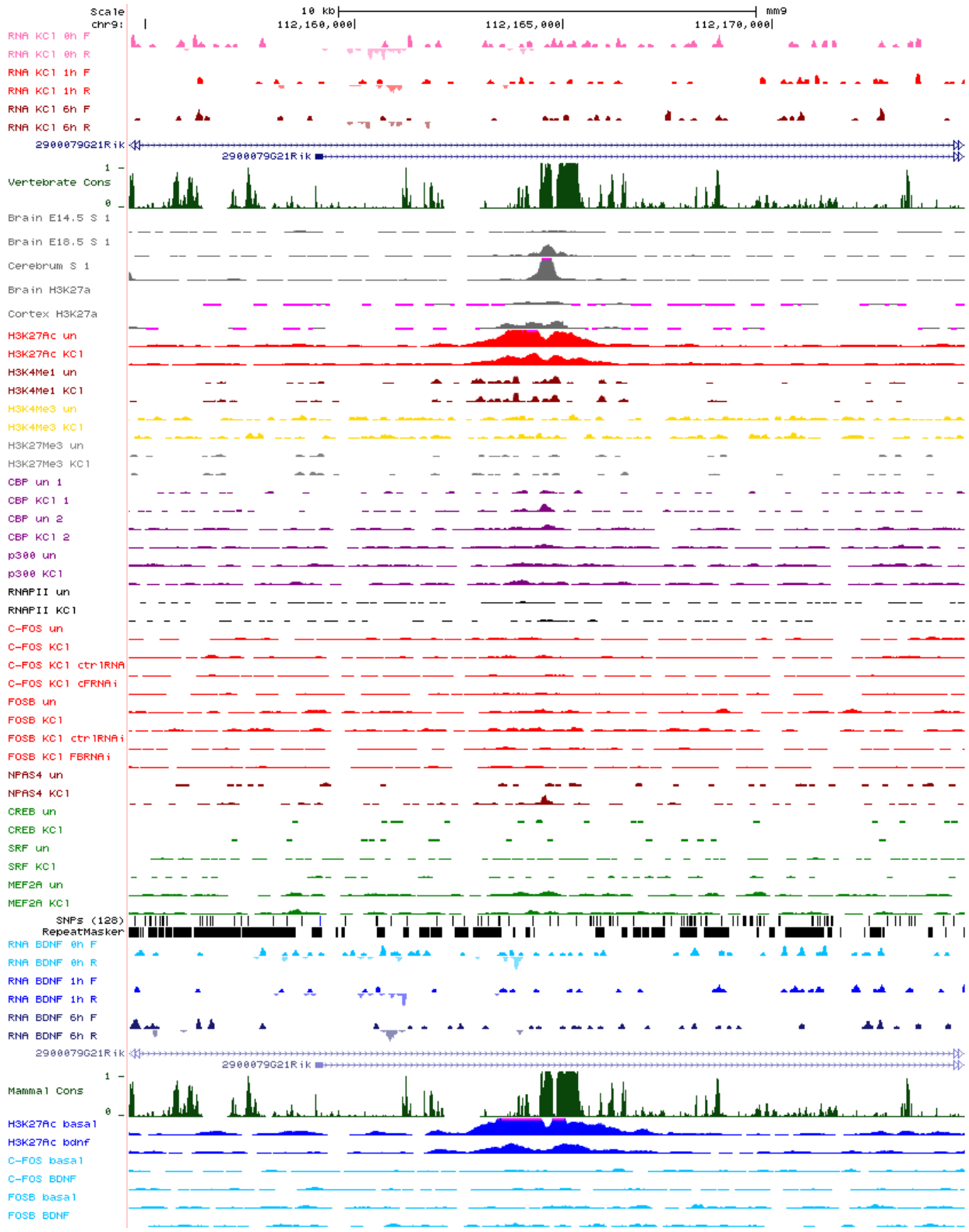

Figure 7.27: Enhancer 27 locus

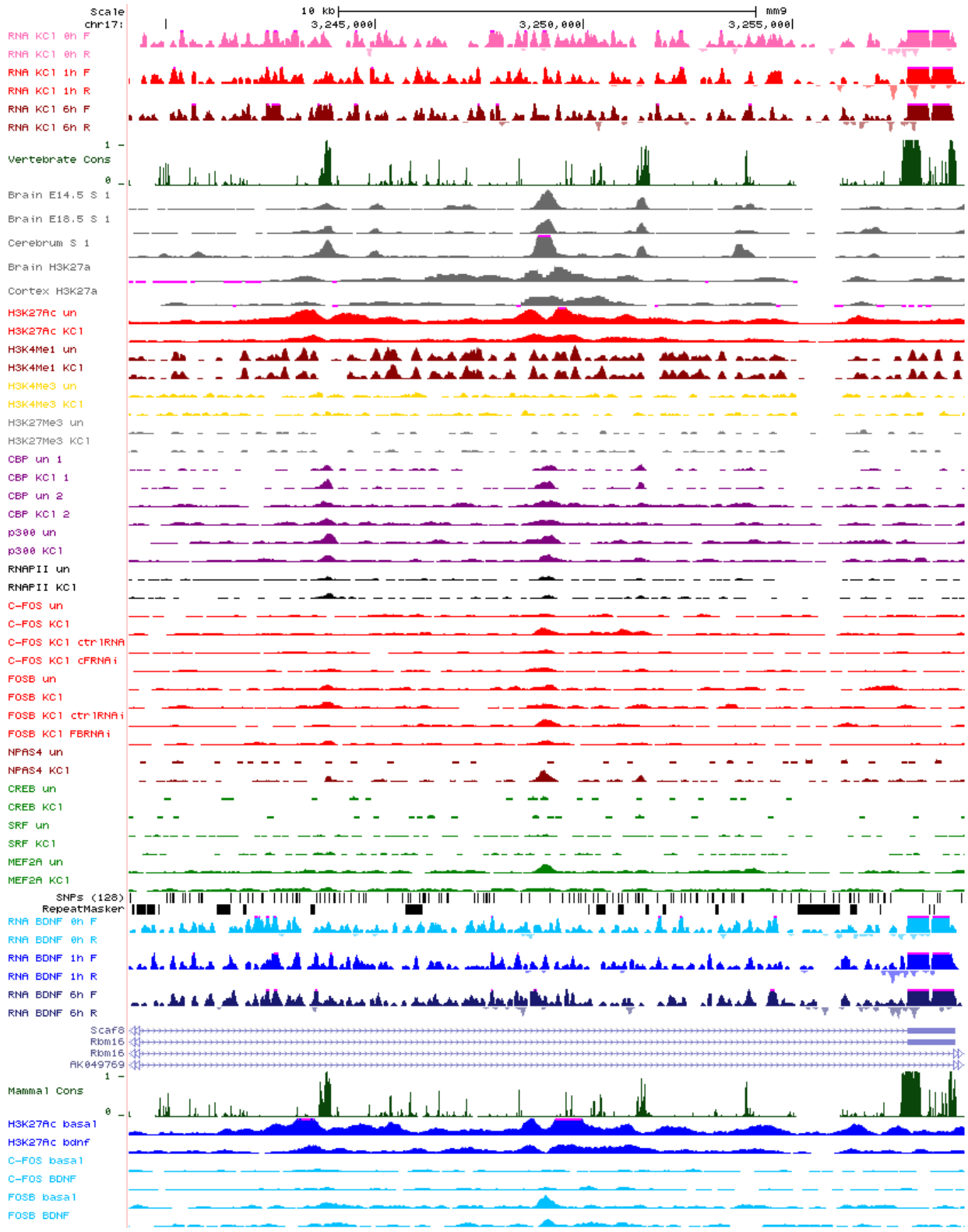

Figure 7.28: Enhancer 28 locus

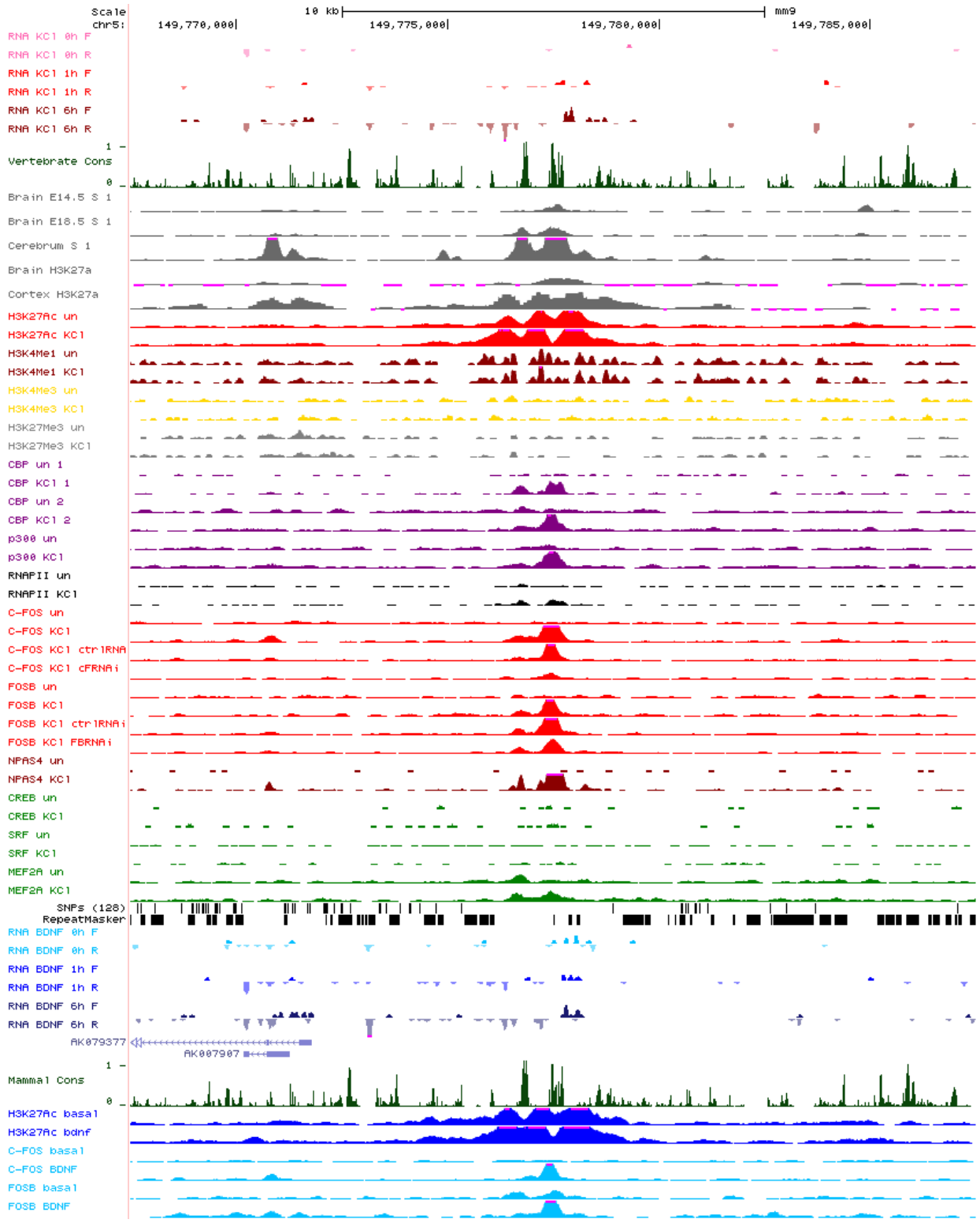

Figure 7.29: Enhancer 29 locus

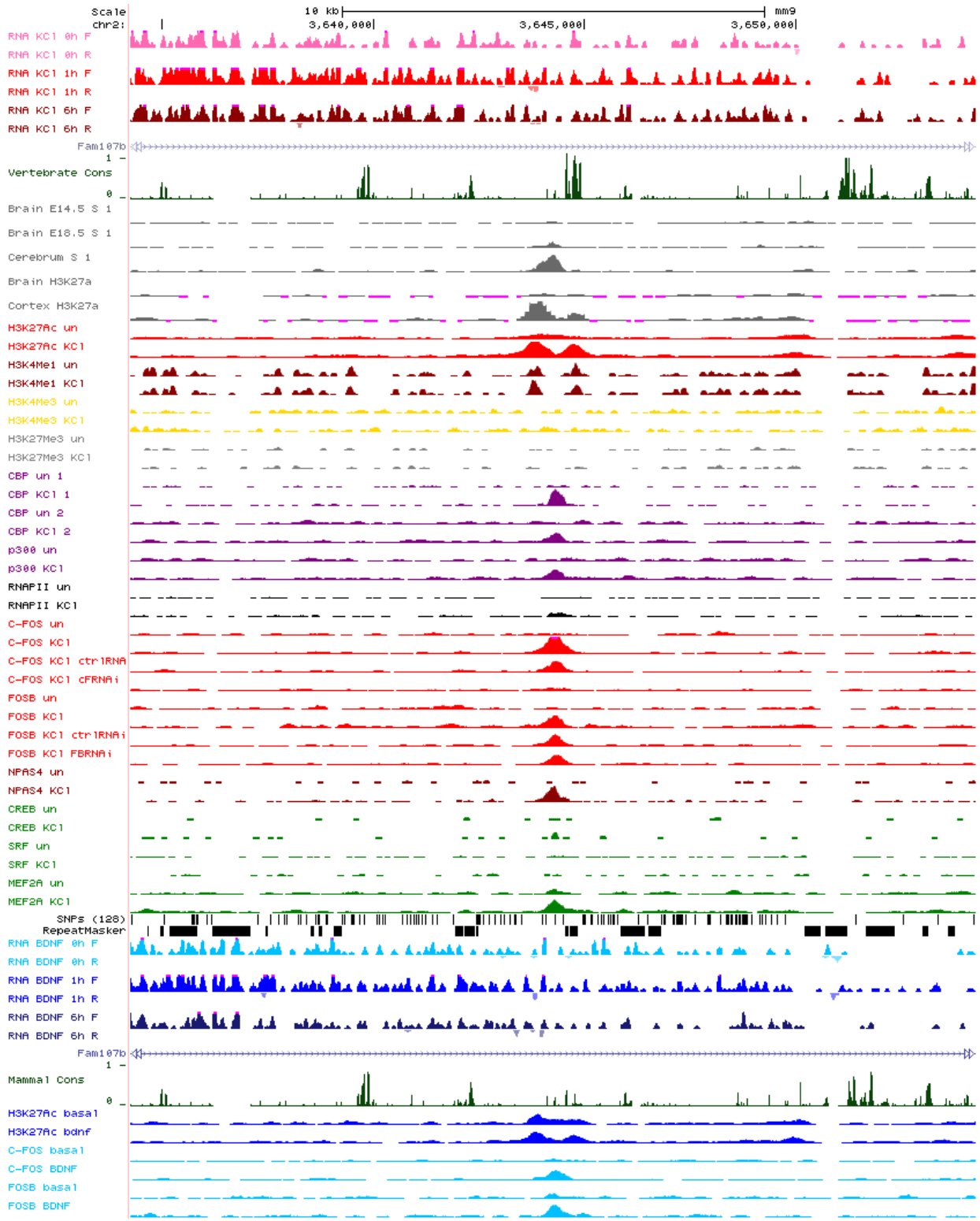

Figure 7.30: Enhancer 30 locus

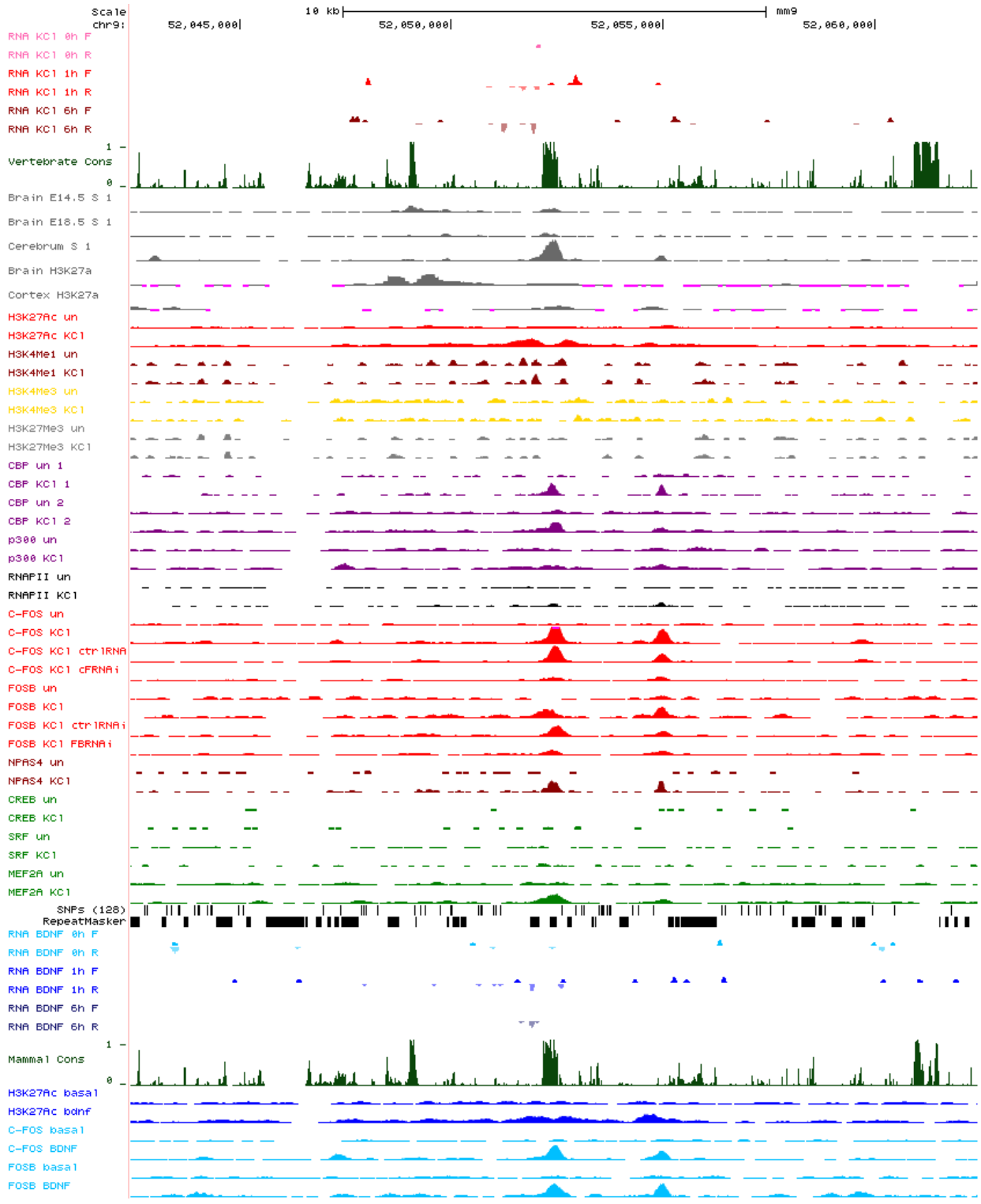

Figure 7.31: Enhancer 31 locus

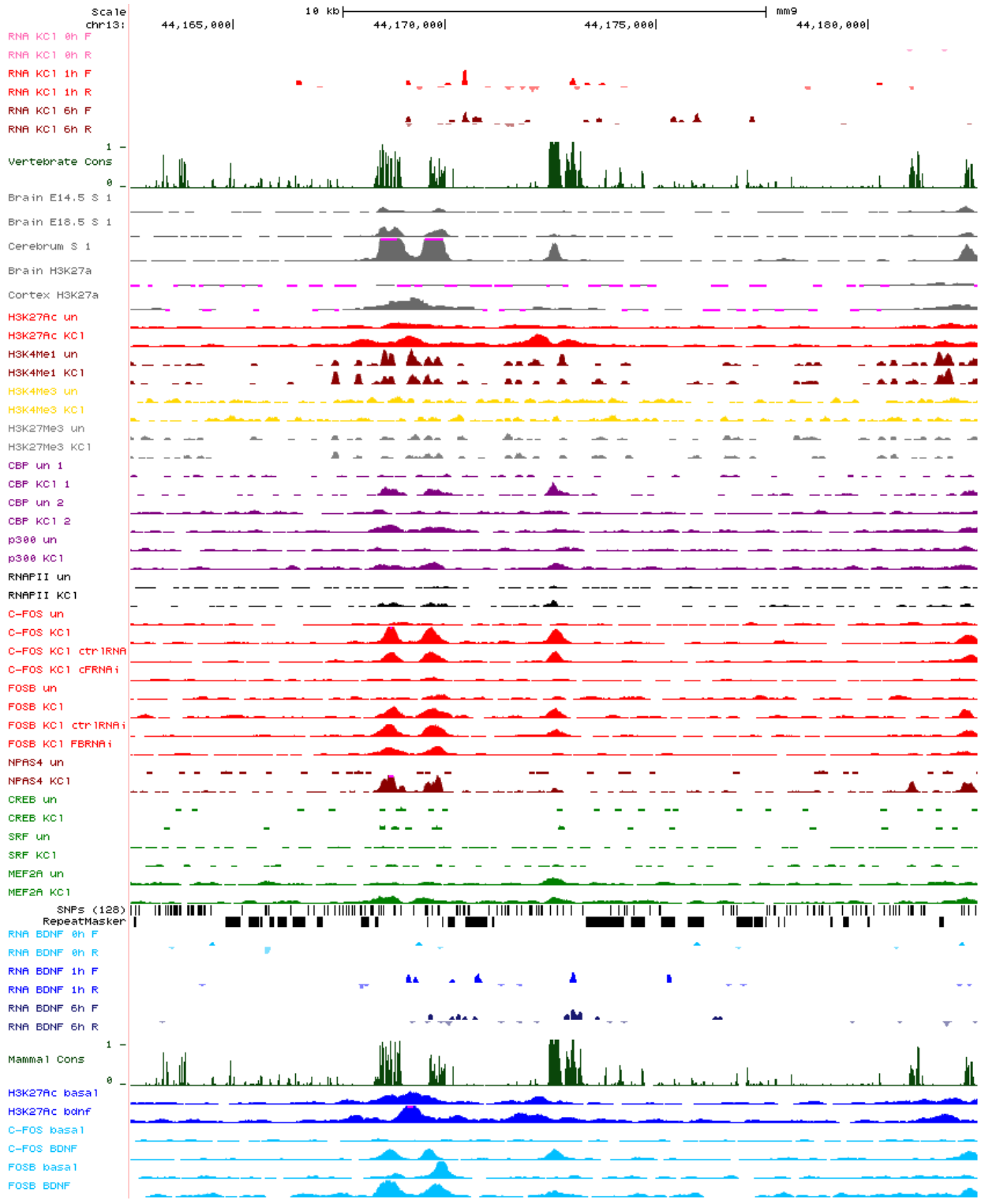

Figure 7.32: Enhancer 32 locus

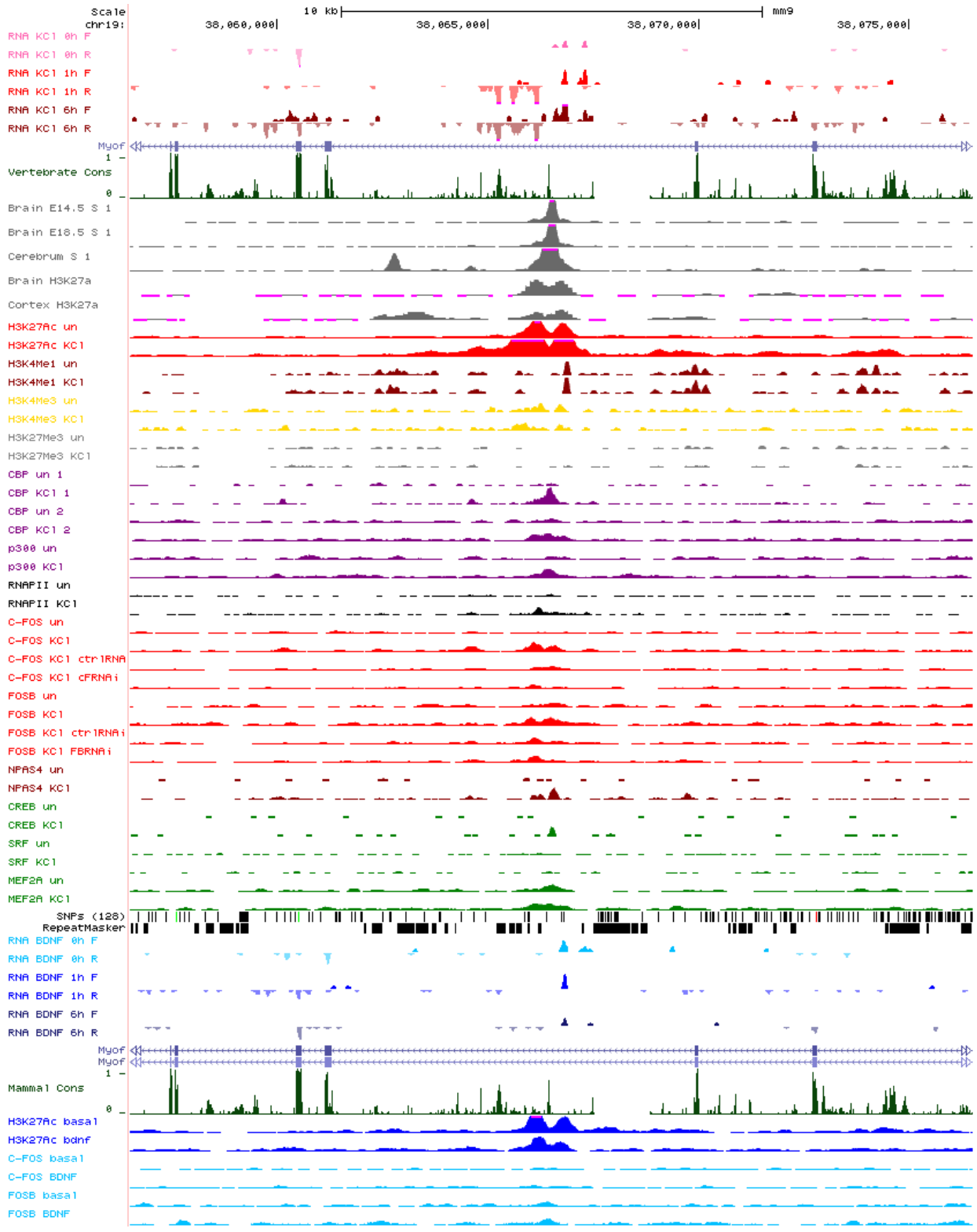

Figure 7.33: Enhancer 33 locus

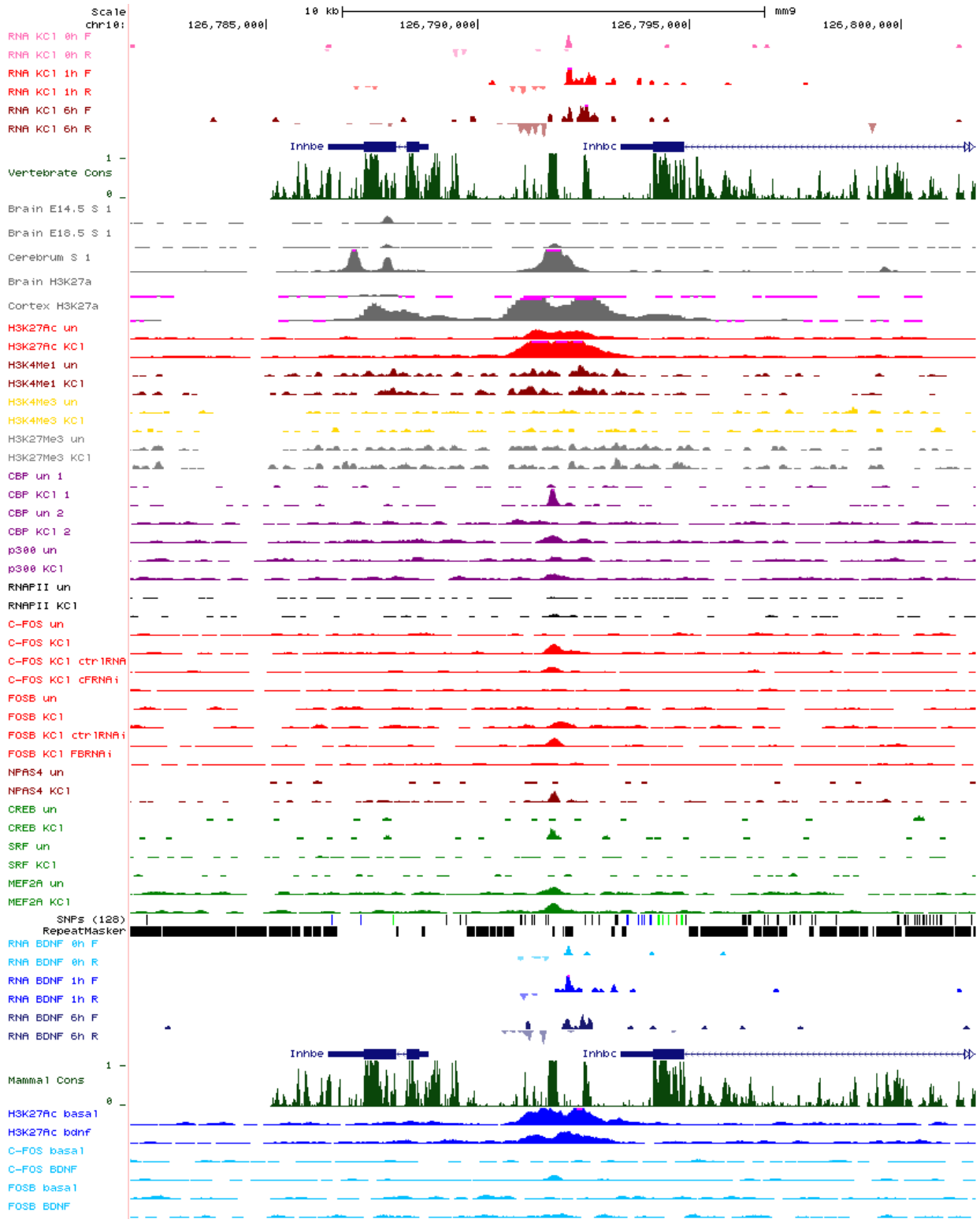

Figure 7.34: Enhancer 34 locus

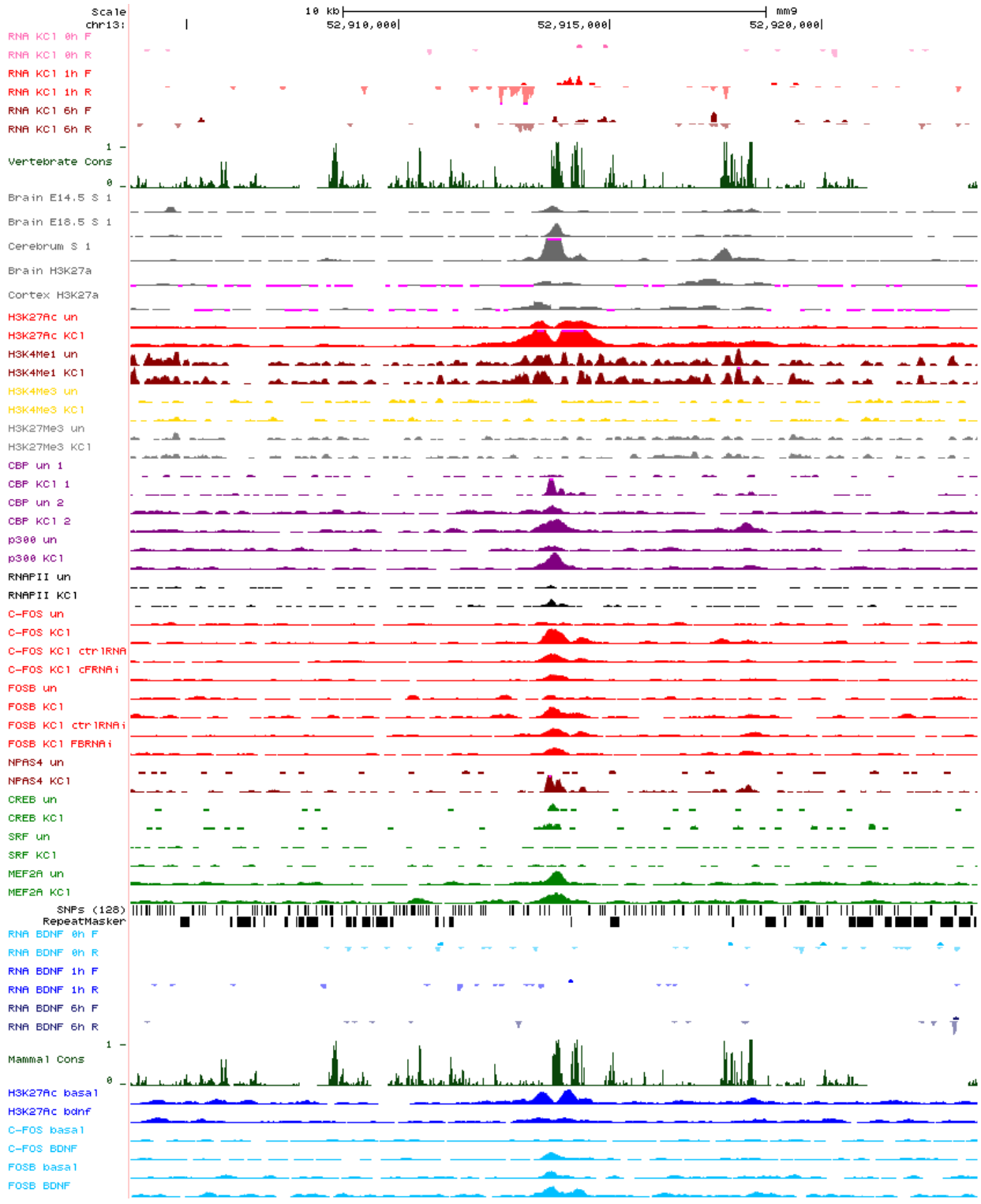

Figure 7.35: Enhancer 35 locus

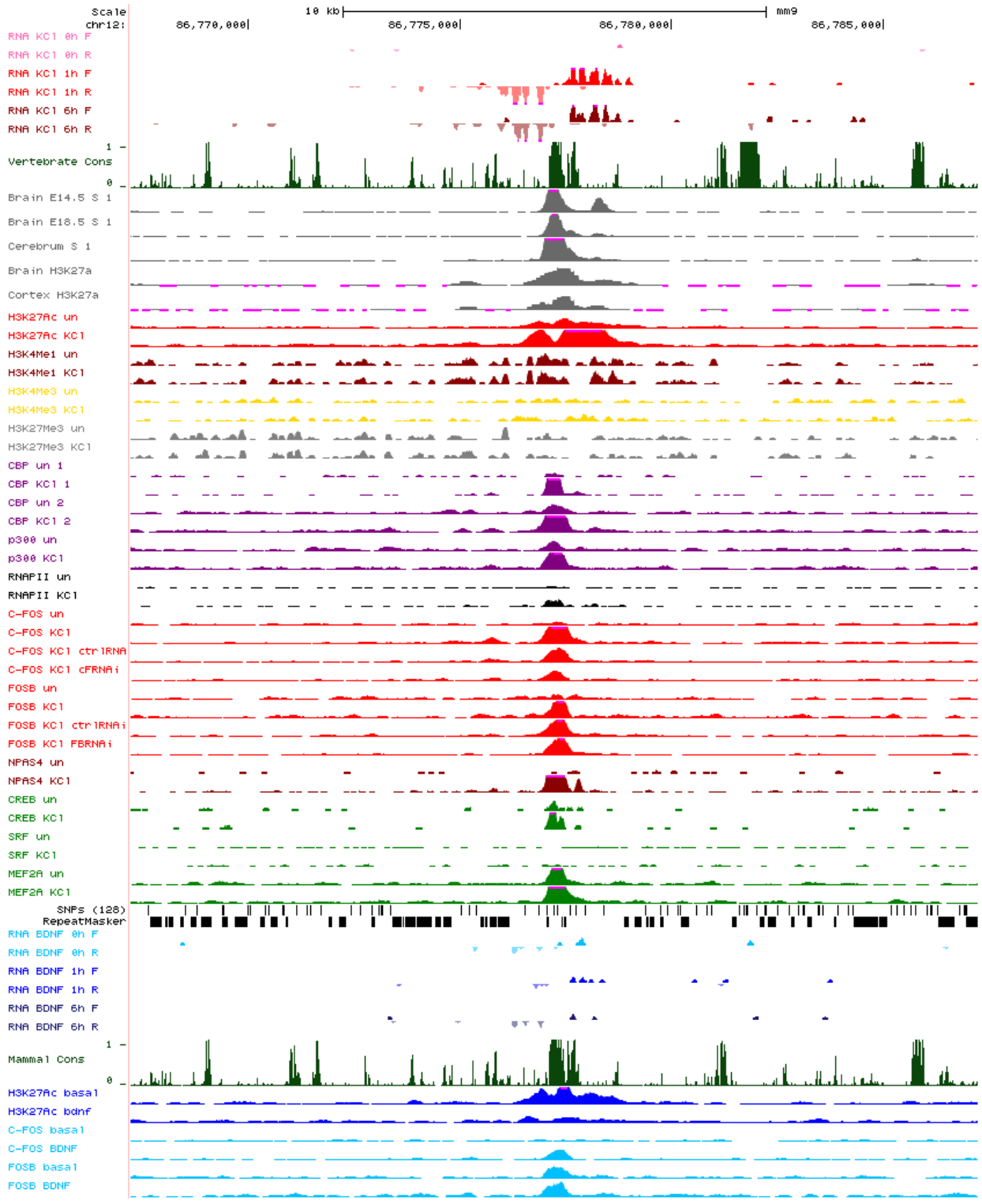

Figure 7.36: Enhancer 36 locus

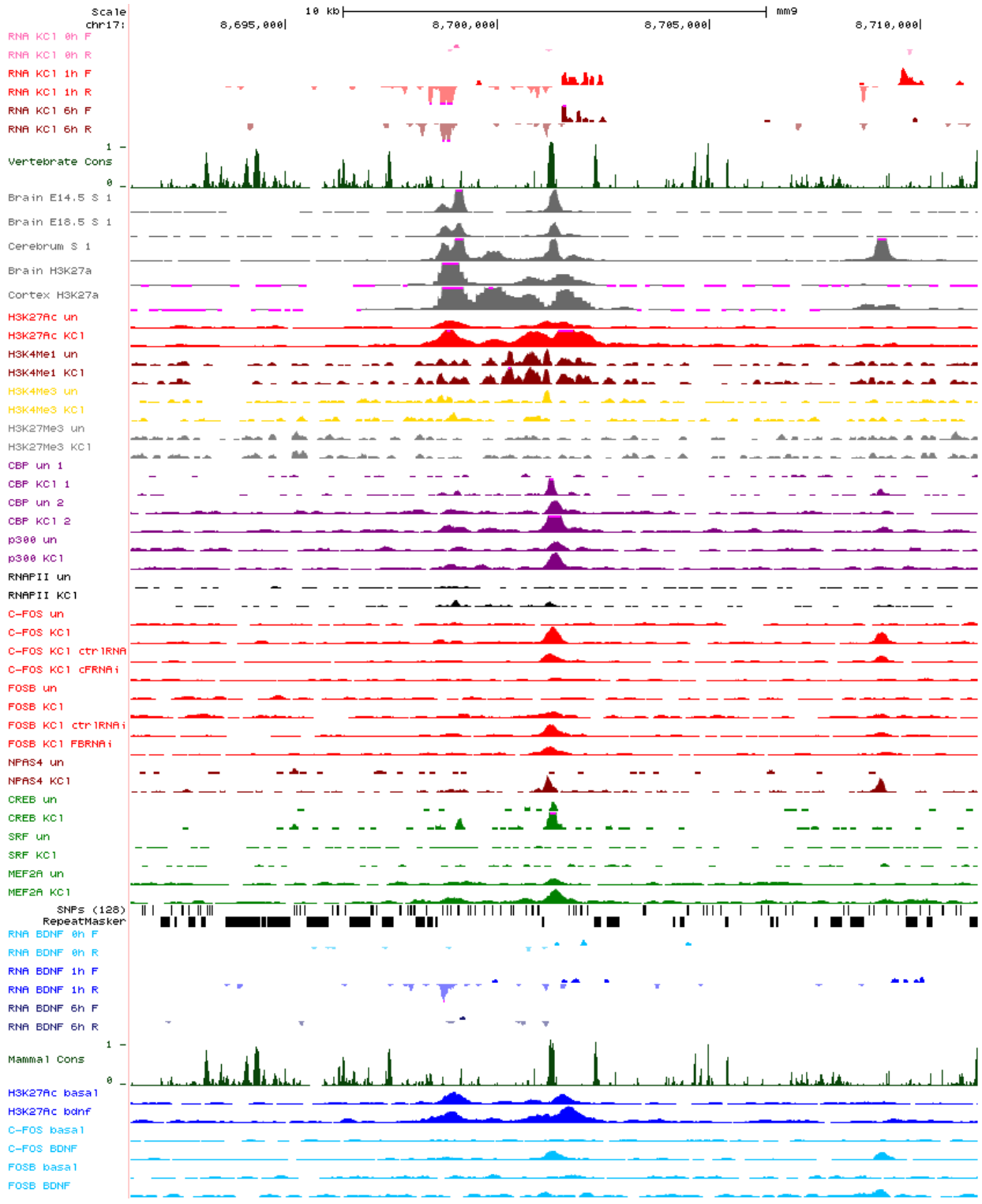

Figure 7.37: Enhancer 37 locus

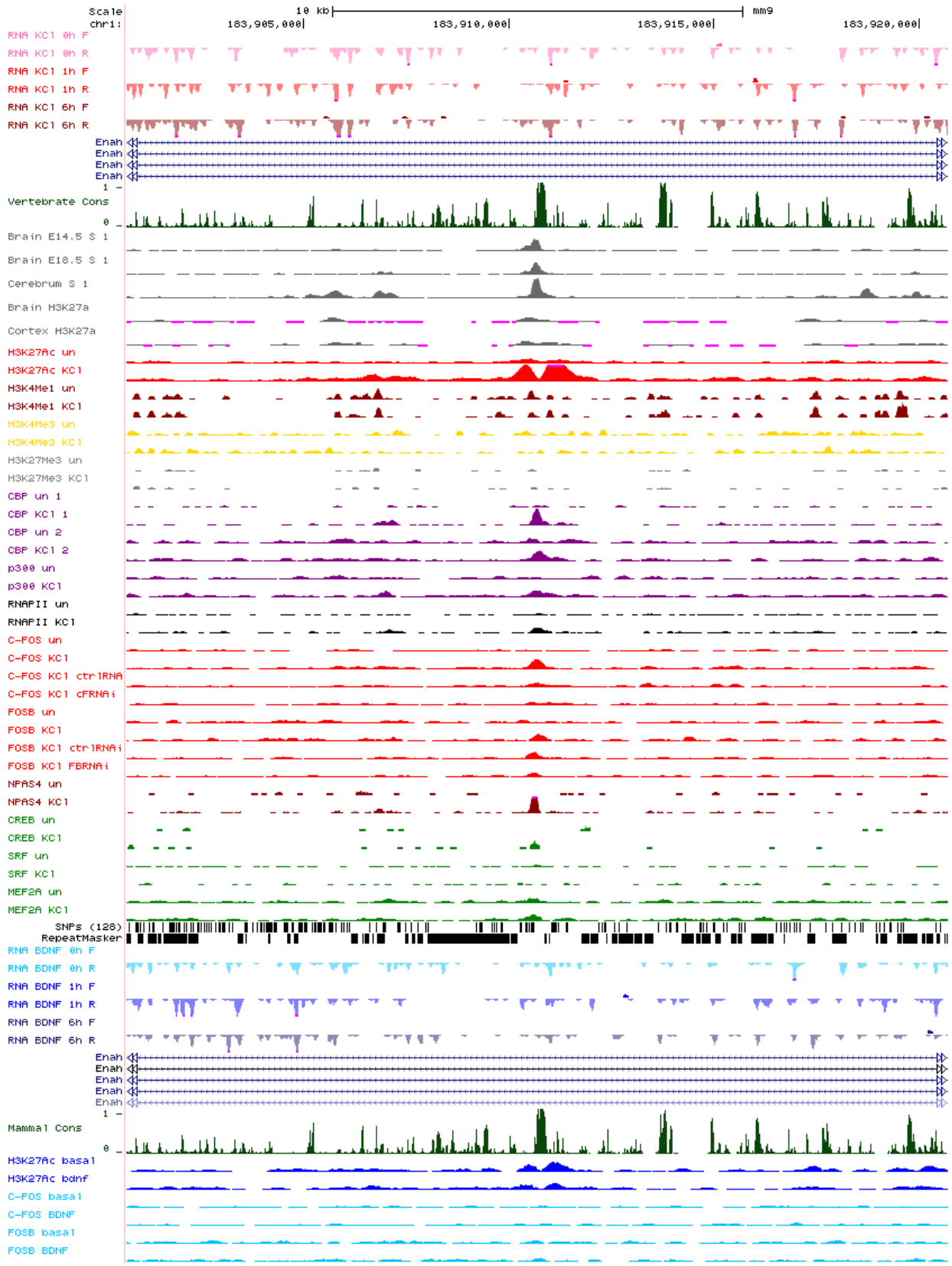

Figure 7.38: Enhancer 38 locus

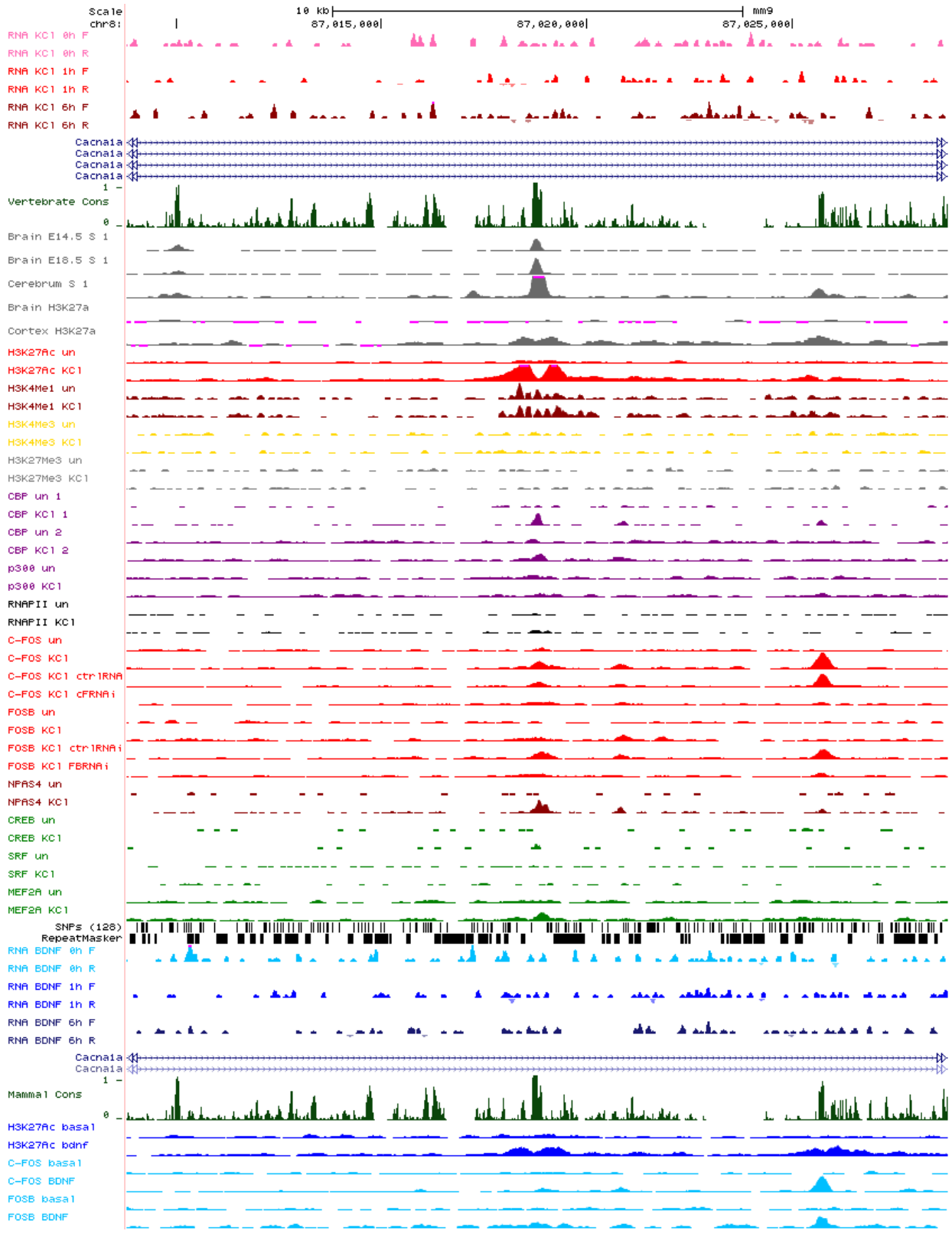

Figure 7.39: Enhancer 39 locus

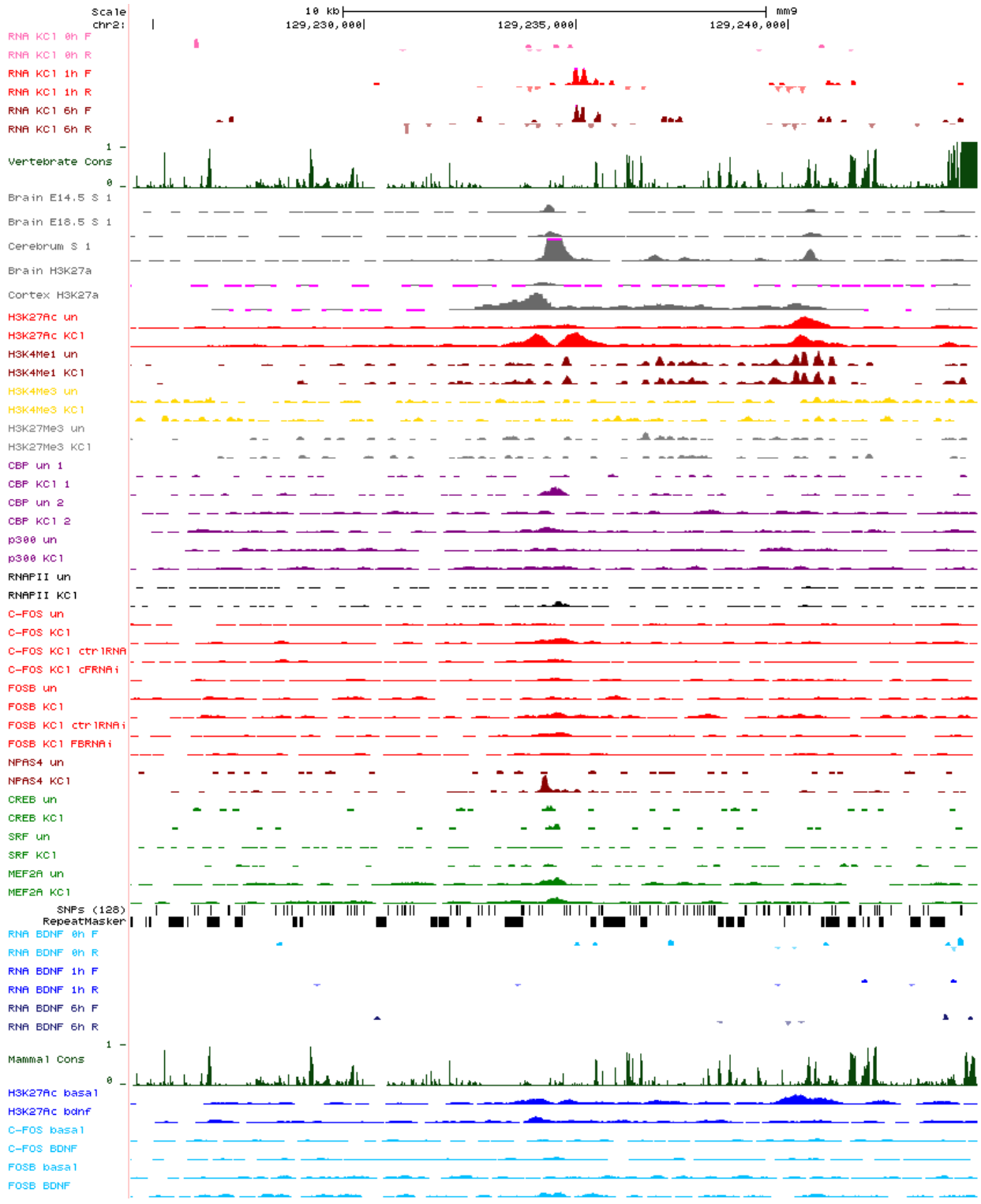

Figure 7.40: Enhancer 40 locus

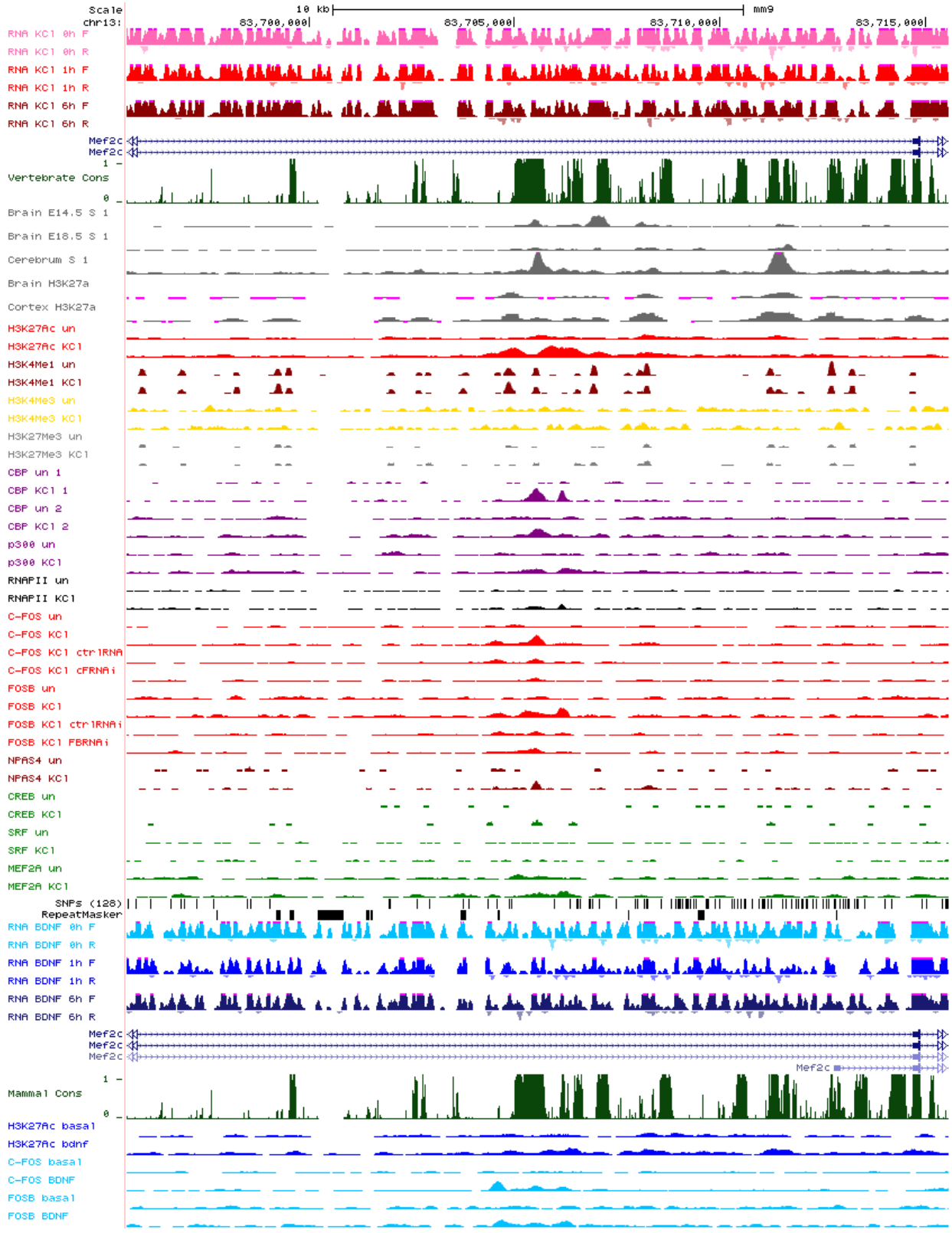

Figure 7.41: Enhancer 41 locus

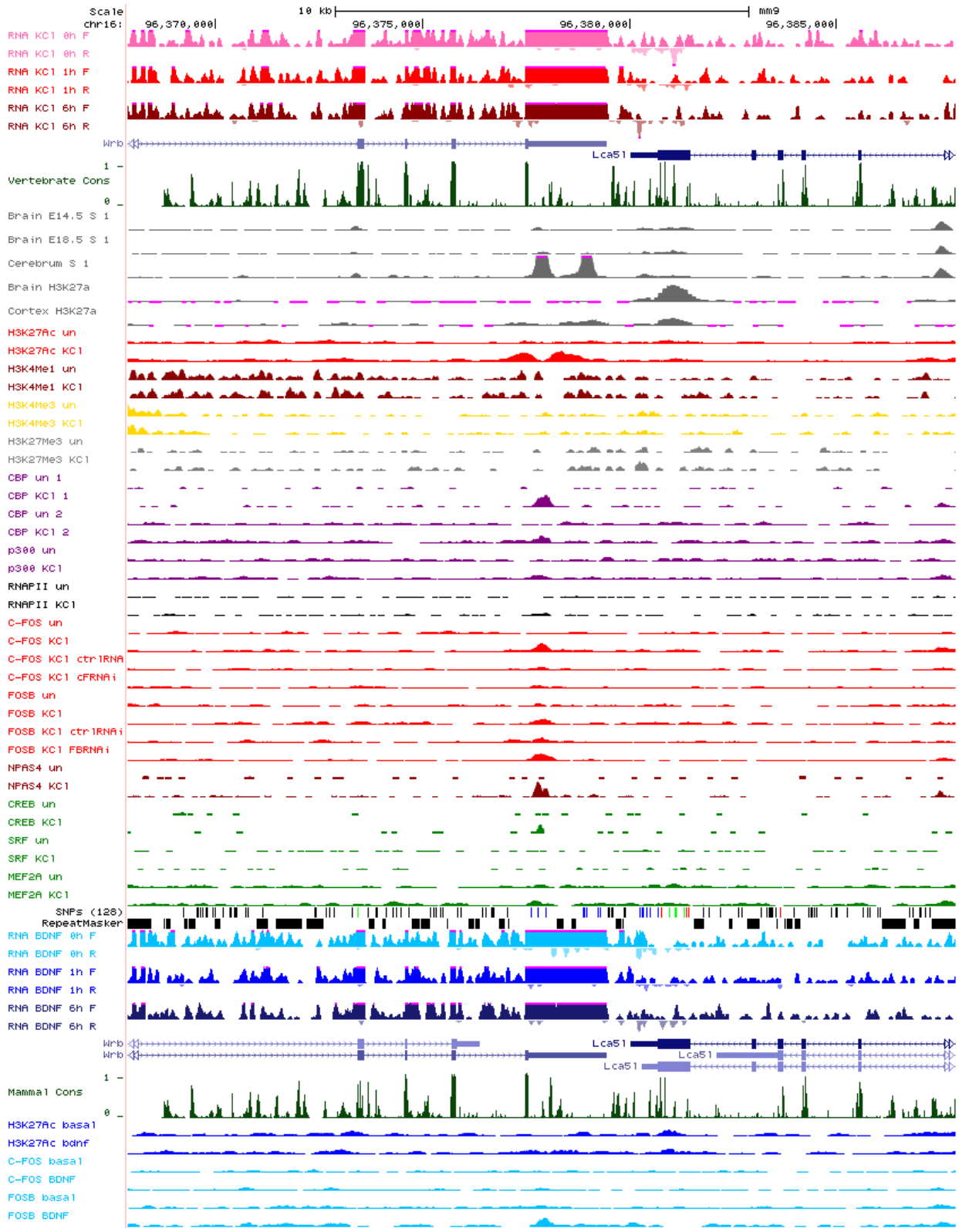

Figure 7.42: Enhancer 42 locus

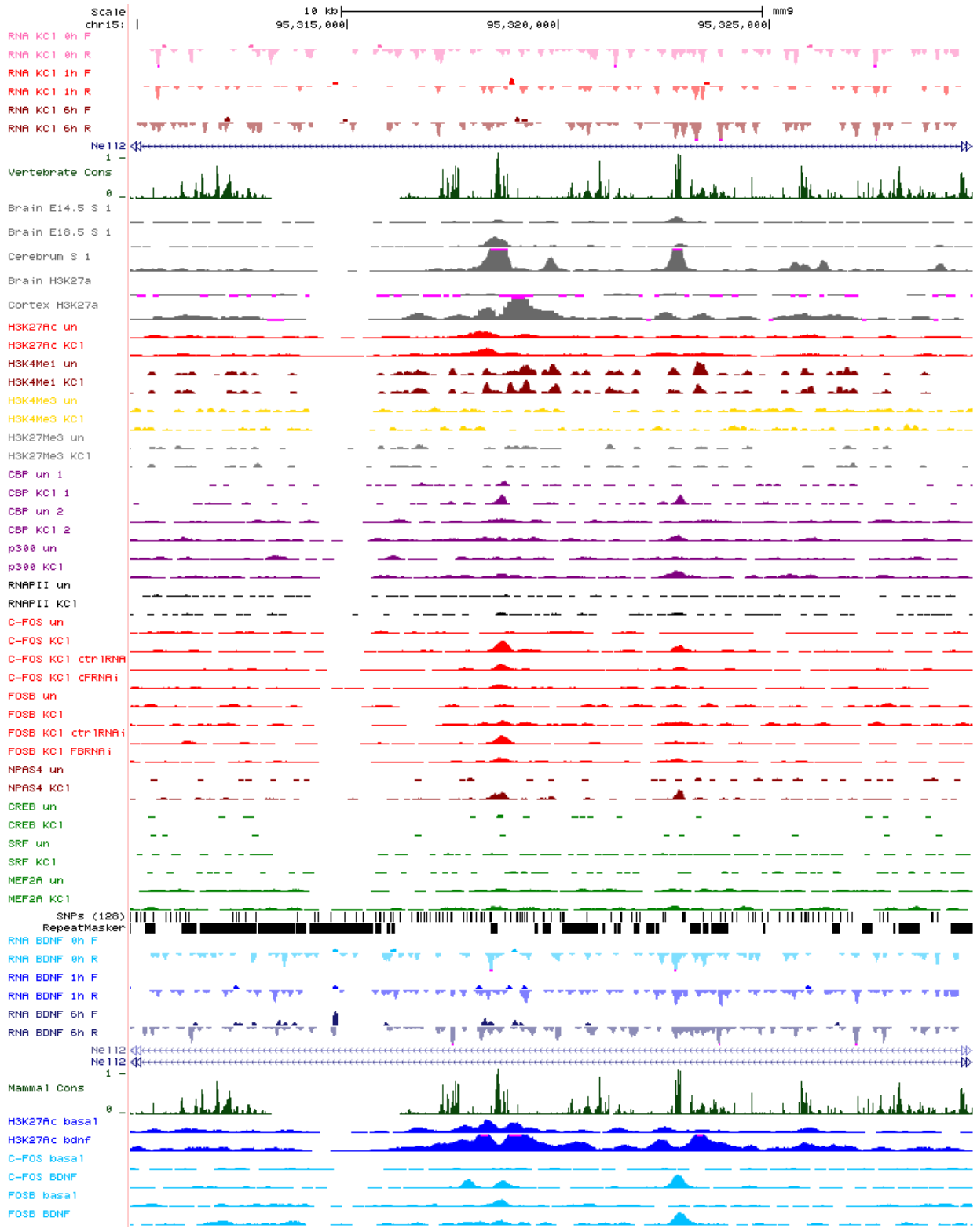

Figure 7.43: Enhancer 43 locus

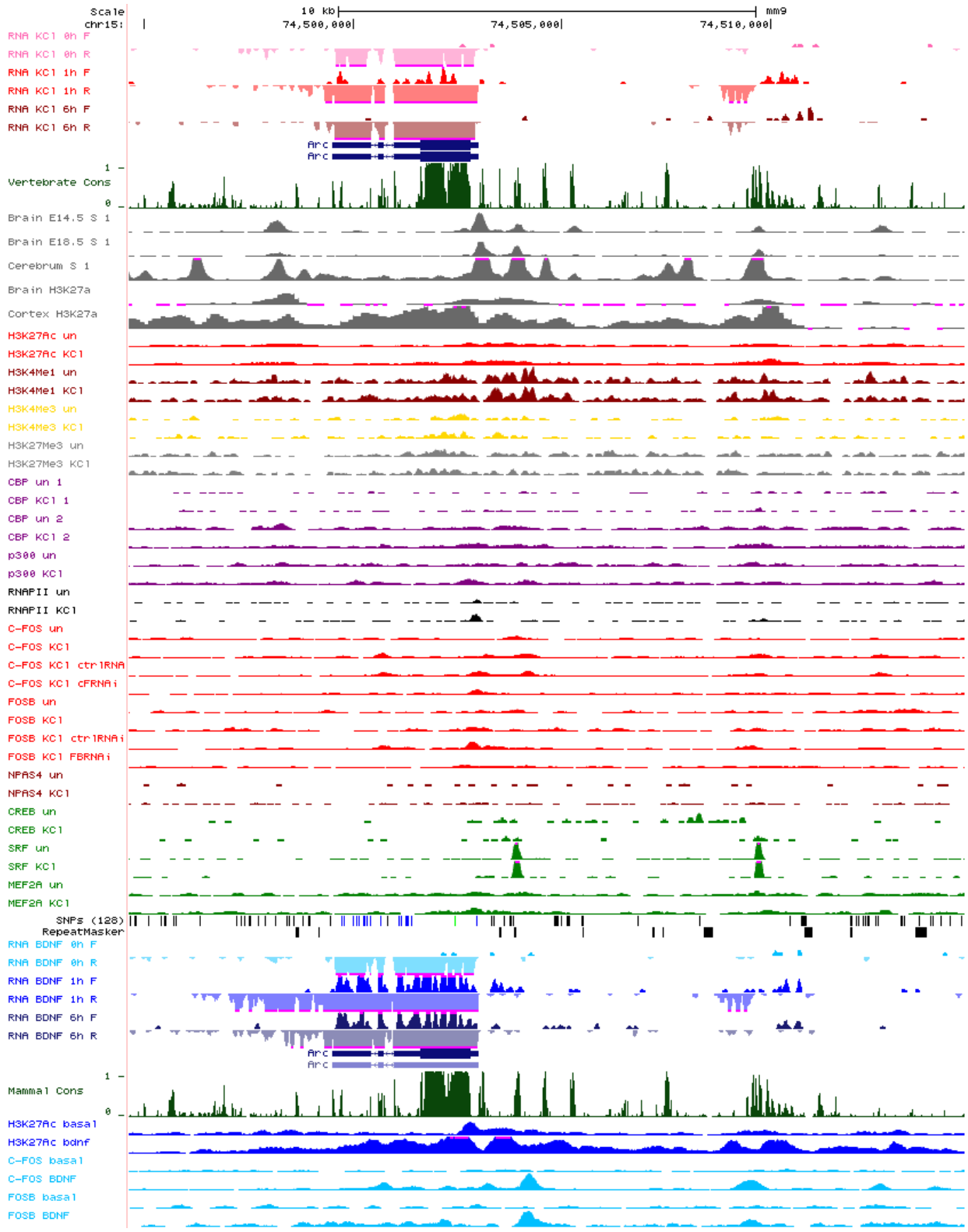

Figure 7.44: Enhancer 44 locus

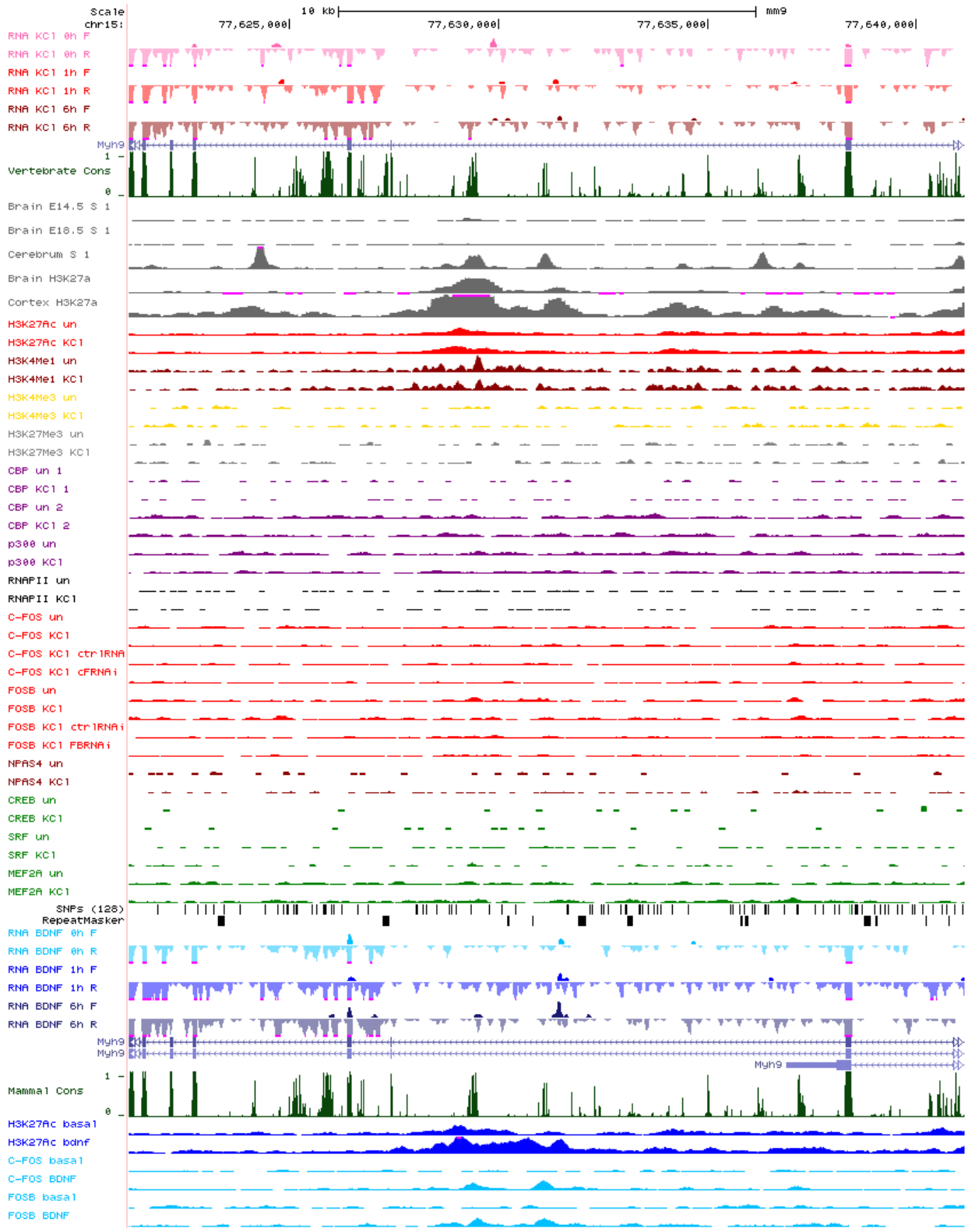

Figure 7.45: Enhancer 45 locus

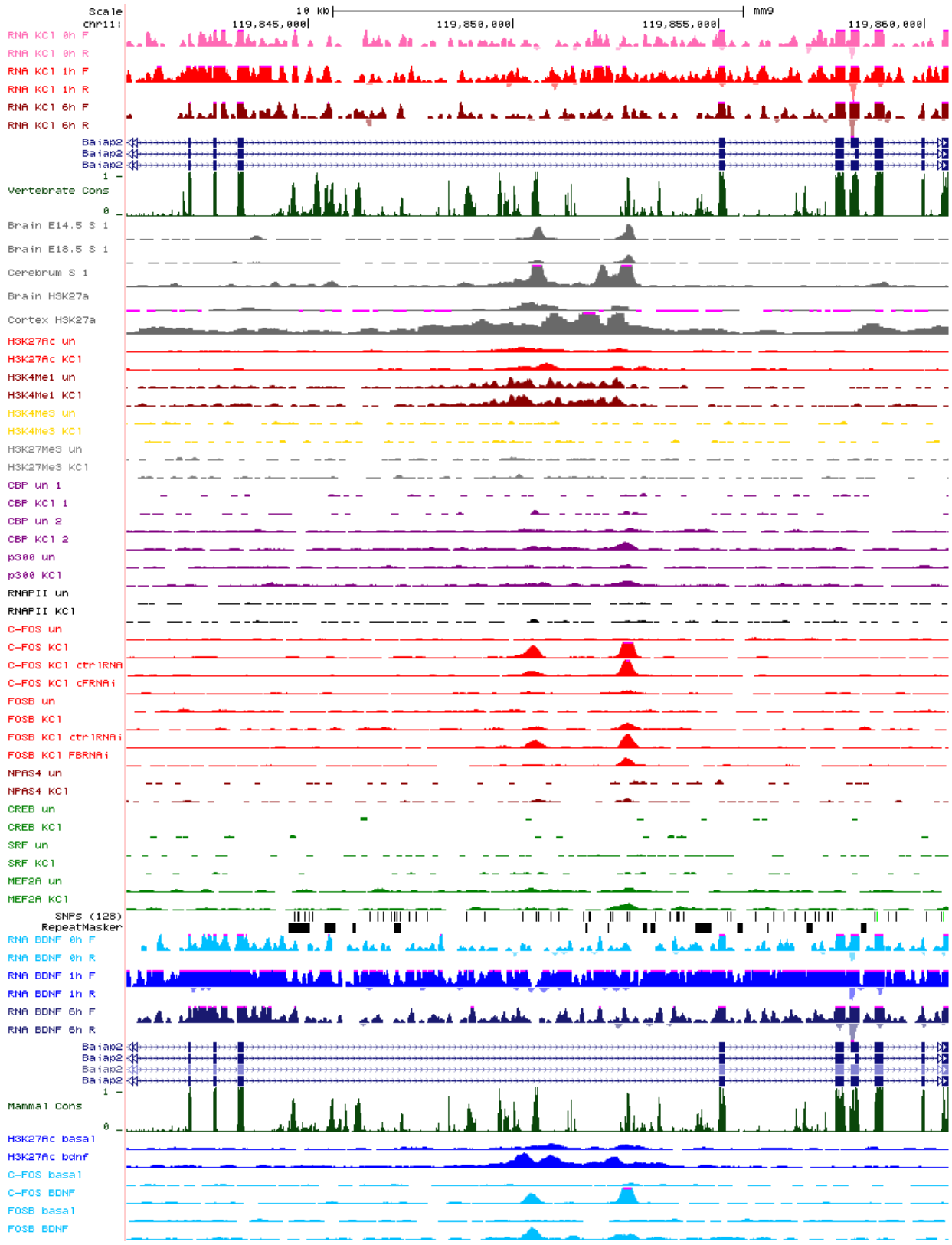

Figure 7.46: Enhancer 46 locus

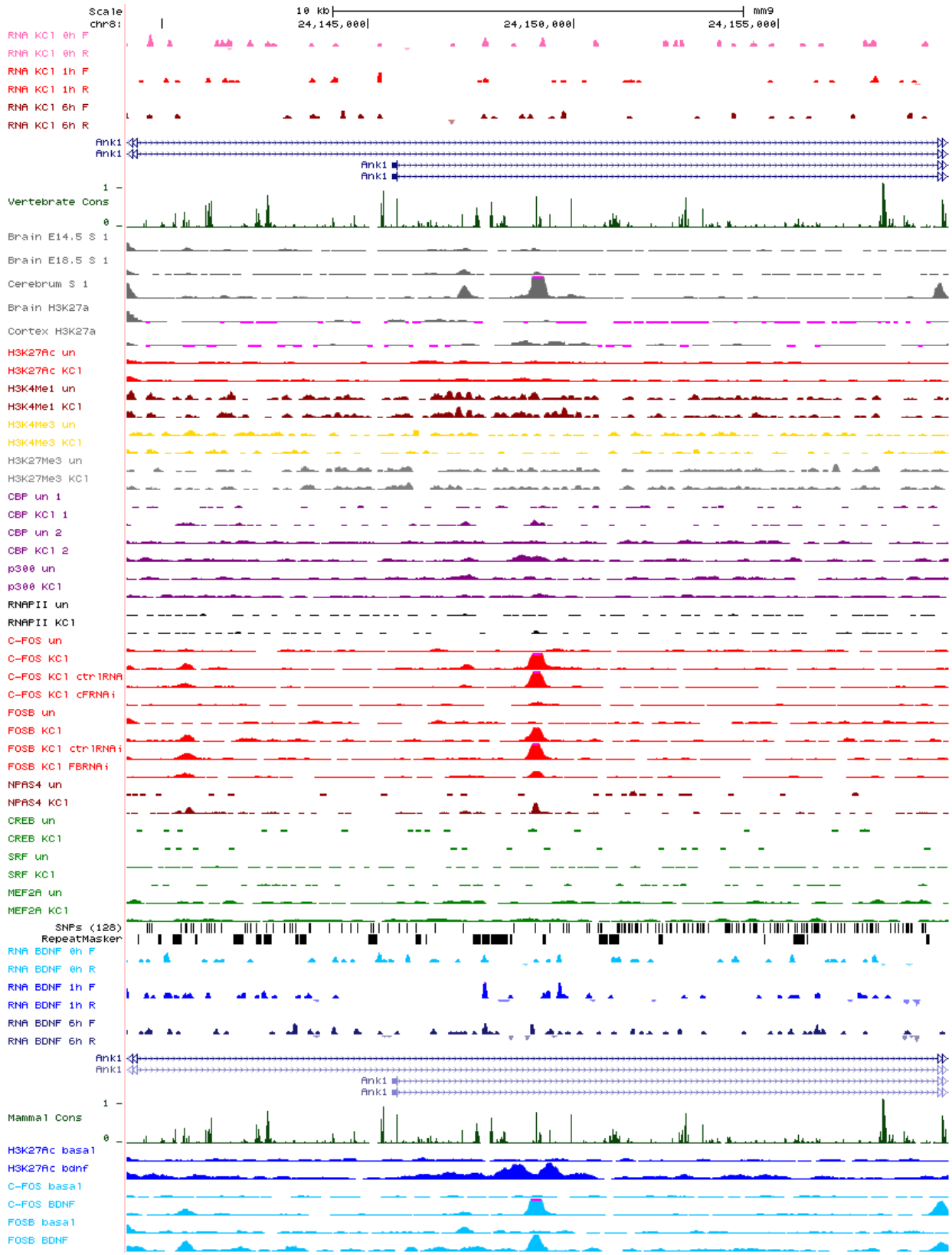

Figure 7.47: Enhancer 47 locus

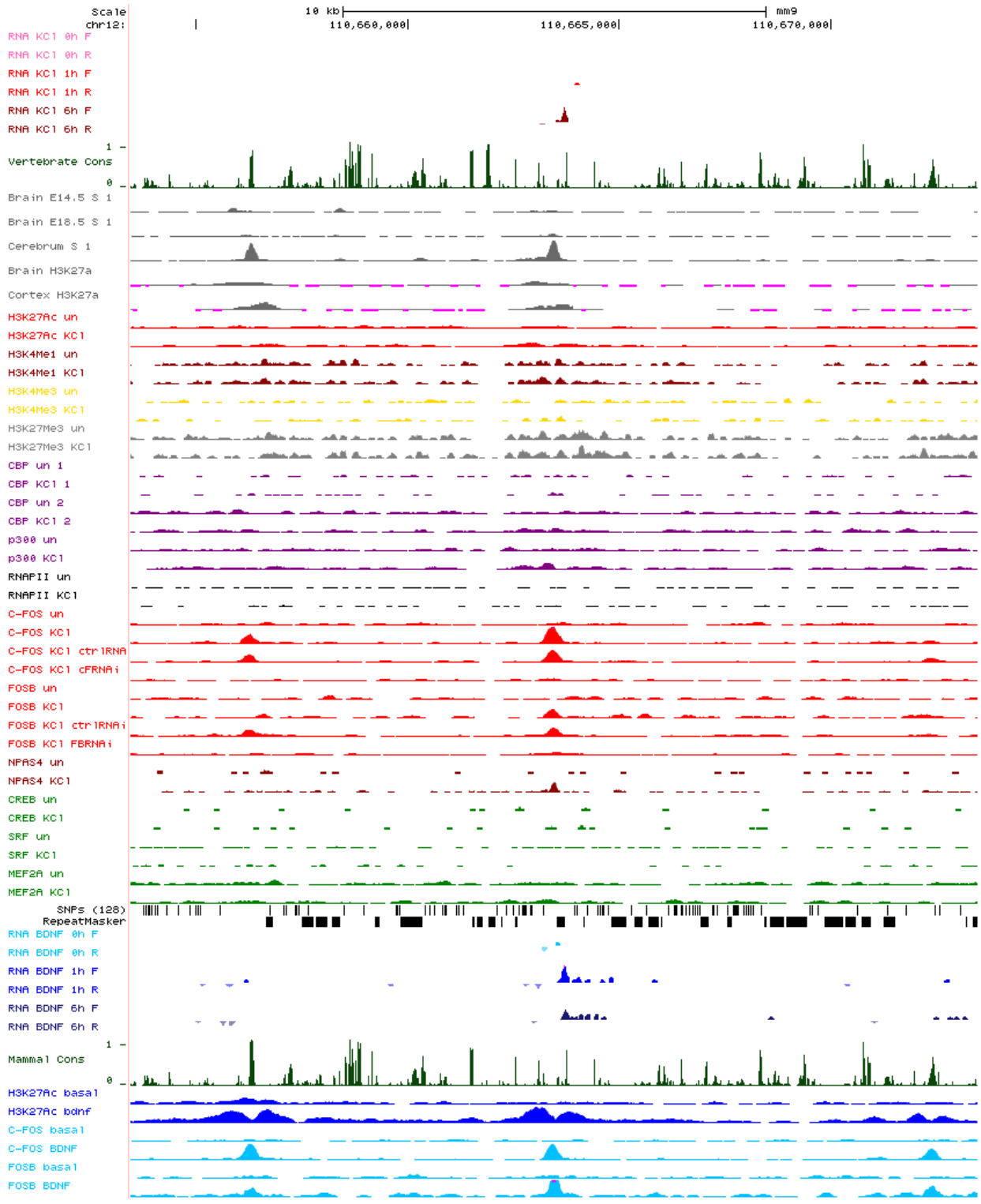

Figure 7.48: Enhancer 48 locus

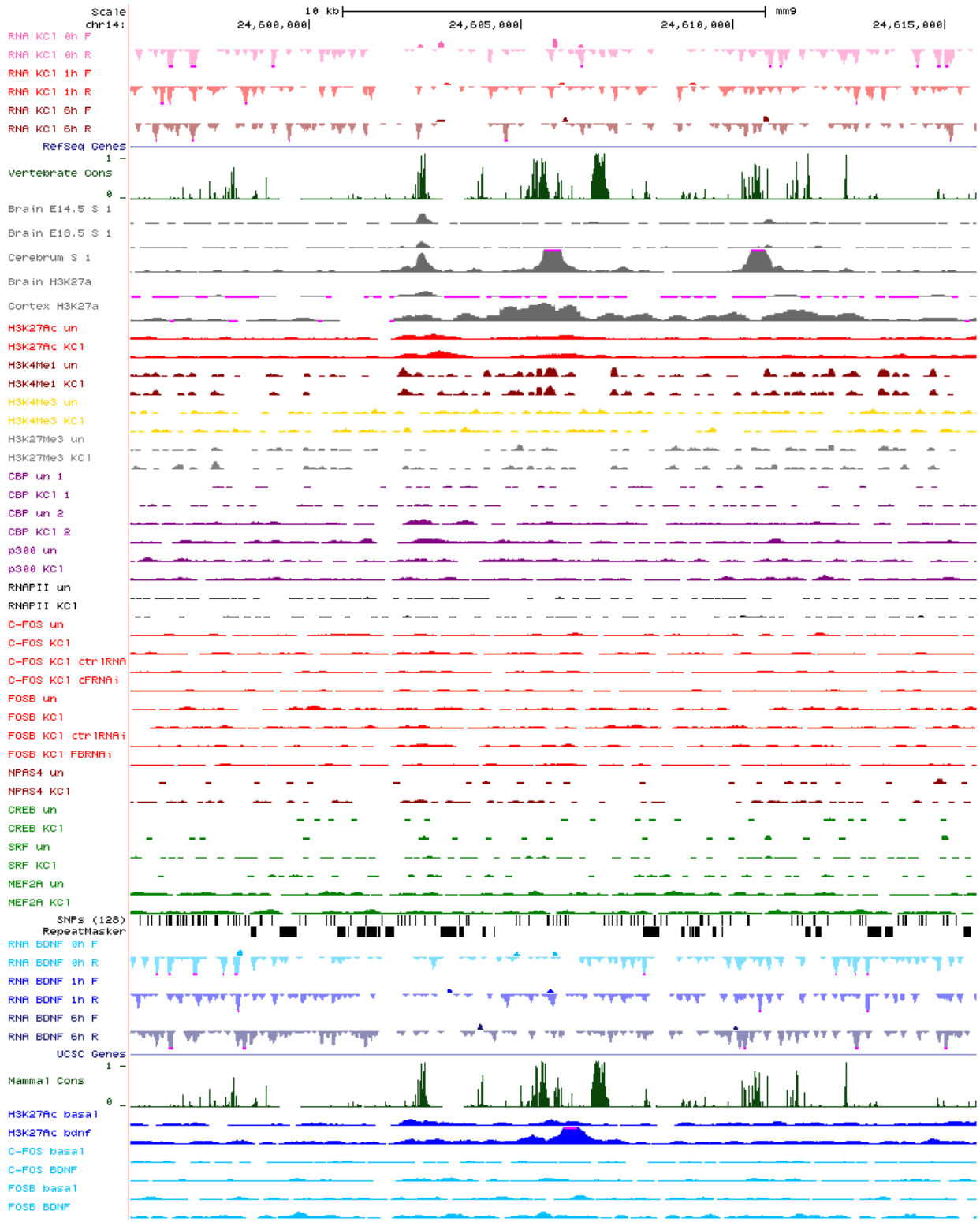

Figure 7.49: Enhancer 49 locus

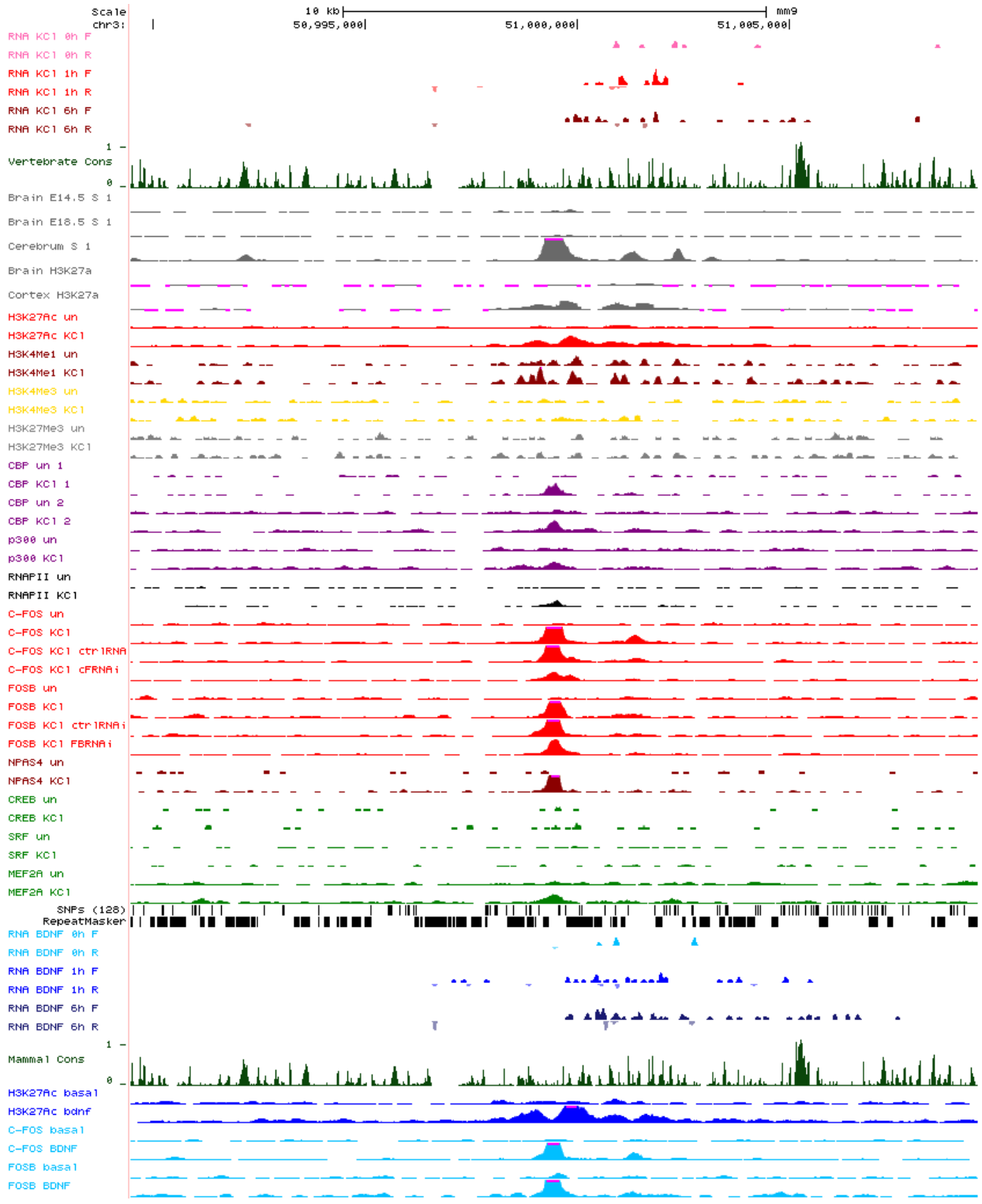

Figure 7.50: Enhancer 50 locus

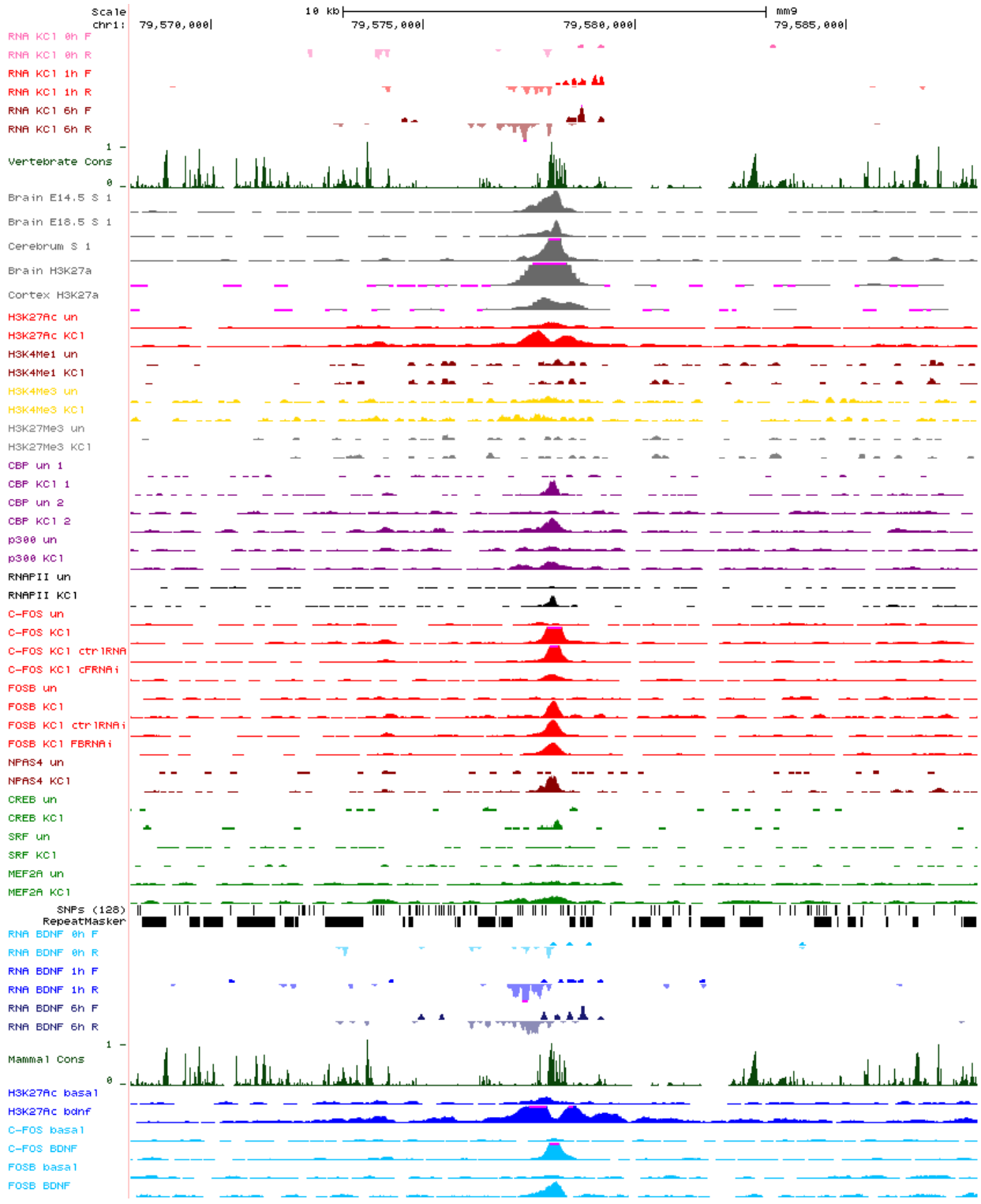

Figure 7.51: Enhancer 51 locus

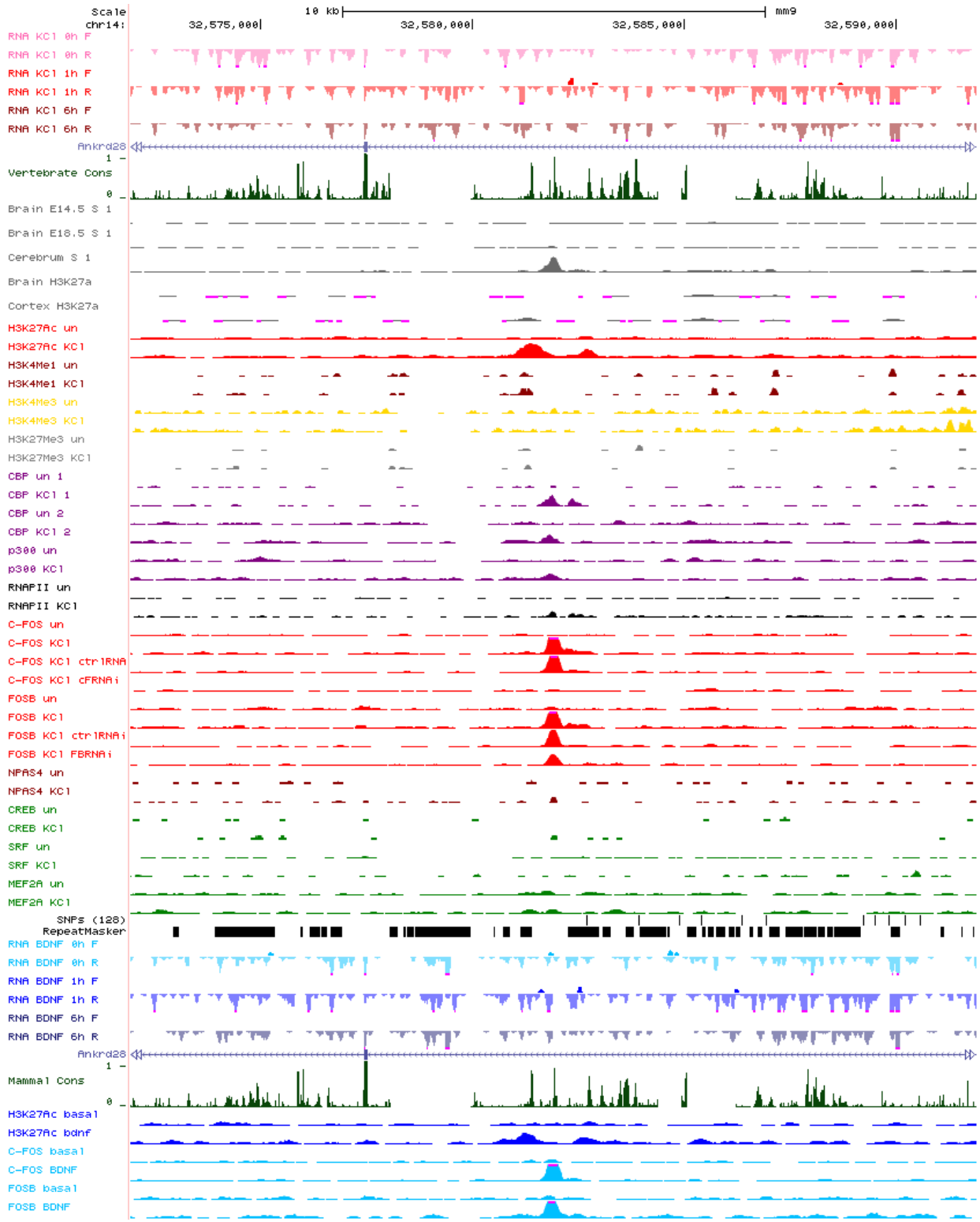

Figure 7.52: Enhancer 52 locus

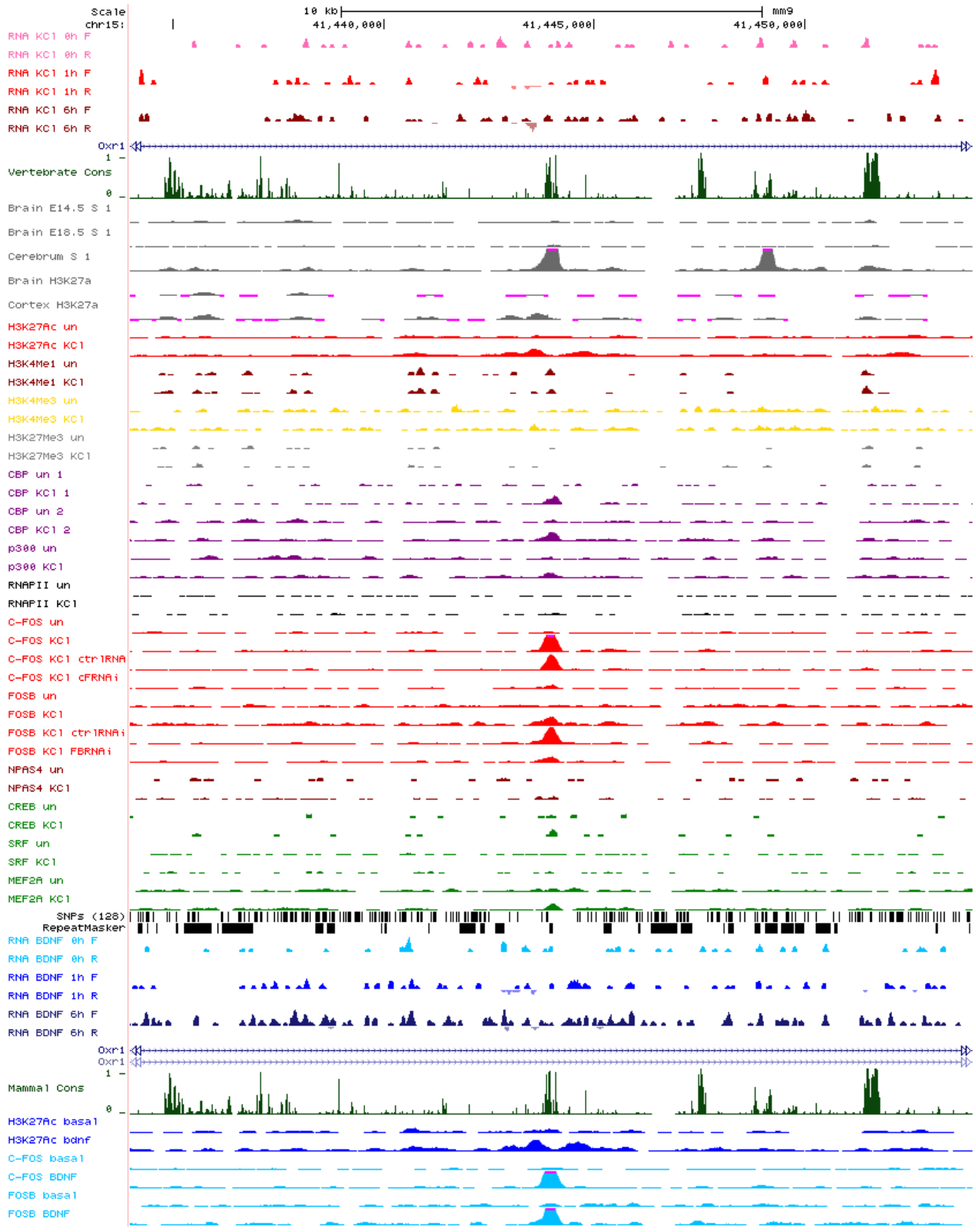

Figure 7.53: Enhancer 53 locus

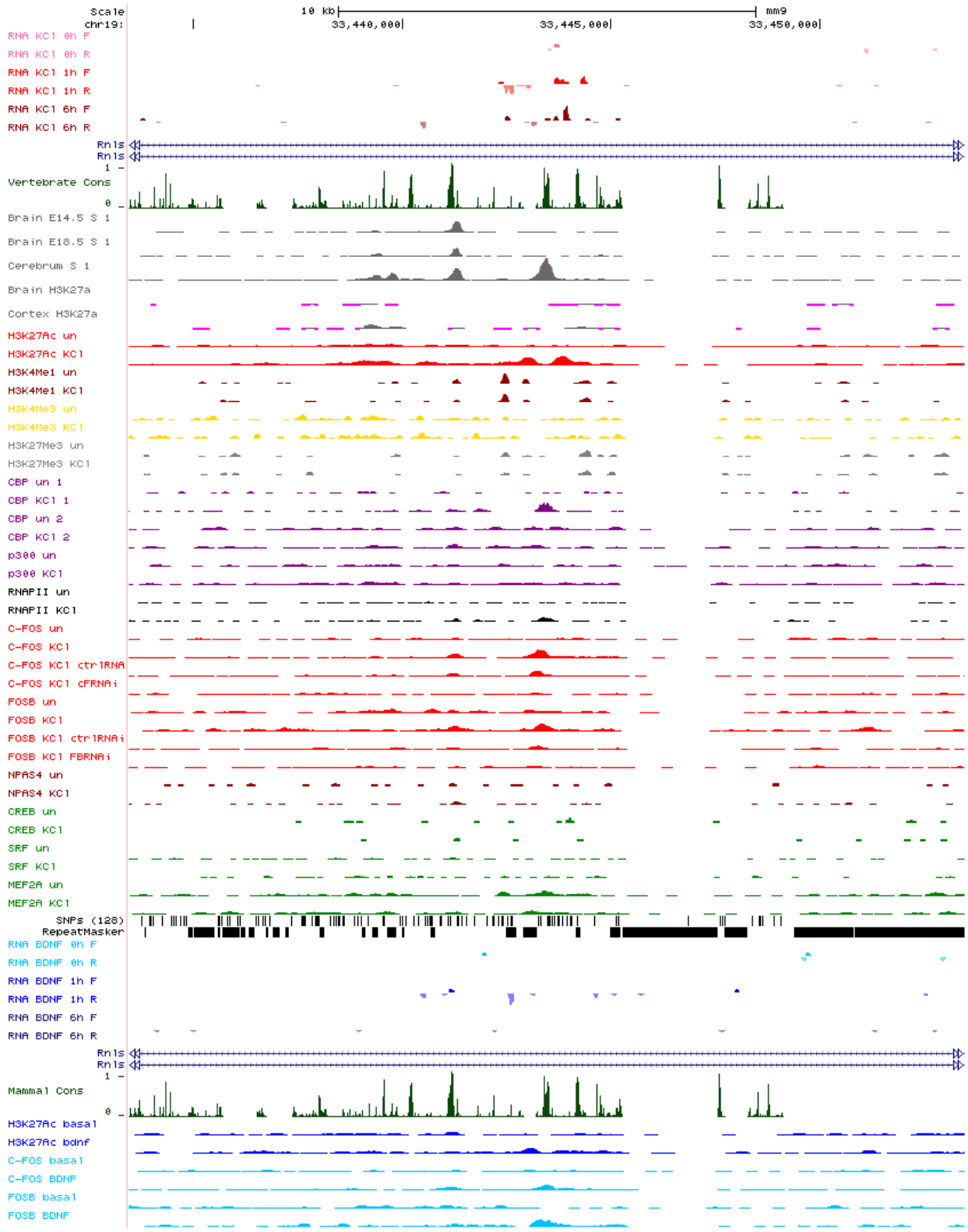

Figure 7.54: Enhancer 54 locus

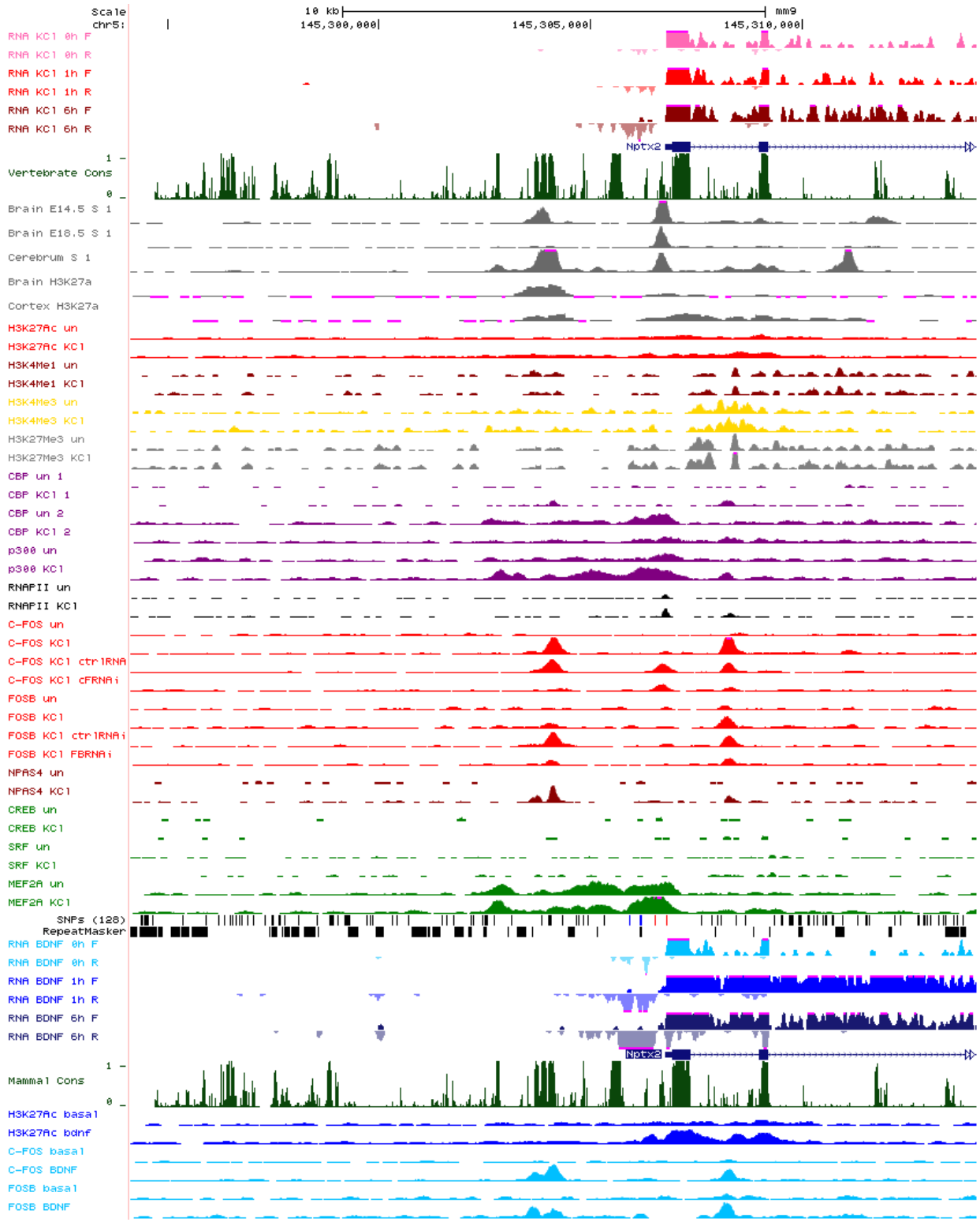

Figure 7.55: *Nptx2* upstream enhancer locus

8 APPENDIX C: ACTIVITY-DEPENDENT LATE RESPONSE GENES LESS INDUCED WITH C-FOS RNAI

On the subsequent pages are displayed all microarray probesets (n=128) that detected activity-dependent genes that were three fold or more induced (6hr/0hr expression>=3) in neurons infected with control RNAi but whose fold induction was reduced by at least 1.75 fold with c-Fos RNAi (fold induction c-Fos RNAi/fold induction control RNAi <= 1/1.75). Probesets are sorted alphabetically by the gene to which they correspond. Fold inductions from control RNAi and c-Fos RNAi infected cells are reported as the average fold induction of two microarray bioreplicates.

				fold induction (6hr/0hr)	
probe.set	gene	Accession	GeneID	control RNAi	c-Fos RNAi
1449363_at	activating transcription factor 3	BC019946	11910	29.4	7.9
1441778_at	adenylate cyclase activating polypeptide 1	BB171354	11516	7.7	3.4
1438936_s_at	angiogenin, ribonuclease A family, member 1	AI385586	11727	8.2	2.5
1438937_x_at	angiogenin, ribonuclease A family, member 1	AI385586	11727	7.6	2.5
1444023_at	ankyrin 2, brain	BB823066	109676	11.8	5.3
1438841_s_at	arginase type II	AV002218	11847	4.6	2.5
1425274_at	aspartate-beta-hydroxylase	AF289490	65973	3.5	1.7
1416250_at	B-cell translocation gene 2, anti-proliferative	NM_007570	12227	5.2	2.0
1448272_at	B-cell translocation gene 2, anti-proliferative	NM_007570	12227	4.6	1.8
1427516_a_at	biregional cell adhesion molecule-related/down-regul	AF388037	117606	4.1	1.9
1422168_a_at	brain derived neurotrophic factor	AY057913	12064	60.0	32.9
1422169_a_at	brain derived neurotrophic factor	AY057913	12064	37.1	18.6
1449031_at	Cbp/p300-interacting transactivator with Glu/Asp-rich	U65091	12705	4.3	2.1
1445128_at	CDNA clone IMAGE:30463708	BQ176646		11.9	5.0
1455947_at	cDNA sequence AK162044	BB667208	211147	4.5	2.4
1426734_at	cDNA sequence BC022623	BB008324	224093	4.7	2.2
1456114_at	CDP-diacylglycerol synthase 1	BI152841	74596	6.6	3.0
1451382_at	ChaC, cation transport regulator-like 1 (E. coli)	BC025169	69065	6.1	2.6
1454770_at	cholecystokinin B receptor	AV221910	12426	4.0	1.3
1424248_at	cyclic AMP-regulated phosphoprotein, 21	BB159263	74100	16.3	3.3
1451280_at	cyclic AMP-regulated phosphoprotein, 21	BB159263	74100	11.3	4.3
1421679_a_at	cyclin-dependent kinase inhibitor 1A (P21)	NM_007669	12575	4.3	2.3
1424638_at	cyclin-dependent kinase inhibitor 1A (P21)	AK007630	12575	4.0	2.0
1457823_at	cysteine rich protein 61	BB533736	16007	11.9	3.9
1442340_x_at	cysteine rich protein 61	BB533736	16007	11.2	4.9
1436125_at	DNA segment, Chr 16, ERATO Doi 472, expressed	AV381575	67102	3.1	1.8
1428834_at	dual specificity phosphatase 4	AK012530	319520	5.0	2.9
1415834_at	dual specificity phosphatase 6	NM_026268	67603	4.1	2.3
1425292_at	dystrobrevin alpha	AF143543	13527	3.3	1.3
1436329_at	early growth response 3	AV346607	13655	5.2	1.4
1416529_at	epithelial membrane protein 1	U25633	13730	11.1	2.2
1417562_at	eukaryotic translation initiation factor 4E binding prot	NM_007918	13685	3.5	1.7
1423100_at	FBJ osteosarcoma oncogene	AV026617	14281	48.6	24.3
1416164_at	fibulin 5	NM_011812	23876	7.5	2.5
1422931_at	fos-like antigen 2	NM_008037	14284	18.8	7.2
1416658_at	frizzled-related protein	U91905	20378	3.5	1.6
1443187_at	gb:AV235077 /DB_XREF=gi:16386187 /DB_XREF=AV23	AV235077		4.2	2.2
1440397_at	gb:BB464523 /DB_XREF=gi:16426998 /DB_XREF=BB46	BB464523		4.4	1.9
1445847_at	gb:BE948333 /DB_XREF=gi:10526092 /DB_XREF=UI-M	BE948333		3.4	1.5
1447100_s_at	gb:C80506 /DB_XREF=gi:2520836 /DB_XREF=C80506 /	C80506		3.3	1.3
1425503_at	glucosaminyl (N-acetyl) transferase 2, I-branching enz	AB037596	14538	3.3	1.8
1460206_at	GRP1 (general receptor for phosphoinositides 1)-assoc	NM_019518	56149	13.4	4.6
1441894_s_at	GRP1 (general receptor for phosphoinositides 1)-assoc	BB071890	56149	12.6	5.1
1457532_at	GTPase activating RANGAP domain-like 1	BB485233	56784	3.6	1.8
1439826_at	heat shock protein 14	BB041480	50497	3.2	1.2
1449872_at	heat shock protein 3	NM_019960	56534	18.5	9.4
1439093_at	Heat shock protein 4 like	BB270852	18415	3.8	1.7
1434572_at	histone deacetylase 9	BB750646	79221	7.7	4.3
1444908_at	hyaluronic acid binding protein 4 /// similar to hyaluro	BM228113	6541 /// 67176	4.7	2.6
1423071_x_at	hypothetical gene supported by BC019681; BC027236	AW549928	/// 624831 ///	4.8	2.7

				fold induction (6hr/0hr)	
probe.set	gene	Accession	GeneID	control RNAi	c-Fos RNAi
1439295_x_at	hypothetical LOC434179	BB371300	434179	4.7	2.6
1442226_at	hypothetical protein 6430702L12	AV348197	330043	4.7	2.1
1419647_a_at	immediate early response 3	NM_133662	15937	3.8	2.0
1452014_a_at	insulin-like growth factor 1	AF440694	16000	13.1	6.6
1419519_at	insulin-like growth factor 1	NM_010512	16000	12.1	5.0
1436066_at	kalirin, RhoGEF kinase	BI965477	545156	3.5	1.8
1445318_at	Kelch-like 4 (Drosophila)	BM251136	237010	11.9	6.1
1439078_at	kelch-like 4 (Drosophila)	BB037068	237010	3.9	2.0
1457397_at	Kruppel-like factor 14	BB022571	101210	8.4	4.2
1436763_a_at	Kruppel-like factor 9	AI267126	16601	4.3	2.2
1458700_at	Leucine rich repeat containing 8 family, member C	BG793487	100604	3.2	1.4
1421262_at	lipase, endothelial	BC020991	16891	8.0	2.7
1450188_s_at	lipase, endothelial	BC020991	16891	7.5	2.7
1429863_at	LON peptidase N-terminal domain and ring finger 3	AK016522	74365	17.2	5.5
1436200_at	LON peptidase N-terminal domain and ring finger 3	BE956940	74365	5.1	2.1
1419254_at	methylenetetrahydrofolate dehydrogenase (NAD+ dep	BG076333	17768	5.4	2.7
1419253_at	methylenetetrahydrofolate dehydrogenase (NAD+ dep	BG076333	17768	4.4	2.5
1418589_a_at	myeloid leukemia factor 1	AF100171	17349	12.8	6.3
1420720_at	neuronal pentraxin 2	NM_016789	53324	11.0	3.7
1449960_at	neuronal pentraxin 2	NM_016789	53324	9.3	4.5
1457198_at	neuropilin 1	AV291009	18186	3.4	1.6
1418932_at	nuclear factor, interleukin 3, regulated	AY061760	18030	10.1	5.7
1428484_at	oxysterol binding protein-like 3	AK004768	71720	6.4	2.6
1429783_at	PDZ and LIM domain 5	AK009464	56376	7.1	2.1
1442710_at	PDZ and LIM domain 5	AV352204	56376	3.5	1.2
1421413_a_at	PDZ and LIM domain 5 /// similar to PDZ and LIM dom	NM_022554	6376 /// 66966	5.4	2.4
1456482_at	phosphatidylinositol 3 kinase, regulatory subunit, poly	AA414954	18710	3.4	1.6
1438588_at	Pleiomorphic adenoma gene-like 1	BB540903	22634	7.4	3.6
1417416_at	potassium voltage-gated channel, shaker-related subfa	NM_010595	16485	8.0	4.0
1438613_at	potassium voltage-gated channel, shaker-related subfa	BB131475	16492	3.9	2.0
1422068_at	POU domain, class 3, transcription factor 1	NM_011141	18991	6.2	3.3
1441764_at	PR domain containing 10	BF730739	382066	3.6	1.5
1416686_at	procollagen lysine, 2-oxoglutarate 5-dioxygenase 2	BC021352	26432	3.3	1.8
1417263_at	prostaglandin-endoperoxide synthase 2	M94967	19225	45.4	6.5
1417262_at	prostaglandin-endoperoxide synthase 2	M94967	19225	19.5	10.5
1437834_s_at	protein kinase C and casein kinase substrate in neuron	BB828106	80708	6.3	3.2
1435460_at	protein kinase, cGMP-dependent, type II	BB363188	19092	3.6	2.0
1439322_at	Protocadherin 9	BB080017	211712	6.1	3.2
1429196_at	RAB GTPase activating protein 1-like	BB431654	29809	10.7	4.8
1429197_s_at	RAB GTPase activating protein 1-like	BB431654	29809	10.6	4.0
1437762_at	RAB39, member RAS oncogene family	BB130995	270160	5.1	2.9
1447830_s_at	regulator of G-protein signaling 2	BB034265	19735	7.3	3.6
1417400_at	retinoic acid induced 14	NM_030690	75646	3.2	1.6
1456203_at	RIKEN cDNA 1110020A10 gene	AI507491	68648	10.0	3.6
1453326_at	RIKEN cDNA 3300001A09 gene /// similar to 3300001A	AK014341	44911 /// 7569	11.7	3.4
1452092_at	RIKEN cDNA 4631426J05 gene	AK019474	77590	3.4	1.4
1429106_at	RIKEN cDNA 4921509J17 gene	AK014853	70857	3.9	2.0
1429900_at	RIKEN cDNA 5330406M23 gene	BM241296	76671	3.2	1.6
1429678_at	RIKEN cDNA 5730508B09 gene	AK017758	70617	3.1	1.4
1453287_at	RIKEN cDNA 5730557B15 gene	AK012871	67434	14.3	3.6

				fold induction (6hr/0hr)	
probe.set	gene	Accession	GeneID	control RNAi	c-Fos RNAi
1430229_at	RIKEN cDNA 6330416L11 gene	AK018183	70713	10.1	5.7
1453334_at	RIKEN cDNA B230216N24 gene	AK021003	78603	10.4	4.8
1439304_at	RIKEN cDNA B230216N24 gene	BM242340	78603	3.8	1.6
1430068_at	RIKEN cDNA C030011L09 gene	BB356045	77316	4.0	1.3
1444324_at	RIKEN cDNA E530001K10 gene	BB559903	414123	40.1	13.8
1455275_at	RIKEN cDNA E530001K10 gene	AW046441	414123	4.6	2.3
1434353_at	Scm-like with four mbt domains 2	BM200222	353282	3.7	1.9
1451599_at	sestrin 2	AV308638	230784	3.8	2.1
1426599_a_at	solute carrier family 2 (facilitated glucose transporter)	BM209618	20525	7.9	3.3
1434773_a_at	solute carrier family 2 (facilitated glucose transporter)	BM207588	20525	7.5	3.3
1426600_at	solute carrier family 2 (facilitated glucose transporter)	BM209618	20525	7.4	3.4
1417750_a_at	solute carrier family 25, member 37	NM_026331	67712	3.5	1.7
1417061_at	solute carrier family 40 (iron-regulated transporter), m	AF226613	53945	6.7	3.8
1417022_at	solute carrier family 7 (cationic amino acid transporter	NM_007515	11989	4.9	2.4
1419503_at	stanniocalcin 2	AF031035	20856	19.2	9.6
1449484_at	stanniocalcin 2	AF031035	20856	14.6	5.5
1417335_at	sulfotransferase family, cytosolic, 2B, member 1	NM_017465	54200	10.7	5.2
1453715_at	synaptic vesicle glycoprotein 2c	AK015921	75209	11.4	3.0
1447421_at	Transcribed locus	BI499978		3.8	1.1
1434413_at	Transcribed locus, weakly similar to XP_328828.1 pred	BG092677		3.6	2.0
1454608_x_at	transthyretin	BG141874	22139	5.5	0.5
1455913_x_at	transthyretin	AV152953	22139	5.4	0.5
1424880_at	tribbles homolog 1 (Drosophila)	AV237242	211770	3.9	2.0
1456225_x_at	tribbles homolog 3 (Drosophila)	BB508622	228775	6.3	1.5
1441969_at	tripartite motif-containing 36	BM933729	28105	7.1	2.7
1436094_at	VGF nerve growth factor inducible	BF458396	381677	32.2	8.5
1422616_s_at	WD repeat domain 54	NM_023790	75659	3.7	2.0
1441787_at	Zinc finger CCCH-type containing 12C	AW764198	244871	6.3	2.8

9 APPENDIX D: WORK RESULTING FROM COLLABORATIONS

nature Vol 455|30 October 2008|doi:10.1038/nature07319

ARTICLES

Activity-dependent regulation of inhibitory synapse development by Npas4

Yingxi Lin[1], Brenda L. Bloodgood[1], Jessica L. Hauser[1]†, Ariya D. Lapan[2], Alex C. Koon[1]†, Tae-Kyung Kim[1], Linda S. Hu[1], Athar N. Malik[1,3] & Michael E. Greenberg[1]

Neuronal activity regulates the development and maturation of excitatory and inhibitory synapses in the mammalian brain. Several recent studies have identified signalling networks within neurons that control excitatory synapse development. However, less is known about the molecular mechanisms that regulate the activity-dependent development of GABA (γ-aminobutyric acid)-releasing inhibitory synapses. Here we report the identification of a transcription factor, Npas4, that plays a role in the development of inhibitory synapses by regulating the expression of activity-dependent genes, which in turn control the number of GABA-releasing synapses that form on excitatory neurons. These findings demonstrate that the activity-dependent gene program regulates inhibitory synapse development, and suggest a new role for this program in controlling the homeostatic balance between synaptic excitation and inhibition.

Sensory experience controls multiple steps in the development and maturation of synapses in the mammalian brain[1–4]. Many of the effects of neuronal activity are mediated by the release of glutamate at excitatory synapses and the subsequent influx of calcium (Ca^{2+}) into the postsynaptic neuron. This results in changes in the number and strength of synapses, a process that underlies learning and memory as well as animal behaviour.

Neurons in the central nervous system receive excitatory synaptic input from glutamatergic neurons and inhibitory input from GABA-releasing (GABAergic) interneurons, except during early development when the first GABAergic synapses are depolarizing and provide the excitatory drive critical for the subsequent development of glutamatergic synapses[5]. The proper balance between excitatory and inhibitory synapses is crucial for representation of sensory information[6,7], execution of motor commands[8,9] and higher-order cognitive functions[10]. Neurological disorders such as autism, schizophrenia and epilepsy are associated with an imbalance between excitatory and inhibitory synapses[11–13]. The number or strength of excitatory synapses can be modified in response to changes in activity, and the molecular mechanisms of these processes have been extensively investigated[14–16]. Less is known about the activity-dependent regulation of inhibitory synapses.

The density of inhibitory synapses in brain regions such as primary sensory cortex, hippocampus and cerebellum is regulated by the level of excitatory synaptic activity and sensory input[17–22]. In addition, initiation of the critical period for synaptic plasticity in the visual cortex is dependent on visual activity and strongly influenced by the maturation of inhibitory synapses[23], suggesting that the activity-dependent regulation of GABAergic synapses is important for the plasticity of the nervous system. Finally, recent studies indicate that regulation of GABAergic synapses in response to neuronal activity may be a critical component of the homeostatic mechanism that maintains a balance between excitation and inhibition in the face of fluctuations in the level of sensory input into neural circuits[24]. Despite the accumulating evidence that neuronal activity regulates the development and maintenance of inhibitory synapses, the molecular mechanisms that control these processes remain to be characterized.

Here we identify a transcription factor, Npas4, that is critical for activity-dependent regulation of GABAergic synapse development. Npas4 expression is rapidly activated by excitatory synaptic activity and turns on a program of gene expression that triggers the formation and/or maintenance of inhibitory synapses on excitatory neurons. These findings provide a molecular link between neuronal excitation and GABAergic synapse development, and suggest a new role for the activity-dependent gene program in controlling inhibitory synapse formation/maintenance on excitatory neurons.

Npas4 is regulated by neuronal activity

The formation of inhibitory synapses onto excitatory neurons is regulated by neuronal activity, takes place over several days, and is a cell-wide process that results in the formation of synapses onto both the cell body and dendrites[18,25]. These features led us to hypothesize that activity-dependent development of inhibitory synapses might be controlled postsynaptically by one or more activity-regulated genes. To test this hypothesis, we used DNA microarrays to identify genes that are induced by membrane depolarization in mouse cortical neurons at the time when inhibitory synapses are developing.

We identified more than 300 genes whose expression levels were altered upon membrane depolarization (Gene Expression Omnibus accession number GSE11256), a third of which were novel activity-regulated genes not seen in previous screens[26,27]. We looked for genes predicted to encode transcription factors, reasoning that, through genome-wide characterization of the targets of an activity-regulated transcription factor that controls inhibitory synapse number, we could gain insight into the biological program that is important for inhibitory synapse development. Among the approximately 20 known or putative transcription factors identified, we focused on genes that are selectively induced by Ca^{2+} influx in neurons but not other cell types, that are transcribed in response to excitatory

[1]F. M. Kirby Neurobiology Center, Children's Hospital and Departments of Neurology and Neurobiology, Harvard Medical School, 300 Longwood Avenue, Boston, Massachusetts 02115, USA. [2]Program in Biological and Biomedical Sciences, Harvard Medical School, 240 Longwood Avenue, Boston, Massachusetts 02115, USA. [3]Program in Neuroscience, Harvard Medical School, 300 Longwood Avenue, Boston, Massachusetts 02115, USA. †Present addresses: Baylor College of Medicine, Medical Scientist Training Program, One Baylor Plaza Suite N201, MS:BCM215, Houston, Texas 77030-7498, USA (J.L.H.); University of Massachusetts Medical School, Lazare Medical Research Building, Room 760C, 364 Plantation Street, Worcester, Massachusetts 06105, USA (A.C.K.).

synaptic activity, and that are expressed coincidently with the development of inhibitory synapses. One transcription factor, the bHLH-PAS family member Npas4 (refs 28–31), fulfilled all these criteria (Fig. 1) and was investigated further.

Unlike other activity-dependent transcription factors such as CREB and c-fos, Npas4 expression in neurons is selectively induced by Ca^{2+} influx but not by several neurotrophic factors, growth factors or forskolin, an activator of protein kinase A (Fig. 1b). Furthermore, Npas4 induction is transient (Fig. 1c), occurs selectively in neurons, and predominately in excitatory neurons (data not shown). Npas4 expression is barely detectable in immature primary hippocampal neurons, when there are few synapses[32], and increases with the formation and maturation of synapses[25] (Fig. 1d).

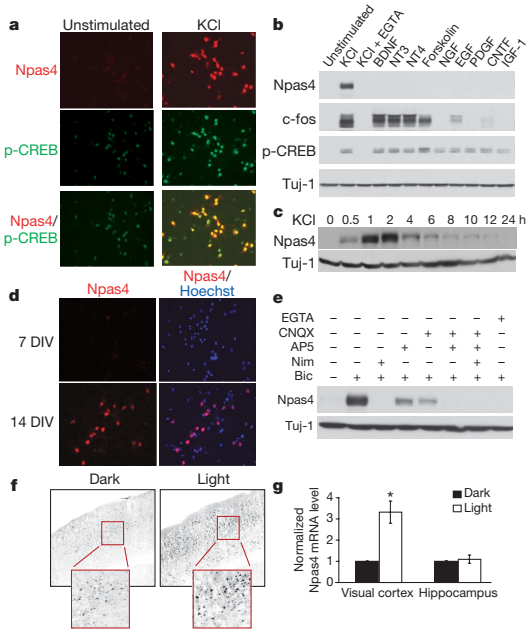

Figure 1 | Npas4 expression is regulated by neuronal activity *in vitro* and *in vivo*. **a**, Immunostaining showing Npas4 protein is induced in rat hippocampal neurons (7 DIV) by depolarization (50 mM KCl, 2 h, right). p-CREB, CREB phosphorylated at Ser 133. **b**, Western blot showing Npas4 is selectively induced by membrane depolarization (50 mM KCl, 7 DIV rat hippocampal neurons), but not by BDNF (50 ng ml^{-1}), NT3 (50 ng ml^{-1}), NT4 (50 ng ml^{-1}), forskolin (10 μM), NGF (100 ng ml^{-1}), EGF (100 ng ml^{-1}), PDGF (100 ng ml^{-1}), CNTF (100 ng ml^{-1}) or IGF-1 (100 ng ml^{-1}). Induction is prevented by pretreatment with the Ca^{2+} chelator EGTA (5 mM, 10 min). **c**, Western blot showing Npas4 (7 DIV rat hippocampal neurons) is transiently induced by membrane depolarization (50 mM KCl, 30 min). **d**, Basal Npas4 expression increases as neurons mature, presumably because of increased endogenous spontaneous activity: compare immunostaining of 7 and 14 DIV rat hippocampal neurons. **e**, Western blot showing stimulation of primary hippocampal neurons (14 DIV) with bicuculline (50 μM, 2 h) increases Npas4 expression levels. This is prevented by pretreatment with nimodipine (5 μM, 1 h) or EGTA (5 μM, 5 min) and reduced by pretreatment (1 h) with antagonists to NMDA receptors (100 μM AP5) or AMPA receptors (50 μM CNQX). **f**, **g**, Mice dark-reared for one week (P21–P28) and then stimulated with strobe lights have greater Npas4 expression levels in the visual cortex than their dark-reared littermates, but there is no difference in the hippocampus. Light stimulation was applied for 2 h for immunocytochemistry analysis (**f**) or 1 h for Npas4 mRNA quantification (**g**). Significance was determined using a one-tailed paired *t*-test, $^*P < 0.05$. Data are shown as mean ± s.e.m.

Npas4 is induced in cultured neurons by the $GABA_A$-receptor antagonist bicuculline, which increases action-potential firing and excitatory synaptic transmission (Fig. 1e). This induction requires an influx of extracellular Ca^{2+} through L-type voltage-sensitive calcium channels (L-VSCCs) and is partly dependent on the activation of *N*-methyl-D-aspartate (NMDA) and α-amino-3-hydroxy-5-methyl-4-isoxazole propionic acid (AMPA) receptors (Fig. 1e). Npas4 expression is also induced in pertinent brain regions *in vivo* in response to specific stimuli: visual stimulation of mice after a period of dark-rearing results in an increase in Npas4 messenger RNA (mRNA) and protein levels specifically in the visual cortex (Fig. 1f, g).

Npas4 regulates the development of inhibitory synapses

The effect of Npas4 on inhibitory synapse development was investigated by RNA interference (RNAi)-mediated knockdown in excitatory neurons of rat dissociated hippocampal cultures, before synapse formation was underway. A small hairpin RNA targeting Npas4 (Npas4-RNAi) effectively reduced Npas4 expression (Fig. 2a) without affecting the overall health of the neurons (Supplementary Fig. 1). To measure inhibitory synapse number, neurons were immunostained for presynaptic GABA-producing enzyme GAD65 and postsynaptic $GABA_A$-receptor γ2 subunit ($GABA_A$-γ2). Co-localization of GAD65 and $GABA_A$-γ2 puncta on a green fluorescent protein (GFP)-transfected glutamatergic neuron was considered indicative of a synapse (Fig. 2b). Expression of Npas4-RNAi, but not a scrambled RNAi (control-RNAi), significantly reduced the number of inhibitory synapses (Fig. 2c). Analysis of synapse number using antibodies that recognize a second pair of inhibitory synaptic proteins (GAD67 and $GABA_A$-β2/3) gave a similar result (data not shown). These data suggest that Npas4 positively regulates the number of inhibitory synapses that form on excitatory neurons.

Different classes of inhibitory neurons synapse onto distinct perisomatic or dendritic regions of pyramidal neurons[33]. We found that Npas4-RNAi leads to a reduction in the number of inhibitory synapses formed on both the perisomatic and dendritic regions, suggesting that Npas4 regulates the number of inhibitory synapses formed by multiple classes of inhibitory neurons (Fig. 2c). In both regions, Npas4-RNAi significantly reduced the density of postsynaptic $GABA_A$-γ2 puncta but had less effect on presynaptic GAD65 puncta, compared with the control-RNAi (Fig. 2d). These findings suggest that Npas4 regulates inhibitory synapse number by controlling the number of postsynaptic specializations, resulting in subsequent remodelling or retraction of the presynaptic terminals.

To test whether Npas4 is important for the development of functional inhibitory synapses in a more intact neural circuit, rat organotypic hippocampal cultures were biolistically co-transfected with GFP and either a control vector or Npas4-RNAi, and whole-cell recordings were performed on GFP-positive CA1 pyramidal neurons to measure spontaneous miniature inhibitory postsynaptic currents (mIPSCs, Fig. 3a). Knocking down Npas4 expression in organotypic cultures significantly increased the inter-event interval and decreased the amplitude of mIPSCs (Fig. 3b, c). This effect of Npas4-RNAi in organotypic slices may be indicative of a decrease in inhibitory synapse number, consistent with our observation that Npas4-RNAi reduces inhibitory synapse number in dissociated cultures. Together, these findings indicate that Npas4 plays an important role in regulating the number of functional inhibitory synapses received by an excitatory neuron.

Consistent with a role for Npas4 in inhibitory synapse development, Npas4 knockout mice ($Npas4^{-/-}$, Supplementary Fig. 2) appear anxious and hyperactive, are prone to seizures and have a shortened lifespan compared with their wild-type littermates, phenotypically resembling other knockout mice lacking genes that control the formation or function of inhibitory circuits[34–36]. However, we found that the frequencies of mIPSCs in acute hippocampal slices prepared from wild-type and $Npas4^{-/-}$ mice were similar (Supplementary Fig. 3), in contrast to the clear change in mIPSC frequency caused by disrupting Npas4 expression acutely in organotypic slices. This difference may

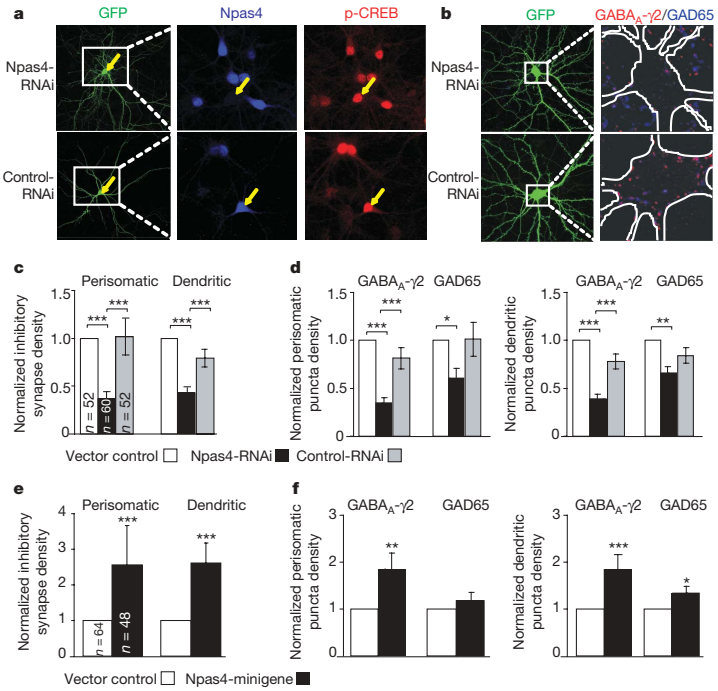

Figure 2 | Npas4 regulates the number of GABAergic synapses in cultured hippocampal neurons. **a**, Npas4-RNAi, but not control-RNAi, reduces the expression of Npas4 in primary hippocampal neurons. Cultures were transfected at 6 DIV and stimulated with bicuculline (50 μM, 2 h) at 14 DIV. **b**, The number of GABAergic synapses is significantly reduced by Npas4-RNAi, as illustrated by two representative rat hippocampal neurons. Cultures were co-transfected (6 DIV) with GFP and either Npas4-RNAi (top) or control-RNAi (bottom). Cultures were subsequently immunostained (25 DIV) with antibodies against GAD65 (blue) and GABA$_A$-γ2 (red). **c**, Quantification of the normalized density of co-localized GABA$_A$-γ2 and GAD65 puncta in 14 DIV rat hippocampal neurons transfected with vector control, Npas4-RNAi or control-RNAi. **d**, Separate quantification of perisomatic and dendritic GABA$_A$-γ2 and GAD65 puncta measured in **c**. **e**, Npas4-minigene increases the density of co-localized GABA$_A$-γ2 and GAD65 puncta. **f**, Separate quantification of perisomatic and dendritic GABA$_A$-γ2 and GAD65 puncta measured in **e**. See Methods for details of data normalization and error propagation. Significance was determined using multifactorial analysis of variance. $*P < 0.05$; $**P < 0.005$; $***P < 0.0005$. Data are presented as mean ± s.e.m. from three (**c**, **d**) or four (**e**, **f**) independent experiments; total numbers of neurons analysed (n) are indicated.

be due to the activation of compensatory pathways during development in the absence of Npas4. Alternatively, it may reflect the fact that Npas4 is absent in both pre- and postsynaptic cells in acute slices from Npas4$^{-/-}$ mice, whereas in the experiments with organotypic slices the disruption of Npas4 expression occurs in postsynaptic neurons only.

To determine conclusively the involvement of Npas4 in inhibitory synapse development, we generated an Npas4 conditional knockout mouse (Npas4$^{flx/flx}$) in which the coding region of Npas4 is flanked by loxP sites and can be acutely removed by Cre-mediated recombination (Supplementary Fig. 4). Organotypic hippocampal slices were prepared from Npas4$^{flx/flx}$ mice and whole-cell recordings made from CA1 pyramidal neurons transfected with GFP and either a control vector or a vector encoding Cre recombinase. Cre expression had no effect on mIPSCs in wild-type neurons (Supplementary Fig. 5). However, compared with transfection with the control construct, transfection of Npas4$^{flx/flx}$ neurons with Cre led to a significant increase in the mIPSC inter-event interval (Fig. 3d, e). This finding provides further evidence that CA1 pyramidal neurons lacking Npas4 receive fewer inhibitory synaptic inputs.

We next investigated whether the number of inhibitory synapses forming onto a cell is controlled by the amount of Npas4 expressed in response to excitatory stimuli. If this is the case, increasing the level of Npas4 should lead to an increase in the number of inhibitory synapses formed on the Npas4-expressing neuron. Additional copies of the Npas4 gene were introduced into neurons using an Npas4-minigene cassette consisting of all Npas4 introns and exons as well as 5 kilobases (kb) of genomic sequence 5′- and 3′- to the coding region. We verified that the Npas4-minigene drives ectopic expression of Npas4 that is activity regulated and functions similarly to the endogenous gene (Supplementary Fig. 6). We found that significantly more inhibitory synapses were formed onto cultured hippocampal neurons expressing the Npas4-minigene than onto neurons transfected with a control vector (Fig. 2e), largely because of an increase in the number of postsynaptic GABA$_A$-γ2 puncta (Fig. 2f). Furthermore, expression of the Npas4-minigene in CA1 pyramidal neurons of hippocampal slices significantly decreases the mIPSC inter-event interval and significantly increases the amplitude (Fig. 3b, c), consistent with the presence of additional and stronger inhibitory synapses on neurons expressing higher levels of Npas4.

Effect of Npas4 on excitatory synapses

The appropriate balance between excitation and inhibition is critical for the function of neural circuits. To maintain this balance, changes in the number or strength of inhibitory synapses are often coupled to changes in excitatory synapses[24]. We next asked whether excitatory synapse number or function is also affected when Npas4 expression is perturbed.

We first determined whether Npas4 regulates the number of excitatory synapses in dissociated hippocampal cultures. As before, neurons were transfected with either Npas4-RNAi or control constructs,

before synaptogenesis was underway and thus before the balance between excitation and inhibition was established. Cultures were immunostained for the presynaptic marker synapsin1 and the excitatory postsynaptic marker PSD95, and the numbers of co-localized synapsin1 and PSD95 puncta on transfected glutamatergic neurons were quantified. Neither the total numbers of excitatory synapses nor the individual numbers of pre- or postsynaptic markers changed significantly upon expression of Npas4-RNAi (Fig. 4a, b), under conditions that significantly decreased the number of inhibitory synapses. Likewise, expression of the Npas4-minigene had no effect on excitatory synapse number (Fig. 4c, d). Because perturbation of the level of Npas4 expression occurred before synaptic connections were established, these experiments suggest that Npas4 is not a major contributor to excitatory synaptogenesis.

We next examined whether Npas4 affects excitatory synapse function in organotypic hippocampal slices, where homeostatic mechanisms are known to control excitatory/inhibitory balance within neural circuits. Deletion of the Npas4 gene from neurons in Npas4$^{flx/flx}$ organotypic hippocampal slices by Cre recombination significantly decreased the inter-event interval of spontaneous miniature excitatory postsynaptic currents (mEPSCs, Fig. 4e, f), whereas elevating the level of Npas4 with the Npas4-minigene significantly increased the inter-event interval and decreased the amplitude of mEPSCs (Fig. 4g, h), compared with control-transfected neurons. Thus, abolishing Npas4 expression in a pyramidal neuron increases, whereas enhancing the level of Npas4 decreases, the number and/or presynaptic release probability of excitatory synapses that form on the neuron. Therefore, the net result of Npas4 activation in an intact neural circuit is an increase in synaptic inhibition and a decrease in excitation of a neuron. We conclude that Npas4 induction in response to increased excitatory input acts to reduce the level of activity, and therefore may function as a negative feedback mechanism to maintain the homeostatic balance between excitation and inhibition.

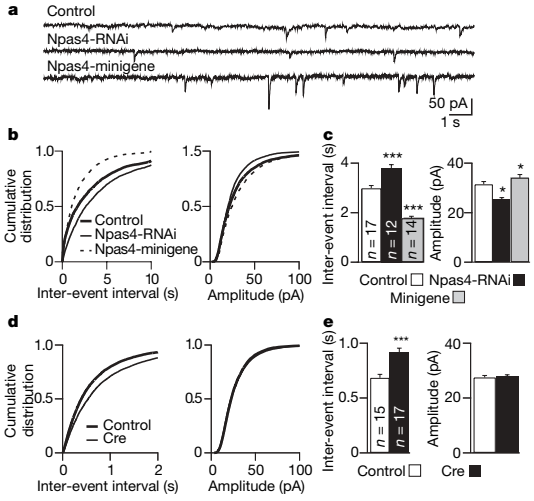

Figure 3 | Npas4 regulates GABAergic synapse development in organotypic hippocampal slices. **a**, Representative mIPSCs recorded from CA1 pyramidal neurons in organotypic hippocampal slices biolistically co-transfected with GFP and either vector control, Npas4-RNAi or Npas4-minigene. **b**, Cumulative distributions of mIPSC inter-event intervals and amplitudes recorded from neurons transfected with vector control, Npas4-RNAi or Npas4-minigene. **c**, Mean ± s.e.m. of data from **b**. mIPSC inter-event intervals: 2986.3 ± 105.7, 3803.0 ± 136.9 and 1776.9 ± 75.1 ms; amplitudes: 31.5 ± 1.1, 25.7 ± 0.8 and 34.1 ± 1.3 pA; for vector control, Npas4-RNAi and Npas4-minigene, respectively. **d**, Cumulative distributions of mIPSC inter-event intervals and amplitudes recorded from Npas4$^{flx/flx}$ neurons co-transfected with GFP and either vector control or Cre recombinase. **e**, Mean ± s.e.m. of data from **d**. mIPSC inter-event intervals: 684.2 ± 31.2 and 917.4 ± 37.7 ms; amplitudes: 27.5 ± 0.7 and 27.9 ± 0.6 pA; for vector control and Cre, respectively. Total numbers of neurons analysed in each condition (n) are indicated in **c** and **e**. $^*P < 0.05$; $^{***}P < 0.001$.

Npas4 regulates genes that control inhibitory synapse development

To uncover the program of gene expression controlled by Npas4, we acutely knocked down Npas4 expression in a high percentage of wild-type neurons using a lentivirus expressing Npas4-RNAi (Supplementary Fig. 7) and performed a second DNA microarray

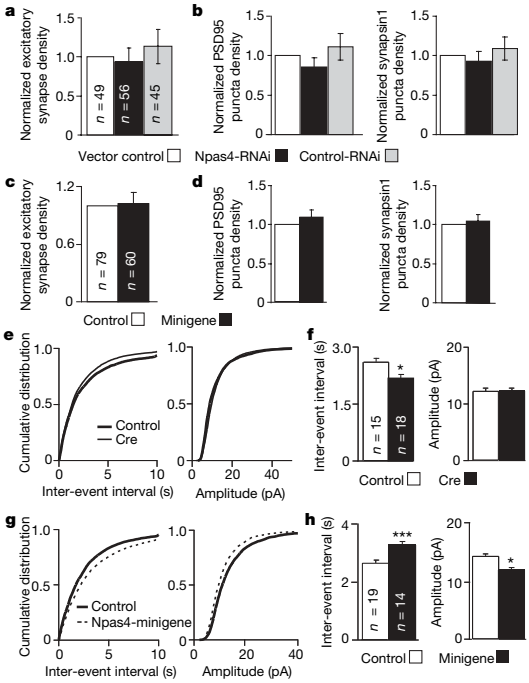

Figure 4 | Npas4 has no effect on excitatory synaptogenesis but affects excitatory/inhibitory balance in neural circuits. **a**, The number of excitatory synapses is not affected by Npas4-RNAi. Quantification of the normalized density of co-localized PSD95 and synapsin1 puncta in 14 DIV rat hippocampal neurons transfected with vector control, Npas4-RNAi or control-RNAi. **b**, Separate quantification of PSD95 and synapsin1 puncta measured in **a**. **c**, Npas4-minigene has no effect on the density of excitatory synapses. Quantification of co-localized synapsin1 and PSD95 puncta is shown. **d**, Separate quantification of PSD95 and synapsin1 puncta measured in **c**. In **a**–**d**, data are presented as mean ± s.e.m. **e**, Cumulative distribution of mEPSC inter-event intervals and amplitudes recorded from Npas4$^{flx/flx}$ neurons co-transfected with GFP and either vector control or Cre. **f**, Mean ± s.e.m. of data from **e**. mEPSC inter-event intervals: 2581.4 ± 104.1 ms and 2140.5 ± 79.7 ms; amplitudes: 12.1 ± 0.4 and 12.4 ± 0.3 pA; for vector control and Cre, respectively. **g**, Cumulative distribution of mEPSC inter-event intervals and amplitudes recorded from neurons transfected with GFP and either vector control or Npas4-minigene. **h**, Mean ± s.e.m. of data from **g**. mEPSC inter-event intervals: 2686.4 ± 89.3 and 3320.7 ± 117.2 ms; amplitudes: 14.3 ± 0.3 and 12.0 ± 0.3 pA; for vector control and Npas4-minigene, respectively. Total numbers of neurons analysed in each condition (n) are indicated. **a**, **b**, Three independent experiments; **c**, **d**, four independent experiments. $^*P < 0.05$; $^{***}P < 0.001$.

experiment to identify activity-regulated genes that are misregulated in the absence of Npas4. The expression levels of 327 microarray probe sets representing 270 unique genes were significantly different in cultures expressing Npas4-RNAi compared with those expressing the control virus (Gene Expression Omnibus accession number GSE11258, Supplementary List). The expression of 182 of these genes was also acutely regulated by membrane depolarization in the absence of Npas4-RNAi, indicating that many putative Npas4-regulated genes are activity regulated (Fig. 5a). Although Npas4 has been shown to function as a transcriptional activator (Supplementary Fig. 6b)[28], we found that many genes are negatively regulated by Npas4 (Fig. 5a). This may reflect the fact that Npas4 functions as a transcriptional repressor as well as an activator, and/or that Npas4 indirectly affects gene expression by altering neuronal excitation.

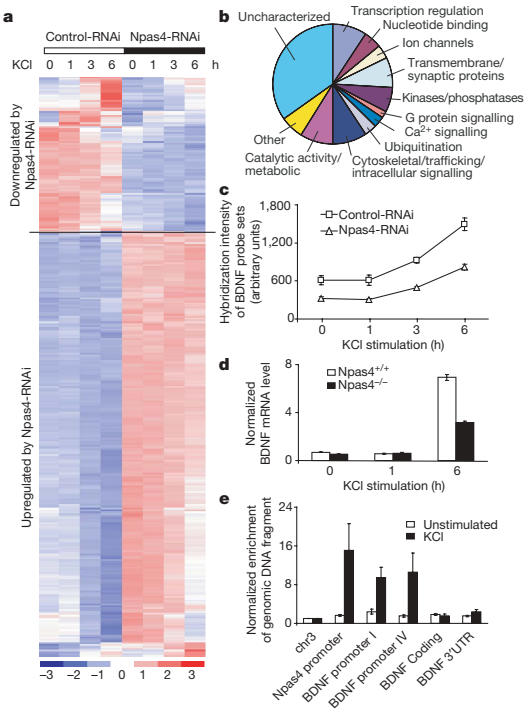

Figure 5 | Npas4 controls a program of gene expression that regulates GABAergic synapses. **a**, Hierarchical clustering of 327 probe sets (270 putative Npas4 target genes) based on their expression profiles using dChip[49]. The expression level of each probe set is normalized to a mean of 0 and a standard deviation of 1. Expression values are displayed within the range [−3, 3] with levels above, equal to or below the mean displayed in red, white and blue, respectively. Dark red represents 3 or higher, and dark blue −3 or lower. **b**, Biological functions of 270 putative Npas4 target genes based on Gene Ontology information provided by Affymetrix (http://www.affymetrix.com). **c**, BDNF expression is reduced by Npas4-RNAi (1.9 ± 0.11-fold reduction, $P < 0.01$, one-tailed paired *t*-test). Mean ± s.e.m. from three independent experiments is shown, and each data point was generated by averaging the hybridization intensity of two BDNF probe sets (1422168_a_at and 1422169_a_at). **d**, BDNF levels are consistently reduced in neurons from Npas4$^{-/-}$ mice compared with their wild-type littermates (58.46 ± 6.49% decrease, 95% confidence interval 30.5–86.4%). Cortical cultures prepared from Npas4$^{+/+}$ and Npas4$^{-/-}$ littermates (7 DIV) were stimulated with KCl (55 mM), and BDNF mRNA levels were measured by quantitative reverse transcriptase PCR using primers in BDNF coding region. Three littermate pairs from three different litters were analysed; data (mean ± s.e.m.) from one representative pair is shown. **e**, Npas4 interacts directly with BDNF promoters I and IV in an activity-dependent manner, as shown by chromatin immunoprecipitation. The Npas4 promoter is used as a positive control. Data are normalized to a control region on chromosome 3 and are presented as mean ± s.e.m. from five independent experiments.

Npas4 appears to regulate a wide variety of genes, such as activity-regulated immediate early genes, various classes of transcription factors, channel proteins, G-protein signalling molecules, kinases and phosphatases, and genes involved in pathways that modulate synaptic functions, such as ubiquitination, trafficking and receptor endocytosis (Fig. 5b and Supplementary List). Interestingly, the functions of 94 of the 270 putative Npas4-regulated genes are uncharacterized (Fig. 5b), suggesting that Npas4 regulates many genes that could affect inhibitory synapses in novel ways.

As a first step towards understanding the genetic program regulated by Npas4, we focused on targets that might be directly involved in the development of GABAergic synapses. Brain-derived neurotrophic factor (BDNF) stood out because it had previously been shown to regulate GABAergic synapse maturation and function[18,20,37–39]. BDNF expression is consistently reduced by almost two-fold in cultures expressing Npas4-RNAi compared with control cultures (Fig. 5c). Primary cultures from Npas4$^{-/-}$ mice showed a similar decrease in depolarization-induced BDNF expression compared with their wild-type littermates (Fig. 5d).

The BDNF gene has many promoters and the activity-dependent BDNF mRNA transcripts are controlled by promoters I and IV[40–42]. Using a chromatin immunoprecipitation assay, we asked whether Npas4 binds to these promoters in primary cortical cultures that were left untreated or membrane-depolarized to trigger Npas4 expression. Although no Npas4 binding was detected in untreated neurons, in membrane-depolarized neurons Npas4 was found to be associated with BDNF promoters I and IV, but not with the coding region or 3′ untranslated region (Fig. 5e), suggesting that Npas4 may directly regulate activity-dependent expression of BDNF.

To determine whether BDNF contributes to the effects of Npas4 on GABAergic synapse development, we tested whether the ability of the Npas4-minigene to increase the number of inhibitory synapses is attenuated by knockdown of BDNF expression, using a previously validated small hairpin RNA that targets the BDNF coding region (BDNF-RNAi)[43]. Confirming that BDNF increases inhibitory synapse number[44], BDNF-RNAi increased mIPSC inter-event intervals compared with control values (2986.3 ± 109.7 and 4086.1 ± 140.7 ms, control and BDNF-RNAi, respectively, $P < 0.01$). Expression of the Npas4-minigene alone led to an approximately 40% decrease in the inter-event interval of mIPSCs recorded from CA1 neurons (Fig. 3b, c), as previously observed, but this was partly attenuated to approximately 20% by the presence of BDNF-RNAi (Fig. 6a). In addition, in the presence of BDNF-RNAi, the effect of the Npas4-minigene on the amplitude of mIPSCs was completely reversed (Fig. 6b). These findings suggest that BDNF mediates a portion of the effect of Npas4 on inhibitory synapse number, but that additional Npas4 targets may also be involved.

Discussion

We have identified the activity-regulated transcription factor Npas4 as a key regulator of GABAergic synapse development. Excitatory synaptic activity induces Npas4 in a Ca^{2+}-dependent manner, and the level of Npas4 determines the number of functional GABAergic synapses by controlling a program of activity-dependent gene expression. Future characterization of Npas4 target genes will help to determine whether Npas4 acts by initiating inhibitory synapse formation, stabilizing nascent inhibitory synapses or promoting the maturation of weak inhibitory synapses. It is possible that different subsets of Npas4 targets control the development of GABAergic synapses formed by distinct classes of interneurons, providing a mechanism for the independent regulation of inhibition received

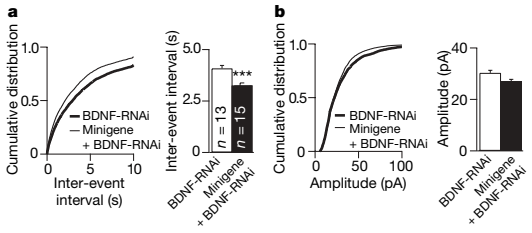

Figure 6 | Knockdown of BDNF partially attenuates the ability of the Npas4-minigene to elevate GABAergic synapses. a, Cumulative distributions (left) and mean ± s.e.m. (right) of mIPSC inter-event intervals in neurons transfected with BDNF-RNAi (4086.1 ± 140.7 ms) or BDNF-RNAi + Npas4-minigene (3257.9 ± 117.7 ms). **b**, Cumulative distributions (left) and mean ± s.e.m. (30.1 ± 0.9 and 27.1 ± 0.7 pA, BDNF-RNAi versus BDNF-RNAi + Npas4-minigene, right) of mIPSC amplitudes. Total numbers of neurons analysed in each condition (n) are indicated. ***$P < 0.001$.

by subregions of a neuron. Another intriguing possibility is that Npas4 controls experience-dependent developmental processes, such as critical period plasticity in the visual cortex, which depend on the function and maturation of GABAergic synapses.

Although Npas4 is not required for the initial formation of excitatory synapses, activation of Npas4 in excitatory neurons within a neural circuit appears to diminish the excitatory synaptic input they receive. It is not known whether this effect is mediated directly by Npas4 or is an indirect consequence of changes in inhibitory input. In either case, our findings suggest that Npas4 functions as part of the homeostatic mechanism that stabilizes the activity of a neuron in the face of changing glutamatergic input. Further investigation of the function of Npas4 and other activity-dependent regulators of inhibitory synapses[45] will provide insight into the mechanism by which neuronal activity controls the balance between excitation and inhibition in the brain, and how the disruption of this balance leads to neurological disorders such as autism, epilepsy and schizophrenia.

METHODS SUMMARY

Dissociated neuron culture and transfection. Dissociated cortical and hippocampal neurons were prepared from E18 rat or E16 mouse embryos as previously described[46]. Cultures were maintained in Neurobasal Medium supplemented with B27 (Invitrogen), penicillin–streptomycin and glutamine. Neurons were plated at 100,000–150,000 per well in a 24-well plate or 15,000,000 per 10-cm plate. For synapse assays, hippocampal neurons (60,000 per well, 24-well plate) were plated on a monolayer of astrocytes[47]. Neurons were transfected at 5–6 days *in vitro* (DIV) using the calcium phosphate method[46].

Organotypic slice culture and transfection. Organotypic hippocampal slice cultures were prepared from P6 rats or mice as previously described[48]. Slices were biolistically transfected with a Helios Gene Gun (Biorad) after 2 days. Bullets for the gene gun were 1.6-μm gold particles coated with 15 μg eGFP and either 5 or 10 μg RNAi construct, 45 μg Npas4-minigene or 30 μg Cre. Empty plasmid was added to bring the total DNA to 60 μg in each case.

Synapse density assay. Hippocampal neurons (14–18 DIV) were immunostained for synaptic markers and imaged on a Zeiss LSM5 Pascal microscope using a ×63 objective lens. Image acquisition and synapse quantification were performed in a blinded manner. Glutamatergic neurons were identified based on morphology and the absence of cytosolic GAD65 staining. Synapse density was measured using Metamorph software as previously described[47]. Within each experiment, density of puncta was normalized against the control, and the error of the control propagated into each experimental condition. Statistical analysis was performed on the raw data (without normalization) using multifactorial analysis of variance in StatView 4.5 (Abacus Concepts).

Electrophysiology. Whole-cell patch clamp recordings were made at room temperature from CA1 pyramidal neurons 7–10 days after transfection. Data were analysed in IgorPro (Wavemetrics) using custom-written macros. Statistical significance was determined by Kolmogorov–Smirnov test and Monte Carlo simulation.

Full Methods and any associated references are available in the online version of the paper at www.nature.com/nature.

Received 5 May; accepted 25 July 2008.
Published online 24 September 2008.

1. Katz, L. C. & Shatz, C. J. Synaptic activity and the construction of cortical circuits. *Science* **274,** 1133–1138 (1996).
2. Spitzer, N. C. Electrical activity in early neuronal development. *Nature* **444,** 707–712 (2006).
3. Wong, R. O. & Ghosh, A. Activity-dependent regulation of dendritic growth and patterning. *Nature Rev. Neurosci.* **3,** 803–812 (2002).
4. Zito, K. & Svoboda, K. Activity-dependent synaptogenesis in the adult mammalian cortex. *Neuron* **35,** 1015–1017 (2002).
5. Ben-Ari, Y. Excitatory actions of GABA during development: the nature of the nurture. *Nature Rev. Neurosci.* **3,** 728–739 (2002).
6. Kenet, T., Froemke, R. C., Schreiner, C. E., Pessah, I. N. & Merzenich, M. M. Perinatal exposure to a noncoplanar polychlorinated biphenyl alters tonotopy, receptive fields, and plasticity in rat primary auditory cortex. *Proc. Natl Acad. Sci. USA* **104,** 7646–7651 (2007).
7. Maffei, A., Nelson, S. B. & Turrigiano, G. G. Selective reconfiguration of layer 4 visual cortical circuitry by visual deprivation. *Nature Neurosci.* **7,** 1353–1359 (2004).
8. Buschges, A. & Manira, A. E. Sensory pathways and their modulation in the control of locomotion. *Curr. Opin. Neurobiol.* **8,** 733–739 (1998).
9. Brown, P., Ridding, M. C., Werhahn, K. J., Rothwell, J. C. & Marsden, C. D. Abnormalities of the balance between inhibition and excitation in the motor cortex of patients with cortical myoclonus. *Brain* **119,** 309–317 (1996).
10. Cline, H. Synaptogenesis: a balancing act between excitation and inhibition. *Curr. Biol.* **15,** R203–R205 (2005).
11. Mohler, H. $GABA_A$ receptors in central nervous system disease: anxiety, epilepsy, and insomnia. *J. Recept. Signal Transduct. Res.* **26,** 731–740 (2006).
12. Rubenstein, J. L. & Merzenich, M. M. Model of autism: increased ratio of excitation/inhibition in key neural systems. *Genes Brain Behav.* **2,** 255–267 (2003).
13. Wassef, A., Baker, J. & Kochan, L. D. GABA and schizophrenia: a review of basic science and clinical studies. *J. Clin. Psychopharmacol.* **23,** 601–640 (2003).
14. Burrone, J., O'Byrne, M. & Murthy, V. N. Multiple forms of synaptic plasticity triggered by selective suppression of activity in individual neurons. *Nature* **420,** 414–418 (2002).
15. Malinow, R. & Malenka, R. C. AMPA receptor trafficking and synaptic plasticity. *Annu. Rev. Neurosci.* **25,** 103–126 (2002).
16. Turrigiano, G. G., Leslie, K. R., Desai, N. S., Rutherford, L. C. & Nelson, S. B. Activity-dependent scaling of quantal amplitude in neocortical neurons. *Nature* **391,** 892–896 (1998).
17. Benevento, L. A., Bakkum, B. W. & Cohen, R. S. Gamma-aminobutyric acid and somatostatin immunoreactivity in the visual cortex of normal and dark-reared rats. *Brain Res.* **689,** 172–182 (1995).
18. Chattopadhyaya, B. *et al.* Experience and activity-dependent maturation of perisomatic GABAergic innervation in primary visual cortex during a postnatal critical period. *J. Neurosci.* **24,** 9598–9611 (2004).
19. Foeller, E. & Feldman, D. E. Synaptic basis for developmental plasticity in somatosensory cortex. *Curr. Opin. Neurobiol.* **14,** 89–95 (2004).
20. Marty, S., Wehrle, R. & Sotelo, C. Neuronal activity and brain-derived neurotrophic factor regulate the density of inhibitory synapses in organotypic slice cultures of postnatal hippocampus. *J. Neurosci.* **20,** 8087–8095 (2000).
21. Micheva, K. D. & Beaulieu, C. Development and plasticity of the inhibitory neocortical circuitry with an emphasis on the rodent barrel field cortex: a review. *Can. J. Physiol. Pharmacol.* **75,** 470–478 (1997).
22. Seil, F. J. & Drake-Baumann, R. Activity-dependent changes in "transplanted" cerebellar cultures. *Exp. Neurol.* **138,** 327–337 (1996).
23. Hensch, T. K. Critical period plasticity in local cortical circuits. *Nature Rev. Neurosci.* **6,** 877–888 (2005).
24. Turrigiano, G. G. & Nelson, S. B. Homeostatic plasticity in the developing nervous system. *Nature Rev. Neurosci.* **5,** 97–107 (2004).
25. Benson, D. L. & Cohen, P. A. Activity-independent segregation of excitatory and inhibitory synaptic terminals in cultured hippocampal neurons. *J. Neurosci.* **16,** 6424–6432 (1996).
26. Nedivi, E., Hevroni, D., Naot, D., Israeli, D. & Citri, Y. Numerous candidate plasticity-related genes revealed by differential cDNA cloning. *Nature* **363,** 718–722 (1993).
27. Worley, P. F., Cole, A. J., Saffen, D. W. & Baraban, J. M. Regulation of immediate early genes in brain: role of NMDA receptor activation. *Prog. Brain Res.* **86,** 277–285 (1990).
28. Ooe, N., Saito, K., Mikami, N., Nakatuka, I. & Kaneko, H. Identification of a novel basic helix-loop-helix-PAS factor, NXF, reveals a Sim2 competitive, positive regulatory role in dendritic-cytoskeleton modulator drebrin gene expression. *Mol. Cell. Biol.* **24,** 608–616 (2004).
29. Flood, W. D., Moyer, R. W., Tsykin, A., Sutherland, G. R. & Koblar, S. A. Nxf and Fbxo33: novel seizure-responsive genes in mice. *Eur. J. Neurosci.* **20,** 1819–1826 (2004).

30. Hester, I. *et al.* Transient expression of Nxf, a bHLH-PAS transactivator induced by neuronal preconditioning, confers neuroprotection in cultured cells. *Brain Res.* **1135,** 1–11 (2007).
31. Shamloo, M. *et al.* Npas4, a novel helix-loop-helix PAS domain protein, is regulated in response to cerebral ischemia. *Eur. J. Neurosci.* **24,** 2705–2720 (2006).
32. Fletcher, T. L., Cameron, P., De Camilli, P. & Banker, G. The distribution of synapsin I and synaptophysin in hippocampal neurons developing in culture. *J. Neurosci.* **11,** 1617–1626 (1991).
33. Huang, Z. J., Di Cristo, G. & Ango, F. Development of GABA innervation in the cerebral and cerebellar cortices. *Nature Rev. Neurosci.* **8,** 673–686 (2007).
34. Gomeza, J. *et al.* Deletion of the mouse glycine transporter 2 results in a hyperekplexia phenotype and postnatal lethality. *Neuron* **40,** 797–806 (2003).
35. Kash, S. F. *et al.* Epilepsy in mice deficient in the 65-kDa isoform of glutamic acid decarboxylase. *Proc. Natl Acad. Sci. USA* **94,** 14060–14065 (1997).
36. Kash, S. F., Tecott, L. H., Hodge, C. & Baekkeskov, S. Increased anxiety and altered responses to anxiolytics in mice deficient in the 65-kDa isoform of glutamic acid decarboxylase. *Proc. Natl Acad. Sci. USA* **96,** 1698–1703 (1999).
37. Huang, Z. J. *et al.* BDNF regulates the maturation of inhibition and the critical period of plasticity in mouse visual cortex. *Cell* **98,** 739–755 (1999).
38. Rutherford, L. C., DeWan, A., Lauer, H. M. & Turrigiano, G. G. Brain-derived neurotrophic factor mediates the activity-dependent regulation of inhibition in neocortical cultures. *J. Neurosci.* **17,** 4527–4535 (1997).
39. Seil, F. J. & Drake-Baumann, R. TrkB receptor ligands promote activity-dependent inhibitory synaptogenesis. *J. Neurosci.* **20,** 5367–5373 (2000).
40. Aid, T., Kazantseva, A., Piirsoo, M., Palm, K. & Timmusk, T. Mouse and rat BDNF gene structure and expression revisited. *J. Neurosci. Res.* **85,** 525–535 (2007).
41. Liu, Q. R. *et al.* Rodent BDNF genes, novel promoters, novel splice variants, and regulation by cocaine. *Brain Res.* **1067,** 1–12 (2006).
42. Tao, X., Finkbeiner, S., Arnold, D. B., Shaywitz, A. J. & Greenberg, M. E. Ca^{2+} influx regulates BDNF transcription by a CREB family transcription factor-dependent mechanism. *Neuron* **20,** 709–726 (1998).
43. Zhou, P. *et al.* Polarized signaling endosomes coordinate BDNF-induced chemotaxis of cerebellar precursors. *Neuron* **55,** 53–68 (2007).
44. Kohara, K. *et al.* A local reduction in cortical GABAergic synapses after a loss of endogenous brain-derived neurotrophic factor, as revealed by single-cell gene knock-out method. *J. Neurosci.* **27,** 7234–7244 (2007).
45. Chubykin, A. A. *et al.* Activity-dependent validation of excitatory versus inhibitory synapses by neuroligin-1 versus neuroligin-2. *Neuron* **54,** 919–931 (2007).
46. Xia, Z., Dudek, H., Miranti, C. K. & Greenberg, M. E. Calcium influx via the NMDA receptor induces immediate early gene transcription by a MAP kinase/ERK-dependent mechanism. *J. Neurosci.* **16,** 5425–5436 (1996).
47. Paradis, S. *et al.* An RNAi-based approach identifies molecules required for glutamatergic and GABAergic synapse development. *Neuron* **53,** 217–232 (2007).
48. Stoppini, L., Buchs, P. A. & Muller, D. A simple method for organotypic cultures of nervous tissue. *J. Neurosci. Methods* **37,** 173–182 (1991).
49. Li, C. & Wong, W. H. Model-based analysis of oligonucleotide arrays: expression index computation and outlier detection. *Proc. Natl Acad. Sci. USA* **98,** 31–36 (2001).

Supplementary Information is linked to the online version of the paper at www.nature.com/nature.

Acknowledgements We thank members of the Greenberg laboratory for suggestions; S. Paradis, J. M. Gray, S. S. Margolis, J. Zieg and C. M. Fletcher for reading the manuscript; S. Vasquez for preparing primary neuronal cell cultures; M. Thompson, Y. Zhou and H. Ye for assistance in generating $Npas4^{-/-}$ mice; T. Diefenbach and the Neurobiology Program Imaging Center for assistance with confocal microscopy; M. Fagiolini for help with dissection of the visual cortex; and X. J. Liu and C. Chen for help with electrophysiology. M.E.G. acknowledges the generous support of the F. M. Kirby Foundation to the Neurobiology Program of the Children's Hospital and support from the Nancy Lurie Marks Family Foundation. This work was supported by a Lefler Foundation postdoctoral fellowship (Y.L.), a Ruth L. Kirschstein National Research Service Award and a Helen Hay Whitney postdoctoral fellowship (B.L.B.), a National Science Foundation Graduate Research Fellowship (A.D.L.), the Jane Coffin Childs Memorial Fund (T.-K.K.) and Mental Retardation Research Center grant HD18655 and National Institutes of Health grants NS27572 and NS48276 (M.E.G.).

Author Contributions Y.L. and M.E.G. conceived and designed the experiments and wrote the manuscript. Y.L. performed or participated in each of the experiments described in the manuscript. B.L.B. performed the electrophysiological recordings and contributed to the writing of the manuscript. J.L.H. quantified Npas4 mRNA levels for the light stimulation experiment, generated the Npas4-minigene construct and performed the luciferase assay to characterize it, managed the Npas4 animal colony and provided extensive technical support. A.D.L. performed immunocytochemistry for the light stimulation experiment and confocal imaging of neurons in the synapse assay with Npas4-RNAi. A.C.K. provided technical support during the early phase of the study and helped generate many reagents used in this study including the Npas4 antibody, Npas4 knockout construct and Npas4-RNAi lentivirus. T.-K.K. performed the chromatin immunoprecipitation experiments. L.S.H. helped generate the Npas4 antibody. A.N.M. performed the initial chromatin immunoprecipitation experiments.

Author Information Data have been placed in the GEO database under accession numbers GSE11256 and GSE11258. Reprints and permissions information is available at www.nature.com/reprints. Correspondence and requests for materials should be addressed to M.E.G. (meg@hms.harvard.edu).

METHODS

DNA constructs. Npas4-RNAi, 5′-GGTTGACCCTGATAATTTA-3′, and control-RNAi with a scrambled sequence (underlined), 5′-GGTTCAGCGTCATAA TTTA-3′, were cloned into the pSuper expression vector (OligoEngine). The same Npas4-RNAi was used to generate the lentivirus construct (Cellogenetics, Inc). The control lentivirus construct, pLenti-shGL3 (Cellogenetics, Inc), targets the luciferase gene, which is not expressed by mouse hippocampal neurons.

The Npas4-minigene was generated by subcloning the mouse genomic region from CTCGGTTTCTATCTTCATGCC to GCCATGTGGCCTGCCGGTAC into a pBluescriptIIk + vector between the *Sac*II and *Kpn*I digestion sites. The sequence targeted by Npas4-RNAi was mutated to AgtCgaTccCgataattta, preserving the amino-acid sequence, to generate an RNAi-resistant Npas4-minigene.

The Npas4 luciferase reporter was constructed by replacing the tandem MEF2 responsive elements with three copies of the Npas4 responsive element[28] in the 3×MRE-luc plasmid[50].

Immunocytochemistry and immunohistochemistry. Cultured neurons were fixed and immunostained as previously described[47]. For immunohistochemistry, mice were perfused intracardially with cold PBS followed by 4% paraformaldehyde in PBS. Brains were post-fixed in 4% paraformaldehyde in PBS at 4 °C overnight followed by incubation in 30% sucrose in PBS at 4 °C for 24 h. These cryo-protected brains were immediately sectioned on a cryostat (Leica) or stored in Tissue-Tec O.C.T. at −80 °C for later sectioning. Matching brain sections (35 μm) were incubated in blocking solution (3% BSA, 3% goat serum, 0.3% Triton X-100, 0.2% Tween-20 in PBS) at room temperature for 2 h. Subsequently, sections were incubated with primary antibodies overnight at 4 °C and with secondary antibodies at room temperature for 2 h, both in blocking solution. Finally, sections were mounted on slides with Aquamount (Lerner Laboratories).

The following antibodies were used: GAD65 (mouse, 1:1,000, Chemicon), $GABA_A$-receptor γ2 subunit (rabbit, 1:400, Chemicon), PSD95 (mouse, 1:300, Affinity BioReagents), synapsin I (rabbit, 1:500, Chemicon), c-fos (rabbit, 1:1,000, Santa Cruz sc-52), phosphor-serine 133 CREB (mouse, 1:2,000, Upstate). The Npas4 antibody (rabbit, 1:2,000) was raised against a carboxy-terminal region of Npas4 (amino acids 597–802) and its specificity was tested in $Npas4^{-/-}$ mice (Supplementary Fig. 2).

Synapse density assay. Confocal image acquisition and synapse density measurement were performed as previously described[47]. The perisomatic region of a neuron was defined as the cell body plus a 20-pixel circumference. Each pixel is approximately 0.143 μm. The perisomatic region was excluded from the excitatory synapse density analysis.

Because synapse density and immunostaining vary significantly between experiments, it is necessary to normalize each experiment before combining them. Normalization and error propagation were performed as previously described[47].

Electrophysiology. Slices were perfused with artificial cerebrospinal fluid containing (in mM) 127 NaCl, 25 $NaHCO_3$, 1.25 Na_2HPO_4, 2.5 KCl, 2 $CaCl_2$, 1 $MgCl_2$, 25 glucose, and saturated with 95% O_2, 5% CO_2. The internal solution for mIPSCs contained (in mM) 147 CsCl, 5 Na_2-phosphocreatine, 10 HEPES, 2 MgATP, 0.3 Na_2GTP and 1 EGTA. The internal solution for mEPSCs contained (in mM) 120 cesium methane sulfonate, 10 HEPES, 4 $MgCl_2$, 4 Na_2ATP, 0.4 Na_2GTP, 10 sodium phosphocreatine and 1 EGTA. Osmolarity and pH were adjusted to 300 mOsm and 7.3 with Millipore water and CsOH, respectively. mIPSCs were pharmacologically isolated by bath application of (in μM) 0.5 tetrodotoxin, 10 (R)-CPP and 10 NBQX disodium salt (all from Tocris Bioscience); mEPSCs were isolated with 0.5 tetrodotoxin and 50 picrotoxin (Tocris Bioscience), and augmented with 10 cyclothiazide. Cells with series resistance larger than 25 MΩ during the recordings were discarded.

Data were analysed in IgorPro (Wavemetrics) using custom-written macros. For each trace, the event threshold was set at 1.5 times the root-mean-square current. Currents were counted as events if they crossed the event threshold, had a rapid rise time (1.5 pA ms^{-1}) and had an exponential decay ($2 < \tau < 200$ ms, $1 < \tau < 50$ ms for mIPSC and mEPSC, respectively).

Statistical significance was determined by two methods. First, 50 random points selected from each cell were concatenated to describe the cumulative distributions of events in each condition and then compared by a Kolmogorov–Smirnov test. Second, a Monte Carlo simulation was performed in which points were randomly sampled from each condition and the mean of these samples compared at least 1,000 times. $P < 0.05$ from both tests was considered significant.

DNA microarrays and data analysis. For all microarray experiments, total RNA was purified using RNeasy mini kits (Qiagen) and biotin-labelled cRNA was generated following Affymetrix standard protocols. Ten micrograms of the labelled cRNA was hybridized to Affymetrix mouse MOE430 arrays.

To identify activity-regulated genes, P0 mouse cortical neurons were cultured for 7 days and then depolarized with 50 mM KCl for 1 and 6 h. To identify Npas4-regulated genes, E16 mouse hippocampal neurons were infected (3 DIV) with Npas4-RNAi or control lentivirus, depolarized (8 DIV) with 50 mM KCl, and total RNA was collected 0, 1, 3 and 6 h later. Drebrin, an Npas4 target previously identified in a neuroblastoma cell line[28] was not affected by Npas4-RNAi in post-mitotic neurons.

The DNA-Chip (dChip) software package[49] was used to analyse the microarray data. Genes were considered candidates if they met the following criteria: (1) there was at least a 1.5-fold difference between the experimental and control conditions (depolarized versus non-depolarized, or Npas4-RNAi virus versus control virus) at any of the time points; and (2) there was an absolute difference of more than 100 normalized hybridization intensity units in the expression level between the experimental and control samples.

Chromatin immunoprecipitation. Rat cortical neurons were treated with 1 μM tetrodotoxin and 100 μM AP5 overnight and then stimulated with 55 mM KCl for 2 h at 8 DIV. Chromatin immunoprecipitation was performed as previously described[49]. The following primers were used for quantitative PCR: Chr3, forward: 5′-GACCCCATCCTGTGGTTATG-3′, reverse: 5′-GCAACAAAGGCA AATGGAAT-3′; Npas4, forward: 5′-CAGGATGACTCACACTGACAGTATT TTTAG-3′, reverse: 5′-GTGGGAGAAGAGCTATTTATATCACCAG-3′; BDNF promoter I, forward: 5′-GTGCCTCTCGCCTAGTCATC-3′, reverse: 5′-AGGG AACAACTGCGTGAATC-3′; BDNF promoter IV, forward: 5′-CAGGGAGC TACTCACCCAAC-3′, reverse: 5′-GCACACAGAAGCCAAACCTT-3′; BDNF coding region, forward: 5′-GACAAGGCAACTTGGCCTAC-3′, reverse: 5′-TC GTCAGACCTCTCGAACCT-3′; BDNF 3′ untranslated region, forward: 5′-GA AACGCCACACCTACGAAT-3′, reverse: 5′-GGCACCGAATCCAATTCTAA-3′.

Quantitative reverse transcriptase PCR. The mRNA level of the gene of interest was normalized against the mRNA level of β-tubulin in the same sample. The following primers were used: Npas4, forward: 5′-GCTATA CTCAGAAGGTCCAGAAGGC-3′, reverse: 5′-TCAGAGAATGAGGGTAGCA CAGC-3′; BDNF, forward: 5′-GATGCCGCAAACATGTCTATGA-3′, reverse: 5′-TAATACTGTCACACACGCTCAGCTC-3′; β-tubulin, forward: 5′-CGAC AATGAAGCCCTCTACGAC-3′, reverse: 5′-ATGGTGGCAGACACAAGGTGG TTG-3′.

50. Flavell, S. W. *et al.* Activity-dependent regulation of MEF2 transcription factors suppresses excitatory synapse number. *Science* **311,** 1008–1012 (2006).

CHMP1A encodes an essential regulator of BMI1-INK4A in cerebellar development

Ganeshwaran H Mochida[1–5,18], Vijay S Ganesh[1–3,6,18], Maria I de Michelena[7], Hugo Dias[8], Kutay D Atabay[1–3], Katie L Kathrein[3,9–11], Hsuan-Ting Huang[3,9–11], R Sean Hill[1–3], Jillian M Felie[1–3], Daniel Rakiec[1–3], Danielle Gleason[1–3], Anthony D Hill[12], Athar N Malik[6], Brenda J Barry[1–3], Jennifer N Partlow[1–3], Wen-Hann Tan[1,4], Laurie J Glader[4,13], A James Barkovich[14], William B Dobyns[15], Leonard I Zon[3,4,9–11,16] & Christopher A Walsh[1–4,17]

Charged multivesicular body protein 1A (CHMP1A; also known as chromatin-modifying protein 1A) is a member of the ESCRT-III (endosomal sorting complex required for transport-III) complex[1,2] but is also suggested to localize to the nuclear matrix and regulate chromatin structure[3]. Here, we show that loss-of-function mutations in human *CHMP1A* cause reduced cerebellar size (pontocerebellar hypoplasia) and reduced cerebral cortical size (microcephaly). *CHMP1A*-mutant cells show impaired proliferation, with increased expression of *INK4A*, a negative regulator of stem cell proliferation. Chromatin immunoprecipitation suggests loss of the normal *INK4A* repression by BMI in these cells. Morpholino-based knockdown of zebrafish *chmp1a* resulted in brain defects resembling those seen after *bmi1a* and *bmi1b* knockdown, which were partially rescued by *INK4A* ortholog knockdown, further supporting links between CHMP1A and BMI1-mediated regulation of *INK4A*. Our results suggest that CHMP1A serves as a critical link between cytoplasmic signals and BMI1-mediated chromatin modifications that regulate proliferation of central nervous system progenitor cells.

As part of ongoing studies of human disorders affecting neural progenitor proliferation, we identified three families characterized by underdevelopment of the cerebellum, pons and cerebral cortex (**Fig. 1a–d**). In a consanguineous pedigree of Peruvian origin, three children in two branches were affected (**Fig. 1e**, family 1). Two additional pedigrees from Puerto Rico showed similar pontocerebellar hypoplasia and microcephaly (**Fig. 1e**, families 2 and 3). Brain magnetic resonance imaging (MRI) of affected individuals from all families showed severe reduction of the cerebellar vermis and hemispheres relative to normal individuals. Notably, the cerebellar folds (folia) were relatively preserved, despite the extremely small cerebellar size (**Fig. 1a–d** and **Supplementary Videos 1** and **2**). All affected individuals had severe pontocerebellar hypoplasia, although affected individuals in family 1 showed better motor and cognitive function than those in families 2 and 3 (**Supplementary Note**).

Genome-wide linkage analysis of families 1 and 2 using SNP microarrays implicated only one region on chromosome 16q as linked and homozygous in all six affected individuals (**Fig. 1e** and **Supplementary Fig. 1**), with a maximum multipoint logarithm of odds (LOD) score of 3.68 (**Fig. 1e**). Although families 2 and 3 are not highly informative for linkage analysis, their shared homozygosity provides additional support for the involvement of this locus. Furthermore, families 2 and 3 shared the same haplotype (**Supplementary Fig. 1**), suggesting a founder effect. Sequencing of 42 genes within the candidate interval at 16q24.3 revealed homozygous variants predicted to be deleterious only in the *CHMP1A* gene. *CHMP1A* (NM_002768) consists of seven exons encoding a 196-amino-acid protein (**Supplementary Note**). Affected individuals in families 2 and 3 had a homozygous nonsense variant in exon 3 predicted to prematurely terminate translation (c.88C>T, p.Gln30*; **Fig. 2a**,**b**). Family 1 showed a homozygous variant in intron 2 of *CHMP1A* (c.28–13G>A; **Fig. 2a**,**b**) predicted to create an aberrant splice acceptor site leading to an 11-bp insertion in the spliced mRNA product (**Supplementary Fig. 2a**). The two mutations were absent from dbSNP, 281 neurologically normal European control DNA samples (562 chromosomes), the 1000 Genomes Project database[4] and approximately 5,000 control exomes from the National Heart, Lung, and Blood Institute (NHLBI) Exome Sequencing Project.

[1]Department of Medicine, Division of Genetics, Boston Children's Hospital, Boston, Massachusetts, USA. [2]Manton Center for Orphan Disease Research, Boston Children's Hospital, Boston, Massachusetts, USA. [3]Howard Hughes Medical Institute, Boston Children's Hospital, Boston, Massachusetts, USA. [4]Department of Pediatrics, Harvard Medical School, Boston, Massachusetts, USA. [5]Pediatric Neurology Unit, Department of Neurology, Massachusetts General Hospital, Boston, Massachusetts, USA. [6]Harvard–Massachusetts Institute of Technology (MIT) Division of Health Sciences and Technology, Cambridge, Massachusetts, USA. [7]Department of Morphologic Sciences, Cayetano Heredia University, Lima, Peru. [8]Institute for Child Development–ARIE, Lima, Peru. [9]Stem Cell Program, Boston Children's Hospital, Boston, Massachusetts, USA. [10]Division of Hematology/Oncology, Boston Children's Hospital, Boston, Massachusetts, USA. [11]Dana-Farber Cancer Institute, Boston, Massachusetts, USA. [12]Department of Neurology, Boston Children's Hospital, Boston, Massachusetts, USA. [13]Complex Care Service, Division of General Pediatrics, Boston Children's Hospital, Boston, Massachusetts, USA. [14]Department of Radiology and Biomedical Imaging, University of California, San Francisco, San Francisco, California, USA. [15]Center for Integrative Brain Research, University of Washington, Seattle, Washington, USA. [16]Harvard Stem Cell Institute, Cambridge, Massachusetts, USA. [17]Department of Neurology, Harvard Medical School, Boston, Massachusetts, USA. [18]These authors contributed equally to the work. Correspondence should be addressed to C.A.W. (christopher.walsh@childrens.harvard.edu).

Received 7 May; accepted 5 September; published online 30 September 2012; doi:10.1038/ng.2425

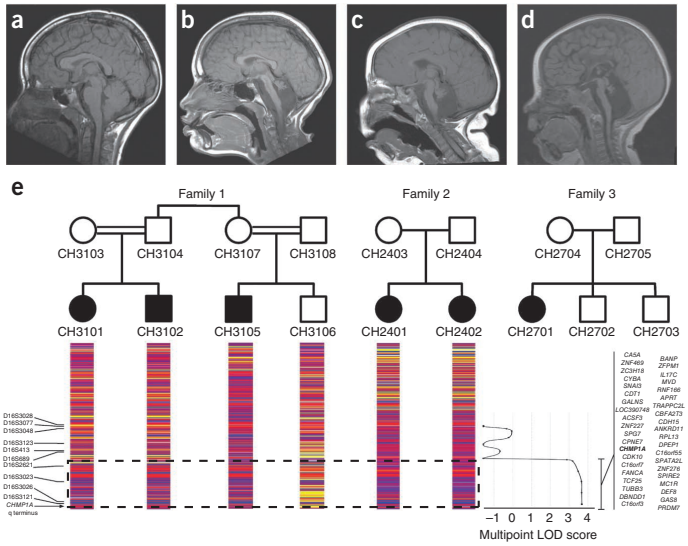

Figure 1 Brain MRI and linkage mapping of pontocerebellar hypoplasia with microcephaly. (**a**–**d**) T1-weighted sagittal brain MRIs of a neurologically normal individual (**a**) and affected individuals CH3102 (**b**), CH2402 (**c**) and CH2701 (**d**). Compared to control, affected individuals show mild reduction in cortical volume, thinning of the corpus callosum and severe hypoplasia of the pons, cerebellar vermis and cerebellar hemispheres. (**e**) Family 1 is a consanguineous pedigree from Peru in which three children from two branches are affected. Families 2 and 3 are both from Puerto Rico. Affymetrix 250K Sty SNP data for each child in families 1 and 2 are shown below (red or blue, homozygous SNP call; yellow, heterozygous SNP call), showing a region of homozygosity (dashed box) shared by all affected individuals in distal chromosome 16q. The graph aligned with the SNP genotyping data shows multipoint LOD scores calculated from microsatellite maker analysis of family 1 (**Supplementary Fig. 1**). Genes in the region of LOD of >3 are indicated to the right of the graph.

We sequenced *CHMP1A* in 64 individuals with other cerebellar anomalies without finding additional mutations, but none of these affected individuals shared the rare and distinctive pattern of hypoplasia seen in the individuals with *CHMP1A* mutations.

RT-PCR analysis of *CHMP1A* in lymphoblastoid cells from affected individuals from family 1 (CH3101 and CH3105) identified the predicted aberrant transcript with the 11-bp insertion and a second aberrant transcript with a 21-bp insertion but no normal *CHMP1A* transcript (**Supplementary Fig. 2b**). In the parents of affected children from family 1 and in unaffected control samples, only the normal transcript was detected, suggesting that the abnormal splice products are unstable. Protein blot analysis revealed a single 24-kDa band in a normal control individual, but no corresponding band was detected in affected individuals from families 1 and 2 (CH3101 and CH2401, respectively; **Fig. 2c**). In the parent (CH3103), the amount of CHMP1A was 50% relative to the amount detected in control lysate. Hence, this genetic study establishes *CHMP1A* null mutations as the cause of pontocerebellar hypoplasia and microcephaly in these pedigrees.

CHMP1A has been assigned two distinct putative functions as both a chromatin-modifying protein and a charged multivesicular

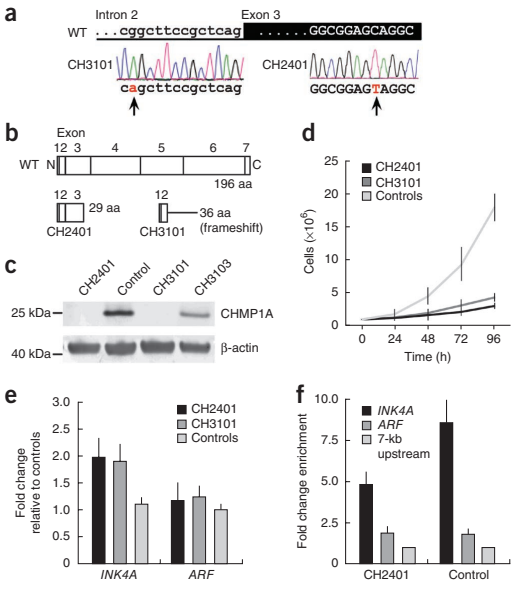

Figure 2 Loss-of-function mutations in *CHMP1A* and dysregulation of *INK4A* in cell lines from affected individuals. (**a**) Chromatograms showing homozygous mutations (red, indicated by arrows) in intron 2 (CH3101; c.28–13G>A; white background) and in exon 3 (CH2401; c.88C>T; black background) of *CHMP1A*. (**b**) Schematic of full-length wild-type (WT) CHMP1A. The mutation in CH2401 leads to premature termination of translation. The intronic mutation in CH3101 creates a novel splice acceptor site, and usage of this novel acceptor site causes a frameshift after exon 2, resulting in termination of translation after 36 amino acids. (**c**) Protein blotting of lysates from lymphoblastoid cell lines from CH2401 and CH3101 showing a complete loss of the 24-kDa band detected by antibody to CHMP1A in control lysate. Lysate from a cell line generated from CH3103 (the mother of CH3101) show 50% of the protein amount relative to the control. Protein amounts were normalized to the 40-kDa β-actin loading control bands. (**d**) Lymphoblastoid cell lines from CH2401 and CH3101 proliferate at a much lower rate than eight control cell lines. (**e**) qPCR analysis of *CDKN2A*-derived cDNA levels in human lymphoblastoid cell lines from CH2401 and CH3101 (normalized to *GAPDH* levels) shows nearly twofold higher expression of *INK4A* in these cells relative to four unrelated, neurologically normal control cell lines. The other transcribed isoform at the locus, *ARF*, shows no significant difference in expression in cells from affected individuals and control cells. (**f**) ChIP-qPCR in lymphoblastoid cell lines using an antibody to BMI1 shows an approximately eightfold enrichment of *INK4A* promoter DNA relative to a probe targeted 7-kb upstream of the locus in a control cell line. Enrichment is nearly half of this in cell lines derived from CH2401 with a homozygous mutation in *CHMP1A*. Enrichment at the *ARF* promoter is not significantly different from that observed in the control cell line. Error bars in **d**–**f**, s.e.m.

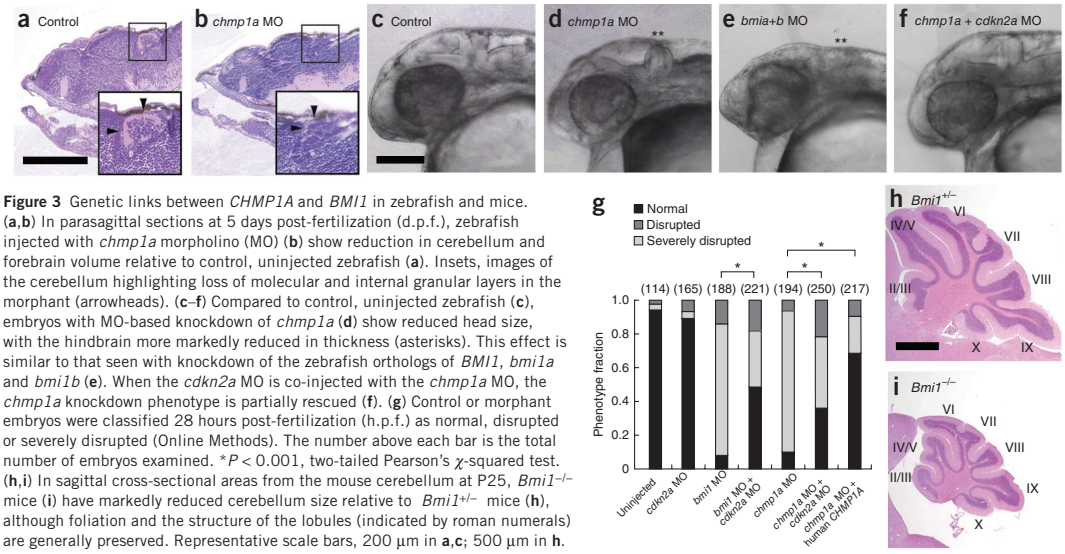

Figure 3 Genetic links between *CHMP1A* and *BMI1* in zebrafish and mice. (**a**,**b**) In parasagittal sections at 5 days post-fertilization (d.p.f.), zebrafish injected with *chmp1a* morpholino (MO) (**b**) show reduction in cerebellum and forebrain volume relative to control, uninjected zebrafish (**a**). Insets, images of the cerebellum highlighting loss of molecular and internal granular layers in the morphant (arrowheads). (**c**–**f**) Compared to control, uninjected zebrafish (**c**), embryos with MO-based knockdown of *chmp1a* (**d**) show reduced head size, with the hindbrain more markedly reduced in thickness (asterisks). This effect is similar to that seen with knockdown of the zebrafish orthologs of *BMI1*, *bmi1a* and *bmi1b* (**e**). When the *cdkn2a* MO is co-injected with the *chmp1a* MO, the *chmp1a* knockdown phenotype is partially rescued (**f**). (**g**) Control or morphant embryos were classified 28 hours post-fertilization (h.p.f.) as normal, disrupted or severely disrupted (Online Methods). The number above each bar is the total number of embryos examined. $^*P < 0.001$, two-tailed Pearson's χ-squared test. (**h**,**i**) In sagittal cross-sectional areas from the mouse cerebellum at P25, *Bmi1*$^{-/-}$ mice (**i**) have markedly reduced cerebellum size relative to *Bmi1*$^{+/-}$ mice (**h**), although foliation and the structure of the lobules (indicated by roman numerals) are generally preserved. Representative scale bars, 200 μm in **a**,**c**; 500 μm in **h**.

body protein[1,3]. CHMP1A was originally identified as a binding partner of the Polycomb group protein Pcl (Polycomblike)[3]. In the nucleus, it has been suggested to recruit the Polycomb group transcriptional repressor BMI1 to heterochromatin, and overexpressed CHMP1A has been shown to arrest cells in S phase[3]. In the cytoplasm, CHMP1A is part of the ESCRT-III complex[1,2]. The ESCRT-III complex localizes to endosomes and interacts with VPS4A and VPS4B[5] to assist in the trafficking of ubiquitinated cargo proteins to the lysosome for degradation[6].

We investigated the potential effects of CHMP1A on Polycomb function by analysis of cell lines from two affected individuals harboring different *CHMP1A* mutations (CH3101 from family 1 and CH2401 from family 2), which show severely impaired doubling times compared to control cell lines, suggesting essential roles for CHMP1A in regulating cell proliferation (**Fig. 2d**). To examine BMI1 function in these cells, we performed quantitative PCR (qPCR) analysis of expression of the BMI1 target locus *CDKN2A*, which encodes alternative transcripts *INK4A* (also known as p16^{INK4A}; NM_000077) and *ARF* (also known as p14^{ARF}; NM_058195) in humans. This analysis revealed abnormally high expression of *INK4A*, the isoform implicated in cerebellar development, but not of *ARF* (**Fig. 2e**), suggesting derepression of *INK4A*. Chromatin immunoprecipitation (ChIP) with an antibody to BMI1 in control cell lines showed an approximately eightfold enrichment of BMI1 binding at *INK4A* promoter DNA relative to a control region 7 kb upstream, whereas cells from an affected individual (CH2401) showed only approximately half this enrichment in BMI1 binding (**Fig. 2f**). Enrichment of BMI1 at the *ARF* promoter was not substantial in this assay and was similar in both control cells and cell lines from affected individuals, consistent with the specificity of regulation of the *INK4A* isoform by BMI1 (**Fig. 2f**). Bmi1 has been shown to suppress the *Cdkn2a* locus and be required for neural stem cell self-renewal[7]. Our evidence suggests a role for CHMP1A in mediating BMI1-directed epigenetic silencing at the *INK4A* promoter but not at the *ARF* promoter.

We further explored the relationship between CHMP1A and BMI1 using morpholino-based knockdown experiments in zebrafish. Knockdown of the zebrafish *CHMP1A* ortholog (*chmp1a*; NM_200563) resulted in reduced cerebellum and forebrain volume compared to control, uninjected zebrafish, similar to the effects of human *CHMP1A* mutations and knockdown in zebrafish of *BMI1* orthologs (*bmi1a*, NM_194366, and *bmi1b*, NM_001080751; **Fig. 3a–e** and **Supplementary Figs. 3** and **4**). A second morpholino targeting *chmp1a* led to a similar phenotype, and both morpholinos were partially rescued by the introduction of human *CHMP1A* mRNA, confirming morpholino specificity (**Supplementary Fig. 4**). The cerebellum consists of five major cell types, with the principal cell, known as the Purkinje cell, deriving from the ventricular epithelium, whereas granule cells derive from a separate progenitor pool known as the rhombic lip. Granule cell precursors then migrate over the outer surface of the cerebellum and form the external germinal layer (EGL) before migrating radially past the Purkinje cells to settle in the internal granule layer (IGL)[8]. Within the *chmp1a*-morphant cerebellum, the internal granule and molecular layers were severely affected (**Fig. 3a**,**b**), which is consistent with the relatively preserved folia pattern of the human cerebellum (thought to primarily be established by Purkinje cells) and severely reduced volume (which is determined mainly by granule cell quantity).

We then tested genetic interactions between *chmp1a* and the zebrafish ortholog of *INK4A* (*cdkn2a*; XM_002660468). Knockdown of *cdkn2a* alone did not result in noticeable abnormalities, and double knockdown of *chmp1a* and *cdkn2a* resulted in partial rescue of the brain morphology defects seen with *chmp1a* knockdown (**Fig. 3f**,**g**). This rescue was analogous to the rescue of the *Bmi1*-knockout mouse cerebellar phenotype in *Bmi1*- and *Cdkn2a*-double knockout mice[9]. Of note, there were also parallels in brain morphology between individuals with *CHMP1A* mutations and *Bmi1*-deficient mice, which show cerebellar hypoplasia[10,11] (**Fig. 3h**,**i**). In *Bmi1*-null mice, the cerebellar architecture was generally preserved, but the thickness of the granular and molecular layers was markedly reduced[10], and *Bmi1*-deficient

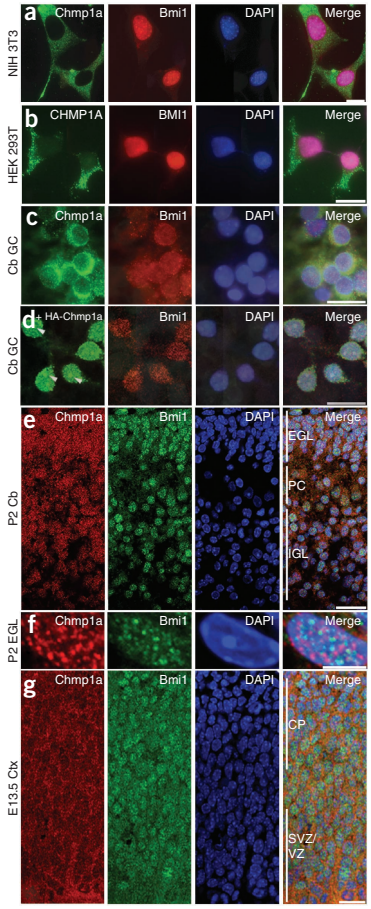

Figure 4 CHMP1A and BMI1 expression in cultured cells and the developing mouse brain. (**a**,**b**) Immunocytochemical analysis of NIH 3T3 cells (**a**) and HEK 293T cells (**b**). (**c**,**d**) Immunocytochemical analysis of mouse dissociated cerebellar granule cells (Cb GC) (**c**) and of these cells transfected with an expression construct encoding HA-tagged Chmp1a (**d**). Arrowheads indicate nuclear punctate staining for HA-Chmp1a. (**e**,**f**) Immunocytochemical analysis in mice of the developing cerebellum at P2 (P2 Cb) (**e**), P2 EGL cells (**f**) and the developing cerebral cortex at E13.5 (E13.5 Ctx) (**g**). EGL, external germinal layer; PC, Purkinje cells; IGL, internal granule layer; SVZ, subventricular zone; VZ, ventricular zone; CP, cortical plate. Scale bars, 20 µm in **a**–**e**,**g**; 5 µm in **f**.

mice show a modest reduction in cerebral volume[10,12], similar to individuals with *CHMP1A* mutations (**Supplementary Note**).

Subcellular localization of CHMP1A seems to vary depending on the cell type. Confocal images of NIH 3T3 cells showed prominent exclusion of Chmp1a from the nucleus (mouse *Chmp1a*, NM_145606), where Bmi1 was detected (**Fig. 4a**). In contrast, confocal images of HEK 293T cells, although also showing predominantly cytoplasmic localization of CHMP1A, showed some nuclear immunoreactivity as well (**Fig. 4b**). Primary cultures of cerebellar granule cells from mice also showed predominantly cytoplasmic localization of Chmp1a, along with a speckled nuclear pattern (**Fig. 4c**). Overexpression of HA-tagged mouse Chmp1a in cultured granule cells resulted in abundant nuclear Chmp1a with a punctate expression pattern, confirming the speckled nuclear localization of endogenous Chmp1a (**Fig. 4d**) and consistent with earlier reports that CHMP1A can be present in the nucleus[3]. Even with Chmp1a overexpression, Chmp1a and Bmi1 do not prominently colocalize within the nucleus, which is also in agreement with previous data[3].

Immunohistochemical studies of the developing cerebellum and cerebral cortex in mice revealed widespread expression of Chmp1a in dividing and postmitotic cells. Chmp1a immunoreactivity was seen in the nucleus and cytoplasm of EGL, Purkinje and IGL cells at postnatal day (P) 2 (**Fig. 4e**,**f** and **Supplementary Fig. 5**). In the nucleus of these cells, Chmp1a immunoreactivity was seen in a speckled pattern. These speckles may be seen adjacent to Bmi1 signals, but they usually did not colocalize (**Fig. 4f** and **Supplementary Fig. 5**). At later stages of cerebellar development (P4, P10 and P29), Chmp1a expression persisted in Purkinje and granule cells (**Supplementary Fig. 6**). Embryonic day (E) 13.5 cerebral cortex showed widespread Chmp1a expression in the neuroepithelial cells (**Fig. 4g**). In the postnatal cerebral cortex (at P4, P10 and P29), Chmp1a expression in postmitotic neurons of the cortical plate gradually decreased and became almost undetectable by P29 (**Supplementary Fig. 6**). These expression studies confirm that Bmi1 and Chmp1a are often expressed in the same cells. However, the absence of widespread subcellular colocalization of Bmi1 and Chmp1a suggests that the regulation of Bmi1 by Chmp1a is perhaps not mediated by direct physical interaction.

Our data implicate CHMP1A as an essential central nervous system regulator of BMI1, which in turn is a key regulator of stem cell self-renewal. The dual cytoplasmic and nuclear localization of CHMP1A and its connection to the ESCRT-III complex position CHMP1A as a potentially crucial link between cytoplasmic signals and the global regulation of stem cells via the Polycomb complex.

URLs. UCSC Human Genome Browser, http://genome.ucsc.edu/; Primer3, http://frodo.wi.mit.edu/primer3/; NetGene2, http://www.cbs.dtu.dk/services/NetGene2/; dbSNP, http://www.ncbi.nlm.nih.gov/projects/SNP/; 1000 Genomes Project, http://www.1000genomes.org/; NHLBI Exome Sequencing Project, http://evs.gs.washington.edu/EVS/.

METHODS

Methods and any associated references are available in the online version of the paper.

Note: Supplementary information is available in the online version of the paper.

ACKNOWLEDGMENTS

We thank the individuals and their families reported herein for their participation in this research. We thank M. van Lohuizen (Netherlands Cancer Institute) for providing the *Bmi1*-knockout mice, A. Wagers for help with breeding the *Bmi1*-knockout mice and P. Baas for sharing human DNA samples. This research was supported by grants from the US National Institute of Neurological Disorders and Stroke (NINDS; R01NS035129) and the Fogarty International Center (R21TW008223) to C.A.W., the Dubai Harvard Foundation for Medical Research, the Simons Foundation and the Manton Center for Orphan Disease Research. G.H.M. was supported by the Young Investigator Award of the National Alliance for Research on Schizophrenia and Depression (NARSAD) as a NARSAD Lieber Investigator. V.S.G. is supported by the Medical Scientist Training Program of Harvard Medical School, with financial support from the US National institute of General Medical Sciences (NIGMS). C.A.W. and L.I.Z. are investigators of the Howard Hughes Medical Institute. Microscopy and image analyses were performed with support from the Cellular Imaging Core of the Boston Children's Hospital Intellectual and Developmental Disabilities Research Center.

AUTHOR CONTRIBUTIONS

G.H.M. designed the study, interpreted clinical information and brain MRIs, identified the disease locus, helped sequence candidate genes, analyzed the sequencing data to identify *CHMP1A* mutations, helped analyze the functional data and wrote the manuscript. V.S.G. performed RT-PCR, protein blots, mouse histology and immunohistochemistry, qPCR, ChIP and zebrafish morpholino experiments and wrote the manuscript. M.I.d.M. and H.D. ascertained family 1 and provided clinical information. K.D.A. performed zebrafish protein blots and mouse immunohistochemistry. K.L.K. performed the morpholino injections. H.-T.H. and L.I.Z. assisted with the morpholino experiments. R.S.H. helped organize genetic data and calculate LOD scores. J.M.F. and D.G. organized human samples and helped perform sequencing experiments. D.R. organized human samples and helped perform microsatellite analysis. A.D.H. assisted in immunohistochemical studies and imaging. A.N.M. assisted in ChIP. B.J.B. and J.N.P. organized clinical information and human samples. W.-H.T. and L.J.G. provided clinical information for family 3. A.J.B. interpreted the brain MRIs of the affected individuals. W.B.D. ascertained family 2 and provided clinical information. C.A.W. directed the overall research and wrote the manuscript.

COMPETING FINANCIAL INTERESTS

The authors declare competing financial interests: details are available in the online version of the paper.

Published online at http://www.nature.com/doifinder/10.1038/ng.2425.
Reprints and permissions information is available online at http://www.nature.com/reprints/index.html.

1. Howard, T.L., Stauffer, D.R., Degnin, C.R. & Hollenberg, S.M. CHMP1 functions as a member of a newly defined family of vesicle trafficking proteins. *J. Cell Sci.* **114**, 2395–2404 (2001).
2. Tsang, H.T. *et al.* A systematic analysis of human CHMP protein interactions: additional MIT domain–containing proteins bind to multiple components of the human ESCRT III complex. *Genomics* **88**, 333–346 (2006).
3. Stauffer, D.R., Howard, T.L., Nyun, T. & Hollenberg, S.M. CHMP1 is a novel nuclear matrix protein affecting chromatin structure and cell-cycle progression. *J. Cell Sci.* **114**, 2383–2393 (2001).
4. 1000 Genomes Project Consortium. A map of human genome variation from population-scale sequencing. *Nature* **467**, 1061–1073 (2010).
5. Stuchell-Brereton, M.D. *et al.* ESCRT-III recognition by VPS4 ATPases. *Nature* **449**, 740–744 (2007).
6. Scita, G. & Di Fiore, P.P. The endocytic matrix. *Nature* **463**, 464–473 (2010).
7. Molofsky, A.V. *et al.* Bmi-1 dependence distinguishes neural stem cell self-renewal from progenitor proliferation. *Nature* **425**, 962–967 (2003).
8. Garel, C., Fallet-Bianco, C. & Guibaud, L. The fetal cerebellum: development and common malformations. *J. Child Neurol.* **26**, 1483–1492 (2011).
9. Jacobs, J.J., Kieboom, K., Marino, S., DePinho, R.A. & van Lohuizen, M. The oncogene and Polycomb-group gene *bmi-1* regulates cell proliferation and senescence through the *ink4a* locus. *Nature* **397**, 164–168 (1999).
10. Leung, C. *et al.* Bmi1 is essential for cerebellar development and is overexpressed in human medulloblastomas. *Nature* **428**, 337–341 (2004).
11. van der Lugt, N.M. *et al.* Posterior transformation, neurological abnormalities, and severe hematopoietic defects in mice with a targeted deletion of the *bmi-1* proto-oncogene. *Genes Dev.* **8**, 757–769 (1994).
12. Zencak, D. *et al. Bmi1* loss produces an increase in astroglial cells and a decrease in neural stem cell population and proliferation. *J. Neurosci.* **25**, 5774–5783 (2005).

ONLINE METHODS

Genetic screening. The genetic study was approved by the Institutional Review Boards of Boston Children's Hospital and the University of Chicago. Appropriate informed consent was obtained from all involved human subjects.

The affected individuals and their parents from family 1 and the affected individuals from family 2 were subjected to genome-wide SNP screening with the Affymetrix GeneChip Human Mapping 250K Sty Array, performed at the Microarray Core of the Dana-Farber Cancer Institute. Microsatellite markers for fine mapping were identified using the UCSC Human Genome Browser[13] and were synthesized with fluorescent labels (Sigma-Genosys). Two-point and multipoint LOD scores were calculated using Allegro[14], assuming recessive inheritance with full penetrance and a disease allele frequency of 0.001. Sequencing primers were designed using Primer3 (ref. 15), and genomic DNA was sequenced using standard Sanger technology. Control DNA samples from neurologically normal individuals of European descent were obtained from the Coriell Cell Repositories (Coriell Institute for Medical Research). All nucleotide numbers are in reference to *CHMP1A* isoform 2 cDNA (NM_002768, with A of the ATG start site corresponding to +1) from the UCSC Genome Browser.

Analysis of *CHMP1A* splicing. Splice prediction software NetGene2 (ref. 16) was used to determine the effect of the family 1 allele on *CHMP1A* splicing. Epstein-Barr virus (EBV)-transformed lymphocytes were grown in RPMI-1640 (Gibco) with 15% FBS (Gibco) and 1% penicillin/streptomycin in (Lonza) a humidified incubator at 37 °C in 5% CO_2. RNA was isolated using the RNeasy Mini kit (Qiagen). Total RNA (5 µg) was used for first-strand synthesis with oligo(dT) primers and SuperScript III First-Strand Synthesis SuperMix (Invitrogen), and 1 µl of the product was used for the subsequent PCR reaction, with primers mapping from the 5′ UTR to exon 6 of *CHMP1A* (NM_002768). Primer sequences are listed in **Supplementary Table 1**.

Proliferation assay of lymphoblastoid cell lines. EBV-transformed lymphoblastoid cell lines from eight control subjects and two affected individuals (CH2401 and CH3101) were grown. For each cell line, 2×10^7 cells were grown, and 1×10^6 cells were aliquoted into 4 sets of 5 T25 flasks filled with 10 ml of medium. Each set was allowed to grow for 24, 48, 72 and 96 h. Cell densities were estimated using a hemocytometer.

qPCR. EBV-transformed lymphoblastoid cell lines were grown, and cDNA was generated. *INK4A* and *ARF* levels were quantified using the StepOnePlus Real-Time PCR System (Applied Biosystems) with *GAPDH* as a control. Primer sequences are listed in **Supplementary Table 1**.

ChIP assays. ChIP was assays were performed as previously described[17] with some modifications. For a single experiment, 2×10^7 EBV-transformed lymphoblastoid cells and 4 µg of the antibody to BMI1 (Abcam, ab14389) were used. qPCR reactions were performed using SYBR Green reagents (Applied Biosystems) and the StepOnePlus Real-Time PCR System. Primers were assessed for specificity by analysis of their melt curves, and a standard curve was determined using four tenfold serial dilutions for each primer using the input DNA samples. The standard curve from the input DNA was determined using 3 µl from each serial dilution as a template. Fold enrichment for each ChIP sample was determined by using 3 µl from each sample as a template and comparing the resultant amplification to the standard curve for that primer pair. Primer sequences are listed in **Supplementary Table 1**.

Zebrafish morpholino experiments. ATG-targeting morpholinos were designed against *chmp1a* (*chmp1a* MO 1), *bmi1a*, *bmi1b* and the *INK4A* zebrafish ortholog (*cdkn2a*) (Gene Tools). In all experiments where *bmi1* morpholinos were used, *bmi1a* and *bmi1b* were injected together. Injections were performed at the one-cell stage. Optimal doses for the *chmp1a* MO 1, *bmi1a* and *bmi1b*, and *cdkn2a* morpholinos were 4.5, 1.2 and 4.0 ng, respectively. At 28 h.p.f., the embryos were visualized using a stereo microscope (Zeiss). To confirm the specificity of the effects of the *chmp1a* MO 1 morpholino, a second ATG-targeting *chmp1a* morpholino (*chmp1a* MO 2) was designed. For this experiment, the dosages of injected *chmp1a* MO 1 and *chmp1a* MO 2 were 6.0 and 3.0 ng, respectively. Morpholino sequences are listed in **Supplementary Table 1**.

For the rescue experiment, morphants were screened at 28 h.p.f. and scored for the presence of a defect in the angle of the head to the tail (measured at the otic vesicle) or a deviation in the straightness of the tail[18]. Human *CHMP1A* cDNA was PCR amplified from control human lymphoblastoid cell total RNA. Primer sequences are listed in **Supplementary Table 1**. The PCR product was subcloned into the pCS2+ vector, and 5′-capped mRNA was synthesized *in vitro* using the mMESSAGE kit (Ambion). mRNA was diluted in 0.1 M KCl and was titrated for the rescue experiments.

For histological preparation, morphants were grown at 28 °C for 5 d, fixed overnight at 4 °C in paraformaldehyde (PFA) and embedded in 3% low-melt agarose blocks (in PBS), which were fixed again in 4% PFA in PBS overnight. The fixed agarose blocks were embedded in paraffin and sectioned at 5-µm thickness in the sagittal plane. Sections were stained by standard techniques with hematoxylin and eosin and were visualized using a bright field microscope (Nikon).

For protein blotting, zebrafish embryos were harvested at 48 h.p.f. They were dechorionated and deyolked as described[19] and treated with lysis buffer (10% SDS and 0.5 M EDTA in 1× PBS) containing Complete Mini Protease Inhibitor Cocktail (Roche). Lysates were mixed with 2× Laemmli sample buffer, loaded onto a NuPage 4–12% Bis-Tris gel (Invitrogen) and run at 100 V for 2 h. Proteins were wet transferred onto Immobilon-P transfer membrane (Millipore) at 300 mA for 1.5 h at 4 °C. The membrane was blocked with Odyssey Blocking Buffer (LI-COR) and was incubated first with antibodies against Chmp1a (1:100 dilution; Abcam, ab104103) and β-actin (1:10,000 dilution; Abcam, ab6276) and then with IRDye secondary antibodies (LI-COR, 926-32212 and 926-68023). The LI-COR Imaging System was used for imaging and quantification.

Immunocytochemistry and immunohistochemistry. NIH 3T3 and HEK 293T cells were grown in DMEM with 10% FBS and 1% penicillin/streptomycin and were fixed and stained with antibodies against Chmp1a (1:200 dilution; Abcam, ab36679) and Bmi1 (1:250 dilution; Abcam, ab14389) using standard techniques. Staining was visualized on a confocal microscope (Nikon).

All animal work was approved by Harvard Medical School, Beth Israel Deaconess Medical School and Boston Children's Hospital Institutional Animal Care and Use Committees.

Cerebellar granule neuron cultures from euthanized, P5 mouse pups were prepared as described[20]. After dissociation, cell density was measured using a hemocytometer, and 1×10^6 cells were plated on each poly-L-ornithine–coated coverslip with 500 µl of plating medium in a 24-well plate. After 1 d *in vitro* (d.i.v.) in a 37 °C incubator, 20 µl of 250 µM AraC (cytosine-1-β-D-arabinofuranoside) was added to each well to arrest mitosis of non-neurons. At 2 d.i.v., conditioned medium was collected from each well, and the wells were washed with DMEM. Cells were then transfected with the HA-Chmp1a mammalian expression construct (GeneCopoeia, EX-Mm15805-M06). Transfection solution (87.6 µl of HBSS and 4.4 µl of 2.5 M calcium chloride with 1.5 µg of plasmid DNA) was prepared at room temperature, and 35 µl of the transfection solution was added to a total of 400 µl of conditioned medium and then added to each well. After an additional 36 h (4 d.i.v.), cells were fixed with 4% PFA for 20 min at room temperature, washed with PBS and stained with antibodies against HA (1:100 dilution; Abcam, ab9110) and Bmi1 (1:250 dilution; Abcam, ab14389). Untransfected cells were processed similarly and were stained with antibodies against Chmp1a (1:200 dilution; Abcam, ab36679) and Bmi1.

Tissues were perfused with 4% PFA, dissected and fixed overnight in 4% PFA and were then embedded in paraffin and sectioned at 5- or 8-µm thickness. After rehydration of the slides in serial washes with xylene, 50% xylene in ethanol, 100% ethanol, 70% ethanol, 50% ethanol, 30% ethanol and finally in PBS, the slides were boiled in antigen-retrieval solution (Retrievagen A, BD Biosciences) for 8 min in the autoclave. Slides were blocked with PBS with 0.1% Triton X-100 supplemented with 1% donkey serum for 1 h at room temperature, and antibodies against Bmi1 (1:400 dilution; Millipore, clone F6), Chmp1a (1:300 dilution; Abcam, ab36679 and ab104103) or calbindin (Swant, CB300) were added in the blocking solution for overnight incubation at 4 °C. Slides were washed three times for 5 min per wash in PBS and were developed with secondary antibodies conjugated to Alexa-Fluor dyes (Invitrogen) for 1.5 h at room temperature. Slides were again washed three times for 5 min per wash in PBS and were mounted with Fluoromount-G

(Southern Biotech) containing DAPI (1:1,000 dilution) and visualized on a confocal microscope (Nikon) or fluorescence microscope (Zeiss). For E13.5 and P2 cerebral cortex, frozen section specimens were used. For frozen sections, heads of E13.5 mouse embryos were directly fixed in 4% PFA, and P2 pups were perfused with 2 ml of 1× PBS and then with 4 ml of 4% PFA in PBS, followed by overnight fixation in 4% PFA. They were then placed in gradually increasing sucrose solutions (10%, 15% and 30%), each overnight, for cryopreservation and were then embedded in optimum cutting temperature (OCT) compound (Sakura Finetek) and sectioned at 20-µm thickness. The same antigen retrieval and staining procedure was used as for the paraffin-embedded sections.

13. Kent, W.J. *et al.* The human genome browser at UCSC. *Genome Res.* **12**, 996–1006 (2002).
14. Gudbjartsson, D.F., Jonasson, K., Frigge, M.L. & Kong, A. Allegro, a new computer program for multipoint linkage analysis. *Nat. Genet.* **25**, 12–13 (2000).
15. Rozen, S. & Skaletsky, H.J. Primer3 on the WWW for general users and for biologist programmers. in *Bioinformatics Methods and Protocols: Methods in Molecular Biology* (eds. Krawetz, S. & Misener, S.) 365–386 (Humana Press, Totowa, New Jersey, 2000).
16. Brunak, S., Engelbrecht, J. & Knudsen, S. Prediction of human mRNA donor and acceptor sites from the DNA sequence. *J. Mol. Biol.* **220**, 49–65 (1991).
17. Flavell, S.W. *et al.* Genome-wide analysis of MEF2 transcriptional program reveals synaptic target genes and neuronal activity–dependent polyadenylation site selection. *Neuron* **60**, 1022–1038 (2008).
18. Kimmel, C.B., Ballard, W.W., Kimmel, S.R., Ullmann, B. & Schilling, T.F. Stages of embryonic development of the zebrafish. *Dev. Dyn.* **203**, 253–310 (1995).
19. Link, V., Shevchenko, A. & Heisenberg, C.P. Proteomics of early zebrafish embryos. *BMC Dev. Biol.* **6**, 1 (2006).
20. Bilimoria, P.M. & Bonni, A. Cultures of cerebellar granule neurons. *CSH Protoc.* **2008**, pdb prot5107 (2008).

A chemical genetic approach reveals distinct EphB signaling mechanisms during brain development

Michael J Soskis[1,5], Hsin-Yi Henry Ho[1,5], Brenda L Bloodgood[1], Michael A Robichaux[2], Athar N Malik[1], Bulent Ataman[1], Alex A Rubin[1], Janine Zieg[1], Chao Zhang[3,4], Kevan M Shokat[3], Nikhil Sharma[1], Christopher W Cowan[2,4] & Michael E Greenberg[1]

EphB receptor tyrosine kinases control multiple steps in nervous system development. However, it remains unclear whether EphBs regulate these different developmental processes directly or indirectly. In addition, given that EphBs signal through multiple mechanisms, it has been challenging to define which signaling functions of EphBs regulate particular developmental events. To address these issues, we engineered triple knock-in mice in which the kinase activity of three neuronally expressed EphBs can be rapidly, reversibly and specifically blocked. We found that the tyrosine kinase activity of EphBs was required for axon guidance *in vivo*. In contrast, EphB-mediated synaptogenesis occurred normally when the kinase activity of EphBs was inhibited, suggesting that EphBs mediate synapse development by an EphB tyrosine kinase–independent mechanism. Taken together, our data indicate that EphBs control axon guidance and synaptogenesis by distinct mechanisms and provide a new mouse model for dissecting EphB function in development and disease.

The EphB family of receptor tyrosine kinases (RTKs) are critical regulators of cell-cell contacts in the developing nervous system, mediating processes as diverse as axon guidance, topographic mapping, neuronal migration and synapse formation[1–3]. In addition to these developmental roles, EphB dysfunction in the mature organism contributes to pathologies such as cancer, Alzheimer's disease and, possibly, autism[4–8]. The signaling mechanisms underlying EphB-mediated development and disease are largely unknown.

As the EphB family of receptors has been shown to regulate a large number of developmental processes, it has been particularly difficult to determine the specific functions of EphBs at defined times during brain development. The presence of at least three partially redundant EphB family members in the nervous system further complicates investigation into the biological functions of EphB proteins. For example, *Ephb1*, *Ephb2* and *Ephb3* single and compound mutant mice have defects in a number of processes, including stem-cell proliferation, axon guidance, filopodial motility, dendritic spine formation, synapse development and long-term potentiation, but it is unclear which of these interdependent phenotypes are direct and which are secondary to the disruption of EphB signaling at an earlier developmental step[9–13].

Another major hurdle in understanding the function of EphBs is the complex nature of their signaling capabilities. EphBs can engage in bidirectional signaling with their transmembrane ligands, the ephrin-Bs. In the forward direction of signaling, the interaction of clustered ephrin-B ligands on one cell with EphB receptors on another leads to EphB oligomerization and auto-phosphorylation, the induction of EphB kinase activity, and the recruitment of cytoplasmic proteins via SH2-binding and PDZ-binding motifs of EphBs[14]. In addition, the extracellular region of EphBs, which contains fibronectin repeat domains, can recruit binding partners such as subunits of the NMDA subtype of glutamate receptor[15,16]. In the reverse direction of EphB and ephrin-B signaling, phosphorylation of the cytoplasmic tail of ephrin-Bs results in the recruitment of SH2 domain–containing proteins and initiation of downstream signal transduction[17]. Thus, through a complex array of potential signaling pathways, EphBs are able to mediate a wide range of processes during nervous system development.

For the most part, it remains unknown which cellular processes require EphB RTK activity and which cellular responses are mediated by EphB tyrosine kinase–independent signaling events. Cytoplasmic deletions of EphBs have been used to assess the requirement of the intracellular domain in mediating specific EphB-regulated processes, but this approach fails to distinguish kinase activity from other modes of cytoplasmic signaling[18]. In particular, given that ephrin-B binding to EphBs induces the formation of EphB oligomers in the plasma membrane, it remains a likely possibility that EphB oligomerization and scaffolding, in the absence of induction of EphB tyrosine kinase activity, mediates some of the biological effects of EphBs[14]. Thus, new ways of selectively inhibiting specific functions of EphBs are critically needed to clarify the kinase-dependent and kinase-independent mechanisms by which EphBs control specific developmental events, such as axon guidance and synapse formation.

[1]Department of Neurobiology, Harvard Medical School, Boston, Massachusetts, USA. [2]Department of Psychiatry, University of Texas Southwestern Medical Center, Dallas, Texas, USA. [3]Department of Cellular and Molecular Pharmacology, University of California, San Francisco, California, USA. [4]Present address: Department of Chemistry, University of Southern California, Los Angeles, California, USA (C.Z.), Department of Psychiatry, McLean Hospital, Harvard Medical School, Belmont, Massachusetts, USA (C.W.C.). [5]These authors contributed equally to this work. Correspondence should be addressed to M.E.G. (michael_greenberg@hms.harvard.edu).

Received 15 August; accepted 1 October; published online 11 November 2012; doi:10.1038/nn.3249

Much of what is currently known about the role of EphB signaling during axon guidance *in vivo* comes from studies of retinal and cortical axon tracts. Notably, genetic deletion of individual or combinations of EphB family members cause marked axon guidance defects that result in the abnormal formation of several axon tracks, including the ipsilateral retinocollicular projection and axonal tracts in the corpus callosum and the anterior commissure[9,19]. However, it remained to be determined whether EphB-dependent axon guidance decisions are mediated by the kinase activity of EphBs or by other modes of EphB signaling, such as PDZ-domain interactions, cytoplasmic domain oligomerization, reverse signaling through ephrin-Bs or EphB extracellular domain interactions.

In general, the mechanisms by which the cytoplasmic domains of axon guidance receptors signal growth cone attraction or repulsion have been difficult to identify. Most axon guidance receptors that have been studied to date, such as Robo, DCC, plexins and neuropilins, do not possess intrinsic kinase activity, suggesting that the predominant mode of axon guidance signaling may be kinase independent[20]. With regard to EphBs, studies in the visual system have suggested a role for the kinase activity, whereas studies in the cortex have suggested kinase-independent roles of EphBs[9,21–24]. However, none of these experiments were able to directly address the requirement of the kinase activity of EphBs when they are expressed at endogenous levels *in vivo*.

In addition to their function in axon guidance, EphBs have been shown to be important for cortical and hippocampal synapse formation. *Ephb* knockout mice or knock-in mice with cytoplasmic domain deletions display defects in dendritic spine and synapse development in dissociated neuronal cultures and in hippocampal slices[13,18]. Overexpression of kinase-defective dominant-negative mutants also results in abnormal spine and synapse development, suggesting that the tyrosine kinase activity of EphBs is involved in these processes[13,15,25]. However, these studies did not directly test the requirement of the kinase activity of EphBs in the regulation of synapse formation under conditions in which ephrin-Bs and EphBs are expressed at physiological levels, thereby complicating the interpretation of the findings and leaving open the possibility that aspects of EphB-dependent synapse development may be kinase independent.

To address the importance of the kinase activity of EphBs for axon guidance and synapse development, we combined chemical biology with mouse genetic engineering to reversibly inhibit EphB tyrosine kinase signaling in cultured neurons, brain slices and live animals. By mutating a bulky gatekeeper residue in the ATP-binding pocket of EphBs to a smaller alanine or glycine, we rendered the enzymatic activity of these kinases sensitive to reversible inhibition by derivatives of the Src inhibitor PP1. These analogs of PP1 do not fit into the ATP-binding pocket of wild-type kinases[26,27] and therefore do not inhibit wild-type EphBs or other kinases. In a previous study, this approach was successfully employed to regulate Trk RTK signaling[28]. We reasoned that this approach would be particularly well suited for investigating the more complex EphB family, allowing us to inhibit the kinase activity of EphBs while preserving extracellular interactions, reverse signaling or other cytoplasmic domain functions of EphBs.

We generated a triple knock-in mouse line that harbors ATP-binding pocket mutations in EphB1, EphB2 and EphB3. By specifically blocking the kinase function of EphBs in these knock-in mice in a temporally controlled manner, we found for the first time, to the best of our knowledge, a requirement for the kinase activity of EphBs in axonal guidance *in vivo*. In contrast, the kinase activity of EphBs was not required for another key EphB-mediated event, the regulation of excitatory synapse formation. Thus, when expressed under physiologically relevant conditions, EphBs differentially regulate key aspects of neuronal development by kinase-dependent and kinase-independent mechanisms.

RESULTS

A chemical genetic approach to studying EphB signaling

To selectively inhibit the tyrosine kinase activity of EphBs, we employed a strategy that combines the advantages of both pharmacology and genetics and in which drug sensitivity can be engineered into a protein[29,30]. The ATP-binding pocket of all kinases contains a bulky hydrophobic gatekeeper residue that is not essential for the catalytic function of the kinase domain. However, this gatekeeper residue, when mutated to an alanine or a glycine, can render the kinase sensitive to inhibition by PP1 analogs that cannot effectively enter the wild-type ATP-binding pocket (**Fig. 1a**)[29,30]. We engineered EphBs with modified gatekeeper residues and refer to these PP1 analog–sensitive EphBs as AS-EphBs.

To design AS-EphB mutants, we compared the amino acid sequence of kinase domains of EphBs with those of related tyrosine kinases for which analog-sensitive versions had been successfully made[26,28]. This analysis revealed a gatekeeper threonine residue in the ATP-binding pocket of mouse EphB1, EphB2 and EphB3 (**Fig. 1b**). We substituted these residues with either alanine or glycine to generate *Ephb1*^{T697G}, *Ephb2*^{T699A} and *Ephb3*^{T706A}.

To verify that the mutations introduced into the EphB ATP-binding pockets did not affect the kinase activity of EphBs in the absence of the PP1 analogs, we assessed the activity of these kinases using a heterologous cell culture system. Activation of EphBs results in receptor auto-phosphorylation on several juxtamembrane tyrosine residues. We previously generated an antibody that specifically recognizes the phosphorylated form of these juxtamembrane tyrosine residues for all EphBs, and used the juxtamembrane tyrosine phosphorylation detected by this antibody as a readout for receptor kinase activation[15]. We overexpressed EphBs in HEK 293 cells in which EphBs cluster spontaneously and become activated in a ligand-independent manner. We probed lysates from cells overexpressing AS-EphBs or wild-type EphBs with antibody to phosphorylated EphB and found that wild-type EphBs and AS-EphBs were phosphorylated at their juxtamembrane tyrosines to a similar extent (**Fig. 1c**). This result indicates that the analog-sensitive mutation does not affect the ability of EphBs to activate their kinase domains in the absence of PP1 analogs.

To test the ability of PP1 analogs to inhibit AS-EphBs, we treated HEK 293 cells overexpressing AS-EphBs or wild-type EphBs with either of two bulky PP1 analogs, 4-amino-1-*tert*-butyl-3-(1′-naphthyl)pyrazolo[3,4-d]pyrimidine (1-NA-PP1) or 1-(*tert*-butyl)-3-(3-methylbenzyl)-1H-pyrazolo[3,4-d]pyrimidin-4-amine (3-MB-PP1) (**Fig. 1a**) and assessed EphB tyrosine phosphorylation. We found that incubation with 1-NA-PP1 (250 nM) or 3-MB-PP1 (1 μM) blocked the phosphorylation of AS-EphBs, but not the phosphorylation of wild-type EphBs (**Fig. 1c**). The drug vehicle DMSO alone did not have any effect on either wild-type EphBs or AS-EphBs. These results indicate that the kinase activity of AS-EphBs was selectively inhibited by PP1 analogs. Inhibition of kinase activity of AS-EphBs was rapid, occurring in minutes (**Fig. 1d**). Given that PP1 analogs act competitively, inhibition was readily reversible following removal of 1-NA-PP1 (**Fig. 1e**). The specificity, rapidity and reversibility of the kinase inhibition make this chemical genetic strategy an ideal platform for studying dynamic biological processes in cells and animals.

To quantify the potency and specificity of 1-NA-PP1 and 3-MB-PP1 with respect to inhibition of EphB1, EphB2 and EphB3, we conducted

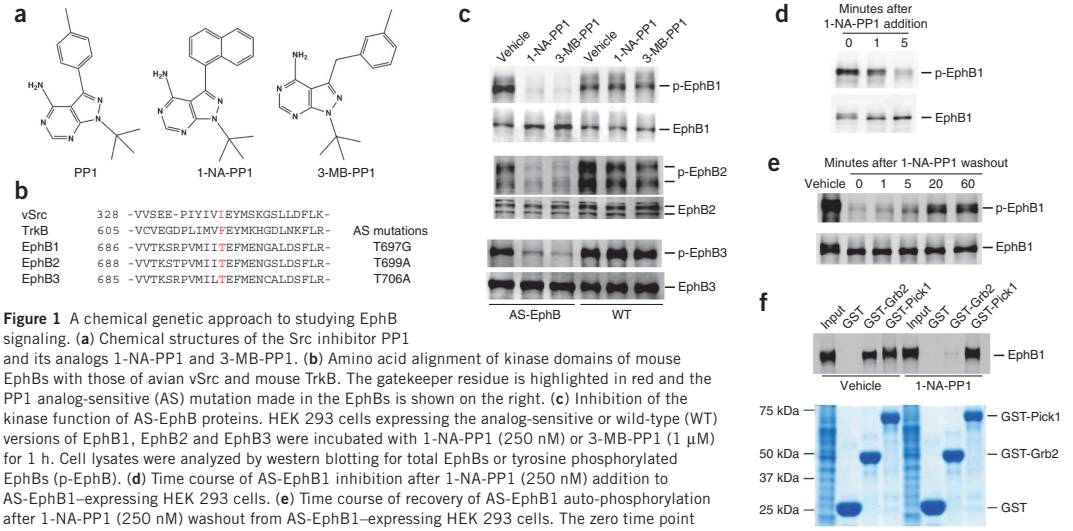

Figure 1 A chemical genetic approach to studying EphB signaling. (**a**) Chemical structures of the Src inhibitor PP1 and its analogs 1-NA-PP1 and 3-MB-PP1. (**b**) Amino acid alignment of kinase domains of mouse EphBs with those of avian vSrc and mouse TrkB. The gatekeeper residue is highlighted in red and the PP1 analog-sensitive (AS) mutation made in the EphBs is shown on the right. (**c**) Inhibition of the kinase function of AS-EphB proteins. HEK 293 cells expressing the analog-sensitive or wild-type (WT) versions of EphB1, EphB2 and EphB3 were incubated with 1-NA-PP1 (250 nM) or 3-MB-PP1 (1 μM) for 1 h. Cell lysates were analyzed by western blotting for total EphBs or tyrosine phosphorylated EphBs (p-EphB). (**d**) Time course of AS-EphB1 inhibition after 1-NA-PP1 (250 nM) addition to AS-EphB1–expressing HEK 293 cells. (**e**) Time course of recovery of AS-EphB1 auto-phosphorylation after 1-NA-PP1 (250 nM) washout from AS-EphB1–expressing HEK 293 cells. The zero time point reflects the moment of 1-NA-PP1 washout after an initial 1-h incubation. (**f**) Effect of 1-NA-PP1 on the ability of AS-EphB1 to bind Grb2 or Pick1. HEK 293 cells expressing AS-EphB1 were incubated with either vehicle or 1-NA-PP1. Cell lysates were incubated with GST, GST-Grb2 or GST-Pick1 proteins immobilized on glutathione beads. Proteins bound to the beads were analyzed by western blotting for EphB1 (top of gel). The same gel (bottom) was stained with Coomassie blue to verify that similar amounts of GST fusion proteins were present in the binding reactions. Uncropped blots are shown in **Supplementary Figure 7**.

dose-response analyses. We determined the half maximal inhibitory concentrations of kinase inhibition, which revealed a preference of the PP1 analogs for inhibiting analog-sensitive kinases (9–48 nM) over wild-type kinases (0.6–8.9 μM) by two orders of magnitude (**Supplementary Fig. 1a**,**b**). These results indicate that the kinase activity of AS-EphBs was selectively inhibited by PP1 analogs.

To confirm that binding of PP1 analogs to AS-EphBs does not affect kinase-independent aspects of EphB function, we performed *in vitro* binding assays to compare the effect of 1-NA-PP1 on tyrosine kinase–dependent and tyrosine kinase–independent protein-protein interactions. The SH2 and SH3 domain–containing adaptor protein Grb2 is a classic example of a signaling molecule that interacts with RTKs, including EphBs, through a tyrosine kinase–dependent mechanism. Following receptor activation and auto-phosphorylation, the phospho-tyrosine residues in the cytoplasmic tails of RTKs, including EphBs, recruit Grb2 through its SH2 domain[31,32]. In contrast, binding of the PDZ domain–containing protein Pick1 to EphBs occurs through the C-terminal PDZ domain–binding motif of EphBs and does not require the tyrosine kinase activity of EphBs[33]. In the binding experiments, we found that EphB1 bound strongly to both GST-Grb2 and GST-Pick1, but not to the negative control, GST alone (**Fig. 1f**). Notably, although 1-NA-PP1 (1 μM) completely abolished the kinase-dependent interaction between AS-EphB1 and GST-Grb2, the inhibitor treatment had no effect on the kinase-independent interaction between AS-EphB1 and GST-Pick1 (**Fig. 1f**). Thus, these observations provide evidence that 1-NA-PP1 specifically targets kinase-dependent functions of EphB proteins.

Generation and validation of AS-EphB TKI mice

Encouraged by these initial experiments, we generated knock-in mice harboring the gatekeeper mutations in EphB1 (T697G), EphB2 (T699A) and EphB3 (T706A), the three catalytically active EphB RTKs expressed in the developing brain. *Ephb1*^{T697G}, *Ephb2*^{T699A} and *Ephb3*^{T706A} single mutant mice were generated individually by homologous recombination in mouse embryonic stem (ES) cells (**Supplementary Fig. 2a–c**). ES cell clones were confirmed by sequencing the targeted alleles in ES cells (**Fig. 2a**).

Previous studies have found substantial functional redundancy of EphBs in several contexts[18,22,34]. To overcome potential compensation by different EphB family members, we intercrossed *Ephb1*^{T697G}, *Ephb2*^{T699A} and *Ephb3*^{T706A} single mutants to generate a line that is triply homozygous for each of the targeted EphB alleles, which we refer to as EphB triple knock-in (AS-EphB TKI) mice.

Although *Ephb1*, *Ephb2* and *Ephb3* triple knockout mice suffer from marked developmental defects, including morphological abnormalities of the palate and the anogenital region[35,36], AS-EphB TKI mice developed normally into healthy, fertile adults, indistinguishable from wild-type mice. Notably, AS-EphB TKI brains exhibited normal morphology and were of equal size to wild-type mouse brains. *In vitro* assays measuring axon guidance, neuronal morphology and synaptic development revealed no differences between wild-type and AS-EphB TKI mice (as shown below), suggesting that AS-EphBs function normally in the absence of PP1 analogs.

Critical to the interpretation of experiments comparing wild-type and AS-EphB TKI mice is evidence that EphB mRNA expression, trafficking and ligand-mediated receptor activation occur normally in AS-EphB TKI neurons in the absence of PP1 analogs. First, we performed quantitative PCR (qPCR) to measure expression of the *Ephb1*, *Ephb2* and *Ephb3* mRNAs in neurons from wild-type and AS-EphB TKI mice. We found that mRNAs isolated from the mutant mice were expressed at the same levels as in wild-type mice (**Fig. 2b**). We conclude that the gene targeting did not affect the expression of *Ephb1*, *Ephb2* and *Ephb3* mRNA in AS-EphB TKI neurons.

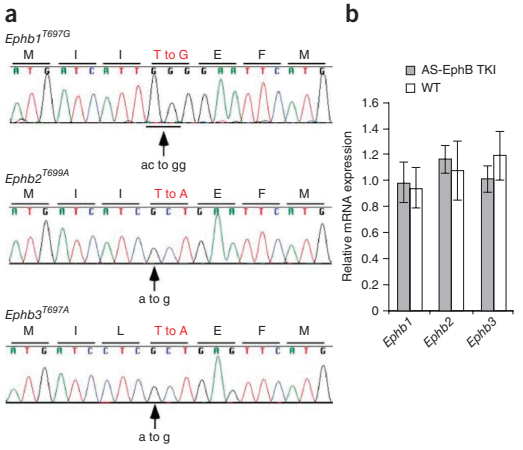

Figure 2 Generation of AS-EphB TKI mice. (**a**) Sequencing reads from AS-EphB knock-in mouse ES cells showing the gatekeeper (analog sensitive) mutation in the *Ephb1*, *Ephb2* and *Ephb3* genes. The mutated amino acids are shown in red. The arrows indicate the DNA base substitutions. (**b**) Relative mRNA expression of *Ephb1*, *Ephb2* and *Ephb3* normalized to *Actb* in AS-EphB TKI and wild-type cultured cortical neurons. Data are mean of two biological replicates ± s.e.m.

We next asked whether neurons from AS-EphB TKI mice could engage in ephrin-B–induced signaling. We cultured dissociated cortical neurons from embryonic day 16.5 to 18.5 (E16.5–18.5) AS-EphB TKI or wild-type mice and stimulated the neurons with clustered ephrin-B1 for 30 min. Western blotting of AS-EphB TKI or wild-type lysates with the antibody to phosphorylated EphB revealed that both wild-type and AS-EphB TKI neurons exhibited robust EphB activation at similar levels, indicating that AS-EphBs are fully competent to engage in ephrin-B–induced kinase signaling in the absence of PP1 analogs (**Fig. 3a**).

To test whether the kinase function of endogenously expressed EphBs from AS-EphB TKI mice can be effectively and selectively inhibited by PP1 analogs, we pre-incubated cultured E16.5–18.5 neurons with vehicle or PP1 analogs for 1 h before ephrin-B1 stimulation. Treatment with 250 nM 1-NA-PP1 or 1 μM 3-MB-PP1 completely abolished ephrin-B1–induced EphB activation in the AS-EphB TKI, but not wild-type, cells, thereby demonstrating the efficacy and selectivity of these PP1 analogs for AS-EphBs expressed at endogenous levels in neurons (**Fig. 3a**).

To more rigorously test the selectivity of PP1 analogs, we assessed the effect of these inhibitors on the kinase activity of EphA4, one of the closest relatives of EphBs. We stimulated wild-type cortical neurons that had been pre-incubated with 250 nM 1-NA-PP1 or 1 μM 3-MB-PP1 with the EphA4 ligand ephrin-A1, immunoprecipitated EphA4 with an antibody to EphA4, and analyzed the immunoprecipitates for phospho-EphA4 or total EphA4. We found no inhibition of EphA4 autophosphorylation at concentrations of PP1 analogs that fully blocked AS-EphB tyrosine kinase function (**Fig. 3b**). The specificity of analog-sensitive inhibition between subfamilies of Eph receptors contrasts with previous unsuccessful attempts at designing selective inhibitors for EphBs relative to EphAs[37,38].

To determine whether PP1 analogs affect the cell surface expression or internalization of AS-EphB proteins, we performed surface biotin labeling for the EphB2 receptor after chronic inhibition from 6–12 days *in vitro* (DIV) in cortical neurons. We found equivalent levels of labeled EphB2 in vehicle and 1-NA-PP1 (1 μM)-treated cells (**Supplementary Fig. 3**). This result indicates that surface expression of EphBs is not altered by the inhibitor treatment.

Kinase cascades can amplify signals greatly. To test whether inhibition of the kinase activity of EphBs effectively blocks the phosphorylation of downstream tyrosine kinase substrates, we examined phosphorylation of the well-characterized EphA and EphB substrate Vav2, a Rho family guanine nucleotide exchange factor that mediates growth cone collapse[39]. Wild-type or AS-EphB TKI neurons were incubated in 1-NA-PP1 (250 nM) or 3-MB-PP1 (1 μM) and stimulated with ephrin-B1 for 30 min to induce Vav2 tyrosine phosphorylation. Immunoprecipitation of Vav2, followed by western blotting with a pan-phospho-tyrosine antibody, revealed a substantial increase in tyrosine phosphorylation of Vav2 after ephrin-B1 stimulation (**Fig. 3c**,**d**). Treatment with 1-NA-PP1 (250 nM) or 3-MB-PP1 (1 μM) selectively blocked the increase in Vav2 phosphorylation in AS-EphB TKI cells, but had no effect in wild-type cells (**Fig. 3c**,**d**). We conclude that PP1 analogs can selectively block the kinase signaling of EphBs and the phosphorylation of their substrates in AS-EphB TKI cells.

EphB RTK signaling is required for growth cone collapse

EphBs have classically been studied in the context of axon guidance[22,40,41]. Although some studies have suggested a role for the kinase activity of EphBs in axon guidance, others have suggested kinase-independent modes of EphB signaling[9,21–24]. To assess the role of EphB kinase activity in axon guidance, we initially chose the visual system because the importance of EphBs in this system is well established. During development of the visual system, most retinal ganglion cell (RGC) axons emanating from the retina enter and cross the optic chiasm at the midline to form the contralateral retinal projections in the lateral geniculate nucleus and superior colliculus[24,40]. However, RGC axons from the ventrotemporal region of the retina, which express EphB1, become repelled by the ephrin-B2–expressing glia of the optic chiasm and form the ipsilateral projection that is required for stereovision[42]. Ephrin-B2 is thought to repel EphB1-expressing axons by inducing the collapse of their growth cones, an activity that can be recapitulated *in vitro*.

To begin to address whether the kinase activity of EphBs is required for repulsive axon guidance, we asked whether the kinase activity of EphBs is required for growth cone collapse. We prepared explants from E14 ventrotemporal retinae and visualized growth cones with fluorescently conjugated phalloidin (to label F-actin) and axons with antibody to neurofilament. In these explants, RGCs extended axons with broad, fan-shaped growth cones over a laminin substrate. We measured the state of growth cones by two methods. First, growth cones were scored as collapsed if they exhibited rod-like morphology and lacked visible lamellipodia. This method allowed us to quantify the percentage of growth cones that were collapsed in each explant. Second, we measured the maximum axial width of each growth cone and calculated the average axial width of the growth cones in each explant.

When treated with clustered ephrin-B2, growth cones from AS-EphB TKI explants exhibited a robust collapse response (**Fig. 4a**,**b**). Treatment of AS-EphB TKI explants with 1-NA-PP1 (250 nM) or 3-MB-PP1 (1 μM) led to a marked decrease in the percentage of collapsed growth cones following ephrin-B treatment (**Fig. 4a**,**b**). In addition, AS-EphB TKI explants showed an ephrin-B2–induced decrease in growth cone width in vehicle-treated explants, but only

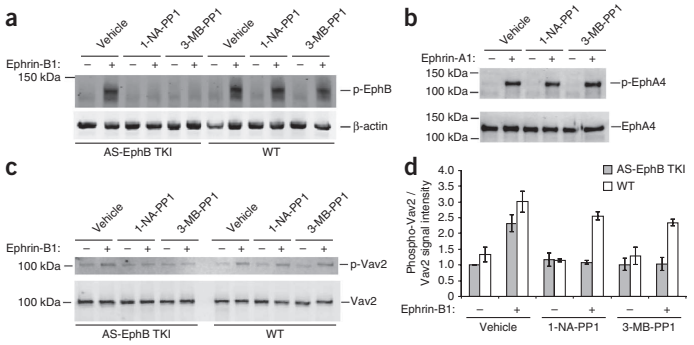

Figure 3 Selective inhibition of the kinase function of EphBs in AS-EphB TKI mice. (**a**) Inhibition of the EphB kinase activity in AS-EphB TKI neurons. We pre-incubated 15 DIV dissociated AS-EphB TKI embryonic cortical neurons with vehicle, 250 nM 1-NA-PP1 or 1 μM 3-MB-PP1 for 1 h before a 30-min ephrin-B1 stimulation. Cell lysates were then analyzed by western blotting for phospho-EphB or β-actin. (**b**) Effect of PP1 analogs on the kinase activity of EphA4. We pre-incubated 4 DIV cortical neurons with vehicle, 250 nM 1-NA-PP1 or 1 μM 3-MB-PP1 for 1 h before a 30-min ephrin-A1 stimulation. Lysates were immunoprecipitated with an antibody to EphA4 and blotted for phospho-EphA4 and EphA4. (**c**) Effect of PP1 analogs on ephrin-B1–induced Vav2 phosphorylation. We stimulated 4 DIV AS-EphB TKI or wild-type cortical neurons with ephrin-B1, immunoprecipitated them with an antibody to Vav2, and blotted them with either a pan-phospho-tyrosine (pY99) or Vav2 antibody. Cells were pre-incubated with vehicle, 250 nM 1-NA-PP1 or 1 μM 3-MB-PP1 for 1 h before a 30-min ephrin-B1 stimulation. (**d**) Quantification of phospho-Vav2/Vav2 band intensity from quantitative western blots in **c**. Data are mean ± s.e.m. ($n = 3$ biological replicates). Values were normalized to the unstimulated AS-EphB TKI vehicle-treated condition. Uncropped blots are shown in **Supplementary Figure 7**.

a slight reduction in explants exposed to 1-NA-PP1 or 3-MB-PP1 (**Fig. 4c**). This inhibitor-dependent blockade of growth cone collapse was not seen in wild-type explants; wild-type cells showed a robust collapse regardless of the presence of inhibitors, as well as a substantial reduction in average growth cone width after stimulation (**Fig. 4a–c**). On the basis of these results, we conclude that the kinase activity of EphBs is required for ephrin-B–induced RGC growth cone collapse.

To verify that treatment of explants with 1-NA-PP1 and 3-MB-PP1 led to inhibition of ephrin-B–dependent EphB tyrosine phosphorylation in RGC axons, we stained explants with antibody to phosphorylated EphB. In the absence of stimulation, minimal phospho-EphB staining was observed in growth cones from wild-type or AS-EphB TKI explants (**Fig. 4a**). Following ephrin-B2 stimulation, punctate patterns of phosphorylated EphB staining were seen in the growth cone and along the axon (**Fig. 4a**). This staining was blocked in AS-EphB TKI explants treated with 1-NA-PP1 (250 nM) or 3-MB-PP1 (1 μM), but not in wild-type explants, indicating that PP1 analogs selectively inhibit the kinase activity of EphBs in AS-EphB TKI RGC explants (**Fig. 4a**).

A crucial feature of this chemical genetic approach is the reversibility of kinase inhibition. To determine whether the inhibitory effect of 1-NA-PP1 on growth cone collapse is indeed reversible, we removed 1-NA-PP1 midway through a 30-min ephrin-B2 stimulation in AS-EphB TKI explants. In the presence of 1-NA-PP1, ephrin-B–stimulated growth cones did not collapse, but did collapse rapidly after washout (**Fig. 4d**). This finding demonstrates the reversibility of PP1 analog inhibition of growth cone collapse in retinal explants from AS-EphB TKI mice and rules out a general health issue as a cause of reduced growth cone collapse.

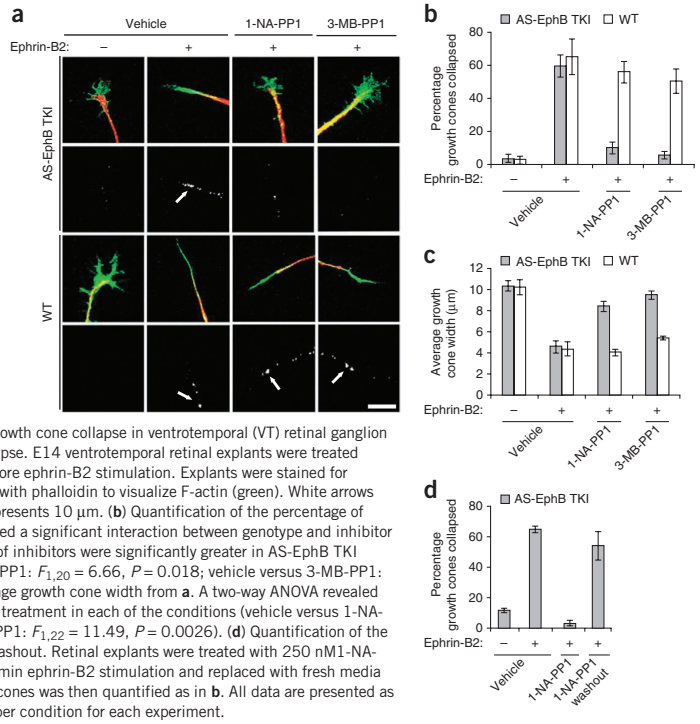

Figure 4 The kinase function of EphBs is required for growth cone collapse in ventrotemporal (VT) retinal ganglion cells. (**a**) Effect of PP1 analog on RGC growth cone collapse. E14 ventrotemporal retinal explants were treated with vehicle, 250 nM 1-NA-PP1 or 1 μM 3-MB-PP1 before ephrin-B2 stimulation. Explants were stained for neurofilament (red), phospho-EphB (white) and labeled with phalloidin to visualize F-actin (green). White arrows denote clusters of phospho-EphB staining. Scale bar represents 10 μm. (**b**) Quantification of the percentage of collapsed growth cones from **a**. A two-way ANOVA revealed a significant interaction between genotype and inhibitor treatment in each condition, indicating that the effects of inhibitors were significantly greater in AS-EphB TKI neurons than in wild-type neurons (vehicle versus 1-NA-PP1: $F_{1,20} = 6.66$, $P = 0.018$; vehicle versus 3-MB-PP1: $F_{1,22} = 7.41$, $P = 0.012$). (**c**) Quantification of the average growth cone width from **a**. A two-way ANOVA revealed a significant interaction between genotype and inhibitor treatment in each of the conditions (vehicle versus 1-NA-PP1: $F_{1,20} = 11.75$, $P = 0.0027$; vehicle versus 3-MB-PP1: $F_{1,22} = 11.49$, $P = 0.0026$). (**d**) Quantification of the percentage of collapsed growth cones after 1-NA-PP1 washout. Retinal explants were treated with 250 nM1-NA-PP1 as in **a**, but media were removed 15 min into a 30-min ephrin-B2 stimulation and replaced with fresh media containing vehicle. The percentage of collapsed growth cones was then quantified as in **b**. All data are presented as mean ± s.e.m. $N = 4–8$ explants (biological replicates) per condition for each experiment.

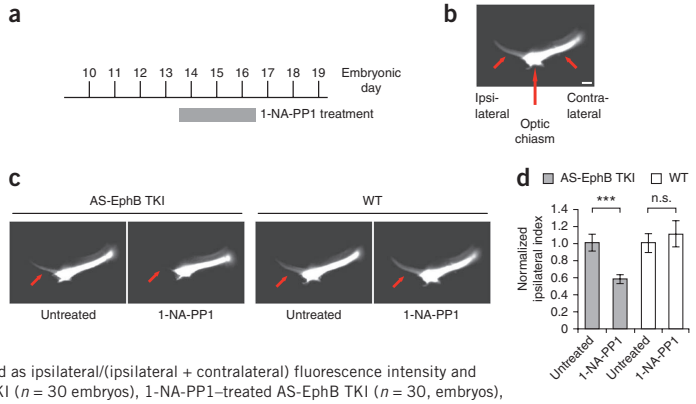

Figure 5 The kinase function of EphBs is required for the formation of the ipsilateral retinal projection *in vivo*. (**a**) Schedule of *in vivo* 1-NA-PP1 administration. Twice-daily subcutaneous injections of 80 mg per kg of body weight 1-NA-PP1 were administered to pregnant females from E13.5–16.5. (**b**) Representative image demonstrating the orientation of the ipsilateral and contralateral retinal projections (short red arrows) of the optic tract with respect to the optic chiasm (long red arrow) as visualized by DiI labeling (white). Scale bar represents 100 μm. (**c**) Representative images of DiI-filled retinal projections at E16.5. Pregnant AS-EphB and C57BL/6 wild-type mice were treated as described in **a**. Red arrows denote the ipsilateral projection. (**d**) Quantification of the ipsilateral phenotype shown in **c**. The ipsilateral index is defined as ipsilateral/(ipsilateral + contralateral) fluorescence intensity and normalized for each genotype (untreated AS-EphB TKI ($n = 30$ embryos), 1-NA-PP1–treated AS-EphB TKI ($n = 30$, embryos), untreated wild-type ($n = 15$, embryos), 1-NA-PP1–treated wild-type ($n = 17$, embryos)). ***$P < 0.001$; n.s., not significant by Student's t test. A two-way ANOVA revealed a significant interaction between genotype and inhibitor treatment, indicating that 1-NA-PP1 treatment effects were significantly greater in AS-EphB TKI embryos than in wild-type embryos ($F_{1,88} = 6.5$, $P = 0.0125$). Data are presented as mean ± s.e.m. Samples are biological replicates.

EphB RTK signaling mediates retinal axon guidance *in vivo*

Having established the requirement of the tyrosine kinase activity of EphBs for growth cone collapse *in vitro*, we next asked whether this requirement is relevant for repulsive guidance *in vivo*, where growth cones exhibit saltatory motion rather than simple extension and collapse. In addition, growth cone collapse *in vivo* is mediated by a number of cues, including membrane-bound ephrin-B rather than ectopically added aggregated soluble ephrin-Bs

To determine whether the kinase activity of EphBs is required for the repulsive guidance of axons under physiological conditions of ephrin-B and EphB signaling *in vivo*, we examined the effect of inhibiting the kinase activity of EphBs on axon repulsion at the optic chiasm. We treated pregnant mice with 1-NA-PP1 from E13.5 to E16.5, the time at which RGC axons encounter the optic chiasm (**Fig. 5a**), and analyzed the retinal projections at E16.5 by DiI labeling.

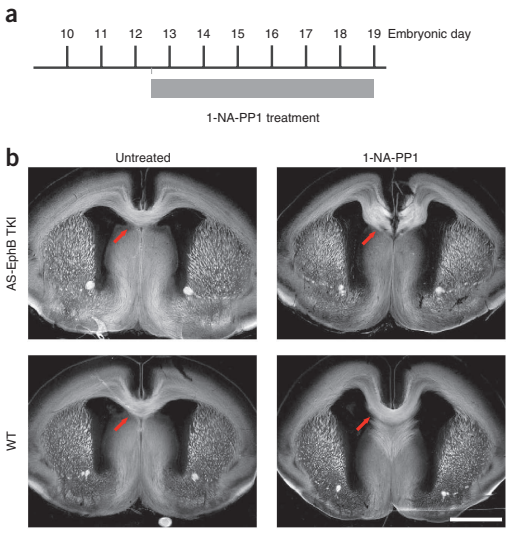

To assess the degree of ipsilateral versus contralateral retinal projection, we measured the fluorescence intensity of a rectangular region in the ipsilateral projection and divided this by the total fluorescence intensity in the combined ipsilateral and contralateral projections to derive the ipsilateral index (**Fig. 5b**)[40]. In 1-NA-PP1–treated AS-EphB TKI embryos, we found that the ipsilateral retinal projection was strongly reduced (by 42%) compared with untreated AS-EphB TKI embryos (**Fig. 5c**,**d**). In many of the AS-EphB TKI embryos treated with 1-NA-PP1, the ipsilateral projection was absent. In contrast, 1-NA-PP1 treatment had no effect on the ipsilateral retinal projection in wild-type embryos, indicating that the observed guidance deficit was a result of specific inhibition of EphBs (**Fig. 5c**,**d**). These findings suggest that the tyrosine kinase activity of EphBs is required for axon repulsion at the optic chiasm. They also illustrate the utility of AS-EphB mice for examining the importance of the tyrosine kinase activity of EphBs in both *in vitro* and *in vivo* settings. Our results demonstrate that PP1 analogs are capable of entering the brain tissue of an intact organism and then effectively and potently inhibiting EphB tyrosine kinase activity. These analogs also completely inhibited EphB tyrosine kinase activity in neuronal cultures, making it possible to use the AS-EphB TKI neurons to investigate the role of the kinase activity of EphBs in a diverse array of neuronal functions.

EphB RTK signaling mediates corpus callosum formation

Based on the finding that EphB tyrosine kinase activity mediates axon guidance at the optic chiasm, we next asked whether a similar mechanism might be used during other axon guidance decisions. We focused on the role of the tyrosine kinase activity of EphBs in the formation of the corpus callosum. Different EphB family members have been suggested to mediate this process

Figure 6 The kinase activity of EphBs is required for the formation of the corpus callosum *in vivo*. (**a**) Schedule of *in vivo* 1-NA-PP1 administration. Twice-daily subcutaneous injections of 80 mg per kg 1-NA-PP1 were administered to pregnant mice from E12.5–19. (**b**) Representative images of brain sections from E19 embryos stained with L1-CAM antibody (white) to visualize axon tracts. Red arrows denote the corpus callosum. Scale bar represents 1 mm.

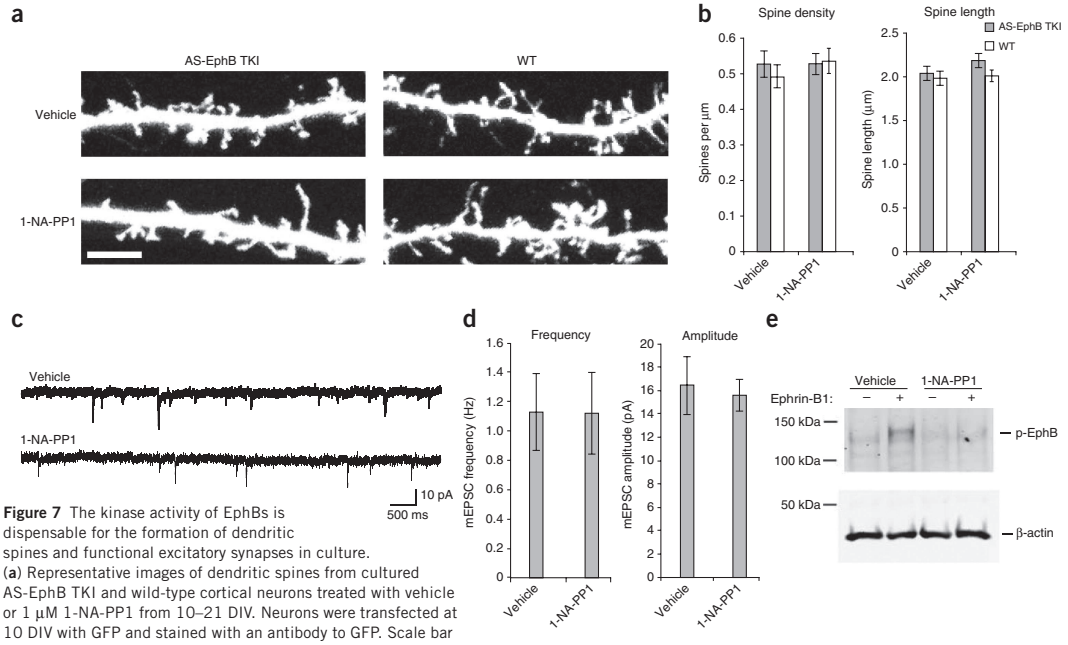

Figure 7 The kinase activity of EphBs is dispensable for the formation of dendritic spines and functional excitatory synapses in culture. (**a**) Representative images of dendritic spines from cultured AS-EphB TKI and wild-type cortical neurons treated with vehicle or 1 µM 1-NA-PP1 from 10–21 DIV. Neurons were transfected at 10 DIV with GFP and stained with an antibody to GFP. Scale bar represents 5 µm. (**b**) Quantification of spine density and spine length from **a**. Data are presented as mean ± s.e.m. $N = 25–33$ neurons from independent biological replicates per condition. (**c**) Representative traces of recordings of mEPSCs from dissociated cortical neurons from AS-EphB TKI embryos at 10–12 DIV. Cultures were treated with vehicle or 1-NA-PP1 (1 µM) from 3 DIV until the time of recording. (**d**) Quantification of mEPSC frequency and amplitude from vehicle and 1-NA-PP1–treated neurons. Data are presented as mean ± s.e.m. $N = 13$ cells from independent biological replicates per condition. (**e**) The tyrosine kinase activity of AS-EphBs was inhibited by 1-NA-PP1. Cultures concurrent with those used in **d** were treated with 1-NA-PP1 under identical culture conditions then stimulated for 30 min with ephrin-B1 at 10 DIV. Cell lysates were analyzed by western blotting for phospho-EphB and β-actin. Uncropped blots are shown in **Supplementary Figure 7**.

through both forward and reverse signaling, but the requirement of the kinase activity has not been tested[22,43].

To address this question, we administered 1-NA-PP1 to pregnant AS-EphB TKI mice from E12.5 to E19.0 and visualized major axon tracts by L1-CAM staining (**Fig. 6a**). As expected, untreated AS-EphB TKI mice had normal corpus callossa (0 of 6 mice with agenesis; **Fig. 6b**). However, AS-EphB TKI mice treated with 1-NA-PP1 had partial corpus callosum agenesis with a gap in the dorsal midline region (11 of 11 mice with agenesis; **Fig. 6b**). Wild-type mice treated with 1-NA-PP1 had a normal corpus callosum (0 of 6 mice with agenesis), indicating that the corpus callosal agenesis phenotype was specific to inhibition of AS-EphBs (**Fig. 6b**). These data indicate that the tyrosine kinase activity of EphBs is essential for proper formation of the corpus callosum *in vivo*. Taken together with our findings on retinal axon guidance, these observations suggest that tyrosine kinase-dependent signaling is likely a general mechanism by which EphB forward signaling mediates repulsive axon guidance *in vivo*.

EphB RTK signaling is not required for synaptogenesis

In addition to their role in axon guidance, EphBs have been shown in numerous studies to control synapse development and function[12,13,15,16,18,25,44,45]. Experiments involving overexpression of kinase-defective EphB mutants and the use of knock-in mice containing cytoplasmic truncations of EphBs have suggested a role for kinase signaling in synaptogenesis[12,13,15,18,25]. However, the relevance of tyrosine kinase activity of EphBs for synaptogenesis has not been examined under conditions in which ephrin-Bs and EphBs are expressed at endogenous levels and engage in physiological signaling.

The most notable synaptic defect observed after perturbation of EphB expression is the loss of dendritic spines, the sites on dendrites where most excitatory synapses form. In neurons from EphB1, EphB2 and EphB3 triple knockout mice, dendritic spine development is severely compromised[13,18]. To assess the importance of EphB tyrosine kinase activity for spine development, we cultured cortical neurons from E15–17 AS-EphB TKI or wild-type embryos and treated them with 1-NA-PP1 (1 µM) between 10–21 DIV, the peak of spinogenesis. To ensure exposure to the full dose of the inhibitor during this long period, we changed the culture medium completely every 3–4 d with fresh 1-NA-PP1. To visualize the fine dendritic structures, we transfected neurons with GFP at 10 DIV and analyzed them at 21 DIV. To assess spine density, we counted spines per unit dendritic length over multiple segments of dendrite totaling more than 50 µm. Notably, we found that 1-NA-PP1 treatment had no detectable effect on spine number and length in AS-EphB TKI or wild-type neurons (**Fig. 7a**,**b**). This result suggests that the tyrosine kinase activity of EphBs is not required for dendritic spine development in dissociated cortical neurons.

To functionally test the effect of 1-NA-PP1 on synaptogenesis, we measured miniature excitatory postsynaptic currents (mEPSCs) in dissociated cortical neurons from AS-EphB TKI mice in the presence or absence of 1-NA-PP1. These cultures were treated with

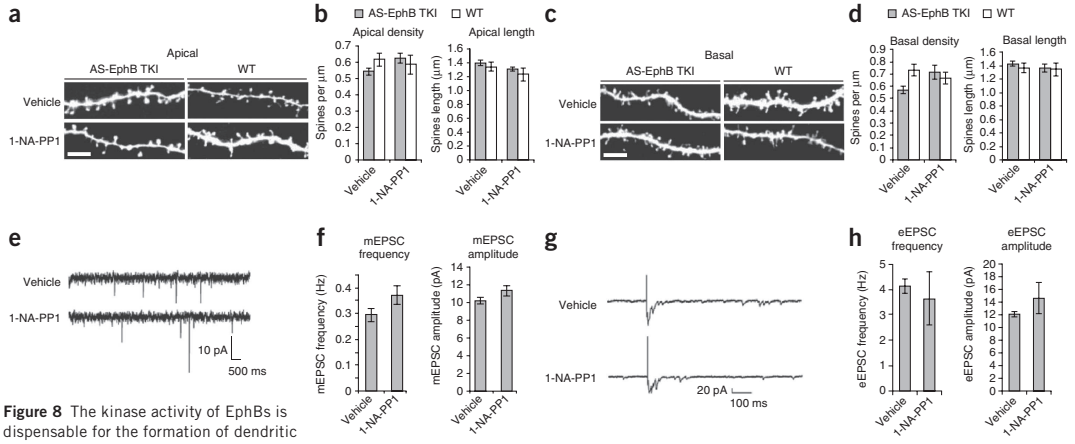

Figure 8 The kinase activity of EphBs is dispensable for the formation of dendritic spines and functional excitatory synapses in hippocampal slices. (**a**) Representative images of apical spines from AS-EphB TKI slices. Slices from postnatal day 5–7 (P5–7) mice were treated with vehicle or 1-NA-PP1 from 0–8 DIV. Scale bar represents 5 µm. (**b**) Quantification of apical spine density and spine length from **a** (wild-type + vehicle, $n = 21$ neurons;, wild-type + 1-NA-PP1, $n = 11$ neurons; AS-EphB TKI + vehicle, $n = 30$ neurons; AS-EphB TKI + 1-NA-PP1, $n = 16$ neurons). (**c**) Representative images of basal spines from slices as described in **a**. (**d**) Quantification of basal spine density and spine length from **c**. (**e**) Representative traces from recordings of mEPSCs from P5–7 AS-EphB TKI slices at 12–14 DIV. (**f**) Quantification of mEPSC frequency and amplitude from **e**. (AS-EphB TKI + vehicle, $n = 16$ neurons; AS-EphB TKI + 1-NA-PP1, $n = 19$ neurons).1-NA-PP1 did not produce a significant change in mEPSC frequency ($P = 0.11$) or amplitude ($P = 0.14$) by Student's t test. (**g**) Representative traces from recordings of eEPSCs from P5–7 AS-EphB TKI slices at 12–14 DIV. (**h**) Quantification of eEPSC frequency and amplitude in hippocampal slices. (AS-EphB TKI + vehicle, $n = 7$ neurons; AS-EphB TKI + 1-NA-PP1, $n = 7$ neurons). 1-NA-PP1 did not produce a significant change in eEPSC frequency ($P = 0.67$) or amplitude ($P = 0.33$) by Student's t test. All experiments were done in organotypic hippocampal slices. The concentration of 1-NA-PP1 was 1 µM. All data are presented as mean ± s.e.m. Samples are independent biological replicates.

1 µM 1-NA-PP1 from 3 to 10–12 DIV, and mEPSCs were measured by whole-cell electrophysiological recordings. Consistent with the spine analysis, we found no difference in mEPSC frequency or amplitude between AS-EphB TKI neurons treated with either vehicle or 1-NA-PP1 (**Fig. 7c**,**d**), which again strongly suggests that the tyrosine kinase activity of EphBs is not required for synaptogenesis, at least in dissociated neurons. To confirm that chronic 1-NA-PP1 treatment inhibits EphB tyrosine phosphorylation in these cultures, we performed western analysis on concurrent cultures and found that exposure of AS-EphB TKI neurons to 1-NA-PP1 (1 µM) resulted in a complete inhibition of ephrin-B–induced EphB autophosphorylation (**Fig. 7e**).

To determine whether the tyrosine kinase activity of EphBs might control excitatory synapse development or function in the context of a more intact neural circuit, we also examined the effect of 1-NA-PP1 inhibition on dendritic spine development, mEPSCs and evoked excitatory postsynaptic currents (eEPSCs) in organotypic hippocampal slices prepared from AS-EphB TKI mice. Expression of shRNAs targeting *Ephb1*, *Ephb2* and *Ephb3* led to pronounced alterations in spine development (**Supplementary Figs. 4a–c** and **5a–d**), and mEPSC and eEPSC currents (**Supplementary Fig. 6a–d**) in organotypic hippocampal slice cultures, indicating that EphBs are important for excitatory synaptic development under these conditions. However, in sharp contrast with these findings, the addition of 1-NA-PP1 to slices from AS-EphB TKI mice had no effect on dendritic spine growth (**Fig. 8a–d**), mEPSC characteristics (**Fig. 8e**,**f**) or eEPSC events (**Fig. 8g**,**h**). Taken together, these findings suggest that, at least under the conditions tested, EphB tyrosine kinase activity is not required for the formation or maintenance of functional synapses.

DISCUSSION

Employing a chemical genetic strategy, we engineered mice in which it is possible to acutely, reversibly and specifically inhibit the kinase signaling of EphBs *in vitro* and *in vivo*. We found that synaptogenesis, a process that requires EphB proteins, did not depend on the tyrosine kinase activity of EphBs. In contrast, we found a clear requirement for the tyrosine kinase activity of EphBs in ephrin-B–mediated growth cone collapse in culture and in the repulsive guidance of retinal and corpus callosal axons *in vivo*. Thus, unlike many other axon guidance receptors, EphBs mediate axon repulsion via a RTK-dependent mechanism.

Our finding that the kinase activity of EphBs is not required for the formation of excitatory synapses was unexpected and suggests a possible role for cytoplasmic domain oligomerization and other forms of protein-protein interactions in this process. For example, the binding of PDZ domain–containing synaptic proteins with the cytoplasmic tail of EphBs or the recruitment of NMDA receptors via the EphB extracellular region may initiate or stabilize the formation of excitatory synapses[13,15]. Alternatively, EphBs could initiate signaling by recruiting other cytoplasmic kinases, such as the Src family of tyrosine kinases[44]. Although our data strongly suggest that the tyrosine kinase activity of EphBs is not required for synaptogenesis under a wide range of experimental conditions tested, we cannot rule out the possibility that EphB kinase signaling has a role in other contexts. It will be important in the future to determine whether the kinase activity of EphBs functions instead in the plasticity of these synapses, as multiple reports have identified a role for EphBs in long-term potentiation in the hippocampus[10,11].

In contrast with synaptogenesis, our results reveal a requirement for the tyrosine kinase activity of EphBs in the formation of the ipsilateral retinal projection and the corpus callosum. Our finding

that EphB tyrosine kinase activity is required for retinal guidance is consistent with data from a previous study that found that overexpression of EphB1 is sufficient to drive retinal axons to ectopically project ipsilaterally and that this function requires an intact EphB1 kinase domain[23]. These findings are also consistent with those of a recent study in which a knock-in mouse was generated with the intracellular region of EphB1 replaced with lacZ[24]. This mouse displays a loss of the ipsilateral retinal projection, which indicates that EphB forward signaling is necessary for the formation of the ipsilateral retinal projection. Using AS-EphB TKI mice, we found that EphB tyrosine kinase activity is directly involved in the formation of the ipsilateral retinal projection.

Mutations of the cytoplasmic domains of EphBs or ephrin-Bs suggest that the formation of the corpus callosum is more complex than the ipsilateral retinal projection and could involve both EphB forward and reverse signaling[22]. However, our finding that inhibition of the kinase activity of EphBs *in vivo* results in a highly penetrant corpus callosum agenesis phenotype provides clear evidence for the requirement of EphB kinase signaling in the development of the corpus callosum.

On the basis of our observations, we favor a model in which EphB tyrosine kinase activity is required for repulsive interactions, such as in axon guidance, but may not be required for adhesive interactions, such as axon fasciculation and synapse formation. This model is consistent with previous theories that have suggested that the amount of kinase activation predicts the strength of repulsion[46]. Furthermore, inhibiting kinase activity in a normally repulsive context (such as axon guidance) may lead to unnatural adhesion. Thus, it will be interesting to study the fate of the misprojected axons that we observed in the optic tract and corpus callosum. It will also be important to search for any counterexamples to our model, such as an adhesive interaction that is EphB tyrosine kinase dependent. The delicate balance between the opposing functionalities of the ephrin-B and EphB signaling system underscores the importance of studying these interactions under physiological conditions.

Understanding the downstream mechanism by which the tyrosine kinase activity of EphBs controls axon guidance represents an important direction for future studies. One crucial mediator of this signaling might be the Vav family of guanine nucleotide exchange factors for the small GTPase Rac. Vav2 is known to control growth cone collapse, and *Vav2* and *Vav3* double mutant mice display defects in the development of the ipsilateral retinocollicular projection[39,47]. We found that the tyrosine kinase activity of EphBs was required for ephrin-B–induced Vav2 tyrosine phosphorylation. A thorough investigation of how EphBs control repulsive axon guidance will require knowledge of the full complement of tyrosine kinase substrates of EphBs. As analog-sensitive kinases accept orthologous ATP analogs that can directly label the targets of the kinase[48], it should be possible to use AS-EphB TKI mice to identify direct kinase substrates of EphBs. Given the general limited knowledge of axon guidance mechanisms, identification of EphB substrates in the relevant neurons could be a powerful approach for uncovering these mechanisms.

Our chemical genetic approach offers several advantages over conventional genetic loss-of-function studies[49]. Given that we were able to block the kinase activity of EphBs while leaving their scaffolding and reverse signaling capabilities intact, it was possible to dissect the role of the kinase activity of EphBs *in vivo* under conditions in which EphBs were expressed at physiological levels. As there are no Cre/*loxP*-based conditional EphB mice of any kind available, AS-EphB TKI mice represent an alternative for many experiments that require conditional regulation of EphB signaling. In addition, the reversible nature and the fine temporal control afforded by the chemical genetic approach should permit investigations into the functions of EphBs in the mature animal, such as in adult neurogenesis and synaptic plasticity, and in pathologies such as Alzheimer's disease, autism and cancer[4,7,50]. This new window into EphB signaling should also provide insights that are crucial for therapeutic drug development for the treatment of EphB-mediated disease.

METHODS

Methods and any associated references are available in the online version of the paper.

Note: Supplementary information is available in the online version of the paper.

ACKNOWLEDGMENTS

We thank M. Thompson, Y. Zhou and H. Ye of the Children's Hospital Boston Intellectual and Developmental Disabilities Research Center Mouse Gene Manipulation Core for ES cell work and blastocyst injection, T. Kuwajima and members of C. Mason's laboratory for advice on retinal explants and DiI labeling, M. Lopez for help selecting and generating PP1 analogs, Z. Wills and A. Mardinly for help with synapse analysis, S. Cohen for advice on electrophysiological recordings, P. Zhang for assistance with animal management, and L. Hu for antibody work. This research was funded by US National Institutes of Health grants RO1-NS-045500 (M.E.G.) and RO1-EY-018207 (C.W.C.). H.-Y.H.H. was supported by the Marion Abbe Fellowship of the Damon Runyon Cancer Research Foundation and US National Institutes of Health training grants in neurodegeneration and cancer biology. M.J.S. was supported by a National Science Foundation Graduate Research Fellowship. M.A.R. was supported by a training grant from the National Institute on Drug Abuse (T32 DA07290).

AUTHOR CONTRIBUTIONS

M.J.S., H.-Y.H.H. and M.E.G. conceived and designed the study. M.J.S. and H.-Y.H.H conducted all of the experiments unless otherwise noted. B.L.B. and N.S. performed electrophysiological recordings. J.Z. generated EphB1 and EphB3 targeting constructs. M.A.R. and C.W.C. contributed to the axon guidance experiments. A.N.M. and A.A.R. generated shRNAs for EphBs. B.A. performed qPCR experiments. C.Z. and K.M.S. designed and synthesized inhibitors. M.J.S., H.-Y.H.H. and M.E.G. wrote the manuscript.

COMPETING FINANCIAL INTERESTS

The authors declare no competing financial interests.

Published online at http://www.nature.com/doifinder/10.1038/nn.3249.
Reprints and permissions information is available online at http://www.nature.com/reprints/index.html.

1. Klein, R. Eph/ephrin signaling in morphogenesis, neural development and plasticity. *Curr. Opin. Cell Biol.* **16**, 580–589 (2004).
2. Lai, K.O. & Ip, N.Y. Synapse development and plasticity: roles of ephrin/Eph receptor signaling. *Curr. Opin. Neurobiol.* **19**, 275–283 (2009).
3. Genander, M. & Frisen, J. Ephrins and Eph receptors in stem cells and cancer. *Curr. Opin. Cell Biol.* **22**, 611–616 (2010).
4. Sanders, S.J. *et al.* De novo mutations revealed by whole-exome sequencing are strongly associated with autism. *Nature* **485**, 237–241 (2012).
5. Merlos-Suárez, A. & Batlle, E. Eph-ephrin signaling in adult tissues and cancer. *Curr. Opin. Cell Biol.* **20**, 194–200 (2008).
6. Pasquale, E.B. Eph receptors and ephrins in cancer: bidirectional signaling and beyond. *Nat. Rev. Cancer* **10**, 165–180 (2010).
7. Cissé, M. *et al.* Reversing EphB2 depletion rescues cognitive functions in Alzheimer model. *Nature* **469**, 47–52 (2011).
8. Sheffler-Collins, S.I. & Dalva, M.B. EphBs: an integral link between synaptic function and synaptopathies. *Trends Neurosci.* **35**, 293–304 (2012).
9. Henkemeyer, M. *et al.* Nuk controls pathfinding of commissural axons in the mammalian central nervous system. *Cell* **86**, 35–46 (1996).
10. Grunwald, I.C. *et al.* Kinase-independent requirement of EphB2 receptors in hippocampal synaptic plasticity. *Neuron* **32**, 1027–1040 (2001).
11. Henderson, J.T. *et al.* The receptor tyrosine kinase EphB2 regulates NMDA-dependent synaptic function. *Neuron* **32**, 1041–1056 (2001).
12. Kayser, M.S., Nolt, M.J. & Dalva, M.B. EphB receptors couple dendritic filopodia motility to synapse formation. *Neuron* **59**, 56–69 (2008).
13. Kayser, M.S., McClelland, A.C., Hughes, E.G. & Dalva, M.B. Intracellular and trans-synaptic regulation of glutamatergic synaptogenesis by EphB receptors. *J. Neurosci.* **26**, 12152–12164 (2006).
14. Himanen, J.P., Saha, N. & Nikolov, D.B. Cell-cell signaling via Eph receptors and ephrins. *Curr. Opin. Cell Biol.* **19**, 534–542 (2007).
15. Dalva, M.B. *et al.* EphB receptors interact with NMDA receptors and regulate excitatory synapse formation. *Cell* **103**, 945–956 (2000).

16. Nolt, M.J. *et al.* EphB controls NMDA receptor function and synaptic targeting in a subunit-specific manner. *J. Neurosci.* **31**, 5353–5364 (2011).
17. Palmer, A. *et al.* EphrinB phosphorylation and reverse signaling: regulation by Src kinases and PTP-BL phosphatase. *Mol. Cell* **9**, 725–737 (2002).
18. Henkemeyer, M., Itkis, O.S., Ngo, M., Hickmott, P.W. & Ethell, I.M. Multiple EphB receptor tyrosine kinases shape dendritic spines in the hippocampus. *J. Cell Biol.* **163**, 1313–1326 (2003).
19. Orioli, D., Henkemeyer, M., Lemke, G., Klein, R. & Pawson, T. Sek4 and Nuk receptors cooperate in guidance of commissural axons and in palate formation. *EMBO J.* **15**, 6035–6049 (1996).
20. O'Donnell, M., Chance, R.K. & Bashaw, G.J. Axon growth and guidance: receptor regulation and signal transduction. *Annu. Rev. Neurosci.* **32**, 383–412 (2009).
21. Cowan, C.A. *et al.* Ephrin-B2 reverse signaling is required for axon pathfinding and cardiac valve formation, but not early vascular development. *Dev. Biol.* **271**, 263–271 (2004).
22. Mendes, S.W., Henkemeyer, M. & Liebl, D.J. Multiple Eph receptors and B-class ephrins regulate midline crossing of corpus callosum fibers in the developing mouse forebrain. *J. Neurosci.* **26**, 882–892 (2006).
23. Petros, T.J., Shrestha, B.R. & Mason, C. Specificity and sufficiency of EphB1 in driving the ipsilateral retinal projection. *J. Neurosci.* **29**, 3463–3474 (2009).
24. Chenaux, G. & Henkemeyer, M. Forward signaling by EphB1/EphB2 interacting with ephrin-B ligands at the optic chiasm is required to form the ipsilateral projection. *Eur. J. Neurosci.* **34**, 1620–1633 (2011).
25. Ethell, I.M. *et al.* EphB/syndecan-2 signaling in dendritic spine morphogenesis. *Neuron* **31**, 1001–1013 (2001).
26. Bishop, A.C. *et al.* A chemical switch for inhibitor-sensitive alleles of any protein kinase. *Nature* **407**, 395–401 (2000).
27. Blethrow, J., Zhang, C., Shokat, K.M. & Weiss, E.L. Design and use of analog-sensitive protein kinases. *Curr. Protoc. Mol. Biol.* **18**, 18.11 (2004).
28. Chen, X. *et al.* A chemical-genetic approach to studying neurotrophin signaling. *Neuron* **46**, 13–21 (2005).
29. Bishop, A.C. *et al.* Design of allele-specific inhibitors to probe protein kinase signaling. *Curr. Biol.* **8**, 257–266 (1998).
30. Alaimo, P.J., Shogren-Knaak, M.A. & Shokat, K.M. Chemical genetic approaches for the elucidation of signaling pathways. *Curr. Opin. Chem. Biol.* **5**, 360–367 (2001).
31. Rozakis-Adcock, M., Fernley, R., Wade, J., Pawson, T. & Bowtell, D. The SH2 and SH3 domains of mammalian Grb2 couple the EGF receptor to the Ras activator mSos1. *Nature* **363**, 83–85 (1993).
32. Moeller, M.L., Shi, Y., Reichardt, L.F. & Ethell, I.M. EphB receptors regulate dendritic spine morphogenesis through the recruitment/phosphorylation of focal adhesion kinase and RhoA activation. *J. Biol. Chem.* **281**, 1587–1598 (2006).
33. Torres, R. *et al.* PDZ proteins bind, cluster, and synaptically colocalize with Eph receptors and their ephrin ligands. *Neuron* **21**, 1453–1463 (1998).
34. Chumley, M.J., Catchpole, T., Silvany, R.E., Kernie, S.G. & Henkemeyer, M. EphB receptors regulate stem/progenitor cell proliferation, migration, and polarity during hippocampal neurogenesis. *J. Neurosci.* **27**, 13481–13490 (2007).
35. Yucel, S., Dravis, C., Garcia, N., Henkemeyer, M. & Baker, L.A. Hypospadias and anorectal malformations mediated by Eph/ephrin signaling. *J. Pediatr. Urol.* **3**, 354–363 (2007).
36. Risley, M., Garrod, D., Henkemeyer, M. & McLean, W. EphB2 and EphB3 forward signalling are required for palate development. *Mech. Dev.* **126**, 230–239 (2009).
37. Choi, Y. *et al.* Discovery and structural analysis of Eph receptor tyrosine kinase inhibitors. *Bioorg. Med. Chem. Lett.* **19**, 4467–4470 (2009).
38. Qiu, R. *et al.* Regulation of neural progenitor cell state by ephrin-B. *J. Cell Biol.* **181**, 973–983 (2008).
39. Cowan, C.W. *et al.* Vav family GEFs link activated Ephs to endocytosis and axon guidance. *Neuron* **46**, 205–217 (2005).
40. Williams, S.E. *et al.* Ephrin-B2 and EphB1 mediate retinal axon divergence at the optic chiasm. *Neuron* **39**, 919–935 (2003).
41. Luria, V., Krawchuk, D., Jessell, T.M., Laufer, E. & Kania, A. Specification of motor axon trajectory by ephrin-B:EphB signaling: symmetrical control of axonal patterning in the developing limb. *Neuron* **60**, 1039–1053 (2008).
42. Williams, S.E., Mason, C.A. & Herrera, E. The optic chiasm as a midline choice point. *Curr. Opin. Neurobiol.* **14**, 51–60 (2004).
43. Bush, J.O. & Soriano, P. Ephrin-B1 regulates axon guidance by reverse signaling through a PDZ-dependent mechanism. *Genes Dev.* **23**, 1586–1599 (2009).
44. Takasu, M.A., Dalva, M.B., Zigmond, R.E. & Greenberg, M.E. Modulation of NMDA receptor–dependent calcium influx and gene expression through EphB receptors. *Science* **295**, 491–495 (2002).
45. McClelland, A.C., Sheffler-Collins, S.I., Kayser, M.S. & Dalva, M.B. Ephrin-B1 and ephrin-B2 mediate EphB-dependent presynaptic development via syntenin-1. *Proc. Natl. Acad. Sci. USA* **106**, 20487–20492 (2009).
46. Holmberg, J. & Frisen, J. Ephrins are not only unattractive. *Trends Neurosci.* **25**, 239–243 (2002).
47. Moon, M.S. & Gomez, T.M. Balanced Vav2 GEF activity regulates neurite outgrowth and branching *in vitro* and *in vivo*. *Mol. Cell. Neurosci.* **44**, 118–128 (2010).
48. Banko, M.R. *et al.* Chemical genetic screen for AMPKα2 substrates uncovers a network of proteins involved in mitosis. *Mol. Cell* **44**, 878–892 (2011).
49. Knight, Z.A. & Shokat, K.M. Chemical genetics: where genetics and pharmacology meet. *Cell* **128**, 425–430 (2007).
50. Batlle, E. *et al.* EphB receptor activity suppresses colorectal cancer progression. *Nature* **435**, 1126–1130 (2005).

ONLINE METHODS

Animals. *EphB1*^{T697G}, *EphB2*^{T699A} and *EphB3*^{T706A} single mutants were generated individually by homologous recombination in mouse ES cells. Mice harboring each of the knock-in mutations were intercrossed to obtain the triple homozygous AS-EphB TKI mice.

To generate the targeting constructs, the 5′ and 3′ arms was PCR amplified from J1 ES cell DNA using primers listed in **Supplementary Table 1** and subcloned into a modified pKSNeoDTA vector (originally constructed in the laboratory of P. Soriano, Mount Sinai Hospital) containing a *loxP-neo-loxP* cassette for positive selection and a diptheria toxin A negative-selection cassette (DTA). The analog-sensitive mutations were introduced by site-directed mutagenesis. The targeting constructs were confirmed by sequencing. Linearized targeting construct was electroporated into J1 ES cells, which were subsequently selected with G418. Correct targeting of ES cells was initially screened by PCR and then confirmed by Southern analysis and direct sequencing of PCR products amplified from the mutated alleles. The positive clones were karyotyped and the neomycin resistance cassette was removed by electroporating targeted ES cells with a Cre expression plasmid. ES cell clones were microinjected into C57BL/6 blastocysts to generate chimeric mice. Male chimeric animals were mated to C57BL/6 wild-type females for germline transmission of the targeted allele.

The ES cell targeting efficiencies were as follows: EphB1 knock-in (17 of 192, 9%), EphB2 knock-in (3 of 186, 2%) and EphB3 knock-in (12 of 96, 13%).

Mice were maintained as homozygotes in a mixed 129 and C57BL/6 background. Unless noted, wild-type mice were F1 offspring of a C57BL/6 × 129sv cross. Animals were housed under a 12-h light/dark cycle. No more than five animals were housed in each cage. Mice and embryos were chosen at random, regardless of sex, for treatment condition.

All experiments with mice were approved by the Animal Care and Use Committee of Harvard Medical School. E0 was defined as midnight preceding the morning a vaginal plug was found.

HEK 293 cell culture and transfection. HEK 293 cells were maintained in DMEM supplemented with 10% fetal bovine serum (vol/vol, Gibco), 2 mM glutamine (Gibco) and penicillin/streptomycin (100 U ml^{-1} and 100 μg ml^{-1}, respectively; Gibco). HEK 293 cells were transfected using the calcium phosphate method, as previously described[15].

Antibodies and western blotting. The following antibodies were purchased commercially: pan-phospho-tyrosine pY99 mouse monoclonal (Santa Cruz), EphB1 (H-80) and EphB3 (H-85) rabbit polyclonal (Santa Cruz), β-actin mouse monoclonal (Abcam), PSD-95 mouse monoclonal (Pierce), and synapsin rabbit polyclonal (Millipore). Mouse monoclonal antibody to neurofilament (2H3) was obtained from the Developmental Studies Hybridoma Bank (T. Jessell, Columbia University). Polyclonal rabbit antibodies to Vav2, pan-phospho-EphB and EphB2 (all at 1:1,000 dilution) were generated in M.E.G.'s laboratory and were described previously[15]. The phospho-specificity of the pan-phospho-EphB antibody was validated in HEK 293 cells for EphB1, EphB2 and EphB3 individually. All western blots were imaged and quantified using the Odyssey Infrared Imaging System (Licor) using fluorescently labeled secondary antibodies (Rockland Immunochemicals).

Protein binding assays. Full-length human Grb2 and rat Pick1 were PCR amplified from plasmids #26085 and #31613 (Addgene), respectively. Grb2 and Pick1 were fused to GST at their N termini by cloning them into a pGEX vector (Pharmacia), expressed in *E. coli*, and affinity purified on glutathione sepharose beads. GST, used as a negative control, was expressed from the empty pGEX vector. AS-EphB1 protein was expressed in HEK 293 cells by transient transfection and the cells were treated with either DMSO or 1 μM 1-NA-PP1 for 16 h. Cells were lysed in lysis buffer (30 mM HEPES (pH 7.7), 100 mM KCl, 1 mM $MgCl_2$, 2 mM DTT, 2 mM sodium orthovandadate, 1% Triton X-100 (vol/vol), protease inhibitor (Roche, 04693159001) and phosphatase inhibitor cocktails (Sigma, P5726, P0044)). The crude lysates were centrifuged at 70,000*g* for 20 min at 4 °C to generate the high-speed supernatants. High-speed supernatant was incubated with glutathione beads coated with approximately GST, GST-Grb2 or GST-Pick1 with rotation at 4 °C for 2 h. The beads were washed three times with lysis buffer and analyzed by SDS-PAGE and western blotting.

Pharmacology. 1-NA-PP1 was synthesized as described previously[27] and dissolved in DMSO. 3-MB-PP1 was synthesized using a similar procedure and dissolved in DMSO. Dose-response curves using 1-NA-PP1 and 3-MB-PP1 were calculated on GraphPad Prism using the least-squares method. The vehicle dose was calculated as two orders of magnitude below the lowest dose (0.05 nM). For wild-type EphBs, 100% inhibition was defined at 1 mM.

Neuronal cell culture. Cortical and hippocampal neurons were prepared from E15–17 mouse embryos as previously described[15]. Cultured neurons were maintained in Neurobasal medium (Invitrogen) supplemented with 1× B27 (Invitrogen), penicillin/streptomycin (100 U ml^{-1} and 100 μg ml^{-1}, respectively) and 2 mM glutamine. For biochemistry, neurons were seeded at a density of 2×10^6 neurons per well of a six-well plate coated with polyornithine (Sigma). For electrophysiology and imaging, neurons were seeded at a density of 7.5×10^4 neurons per well on a glial monolayer on glass coverslips coated with polyornithine and laminin (Invitrogen).

Organotypic slices. Hippocampal organotypic slices were prepared in ice-cold dissection media (1 mM $CaCl_2$, 5 mM $MgCl_2$, 10 mM D-glucose, 4 mM KCl, 26 mM $NaHCO_3$, 218 mM sucrose, 1.3 mM sodium phosphate and 30 mM HEPES, pH 7.4). Brains were isolated from P5–7 pups, and hippocampi were excised and chopped into 400-μm sections. Slices were cultured on Millicell cell culture inserts (Millipore) in media containing 20% horse serum, 1 mM L-glutamine, 0.0012% ascorbic acid (wt/vol), 1 μg ml^{-1} insulin, 1 mM $CaCl_2$, 2 mM $MgCl_2$, 2.3 mg ml^{-1} glucose, 0.44 mg ml^{-1} $NaHCO_3$ and 7.16 mg ml^{-1} HEPES in MEM.

Ephrin stimulation. For ephrin stimulations in dissociated cultured neurons and retinal explants, mouse ephrin-B1–Fc or ephrin-B2–Fc (R&D Systems) was pre-clustered for 50 min with goat antibody to human IgG Fc (Jackson ImmunoResearch, 109-001-008) at 22–25 °C in phosphate-buffered saline (PBS) at a molar ratio of 1:1 before stimulation. Pre-clustered ephrin-B1–Fc or ephrin-B2–Fc was added to the appropriate medium at a final concentration of 2.5 μg ml^{-1}. As a control, clustered human Fc in media was applied to neurons where specified.

Cell lysis and immunoprecipitation. Cultured cells were collected and homogenized in RIPA buffer (50 mM Tris (pH 8.0), 150 mM NaCl, 1% Triton X-100, 0.5% sodium deoxycholate, 0.1% SDS (wt/vol), 10 mM NaF, complete protease inhibitor cocktail tablet (Roche), 1 mM sodium orthovanadate, and phosphatase inhibitor cocktails 1 and 2 (1×, Sigma)). After clearing lysates, supernatants were incubated with the appropriate antibody for 1 h at 4 °C, followed by addition of Protein-A Fastflow agarose beads (Sigma) for 1 h. Beads were washed in lysis buffer or PBS three times and eluted in 2× SDS sample buffer followed by boiling.

Surface labeling. Labeling of surface proteins was performed using the Pierce Cell Surface Protein Isolation Kit (Thermo Scientific). After chronic treatment with vehicle or 1 μM 1-NA-PP1, cultured cortical neurons were incubated with EZ-link biotin for 30 min at 22–25 °C , washed with PBS, and lysed in RIPA buffer. Lysates were immunoprecipitated with an antibody to EphB2 or a control antibody, and probed with either antibody to EphB2 or fluorescently labeled streptavidin (Invitrogen).

Retinal explants. Ventrotemporal segments of retina were microdissected from E14.5 mouse embryos and cultured as previously described[51]. Embryos were removed from the uterus and decapitated, and heads were placed in ice-cold DMEM/F12 (Gibco). Ventrotemporal sections of the retina were excised and placed on glass coverslips coated with polyornithine and laminin. Explants were maintained in serum free medium (10 mg ml^{-1} BSA (Sigma), 1% ITS supplement (vol/vol) (Sigma), penicillin/streptomycin (20 U ml^{-1} and 20 μg ml^{-1}, respectively, Gibco) in DMEM/F12) supplemented with 0.2% methyl cellulose (wt/vol, Sigma) to increase media viscosity and minimize explant movement. All experiments were conducted 18–24 h after initial plating.

Immunocytochemistry and growth cone collapse assay. For experiments with inhibitor treatment, explants were pre-incubated with vehicle or PP1 analogs for 1 h, followed by a 30-min ephrin-B2 stimulation, with variations as described in the text. Following stimulation, retinal explants were fixed for 20 min at 25 °C with 4% paraformaldehyde (PFA)/2% sucrose (wt/vol) in PBS. Explants were

then blocked in 10% goat serum (vol/vol), 0.2% Tween-20 (vol/vol) in PBS for 1 h, followed by incubation with antibody to either neurofilament phospho-EphB in 50% blocking solution overnight. After PBS washes, explants were incubated in Alexa Fluor–conjugated secondary antibodies (Invitrogen) and Alexa Fluor 488–conjugated phalloidin (Invitrogen). Explants on coverslips were mounted on glass slides using Fluoromount-G (Southern Biotech). Neurons were imaged using a laser-scanning Zeiss Pascal microscope using a 40× objective with sequential acquisition settings at 1,024 × 1,024 pixel resolution. All imaging and image analysis were performed blind to the genotype and treatment condition of the samples. At least ten growth cones were analyzed per explant.

***In vivo* 1-NA-PP1 delivery.** Pregnant wild-type or AS-EphB TKI mice were injected subcutaneously twice daily with 80 mg per kg of body weight 1-NA-PP1 dissolved in 10% DMSO, 20% Cremaphor-EL and 70% saline (vol/vol) from E13.5–16.5 for optic tract experiments or from E12.5–19 for cortical tract experiments. All experiments included data from at least two separate litters of embryos per condition. Animals used for *in vivo* 1-NA-PP1 treatment had no prior exposure to 1-NA-PP1 or other drugs.

DiI labeling. DiI labeling was performed as previously described[52]. At E16.5, embryo heads were fixed in 4%PFA/2% sucrose in PBS overnight and then washed with PBS. The lens and retina were removed from the left eye and a small crystal of DiI (Invitrogen) was placed in the optic disc. The retina was then replaced securely and the heads were stored in PBS + 0.1% azide (wt/vol) at 22–25 °C for 12 d. After labeling, brains were removed and fluorescent optic tracts were imaged on a Leica MZ16F fluorescent stereomicroscope. Images were captured using Spot Advanced software. Labeling was quantified using Metamorph software by drawing rectangular regions of interest around the ipsilateral and contralateral tracts, subtracting background, and calculating the ipsilateral index on the basis of the integrated intensity of fluorescence: ipsilateral index = ipsilateral / (ipsilateral + contralateral). To compare wild-type and AS-EphB TKI responses with respect to 1-NA-PP1 treatment, each genotype was normalized to its untreated condition, producing a normalized ipsilateral index.

Analysis of corpus callosum phenotypes. E19.0 embryos were fixed in 4% PFA/2% sucrose in PBS for 2 d, then stored in PBS + 0.02% sodium azide at 4 °C. Brains were removed and vibratome sectioned to 70 µm. Sections were blocked in 5% normal donkey serum, 1% BSA, 0.2% glycine (wt/vol), 0.2% lysine (wt/vol) with 0.3% Triton X-100 in PBS at 22–25 °C for 1 h. To stain axon tracts, sections were incubated with rat antibody to L1-CAM (Millipore, MAB5272MI) at a 1:200 dilution in blocking solution at 4 °C overnight. Sections were washed three times with PBS and incubated with Cy3-conjugated donkey antibody to rat IgG (Jackson) for 1.5 h. Sections were washed 7–8 times with PBS and mounted with Aqua-mount (Lerner laboratories). Sections were imaged on an Olympus Bx51 epifluorescent microscope at 4× magnification. Corpus callosum partial agenesis was scored as the apparent failure of corpus callosal axons to cross the midline in a specific region along the rostral-caudal brain axis, and was evident by a gap in the dorsal midline region.

qPCR. Total RNA was isolated from mouse 7 DIV cortical cultures using Trizol reagent (Invitrogen) according to the manufacturer's instructions. Isolated RNA was treated with DNAseI Amplification Grade (Invitrogen) and a cDNA library was synthesized by cDNA High Capacity cDNA Reverse Transcription Kit (Applied Biosystems). The cDNA was the source of input for qPCR, using a Step One Plus Real-Time PCR Instrument and SYBR Green reagents (Applied Biosystems). The relative expression plot was generated using concentration values that were normalized to corresponding actin concentrations. The following qPCR primer pairs were used: EphB1 forward, ACTGCAGAGTTGGGATGGAC; EphB1 reverse, CATCATAGCCACTGACTTCTTCC; EphB2 forward, TTCATGG AGAACGGATCTCTG; EphB2 reverse, GACTGTGAACTGCCCATCG; EphB3 forward, CCCTGGACTCCTTTCTACGG; EphB3 reverse, GCAATGCC TCGTAACATGC.

Analysis of dendritic spines. For dissociated neuron experiments, cortical neurons were cultured as described above and grown on a monolayer of astrocytes on glass coverslips. Neurons were treated with vehicle or PP1 analogs at 10 DIV and media was changed entirely every 3–4 d (using neuronally pre-conditioned media). Neurons were transfected with GFP at 10 DIV using Lipofectamine 2000 and fixed with 4% PFA/2% sucrose in PBS at 21 DIV. Cells on coverslips were stained for GFP and mounted on slides using Fluoromount-G.

Neurons were imaged on a Zeiss Pascal confocal microscope, using a 63× objective, and maximal *z* projections were analyzed using Metamorph software. Multiple sections of dendrite totaling >50 µM were counted for each neuron.

For experiments in slice, hippocampal slices were treated with vehicle or PP1 derivatives at 2 DIV and media/drug were fully replaced every 2–3 d. At 2–3 DIV, plasmids encoding GFP (or GFP and EphB shRNAs) was biolistically transfected using a Helios gene gun. DNA bullets were prepared from 1.6-µm gold microcarrier particles (Biorad). After 8–9 DIV, slices were fixed in 3.2% PFA/5% sucrose in PBS for 1 h and stained with chicken antibody to GFP (Aves Labs) and rabbit antibody to NeuN (Millipore, clone A60, 1:1,000 dilution) to visualize the structure of hippocampal fields. Basal and apical dendrites were analyzed separately and sections of dendrite totaling >50 µM were counted for each neuron.

Electrophysiology. For experiments in dissociated neurons, whole-cell voltage-clamp recordings were obtained using an Axopatch 200B amplifier at 25 °C. During recordings, neurons were perfused with artificial cerebrospinal fluid containing 127 mM NaCl, 25 mM $NaHCO_3$, 1.25 mM Na_2HPO_4, 2.5 mM KCl, 2 mM $CaCl_2$, 1 mM $MgCl_2$, 25 mM glucose, and saturated with 95% O_2, 5% CO_2. Vehicle or 1-NA-PP1 treatment was initiated at 3 DIV and continued throughout recordings. The internal solution used in all eletrophysiological experiments contained 120 mM cesium methane sulfonate, 10 mM HEPES, 4 mM $MgCl_2$, 4 mM Na_2ATP, 0.4 mM Na_2GTP, 10 mM sodium phosphocreatine and 1 mM EGTA. Osmolarity and pH were adjusted to 310 mOsm and 7.3 with Millipore water and CsOH, respectively.

mEPSCs were isolated by exposing neurons to 0.5 µM tetrodotoxin, 50 µM picrotoxin, and 10 µM cyclothiazide (all from Tocris Bioscience). Cells with series resistance larger than 25 MΩ during the recordings were discarded. Data were analyzed in IgorPro (Wavemetrics) using custom-written macros. For each trace, the event threshold was set 1.5-fold greater than the root-mean-square current. Currents were counted as events if they crossed the event threshold, had a rapid rise time (1.5 pA ms^{-1}) and had an exponential decay ($\tau < 50$ ms for mEPSC).

As a control for inhibition of EphBs, concurrent plates of neurons were treated with inhibitor and at the time of recording were stimulated with ephrin-B1 for 30 min. Neurons were lysed in 1× SDS-sample buffer, run on western blot and probed with rabbit antibody to phospho-Eph and mouse antibody to β-actin (Abcam).

For mEPSC experiments in organotypic hippocampal slices, whole-cell voltage-clamp recordings were made from visually identified CA1 pyramidal neurons and the mEPSC amplitude and frequency measured. Slices were treated with vehicle or 1-NA-PP1 from 2 DIV until the time of recording.

To evaluate evoked synaptic transmission, the Schafer collaterals were depolarized with an extracellular stimulating electrode and the postsynaptic eEPSC response measured from CA1 neurons[53]. In these experiments, the artificial cerebrospinal fluid contained 4 mM Sr^{2+} instead of $CaCl_2$ and 4 mM $MgCl_2$ so that the extracellular stimulation resulted in asynchronous presynaptic vesicle fusion. The stimulus strength was set so that the initial postsynaptic response was 50–100 pA and the current amplitude and frequency of the asynchronous EPSCs occurring 400–900 ms post-stimulation was measured. Slices were treated with vehicle or 1-NA-PP1 from 2 DIV until the time of recording. Analysis of eEPSCs was performed using custom-written macros in IgorPro.

Statistical analysis. All animal experiments contained pups from multiple litters. All imaging analyses were done blind to condition. No data points were excluded in any experiment. Unpaired *t* tests and two-way ANOVA (for comparing effect of drug on AS EphB TKI versus wild-type neurons) analyses were conducted using GraphPad Prism software. All tests are two-sided (standard).

51. Petros, T.J., Bryson, J.B. & Mason, C. Ephrin-B2 elicits differential growth cone collapse and axon retraction in retinal ganglion cells from distinct retinal regions. *Dev. Neurobiol.* **70**, 781–794 (2010).
52. Plump, A.S. *et al.* Slit1 and Slit2 cooperate to prevent premature midline crossing of retinal axons in the mouse visual system. *Neuron* **33**, 219–232 (2002).
53. Xu-Friedman, M.A. & Regehr, W.G. Presynaptic strontium dynamics and synaptic transmission. *Biophys. J.* **76**, 2029–2042 (1999).

Neuron
Article

Using Whole-Exome Sequencing to Identify Inherited Causes of Autism

Timothy W. Yu,[1,2,3,4,5,6,7,32,*] Maria H. Chahrour,[1,2,3,4,5,7,32] Michael E. Coulter,[1,2,3,5] Sarn Jiralerspong,[8] Kazuko Okamura-Ikeda,[9] Bulent Ataman,[10] Klaus Schmitz-Abe,[1,2,5] David A. Harmin,[10] Mazhar Adli,[11] Athar N. Malik,[10] Alissa M. D'Gama,[5] Elaine T. Lim,[12] Stephan J. Sanders,[13] Ganesh H. Mochida,[1,2,3,5,6] Jennifer N. Partlow,[1,2,3] Christine M. Sunu,[1,2,3] Jillian M. Felie,[1,2,3] Jacqueline Rodriguez,[1,2,3] Ramzi H. Nasir,[5,14] Janice Ware,[5,14] Robert M. Joseph,[4,15] R. Sean Hill,[1,2,3,5] Benjamin Y. Kwan,[16] Muna Al-Saffar,[1,2,17] Nahit M. Mukaddes,[18] Asif Hashmi,[19] Soher Balkhy,[20] Generoso G. Gascon,[6,18,21] Fuki M. Hisama,[22] Elaine LeClair,[5,14] Annapurna Poduri,[5,23] Ozgur Oner,[24] Samira Al-Saad,[25] Sadika A. Al-Awadi,[26] Laila Bastaki,[26] Tawfeg Ben-Omran,[27,28] Ahmad S. Teebi,[27,28] Lihadh Al-Gazali,[17] Valsamma Eapen,[29] Christine R. Stevens,[7] Leonard Rappaport,[4,5,14] Stacey B. Gabriel,[7] Kyriacos Markianos,[1,2,5] Matthew W. State,[13] Michael E. Greenberg,[10] Hisaaki Taniguchi,[9] Nancy E. Braverman,[8] Eric M. Morrow,[4,30,31] and Christopher A. Walsh[1,2,3,4,5,7,*]

[1]Division of Genetics, Department of Medicine
[2]Manton Center for Orphan Disease Research
[3]Howard Hughes Medical Institute
Boston Children's Hospital, Boston, MA 02115, USA
[4]The Autism Consortium, Boston, MA 02115, USA
[5]Harvard Medical School, Boston, MA 02115, USA
[6]Department of Neurology, Massachusetts General Hospital, Boston, MA 02114, USA
[7]Program in Medical and Population Genetics, Broad Institute of Massachusetts Institute of Technology and Harvard University, Cambridge, MA 02142, USA
[8]Department of Human Genetics and Pediatrics, McGill University, Montreal Children's Hospital Research Institute, Montreal, QC H3H 1P3, Canada
[9]Institute for Enzyme Research, The University of Tokushima, Tokushima 770-8501, Japan
[10]Department of Neurobiology, Harvard Medical School, Boston, MA 02115, USA
[11]Department of Biochemistry and Molecular Genetics, School of Medicine, University of Virginia, Charlottesville, VA 22908, USA
[12]Analytic and Translational Genetics Unit, Center for Human Genetic Research, Massachusetts General Hospital, Boston, MA 02114, USA
[13]Department of Genetics, Center for Human Genetics and Genomics and Program on Neurogenetics, Yale University School of Medicine, New Haven, CT 06510, USA
[14]Division of Developmental Medicine, Boston Children's Hospital, Boston, MA 02115, USA
[15]Department of Anatomy and Neurobiology, Boston University School of Medicine, Boston, MA 02118, USA
[16]Schulich School of Medicine and Dentistry, Western University, London, ON N6A 5C1, Canada
[17]Department of Paediatrics, Faculty of Medicine and Health Sciences, United Arab Emirates University, Al Ain, United Arab Emirates
[18]Istanbul Faculty of Medicine, Department of Child Psychiatry, Istanbul University, Istanbul 34452, Turkey
[19]Armed Forces Hospital, King Abdulaziz Naval Base, Jubail 31951, Kingdom of Saudi Arabia
[20]Department of Neurosciences and Pediatrics, King Faisal Specialist Hospital and Research Center, Jeddah 21499, Kingdom of Saudi Arabia
[21]Clinical Neurosciences and Pediatrics, Brown University School of Medicine, Providence, RI 02912, USA
[22]Division of Medical Genetics, Department of Medicine, University of Washington, Seattle, WA 98195, USA
[23]Department of Neurology, Boston Children's Hospital, Boston, MA 02115, USA
[24]Department of Child and Adolescent Psychiatry, Dr Sami Ulus Childrens' Hospital, Telsizler, Ankara 06090, Turkey
[25]Kuwait Center for Autism, Kuwait City 73455, Kuwait
[26]Kuwait Medical Genetics Center, Kuwait City 72458, Kuwait
[27]Section of Clinical and Metabolic Genetics, Department of Pediatrics, Hamad Medical Corporation, Doha, Qatar
[28]Departments of Pediatrics and Genetic Medicine, Weill Cornell Medical College, New York, NY 10065, USA, and Doha, Qatar
[29]Academic Unit of Child Psychiatry South West Sydney (AUCS), University of New South Wales, Sydney, New South Wales 2170, Australia
[30]Department of Molecular Biology, Cell Biology and Biochemistry
[31]Department of Psychiatry and Human Behavior
Brown University, Providence, RI 02912, USA
[32]These authors contributed equally to this work
*Correspondence: timothy.yu@childrens.harvard.edu (T.W.Y.), christopher.walsh@childrens.harvard.edu (C.A.W.)
http://dx.doi.org/10.1016/j.neuron.2012.11.002

SUMMARY

Despite significant heritability of autism spectrum disorders (ASDs), their extreme genetic heterogeneity has proven challenging for gene discovery. Studies of primarily simplex families have implicated de novo copy number changes and point mutations, but are not optimally designed to identify inherited risk alleles. We apply whole-exome sequencing (WES) to ASD families enriched for inherited causes due to consanguinity and find familial ASD associated

with biallelic mutations in disease genes (*AMT*, *PEX7*, *SYNE1*, *VPS13B, PAH*, and *POMGNT1*). At least some of these genes show biallelic mutations in nonconsanguineous families as well. These mutations are often only partially disabling or present atypically, with patients lacking diagnostic features of the Mendelian disorders with which these genes are classically associated. Our study shows the utility of WES for identifying specific genetic conditions not clinically suspected and the importance of partial loss of gene function in ASDs.

INTRODUCTION

Despite studies suggesting that autism spectrum disorders (ASDs) are significantly heritable, the basis of this heritability remains largely unexplained (Devlin and Scherer, 2012). Autism is characterized by the triad of communication deficits, abnormal social interests, and restricted and repetitive behaviors. Genome-wide association studies (GWAS) have so far detected no strong contribution of common alleles (State, 2010), motivating renewed interest in rare variants (Malhotra and Sebat, 2012). Transmitted, rare copy number variants (CNVs), such as 16p11.2 microdeletion/duplication and 15q11.2–q13 duplication have been found to contribute, although the total number of cases accounted for by these conditions is small (Levy et al., 2011; Pinto et al., 2010; Weiss et al., 2008). Significant roles have also been demonstrated for diverse, de novo CNVs (Levy et al., 2011; Sanders et al., 2011; Sebat et al., 2007) and more recently, de novo, protein-altering point mutations (Iossifov et al., 2012; Neale et al., 2012; O'Roak et al., 2011; O'Roak et al., 2012; Sanders et al., 2012). In the cohorts examined, de novo events may be projected to account for up to 15%–20% of ASD cases. Despite the high total rate of de novo point mutations, estimates of the number of contributing loci to autism susceptibility are in the several hundreds, so that validating specific causative genes is a significant challenge, since recurrent mutation in any given gene is so uncommon. Nonetheless, these studies have been successful at elucidating gene dosage-sensitive ASD molecular pathways, since the typical mutations observed are loss/disruption, or sometimes gain, of one functional copy of a gene or contiguous genes, rather than biallelic mutations of both copies of a gene. However, despite the importance of de novo mutations, much of the heritability of ASDs remains unaccounted for (Devlin and Scherer, 2012).

We hypothesized that at least some cases of autism reflect rare, inherited point mutations that existing study designs, often involving families with one or two affected individuals, are not designed to capture. Consanguineous and multiplex pedigrees have been extremely useful for identifying inherited mutations responsible for rare heritable conditions in the setting of extreme genetic heterogeneity, because single families can provide substantial genetic linkage evidence (Lander and Botstein, 1987; Woods et al., 2006). Applying high-throughput sequencing to such families has been extremely useful in identifying recessive causes of intellectual disability (Najmabadi et al., 2011). The potential role of biallelic mutations in ASDs is strongly supported by a number of syndromic recessive conditions that have already been associated with autistic symptoms (Betancur, 2011). Additional evidence supporting a role of biallelic mutations comes from studies that have implicated homozygous CNVs (Levy et al., 2011; Morrow et al., 2008) and long homozygous intervals as significantly associated with ASDs (Casey et al., 2012). Finally, a recent whole-exome sequencing (WES) study has suggested a role for biallelic point mutations in a subset of patients with ASDs that show long runs of homozygosity (Chahrour et al., 2012).

In this study, we apply WES to a cohort of consanguineous and/or multiplex families with ASD that also show shared ancestry between the parents, typically as cousins. We find several families where mapping and sequence analysis allow the identification of specific causative mutations and show that many of these mutations represent partial loss of function in genes where null mutations cause distinctive Mendelian disorders. These hypomorphic mutations confirm the complex and heterogeneous nature of ASDs, but also highlight the importance of WES in identifying specific genetic causes underlying this heterogeneity.

RESULTS

Identifying Inherited Mutations in Three ASD Families

We studied an ASD cohort recruited by the Homozygosity Mapping Collaborative for Autism (HMCA), an international, multicenter effort to identify genetically informative ASD families with consanguinity and/or multiple affected individuals (Morrow et al., 2008). We first performed genome-wide linkage analysis on the most informative families, using high-resolution single nucleotide polymorphism (SNP) arrays, reasoning that some families would show homozygous, biallelic mutations embedded within larger blocks of homozygosity inherited from the ancestor common to both parents. Families were prescreened to exclude those harboring autism-associated CNVs or other known diagnoses (Supplemental Experimental Procedures). Three families provided particularly strong genetic power to localize potential disease loci.

The first family had three children affected with ASD and two unaffected children, born to parents who were first cousins (Figure 1A; Table 1B; see Supplemental Text available online). Mapping under a single locus, biallelic model (i.e., allowing for both homozygous and compound heterozygous mutations) excluded 99.3% of the genome and revealed a single linkage peak centered at 3p21.31, in a large homozygous interval, reaching the maximum LOD score obtainable in the pedigree, 2.96 (Figure 1B), suggesting a >900:1 likelihood that the responsible mutation was contained within this homozygous interval. WES of a single affected child was performed. The linked interval contained only a single rare, nonsynonymous change that was absent from known databases and population-matched controls: a homozygous single base substitution in the aminomethyltransferase (*AMT*) gene, encoding an enzyme essential for the degradation of glycine. The mutation resulted in p.I308F, altering an Ile residue that is highly conserved in all *AMT* orthologs (Figure 1C) and is packed tightly into a hydrophobic pocket

(Figure 1D; Okamura-Ikeda et al., 2005). Sanger validation confirmed that the mutation was heterozygous in both parents, homozygous in all affected children, and absent or heterozygous in the two unaffected children.

Mutations in *AMT* classically cause nonketotic hyperglycinemia (NKH) (Applegarth and Toone, 2004), a neonatal syndrome leading to progressive lethargy, hypotonia, severe seizures, and death within the first year of life (Hamosh and Johnston, 2001). Patients with neonatal NKH have impaired activity of the glycine cleavage system, leading to abnormal elevation of glycine levels in serum or cerebrospinal fluid (CSF). Rarer, atypical forms of NKH have been described in association with hypomorphic, missense *AMT* mutations (Applegarth and Toone, 2001; Dinopoulos et al., 2005), manifesting as later age of clinical onset, delays in expressive language, behavioral problems, and variable or absent seizures. Clinical and biochemical evidence suggests that the p.I308F mutation is hypomorphic. While individually nondiagnostic, the three affected children in this family exhibited a range of neurologic symptoms that in aggregate were strongly suggestive of NKH (Supplemental Text). The eldest child was twelve years old and had, in addition to a diagnosis of ASD, a history of severe epilepsy, with first seizures presenting by age 10 months, very consistent with NKH. The second child was nine years old and also suffered from a combination of autism and epilepsy, though her seizures were milder. The third child was two years old, suffered from language and motor delays, and carried a presumptive PDD diagnosis. He had had only a single febrile seizure. Though the two older children had had plasma amino acid screening that disclosed no abnormalities, milder forms of NKH typically have no abnormalities on serum biochemical analyses (Applegarth and Toone, 2001; Dinopoulos et al., 2005).

Direct biochemical analysis of the p.I308F mutation confirms that it has reduced activity. While wild-type AMT is fully soluble at 30°C when expressed in bacteria, mutant AMT p.I308F was very poorly soluble (Figure 1E), indicating a protein folding defect, similar to that observed with NKH-associated AMT mutations (Figure S1; Table S1). This defect could be rescued by co-expressing GroES and GroEL heat-shock proteins at 22°C (Figure 1E). AMT p.I308F, even after solubilization, retained only 45% (SD 4.1%) and 1.8% (SD 0.5%) of wild-type glycine cleavage and glycine synthesis specific activity, respectively, when assayed enzymatically (Figures 1F and S2). When compared to classical NKH-associated alleles, glycine cleavage activity of AMT p.I308F is at the mild end of the range of previously reported values (Figures 1F and S2), further suggesting that the affected autistic children in this family suffer from undiagnosed, atypical NKH presenting as ASD and seizures.

A second consanguineous family had three children diagnosed with ASD and three unaffected children, born to unaffected parents who were first cousins (Figure 2A; Table 1B; Supplemental Text). Parametric mapping excluded 97.2% of the genome and established linkage to a homozygous interval on 6p23 (Figure 2B) (LOD 2.78, the maximum obtainable in the pedigree, under a recessive model, indicating a >600:1 likelihood that this interval contained the disease-causing mutation). WES identified only one variant, absent from known databases and population-matched controls, in this region that was predicted to be pathogenic: *PEX7* p.W75C. This change was homozygous and altered a highly conserved Trp residue within a WD-40 repeat of the predicted protein (Figures 2C and 2D). Sanger validation confirmed that this mutation was heterozygous in both parents, and heterozygous or wild-type in unaffected children.

PEX7 encodes a receptor required for import of PTS2 (peroxisome targeting signal 2)-containing proteins into the peroxisome (Braverman et al., 1997). Null mutations in *PEX7* cause rhizomelic chondrodysplasia punctata (RCDP), an inborn metabolic syndrome of abnormal facies, cataracts, skeletal dysplasia, epilepsy, and severe psychomotor defects, with most cases not surviving beyond two years of age (Braverman et al., 2002; Braverman et al., 1997; Motley et al., 1997). The affected children in this family, however, ranged in age from 18 to 31 years. They were not dysmorphic and did not exhibit skeletal dysplasia, though two had cataracts and two had epilepsy (Supplemental Text). The cataracts and seizures in particular suggested partial loss of *PEX7* function, since rare, atypical RCDP cases associated with hypomorphic compound heterozygous or homozygous mutations have been described that have some but not all of the features of the classical syndrome, lacking dysmorphic features and showing only intellectual disability with variable cataracts (Braverman et al., 2002).

To evaluate whether the p.W75C missense change in this family could be pathogenic, we assayed its ability to rescue peroxisomal import in cultured fibroblasts from a RCDP patient. In RCDP fibroblasts, fluorescent mCherry fused to the PTS2 peroxisomal targeting sequence fails to be imported into peroxisomes and remains cytosolic (Figure 2E). Cotransfection of wild-type *PEX7* fully restores peroxisomal import (Figure 2E). In contrast, transfection with *PEX7* p.W75C failed to rescue (Figure 2E): the majority of cells showed cytosolic PTS2-mCherry, although a fraction showed partial rescue. To characterize this effect, we utilized a semiquantitative assay of peroxisomal import. The PTS2 proteins thiolase, phytanoyl-CoA hydroxylase (PhyH), and alkylglycerone phosphate synthase (AGPS) are imported into the peroxisome and proteolytically processed into smaller, mature forms (Figure 2F). Peroxisomal uptake is thus reflected in the ratio of the mature protein to the preprotein. In RCDP cells, these three proteins all remain in the preprotein state, reflecting failure of peroxisomal import. Transfection of wild-type *PEX7* fully restores processing, whereas transfection of *PEX7* p.W75C produced only partial processing (Figure 2F). These results demonstrate that this allele is pathogenic, but partial loss of function, consistent with these individuals not exhibiting full features of the RCDP syndrome.

To our knowledge, a link between mild RCDP and ASDs has not been described previously. However, two previously reported patients with biochemical evidence of RCDP and cataracts, but lacking the dysmorphic features of RCDP, were found to be compound heterozygous for partial loss-of-function *PEX7* mutations (Braverman et al., 2002); one was originally described as intellectually disabled and the second as neurotypical. We recontacted these patients. A review of clinical records and reexamination of the first child revealed that she had subsequently been diagnosed with ASD, and the second child was diagnosed with severe ADHD, providing additional examples of the range of clinical expressivity of mild mutations in *PEX7*. Partial loss of

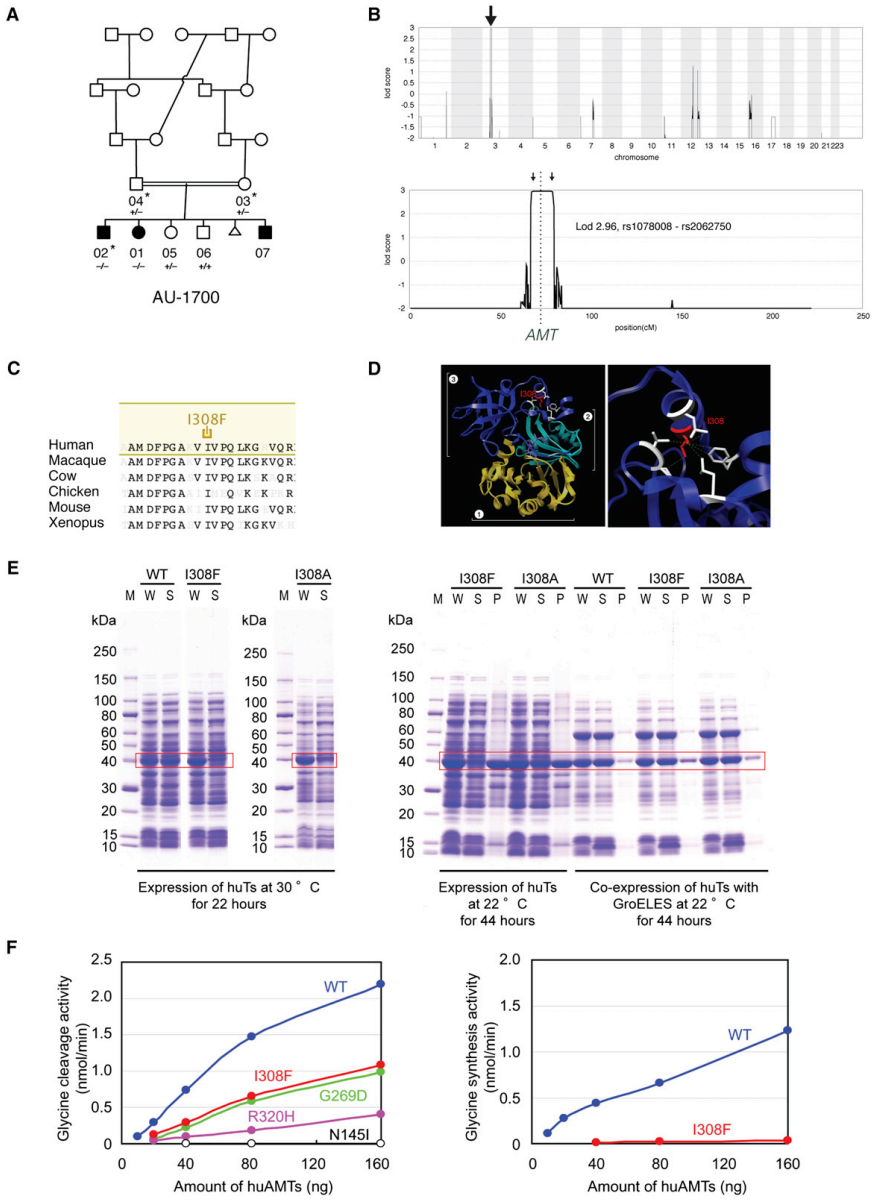

Figure 1. Identification of Mutations in *AMT* in a Family with ASD

(A) AU-1700, a Saudi family with three children affected by autism. Shaded symbols indicate affected individuals. The triangle represents a miscarriage. WES was performed on samples from individuals indicated with a star. Genotyping by Sanger sequencing in additional family members was performed where indicated (+, reference allele; −, alternate allele).

(B) Mapping to a locus on chromosome 3. Genome-wide linkage plot (top) and maximum obtainable LOD score in the family across the interval (bottom).

(legend continued on next page)

function for one of the alleles in these patients, S25F, was verified in fibroblast assays (Figures 2E and 2F).

Analysis of a third large family pointed to a candidate autism gene potentially implicated in synaptic plasticity, *SYNE1*. In this family, five children were born to parents who were double first cousins. Four were affected with autism and the fifth child was unaffected (Figure 3A; Supplemental Text). The family showed linkage to two loci on chromosome 6q25 and 7q33 (LOD 2.83, maximal obtainable in the pedigree, indicating a >670:1 chance that the disease-causing gene lies in one of these intervals) (Figure 3B). WES was performed for the entire nuclear family. No rare, protein-altering variants were found in the 7q33 linkage interval, whereas 6q25 harbored only one protein-altering variant, absent from known databases and population-matched controls, that segregated with disease: a homozygous missense change in *SYNE1* (p.L3206M) (Table 1). *SYNE1* has previously been implicated as an ASD gene candidate by the presence of a de novo single nucleotide variant in a patient with ASD (O'Roak et al., 2011) and has been implicated in bipolar disorder in a GWAS study (Sklar et al., 2011; Figure 3C). Truncating, presumably null, mutations in *SYNE1* cause cerebellar ataxia (Gros-Louis et al., 2007) and a recessive form of arthrogryposis multiplex congenita (Attali et al., 2009; Figure 3C), again suggesting that the ASD-associated allele may be hypomorphic, since the phenotype is milder. *SYNE1* p.L3206M alters a highly conserved residue that lies within a spectrin repeat (Figure 3D; SIFT score 0.01).

Full-length *SYNE1* encodes a large 8,797 amino acid protein with two N-terminal actin-binding domains, multiple spectrin repeats, a transmembrane domain, and a C-terminal KASH domain. The *SYNE1* mutation identified here is predicted to map to exon 61 of the full-length transcript (RefSeq NM_182961), although the *SYNE1* locus is complex, with many predicted alternative splice forms (Simpson and Roberts, 2008).

To identify what human transcript(s) might be affected by the p.L3206M mutation, we mapped transcriptional start sites in human neurons using ChIPseq (Figure 3E). ChIPseq using antibodies to H3K4Me3, a mark associated with active promoter sites (Ernst et al., 2011), and to H3K27Ac, a mark associated with enhancer elements (Heintzman et al., 2009), demonstrated mapped read peaks corresponding to at least four major transcriptional start sites within the *SYNE1* locus (P1–P4), one of which (P3) lies immediately upstream of the p.L3206M mutation (Figure 3E). 5′ and 3′ RACE (data not shown) confirmed the existence of at least one polyadenylated transcript emanating from this promoter, corresponding to GenBank mRNA clone BC039121, encompassing exons 57–63 of the predicted full-length *SYNE1* mRNA. This is the minimal confirmed transcript that overlaps the p.L3206M mutation, although contributions of additional or even full-length transcripts cannot be excluded.

SYNE1 has been shown to have roles in cellular nuclear migration in *C. elegans* and *Drosophila* (Starr and Han, 2002; Zhang et al., 2002), anchoring of synaptic nuclei with postsynaptic membranes at the vertebrate neuromuscular junction (Grady et al., 2005), although based upon patients with SYNE1-associated cerebellar ataxia, it has been suggested that vertebrates may have compensatory mechanisms for these two processes and that SYNE1 may have adapted to perform a specialized function in the brain (Gros-Louis et al., 2007). In rodents, a spectrin-rich splice form of *SYNE1* called *CPG2* has been shown to control dendritic spine shape and glutamate receptor turnover in response to neuronal activity (Cottrell et al., 2004). To test whether *SYNE1* might be responsive to neuronal activity, we performed RNaseq on cultured human primary neurons, before and after depolarization. Transcription of full-length *SYNE1* was induced 1.27-fold (n = 5, SE 0.06, p = 0.0203, t test, one-tailed) by neuronal activity, and transcription of BC039121 was induced by 1.50-fold (n = 5, SE 0.11, p = 0.0225, t test, one-tailed) across five biological replicates (Figures 3E and S2). This suggests that both full-length *SYNE1* and the shorter BC039121 isoform may have neuronal activity-dependent roles in regulating synaptic strength, like other synaptic genes implicated in autism.

WES for Known Disease Genes

Our findings of inherited, biallelic, hypomorphic ASD mutations in larger families prompted us to ask whether additional cases of ASD might be explained by either unsuspected or atypical presentations of known diseases. Over 450 genes have been identified that, when mutated, have neurocognitive impact (van Bokhoven, 2011). To increase the specificity of our analysis, we chose to analyze a limited subset of 70 of these genes, each associated with a monogenic, autosomal recessive or X-linked neurodevelopmental syndrome in which autistic features have been previously described (Table S2; Betancur, 2011). We also screened for additional alleles of *AMT*, *PEX7*, and *SYNE1*. We used WES to screen for mutations in these genes in a total of 163 consanguineous and/or multiplex families using established heuristic filtering for rare, high penetrance disease (Bamshad et al., 2011; Stitziel et al., 2011) to identify homozygous, compound heterozygous, or hemizygous variants

(C) Ile308 residue is highly conserved across species.
(D) Mapping of the I308F missense mutation onto the human AMT crystal structure (PDB accession 1WSV). (Left) Overview showing I308 in domain 3 of AMT. (Right) Detail illustrating the hydrophobic pocket in which I308 resides. Neighboring hydrophobic residues are shown in white. The white brackets indicate the different domains: AMT domain 1 (folding); AMT domain 2 (catalytic); AMT domain 3 (capping).
(E) I308F results in protein misfolding and aggregation. C-terminal 6xHis-tagged human AMT, AMT I308F, and AMT I308A were expressed in *E. coli*. (Left) When overexpressed at 30°C by induction with 25 μM IPTG, wild-type AMT was fully soluble, but I308F and I308A segregated to inclusion bodies despite overall similar expression levels. W, whole-cell extract; S, supernatant; P, pellet. Right panel, slower induction at 22°C for 44 hr resulted in partially soluble mutants. Near-wild-type solubility could be achieved by coexpression with GroEL and GroES.
(F) AMT I308F results in partial loss-of-function of glycine cleavage and synthesis activity. Wild-type and mutant 6xHis-human AMT were expressed in *E. coli*, purified, and assayed for glycine cleavage and glycine synthesis activity. Relative to wild-type (blue traces), AMT I308F (red traces) demonstrates significant reduction of activity in glycine cleavage (left) and glycine synthesis (right) assays. R320H, N145I, and G269D are previously reported NKH-associated alleles (Okamura-Ikeda et al., 2005).
See also Figures S1, S2, and S5 and Table S1.

Table 1. Inherited Mutations Identified in ASDs

(A) Severe Mutations

Mutation	Known Disease Association	Family	Structure	Consanguinity	# Affected	# Unaffected	Linkage	Primary Phenotype	Additional Phenotypes
MECP2 p.E483X	Rett syndrome, ASD	AU-5400	Multiplex	No	2 (2M)	–	Yes	Autism	–
NLGN4X p.Q329X	Nonsyndromic X-linked ID and/or ASD	AU-5700	Simplex	Yes	1 (M)	1	Yes	Autism	–
PAH p.198_205 del	Phenylketonuria	AU-13100	Simplex	Yes	1 (M)	2	Yes	Autism	ID
PAH p.Q235X	Phenylketonuria	AU-4100	Multiplex	Yes	2 (2F)	–	Yes	Autism	–
VPS13B p.A3943fs	Cohen syndrome	AU-21100	Simplex	Yes	1 (M)	3	Yes	Autism	ID, dysmorphic features, hyperextensible joints

(B) Hypomorphic Mutations

Mutation	Known Disease Association	Family	Structure	Consanguinity	#Affected	# Unaffected	Linkage	Primary Phenotype	Additional Phenotypes
AMT p.I308F	Nonketotic hyperglycinemia	AU-1700	Multiplex	Yes	3 (2M, 1F)	2	Yes	Autism	ID, seizures
AMT p.D198G	Nonketotic hyperglycinemia	AU-11800	Simplex	Yes	1 (M)	1	Yes	Autism	ID, seizures
PEX7 p.W75C	Rhizomelic chondrodysplasia punctata	AU-3500	Multiplex	Yes	3 (2M, 1F)	3	Yes	PDD-NOS	ID, seizures, cataracts
POMGNT1 p.R367H	Muscle-eye-brain disease	AU-13300	Simplex	Yes	1 (M)	1	Yes	Autism	ID
SYNE1 p.L3206M	Autosomal recessive cerebellar ataxia type 1, arthrogryposis congenita, ASD, bipolar disease	AU-1600	Multiplex	Yes	4 (1M, 3F)	1	Yes	Autism	ID
VPS13B p.S824A	Cohen syndrome	AU-17800	Simplex	Yes	1 (M)	1	Yes	Autism	ID, dysmorphic features, hyperextensible joints

Severe (nonsense, frameshift) (A) and hypomorphic (missense) (B) mutations in known disease genes were identified in 11 ASD families. M, male; F, female; ID, intellectual disability. See also Tables S3 and S4.

with allele frequencies of less than 1% (dbSNP132, 1000 Genomes Project, NHLBI Exome Sequencing Project, and population-matched controls consisting of 831 exomes from the Middle Eastern population; see Experimental Procedures for details) and which were predicted to be protein altering (missense, nonsense, splice site, or frameshift). Candidate mutations were confirmed by Sanger sequencing in the entire family and were required to segregate with disease status within the family (i.e., homozygous or hemizygous in the affected individuals, inherited in the heterozygous state from parents, and heterozygous or absent from unaffected siblings). An overview of the analytic strategy is shown in Figure 4.

In five families (Tables 1A and S4), our screen revealed molecular genetic diagnoses due to severe loss of function (nonsense or frameshift) hemizygous or homozygous mutations in known genes. One of these was a nonsense mutation in *NLGN4X* (p.Q329X), found in a single affected male child. *NLGN4X* is an X-linked gene encoding a neuronal synaptic adhesion molecule, and mutations in *NLGN4X* have been described in individuals with autism, Asperger syndrome, and intellectual disability (Jamain et al., 2003). This mutation was inherited from an unaffected mother, consistent with prior observations that carrier females may be asymptomatic (Südhof, 2008; Table 1A; Figure S4).

In another family, two male children affected with autism carried a nonsense mutation in the X-linked gene *MECP2* (p.E483X), the gene responsible for Rett syndrome (Table 1A). Their mutation was also inherited from the unaffected mother, who was heterozygous (Figure S4). The finding of *MECP2* nonsense mutations in this family was unusual since these are typically lethal in males (Chahrour and Zoghbi, 2007), suggesting that this allele is likely hypomorphic. Consistent with this idea, p.E483X is a late truncation predicted to remove only the last four amino acids of the full-length protein.

Two consanguineous families had homozygous nonsense or frameshift mutations in *PAH* (Table 1A; Figure S4), the cause of phenylketonuria and one of the earliest neurometabolic syndromes described as a cause of ASD (Zecavati and Spence, 2009). These families were confirmed to have phenylketonuria by clinical laboratory testing.

An additional ASD family implicated a syndrome associated with dysmorphic features and microcephaly. We found a homozygous frameshift alteration in *VPS13B/COH1* in the proband in a consanguineous family who had ASD and mild dysmorphic features (Figure 5A; Table 1A). The mutation (p.A3943fs) causes truncation of the C-terminal 54 amino acids of VPS13B/COH1. Recessive mutations in *VPS13B/COH1* cause Cohen syndrome, characterized by a constellation of intellectual disability, facial dysmorphism, retinal dystrophy, truncal obesity, joint laxity, intermittent neutropenia, and postnatal microcephaly (Hennies et al., 2004) that has previously been associated with autistic symptoms in some cases (Douzgou and Petersen, 2011). However, significant variability in the features associated with Cohen syndrome makes clinical diagnosis challenging (Mochida et al., 2004; Seifert et al., 2006). The affected child in our cohort had several features that suggest a diagnosis of Cohen syndrome, including microcephaly (head circumference 49 cm at age 9, $\ll 3^{rd}$ percentile) and the characteristic facial dysmorphisms typically seen in Cohen syndrome (Figures 5B and 5C; Supplemental Text).

In addition to severe loss-of-function mutations, a significant proportion of rare missense variants are also expected to be significantly deleterious (Kryukov et al., 2007), as underscored by our *AMT* and *PEX7* findings. Eleven families were found to have rare, segregating, homozygous or hemizygous missense changes in known genes (Tables 1B, S3, and S4). While some of these may be expected to be functionally silent, we found clinical and/or biochemical evidence supporting their pathogenicity in at least four instances (Table 1B).

In one consanguineous ASD family, we identified a linked homozygous missense change in *AMT* (p.D198G) in a single affected child with ASD and intellectual disability (Table 1B). This variant was heterozygous in both parents and an unaffected sibling, and disrupts a highly conserved residue of AMT (SIFT score 0.01). Functional assays of AMT p.D198G demonstrated that, like p.I308F and other NKH-associated mutations, p.D198G is poorly soluble (Figure S5). AMT p.D198G also exhibited a temperature-sensitive protein stability defect (Figure S5). Enzyme specific activity was preserved (Figure S5), suggesting that pathogenicity may be due to protein misfolding/stability and not catalytic dysfunction, similar to what is observed for p.G47R, a known NKH-associated AMT mutation (Figure S1; Table S1). These findings suggest that this child may have also suffered from undiagnosed, atypical NKH.

A child affected with ASD and moderate intellectual disability was found to have a homozygous missense change (p.R367H) in *POMGNT1* (Table 1B; Figure S4). *POMGNT1* is responsible for an inherited dystroglycanopathy characterized by brain malformation, intellectual disability, developmental delay, hypotonia, and myopia; interestingly, rare patients have been reported with severe autistic features (Haliloglu et al., 2004; Hehr et al., 2007). The p.R367H missense variant in this patient disrupts a highly conserved residue, and this exact allele has been reported as causative in a patient with relatively mild clinical disease, as a compound heterozygous mutation in combination with a splice site mutation (Godfrey et al., 2007).

Finally, in another consanguineous family, the single affected child was homozygous for a rare missense variant (p.S824A) in *VPS13B* (Table 1B; Figure S4). The proband had in retrospect some but not all features of Cohen syndrome (autism with mild facial dysmorphism and joint laxity), consistent with mild versions reported previously (Hennies et al., 2004).

To begin to explore how these results might extend to nonconsanguineous families, we screened for mutations in genes implicated from our cohort (*AMT*, *PEX7*, *SYNE1*, *VPS13B*, *PAH*, and *POMGNT1*) in 612 families from the Simons Simplex Collection (193 trios with parents and affected child, plus 419 quartets with parents, affected child, and unaffected sibling). An analysis of publicly released whole-exome sequence data (Iossifov et al., 2012; O'Roak et al., 2012; Sanders et al., 2012) showed a modest trend toward an excess of biallelic, inherited, rare (MAF < 1%), protein-altering variants in cases (8/612) compared to control siblings (2/419) ($p = 0.21$, Fisher's exact test, two-tailed) in at least one of the genes we screened (Table S5). As expected for a nonconsanguineous cohort, all but one were found in the compound heterozygous state. Although functional validation

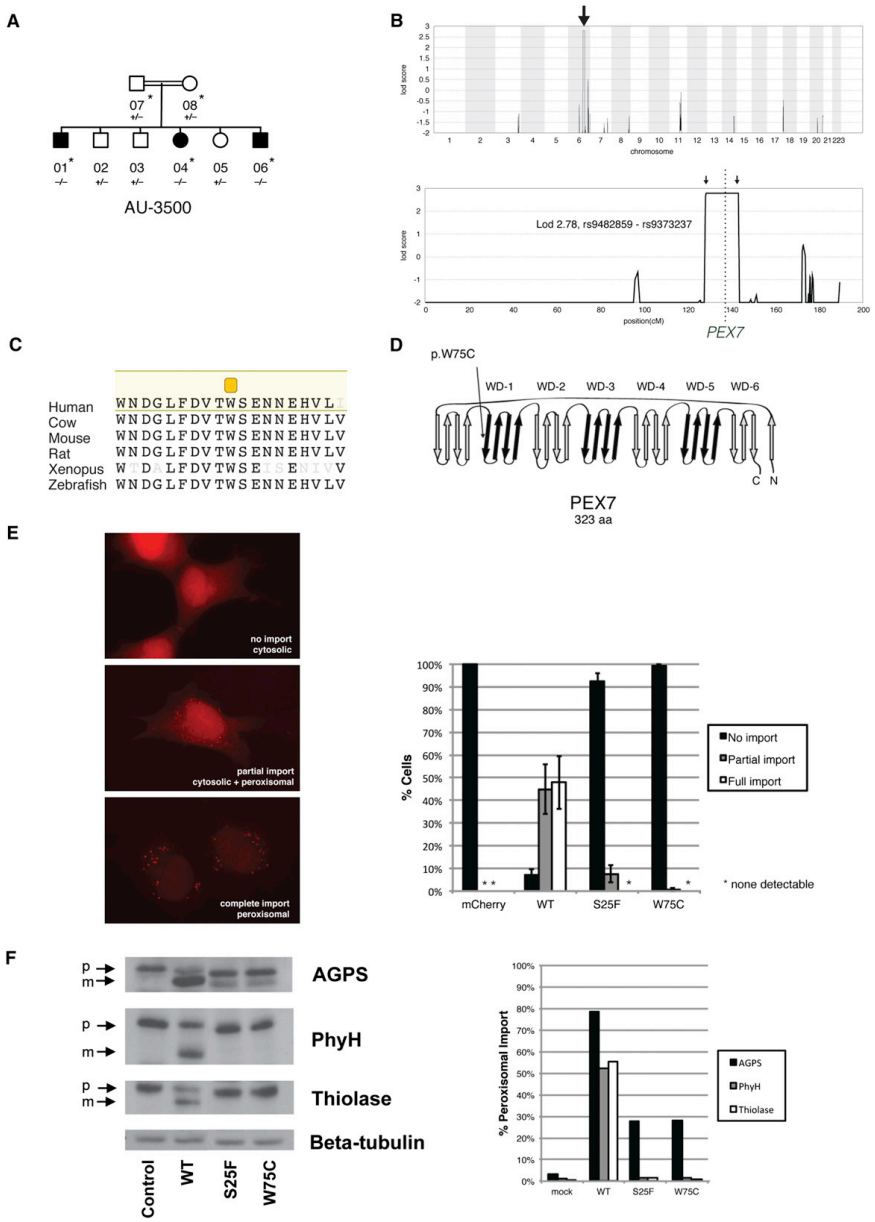

Figure 2. Identification of Mutations in *PEX7* in a Family with ASD

(A) AU-3500, a family with three children affected with ASD. Shaded symbols indicate affected individuals. WES was performed on samples from individuals indicated with a star. Genotyping by Sanger sequencing in additional family members was performed where indicated (+, reference allele; –, alternate allele).

(legend continued on next page)

of all of these mutations is not available, in at least two cases, phenotype data are supportive of the mutations' pathogenicity. One affected male child was compound heterozygous for two different mutations in *VPS13B* (p.W963X/p.G2704R). Gly2704 is a highly conserved residue, while p.W963X leads to early truncation of the protein and has been previously reported in Cohen syndrome (Kolehmainen et al., 2004). Review of the clinical phenotype of this individual confirmed that he manifested, in addition to autism, features of Cohen syndrome including prominent microcephaly (<3 SD) and somatic dysmorphisms (Supplemental Text), making the diagnosis of a Cohen syndrome mutation highly likely. A second, unrelated male child affected with autism was compound heterozygous for two rare point mutations in *VPS13B*, p.S3303R and p.A3691T, both altering highly conserved residues. In addition to being autistic, this child also manifested dysmorphisms of the face and extremities as well as an abnormal hair growth pattern, known to characterize Cohen syndrome. These data confirm that biallelic mutations are also found in nonconsanguineous autism cohorts, but analysis of much larger numbers of genes and patients will be needed to quantify their prevalence.

DISCUSSION

Our data combine WES with segregation analysis to demonstrate that biallelic, hypomorphic mutations underlie at least a subset of ASDs (Chahrour et al., 2012; Morrow et al., 2008), and together with a report on biallelic null mutations in this same issue of *Neuron* (Lim et al., 2013), provide strong evidence for a role of inherited recessive mutations in contributing to ASD. We demonstrate the utility of our approach in identifying three new ASD genes from a relatively small sample enriched for recessive inheritance. We present three families that simplify the identification of causative genes by narrowing genetic loci to 1%–3% of the genome and allow identification of single mutations that are rare and likely to be functional. These analyses demonstrate a strategy for dissection of an otherwise highly heterogeneous disorder. We present additional evidence that biallelic mutations occur in other smaller families, as well as in European American families from the Simons Simplex Collection. As high-quality whole-exome sequencing data from additional cohorts becomes available, it will be valuable to quantify the prevalence of these biallelic mutations in ASD in general. A common theme of many of the mutations identified in this cohort is hypomorphic mutations that partially impair gene function, though one or two null mutations are also identified.

The finding of partially disabling mutations in *AMT* and *PEX7* suggests that mild forms of neurometabolic conditions may present with autistic symptoms, although such very mild mutations may be quite rare, especially in nonconsanguineous populations. Although several neurometabolic disorders have been associated with autistic symptoms (Zecavati and Spence, 2009; Novarino et al., 2012), milder forms of other metabolic conditions may also be potentially missed by current newborn or biochemical screening tests, which have limits to their sensitivity (Watson et al., 2006). In analogous fashion, the rare biallelic variants we identified in other syndromic neurodevelopmental genes (*VPS13B/COH1*, *SYNE1*, *MECP2*, *POMGNT1*) also seem to represent mutations in genes in which complete knockout causes more severe syndromes, but which present with milder ASD phenotypes when partially inactivated. Exome sequencing will likely improve our ability to recognize these difficult-to-diagnose cases. Metabolic conditions are especially critical to identify since for some neurometabolic conditions, interventions may be available.

In this study, we focused on identifying rare, deleterious, penetrant variants that are causative of ASD in the families in question. Our data does not rule out contributions of common variation to ASD in other cases. While common variants are under less selective pressure than rare variants and are more likely to be benign, the functional impact of most common variants is poorly understood. Some might be expected to lie in autism gene pathways, impact biochemical function, and modify disease risk. For example, a common deletion in *TMLHE*, encoding the first enzyme in carnitine biosynthesis, has been recently implicated as a risk factor for autism (Celestino-Soper et al., 2012).

Genes implicated in this study include ones known to regulate or be regulated by synaptic activity (*MECP2*, *SYNE1*) but also genes not traditionally thought of as having synaptic roles (*AMT*, *PEX7*, *VPS13B/COH1*). This could reflect an important role for nonsynaptic genes and suggest the involvement of hitherto unexpected pathways in ASDs. Alternatively, given the strength of genetic evidence implicating genes of the synapse as causative in ASDs, *AMT*, *PEX7*, and *VPS13B/COH1* may have involvement in synaptic pathways that have yet to be characterized. *AMT* for example, regulates turnover of glycine, a crucial inhibitory neurotransmitter (Baer, 2009; Keck and White, 2009). *PEX7* regulates peroxisomal protein import, and peroxisomes are abundant in dendrites (Kou et al., 2011). Finally, VPS13B/COH1 has essential roles in vesicle trafficking through the Golgi apparatus (Seifert et al., 2011). Hence, while null

(B) Mapping to a locus on chromosome 6. Genome-wide linkage plot (top) and maximum obtainable LOD score in the family across the interval (bottom).
A homozygous missense mutation in the AU-3500 family disrupts a conserved tryptophan (p.W75C) (C) in the first WD40 repeat of *PEX7*, the receptor responsible for import of PTS2-containing proteins into the peroxisome (D), and an established cause of rhizomelic chondrodysplasia punctata.
(E) PEX7 W75C and S25F, a previously characterized mutation from a patient with mild RCDP and ASD, result in partial loss of function in a peroxisomal import assay. In fibroblasts from patients with RCDP, PTS2-tagged mCherry accumulates in the cytoplasm due to lack of PEX7 transport activity (top). Transfection of wild-type PEX7 cDNA causes PTS2-mCherry to redistribute to small puncta, indicative of restoration of peroxisomal import (bottom). Transfection of mutant PEX7 W75C or S25F does not restore complete import, with a minority of cells showing partial import (middle). Quantification of defects in peroxisomal import mediated by ASD-associated PEX7 alleles, scored by visual assay. Error bars represent standard error (right).
(F) Immunoblotting of whole cell lysates illustrates deficient maturation of PTS2-targeted proteins in a RCDP cell line transfected with ASD-associated PEX7 alleles. AGPS, PhyH, and thiolase are imported into the peroxisome and undergo cleavage into a smaller, mature peptide. p, preprotein; m, mature protein; Beta-tubulin, loading control. Quantification of processing defects by densitometry of transfected cell lysates (right).

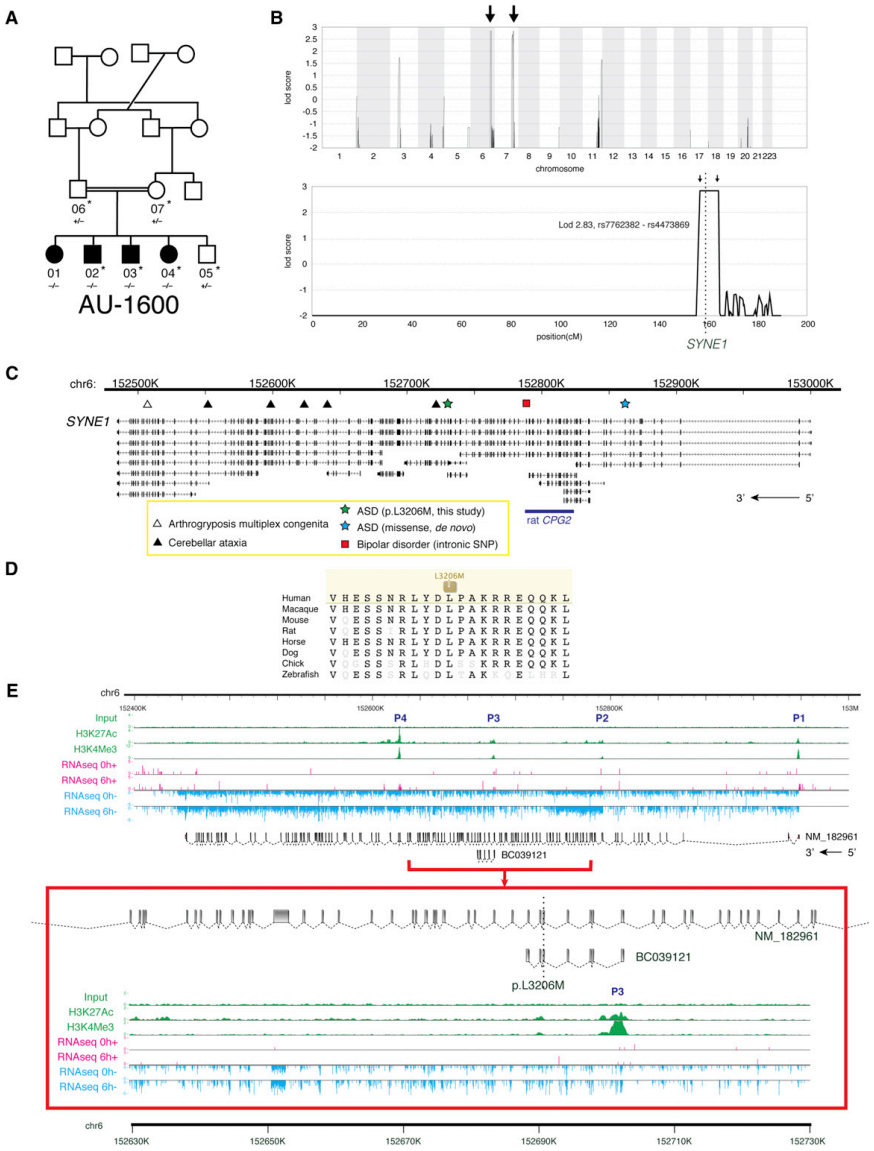

Figure 3. Identification of Mutations in *SYNE1* in a Family with ASD

(A) AU-1600, a family with four children affected with ASD. Shaded symbols indicate affected individuals. WES was performed on samples from individuals indicated with a star. Genotyping by Sanger sequencing in additional family members was performed where indicated (+, reference allele; –, alternate allele).

(B) Mapping rules out the majority of the genome and points out to only two candidate loci, one on chromosome 6 and the other on chromosome 7. Genome-wide linkage plot (top) and maximum obtainable LOD score in the family across the interval (bottom).

(C) *SYNE1* is a complex locus implicated in neuropsychiatric disease. *SYNE1* encompasses multiple alternative transcripts (Known Genes, UCSC Genome Browser), and mutations have been associated with a wide range of neurodevelopmental phenotypes. The location of the recessively inherited missense change

(legend continued on next page)

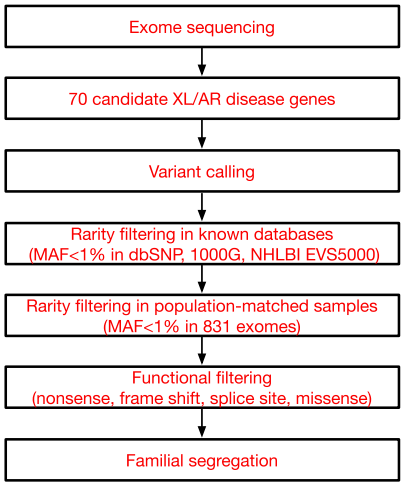

Figure 4. Schematic of the Analytical Pipeline
Tiered strategy for examining the cohort of ASD families for inherited mutations in known disease genes. Whole-exome sequencing data were used to systematically survey 70 genes (listed in Table S2) known to be associated with autosomal recessive or X-linked neurodevelopmental illness and autistic features. Variants were filtered based on rarity (MAF < 1%) in known databases and our internal, population-matched data set (see Experimental Procedures for details), and predicted functional effect on the protein. All candidate variants were validated by Sanger sequencing and were required to segregate within the family. XL, X-linked; AR, autosomal recessive; MAF, minor allele frequency; 1000G, 1000 Genomes Project; NHLBI EVS5000, NHLBI Exome Sequencing Project. See also Figure S4.

mutations in these genes have effects in many tissues, hypomorphic mutations may cause subtler defects primarily limited to neurons.

Our data support the interpretation that biallelic mutations in the proper setting can cause a spectrum of clinical phenotypes, which at one extreme cause a Mendelian disorder, but at the other extreme represent risk alleles for ASDs. In our multiplex pedigrees, siblings who share homozygosity for the identical biallelic mutation still can show a variety of phenotypes, ranging from ASD to intellectual disability, and including epilepsy and/or other features. This variable expressivity has parallels in known associations of ASD with Mendelian genes like *FMR1* or *TSC2*, which are near fully penetrant for syndromic features of Fragile X or Tuberous Sclerosis, respectively, but only partially penetrant for ASD (Hagerman et al., 2010; Wiznitzer, 2004). Variability of phenotype is also characteristic of recurrent ASD-associated CNVs, such as 16p11.2, which has been linked not only to ASD but also to schizophrenia, epilepsy, ADHD, and obesity (McCarthy et al., 2009; Shinawi et al., 2010; Walters et al., 2010; Weiss et al., 2008). The common theme of variability of phenotype despite underlying shared genetic susceptibility increasingly suggests that highly penetrant mutations associated strictly with ASD, and never with other conditions, may be extremely rare or nonexistent.

Our data extend the observation that hypomorphic alleles can commonly cause conditions that may be dramatically different from null mutations in the same gene (Walsh and Engle, 2010). Hypomorphic, biallelic mutations, combined with CNVs and heterozygous stop mutations (Neale et al., 2012; O'Roak et al., 2012; Sanders et al., 2012) which completely inactivate one of two alleles, suggest that a common theme for ASD mutations in general might be partial loss of gene function and/or dosage sensitivity. In other words, ASD, and potentially other neuropsychiatric conditions, may be united by incomplete loss of function of specific synaptic genes. Such incomplete loss might provide a general model for the complex genetic architecture, and genetic heterogeneity, of ASDs. In this respect, neuropsychiatric conditions may increasingly come to be understood as much by their allelic architecture as by the specific causative genes.

EXPERIMENTAL PROCEDURES

Human Studies
All human studies were reviewed and approved by the institutional review board of the Boston Children's Hospital, Beth Israel Deaconess Medical Center, and local institutions.

Patient Recruitment
The families presented were collected by the Homozygosity Mapping Collaborative for Autism (HMCA) (Morrow et al., 2008), with referral centers in Turkey, the Kingdom of Saudi Arabia, Kuwait, United Arab Emirates, Oman, Jordan, and Pakistan. Inclusion criteria included a diagnosis of autism or ASD by a neurologist, child psychiatrist, or psychologist and families with multiple affected children and/or suspected consanguinity. See Supplemental Experimental Procedures for further phenotyping details. Additional clinical information on families described here is provided in Supplemental Text.

Genome-wide Linkage and Homozygosity Scans
Genome-wide SNP screens were performed at the Broad Institute and Dana Farber Cancer Institute. Families were genotyped using Affymetrix 500K (NspI/Sty) or Affymetrix 6.0 microarrays. Linkage disequilibrium-based

in this study is denoted by the green star. Late truncation (open triangle) causes autosomal recessive arthrogyroposis multiplex congenita (Attali et al., 2009), while truncating mutations further upstream (closed triangles) cause autosomal recessive cerebellar ataxia (Gros-Louis et al., 2007). An intronic SNP (red square) is a putative bipolar disorder susceptibility locus (Sklar et al., 2011). A de novo missense change was previously reported in ASD (blue star) (O'Roak et al., 2011). (D) The homozygous missense mutation p.L3206M disrupts a highly conserved residue.
(E) Human neuronal ChIPseq and RNaseq data demonstrate transcriptional complexity and activity-dependent regulation of the *SYNE1* locus. ChIPseq with antibodies to H3K4Me3 (active promoters) and H3K27Ac (enhancers) demonstrates at least four active promoters (P1-P4) for *SYNE1*. P3 lies immediately upstream of the residue mutated in AU-1600 (p.L3206M) and corresponds to the active promoter site for BC039121. RNAseq of cultured human neurons was performed before (0h, 0 hr) and after (6h, 6 hr) depolarization with KCl. Depolarization induces upregulation of full-length *SYNE1* and the BC039121 isoform compared to untreated neurons (also see Figure S3). The experiment was performed on five biological replicates. Representative tracks are shown. The red square represents a magnification of the region around BC039121. Sense (+, pink) and antisense (–, blue) transcripts are indicated.
See also Table S5.

Figure 5. Identification of a Mutation in *VPS13B*, the Cohen Syndrome Gene, in a Patient with ASD

(A) AU-21100, a family with one child affected with ASD. Shaded symbol indicates affected individual. The triangle represents a miscarriage. WES was performed on samples from individuals indicated with a star. Genotyping by Sanger sequencing in additional family members was performed where indicated (+, reference allele; –, alternate allele).

(B) Photographs of proband, demonstrating mild facial dysmorphisms consistent with Cohen syndrome: prominent nasal tip, protruding maxilla, and short philtrum. For additional clinical details, see Supplemental Text.

(C) Head circumference for proband compared to published population normative data (reprinted with permission from Schienkiewitz et al., 2011). KiGGS: norms from German Health Interview and Examination Survey for Children and Adolescents, 2003–2006. Prader: previously published Swiss growth curves from 1989. See also Table S5.

SNP pruning was performed with PLINK, followed by filtering of loci homozygous in all samples and those with Mendelian inheritance errors. Multipoint LOD scores were calculated using MERLIN, assuming a recessive mode of disease inheritance, full penetrance, and a disease allele frequency of 0.0001. Runs of homozygosity were calculated using custom Perl scripts, allowing for no more than two consecutive heterozygous SNPs in a run and three heterozygous calls in every ten consecutive SNPs. Intervals homozygous for the same haplotype and shared by all affected individuals were used to narrow the locus in each family. See Supplemental Experimental Procedures for details.

Whole-Exome Sequencing and Data Analysis

DNA samples were sequenced at the Broad Institute. Whole blood DNA was subject to exome capture (SureSelect v2, Agilent Technologies) and whole-exome sequence (Illumina HiSeq) was obtained on a total of 277 affected children and 409 parents, with a mean target coverage of 85.6% at $\geq$20× and a mean read depth of 158×. For this study, families harboring known autism-associated CNVs were excluded (Supplemental Experimental Procedures). Reads were aligned to NCBI human genome build v37 and variants were called and annotated using GATK. ANNOVAR (Wang et al., 2010) and custom pipelines. All reported variants were confirmed by Sanger sequencing. See Supplemental Experimental Procedures for additional details.

SSC Exome Reanalysis

Exome data from 612 families from the Simons Simplex Collection were obtained from dbGAP and NDAR. Raw sequence reads were aligned with BWA and variants were called with Samtools and annotated as previously described (Sanders et al., 2012).

Sanger Resequencing

See Supplemental Experimental Procedures for details.

Data Visualization

See Supplemental Experimental Procedures for details.

AMT Expression and Enzymatic Assays

Wild-type and mutant human AMT proteins with a C-terminal His6-tag were expressed and purified as previously described (Okamura-Ikeda et al., 2005). I308F, I308A, D198G, or D198A substitutions were introduced using site-directed mutagenesis, and enzymatic activities were determined as previously described (Okamura-Ikeda et al., 2010).

For heat stability studies, wild-type and mutant AMTs (about 0.5 mg/ml in 20 mM Tris-HCl [pH 7.5], 1 mM DTT, 20 mM (p-amidinophenyl) methanesulfonyl fluoride, and 10% glycerol) were incubated for 1, 2, and 3 hr at 37°C and 42°C. After incubation, the solutions were centrifuged and the protein concentrations in the supernatants were determined using Coomassie Plus (Thermo Scientific, USA) with BSA as standard. The remaining protein concentrations in the supernatant were showed as a percent of the initial concentrations.

PEX7 Peroxisomal Import Assays

A peroxisomal import marker was generated by fusing mCherry fluorescent protein to the PTS2 signal located in the first 26 amino acids of rat 3-ketoacyl-CoA thiolase [P07871.2] (Tsukamoto et al., 1994). N-terminal c-*myc* tagged variants of PEX7 (W75C and S25F) were engineered using PCR based site-directed mutagenesis of the N-myc-PEX7 cDNA [NM_000288] in pCDNA1. PEX7 and PTS2-mCherry were transiently transfected into an immortalized RCDP1 fibroblast line with a *PEX7* null genotype (p.L292X]; [S132X) and processed at 3 days for direct and indirect immunofluorescence as previously reported (Braverman et al., 2002). Recovery of peroxisomal import was assessed by blinded visual scoring of 100 cells each from 3 separate transfections. Peroxisomal import was confirmed by colocalization of the peroxisome membrane protein PEX14. Whole cell lysates from similarly transfected fibroblasts were used for immunoblotting with antibodies to the endogenous PTS2 proteins thiolase, PhyH, and AGPS (Zhang et al., 2010). PEX7 protein expression was confirmed with a c-*myc* antibody (SC789, Santa Cruz Biotechnology Inc., Santa Cruz, CA).

RNaseq of Human Neurons

Primary human neuronal cells were purchased from Sciencell (Carlsbad, CA). For RNaseq experiments, neuronal cultures from three biological replicates were grown for around two weeks (DIV13–16). At the final day in culture, neurons in the experimental group were stimulated for 6 hr with 55 mM KCl and were harvested along with the unstimulated control neurons using Trizol (Invitrogen). Strand-specific and paired-end cDNA libraries were generated using the PE RNaseq library kit (Illumina). RNaseq was performed using HiSeq 2000 at the Broad Institute. 76-bp RNaseq reads were aligned to the human GRCh37/hg19 assembly using BWA. See Supplemental Experimental Procedures for details. For quantification of *SYNE1* expression in response to depolarization, for each biological replicate, expression levels (normalized reads per bp) of individual exons were calculated, which allowed the calculation of the average expression level over any isoform of *SYNE1* comprising subsets of

these exons. Then fold-change ratios (6 hr/unstimulated) of these levels were calculated for each replicate and isoform, and finally each isoform's mean and standard error over the replicates' fold changes.

ChIPseq of Human Neurons

The mini-ChIP assays were performed as previously described (Adli and Bernstein, 2011) on human neuronal cells that had been cultured for around two weeks. Briefly, cells were cross-linked, lysed, and the fragmented chromatin was then immunoprecipated with H3K27Ac (Abcam Cat# ab4728) and H3K27me3 (Millipore Cat# 074490) antibodies. The ChIP DNA was recovered and precipitated following standard procedures. The ChIP DNA libraries were then constructed using ChIP-Seq DNA Sample Prep Kit (Illumina) and subsequently sequenced using HiSeq 2000 (Illumina) in Biopolymers facility at Harvard Medical School. ChIPseq reads were aligned to the human genome (GRCh37/hg19 assembly). See Supplemental Experimental Procedures for details.

Data Access

Whole-exome sequence data is available online (The National Database for Autism Research [NDAR] Collection ID: NDARCOL0001918).

SUPPLEMENTAL INFORMATION

Supplemental Information includes five figures, five tables, Supplemental Experimental Procedures, and Supplemental Text and can be found with this article online at http://dx.doi.org/10.1016/j.neuron.2012.11.002.

ACKNOWLEDGMENTS

We are grateful to Ed Gilmore, Chiara Manzini, Jenny Yang, and Mark Daly for stimulating discussions and helpful comments on the manuscript and Thomas Lehner for support from the National Institute of Mental Health (NIMH). We are also grateful for the participation of the many families that enrolled in our studies as well as for the collaborative support of the Kuwait Center for Autism and the Dubai Autism Center. T.W.Y. was supported by a National Institute of Health (NIH) T32 grant (T32 NS007484-08), the Clinical Investigator Training Program (CITP) at Harvard-MIT Health Sciences and Technology and Beth Israel Deaconess Medical Center in collaboration with Pfizer, Inc. and Merck and Company, Inc., and the Nancy Lurie Marks Junior Faculty MeRIT Fellowship. M.H.C. was supported by a NIH T32 grant (T32 NS007473-12). G.H.M. was supported by the Young Investigator Award of NARSAD as a NARSAD Lieber Investigator. A.P. was supported by the National Institutes of Neurological Disease and Stroke (K23NS069784). A.M.D. was supported by the National Institute of General Medical Sciences (T32GM07753). Research was supported by grants from the National Institute of Mental Health (RO1 MH083565; 1RC2MH089952) to C.A.W., the NIH to M.E.G. (RO1 NS048276), the NIMH to E.M.M. (1K23MH080954-01), the Dubai Harvard Foundation for Medical Research, the Nancy Lurie Marks Foundation, the Simons Foundation, the Autism Consortium, and the Manton Center for Orphan Disease Research. Sequencing at the Broad Institute was supported by the ARRA Grand Opportunities grant 1RC2MH089952. C.A.W. is an Investigator of the Howard Hughes Medical Institute. T.W.Y. identified *AMT*, *PEX7*, and *SYNE1* mutations, helped design *AMT* and *PEX7* functional studies, designed and performed exome sequencing analyses for candidate genes, contributed to CNV analyses, and wrote the manuscript. M.H.C. designed and performed exome sequencing analyses for candidate genes, analyzed Sanger validation data and SSC exome data, and wrote the manuscript. M.E.C. helped analyze AU-1700 and AU-3500. S.J. designed PEX7 functional experiments with N.E.B., and S.J. performed them. K.O.-I. designed and performed AMT functional studies and analyzed results. B.A. designed and analyzed RNAseq, ChIPseq, and qPCR experiments. D.A.H. analyzed RNAseq and qPCR experiments. M.A. performed ChIPseq experiments, and A.N.M. analyzed the data. A.M.D. performed RACE experiments for *SYNE1*. K.S.-A. and K.M. designed the CNV analysis, and K.S.-A. compiled the CNV catalog and identified pathogenic CNVs. E.T.L. and S.J.S. helped analyze SSC whole-exome data. G.H.M. performed clinical phenotyping of Middle Eastern families as well as detailed molecular analyses of AU-8600. J.N.P. organized clinical information and patient samples. C.M.S. assisted with exome sequencing analyses and performed follow-up Sanger validation. J.M.F. and J.R. performed follow-up Sanger validation. R.H.N. performed clinical phenotyping of AU-17800. J.W performed clinical phenotyping of AU-17700 and AU-17800. R.M.J. performed clinical phenotyping of AU-1600, AU-10000, and AU-10200. R.S.H. performed genome-wide linkage studies and homozygosity analyses. B.Y.K. assisted with characterization of the *AMT* mutation. M.A.-S. organized clinical information and patient samples and referred AU-17700 and AU-17800. N.M.M. referred and clinically characterized AU-4200, AU-4400, AU-4900, AU-5700, AU-6100, AU-6200, AU-6300, AU-8600, AU-11100, AU-11800, AU-11900, AU-12100, AU-12400, AU-14900, AU-15800, AU-16700, AU-20700, AU-22500, AU-23400, and AU-24300. A.H. referred and characterized AU-3500 and AU-3600. S.B. referred and characterized AU-1700. G.G. referred and characterized AU-1700, AU-3100, AU-4100, and AU-6000. F.M.H. helped characterize AU-17700 and AU-17800. E.L. and A.P. performed clinical phenotyping of AU-1600, AU-10000, and AU-10200. O.O. referred and characterized AU-13100, AU-13400, AU-18000, AU-20300, and AU-22000. S.A.-S., S.A.A.-A., and L.B. referred and characterized AU-1600. S.A.-S. referred and characterized AU-9600. T.B.-O. and A.S.T. referred and characterized AU-21100. L.A.-G. and V.E. referred and characterized AU-3200. C.R.S. organized and coordinated exome sequencing. L.R. evaluated the second compound heterozygous *PEX7* family. S.B.G. directed exome sequencing. K.M. designed the CNV analysis. M.W.S. oversaw SSC exome analyses. M.E.G. oversaw *SYNE1* RNAseq and qPCR experiments. H.T. designed and performed AMT functional experiments. N.E.B. designed PEX7 functional experiments, recruited the nonconsanguineous family with two sisters affected by *PEX7* mutation, and contributed to interpretation of *PEX7* sequencing data. E.M.M. helped characterize AU-1700, performed linkage studies on AU-1600, AU-1700, and AU-3500, helped design the exome sequencing experiment, and contributed to finding the *SYNE1* mutation. C.A.W. directed the overall research and wrote the manuscript.

Accepted: November 2, 2012
Published: January 23, 2013

REFERENCES

Adli, M., and Bernstein, B.E. (2011). Whole-genome chromatin profiling from limited numbers of cells using nano-ChIP-seq. Nat. Protoc. *6*, 1656–1668.

Applegarth, D.A., and Toone, J.R. (2001). Nonketotic hyperglycinemia (glycine encephalopathy): laboratory diagnosis. Mol. Genet. Metab. *74*, 139–146.

Applegarth, D.A., and Toone, J.R. (2004). Glycine encephalopathy (nonketotic hyperglycinaemia) : review and update. J. Inherit. Metab. Dis. *27*, 417–422.

Attali, R., Warwar, N., Israel, A., Gurt, I., McNally, E., Puckelwartz, M., Glick, B., Nevo, Y., Ben-Neriah, Z., and Melki, J. (2009). Mutation of SYNE-1, encoding an essential component of the nuclear lamina, is responsible for autosomal recessive arthrogryposis. Hum. Mol. Genet. *18*, 3462–3469.

Baer, K. (2009). Localisation of glycine receptors in the human forebrain, brainstem, and cervical spinal cord: an immunohistochemical review. Front. Mol. Neurosci. *2*. http://dx.doi.org/10.3389/neuro.02.025.2009.

Bamshad, M.J., Ng, S.B., Bigham, A.W., Tabor, H.K., Emond, M.J., Nickerson, D.A., and Shendure, J. (2011). Exome sequencing as a tool for Mendelian disease gene discovery. Nat. Rev. Genet. *12*, 745–755.

Betancur, C. (2011). Etiological heterogeneity in autism spectrum disorders: more than 100 genetic and genomic disorders and still counting. Brain Res. *1380*, 42–77.

Braverman, N., Steel, G., Obie, C., Moser, A., Moser, H., Gould, S.J., and Valle, D. (1997). Human PEX7 encodes the peroxisomal PTS2 receptor and is responsible for rhizomelic chondrodysplasia punctata. Nat. Genet. *15*, 369–376.

Braverman, N., Chen, L., Lin, P., Obie, C., Steel, G., Douglas, P., Chakraborty, P.K., Clarke, J.T.R., Boneh, A., Moser, A., et al. (2002). Mutation analysis of PEX7 in 60 probands with rhizomelic chondrodysplasia punctata and functional correlations of genotype with phenotype. Hum. Mutat. *20*, 284–297.

Casey, J.P., Magalhaes, T., Conroy, J.M., Regan, R., Shah, N., Anney, R., Shields, D.C., Abrahams, B.S., Almeida, J., Bacchelli, E., et al. (2012). A novel approach of homozygous haplotype sharing identifies candidate genes in autism spectrum disorder. Hum. Genet. *131*, 565–579.

Celestino-Soper, P.B.S., Violante, S., Crawford, E.L., Luo, R., Lionel, A.C., Delaby, E., Cai, G., Sadikovic, B., Lee, K., Lo, C., et al. (2012). A common X-linked inborn error of carnitine biosynthesis may be a risk factor for nondysmorphic autism. Proc. Natl. Acad. Sci. USA *109*, 7974–7981.

Chahrour, M., and Zoghbi, H.Y. (2007). The story of Rett syndrome: from clinic to neurobiology. Neuron *56*, 422–437.

Chahrour, M.H., Yu, T.W., Lim, E.T., Ataman, B., Coulter, M.E., Hill, R.S., Stevens, C.R., Schubert, C.R., Greenberg, M.E., Gabriel, S.B., and Walsh, C.A.; ARRA Autism Sequencing Collaboration. (2012). Whole-exome sequencing and homozygosity analysis implicate depolarization-regulated neuronal genes in autism. PLoS Genet. *8*, e1002635.

Cottrell, J.R., Borok, E., Horvath, T.L., and Nedivi, E. (2004). CPG2: a brain- and synapse-specific protein that regulates the endocytosis of glutamate receptors. Neuron *44*, 677–690.

Devlin, B., and Scherer, S.W. (2012). Genetic architecture in autism spectrum disorder. Curr. Opin. Genet. Dev. *22*, 229–237.

Dinopoulos, A., Matsubara, Y., and Kure, S. (2005). Atypical variants of nonketotic hyperglycinemia. Mol. Genet. Metab. *86*, 61–69.

Douzgou, S., and Petersen, M.B. (2011). Clinical variability of genetic isolates of Cohen syndrome. Clin. Genet. *79*, 501–506.

Ernst, J., Kheradpour, P., Mikkelsen, T.S., Shoresh, N., Ward, L.D., Epstein, C.B., Zhang, X., Wang, L., Issner, R., Coyne, M., et al. (2011). Mapping and analysis of chromatin state dynamics in nine human cell types. Nature *473*, 43–49.

Godfrey, C., Clement, E., Mein, R., Brockington, M., Smith, J., Talim, B., Straub, V., Robb, S., Quinlivan, R., Feng, L., et al. (2007). Refining genotype phenotype correlations in muscular dystrophies with defective glycosylation of dystroglycan. Brain *130*, 2725–2735.

Grady, R.M., Starr, D.A., Ackerman, G.L., Sanes, J.R., and Han, M. (2005). Syne proteins anchor muscle nuclei at the neuromuscular junction. Proc. Natl. Acad. Sci. USA *102*, 4359–4364.

Gros-Louis, F., Dupré, N., Dion, P., Fox, M.A., Laurent, S., Verreault, S., Sanes, J.R., Bouchard, J.-P., and Rouleau, G.A. (2007). Mutations in SYNE1 lead to a newly discovered form of autosomal recessive cerebellar ataxia. Nat. Genet. *39*, 80–85.

Hagerman, R., Hoem, G., and Hagerman, P. (2010). Fragile X and autism: intertwined at the molecular level leading to targeted treatments. Molecular Autism *1*, 12.

Haliloglu, G., Gross, C., Senbil, N., Talim, B., Hehr, U., Uyanik, G., Winkler, J., and Topaloglu, H. (2004). Clinical spectrum of muscle-eye-brain disease: from the typical presentation to severe autistic features. Acta Myologica: Myopathies and Cardiomyopathies *23*, 137–139.

Hamosh, A., and Johnston, M. (2001). Non-ketotic hyperglycinemia. In The metabolic and molecular bases of inherited disease, C.R. Scriver, A.L. Beaudet, W.S. Sly, and D. Valle, eds. (New York: McGraw-Hill), pp. 2065–2078.

Hehr, U., Uyanik, G., Gross, C., Walter, M.C., Bohring, A., Cohen, M., Oehl-Jaschkowitz, B., Bird, L.M., Shamdeen, G.M., Bogdahn, U., et al. (2007). Novel POMGnT1 mutations define broader phenotypic spectrum of muscle–eye–brain disease. Neurogenetics *8*, 279–288.

Heintzman, N.D., Hon, G.C., Hawkins, R.D., Kheradpour, P., Stark, A., Harp, L.F., Ye, Z., Lee, L.K., Stuart, R.K., Ching, C.W., et al. (2009). Histone modifications at human enhancers reflect global cell-type-specific gene expression. Nature *459*, 108–112.

Hennies, H.C., Rauch, A., Seifert, W., Schumi, C., Moser, E., Al-Taji, E., Tariverdian, G., Chrzanowska, K.H., Krajewska-Walasek, M., Rajab, A., et al. (2004). Allelic heterogeneity in the COH1 gene explains clinical variability in Cohen syndrome. Am. J. Hum. Genet. *75*, 138–145.

Iossifov, I., Ronemus, M., Levy, D., Wang, Z., Hakker, I., Rosenbaum, J., Yamrom, B., Lee, Y.H., Narzisi, G., Leotta, A., et al. (2012). De novo gene disruptions in children on the autistic spectrum. Neuron *74*, 285–299.

Jamain, S., Quach, H., Betancur, C., Råstam, M., Colineaux, C., Gillberg, I.C., Soderstrom, H., Giros, B., Leboyer, M., Gillberg, C., and Bourgeron, T.; Paris Autism Research International Sibpair Study. (2003). Mutations of the X-linked genes encoding neuroligins NLGN3 and NLGN4 are associated with autism. Nat. Genet. *34*, 27–29.

Keck, T., and White, J.A. (2009). Glycinergic inhibition in the hippocampus. Rev. Neurosci. *20*, 13–22.

Kolehmainen, J., Wilkinson, R., Lehesjoki, A.-E., Chandler, K., Kivitie-Kallio, S., Clayton-Smith, J., Träskelin, A.-L., Waris, L., Saarinen, A., Khan, J., et al. (2004). Delineation of Cohen syndrome following a large-scale genotype-phenotype screen. Am. J. Hum. Genet. *75*, 122–127.

Kou, J., Kovacs, G.G., Höftberger, R., Kulik, W., Brodde, A., Forss-Petter, S., Hönigschnabl, S., Gleiss, A., Brügger, B., Wanders, R., et al. (2011). Peroxisomal alterations in Alzheimer's disease. Acta Neuropathol. *122*, 271–283.

Kryukov, G.V., Pennacchio, L.A., and Sunyaev, S.R. (2007). Most rare missense alleles are deleterious in humans: implications for complex disease and association studies. Am. J. Hum. Genet. *80*, 727–739.

Lander, E.S., and Botstein, D. (1987). Homozygosity mapping: a way to map human recessive traits with the DNA of inbred children. Science *236*, 1567–1570.

Levy, D., Ronemus, M., Yamrom, B., Lee, Y.H., Leotta, A., Kendall, J., Marks, S., Lakshmi, B., Pai, D., Ye, K., et al. (2011). Rare de novo and transmitted copy-number variation in autistic spectrum disorders. Neuron *70*, 886–897.

Lim, E.T., Raychaudhuri, S., Sanders, S.J., Stevens, C., Sabo, A., MacArthur, D.G., Neale, B.M., Kirby, A., Ruderfer, D.M., Fromer, M., et al. (2013). Rare complete knockouts in humans: population distribution and significant role in autism spectrum disorders. Neuron *77*, this issue, 235–242.

Malhotra, D., and Sebat, J. (2012). CNVs: harbingers of a rare variant revolution in psychiatric genetics. Cell *148*, 1223–1241.

McCarthy, S.E., Makarov, V., Kirov, G., Addington, A.M., McClellan, J., Yoon, S., Perkins, D.O., Dickel, D.E., Kusenda, M., Krastoshevsky, O., et al.; Wellcome Trust Case Control Consortium. (2009). Microduplications of 16p11.2 are associated with schizophrenia. Nat. Genet. *41*, 1223–1227.

Mochida, G.H., Rajab, A., Eyaid, W., Lu, A., Al-Nouri, D., Kosaki, K., Noruzinia, M., Sarda, P., Ishihara, J., Bodell, A., et al. (2004). Broader geographical spectrum of Cohen syndrome due to COH1 mutations. J. Med. Genet. *41*, e87.

Morrow, E.M., Yoo, S.-Y., Flavell, S.W., Kim, T.-K., Lin, Y., Hill, R.S., Mukaddes, N.M., Balkhy, S., Gascon, G., Hashmi, A., et al. (2008). Identifying autism loci and genes by tracing recent shared ancestry. Science *321*, 218–223.

Motley, A.M., Hettema, E.H., Hogenhout, E.M., Brites, P., ten Asbroek, A.L., Wijburg, F.A., Baas, F., Heijmans, H.S., Tabak, H.F., Wanders, R.J., and Distel, B. (1997). Rhizomelic chondrodysplasia punctata is a peroxisomal protein targeting disease caused by a non-functional PTS2 receptor. Nat. Genet. *15*, 377–380.

Najmabadi, H., Hu, H., Garshasbi, M., Zemojtel, T., Abedini, S.S., Chen, W., Hosseini, M., Behjati, F., Haas, S., Jamali, P., et al. (2011). Deep sequencing reveals 50 novel genes for recessive cognitive disorders. Nature *478*, 57–63.

Neale, B.M., Kou, Y., Liu, L., Ma'ayan, A., Samocha, K.E., Sabo, A., Lin, C.-F., Stevens, C., Wang, L.-S., Makarov, V., et al. (2012). Patterns and rates of exonic de novo mutations in autism spectrum disorders. Nature *485*, 242–245.

Novarino, G., El-Fishawy, P., Kayserili, H., Meguid, N.A., Scott, E.M., Schroth, J., Silhavy, J.L., Kara, M., Khalil, R.O., Ben-Omran, T., et al. (2012). Mutations in BCKD-kinase lead to a potentially treatable form of autism with epilepsy. Science *338*, 394–397.

O'Roak, B.J., Deriziotis, P., Lee, C., Vives, L., Schwartz, J.J., Girirajan, S., Karakoc, E., Mackenzie, A.P., Ng, S.B., Baker, C., et al. (2011). Exome sequencing in sporadic autism spectrum disorders identifies severe de novo mutations. Nat. Genet. *43*, 585–589.

O'Roak, B.J., Vives, L., Girirajan, S., Karakoc, E., Krumm, N., Coe, B.P., Levy, R., Ko, A., Lee, C., Smith, J.D., et al. (2012). Sporadic autism exomes reveal a highly interconnected protein network of de novo mutations. Nature *485*, 246–250.

Okamura-Ikeda, K., Hosaka, H., Yoshimura, M., Yamashita, E., Toma, S., Nakagawa, A., Fujiwara, K., Motokawa, Y., and Taniguchi, H. (2005). Crystal structure of human T-protein of glycine cleavage system at 2.0 A resolution and its implication for understanding non-ketotic hyperglycinemia. J. Mol. Biol. *351*, 1146–1159.

Okamura-Ikeda, K., Hosaka, H., Maita, N., Fujiwara, K., Yoshizawa, A.C., Nakagawa, A., and Taniguchi, H. (2010). Crystal structure of aminomethyltransferase in complex with dihydrolipoyl-H-protein of the glycine cleavage system: implications for recognition of lipoyl protein substrate, disease-related mutations, and reaction mechanism. J. Biol. Chem. *285*, 18684–18692.

Pinto, D., Pagnamenta, A.T., Klei, L., Anney, R., Merico, D., Regan, R., Conroy, J., Magalhaes, T.R., Correia, C., Abrahams, B.S., et al. (2010). Functional impact of global rare copy number variation in autism spectrum disorders. Nature *466*, 368–372.

Sanders, S.J., Ercan-Sencicek, A.G., Hus, V., Luo, R., Murtha, M.T., Moreno-De-Luca, D., Chu, S.H., Moreau, M.P., Gupta, A.R., Thomson, S.A., et al. (2011). Multiple recurrent de novo CNVs, including duplications of the 7q11.23 Williams syndrome region, are strongly associated with autism. Neuron *70*, 863–885.

Sanders, S.J., Murtha, M.T., Gupta, A.R., Murdoch, J.D., Raubeson, M.J., Willsey, A.J., Ercan-Sencicek, A.G., DiLullo, N.M., Parikshak, N.N., Stein, J.L., et al. (2012). De novo mutations revealed by whole-exome sequencing are strongly associated with autism. Nature *485*, 237–241.

Schienkiewitz, A., Schaffrath Rosario, A., Dortschy, R., Ellert, U., and Neuhauser, H. (2011). German head circumference references for infants, children and adolescents in comparison with currently used national and international references. Acta Paediatrica *100*, e28–e33.

Sebat, J., Lakshmi, B., Malhotra, D., Troge, J., Lese-Martin, C., Walsh, T., Yamrom, B., Yoon, S., Krasnitz, A., Kendall, J., et al. (2007). Strong association of de novo copy number mutations with autism. Science *316*, 445–449.

Seifert, W., Holder-Espinasse, M., Spranger, S., Hoeltzenbein, M., Rossier, E., Dollfus, H., Lacombe, D., Verloes, A., Chrzanowska, K.H., Maegawa, G.H.B., et al. (2006). Mutational spectrum of COH1 and clinical heterogeneity in Cohen syndrome. J. Med. Genet. *43*, e22.

Seifert, W., Kühnisch, J., Maritzen, T., Horn, D., Haucke, V., and Hennies, H.C. (2011). Cohen syndrome-associated protein, COH1, is a novel, giant Golgi matrix protein required for Golgi integrity. J. Biol. Chem. *286*, 37665–37675.

Shinawi, M., Liu, P., Kang, S.-H.L., Shen, J., Belmont, J.W., Scott, D.A., Probst, F.J., Craigen, W.J., Graham, B.H., Pursley, A., et al. (2010). Recurrent reciprocal 16p11.2 rearrangements associated with global developmental delay, behavioural problems, dysmorphism, epilepsy, and abnormal head size. J. Med. Genet. *47*, 332–341.

Simpson, J.G., and Roberts, R.G. (2008). Patterns of evolutionary conservation in the nesprin genes highlight probable functionally important protein domains and isoforms. Biochem. Soc. Trans. *36*, 1359–1367.

Sklar, P., Ripke, S., Scott, L.J., Andreassen, O.A., Cichon, S., Craddock, N., Edenberg, H.J., Nurnberger, J.I., Rietschel, M., Blackwood, D., et al. (2011). Large-scale genome-wide association analysis of bipolar disorder identifies a new susceptibility locus near ODZ4. Nat. Genet. *43*, 977–983.

Starr, D.A., and Han, M. (2002). Role of ANC-1 in tethering nuclei to the actin cytoskeleton. Science *298*, 406–409.

State, M.W. (2010). The genetics of child psychiatric disorders: focus on autism and Tourette syndrome. Neuron *68*, 254–269.

Stitziel, N.O., Kiezun, A., and Sunyaev, S. (2011). Computational and statistical approaches to analyzing variants identified by exome sequencing. Genome Biol. *12*, 227.

Südhof, T.C. (2008). Neuroligins and neurexins link synaptic function to cognitive disease. Nature *455*, 903–911.

Tsukamoto, T., Hata, S., Yokota, S., Miura, S., Fujiki, Y., Hijikata, M., Miyazawa, S., Hashimoto, T., and Osumi, T. (1994). Characterization of the signal peptide at the amino terminus of the rat peroxisomal 3-ketoacyl-CoA thiolase precursor. J. Biol. Chem. *269*, 6001–6010.

van Bokhoven, H. (2011). Genetic and epigenetic networks in intellectual disabilities. Annu. Rev. Genet. *45*, 81–104.

Walsh, C.A., and Engle, E.C. (2010). Allelic diversity in human developmental neurogenetics: insights into biology and disease. Neuron *68*, 245–253.

Walters, R.G., Jacquemont, S., Valsesia, A., de Smith, A.J., Martinet, D., Andersson, J., Falchi, M., Chen, F., Andrieux, J., Lobbens, S., et al. (2010). A new highly penetrant form of obesity due to deletions on chromosome 16p11.2. Nature *463*, 671–675.

Wang, K., Li, M., and Hakonarson, H. (2010). ANNOVAR: functional annotation of genetic variants from high-throughput sequencing data. Nucleic Acids Res. *38*, e164.

Watson, M., Mann, M., Lloyd-Puryear, M., Rinaldo, P., and Howell, R.; American College of Medical Genetics Newborn Screening Expert Group. (2006). Newborn screening: toward a uniform screening panel and system—executive summary. Pediatrics *117*, S296–S307.

Weiss, L.A., Shen, Y., Korn, J.M., Arking, D.E., Miller, D.T., Fossdal, R., Saemundsen, E., Stefansson, H., Ferreira, M.A.R., Green, T., et al.; Autism Consortium. (2008). Association between microdeletion and microduplication at 16p11.2 and autism. N. Engl. J. Med. *358*, 667–675.

Wiznitzer, M. (2004). Autism and tuberous sclerosis. J. Child Neurol. *19*, 675–679.

Woods, C.G., Cox, J., Springell, K., Hampshire, D.J., Mohamed, M.D., McKibbin, M., Stern, R., Raymond, F.L., Sandford, R., Malik Sharif, S., et al. (2006). Quantification of homozygosity in consanguineous individuals with autosomal recessive disease. Am. J. Hum. Genet. *78*, 889–896.

Zecavati, N., and Spence, S.J. (2009). Neurometabolic disorders and dysfunction in autism spectrum disorders. Curr. Neurol. Neurosci. Rep. *9*, 129–136.

Zhang, Q., Ragnauth, C., Greener, M.J., Shanahan, C.M., and Roberts, R.G. (2002). The nesprins are giant actin-binding proteins, orthologous to Drosophila melanogaster muscle protein MSP-300. Genomics *80*, 473–481.

Zhang, R., Chen, L., Jiralerspong, S., Snowden, A., Steinberg, S., and Braverman, N. (2010). Recovery of PEX1-Gly843Asp peroxisome dysfunction by small-molecule compounds. Proc. Natl. Acad. Sci. USA *107*, 5569–5574.